

CARBON MATERIALS:
CHEMISTRY AND PHYSICS

01

Series Editors F. Cataldo · P. Milani
Volume Editors F. Cataldo · T. Da Ros

Medicinal Chemistry and Pharmacological Potential of Fullerenes and Carbon Nanotubes

 Springer

Medicinal Chemistry and Pharmacological Potential of Fullerenes and Carbon Nanotubes

CARBON MATERIALS: CHEMISTRY AND PHYSICS

A comprehensive book series which encompasses the complete coverage of carbon materials and carbon-rich molecules from elemental carbon dust in the interstellar medium to the most specialized industrial applications of elemental carbon and its derivatives. A great emphasis is placed on the most advanced and promising applications ranging from electronics to medicinal chemistry. The aim is to offer the reader a book series which not only consists of self-sufficient reference works, but one which stimulates further research and enthusiasm.

Series Editors

Dr. Prof. Franco Cataldo
Director of Lupi Chemical Research Institute
Via Casilina 1626/A
00133 Rome,
Italy

Professor Paolo Milani
University of Milan
Department of Physics
Via Celoria, 26
20133, Milan, Italy

VOLUME 1: MEDICINAL CHEMISTRY AND PHARMACOLOGICAL POTENTIAL OF FULLERENES AND CARBON NANOTUBES

Volume Editors

Dr. Prof. Franco Cataldo
Director of Lupi Chemical Research
Institute
Via Casilina 1626/A,
00133 Rome,
Italy

Dr. Tatiana Da Ros
Dipartimento di Scienze
Farmaceutiche
University of Trieste
Piazzale Europe,
I-34127 Trieste, Italy

Franco Cataldo • Tatiana Da Ros

Editors

Medicinal Chemistry and Pharmacological Potential of Fullerenes and Carbon Nanotubes

 Springer

Editors

Dr. Franco Cataldo
Lupi Chemical Research Institute
Rome, Italy

Dr. Tatiana Da Ros
University of Trieste
Trieste, Italy

ISBN 978-1-4020-6844-7

e-ISBN 978-1-4020-6845-4

Library of Congress Control Number: 2008930078

© 2008 Springer Science + Business Media B.V.

No part of this work may be reproduced, stored in a retrieval system, or transmitted in any form or by any means, electronic, mechanical, photocopying, microfilming, recording or otherwise, without written permission from the Publisher, with the exception of any material supplied specifically for the purpose of being entered and executed on a computer system, for exclusive use by the purchaser of the work.

Printed on acid-free paper

9 8 7 6 5 4 3 2 1

springer.com

Preface

The emerging field of nanotechnology is affirming its increasing importance day by day. In this context fullerenes and carbon nanotubes (CNTs) play an important role. These new allotropic forms of carbon have been discovered in the last two decades, and, since then, they have stimulated the curiosity and interest of physicists and chemists.

This book is the first of a new series entitled “Carbon Materials: Chemistry and Physics”, the purpose of which is to analyze the new frontiers of carbon.

This volume summarizes the more recent advances on fullerenes and carbon nanotubes facing the biological-medical horizon, an important and interesting area to the scientific community.

We will present general overviews of fullerenes and CNTs that are state-of-the-art in biomedical applications, deepening their principal and more promising exploitations.

In particular for fullerenes, antioxidant properties and photodynamic activity are presented in detail, together with the analysis of gadolinium endohedrals as magnetic resonance imaging (MRI) contrast agents. Moreover, drug delivery based on carbon nanomaterials has been illustrated.

Few chapters are dedicated to toxicity and to the use of nanomaterials as pollutant probes. The debate on fullerene and CNT toxicity is open and reports different results, which are not always able to abolish the concern about pollution related to the industrial production and their impact on the environment. However, it is possible to state that positive evidence for their favorable applications in medicine has emerged.

Theoretical calculation potentialities have been examined in few chapters, giving new instruments to predict fullerene solubility in different solvents, such as fatty acid esters. Visualization approaches necessary to study unusual compounds such as CNT are herein presented. Despite the structural novelty of CNT, its resemblance to cellular structures is highlighted, launching or confirming the hypothesis of using CNTs as communication devices between cells.

Considering the specificity of the field, this book is mainly addressed to researchers who have delved, or who want to delve, into carbon nanoworld, but at

the same time, it presents a general and accurate view of carbon nanotechnology accessible to researchers intrigued by this topic, but not yet experts in the field.

April 2008

Tatiana Da Ros
Franco Cataldo

Contents

Preface	v
1 Twenty Years of Promises: Fullerene in Medicinal Chemistry	1
Tatiana Da Ros	
2 Biomedical Applications of Functionalised Carbon Nanotubes	23
Alberto Bianco, Raquel Sainz, Shouping Li, Hélène Dumortier, Lara Lacerda, Kostas Kostarelos, Silvia Giordani, and Maurizio Prato	
3 Antioxidant Properties of Water-Soluble Fullerene Derivatives	51
Florian Beuerle, Russell Lebovitz, and Andreas Hirsch	
4 Fullerenes as Photosensitizers in Photodynamic Therapy	79
Pawel Mroz, George P. Tegos, Hariprasad Gali, Timothy Wharton, Tadeusz Sarna, and Michael R. Hamblin	
5 Photodynamic Inactivation of Enveloped Viruses by Fullerene: Study of Efficacy and Safety	107
Vladimir V. Zarubaev, Inna Belousova, Vladimir Rylkov, Alexander Slita, Alexey Sirotkin, Pavel Anfimov, Tatyana Muraviova, and Andrey Starodubtsev	
6 Effects of Photoexcited Fullerene C₆₀-Composites in Normal and Transformed Cells	123
S.V. Prylutska, I.I. Grynyuk, O.P. Matyshevskaya, A.A. Golub, A.P. Burlaka, Yu.I. Prylutskiy, U. Ritter, and P. Scharff	
7 Biological Effects in Cell Cultures of Fullerene C₆₀: Dependence on Aggregation State	139
Levon B. Piotrovsky, Mikhail Yu. Erokin, Elena M. Eropkina, Marina A. Dumpis, and Oleg I. Kiselev	

8 Gadolinium Endohedral Metallofullerene-Based MRI Contrast Agents	157
Robert D. Bolskar	
9 Biomolecules Functionalized Carbon Nanotubes and Their Applications	181
Daxiang Cui	
10 Applications of Carbon-Based Nanomaterials for Drug Delivery in Oncology	223
Nicole H. Levi-Polyachenko, David L. Carroll, and John H. Stewart, IV	
11 Visualization of Carbon Nanoparticles Within Cells and Implications for Toxicity	267
Alexandra Porter and Mhairi Gass	
12 Pharmacological Applications of Biocompatible Carbon Nanotubes and Their Emerging Toxicology Issues	283
Tae-Joon Park, Jeffrey G. Martin, and Robert J. Linhardt	
13 Solubility of Fullerenes in Fatty Acids Esters: A New Way to Deliver <i>In Vivo</i> Fullerenes. Theoretical Calculations and Experimental Results	317
Franco Cataldo	
14 New Approach to QSPR Modeling of Fullerene C₆₀ Solubility in Organic Solvents: An Application of SMILES-Based Optimal Descriptors	337
A.A. Toropov, B.F. Rasulev, D. Leszczynska, and J. Leszczynski	
15 Functionalized Nanomaterials to Sense Toxins/Pollutant Gases Using Perturbed Microwave Resonant Cavities	351
Aman Anand, J.A. Roberts, and J.N. Dahiya	
16 Cellular Nanotubes: Membrane Channels for Intercellular Communication	363
Raquel Negrão Carvalho and Hans-Hermann Gerdes	
Index	373
Color Plates	379

Chapter 1

Twenty Years of Promises: Fullerene in Medicinal Chemistry

Tatiana Da Ros

Abstract Many biological activities have been envisioned for fullerenes and some of them seem to be very promising. The lack of solubility in biologically friendly environments is the major obstacle in the development of this field. The possibility of multiple functionalization can be exploited to get more soluble compounds but, up to now, only a few polyadducts, presenting perfectly defined geometry, can be selectively prepared avoiding long purification processes.

The toxicity of this third allotropic form of carbon is an aspect related to application in medicine and biology, while the concern about the environmental impact is due to the industrial production of fullerenes. Many studies are dedicated to both aspects and, so far, it is not possible to have a definitive answer although the current findings allow some optimistic vision.

In this chapter the main biological applications of fullerene and fullerene derivatives will be reviewed, with special attention to the most recent advances in this field. Antiviral and antibacterial activity, enzymatic inhibition, and DNA photocleavage are some aspects considered herein, together with the use of these nanostructures as possible vectors for drug and gene delivery. The most promising applications include the use of endohedral fullerenes, filled by gadolinium, in magnetic resonance imaging (MRI) and the antioxidant capacity exploitation of some tris-adducts and fullerols.

Keywords Antibacterial activity, anticancer activity, antioxidant properties, antiviral activity, cell protection, contrast agent, drug delivery, photodynamic therapy, protein interaction, radiotherapy, toxicity

1.1 Introduction

Fullerene reactivity and applications have been explored since being discovered in 1985. Nowadays, this chemistry has been intensely developed, although there is still the possibility to find some new reactions, as recently underlined by Martín

University of Trieste, Italy
Email: daros@units.it

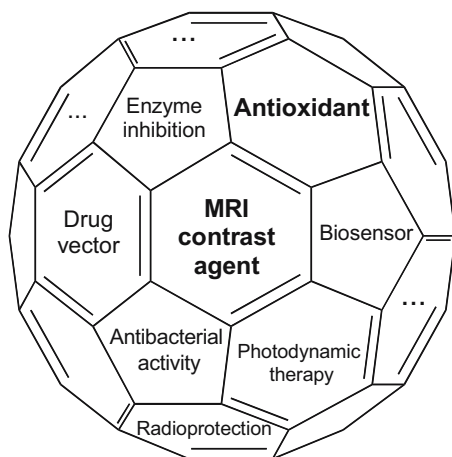


Fig. 1.1 Potential biological applications of fullerene

(2006). The main efforts are now devoted to broaden the applications of the fullerene family and its derivatives (Fig. 1.1). It is evident that the interest in C_{60} suffers from the advent of carbon nanotubes (CNTs) and many researchers involved in fullerene studies are moving toward CNT as a natural evolution of their research.

In this chapter we consider, above all, the most recent developments of biological and toxicological aspects of fullerene and related compounds of the last few years, considering that many reviews and books cover this topic up to 2006 (Jensen et al., 1996; Nakamura et al., 1996; Da Ros and Prato, 1999; Tagmatarchis and Shinohara, 2001; Bosi et al., 2003; Nakamura and Isobe, 2003; Sarova et al., 2006; Bianco and Da Ros, 2007).

1.2 Cell Protection and Antioxidant Properties

The possibility to employ C_{60} as cytoprotective agents can be considered both one of the most promising applications and one of the most studied since the publication of the fundamental works of Dugan and coworkers, who analyzed fullerene capability of scavenging reactive oxygen species (ROS) (Dugan et al., 1996, 1997, 2000; Quick and Dugan, 2004; Ali et al., 2004).

The antioxidant properties of water-soluble fullerene derivatives, mainly inspired to tris-malonic acid fullerene derivatives and dendrofullerene (Fig. 1.2), have been studied in detail (Witte et al., 2007). A library has been created, containing positively and negatively charged derivatives, which can be synthesized in an easy scalable way, overcoming the main problems of polyadduct purification. In the proposed series, dendrofullerenes are more active than polyadducts and, among polyfunctionalized fullerenes, anionic compounds give higher protection than cationic

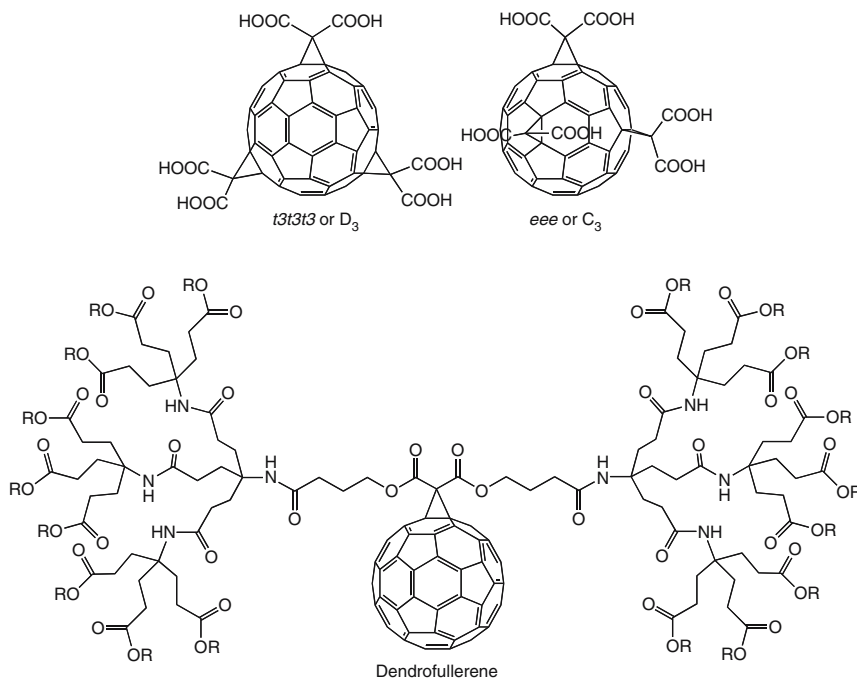


Fig. 1.2 Tris-malonic acids D₃ and C₃, and dendrofullerene

ones. The authors analyzed the interactions with cytochrome *c* and it appears evident that fullerene derivatives directly interact with this biomolecule, employed in the assay for determination of superoxide concentration. Considering the biological importance of this macromolecule, involved in many cellular pathways as apoptosis, it is fundamental to clarify the role that anionic fullerene derivatives can play in binding cytochrome *c*.

The cytoprotective activities of the same compounds have been studied by Beuerle et al. (2007) on zebra fishes. The authors analyzed the intrinsic toxicity of the fullerene derivatives and their action against four different toxicity models, as protection of neuromast hair cells from gentamicin-induced toxicity, from cisplatinum-induced toxicity, protection of tyrosine hydroxylase-containing dopaminergic CNS neurons, and protection of total CNS neurons from 6-hydroxydopamine. A general higher toxicity was noticed for positively charged derivatives with respect to negative ones; however, it is necessary to underline that some anionic derivatives (i.e., tris-malonic acid derivatives) can lead to decarboxylation and this instability increases the toxicity. In the model used the anionic compounds can block the drug-induced apoptosis. Dendrofullerene derivatives show good cytoprotection against cisplatinum toxicity, while gentamicin can be antagonized by C₃ (*e,e,e*-tris-malonic acid fullerene derivative, Fig. 1.2). The mechanism depends on the processes activated by drug administration, so it is not possible to recognize one common way. The differences for gentamicin with

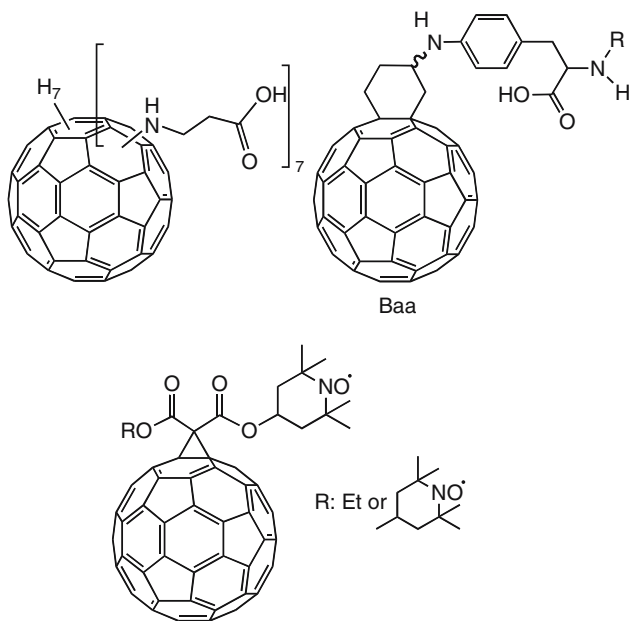


Fig. 1.3 Fullerene bearing 7 β -alanine, Baa, and nitroxide malonate methanofullerene

respect to cisplatinum can be related to differences in cellular compartmentalization of fullerene derivatives, in reactivity and in interaction with proteins.

Water-soluble fullerene derivatives bearing seven β -alanine groups (Fig. 1.3) have been used to avoid hydrogen peroxide-induced apoptosis (Hu et al., 2007a). The use of alanine–fullerene derivative reduces the extra and intracellular accumulation of ROS, a characteristic that could have as a consequence the prevention of the apoptosis trigger. Previously, α -alanine was also used to prepare water-soluble fullerene derivatives, which have been tested as a radical scavenger as well (Sun and Xu, 2006). In this case, positive results were obtained, thus demonstrating the capability to remove hydroxyl radicals and superoxide anions with high efficiency. Other amino acidic derivatives have been studied: fullerene derivatives bearing five cysteine residues are able to scavenge superoxide and hydroxyl radicals preventing apoptosis (Hu et al., 2007); a compound bearing a polypeptide chain (polyglutamic acid) self-assembled with a stable aggregation of fullerene in aqueous solution. This structure is supposed to favor electron transfer from superoxide, with good efficiency of radical scavenging (Higashi et al., 2006).

Yang et al. reported the synthesis of a fullerene derivative, called bucky amino acid (Baa, Fig. 1.3), using the (4-amino)phenylalanine (Yang et al., 2007b), which could be used as a building block for solid phase peptide synthesis, following the line traced by Prato and coworkers (Pellarini et al., 2001; Pantarotto et al., 2002). In the complete study of Baa, its antioxidant properties were also studied in dimethyl sulfoxide/phosphate buffered saline (DMSO/PBS) 1:1 and the resulting IC₅₀ is

impressive ($55.88 \mu\text{M}$). Baa is ten times more active than Trolox, a currently commercialized potent antioxidant. The antioxidant properties of a peptide containing Baa [Baa-(Glu)₄-(Gly)₃-Ser-OH] have been measured, obtaining good result (IC_{50} $90 \mu\text{M}$), but it is not clear why the activity is reduced with respect to Baa alone. A possible explanation is the aggregation of this peptide, which shelters the fullerene portion inside the aggregates.

Enes et al. (2006) recently presented new fulleropyrrolidines bearing one or two 3,5-di-*tert*-butyl-4-hydroxyphenyl units, the EPR studies of which demonstrated that these derivatives are antioxidants. In this case, the presence of the fullerene unit seems to play a marginal role in the reaction with peroxy radicals, which is governed by the phenol portion. Despite this, the presence of C_{60} should contribute to scavenge radicals in hypoxic conditions, where alkyl radicals could be the main oxidative products to be removed.

Novel nitroxide malonate methanofullerenes (Fig. 1.3), thanks to the presence of nitroxide radicals and fullerene moiety, are able to protect cells from toxic side effects of cyclophosphamide (Gubskaya et al., 2007). Experiments were carried out on mice, in which leukemia P-388 was transplanted. Cyclophosphamide or fullerene individually injected did not increase the average life span of the animals, while the combination of the anticancer drug and nitroxide fullerene derivative resulted in the survival of 70% animals, classifying these compounds as promising modifiers of biological reaction for tumor therapy.

For the first time in 2007 a new action of fullerene as antiallergic compound, probably due to its radical scavenging properties, was reported. The effect of water-soluble derivatives [$\text{C}_{60}(\text{OH})_x$ and $\text{C}_{60}(\text{NEt})_x$] was studied on human mast cell (MC) and peripheral blood basophils (PBB). The cell growth was regular in presence of concentrations up to $1 \mu\text{g/mL}$, excluding any cytotoxic effect of the compounds under investigation. Incubation using these substances did not induce MC or PBB mediator release, but in some conditions there was an inhibition of degranulation and cytokine production. At the same time the pretreatment with fullerene derivatives did not inhibit IgE binding to mast cells. In *in vivo* experiments, the administration of 2 ng/g of fullerene derivatives into mice inhibits anaphylaxis, without presenting toxic effects. Considering that the concentrations necessary to stop the anaphylaxis process are 400–300,000 times lower than the toxic values, this potential antiallergic compound would have a very good therapeutic index (Ryan et al., 2007).

Recently, the possibility to use C_{60} as anti-inflammatory compound has been reported (Huang et al., 2008). Fullerene–xanthine hybrids have been studied to determine if nitric oxide (NO) and tumor necrosis factor- α (TNF- α) production in lipopolysaccharide (LPS)-activated macrophages can be inhibited by hybrid administration, finding positive results. The presence of xanthine moiety seems to be essential for the inhibition of LPS-induced TNF- α production, while the fullerene portion ameliorates the efficiency in LPS-induced NO production blockage, leading to a new promising class of potent anti-inflammatory agents. It is necessary to mention also the opposite results obtained by an amino acid fullerene derivative tested on human epidermal keratinocytes at concentration from 0.4 to $400 \mu\text{g/mL}$.

These concentrations, in fact, decrease cell viability and promote pro-inflammatory response (Rouse et al., 2006).

Thanks to its radical sponge behavior, fullerene can find application in radioprotection. Zebra fish embryos were exposed to ionizing radiations, with consequent dose- and time-dependent alterations of morphology and physiology. The pretreatment with dendrofullerene, the toxicity of which was previously excluded at the used concentrations, decreased the radiation damage, with an efficacy comparable to amifostine, a well-known radioprotector currently in use. Also the administration of fullerene derivatives 15 min after irradiation gives protection (Daroczi et al., 2006). On the contrary, its administration 30 min after radiation exposure results to be ineffective. The accredited mechanism involves the scavenging of reactive oxygen species, which are produced by irradiation. Other experiments were carried out on keratinocytes irradiated by UV A and B. In these cases, the fullerene was entrapped in polyvinylpyrrolidone (PVP) in a molar ratio range of 0.42–0.67:1 (Xiao et al., 2005, 2006). The “Radical Sponge®” was active at 10–40 μM concentrations with better activity if administrated and washed off before irradiation, while treatments during or after irradiation were not equally effective, demonstrating its better ability in preventing than in sheltering the radiation toxicity.

1.3 Oxidative Stress and Photodynamic Therapy

The above-quoted behavior is not surprising if we consider the paradoxical properties of fullerene moiety. In fact C_{60} can be a real effective radical scavenger but, at the same time, it is known to induce radical production upon photoirradiation. The light radiation excites C_{60} from the ground state to $^1\text{C}_{60}$, a short-lived species readily converted to the long-lived $^3\text{C}_{60}$. The latter can transfer energy to molecular oxygen, if present, going back to the ground state. In this way toxic $^1\text{O}_2$ is generated. Moreover, fullerene in singlet and triplet states can be easily reduced to C_{60}^- by electron transfer. All the reactive species herein described can attach biomolecules as lipids, proteins, and nucleic acids, classical targets in photodynamic therapy. The mechanisms of action are two: when the damage is induced by reactive species other than singlet oxygen, type I mechanism takes place, while it is possible to refer to type II mechanism when the damage is directly attributable to $^1\text{O}_2$. For DNA both pathways lead to guanosine oxidation and these modifications decrease the stability of phosphodiesteric bonds, which become easily hydrolyzed in alkaline conditions.

Many different preparations have been used to study photodynamic potentialities, starting from *N*-vinylpyrrolidone linked to fulleropyrrolidines. The obtained copolymer is water-soluble when the C_{60} to NVP ratio is more than 1:100. A photoinduced cleaving test on pBR322 supercoiled DNA gives nicked DNA in good yield, as a function of fullerene concentration and light dose (Iwamoto and Yamakoshi, 2006). Unmodified C_{60} complexed with PVP, cyclodextrins, or a new carbohydrate-containing nonionic homooxacalix[3]arene gives interesting results, especially the latter (Ikeda et al., 2005). Ikeda et al. reported further developments in this field, incorporating

fullerenes (both C_{60} and C_{70}) into liposomes. These are constituted by cationic phospholipids and can easily interact with DNA. Their photoirradiation leads to nicked DNA with good efficiency although better results correspond to C_{70} incorporation (Ikeda et al., 2007a, b).

Radical polymerization of maleic anhydride and fullerene was used to obtain a new material, the photodynamic properties of which have been studied *in vitro* and *in vivo*. HeLa and bone tumor cell growth were inhibited by treatment with fullerene and light, so the polymer was tested on mice affected by bone tumor. After injection and irradiation, tumor size and weight were reduced and the mouse survival time was extended (Jiang and Li, 2007). The photodynamic properties of a supramolecular cucurbit[8]uril–fullerene complex have been studied by the same authors (Jiang and Li, 2006) who attributed HeLa cell death mainly to the damage of membrane phospholipids and proteins.

The equatorial di-malonic acid C_{60} (DMA- C_{60}), if irradiated by laser source, can induce membrane damage in HeLa cells. The laser power necessary to obtain this result is quite low (≤ 1 mW) and the time necessary for the cells to become permeable to propidium iodide is inversely proportional to fullerene concentration. Cytoplasmic calcium concentration transiently increases after exposition to DMA- C_{60} , by afflux of Ca^{2+} present in the external medium, followed by an abrupt depletion, and mitochondrial membrane damage has also been reported. Laser light at low power, together with low concentration of DMA- C_{60} and short time of irradiation, can give strong effect with potential application in photodynamic therapy although this derivative did not show specific tropism for tumors (Yang et al., 2007c).

Both type I and II mechanisms are involved in the lipidic peroxidation of erythrocytes caused by irradiation of anionic fullerene derivatives (bearing carboxylic or phosphonate residues) (Yang et al., 2007e), with a significant activity at $10 \mu\text{M}$ concentration and 30 min of irradiation, or at half concentration and double exposure time. The bis-methanophosphonate fullerene is the most effective, but no structure–activity correlations were reported.

An original approach conjugates polyethylene glycol (PEG)-fullerene derivative to Gd^{3+} , used as magnetic resonance imaging (MRI) contrast agent (see paragraph 1.8). After addition of gadolinium, chelated by the diethylenetriaminepentaacetic acid (DTPA), this compound (C_{60} -PEG-Gd) has been intravenously administered in mice affected by cancer and the tumor mass has been visualized by MRI with good resolution, indicating that gadolinium accumulates in the altered tissue. Photoirradiation causes superoxide anion generation with consequent cytotoxicity, as previously determined in *in vitro* experiments, even though it is necessary to irradiate the tumor after the maximum concentration of C_{60} -PEG-Gd has been reached (in this case 3 h after injection), but it is worthy to note that the accumulation can be monitored by MRI (Liu et al., 2007).

It is interesting to cite also the antitumoral effect of water suspension of nC_{60} in absence of photoirradiation (Harhaji et al., 2007). Depending on the concentration, in glioma cell cultures it is possible to have reactive oxygen/extracellular signal-regulated kinases (ERK)-mediated necrosis (at high fullerene concentrations), or reactive oxygen/ERK-independent cell proliferation block and autophagy

(at low concentrations). Moreover, primary rat astrocytes are less sensitive to low nC_{60} concentrations than transformed ones, paving the way to fullerenes as anticancer agents.

1.4 Interaction with Proteins

As mentioned earlier, there is an interaction of fullerene derivatives with cytochrome *c* (Witte et al., 2007). The importance of these interactions is quite evident, considering that drugs, before reaching their target, interact with serum proteins, cross cellular barriers, and come in contact with enzymes of the metabolic path such as cytochrome P450. Therefore, these studies are really important to develop new fullerene derivatives as potential drugs.

C_3 derivative has been complexed with equine skeletal muscle apomyoglobin. The complex has been purified and it is stable. Its full characterization permits a better comprehension of the binding characteristics of apomyoglobin (Kolsenik et al., 2007). The interaction of a water-soluble fullerene derivative bearing phosphate residues $[C_{60}O_m(OH)_nC(PO_3Et_2)_2]$ with human serum albumin (HSA) has been explored (Zhang et al., 2007). A quenching of HSA fluorescence is registered in presence of fullerene and it has been possible to predict the binding position of the phosphate derivative, which is likely at the site of the subdomain IIA. The interaction of fullerene with the protein leads to a more compact structure of the protein itself.

Docking studies have been performed on four different proteins as HIV-protease, fullerene-specific antibody, human serum albumin, and bovine serum albumin. The patterns common to all four proteins are not specific enough to represent the essential feature to bind fullerene, but in all cases the protein backbones undergo conformational variations due to the binding with fullerene (Benyamini et al., 2006). This is not surprising for biomolecules as receptors, which use these changes as “response” to the messenger binding. The *e,e,e*-tris-malonic acid fullerene derivative and dendrofullerene interactions with serum have also been analyzed by capillary electrophoresis. In the case of C_3 it is possible to disrupt its interactions with proteins by adding sodium dodecyl sulfate (SDS), while for dendrofullerene the concentration of SDS is critical (Chan et al., 2007).

Belgorodsky et al. (2006) studied the binding of pristine fullerene complexed with cyclodextrin on bovine serum albumin protein demonstrating that the binding is a multistep process. First, the cyclodextrin dissociation from C_{60} takes place, exposing a fullerene hydrophobic portion, than this portion binds to the protein.

The curved surface of fullerene has been found to stabilize enzymes in denaturing environments. Soybean peroxidase has been chosen as prototype and its half-life, when adsorbed on C_{60} , is 13-fold higher than the native enzyme (Asuri et al., 2007). These findings are really important for the applications of fullerene, not only in biomedical fields.

1.5 Antibacterial Activity

Fullerene showed antibacterial activity, which can be attributed to different interactions of C_{60} with biomolecules (Da Ros et al., 1996). In fact, there is a possibility to induce cell membrane disruption. The fullerene sphere seems not really adaptable to planar cellular surface, but for sure the hydrophobic surface can easily interact with membrane lipids and intercalate into them. However, it has been demonstrated that fullerene derivatives can inhibit bacterial growth by unpairing the respiratory chain. There is, first, a decrease of oxygen uptake at low fullerene derivative concentration, and then an increase of oxygen uptake, which is followed by an enhancement of hydrogen peroxide production. The higher concentration of C_{60} seems to produce an electron leak from the bacterial respiratory chain (Mashino et al., 2003).

A recent study performed with three different classes of fullerene compounds (positively charged, neutral, and negatively charged) showed that the main effect on *Escherichia coli* and *Shewanella oneidensis* is obtained with cationic derivatives, while the anionic derivatives are ineffective. Also the analysis of bacterial metabolism is reported, demonstrating that, in these conditions, the central metabolism does not change. The possible explanation of the best activity of cationic derivatives can be found considering that the bacteria cellular surface is negatively charged and the interactions with cationic fullerenes are strong, confirming the membrane stress hypothesis (Tang et al., 2007).

In other cases fullerene antibacterial action takes place after photoirradiation of fulleropyrrolidinium salts. It is not yet clear if the photodynamic action implies the participation of superoxide and hydroxyl radicals (type I mechanism) or singlet oxygen (type II mechanism) but the efficacy is really interesting with the death of more than 99.9% of bacterial and fungal cells and a special selectivity for microbes over mammalian cells (Tegos et al., 2005). Also a sulfobutyl fullerene derivative is able to inhibit environmental bacteria after photoirradiation and it exerts its action on *E. coli* even if incorporated in coated polymer (Yu et al., 2005).

1.6 Enzymatic Inhibition and Antiviral Activity

The work that paved the way toward enzymatic inhibition was published in the early 1990s by Wudl and coworkers (Schinazi et al., 1993; Friedman et al., 1993; Sijbesma et al., 1993) and since then studies regarding antiviral activity, mainly HIV-protease inhibition, have been carried out to find active compounds. Up to now, the most effective fullerene derivatives are the *trans*-2 *N,N*-dimethyl-bis-fulleropyrrolidinium salt (Fig. 1.4) (Marchesan et al., 2005) and the dendrofullerene reported by Hirsch (Schuster et al., 2000): both of them present an EC_{50} of 0.2 μ M. Also HIV reverse transcriptase can be inhibited by *N,N*-dimethyl-bis-fulleropyrrolidinium salts (Mashino et al., 2005). The same compounds are also active against acetylcholine esterase (AChE), an enzyme that hydrolyzes a very important neurotransmitter.

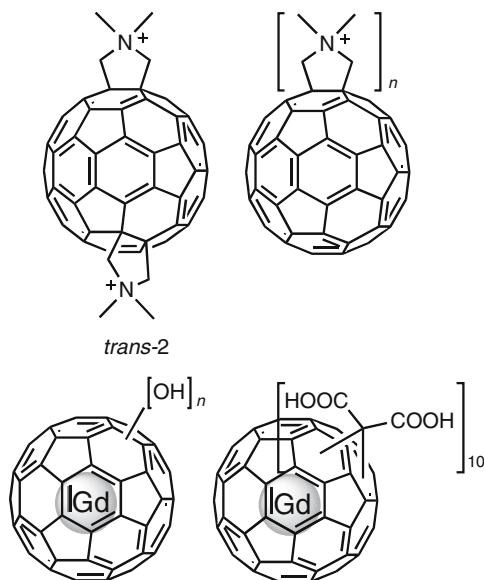


Fig. 1.4 *N,N*-dimethylpyrrolidinium salts (*trans-2* and poly) and variously functionalized Gd@C₆₀

The fullerene derivatives result to be noncompetitive inhibitors, meaning that, although the catalytic site of AChE could bind cationic fullerenes, the binding of C₆₀ derivatives should take place in allosteric sites (Pastorin et al., 2006). Considering all these actions, with important biomedical applications, the question about selectivity naturally arises, but no answer has been proposed as yet.

The most recent advances on enzymatic inhibition are related to endonucleases and polymerases. A tris-malonic acid fullerene derivative can interfere with DNA restrictive enzymatic reactions, demonstrating a dose-dependent inhibition of these enzymes, with an IC₅₀ in the micromolar range. The addition of ROS scavenger does not revert the enzymatic activity, indicating that the fullerene action should be exerted in a direct way (Yang et al., 2007d).

Although HIV infection inhibition is mainly due to interaction of fullerene derivatives with viral enzymes, it is necessary to consider that this is not the only exploitable mechanism. In fact, the photodynamic inactivation of influenza virus has also been proposed (Zarubaev et al., 2007). The outer viral membrane is destroyed, while it seems that the protein profile of allantoic fluid, in which the virus was propagated, remains unchanged, confirming one more time the great potentiality of fullerene.

1.7 Drug Delivery

Fullerene was also studied as a possible drug delivery system. The hypothesis of C₆₀ as drug vector has been developed considering that the hydrophobic fullerene portion could help the membrane crossing. Venkatesan et al. (2005) utilized fullerene as

adsorbent to study the bioavailability of erythropoietin (EPO, a peptide hormone) on rats, after intraperitoneal administration. Usually erythropoietin is administered by intravenous or subcutaneous injection because of bioavailability problems, barrier penetration difficulties, and enzymatic degradation. In this study the pharmacokinetics and the increase of erythropoietin adsorption were determined. The maximum reached concentration was double in the presence of fullerene with respect to erythropoietin alone, leading to a bioavailability of 5.7%, almost three times higher than EPO administration.

Ionic bonds are exploited to link oligonucleotides on cationic fullerene derivatives. Nakamura et al. reported the first attempt in this direction in 2000 (Nakamura et al., 2000). Recently, a library of fullerene derivatives has been tested (Isobe et al., 2006a, b). Some characteristics seem to be necessary to exert this function, such as a specific distance between positive charges. The transfection induced by C_{60} derivatives is better than transfection with lipofectin, probably because the fullerene presence can shelter genetic materials from the lysosomal enzymes by aggregation in nanometer and micrometer scale, a process that would not be detrimental for the membrane over-crossing in this dimension range. This hypothesis was confirmed by Ying (Ying et al., 2005) and Burger (Burger and Chu, 2007), who studied fullerene capability of decorating and stabilizing DNA coils in aqueous solution. Also Klumpp et al. (2007) reported interesting achievements in gene delivery by using poly-fulleropyrrolidinium salts (Fig. 1.4), which are completely soluble in water. The use of surface plasmon resonance technique permitted the determination of affinity and the corresponding equilibrium association constant results of $7.74 \cdot 10^8 M^{-1}$, indicative of a good interaction.

A paclitaxel fullerene derivative has been obtained by covalent linkage of the drug to the C_{60} by means of an ester, the hydrolysis of which presents a favorable kinetic profile, with consequent release of paclitaxel (Zakharian et al., 2005). The *in vitro* tests show a good anticancer activity, holding out hope for enhancing the drug efficacy *in vivo*.

In this context, it is worthy to note that the already mentioned Baa behaves as a new cell-penetrating unit, because its presence permits the delivery into cells of both cationic and anionic peptides, which are not able to cross the membrane by themselves, further increasing the potentiality of fullerene derivatives (Yang et al., 2007a).

1.8 Endohedrals

Fullerene structure leads to the opportunity of filling its cavity using different elements. The filler is added contextually to the carbon source, during the production procedure. The processes of opening, filling, and the subsequent closure of the cage after fullerene production are still rather far away. The so-called endohedrals can present transition metals as scandium or lanthanoids as holmium or gadolinium entrapped inside the cage. The latter represents one of the most useful elements for biological applications of endohedrals. Gadolinium is currently used as an MRI contrast agent, but the possibility of undesired releasing of toxic metal from the

chelates raises some concerns. The opportunity to confine Gd to the carbon cage, which is virtually unbreakable, would really improve safety. $\text{Gd}@C_{60}(\text{OH})_x$ and $\text{Gd}@C_{60}[\text{C}(\text{COOH})_2]_{10}$ (Fig. 1.4) are water-soluble derivatives and present interesting properties of proton relaxivity, which varies with the variation of pH conditions. This behavior can be exploited to analyze pH differences in cells and is due to the aggregation of fullerene derivatives, which is pH-dependent, as demonstrated by dynamic light-scattering measurements (Tóth et al., 2005). Further studies have been performed demonstrating that addition of salts can disrupt endohedral aggregates in water solutions and that the presence of phosphates exerts a greater effect than sodium halides (Laus et al., 2005).

Distribution experiments in *in vitro* agarose gel infusion and *in vivo* infusion in rat brain have been carried out (Fatouros et al., 2006). In this case $\text{Gd}_3\text{N}@C_{80}$, functionalized with PEG and hydroxyl groups, was examined. Its water hydrogen MRI relaxivity is much higher than the one reported for commercially available agents. To get the same visualization in agarose gel infusion, gadofullerene derivative was used in a concentration one order of magnitude lower than commonly used compounds. The diffusion *in vivo* demonstrated a prolonged residence of endohedral fullerene within the tumor volume, with interesting therapeutic possibilities.

Endohedrals can find application not only as contrast agents, but also in radioimmunotherapy. In this case radionuclides are encapsulated into the carbon cage, without the possibility to be released, as for $^{212}\text{Pb}@C_{60}[\text{C}(\text{COOH})_2]_x$ which contain the ^{212}Pb β -emitter, parent of the α -emitter ^{212}Bi (Diener et al., 2007). In biodistribution studies, the slow clearance of this compound can be considered an unfavorable event, but its accumulation in liver, kidneys, and spleen overrules the main adverse effect of ^{212}Pb , due to accumulation in the bone marrow, making $^{212}\text{Pb}@C_{60}[\text{C}(\text{COOH})_2]_x$ really attractive.

1.9 Toxicology

In recent years, because of the increasing fullerene industrial production and also considering the development of technologies based on nanoparticles (including C_{60}), a great concern has arisen about their toxicological effects. This anxiety is reflected in the high numbers of articles published on this topic and the general toxicology of fullerene nanoparticles (nC_{60}) is the subject of many recent papers. Less general attention is devoted to functionalized derivatives, apart from the polyhydroxylated fullerenes or fullerols. This is not surprising if we consider that usually the toxicity of fullerene derivatives is analyzed together with their biological properties and that they are prepared in small quantity with consequent minor environmental impact.

Fortner et al. (2005) reported an inhibitory effect on bacterial growth due to the presence of fullerene nanoparticles at concentration ≥ 4 mg/L, while recently the impact of C_{60} pollution on soil was described (Tong et al., 2007). The authors analyzed the soil respiration, as well as the enzymatic and the microbial activity

and, although the necessity to extend this analysis for a long-term period emerged, their findings demonstrate a low impact of C_{60} on structure and function of soil microbial population and processes. Different results have been obtained with water suspensions of nC_{60} on *Bacillus subtilis*. In this case there is a relatively strong antibacterial activity (MIC 0.1 mg/L) and the smaller nanoparticles result to be the most active (Lyon et al., 2006).

Experiments have also been performed to analyze what impact fullerene nanoparticles can produce on aquatic environment. After the first report by Oberdörster (2004), in which important evidences of lipid peroxidation in largemouth bass brain were described, the research was expanded to freshwater crustaceans as *Daphnia magna*, copepods, and different fish species (Oberdörster et al., 2006). Tested concentrations reach 35 ppm in freshwater and 22.5 ppm in seawater, which are the highest concentrations obtained without using organic solvents to prepare the suspension. At the moment, it is not possible to determine if these values can be overcome in case of pollution. In these conditions it was not possible to determine the LD_{50} for fullerene nanoparticles. The most affected specie was *D. magna*, in which sublethal effects, as altered moult, were noticed. In fish species no differences were reported for P450 isoenzymes, while few changes in lipid metabolism were found, but new studies are suggested to better define targets for the analysis.

Different results on *D. magna* have been reported (Lovern and Klaper, 2006). Mortality has been described in presence of fullerene nanoparticles obtained by tetrahydrofuran (THF) dispersion in water, subsequent filtration, and removal of the organic solvent. This effect was concentration-dependent, reaching total mortality at 880 ppb. On the contrary, C_{60} nanoparticles prepared by sonication gave nonuniform lethal effects, without concentration dependence.

A more recent study performed on nC_{60} and hydrogenated fullerenes presents more detailed effects on hopping frequency, heart rate, appendage movement, and post-abdominal claw curling. The results show intoxication effects, which lead an invertebrate population to be more easily plundered (Lovern et al., 2007).

Bacterial phospholipids can be altered after fullerene water suspension incubation, with different degrees of variation, depending on bacterial species (Fang et al., 2007). *B. subtilis* (Gram positive) is less sensitive (MIC 0.5–0.75 mg/L) than *Pseudomonas putida* (Gram negative, MIC 0.25–0.5 mg/L). The first shows an increased presence of branched fatty acids and a decreased concentration of saturated and unsaturated lipids, while in *P. putida* a higher percentage of saturated fatty acids and corresponding higher membrane fluidity were detected. It is worthy to note that in both cases peroxidation of lipids was not reported.

Experiments on human dermal fibroblast, human liver carcinoma cell (HepG2), and neuronal human astrocytes performed with pristine C_{60} , as nanoparticles, demonstrate toxicity due to lipid peroxidation, while mitochondrial activity is unaffected (Sayes et al., 2005). In experiments performed on alveolar macrophages, C_{60} shows really low cytotoxicity when used to incubate cell cultures but, after this treatment, the macrophages present a decreased phagocytic activity (Jia et al., 2005). Other experiments on eukaryotic cells as human monocyte macrophages show accumulation of nC_{60} without significant toxicity using concentration up to 10 $\mu\text{g/mL}$ (Porter et al., 2006).

Interestingly, the cellular distribution was analyzed by energy-filtered transmission electron microscopy and electron tomography, demonstrating the presence of free fullerene in the cytoplasm, or associated with nuclear membrane, plasma membrane, lysosomes and, rather surprisingly, with the nucleus (Porter et al., 2006, 2007).

The different toxicity revealed in many studies could be associated or strongly related to the different methodologies in the preparation of fullerene nanoparticles. The negative effect has been imputed to the presence of THF into the preparation (Isakovic et al., 2006a). Fullerene nanoparticle preparation obtained after solubilization of C_{60} into THF has been treated by γ -irradiation (γ - nC_{60}). The carbon cage does not present changes due to the irradiation but the IR signals related to the presence of THF as intercalating agent in the nC_{60} disappears. The γ - nC_{60} preparation does not exert cytotoxic activity in the same condition in which nC_{60} induces a decrease of cell number, both for primary and tumor cell lines. Release of lactate dehydrogenase (LDH), reactive oxygen species, lipid peroxidation, and necrotic processes are reported only for nonirradiated preparation. On the contrary, γ - nC_{60} exerts a partial effect of cytoprotection against treatment by oxidative stress-inducing agents. The antioxidant properties of pristine fullerene have been illustrated: *in vivo* acute intoxication by CCl_4 can be prevented by pretreatment of the animals with C_{60} , in a dose-dependent manner (Gharbi et al., 2005).

A new technique to prepare nC_{60} (fullerene sonication in methanol) has been used, but in this case the cluster sizes are not homogeneous. This preparation permeates the cell membrane of normal and malignant breast epithelial cells (MCF10A and MDA MB 231 or MDA MB 435, respectively) without interfering with cellular events. Also the incubation with high concentration (200 ppm) does not adversely impact cell proliferation (Levi et al., 2006).

In rats, the administration of fullerene by inhalation, as nano- and microparticles generated by aerosol, does not lead to lesions and only a little increase of protein concentration in bronchoalveolar lavage fluid was obtained (Baker et al., 2007). Recently, Sayes et al. (2007) analyzed *in vivo* pulmonary toxicity of nC_{60} and $C_{60}(OH)_{24}$, after intratracheal instillation in rats. They verified only transient inflammatory and cell injury effects, 1 day postexposure, without differences from water-instilled controls. No adverse lung tissue effects were measured, and the results demonstrated little or no differences in lung toxicity effects between the nC_{60} and fullerols, compared to controls.

Embryonic zebra fish model was employed to study fullerene toxicity. This model is quite convenient because the embryos are transparent in the first week of life and their rate of development is rather fast. C_{60} , C_{70} , and $C_{60}(OH)_{24}$ have been tested on early embryogenesis (Usenko et al., 2007), presenting effects on this process with malformations, pericardial edema, and mortality. The results for fullerols are milder, but it is difficult to attribute this effect to the presence of the functionalizations themselves or to the easier solubilization, implying diminished cluster formations and avoiding the use of solvents as toluene or THF, the presence of which can play an important role in toxicity, as already demonstrated.

The use of nC_{60} (obtained using THF solution) and fullerols to treat different cell lines has been studied by Isakovic et al. (2006b) who reported ROS-associated cell death for nC_{60} and cell death independent of ROS concentrations when fullerols are

used. In the first case the death mechanism is necrosis, while in the second case the involved process is apoptosis. On these bases pristine fullerene seems to exert strong pro-oxidant capacity and fullerols seem to be endowed with antioxidant activity. Fullerol cytotoxicity has also been studied on *Tetrahymena pyriformis*, as a model organism. A dose-dependent inhibition of growth is reported; in fact the generation time in standard conditions is of 7.23 ± 0.03 h while in the presence of fullerols (0.25 mg/mL) it increases up to 9.97 ± 1.54 h (Zhao et al., 2006). The macronucleus is not anymore evident, glutathione peroxidase and glutathione reductase concentrations decrease, while superoxide dismutase is constant.

Fullerols have been tested on endothelial cells and in this case cytotoxic morphological changes, such as decreased cell density or cytosolic vacuole formation, take place in a concentration-dependent manner. The chronic treatment with $1 \mu\text{g}/\text{mL}$ of fullerols for 10 days had no significant toxicity on endothelial cells, but at the maximal concentration ($100 \mu\text{g}/\text{mL}$, 24h) endothelial LDH is released, indicating cell death. The apoptosis is not triggered, but a mechanism of autophagy seems to be activated (Yamawaki and Iwai, 2006), indicating the risk of atherosclerosis and ischemic heart disease due to $\text{C}_{60}(\text{OH})_{24}$ administration. The effect of $\text{C}_{60}(\text{OH})_{24}$ chronic administration, at very low concentration, has been studied (Niwa and Iwai, 2006). The exposure at picograms per milliliter (pg/mL) concentration does not have oncogenic or antioncogenic activity, while at nanograms per milliliter (ng/mL) there is evidence of antioncogenic functions, with cell growth inhibition. LDH activity is suppressed in a dose-dependent concentration and micronucleus generation takes place. This phenomenon leads to genotoxic effects and is attributed to difficulties in chromosomal DNA division, excluding any participation of ROS-increased production in the toxic effect.

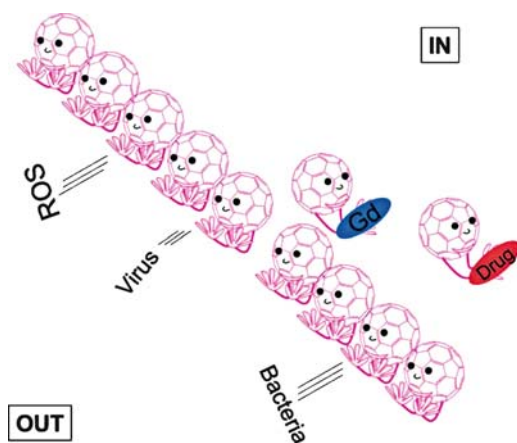


Fig. 1.5 Fullerene's activity (See Color Plates)

1.10 Conclusions

Once upon a time there were three brilliant researchers who isolated and identified the third allotropic form of carbon. C₆₀ fullerene is the most common compound of this family and, since its discovery it has attracted glances and attentions from the scientific community for its biological potentialities (Fig. 1.5).

Considering that medicine and biology are not exact sciences, it is not surprising to find discordant results in the literature: there is still a lot of room for further studies and analyses to discover, rationalize, and explain the activities and the behaviors of fullerenes in cells, animals, and human beings. Despite all the hopes we still feed on, it is honest to admit that, up to now, no decisive medical application has been so deeply developed to be currently in use, but, with all the energies the “fullerene community” is spending on this field, we are sure that this will not be the unhappy end of the C₆₀ fairytale: derivatives as Gd@C₆₀ have qualities and characteristics that render the effective application in therapy or diagnostics a goal very close to be reached.

References

- Ali SS, Hardt JI, Quick KL, Kim-Han JS, Erlanger BF, Huang TT, Epstein CJ, Dugan LL (2004) A biologically effective fullerene (C₆₀) derivative with superoxide dismutase mimetic properties. *Free Rad. Biol. Med.* 37:1191–1202.
- Asuri P, Karajanagi SS, Vertegel AA, Dordick JS, Kane RS (2007) Enhanced stability of enzymes adsorbed onto nanoparticles. *J. Nanosci. Nanotechnol.* 7:1675–1678.
- Baker G, Gupta A, Clark M, Valenzuela B, Staska L, Harbo S, Pierce J, Dill J (2007) Inhalation toxicity and lung toxicokinetics of C₆₀ fullerene nanoparticles and microparticles. *Toxicol. Sci.*: doi:10.1093/toxsci/kfm1243
- Belgorodsky B, Fadeev L, Kolsenik J, Gozin M (2006) Formation of a soluble stable complex between pristine C₆₀-fullerene and a native blood protein. *Chem. Biol. Chem.* 7:1783–1789.
- Benyamini H, Shulman-Peleg A, Wolfson HJ, Belgorodsky B, Fadeev L, Gozin M (2006) Interaction of C₆₀-fullerene and carboxyfullerene with proteins: Docking and binding site alignment. *Bioconjug. Chem.* 17:378–386.
- Beuerle F, Witte P, Hartnagel U, Lebovitz R, Parnig C, Hirsch A (2007) Cytoprotective activities of water-soluble fullerenes in zebrafish models. *J. Exp. Nanosci.* 2:147–170.
- Bianco A, Da Ros T (2007) Biological applications of fullerenes. In: Langa F, Nierengarten J-F (eds.) *Fullerenes – Principles and Applications*. Royal Chemical Society, Cambridge, pp. 301–328.
- Bosi S, Da Ros T, Spalluto G, Prato M (2003) Fullerene derivatives: An attractive tool for biological applications. *Eur. J. Med. Chem.* 38:913–923.
- Burger C, Chu B (2007) Functional nanofibrous scaffolds for bone reconstruction. *Colloid. Surf. B* 56:134–141.
- Chan KC, Patri AK, Veenstra TD, McNeil SE, Issaq HJ (2007) Analysis of fullerene-based nanomaterial in serum matrix by CE. *Electrophoresis* 28:1518–1524.
- Da Ros T, Prato M (1999) Medicinal chemistry with fullerenes and fullerene derivatives. *Chem. Commun.* 8:663–669.
- Da Ros T, Prato M, Novello F, Maggini M, Banfi E (1996) Easy access to water soluble fullerene derivatives via 1,3-dipolar cycloadditions of azomethine ylides to C₆₀. *J. Org. Chem.* 61:9070–9072.

- Daroczi B, Kari G, McAleer MF, Wolf JC, Rodeck U, Dicker AP (2006) In vivo radioprotection by the fullerene nanoparticle DF-1 as assessed in a zebrafish model. *Clin. Cancer Res.* 12:7086–7091.
- Diener MD, Afford JM, Kennel SJ, Mirzadeh S (2007) 212Pb@C60 and its water-soluble derivatives: Synthesis, stability, and suitability for radioimmunotherapy. *J. Am. Chem. Soc.* 129: 5131–5138.
- Dugan L, Gabrielsen J, Yu S, Lin T, Choi D (1996) Buckminsterfullerenol free radical scavengers reduce excitotoxic and apoptotic death of cultured cortical neurons. *Neurobiol. Dis.* 3:129–135.
- Dugan LL, Turetsky DM, Du C, Lobner D, Wheeler M, Almlı CR, Shen CK-F, Luh T-Y, Choi DW, Lin T-S (1997) Carboxyfullerenes as neuroprotective agents. *Proc. Natl. Acad. Sci. USA* 94:9434–9439.
- Dugan LL, Lovett E, Cuddihy S, Ma B-W, Lin T-S, Choi DW (2000) Carboxyfullerenes as neuroprotective antioxidants. In: Kadish KM, Ruoff RS (eds.) *Fullerenes: Chemistry, Physics, and Technology*. Wiley, New York, pp. 467–479.
- Enes RF, Tome AC, Cavaleiro JAS, Amorati R, Fumo MG, Pedulli GF, Valgimigli L (2006) Synthesis and antioxidant activity of [60]fullerene-BHT conjugates. *Chem. Eur. J.* 12:4646–4653.
- Fang J, Lyon DY, Wiesner MR, Dong J, Alvarez PJJ (2007) Effect of a fullerene water suspension on bacterial phospholipids and membrane phase behavior. *Environ. Sci. Technol.* 41:2636–2642.
- Fatouros PP, Corwin FD, Chen ZJ, Broaddus WC, Tatum JL, Kettenmann B, Ge Z, Gibson HW, Russ JL, Leonard AP, Duchamp JC, Dorn HC (2006) *In vitro* and *in vivo* imaging studies of a new endohedral metallofullerene nanoparticle. *Radiology* 240:756–764.
- Fortner JD, Lyon DY, Sayes CM, Boyd AM, Falkner JC, Hotze EM, Alemany LB, Tao YJ, Guo W, Ausman KD, Colvin VL, Hughes JB (2005) C₆₀ in water: Nanocrystal formation and microbial response. *Environ. Sci. Technol.* 39:4307–4316.
- Friedman SH, DeCamp DL, Sijbesma RP, Srdanov G, Wudl F, Kenyon GL (1993) Inhibition of the HIV-1 protease by fullerene derivatives: Model building studies and experimental verification. *J. Am. Chem. Soc.* 115:6506–6509.
- Gharbi N, Pressac M, Hadchouel M, Szwarz H, Wilson SR, Moussa F (2005) [60]Fullerene is a powerful antioxidant *in vivo* with no acute or subacute toxicity. *Nano Lett.* 5:2578–2585.
- Gubskaya VP, Berezhnaya LS, Gubaidullin AT, Faingold II, Kotelnikova RA, Konovalova NP, Morozov VI, Litvinov IA, Nuretdinov IA (2007) Synthesis, structure and biological activity of nitroxide malonate methanofullerenes. *Org. Biomol. Chem.* 5:976–981.
- Harhaji L, Isakovic A, Raicevic N, Markovic Z, Todorovic-Markovic B, Nikolic N, Vranjes-Djuric S, Markovic I, Trajkovic V (2007) Multiple mechanisms underlying the anticancer action of nanocrystalline fullerene. *Eur. J. Pharmacol.* 568:89–98.
- Higashi N, Shosu T, Koga T, Niwa M, Tanigawa T (2006) pH-responsive, self-assembling nanoparticle from a fullerene-tagged poly(L-glutamic acid) and its superoxide dismutase mimetic property. *J. Colloid Interface Sci.* 298:118–123.
- Hu Z, Guan W, Wang W, Huang L, Xing H, Zhu Z (2007a) Synthesis of β -alanine C₆₀ derivative and its protective effect on hydrogen peroxide-induced apoptosis in rat pheochromocytoma cells. *Cell Biol Int.* 31:798–804.
- Hu Z, Guan W, Wang W, Huang L, Xing H, Zhu Z (2007b) Protective effect of a novel cystine C₆₀ derivative on hydrogen peroxide-induced apoptosis in rat pheochromocytoma PC12 cells. *Chem. Biol. Interact.* 167:135–144.
- Huang S-T, Liao J-S, Fang H-W, Lin C-M (2008) Synthesis and anti-inflammation evaluation of new C₆₀ fulleropyrrolidines bearing biologically active xanthine. *Bioorg. Med. Chem. Lett.* 18:99–103.
- Ikeda A, Ejima A, Nishiguchi K, Kikuchi JI, Matsumoto T, Hatano T, Shinkai S, Goto M (2005) DNA-photocleaving activities of water-soluble carbohydrate-containing nonionic homooxacalix[3]arene [60]fullerene complex. *Chem. Lett.* 34:308–309.
- Ikeda A, Doi Y, Hashizume M, Kikuchi JI, Konishi T (2007a) An extremely effective DNA photocleavage utilizing functionalized liposomes with a fullerene-enriched lipid bilayer. *J. Am. Chem. Soc.* 129:4140–4141.

- Ikeda A, Doi Y, Nishiguchi K, Kitamura K, Hashizume M, Kikuchi JI, Yogo K, Ogawa T, Takeya T (2007b) Induction of cell death by photodynamic therapy with water-soluble lipid-membrane-incorporated [60]fullerene. *Org. Biomol. Chem.* 5:1158–1160.
- Isakovic A, Markovic Z, Nikolic N, Todorovic-Markovic B, Vranjes-Djuric S, Harhaji L, Raicevic N, Romcevic N, Vasiljevic-Radovic D, Dramicanin M, Trajkovic V (2006a) Inactivation of nanocrystalline C₆₀ cytotoxicity by γ -irradiation. *Biomaterials* 27:5049–5058.
- Isakovic A, Markovic Z, Todorovic-Marcovic B, Nikolic N, Vranjes-Djuric S, Mirkovic M, Dramicanin M, Harhaji L, Raicevic N, Nikolic Z, Trajkovic V (2006b) Distinct cytotoxic mechanisms of pristine versus hydroxylated fullerene. *Toxicol. Sci.* 91:173–183.
- Isobe H, Nakanishi W, Tomita N, Jinno S, Okayama H, Nakamura E (2006a) Gene delivery by aminofullerenes: Structural requirements for efficient transfection. *Chem. Asian J.* 1:167–175.
- Isobe H, Nakanishi W, Tomita N, Jinno S, Okayama H, Nakamura E (2006b) Nonviral gene delivery by tetraamino fullerene. *Mol. Pharm.* 3:124–134.
- Iwamoto Y, Yamakoshi Y (2006) A highly water-soluble C60-NVP copolymer: A potential material for photodynamic therapy. *Chem. Commun.* 4805–4807.
- Jensen AW, Wilson SR, Schuster DI (1996) Biological applications of fullerenes. A review. *Bioorg. Med. Chem.* 4:767–779.
- Jia G, Wang HF, Yan L, Wang X, Pei RJ, Yan T, Zhao YL, Guo XB (2005) Cytotoxicity of carbon nanomaterials: Single-wall nanotube, multi-wall nanotube, and fullerene. *Environ. Sci. Technol.* 39:1378–1383.
- Jiang G, Li G (2006) Preparation and biological activity of novel cucurbit[8]uril-fullerene complex. *J. Photochem. Photobiol. B* 85:223–227.
- Jiang G, Li G (2007) Synthesis, characterization and biological activity of C₆₀ derivative. *J. Appl. Polym. Sci.* 104:3120–3123.
- Klump C, Lacerda L, Chaloin O, Da Ros T, Kostarelos K, Prato M, Bianco A (2007) Multifunctionalised cationic fullerene adducts for gene transfer: Design, synthesis and DNA complexation. *Chem. Commun.* 3762–3764.
- Kolsenik J, Belgorodsky B, Fadeev L, Gozin M (2007) Can apomyoglobin form a complex with a spherical ligand? Interactions between apomyoglobin and [C₆₀] fullerene derivative. *J. Nanosci. Nanotechnol.* 7:1389–1394.
- Laus S, Sitharaman B, Toth V, Bolskar RD, Helm L, Asokan S, Wong MS, Wilson LJ, Merbach AE (2005) Destroying gadofullerene aggregates by salt addition in aqueous solution of Gd@C₆₀(OH)_x and Gd@C₆₀(C(COOH)₂)₁₀. *J. Am. Chem. Soc.* 127:9368–9369.
- Levi N, Hantgan RR, Lively MO, Carroll DL, Prasad GL (2006) C₆₀-Fullerenes: Detection of intracellular photoluminescence and lack of cytotoxic effects. *J. Nanobiotechnol.* 4:14.
- Liu J, Ohta Si, Sonoda A, Yamada M, Yamamoto M, Nitta N, Murata K, Tabata Y (2007) Preparation of PEG-conjugated fullerene containing Gd³⁺ ions for photodynamic therapy. *J. Controlled Rel.* 117:104–110.
- Lovern SB, Klaper R (2006) *Daphnia magna* mortality when exposed to titanium dioxide and fullerene (C₆₀) nanoparticles. *Environ. Toxicol. Chem.* 25:1132–1137.
- Lovern SB, Strickler JR, Klaper R (2007) Behavioral and physiological changes in *Daphnia magna* when exposed to nanoparticle suspensions (titanium dioxide, nano-C₆₀, and C₆₀H_xC₇₀H_x). *Environ. Sci. Technol.* 41:4465–4470.
- Lyon DY, Adams LK, Falkner JC, Alvarez PJJ (2006) Antibacterial activity of fullerene water suspensions: Effects of preparation method and particle size. *Environ. Sci. Technol.* 40:4360–4366.
- Marchesan S, Da Ros T, Spalluto G, Balzarini J, Prato M (2005) Anti-HIV properties of cationic fullerene derivatives. *Bioorg. Med. Chem. Lett.* 15:3615–3618.
- Martín N (2006) New challenges in fullerene chemistry. *Chem. Commun.* 2093–2104.
- Mashino T, Usui N, Okuda K, Hirota T, Mochizuki M (2003) Respiratory chain inhibition by fullerene derivatives: Hydrogen peroxide production caused by fullerene derivatives and a respiratory chain system. *Bioorg. Med. Chem.* 11:1433–1438.
- Mashino T, Shimotohno K, Ikegami N, Nishikawa D, Okuda K, Takahashi K, Nakamura S, Mochizuki M (2005) Human immunodeficiency virus-reverse transcriptase inhibition and

- hepatitis C virus RNA-dependent RNA polymerase inhibition activities of fullerene derivatives. *Bioorg. Med. Chem. Lett.* 15:107–1109.
- Nakamura E, Isobe H (2003) Functionalized fullerenes in water. The first 10 years of their chemistry, biology, and nanoscience. *Acc. Chem. Res.* 36:807–815.
- Nakamura E, Tokuyama H, Yamago S, Shiraki T, Sugiura Y (1996) Biological activity of water-soluble fullerenes. Structural dependence of DNA cleavage, cytotoxicity, and enzyme inhibitory activities including HIV-Protease inhibition. *Bull. Chem. Soc. Jpn.* 69:2143–2151.
- Nakamura E, Isobe H, Tomita N, Sawamura M, Jinno S, Okayama H (2000) Functionalized fullerene as an artificial vector for transfection. *Angew. Chem. Int. Edit.* 39:4254–4257.
- Niwa Y, Iwai N (2006) Genotoxicity in cell lines induced by chronic exposure to water-soluble fullerenes using micronucleus test. *Environ. Health Prev. Med.* 11:292–297.
- Oberdörster E (2004) Manufactured nanomaterials (Fullerenes, C₆₀) induce oxidative stress in the brain of juvenile Largemouth Bass. *Environ. Health Perspect.* 112:1058–1062.
- Oberdörster E, Zhu S, Blickey TM, McClellan-Green P, Haasch ML (2006) Ecotoxicology of carbon-based engineered nanoparticles: Effects of fullerene (C₆₀) on aquatic organisms. *Carbon* 44:1112–1120.
- Pantarotto D, Bianco A, Pellarini F, Tossi A, Giangaspero A, Zelezetsky I, Briand J-P, Prato M (2002) Solid-phase synthesis of fullerene-peptides. *J. Am. Chem. Soc.* 124:12543–12549.
- Pastorin G, Marchesan S, Hoebeke J, Da Ros T, Ehret-Sabatier L, Briand J-P, Prato M, Bianco A (2006) Design and activity of cationic fullerene derivatives as inhibitors of acetylcholinesterase. *Org. Biomol. Chem.* 4:2556–2562.
- Pellarini F, Pantarotto D, Da Ros T, Giangaspero A, Tossi A, Prato M (2001) A novel [60]fullerene amino acid for use in solid-phase peptide synthesis. *Org. Lett.* 3:1845–1848.
- Porter AE, Muller K, Skepper J, Midgley P, Welland M (2006) Uptake of C₆₀ by human monocyte macrophages, its localization and implications for toxicity: Studied by high resolution electron microscopy and electron tomography. *Acta Biomaterialia* 2:409–419.
- Porter AE, Gass M, Muller K, Skepper JN, Midgley P, Welland M (2007) Visualizing the uptake of C₆₀ to the cytoplasm and nucleus of human monocyte-derived macrophage cells using energy-filtered transmission electron microscopy and electron tomography. *Environ. Sci. Technol.* 41:3012–3017.
- Quick K, Dugan L (2004) Fullerene derivative (C₃) functions as a SOD mimetic by reducing age-related increase in superoxide levels and prevention of age-related loss of mitochondrial membrane potential in brain. *Free Rad. Biol. Med.* 37:S163–S163.
- Rouse JG, Yang J, Barron AR, Monteiro-Riviere NA (2006) Fullerene-based amino acid nanoparticle interactions with human epidermal keratinocytes. *Toxicol. In Vitro* 20:1313–1320.
- Ryan JJ, Bateman HR, Stover A, Gomez G, Norton SK, Zhao W, Schwartz LB, Lenk R, Kepley CL (2007) Fullerene nanomaterials inhibit the allergic response. *J. Immunol.* 179:665–672.
- Sarova GH, Da Ros T, Guldi DM (2006) Fullerene-based devices for biological applications. In: Kumar C (ed.) *Nanodevices for the Life Science*, Vol. 4. Wiley-VCH Verlag GmbH & Co. KGaA, Weinheim, pp. 352–389.
- Sayes C, Marchione A, Reed K, Warheit DB (2007) Comparative pulmonary toxicity assessments of C₆₀ water suspensions in rats: Few differences in fullerene toxicity in vivo in contrast to in vitro profiles. *Nano Lett.* 7:2399–2403.
- Sayes CM, Gobin AM, Ausman KD, Mendez J, West JL, Colvin VL (2005) Nano-C₆₀ cytotoxicity is due to lipid peroxidation. *Biomaterials* 26:7587–7595.
- Schinazi RF, Sijbesma RP, Srdanov G, Hill CL, Wudl F (1993) Synthesis and virucidal activity of a water soluble, configurationally stable, derivatized C₆₀ fullerene. *Antimicrob. Agents Chemother.* 37:1707–1710.
- Schuster DI, Wilson LJ, Kirschner AN, Schinazi RF, Schlueter-Wirtz S, Tharnish P, Barnett T, Ermoloeff J, Tang J, Brettreich M, Hirsch A (2000) In: Martin N, Maggini M, Guldi DM (eds.) *Fullerene 2000 – Functionalized Fullerenes*, Vol. 9. The Electrochemical Society, Pennington, NJ, pp. 267–270.

- Sijbesma R, Srdanov G, Wudl F, Castoro JA, Wilkins C, Friedman SH, DeCamp DL, Kenyon GL (1993) Synthesis of a fullerene derivative for the inhibition of HIV enzymes. *J. Am. Chem. Soc.* 115:6510–6512.
- Sun T, Xu Z (2006) Radical scavenging activities of alpha-alanine C₆₀ adduct. *Bioorg. Med. Chem. Lett.* 16:3731–3734.
- Tagmatarchis N, Shinohara H (2001) Fullerene in medicinal chemistry and their biological applications. *Mini Rev. Med. Chem.* 1:339–348.
- Tang YJ, Ashcroft JM, Chen D, Min G, Kim CH, Murkhejee B, Larabell C, Keasling JD, Chen FF (2007) Charge-associated effects of fullerene derivatives on microbial structural integrity and central metabolism. *Nano Lett.* 7:754–760.
- Tegos GP, Demidova TN, Arcila-Lopez D, Lee H, Wharton T, Gali H, Hamblin MR (2005) Cationic fullerenes are effective and selective antimicrobial photosensitizers. *Chem. Biol.* 12:1127–1135.
- Tóth E, Bolskar RD, Borel A, Gonzalez G, Helm L, Merbach AE, Sitharaman B, Wilson LJ (2005) Water-soluble gadofullerenes: Toward high-relaxivity, pH-responsive MRI contrast agents. *J. Am. Chem. Soc.* 127:799–805.
- Tong Z, Bischoff M, Nies L, Applegate B, Turco RF (2007) Impact of fullerene (C₆₀) on a soil microbial community. *Environ. Sci. Technol.* 41:2985–2991.
- Usenko CY, Harper SL, Tanguay RL (2007) In vivo evaluation of carbon fullerene toxicity using embryonic zebrafish. *Carbon* 45:1891–1898.
- Venkatesan N, Yoshimitsu J, Ito Y, Shibata N, Takada K (2005) Liquid filled nanoparticles as a drug delivery tool for protein therapeutics. *Biomaterials* 26:7154–7163.
- Witte P, Beuerle F, Hartnagel U, Lebovitz R, Savouchkina A, Sali S, Guldi D, Chronakis N, Hirsch A (2007) Water-solubility, antioxidant activity and cytochrome C binding of four families of exohedral adducts of C₆₀ and C₇₀. *Org. Biomol. Chem.* 5:3599–3613.
- Xiao L, Takada H, Maeda K, Haramoto M, Miwa N (2005) Antioxidant effects of water-soluble fullerene derivatives against ultraviolet ray or peroxy lipid through their action of scavenging the reactive oxygen species in human skin keratinocytes. *Biomed. Pharmacother.* 59:351–358.
- Xiao L, Takada H, Gan XH, Miwa N (2006) The water-soluble fullerene derivative ‘Radical Sponge®’ exerts cytoprotective action against UVA irradiation but not visible-light-catalyzed cytotoxicity in human skin keratinocytes. *Bioorg. Med. Chem. Lett.* 16:1590–1595.
- Yamawaki H, Iwai N (2006) Cytotoxicity of water-soluble fullerene in vascular endothelial cells. *Am. J. Physiol. Cell Physiol.* 290:1495–1502.
- Yang J, Alemany LB, Driver J, Hartgerink JD, Barron AR (2007a) Fullerene-derivatized amino acids: Synthesis, characterization, antioxidant properties, and solid-phase peptide synthesis. *Chem. Eur. J.* 13:2530–2545.
- Yang J, Wang K, Driver J, Yang J, Barron AR (2007b) The use of fullerene substituted phenylalanine amino acid as a passport for peptides through cell membranes. *Org. Biomol. Chem.* 5:260–266.
- Yang X, Chen L, Qiao X, Fan C (2007c) Photo-induced damages of cytoplasmic and mitochondrial membranes by a [C₆₀]fullerene malonic acid derivative. *Int. J. Toxicol.* 26:197–201.
- Yang X, Chen Z, Meng X, Li B, Tan X (2007d) Inhibition of DNA restrictive endonucleases and Taq DNA polymerase by trimalonic acid C₆₀. *Chin. Sci. Bull.* 52:1802–1806.
- Yang XL, Huang C, Qiao XG, Yao L, Zhao DX, Tan X (2007e) Photo-induced lipid peroxidation of erythrocyte membranes by a bis-methanophosphonate fullerene. *Toxicol. In Vitro* 21:1493–1498.
- Ying Q, Zhang J, Liang D, Nakanishi W, Isobe H, Nakamura E, Chu B (2005) Fractal behavior of functionalized fullerene aggregates. I. Aggregation of two-handed tetraaminofullerene with DNA. *Langmuir* 21:9824–9831.
- Yu C, Canteenwala T, Chiang LY, Wilson B, Pritzker K (2005) Photodynamic effect of hydrophilic C₆₀-derived nanostructures for catalytic antitumoral antibacterial applications. *Synth. Metals* 153:37–40.

- Zakharian T, Seryshev A, Sitharaman B, Gilbert B, Knight V, Wilson L (2005) A fullerene-paclitaxel chemotherapeutic: Synthesis, characterization, and study of biological activity in tissue culture. *J. Am. Chem. Soc.* 127:12508–12509.
- Zarubaev VV, Belousova IM, Kiselev OI, Piotrovsky LB, Anfimov PM, Krisko TC, Muraviova TD, Rylkov VV, Starodubzev AM, Sirotkin AC (2007) Photodynamic inactivation of influenza virus with fullerene C₆₀ suspension in allantoic fluid. *Photodiagn. Photodyn. Ther.* 4:31–35.
- Zhang X-F, Shu C-Y, Xie L, Wang C-R, Zhang Y-Z, Xiang J-F, Li L, Tang Y-I (2007) Protein conformation changes induced by a novel organophosphate-containing water-soluble derivative of a C₆₀ fullerene nanoparticle. *J. Phys. Chem. C* 111:14327–14333.
- Zhao QF, Zhu Y, Ran TC, Li JG, Li QN, Li WX (2006) Cytotoxicity of fullerenols on *Tetrahymena pyriformis*. *Nucl. Sci. Technol./Hewuli* 17:280–284.

Chapter 2

Biomedical Applications of Functionalised Carbon Nanotubes

Alberto Bianco¹, Raquel Sainz¹, Shouping Li¹, H el ene Dumortier¹, Lara Lacerda², Kostas Kostarelos², Silvia Giordani^{3,4}, and Maurizio Prato⁴

Abstract This chapter describes the developing potential of carbon nanotubes (CNTs) in biomedicine. Methodologies to render nanotubes biocompatible, the related studies on cell uptake, applications in vaccine delivery, interaction with nucleic acids and impact on health will be described. The use of CNTs for biomedical applications is acquiring more and more substantiating evidence for efficient development. It is clear that some important issues related to the health impact including the biodistribution, accumulation and elimination have to be addressed more thoroughly before CNTs can be proposed for clinical trials. However, CNTs show remarkable carrier properties, with a very strong tendency to cross cell membranes. Although, the toxicological studies on pristine CNTs are contradictory, showing a certain degree of risk, it is becoming evident that functionalised CNTs have reduced toxic effects. Therefore, the combination of cell uptake capacity with high loading of cargo molecules achievable with CNTs makes this new carbon nanomaterial a promising candidate for innovative therapies.

Keywords Carbon nanotubes, Functionalization, Drug Delivery, Gene transfer, Health, Biodistribution

2.1 Introduction

Nanotechnology is expected to impact all current industries including semiconductors, manufacturing and biotechnology, and it may also create several new ones. Major challenges remain, before these opportunities can be realised and some of them include the

¹CNRS, Institut de Biologie Mol culaire et Cellulaire, Laboratoire d'Immunologie et Chimie Th rapeutiques, 67084 Strasbourg, France
Email: a.bianco@ibmc.u-strasbg.fr

²Nanomedicine Laboratory, Centre for Drug Delivery Research, The School of Pharmacy, University of London, London WC1N 1AX, United Kingdom
Email: kostas.kostarelos@pharmacy.ac.uk

³School of Chemistry/Centre for Research on Adaptive Nanostructures and Nanodevices (CRANN), Trinity College Dublin, College Green, Dublin 2, Ireland

⁴Dipartimento di Scienze Farmaceutiche, Universit  di Trieste, 34127 Trieste, Italy
Email: prato@units.it

ability to assemble, characterise and manipulate materials at the nanoscale level. Nanomedicine is an area with particular promise and may inspire the construction of nanostructured carriers for the targeted delivery of small-molecule ‘passengers’ to a desired area. Nanosized delivery vehicles may also offer better or more efficient use of an active molecule (i.e. drugs, antigens, proteins, enzymes and nucleic acids) by controlling release rates, by protecting it from unwanted metabolic processes or through targeted delivery processes that can reduce side effects. A drug delivery system is usually designed to improve the pharmacological and therapeutic properties of conventional drugs and to overcome problems such as limited solubility, poor distribution, lack of selectivity and tissue damage. Cell membranes act as barriers and allow only certain structures with the right hydrophilicity to hydrophobicity ratio to pass. Among the currently available delivery systems, which include liposomes, emulsions, polymers and microparticles (Lavan et al., 2003; Martin and Kohli, 2003; Allen and Cullis, 2004), carbon nanotubes (CNTs) have recently gained popularity as potential drug carriers, therapeutic agents and diagnostic tools (Gref et al., 1994; Langer, 1998; Lavan et al., 2002; Duncan, 2003; Savic et al., 2003; Murthy et al., 2003; Varde and Pack, 2004). They have nanoscale dimensions, and can be modified through covalent bonding of functional organic molecules. CNTs have been shown to penetrate easily through cell membranes (Bianco et al., 2005b; Kostarelos et al., 2007), have been proposed as components for DNA and protein biosensors, ion channel blockers and as bioseparators and biocatalysts (Chen et al., 2001b; Williams et al., 2002; Cai et al., 2003; Gooding et al., 2003; Patolsky et al., 2004; Wang et al., 2004). CNTs have also been used as platforms to detect antibodies associated with human autoimmune diseases (Chen et al., 2003).

This chapter will describe the potential of carbon nanotubes in biomedicine. It will illustrate the methodologies to render nanotubes biocompatible, the studies on their cell uptake, their application in vaccine delivery, their interaction with nucleic acids and their impact on health.

2.2 Carbon Nanotubes

2.2.1 *Structure and Characteristics*

CNTs, discovered in 1991 by Iijima (Iijima, 1991; Iijima and Ichihashi, 1993), display unique structures and remarkable physical (mechanical, thermal and electronic) properties (Ajayan, 1999; Baughman et al., 2002). As a result, a variety of applications of these architectures can be envisioned in both the physical and life sciences. They can be classified into two main types: single-walled carbon nanotubes (SWNTs), which consist of one single layer of graphene sheet seamlessly rolled into a cylindrical tube, and multi-walled carbon nanotubes (MWNTs), which are made up of several concentric graphene layers (Fig. 2.1). They have nanoscale dimensions, with diameters in the range of 0.5–1.5 nm and 2–100 nm and lengths in the range of 20–1,000 nm, and 1–50 μm for SWNTs and MWNTs, respectively.

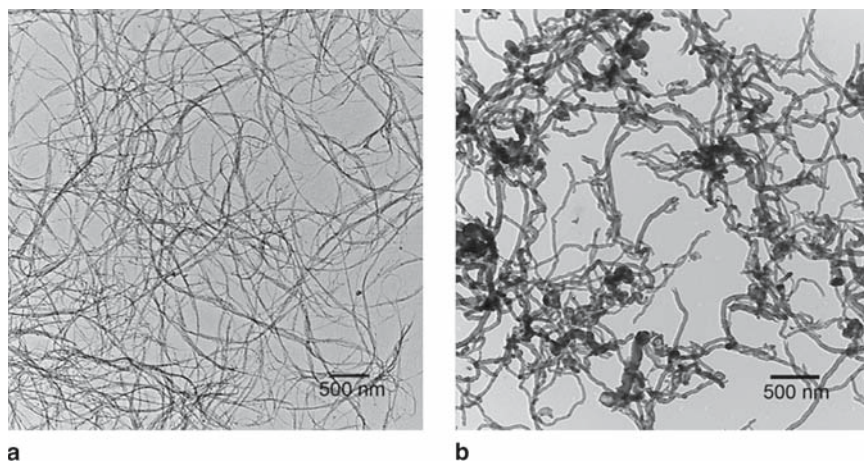


Fig. 2.1 Transmission electron microscopy (TEM) images of pristine single-walled (a) and multi-walled carbon nanotubes (b)

Several methods for the production of both types of tubes and the modulation of their dimensions are available in the literature (Special issue on Carbon Nanotubes, 2002). They can be classified into three main techniques: arc-discharge, laser ablation and chemical vapour deposition. The nanotubes produced by the different methods are usually a mixture of tubes with different diameters, lengths, chirality and often contain impurities, mainly amorphous carbon and catalyst particles. They have limited solubility in organic solvents (Giordani et al., 2006) and are basically insoluble in aqueous solutions. In addition, pristine isolated SWNTs are rarely available in sufficient quantities. Due to their great flexibility and high surface energy, they tend to aggregate into bundles and superstructures of bundles with still a higher degree of entanglement (ropes, mats). These bundles contain huge numbers of both metallic and semiconducting SWNTs in a mixture of one third and two thirds, respectively. Bundle properties are generally inferior to those of isolated SWNTs and effective separation of aggregates must be achieved prior to functionalisation and construction of nanodevices.

In order to be used in biology and medicinal chemistry, carbon nanotubes need to be purified and soluble in physiological media. Various methods have been developed to purify CNTs, such as oxidation, microfiltration, chromatography and microwave irradiation (Ajayan, 1999; Xie et al., 1999). The solubilisation of CNTs can be achieved following two major pathways: (1) noncovalent supramolecular modifications, and (2) covalent functionalisation. Both types of approach give rise to soluble conjugates, in which one component is constituted by CNTs and the counterpart is, for example, a biopolymer (i.e. peptide, protein and DNA). There are advantages and drawbacks related to the two strategies of solubilisation, which will be tackled in the following paragraphs.

2.2.2 *Noncovalent Functionalisation*

Because offering the possibility of both exfoliating bundles, which affords individual CNTs, and attaching chemical or biological molecules without affecting the electronic network of the nanotubes, noncovalent functionalisation of CNTs is considered a very promising method in the fields such as the preparation of functional and composite materials and biomedical technologies. Many groups have reported the noncovalent interactions between biomolecules and CNTs using both computational and experimental approaches.

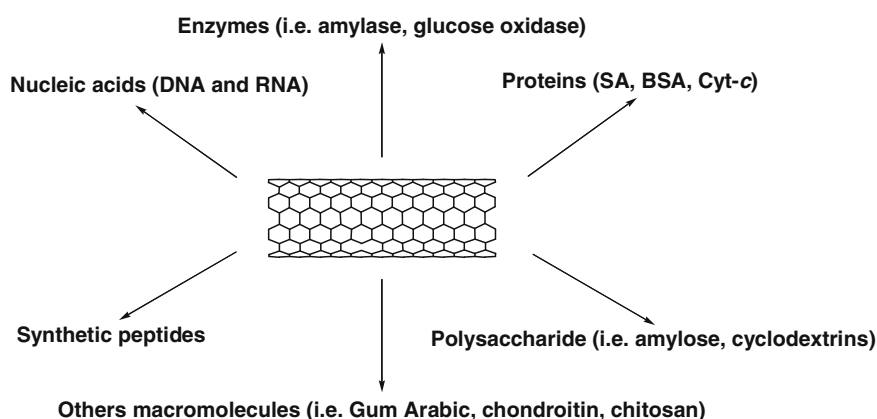
Molecular dynamics (MD) simulations indicated that in the single-strand DNA (ssDNA)–CNT interaction, both the van der Waals and hydrophobic forces are important. The former play a more dominant role, while the hydrophobic effect alone is insufficient to guarantee the binding between the DNA and CNTs in water, either encapsulating DNA inside or wrapping it outside CNTs (Gao et al., 2003; Gao and Kong, 2004). Utilising molecular modelling simulations, it has been demonstrated that double-stranded DNA (dsDNA) could also wrap around the surface of CNTs (Lu et al., 2005). MD simulations were also performed on the complexes constituted by the amylase–nanotube system to study the mode of interaction between the initially separated amylase and SWNT fragments. It has been found that the van der Waals forces are dominant and they always play an important role in promoting noncovalent association (Xie and Soh, 2005). Experimentally, Tsang and co-workers studied the interaction of protein, enzymes and DNA with carbon nanotubes. They found that DNA molecules tended to cover the surface of nanotubes and the small proteins and enzymes could be readily placed on the outer surface and also within the interior cavity of opened CNTs, as evidenced by high-resolution transmission electron microscopy (HRTEM) (Tsang et al., 1997; Davis et al., 1998; Guo et al., 1998). Alternatively to electron microscopy techniques, fluorescence microscopy was used to observe DNA transport through a MWNT channel (Ito et al., 2003). Kam et al. reported that DNA and various proteins, such as streptavidin (SA), protein A (SpA), bovine serum albumin (BSA) and cytochrome *c* (cyt-*c*), adsorb spontaneously on the sidewalls of CNTs. These functionalised CNTs are capable of carrying proteins and DNA into cells via the endocytosis pathway (Kam and Dai, 2005; Kam et al., 2006). Star et al. analysed the interaction of CNTs with the starch. In particular, the amylose linear component is able to disperse CNTs in water. This polysaccharide adopts a helical conformation in water. The initial experiments showed that CNTs were not soluble in an aqueous solution of starch, but were soluble in an aqueous solution of a starch–iodine complex. The authors suggested that the preorganisation of amylose in a helical conformation through complexation with small molecules like iodine was critical for single nanotube or bundles to enter into the cavity of the helix (Star et al., 2002). The helical amylose could be used as an effective dispersant to solubilise SWNTs by supramolecular encapsulation. It has been demonstrated that 10–20% dimethyl sulfoxide (DMSO) mixture with water was the best solvent, in which amylose assumed an interrupted loose helix (Kim et al., 2003). Cyclodextrins, the macrocyclic analogues of amylose, were

also selected to study the complexation with CNTs (Dodziuk et al., 2003; Ikeda et al., 2004). The first samples were prepared by a simple grinding procedure to efficiently cut SWNTs (Chen et al., 2001a). A refluxing procedure was also performed to obtain the complexation, and the samples were analysed using absorption spectroscopy, Raman spectroscopy and differential scanning calorimetry (DSC). The results showed an intermolecular interaction between CNTs and cyclodextrins (Chambers et al., 2003).

An alternative efficient approach to disperse CNTs relies on the use of synthetic peptides. Peptides were designed to coat and solubilise the CNTs by exploiting a noncovalent interaction between the hydrophobic face of amphiphilic helical peptides and the graphitic surface of CNTs (Dieckmann et al., 2003; Zorbas et al., 2004; Dalton et al., 2004; Arnold et al., 2005). Peptides showed also selective affinity for CNTs and therefore may provide them with specifically labelled chemical handles (Wang et al., 2003). Other biomolecules, such as Gum Arabic (GA) (Bandyopadhyaya et al., 2002), salmon sperm DNA, chondroitin sulphate sodium salt and chitosan (Zhang et al., 2004; Moulton et al., 2005), were selected as surfactants to disperse CNTs (Scheme 2.1).

Through van der Waals and hydrophobic interactions, CNTs were functionalised and made water soluble by the strong adsorption of phospholipids (PLs) grafted onto amino-terminated polyethylene glycol (PEG). The group of Dai bound nucleic acids (DNA and RNA) and proteins to CNTs for specific detection of antibodies (Chen et al., 2003; Kam et al., 2005a, b; Liu et al., 2007b).

Our group reported a method of functionalisation of CNTs to generate positively charged CNTs (CNT-NH₃⁺) (Georgakilas et al., 2002). Plasmid DNA (pDNA) was selected to study the interaction with CNT-NH₃⁺. It was found that strong complexes were formed between CNTs and pDNA primarily through electrostatic forces and pDNA was condensed around the CNTs (Pantarotto et al., 2004b; Singh



Scheme 2.1 Examples of noncovalent functionalisation of carbon nanotubes (CNTs) with different biomolecules

et al., 2005; Lacerda et al., 2006b) (see Paragraph 6). In another approach, Liu et al. (2005) prepared polyethyleneimine-functionalised CNTs for immobilisation and efficient delivery of DNA. Gao et al. (2006) used cationic CNTs to create a complex with GFT-encoding pDNA and delivered the latter into mammalian cells showing a certain degree of transfection.

Recently, Zhang et al. (2007) reported a hybrid nanocomposite with sandwich structure by alternative electrostatic assembly of haemoglobin (Hb) and DNA on the surface of oxidised CNTs. Valenti et al. studied the adsorption–desorption process of protein (BSA) on CNTs by reflectometry. Different BSA concentrations, pH values and ionic strengths affect this process in different conditions (Valenti et al., 2007). The adsorption of proteins onto CNTs was used to control the formation of silver nanoparticles on carbon nanotubes (Bale et al., 2007). Several groups have reported the binding of biomolecules to carbon nanotubes through π -stacking. Due to the high aromatic character and the strong interaction with the sidewalls of CNTs, pyrenyl groups were selected as a suitable bridge possessing additional functional groups. Proteins (Chen et al., 2001b), enzymes (Besteman et al., 2003) and DNA (Taft et al., 2004) were successfully immobilised on the sidewall of CNTs using bifunctional pyrene derivatives. Zheng et al. reported effective dispersion and separation of CNTs via the assistance of DNA. Molecular modelling suggested that ssDNA could bind to CNTs through π -stacking, resulting in helical wrapping around the surface (Zheng et al., 2003a, b). The interactions between RNA and CNTs were also investigated by Rao and co-workers (Rao et al., 2004) (see Paragraph 6).

Concluding, the noncovalent functionalisation is a versatile and useful strategy for increasing the solubility of CNTs. Furthermore, it permits their conjugation with different molecules while conserving their electronic structure and properties, opening up a range of potential applications of CNTs in nanomedicine.

2.2.3 Covalent Functionalisation

The covalent functionalisation of CNTs is the alternative and extremely promising approach for applications in fields such as that of functional and composite materials and that of biology. According to the location of the functional groups, two main strategies are used to covalently functionalise CNTs with biomolecules: (i) defect functionalisation, and (ii) sidewall functionalisation.

2.2.3.1 Defect Functionalisation

Chemical treatments, such as strong oxidising acid mixtures of $\text{HNO}_3/\text{H}_2\text{SO}_4$ under sonication, modify CNT surfaces with anchor groups, including carboxylic, carbonyl and hydroxyl functions, eventually used to covalently connect molecules to the tubes. The carboxylic acid groups are often the most common

choice to connect the CNTs with the amino-terminated sites present on the biomolecules. Before covalent modification, the carboxylic acids are often activated by thionyl or oxalyl chloride, carbodiimides or active esters, to get highly reactive intermediate groups, to link different types of biomolecules to CNTs via stable covalent bonds. The carboxyl groups of CNTs were activated, for example, in the presence of *N*-hydroxysuccinimide and carbodiimide and used to conjugate peptide nucleic acid (PNA, an uncharged DNA analogue) to the end of CNTs via a stable amide bond. PNAs were then hybridised with complementary DNA sequences, showing the possibility of recognition-based assembly and the potential use as biological sensors (Williams et al., 2002). Similar methods based on the amide linkage were used to immobilise DNA (Nguyen et al., 2002; Baker et al., 2002; Hazani et al., 2003; Li et al., 2005), proteins, such as BSA (Huang et al., 2002; Jiang et al., 2004) and streptavidin (Wohlstadter et al., 2003), and glucose oxidase (Lin et al., 2004) to CNTs. Streptavidin was also complexed to CNTs prefunctionalised with biotin through carbodiimide-activated amidation (Kam et al., 2004). Similarly, a biotinylated DNAzyme was covalently attached to CNTs using streptavidin as a bridge (Yim et al., 2005) (Scheme 2.2).

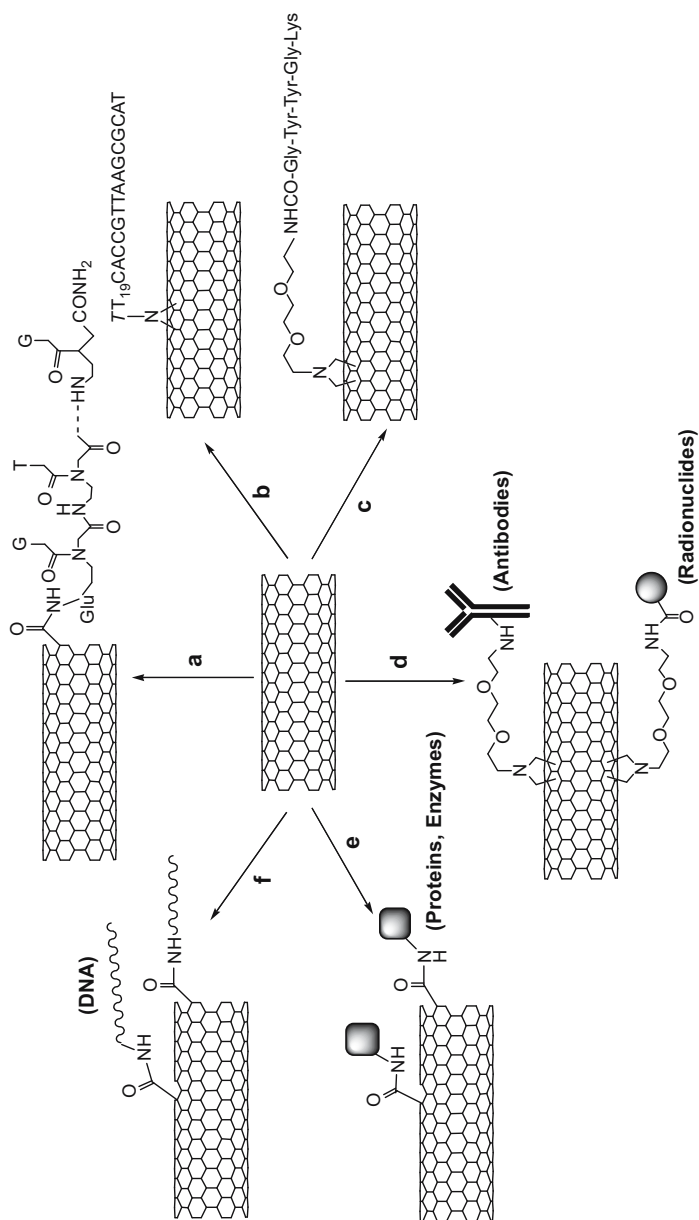
An interesting work carried out by Patolsky et al. (2004) by anchoring redox enzymes to the edges of CNTs via amino coupling, as evidenced by AFM and high-resolution TEM. With the carboxylic acids activated by a coupling reagent, Taft et al. (2004) bonded ssDNA on arrayed carbon nanotube via amino coupling.

2.2.3.2 Sidewall Functionalisation

Several different methods of sidewall functionalisation, such as fluorination, radical addition, nucleophilic addition, electrophilic addition and cycloaddition, have been developed (Tasis et al., 2006). The sidewalls of vertically aligned CNTs have been functionalised with DNA using azide units as photoactive components. The azidothymidine reacted photochemically with sidewalls of CNTs utilising [2+1] cycloaddition. The oligonucleotides were grown *in situ* on the sidewalls of CNTs and the DNA-modified CNTs were obtained after the deprotection of the nucleic acid (Moghaddam et al., 2004).

1,3-Dipolar cycloaddition of azomethine ylides, generated by the condensation of an α -amino acid and an aldehyde, is an efficient method for covalent sidewall functionalisation and has been successfully used to solubilise CNTs in most organic solvents (Tasis et al., 2003; Holzinger et al., 2003). This particular technique has also been utilised to obtain the first example of a bioactive peptide covalently linked to CNTs by the prospect for the potential applications in immunology (Bianco and Prato, 2003; Pantarotto et al., 2003a, b; Bianco et al., 2005b).

McDevitt et al. (2007) reported that the tumour-targeting CNT constructs were synthesised via sidewall covalent functionalisation using 1,3-dipolar cycloaddition to attach the antibody IgG, radiometal-ion chelates and fluorescent probes.



Scheme 2.2 Examples of covalent functionalisation of carbon nanotubes (CNTs) with different types of therapeutic agents. (a) Williams et al. (2002); (b) Moghaddam et al. (2004); (c) Pantarotto et al. (2003a); (d) McDevitt et al. (2007); (e) Huang et al. (2002), Jiang et al. (2004), Wohlstadter et al. (2003), Lin et al. (2004), Kam et al. (2004), Yim et al. (2005), Patolsky et al. (2004), Baker et al. (2002), Hazami et al. (2003), Li et al. (2005), Taft et al. (2004)

Great effort has been made to overcome the barriers of CNTs towards bioapplications, especially those concerning the aqueous dispersion and biocompatibility. As a consequence the number of reactions that involve chemical modification of the tubes is progressively increasing. Besides the advantage of obtaining soluble CNTs, the covalent functionalisation also provides the possibility of linking a large number of biomolecules to the surface of the tubes.

2.3 Carbon Nanotube Cell Uptake: Mechanisms and Trafficking

Determination of the exact mechanism leading to cellular internalisation of CNTs is considered very important in their development as components of biomedical devices and therapeutics intended for implantation or administration to patients. One of the most important parameters in all such studies is the type of nanotubes used, determined by the process by which they are made biocompatible. Interactions with cells have to be performed using biocompatible CNTs, achieved by either covalent or noncovalent surface functionalisation that results in water-dispersible CNTs. A variety of different functionalisation strategies for CNTs have been reported by different groups, therefore direct comparisons are often hampered by the inability to correlate experimental conditions.

In the CNT literature there are already published reports of cellular internalisation using multiple types of cells (fibroblasts, epithelial and cancer cells, phagocytes, bacteria and fungi) in various studies and under different experimental conditions (Cherukuri et al., 2004; Rojas-Chapana et al., 2005; Kostarelos et al., 2007). Such interesting properties of water-dispersible, individualised CNTs can be used in biomedical applications, such as their consideration as novel carrier systems of therapeutics and diagnostics because: (a) CNTs can be internalised by a wide range of cell types; and (b) their high surface area can potentially act as a template of cargo molecules such as peptides, proteins, nucleic acids and drugs. Although the exact mechanisms responsible for the observed CNT entrance into the cells are still unclear and remain to be elucidated, in Fig. 2.2 some pathways that have been proposed to explain how cellular uptake of CNT occurs are schematically represented. The main internalisation pathways to accomplish internalisation of CNT within cells are as follows: (A) phagocytosis; (B) membrane piercing by passive diffusion; (C) caveolae-mediated endocytosis and (D) clathrin-mediated endocytosis.

Several groups have been mainly concerned with studying *in vitro* detection techniques for CNTs. For this reason phagocytic-competent cells were used in their studies to guarantee that the CNTs are internalised in high percentages. Cherukuri et al. (2004) have shown that CNTs wrapped with Pluronic F108 were actively phagocytosed by macrophages and that the near-infrared (NIR) signal of the CNTs was well captured. In addition, Choi et al. (2007) have also studied the NIR signal of CNTs in macrophages, but in this case the CNTs used were wrapped by ssDNA.

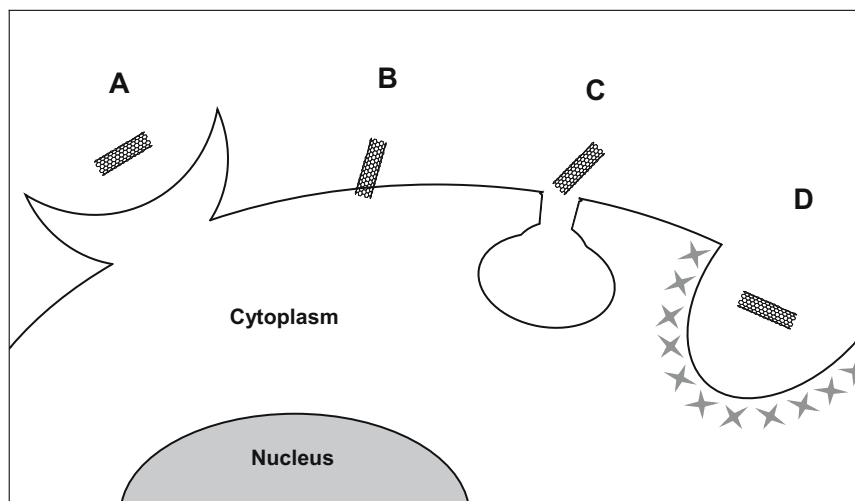


Fig. 2.2 Cellular internalisation pathways proposed for carbon nanotubes (CNTs): (A) phagocytosis; (B) membrane piercing by passive diffusion; (C) caveolae-mediated endocytosis; and (D) clathrin-mediated endocytosis

There have been a few published studies using ssDNA as the CNTs coating material to render CNTs water-dispersible. Such nucleic acids do not encode for exogenous genes, therefore are not relevant to therapeutic applications, however, they have been described to translocate intracellularly. Kam et al. have reported the translocation of ssDNA into the nucleus of HeLa cells by two different CNT structures: (a) Cy3-labelled ssDNA directly linked to CNT through a noncovalent adsorption (Kam et al., 2005b, 2006), and (b) Cy3-labelled ssDNA covalently linked to a polyethylene glycol chain that was part of a phospholipid molecule, which was adsorbed onto the CNT (Kam et al., 2005a). The authors of these studies postulated endocytotic uptake of the whole ssDNA–CNT constructs. In addition, Heller et al. (2005, 2006) have also reported the cellular internalisation of CNTs coated by ssDNA via an endocytic pathway. Although the long-term goal of this team was to develop resilient optical sensors based on CNTs for *in vitro* and *in vivo* applications, they have used ssDNA to achieve the solubilisation of the CNTs in aqueous solutions and demonstrated an endocytosis-dependent internalisation and perinuclear localisation without penetration into the nuclear envelope of the ssDNA–CNT complexes incubated with mammalian cells.

Studies from our laboratories by Pantarotto et al. (2004a, b), Wu et al. (2005) and Kostarelos et al. (2007) using covalently functionalised CNTs (1,3-dipolar cycloaddition reaction chemistry) have reproducibly described that CNTs were taken up by cells via pathways other than endocytosis. This work has experimentally observed that CNTs were able to interact with plasma membranes and cross into the cytoplasm without the apparent need of engulfment into a cellular compartment

to facilitate intracellular transport. The nanotubes were observed by transmission electron microscopy (TEM) during the process of cellular internalisation to obtain a perpendicular orientation relative to the axis of the plasma membrane (Pantarotto et al., 2004b). In addition, the effect of different functional groups at the surface of functionalised CNTs was investigated using techniques such as confocal microscopy, fluorescence-activated cell sorting (FACS) and protocols, which inhibit energy-dependent internalisation mechanisms (incubation at 4 °C and addition of sodium azide or 2,4-dinitrophenol to cell culture media). Interestingly, such studies confirmed the ability of CNTs to be uptaken by cells, regardless of cell type or characteristics (e.g. surface charge) of the functional group attached onto the CNTs (Kostarelos et al., 2007).

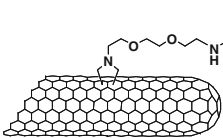
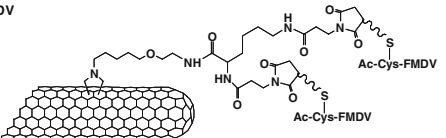
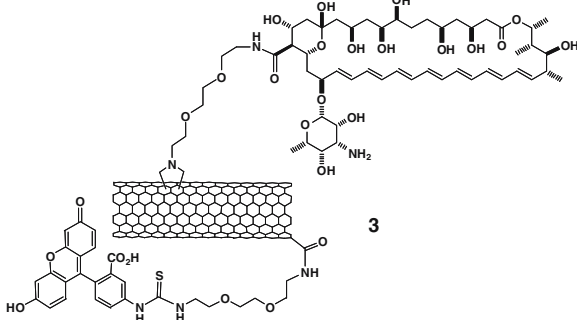
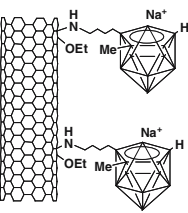
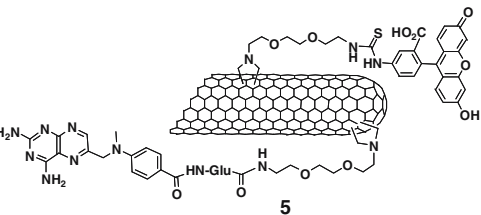
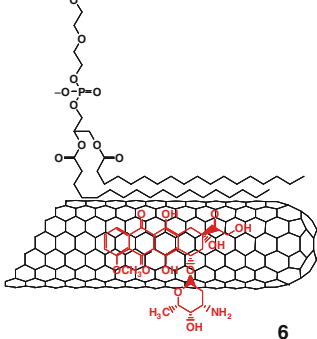
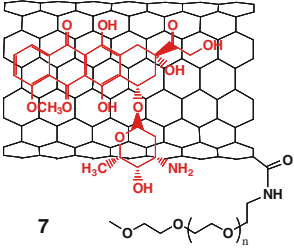
Very recently, the hypothesis of CNT-piercing cells as ‘nanoneedles’ on the plasma membrane has been experimentally observed independently for two different types of CNTs: (a) block copolymer-coated noncovalently functionalised MWNTs binding studies using microglia cells (Kateb et al., 2007); and (b) oxidised, water-soluble CNTs interacting with *Escherichia coli* under application of microwaves (Rojas-Chapana et al., 2005). The work accumulating gradually by different groups is confirming that novel, very interesting mechanisms other than ‘classical’ endocytosis are contributing to the high levels of cellular internalisation of CNTs. What should be highlighted, however, from these studies using CNT dispersions coated with macromolecules is that the surface coating on the CNTs, such as ssDNA, PEGylated lipid or block copolymers, in the cases above is – as expected – critically important for the interactions between cells and CNTs. The endocytotic mechanism of uptake reported is thought to be a result of the nucleic acid or lipid coat on the CNT surface recognised by the cells instead of the CNT backbone. The possible cellular uptake mechanism of CNTs is thought to be due to various different contributing pathways. Transforming the surface of the CNTs with large macromolecules leads to modification of the inherent abilities of these nanostructures and their interactions with cells by masking the CNT structure (Nimmagadda et al., 2006).

2.4 Carbon Nanotubes and Immunological Response

2.4.1 Carbon Nanotubes for Peptide Delivery

In recent years, CNTs have been receiving considerable attention because of their potential use in biomedical applications. Solubility of CNTs in aqueous media is a fundamental prerequisite to increase their biocompatibility. For this purpose several methods of dispersion and solubilisation have been developed leading to chemically modified CNTs (see Paragraph 2). The modification of carbon nanotubes also provides multiple sites for the attachment of several kinds of molecules, making functionalised CNTs a promising alternative for the delivery of therapeutic compounds.

Table 2.1 Structures of carbon nanotubes (CNTs) conjugated to several therapeutic agents (*See Color Plates*)

 <p style="text-align: center;">1</p>	 <p style="text-align: center;">2</p>
<p style="text-align: center;">Peptide-vaccine delivery (Pantarotto et al. 2003a and 2003b) (FMDV peptide corresponds to the 141-159 region of the viral envelope protein VP1 from foot-and-mouth disease virus)</p>	
 <p style="text-align: center;">3</p> <p style="text-align: center;">Antibiotic delivery (Wu et al. 2005)</p>	
 <p style="text-align: center;">4</p>	 <p style="text-align: center;">5</p>
<p style="text-align: center;">Cancer therapy (Yinghui et al. 2005)</p>	<p style="text-align: center;">Cancer therapy (Pastorin et al. 2006)</p>
 <p style="text-align: center;">6</p>	 <p style="text-align: center;">7</p>
<p style="text-align: center;">Cancer therapy (Liu et al. 2007a, Ali-Boucetta et al. 2008)</p>	

Biologically active peptides can be linked through a stable covalent bond to CNTs suggesting their application on peptide-vaccine delivery. Our groups have developed a vaccine delivery system by covalently linking amino-derivatised CNTs to a series of peptides (Pantarotto et al., 2003a, b). In particular, a B-cell epitope from the VP1 coat protein of the foot-and-mouth disease virus (FMDV) was attached to the maleimide moieties of mono- and bis-derivatised CNTs (see Table 2.1, structures 1 and 2). The secondary conformation of the peptide was maintained and recognised by specific monoclonal and polyclonal antibodies as assessed by enzyme-linked immunosorbent assay (ELISA) and surface plasmon resonance (SPR). Following the administration of the peptide–CNT conjugates in animal models, there was no immune response to the CNTs devoid of the peptide moiety, suggesting that nanotubes do not possess intrinsic immunogenicity. In addition, derivatised peptide–CNTs elicited high virus-neutralising antibody responses *in vivo*, thus demonstrating the potential use of peptide–CNT conjugates for their application in vaccine delivery.

2.4.2 Immunopotentiality by Cytosine-Phosphodiester-Guanine-Containing Oligodeoxynucleotides

Bacterial DNA is recognised as a ‘danger’ signal by the immune system of mammals and, as a consequence, induces the stimulation of a variety of immune cells. This has been attributed to the presence of unmethylated cytosine-phosphodiester-guanine (CpG) motifs (Krieg et al., 1995; Klinman et al., 1997). Synthetic oligodeoxynucleotides (ODN) containing CpG motifs have been shown to be effective immunoprotective agents against a variety of pathogens and enhancers of antigen-specific immune responses. For these reasons they have been considered as candidate adjuvants for vaccines or immunomodulators for therapeutic applications against infectious diseases, tumours, asthma and allergy (Krieg, 2002) or to combat bioterrorist threats (Klinman et al., 1999). However, their biological activity is often transient and several administrations or high doses are required to achieve the desired effects (Mutwiri et al., 2004). Therefore, there is a great interest in developing delivery systems to improve the stimulatory activity of ODN CpGs.

Our group has evaluated the interaction of functionalised CNTs with one specific ODN immunostimulatory CpG motif (Bianco et al., 2005a) using SPR technology. Two types of cationic-functionalised CNTs were used. Mono- and bis-ammonium-derivatised CNTs displayed no toxic effects on mouse splenocytes. More importantly, high ratios of functionalised CNTs over a minimum immunostimulatory dose of a specific ODN CpG increased the immunopotentiating activity *in vitro*, while decreasing the secretion of proinflammatory interleukine-6. The positive charge of the functionalised nanotubes neutralises the negative charge of ODN CpG, and as a consequence the repulsion by the negatively charged cell membrane should be reduced, facilitating the cellular uptake of ODN CpG.

2.5 Carbon Nanotubes for Drug Delivery

To maximise the efficacy of a drug, the choice of the delivery system is of fundamental importance. Conventional drug administration often fails due to low drug solubility, instability in biological milieu, poor distribution among the cells and lack of selectivity and damage of healthy tissues. Drug delivery systems are aimed to minimise the drug degradation, to increase its bioavailability, to target it to specific cells and to reduce the amount of drug needed, decreasing toxicity and harmful side effects. CNTs possess an enormous aspect ratio (ratio between the length and the diameter) compared to classical drug delivery systems such as liposomes or polymer-based carriers, and are becoming a promising alternative in this field, since the first demonstration of their capacity to penetrate into cells (see Paragraph 3). CNTs can be functionalised with antibiotics to deliver them into the cells. In particular, CNTs were employed in the administration of amphotericin B (AmB). AmB is a potent antifungal agent for the treatment of chronic fungal infections, but highly toxic for mammalian cells (Zotchev, 2003) due to the formation of aggregates, which reduce the solubility in water (Szlinder-Richert et al., 2004). A double functionalisation approach of CNTs with AmB and a fluorescence dye was performed by our group in order to study cell uptake and the toxicity towards human Jurkat lymphoma T-cells (See Table 2.1, structure 3). The antifungal activity was eventually evaluated (Wu et al., 2005). We have shown that the conjugation of AmB to CNTs clearly reduces the cytotoxicity of AmB on mammalian cells, while enhancing the antifungal activity against different types of micro-organisms.

Another application of CNTs as drug delivery systems concerns cancer therapy. Yinghuai et al. (2005) have studied the utility of CNTs as boron delivery agents for their use in boron neutron capture therapy (BNCT). Substituted carborane cages were attached to the walls of SWNTs via nitrene cycloaddition followed by a treatment with sodium hydroxide, obtaining water-soluble carborane-appended SWNTs (Table 2.1, structure 4). Boron tissue distribution studies showed that there is an enhanced boron uptake and retention of the carborane nanotubes in tumour tissue compared to blood, lung, liver or spleen. Although the mechanism of the accumulation of carborane nanotubes in tumour is not yet understood, these results are promising for the future use of CNTs as boron delivery vehicles in BNCT treatment of cancer.

In an alternative approach, our group introduced around the CNT sidewalls the anticancer agent methotrexate (MTX) together with a fluorescent probe (Pastorin et al., 2006) (Table 2.1, structure 5). MTX is a drug widely used against cancer; however, due to its low cellular uptake (Sirotnak et al., 1981; Pignatello et al., 2001) high concentrations of drug are required. Our results show that MTX is rapidly internalised inside the cell by carbon nanotubes. Preliminary results have shown that MTX conjugated to the CNTs is as active as MTX alone in a cell culture assay (Prato et al., 2008). The stable amide bond between the MXT and the tubes could be the reason for lack of enhanced efficacy, releasing the drug too slowly from the CNTs into the cytoplasm. One solution to this problem could be to introduce a cleavable linker or a more enzymatically sensitive bond.

Another anticancer agent, doxorubicin (DOX), noncovalently linked to CNTs has recently been investigated by Liu et al. (a) and by our group (Ali-Boucetta et al., 2008) in two simultaneous and independent studies. Our group used MWNTs dispersions in Pluronic F127, while Liu et al. used SWNTs functionalised either noncovalently with polyethylene glycol (PEG) (Table 2.1, structure 6) or covalently by PEGylation of carboxylic groups introduced by preoxidation of the CNTs (Table 2.1, structure 7). The DOX–CNT complexes exhibit cytotoxic activity against cancer cells. The potential advantage of using CNTs as drug carrier resides on the ability to deliver the drug to certain types of cells by conjugation with tumour-targeting peptides, therefore reducing the toxicity towards non-targeted cells.

Venkatesan et al. (2005) studied, among other porous adsorbents, the use of CNTs as a drug carrier system for oral administration of erythropoietin (EPO). EPO is a glycoprotein hormone that regulates red blood cell production and it is used to treat certain types of anaemia. However, low oral bioavailability, i.e. poor membrane permeability and enzymatic degradation, is the main problem in achieving patient-friendly routes of administration of this drug. The results of this work showed that the use of CNTs as adsorbent, combined with casein as enzyme inhibitor and Labrasol as absorption enhancer, gave the best bioavailability of EPO, opening many possibilities for the oral administration of this drug.

In a different approach CNTs can act as containers by inserting molecules inside the tubes and releasing them into the cells. Recently, the reversible filling of CNTs with fullerenes was reported by two independent groups (Fan et al., 2007; Simon et al., 2007). Although fullerenes and their derivatives have a broad range of medical applications, the reversible filling reported by these groups should be applied to water-soluble functionalised fullerenes in order to be useful for drug delivery applications.

2.6 Interaction Between Carbon Nanotubes and Nucleic Acids

The physicochemical interactions between CNTs and DNA have been studied under different contexts for a long time, particularly towards efforts to achieve well-dispersed nonfunctionalised CNTs and more recently for the construction of sensors, nanocircuits, nanocomposites and gene delivery vectors. Towards this latter aim, in the quest for a useful non-viral gene transfer system, the interaction between a cationic component, such as an amino-functionalised CNTs, and the negatively charged nucleic acid to be delivered is critical for the eventual effectiveness of a gene transfer construct. Theoretical predictions of DNA interactions with CNTs by molecular dynamics simulations have shown that ssDNA spontaneously inserts into nonfunctionalised CNTs through a combination of van der Waals and hydrophobic forces (Gao et al., 2003). Moreover, molecular modelling has demonstrated that dsDNA can also wrap around nonfunctionalised CNTs or, in the case of positively charged CNTs in an aqueous environment, DNA molecules could be electrostatically adherent onto the CNT surface (Lu et al., 2005). In addition, it was very

recently reported that CNTs induce a spontaneous conformational change of ssDNA, which allows it to wrap around the nanotubes via π - π stacking interactions (Johnson et al., 2008).

Experimentally, a range of different techniques have been used to understand the CNT-DNA interactions and the ensuing supramolecular structures between these two components. However, most studies agree that the nature and mechanism of such interactions will be highly dependent on the type of CNTs, its surface functionalisation and the characteristics of the nucleic acids. UV and IR spectroscopy have both been used to show that nonfunctionalised SWNTs and dsDNA interact through hydrogen bonds (Matyshevska et al., 2001; Buzaneva et al., 2002). In these studies changes in the electronic levels in the nucleotide bases of the DNA molecule were found and the DNA acquired a chaotic spherical conformation upon interaction with CNTs. π - π interactions between the CNT sidewalls and the nucleic acid bases have been proposed as the mechanistic basis for this wrapping effect. Moreover, the ability of DNA to wrap around the CNT surface has been described for both dsDNA (Dovbeshko et al., 2003; Nepal et al., 2005) and ssDNA (Zheng et al., 2003a) and has been utilised to disperse CNT in solvents of varying polarity.

Several studies described that oxidised CNTs covalently bond DNA-NH₂ in a controllable assembling process (Dwyer et al., 2002; Hazani et al., 2003; Taft et al., 2004; Guo et al., 2004) or are helically wrapped (π - π interactions) by dsDNA and ssDNA (Nakashima et al., 2003; Rajendra et al., 2004; Rajendra and Rodger, 2005). An alternative functionalisation reaction described by Georgakilas et al. (2002) produces positively charged ammonium-functionalised CNT (CNT-NH₃⁺). The interaction of CNT-NH₃⁺ with pDNA was studied in detail in our laboratories (Singh et al., 2005; Lacerda et al., 2006b). We have found that these functionalised CNTs interact with pDNA to form complexes primarily through electrostatic forces and that the pDNA was condensed around the CNT-NH₃⁺. Moreover, these studies have indicated that the total available surface area and the surface charge density of CNTs were critical parameters in the interaction and complexation of pDNA.

With regards to the interactions between RNA and CNTs, to our knowledge there has only been one published report describing the interaction between non-functionalised SWNTs and the RNA polymer poly(rU) (Rao et al., 2004). In this study, the RNA polymer poly(rU) is observed in a blob-like conformation when bound at the surface of CNTs as imaged by scanning electron microscopy resembling the condensation of pDNA strands. It was suggested that the binding occurs through π -stacking and hydrophobic interactions; however, no detailed mechanistic study has been published so far describing how the CNT-RNA interactions occur.

Concerning utilisation of CNTs for the delivery of nucleic acids, CNTs have already been shown to be versatile platforms for nucleic acid delivery *in vitro* and *in vivo* because of their high surface area, facile functionalisation of their surface and their ability to cross the cell membranes. To our knowledge, it is crucial to functionalise the surface of CNTs, in order to transform nonfunctionalised CNTs (insoluble in most solvents) into water-soluble and biocompatible CNTs. On the other hand, with a growing number of functionalisation routes, many important questions remain unanswered. Each functionalisation method is probably producing

CNTs with different characteristics, which will lead to differences in the mechanism of CNT metabolism, degradation or dissolution, clearance and bioaccumulation. On the other hand, most non-viral gene delivery systems today suffer from both limited levels of gene expression and an unfavourable toxicity profile due to their highly cationic surface character. Therefore, opportunities for CNT-based gene transfer systems are still ample.

The development of CNTs as delivery systems for nucleic acids is still in its nascent stages and many more studies are needed to determine the advantages and limitations offered by these novel materials. Most challenges are still ahead for the biomedical utilisation of CNTs. The administration or implantation of CNTs and their complexes with gene encoding or silencing constructs in an *in vivo* setting are almost completely unexplored, despite the groundbreaking, but always proof-of-concept, work by several groups (Lacerda et al., 2006a). Moreover, the toxicological and pharmacological profile of CNT systems used as therapeutics will have to be better elucidated prior to any clinical studies undertaken. In conclusion, we would like to stress that although we are still in very early stages of development, nucleic acid delivery systems based on CNTs may well become viable and effective, particularly in combination with their electrical or semiconducting properties and an improved toxicity profile.

2.6.1 DNA Therapeutics

There are several studies that have reported cellular internalisation of DNA using CNTs. In 2004, our groups published the first studies (Pantarotto et al., 2004b; Singh et al., 2005) to demonstrate that CNT-mediated gene delivery and expression leading to production of marker proteins encoded in pDNA was possible. In these initial studies we observed that pDNA was able to associate in a condensed globular conformation through electrostatic interactions at the surface of CNTs covalently functionalised with ammonium groups. The delivery of pDNA and expression of β -galactosidase (marker gene) in CHO cells was found to be approximately ten times higher than naked pDNA alone. Furthermore, it was found that the charge ratio (+/-) CNT-NH₃⁺-pDNA was an important factor determining the level of gene expression. Later, Liu et al. (2005) also reported the noncovalent association of pDNA with CNT functionalised with polyethylenimine (PEI) groups, which contain a high density of terminal amine groups, an overall highly cationic macromolecule commonly used as a transfection agent. The CNT-PEI-pDNA complexes tested at different charge ratios in different cell lines were shown to produce much higher levels of gene expression than pDNA alone. Furthermore, it was reported that the transfection efficiency with the CNT-PEI constructs was about three times higher than with PEI alone.

Interestingly, it has been subsequently shown that the functionalisation group on the CNT surface also plays a role in the formation of the complexes between the CNTs and pDNA. Gao et al. (2006) studied the gene delivery of pDNA by CNT

functionalised with four different chemical groups: amino, carboxyl, hydroxyl and alkyl. However, only the positively charged, amine-functionalised CNTs were able to complex and deliver the pDNA. Although the complexes between CNTs and pDNA enhanced the gene delivery and expression compared to naked DNA alone, they did not improve the transfection efficiency compared to commercially available transfection agent (Lipofectamine 2000).

Cai et al. (2005) proposed an alternative strategy to introduce exogenous pDNA immobilised on CNTs into mammalian cells. The CNTs used in these studies contained Ni particles enclosed in their tips, which allowed a magnetic 'spearing' technique (exposure to an external magnetic field followed by centrifugation) onto the CNT-pDNA complexes. The results from these investigations reported gene expression in 80–100% of the cell population for the CNTs with Ni, while CNTs deprived of Ni particles did not produce any gene expression. However, the use of such technique is limited to *in vitro* or *ex vivo* gene transfer.

Interestingly, CNTs have been shown to be able to deliver exogenous genes not only in mammalian cells, but also in bacteria. Rojas-Chapana et al. (2005) demonstrated that oxidised, water-dispersible CNTs can deliver pDNA into *E. coli* (ratio of transformation efficiency/transformants of about 32) by opening up temporary nanochannels across the cell envelope. The authors described that addition of CNTs in a suspension containing *E. coli* and pDNA and application of a microwave frequency resulted in the orientation of the CNT tips perpendicularly to the cell surface and subsequently plasmid delivery into the bacteria.

To our knowledge there is no study in the literature describing *in vivo* gene expression by CNT-mediated delivery of DNA yet. However, Zhang et al. (2006) have recently injected intratumourally FAM-labelled dsDNA-CNT conjugates in mice bearing Lewis lung carcinoma tumours. The study has confirmed the uptake of the conjugates by observing that almost all tumour cells were fluorescent, nevertheless, the experiment was performed only for the purpose of *in vivo* imaging and tracking of the CNTs. No further attempt has been reported to deliver gene-expressing DNA in live tissue.

2.6.2 RNA Therapeutics

In the last few years, a great effort has been invested in the discovery of effective ways to deliver small-interference RNA (siRNA) into cells and tissues. Kam et al. (2005a) have studied a siRNA-CNT conjugate linked with disulfide bonds to PEGylated lipids coating the CNT surface, and have shown that the conjugates were internalised into HeLa cells and also reported siRNA-mediated gene silencing. In these studies, different siRNA constructs were successfully delivered by CNTs, and two targeted genes were silenced: (a) the gene encoding laminin A/C protein (localised inside the nuclear lamina of cells), and (b) the luciferase gene. This work also compared the gene silencing efficiency between the siRNA-CNT conjugates and the more conventional Lipofectamine-siRNA complexes to find that the CNTs

improved the degree of gene silencing. More recently, Liu et al. (2007b) have shown the delivery of siRNA molecules able to silence the expression of the cell-surface receptors CD4 and co-receptors CXCR4 in human T-cells and peripheral blood mononuclear cells by CNTs. Because both cell-surface receptors are necessary for HIV binding and infection of T-cells, the authors have suggested that siRNA–CNT conjugates can potentially be used for the treatment of HIV. Furthermore, they observed that conjugates of CNTs covalently linked by disulphide bonds to siRNA had greatly improved the silencing in T-cells compared to Lipofectamine 2000 and other liposome-based formulations.

Very recently, Zhang et al. (2006) pushed the development of CNTs as siRNA delivery systems further, as they employed ammonium-functionalised CNTs to mediate the delivery of *TERT*siRNA into tumor cells (murine and human) and silence the *TERT* gene, which is critical for the development and growth of tumours. They observed that treatment of different tumour cells with the *TERT*siRNA–CNT complexes led to the suppression of the cell growth. These *in vitro* studies were extended to *in vivo* studies in the same report. The activity of *TERT*siRNA–CNTs was verified after intratumoural injections in mice bearing Lewis lung carcinoma tumours or HeLa cell xenografts. Tumour growth was inhibited after treatment with *TERT*siRNA–CNT complexes and average tumour weight was significantly reduced when compared to that of tumours from untreated animals.

In conclusion, CNTs can offer a promising new technology for the development of advanced cancer treatment applications. However, much more work is definitely needed and will surely appear in order to explore and carefully define the opportunities and limitations of CNTs as delivery systems of nucleic acids using *in vivo* models.

2.7 Impact of Carbon Nanotubes on Health

What is the actual impact of CNTs on health? This is an essential but still partially unanswered question (Tsuji et al., 2006; Helland et al., 2007; Boczkowski and Lanone, 2007). As emerged from the previous paragraphs, a tremendous enthusiasm has been developed around the very promising applications of CNTs particularly in biomedicine. However, one should keep in mind that this extending manufacturing and use of CNTs will necessarily lead to an increased frequency of people being exposed to these nano-materials, in an accidental (e.g. during production processes) or voluntary (e.g. if they are used as contrast agents or for drug delivery) way, and that this might have harmful consequences. Therefore, in order to guarantee a safe use of CNTs for future biomedical applications, we should gain a thorough knowledge of their physiological impact and of their potential adverse effects on animal and human health. This major concern has started to be taken into consideration for the last few years and a wide range of mainly *in vitro* studies have been undertaken to answer the following simple question: are CNTs toxic? Most of these experiments first concluded that CNTs exert some cytotoxic activity, as measured by a loss in cell viability and induction of some oxidative stress, and that CNTs could therefore constitute a danger for health (Shvedova et al., 2003;

Monteiro-Riviere et al., 2005; Cui et al., 2005; Manna et al., 2005; Ding et al., 2005; Bottini et al., 2006). Moreover, a few very recent studies have demonstrated some genotoxic impact of CNTs (Kisin et al., 2007; Muller et al., 2008). However, it appears that CNT toxicity is a much more complex issue than expected. Indeed, the diversity of CNT products is not simply limited to SWNTs or MWNTs, but depending on the synthesis method and the cleaning process employed, CNTs harbour varied physical and chemical properties. For example, the level of metallic impurities, such as iron and nickel, which are contained in CNT preparations, can vary a lot and this has a great influence on the toxicity measured since these contaminants can be active *per se* (Kagan et al., 2006). This heterogeneity, combined with the use of different *in vitro* cell models (i.e. keratinocytes, macrophages, epithelial cells and smooth muscle cells) and biological tests, has sometimes led to results which look contradictory but which are actually difficult to compare. However, a parameter, which emerged as a key determinant for CNT toxicity, consists in their surface modification, which directly affects their agglomeration/dispersion state in solution. The highly hydrophobic pristine CNTs form rather large aggregates with cytotoxic affect that can be reduced when the tubes are well dispersed (Wick et al., 2007). Some groups have used CNTs surrounded by surfactants to improve their dispersion, but surfactants themselves could have a significant influence on cell behaviour (Cherukuri et al., 2004). Therefore, one of the best ways, which has been settled to ameliorate the aqueous solubility of CNTs and their compatibility with living systems consists in functionalising them, i.e. chemically modifying their surface. Sayes et al. (2006) have shown that the level of cytotoxicity exerted by SWNTs is directly related to the density of functional groups around the tubes. In this context, our group has developed several functionalisation methods (see Paragraph 2) and we have evidenced that fully water-soluble SWNTs do not exert any deleterious effect on the survival and functionality of cell lines and primary mouse immune cells (Pantarotto et al., 2004a; Dumortier et al., 2006). We also used these soluble functionalised CNTs to perform one of the first complete *in vivo* biodistribution studies of CNTs (Singh et al., 2006; Lacerda et al., 2008). The intravenous administration of indium-labelled functionalised SWNTs and MWNTs to mice showed a rapid clearance via the renal excretion route without neither accumulation in the reticuloendothelial system organs (liver or spleen) nor severe toxic side effects. Recently, Guo et al. (2007) published biodistribution data of technetium-labelled glucosamine-functionalised MWNTs, which also underscored an absence of toxicity and a natural elimination process via urine and faeces. These results are very promising considering the potential clinical use of CNTs and reinforce the importance of functionalisation to improve biocompatibility. Indeed, a few articles describe the *in vivo* toxicity of CNTs, but they are mostly based on the use of non-soluble pristine CNTs. Most of these studies focused on the pulmonary exposure of animals to CNTs, by intratracheal instillation or pharyngeal aspiration, thus mimicking what could happen upon accidental exposure by inhalation. In most cases, inflammatory responses, accompanied by interstitial fibrosis and granulomas formation, were observed (Lam et al., 2004; Warheit et al., 2004; Muller et al., 2005). One study even suggested that in addition to these primary effects, CNTs may also have an impact on the resistance to pathogens as co-inhalation of pathogenic bacteria and SWNTs slows down the clearance of bacteria from the lungs (Shvedova et al., 2005).

Altogether, the data which have been accumulated till today, evidence the potential toxicity of CNTs, which should not be neglected. However, they also clearly point out the functionalisation and the resulting solubility of CNTs as key parameters for controlling their biocompatibility, giving hope for their future use as medical tools. Our knowledge in the field of nanotoxicology has considerably improved, but we are still far from getting a full comprehensive view of what is the global impact of CNTs on health and further experiments are required before CNTs can be used in a completely safe manner.

2.8 Conclusions

The use of CNTs for biomedical applications is acquiring more and more substantiating evidence for efficient development. It is clear that some important issues related to the health impact including the biodistribution, accumulation and elimination have to be addressed more thoroughly before CNTs can be proposed for clinical trials. However, CNTs show remarkable carrier properties, with a very strong tendency to cross cell membranes, and seem to perfectly fit into the emerging discipline of nanomedicine. Although, the toxicological studies on pristine CNTs are contradictory, showing a certain degree of danger, it is becoming evident that functionalised CNTs have reduced toxic effects. Therefore, the combination of cell uptake capacity with high loading of cargo molecules achievable with CNTs makes this new carbon nanomaterial a promising candidate for innovative therapies. In conclusion, we do hope that, in a few years, functionalised CNTs will be considered as valuable scaffolds for pharmaceutical applications.

Acknowledgements The authors are deeply indebted to all their co-workers who have partly contributed to the development of the research described in this chapter and whose names are cited in the references. This work was supported by the 'Centre National de la Recherche Scientifique' and the French 'Agence Nationale de la Recherche' (grant ANR-05-JCJC-0031-01), the University of Trieste, Italian MUR (PRIN 2006, prot.2006034372 and FIRB RBIN04HC3S) and Regione Friuli Venezia-Giulia. This work was also supported by the European Union, NEURONANO program (NMP4-CT-2006-031847).

References

- Ajayan PM (1999) Nanotubes from carbon. *Chem. Rev.* 99: 1787–1799.
- Ali-Boucetta H, Al-Jamal KT, McCarthy D, Prato M, Bianco A, Kostarelos K (2008) Multiwalled carbon nanotube–doxorubicin supramolecular complexes for cancer therapeutics. *Chem. Commun.* 459–461.
- Allen TM, Cullis PR (2004) Drug delivery systems: Entering the mainstream. *Science* 303: 1818–1822.
- Arnold MS, Guler MO, Hersam MC, Stupp SI (2005) Encapsulation of carbon nanotubes by self-assembling peptide amphiphiles. *Langmuir* 21: 4705–4709.

- Baker SE, Cai W, Lassetter TL, Weidkamp KP, Hamers RJ (2002) Covalently bonded adducts of deoxyribonucleic acid (DNA) oligonucleotides with single-wall carbon nanotubes: Synthesis and hybridization. *Nano Lett.* 2: 1413–1417.
- Bale SS, Asuri P, Karajanagi SS, Dordick JS, Kane RS (2007) Protein-directed formation of silver nanoparticles on carbon nanotubes. *Adv. Mater.* 19: 3167–3170.
- Bandyopadhyaya R, Nativ-Roth E, Regev O, Yerushalmi-Rozen R (2002) Stabilization of individual carbon nanotubes in aqueous solutions. *Nano Lett.* 2: 25–28.
- Baughman RH, Zakhidov AA, de Heer WA (2002) Carbon nanotubes – the route toward applications. *Science* 297: 787–792.
- Besteman K, Lee JO, Wiertz FGM, Heering HA, Dekker C (2003) Enzyme-coated carbon nanotubes as single-molecule biosensors. *Nano Lett.* 3: 727–730.
- Bianco A, Prato M (2003) Can carbon nanotubes be considered useful tools for biological applications? *Adv. Mater.* 15: 1765–1768.
- Bianco A, Hoebeke J, Godefroy S, Chaloin O, Pantarotto D, Briand JP, Muller S, Prato M, Partidos CD (2005a) Cationic carbon nanotubes bind to CpG oligodeoxynucleotides and enhance their immunostimulatory properties. *J. Am. Chem. Soc.* 127: 58–59.
- Bianco A, Kostarelos K, Partidos CD, Prato M (2005b) Biomedical applications of functionalised carbon nanotubes. *Chem. Commun.* 571–577.
- Boczkowski J, Lanone S (2007) Potential uses of carbon nanotubes in the medical field: How worried should patients be? *Nanomedicine* 2: 407–410.
- Bottini M, Bruckner S, Nika K, Bottini N, Bellucci S, Magrini A, Bergamaschi A, Mustelin T (2006) Multi-walled carbon nanotubes induce T lymphocyte apoptosis. *Toxicol. Lett.* 160: 121–126.
- Buzaneva E, Karlash A, Yakovkin K, Shtogun Y, Putselyk S, Zhrebetskiy D, Gorchinskiy A, Popova G, Prilutska S, Matyshevska O, Prilutskyy Y, Lytvyn P, Scharff P, Eklund P (2002) DNA nanotechnology of carbon nanotube cells: Physico-chemical models of self-organization and properties. *Mater. Sci. Eng. C* 19: 41–45.
- Cai D, Mataraza JM, Qin ZH, Huang ZP, Huang JY, Chiles TC, Carnahan D, Kempa K, Ren ZF (2005) Highly efficient molecular delivery into mammalian cells using carbon nanotube spearing. *Nat. Methods* 2: 449–454.
- Cai H, Cao XN, Jiang Y, He PG, Fang YZ (2003) Carbon nanotube-enhanced electrochemical DNA biosensor for DNA hybridization detection. *Anal. Bioanal. Chem.* 375: 287–293.
- Chambers G, Carroll C, Farrell GF, Dalton AB, McNamara M, Panhuis MIH, Byrne HJ (2003) Characterization of the interaction of gamma cyclodextrin with single-walled carbon nanotubes. *Nano Lett.* 3: 843–846.
- Chen J, Dyer MJ, Yu MF (2001a) Cyclodextrin-mediated soft cutting of single-walled carbon nanotubes. *J. Am. Chem. Soc.* 123: 6201–6202.
- Chen RJ, Zhang YG, Wang DW, Dai HJ (2001b) Noncovalent sidewall functionalization of single-walled carbon nanotubes for protein immobilization. *J. Am. Chem. Soc.* 123: 3838–3839.
- Chen RJ, Bangsaruntip S, Drouvalakis KA, Kam NWS, Shim M, Li YM, Kim W, Utz PJ, Dai HJ (2003) Noncovalent functionalization of carbon nanotubes for highly specific electronic biosensors. *Proc. Natl. Acad. Sci. USA* 100: 4984–4989.
- Cherukuri P, Bachilo SM, Litovsky SH, Weisman RB (2004) Near-infrared fluorescence microscopy of single-walled carbon nanotubes in phagocytic cells. *J. Am. Chem. Soc.* 126: 15638–15639.
- Choi JH, Nguyen FT, Barone PW, Heller DA, Moll AE, Patel D, Boppart SA, Strano MS (2007) Multimodal biomedical imaging with asymmetric single-walled carbon nanotube/iron oxide nanoparticle complexes. *Nano Lett.* 7: 861–867.
- Cui DX, Tian FR, Ozkan CS, Wang M, Gao HJ (2005) Effect of single wall carbon nanotubes on human HEK293 cells. *Toxicol. Lett.* 155: 73–85.
- Dalton AB, Ortiz-Acevedo A, Zorbas V, Brunner E, Sampson WM, Collins L, Razal JM, Yoshida MM, Baughman RH, Draper RK, Musselman IH, Jose-Yacaman M, Dieckmann GR (2004) Hierarchical self-assembly of peptide-coated carbon nanotubes. *Adv. Funct. Mater.* 14: 1147–1151.

- Davis JJ, Green MLH, Hill HAO, Leung YC, Sadler PJ, Sloan J, Xavier AV, Tsang SC (1998) The immobilisation of proteins in carbon nanotubes. *Inorg. Chim. Acta* 272: 261–266.
- Dieckmann GR, Dalton AB, Johnson PA, Razal J, Chen J, Giordano GM, Munoz E, Musselman IH, Baughman RH, Draper RK (2003) Controlled assembly of carbon nanotubes by designed amphiphilic peptide helices. *J. Am. Chem. Soc.* 125: 1770–1777.
- Ding LH, Stilwell J, Zhang TT, Elboudwarej O, Jiang HJ, Selegue JP, Cooke PA, Gray JW, Chen FQF (2005) Molecular characterization of the cytotoxic mechanism of multiwall carbon nanotubes and nano-onions on human skin fibroblast. *Nano Lett.* 5: 2448–2464.
- Dodziuk H, Ejchart A, Anczewski W, Ueda H, Krinichnaya E, Dolgonos G, Kutner W (2003) Water solubilization, determination of the number of different types of single-wall carbon nanotubes and their partial separation with respect to diameters by complexation with α -cyclodextrin. *Chem. Commun.* 986–987.
- Dovbeshko GI, Repnytska OP, Obratsova ED, Shtogun YV (2003) DNA interaction with single-walled carbon nanotubes: A SEIRA study. *Chem. Phys. Lett.* 372: 432–437.
- Dumortier H, Lacotte S, Pastorin G, Marega R, Wu W, Bonifazi D, Briand JP, Prato M, Muller S, Bianco A (2006) Functionalized carbon nanotubes are non-cytotoxic and preserve the functionality of primary immune cells. *Nano Lett.* 6: 1522–1528.
- Duncan R (2003) The dawning era of polymer therapeutics. *Nat. Rev. Drug Discov.* 2: 347–360.
- Dwyer C, Guthold M, Falvo M, Washburn S, Superfine R, Erie D (2002) DNA-functionalized single-walled carbon nanotubes. *Nanotechnology* 13: 601–604.
- Fan J, Yudasaka M, Yuge R, Futaba DN, Hata K, Iijima S (2007) Efficiency of C-60 incorporation in and release from single-wall carbon nanotubes depending on their diameters. *Carbon* 45: 722–726.
- Gao HJ, Kong Y (2004) Simulation of DNA-nanotube interactions. *Annu. Rev. Mater. Res.* 34: 123–150.
- Gao HJ, Kong Y, Cui DX, Ozkan CS (2003) Spontaneous insertion of DNA oligonucleotides into carbon nanotubes. *Nano Lett.* 3: 471–473.
- Gao LZ, Nie L, Wang TH, Qin YJ, Guo ZX, Yang DL, Yan XY (2006) Carbon nanotube delivery of the GFP gene into mammalian cells. *Chembiochem* 7: 239–242.
- Georgakilas V, Tagmatarchis N, Pantarotto D, Bianco A, Briand JP, Prato M (2002) Amino acid functionalisation of water soluble carbon nanotubes. *Chem. Commun.* 3050–3051.
- Giordani S, Bergin SD, Nicolosi V, Lebedkin S, Kappes MM, Blau WJ, Coleman JN (2006) Debundling of single-walled nanotubes by dilution: Observation of large populations of individual nanotubes in amide solvent dispersions. *J. Phys. Chem. B* 110: 15708–15718.
- Gooding JJ, Wibowo R, Liu JQ, Yang WR, Losic D, Orbons S, Mearns FJ, Shapter JG, Hibbert DB (2003) Protein electrochemistry using aligned carbon nanotube arrays. *J. Am. Chem. Soc.* 125: 9006–9007.
- Gref R, Minamitake Y, Peracchia MT, Trubetsky V, Torchilin V, Langer R (1994) Biodegradable long-circulating polymeric nanospheres. *Science* 263: 1600–1603.
- Guo J, Zhang X, Li Q, Li W (2007) Biodistribution of functionalized multiwall carbon nanotubes in mice. *Nucl. Med. Biol.* 34: 579–583.
- Guo ML, Chen JH, Liu DY, Nie LH, Yao SZ (2004) Electrochemical characteristics of the immobilization of calf thymus DNA molecules on multi-walled carbon nanotubes. *Bioelectrochemistry* 62: 29–35.
- Guo ZJ, Sadler PJ, Tsang SC (1998) Immobilization and visualization of DNA and proteins on carbon nanotubes. *Adv. Mater.* 10: 701–703.
- Hazani M, Naaman R, Henrich F, Kappes MM (2003) Confocal fluorescence imaging of DNA-functionalized carbon nanotubes. *Nano Lett.* 3: 153–155.
- Helland A, Wick P, Koehler A, Schmid K, Som C (2007) Reviewing the environmental and human health knowledge base of carbon nanotubes. *Environ. Health Perspect.* 115: 1125–1131.
- Heller DA, Baik S, Eurell TE, Strano MS (2005) Single-walled carbon nanotube spectroscopy in live cells: Towards long-term labels and optical sensors. *Adv. Mater.* 17: 2793–2799.

- Heller DA, Jeng ES, Yeung TK, Martinez BM, Moll AE, Gastala JB, Strano MS (2006) Optical detection of DNA conformational polymorphism on single-walled carbon nanotubes. *Science* 311: 508–511.
- Holzinger M, Abraha J, Whelan P, Graupner R, Ley L, Hennrich F, Kappes M, Hirsch A (2003) Functionalization of single-walled carbon nanotubes with (R)-oxycarbonyl nitrenes. *J. Am. Chem. Soc.* 125: 8566–8580.
- Huang WJ, Taylor S, Fu KF, Lin Y, Zhang DH, Hanks TW, Rao AM, Sun YP (2002) Attaching proteins to carbon nanotubes via diimide-activated amidation. *Nano Lett.* 2: 311–314.
- Iijima S (1991) Helical microtubules of graphitic carbon. *Nature* 354: 56–58.
- Iijima S, Ichihashi T (1993) Single-shell carbon nanotubes of 1-nm diameter. *Nature* 363: 603–605.
- Ikeda A, Hayashi K, Konishi T, Kikuchi J (2004) Solubilization and debundling of purified single-walled carbon nanotubes using solubilizing agents in an aqueous solution by high-speed vibration milling technique. *Chem. Commun.* 1334–1335.
- Ito T, Sun L, Crooks RM (2003) Observation of DNA transport through a single carbon nanotube channel using fluorescence microscopy. *Chem. Commun.* 7: 1482–1483.
- Jiang KY, Schadler LS, Siegel RW, Zhang XJ, Zhang HF, Terrones M (2004) Protein immobilization on carbon nanotubes via a two-step process of diimide-activated amidation. *J. Mater. Chem.* 14: 37–39.
- Johnson RR, Johnson ATC, Klein ML (2008) Probing the Structure of DNA-Carbon Nanotube Hybrids with Molecular Dynamics. *Nano Lett.* 8: 69–75.
- Kagan VE, Tyurina YY, Tyurin VA, Konduru NV, Potapovich AI, Osipov AN, Kisin ER, Schwegler-Berry D, Mercer R, Castranova V, Shvedova AA (2006) Direct and indirect effects of single walled carbon nanotubes on RAW 264.7 macrophages: Role of iron. *Toxicol. Lett.* 165: 88–100.
- Kam NWS, Dai HJ (2005) Carbon nanotubes as intracellular protein transporters: Generality and biological functionality. *J. Am. Chem. Soc.* 127: 6021–6026.
- Kam NWS, Jessop TC, Wender PA, Dai HJ (2004) Nanotube molecular transporters: Internalization of carbon nanotube-protein conjugates into mammalian cells. *J. Am. Chem. Soc.* 126: 6850–6851.
- Kam NWS, Liu Z, Dai HJ (2005a) Functionalization of carbon nanotubes via cleavable disulfide bonds for efficient intracellular delivery of siRNA and potent gene silencing. *J. Am. Chem. Soc.* 127: 12492–12493.
- Kam NWS, O'Connell M, Wisdom JA, Dai HJ (2005b) Carbon nanotubes as multifunctional biological transporters and near-infrared agents for selective cancer cell destruction. *Proc. Natl. Acad. Sci. USA* 102: 11600–11605.
- Kam NWS, Liu ZA, Dai HJ (2006) Carbon nanotubes as intracellular transporters for proteins and DNA: An investigation of the uptake mechanism and pathway. *Angew. Chem. Int. Ed.* 45: 577–581.
- Kateb B, Van Handel M, Zhang LY, Bronikowski MJ, Manohara H, Badie B (2007) Internalization of MWCNTs by microglia: Possible application in immunotherapy of brain tumors. *NeuroImage* 37: S9-S17.
- Kim OK, Je JT, Baldwin JW, Kooi S, Pehrsson PE, Buckley LJ (2003) Solubilization of single-wall carbon nanotubes by supramolecular encapsulation of helical amylose. *J. Am. Chem. Soc.* 125: 4426–4427.
- Kisin ER, Murray AR, Keane MJ, Shi XC, Schwegler-Berry D, Gorelik O, Arepalli S, Castranova V, Wallace WE, Kagan VE, Shvedova AA (2007) Single-walled Carbon Nanotubes: Geno- and Cytotoxic Effects in Lung Fibroblast V79 Cells. *J. Toxicol. Environ. Health A* 70: 2071–2079.
- Klinman DM, Yamshchikov G, Ishigatsubo Y (1997) Contribution of CpG motifs to the immunogenicity of DNA vaccines. *J. Immunol.* 158: 3635–3639.
- Klinman DM, Verthelyi D, Takeshita F, Ishii KJ (1999) Immune recognition of foreign DNA: A cure for bioterrorism? *Immunity* 11: 123–129.

- Kostarelos K, Lacerda L, Pastorin G, Wu W, Wieckowski S, Luangsilavay J, Godefroy S, Pantarotto D, Briand JP, Muller S, Prato M, Bianco A (2007) Cellular uptake of functionalized carbon nanotubes is independent of functional group and cell type. *Nat. Nanotechnol.* 2: 108–113.
- Krieg AM (2002) CpG motifs in bacterial DNA and their immune effects. *Annu. Rev. Immunol.* 20: 709–760.
- Krieg AM, Yi AK, Matson S, Waldschmidt TJ, Bishop GA, Teasdale R, Koretzky GA, Klinman DM (1995) CpG motifs in bacterial DNA trigger direct B-cell activation. *Nature* 374: 546–549.
- Lacerda L, Bianco A, Prato M, Kostarelos K (2006a) Carbon nanotubes as nanomedicines: From toxicology to pharmacology. *Adv. Drug. Deliv. Rev.* 58: 1460–1470.
- Lacerda L, Pastorin G, Wu W, Prato M, Bianco A, Kostarelos K (2006b) Luminescence of functionalized carbon nanotubes as a tool to monitor bundle formation and dissociation in water: The effect of plasmid-DNA complexation. *Adv. Funct. Mater.* 16: 1839–1846.
- Lacerda L, Soundararajan A, Singh R, Pastorin G, Al-Jamal KT, Turton J, Frederik P, Herrero MA, Li S, Bao A, Emfietzoglou D, Mather S, Phillips WT, Prato M, Bianco A, Goins B, Kostarelos K (2008) Dynamic imaging of functionalized multi-walled carbon nanotube systemic circulation and urinary excretion. *Adv. Mater.* 20: 225–230.
- Lam CW, James JT, McCluskey R, Hunter RL (2004) Pulmonary toxicity of single-wall carbon nanotubes in mice 7 and 90 days after intratracheal instillation. *Toxicol. Sci.* 77: 126–134.
- Langer R (1998) Drug delivery and targeting. *Nature* 392: 5–10.
- Lavan DA, Lynn DM, Langer R (2002) Moving smaller in drug discovery and delivery. *Nat. Rev. Drug Discov.* 1: 77–84.
- Lavan DA, McGuire T, Langer R (2003) Small-scale systems for in vivo drug delivery. *Nat. Biotechnol.* 21: 1184–1191.
- Li SN, He PG, Dong JH, Guo ZX, Dai LM (2005) DNA-directed self-assembling of carbon nanotubes. *J. Am. Chem. Soc.* 127: 14–15.
- Lin YH, Lu F, Tu Y, Ren ZF (2004) Glucose biosensors based on carbon nanotube nanoelectrode ensembles. *Nano Lett.* 4: 191–195.
- Liu Y, Wu DC, Zhang WD, Jiang X, He CB, Chung TS, Goh SH, Leong KW (2005) Polyethylenimine-grafted multiwalled carbon nanotubes for secure noncovalent immobilization and efficient delivery of DNA. *Angew. Chem. Int. Ed.* 44: 4782–4785.
- Liu Z, Sun X, Nakayama-Ratchford N, Dai H (2007a) Supramolecular Chemistry on Water-Soluble Carbon Nanotubes for Drug Loading and Delivery. *ACS Nano* 1: 50–56.
- Liu Z, Winters M, Holodniy M, Dai HJ (2007b) siRNA delivery into human T cells and primary cells with carbon-nanotube transporters. *Angew. Chem. Int. Ed.* 46: 2023–2027.
- Lu G, Maragakis P, Kaxiras E (2005) Carbon nanotube interaction with DNA. *Nano Lett.* 5: 897–900.
- Manna SK, Sarkar S, Barr J, Wise K, Barrera EV, Jejelowo O, Rice-Ficht AC, Ramesh GT (2005) Single-walled carbon nanotube induces oxidative stress and activates nuclear transcription factor-kappa B in human keratinocytes. *Nano Lett.* 5: 1676–1684.
- Martin CR, Kohli P (2003) The emerging field of nanotube biotechnology. *Nat. Rev. Drug Discov.* 2: 29–37.
- Matyshevska OP, Karlash AY, Shtogun YV, Benilov A, Kirgizov Y, Gorchinskyy KO, Buzaneva EV, Prylutskyy YI, Scharff P (2001) Self-organizing DNA/carbon nanotube molecular films. *Mater. Sci. Eng. C* 15: 249–252.
- McDevitt MR, Chattopadhyay D, Kappel BJ, Jaggi JS, Schiffman SR, Antczak C, Njardarson JT, Brentjens R, Scheinberg DA (2007) Tumor targeting with antibody-functionalized, radiolabeled carbon nanotubes. *J. Nucl. Med.* 48: 1180–1189.
- Moghaddam MJ, Taylor S, Gao M, Huang SM, Dai LM, Mccall MJ (2004) Highly efficient binding of DNA on the sidewalls and tips of carbon nanotubes using photochemistry. *Nano Lett.* 4: 89–93.
- Monteiro-Riviere NA, Nemanich RJ, Inman AO, Wang YYY, Riviere JE (2005) Multi-walled carbon nanotube interactions with human epidermal keratinocytes. *Toxicol. Lett.* 155: 377–384.

- Moulton SE, Minett AI, Murphy R, Ryan KP, McCarthy D, Coleman JN, Blau WJ, Wallace GG (2005) Biomolecules as selective dispersants for carbon nanotubes. *Carbon* 43: 1879–1884.
- Muller J, Huaux F, Moreau N, Misson P, Heilier JF, Delos M, Arras M, Fonseca A, Nagy JB, Lison D (2005) Respiratory toxicity of multi-wall carbon nanotubes. *Toxicol. Appl. Pharmacol.* 207: 221–231.
- Muller J, Decordier I, Hoet P, Lombaert N, Thomassen L, Huaux F, Lison D, Kirsch-Volders M (2008) Clastogenic and aneugenic effects of multi-wall carbon nanotubes in epithelial cells. *Carcinogenesis* 29: 427–433.
- Murthy N, Xu MC, Schuck S, Kunisawa J, Shastri N, Frechet JMJ (2003) A macromolecular delivery vehicle for protein-based vaccines: Acid-degradable protein-loaded microgels. *Proc. Natl. Acad. Sci. USA* 100: 4995–5000.
- Mutwiri GK, Nichani AK, Babiuk S, Babiuk LA (2004) Strategies for enhancing the immunostimulatory effects of CpG oligodeoxynucleotides. *J. Contr. Rel.* 97: 1–17.
- Nakashima N, Okuzono S, Murakami H, Nakai T, Yoshikawa K (2003) DNA dissolves single-walled carbon nanotubes in water. *Chem. Lett.* 32: 456–457.
- Nepal D, Sohn JJ, Aicher WK, Lee S, Geckeler KE (2005) Supramolecular conjugates of carbon nanotubes and DNA by a solid-state reaction. *Biomacromolecules* 6: 2919–2922.
- Nguyen CV, Delzeit L, Cassell AM, Li J, Han J, Meyyappan M (2002) Preparation of nucleic acid functionalized carbon nanotube Arrays. *Nano Lett.* 2: 1079–1081.
- Nimmagadda A, Thurston K, Nollert MU, McFetridge PSF (2006) Chemical modification of SWNT alters in vitro cell-SWNT interactions. *J. Biomed. Mater. Res. A* 76A: 614–625.
- Pantarotto D, Partidos CD, Graff R, Hoebeke J, Briand JP, Prato M, Bianco A (2003a) Synthesis, structural characterization, and immunological properties of carbon nanotubes functionalized with peptides. *J. Am. Chem. Soc.* 125: 6160–6164.
- Pantarotto D, Partidos CD, Hoebeke J, Brown F, Kramer E, Briand JP, Muller S, Prato M, Bianco A (2003b) Immunization with peptide-functionalized carbon nanotubes enhances virus-specific neutralizing antibody responses. *Chem. Biol.* 10: 961–966.
- Pantarotto D, Briand JP, Prato M, Bianco A (2004a) Translocation of bioactive peptides across cell membranes by carbon nanotubes. *Chem. Commun.* 16–17.
- Pantarotto D, Singh R, McCarthy D, Erhardt M, Briand JP, Prato M, Kostarelos K, Bianco A (2004b) Functionalized carbon nanotubes for plasmid DNA gene delivery. *Angew. Chem. Int. Ed.* 43: 5242–5246.
- Pastorin G, Wu W, Wieckowski S, Briand JP, Kostarelos K, Prato M, Bianco A (2006) Double functionalisation of carbon nanotubes for multimodal drug delivery. *Chem. Commun.* 1182–1184.
- Patolsky F, Weizmann Y, Willner I (2004) Long-range electrical contacting of redox enzymes by SWCNT connectors. *Angew. Chem. Int. Ed.* 43: 2113–2117.
- Pignatello R, Toth I, Puglisi G (2001) Structural effects of lipophilic methotrexate conjugates on model phospholipid biomembranes. *Thermochim. Acta* 380: 255–264.
- Prato M, Kostarelos K, Bianco A (2008) Functionalized carbon nanotubes in drug design and discovery. *Acc. Chem. Res.* 41: 60–68.
- Rajendra J, Rodger A (2005) The binding of single-stranded DNA and PNA to single-walled carbon nanotubes probed by flow linear dichroism. *Chem. Eur. J.* 11: 4841–4847.
- Rajendra J, Baxendale M, Rap LGD, Rodger A (2004) Flow linear dichroism to probe binding of aromatic molecules and DNA to single-walled carbon nanotubes. *J. Am. Chem. Soc.* 126: 11182–11188.
- Rao R, Lee J, Lu Q, Keskar G, Freedman KO, Floyd WC, Rao AM, Ke PC (2004) Single-molecule fluorescence microscopy and Raman spectroscopy studies of RNA bound carbon nanotubes. *Appl. Phys. Lett.* 85: 4228–4230.
- Rojas-Chapana J, Troszczynska J, Firkowska I, Morszeck C, Giersig M (2005) Multi-walled carbon nanotubes for plasmid delivery into *Escherichia coli* cells. *Lab Chip* 5: 536–539.
- Savic R, Luo LB, Eisenberg A, Maysinger D (2003) Micellar nanocontainers distribute to defined cytoplasmic organelles. *Science* 300: 615–618.

- Sayes CM, Liang F, Hudson JL, Mendez J, Guo WH, Beach JM, Moore VC, Doyle CD, West JL, Billups WE, Ausman KD, Colvin VL (2006) Functionalization density dependence of single-walled carbon nanotubes cytotoxicity in vitro. *Toxicol. Lett.* 161: 135–142.
- Shvedova AA, Castranova V, Kisin ER, Schwegler-Berry D, Murray AR, Gandelsman VZ, Maynard A, Baron P (2003) Exposure to carbon nanotube material: Assessment of nanotube cytotoxicity using human keratinocyte cells. *J. Toxicol. Environ. Health A* 66: 1909–1926.
- Shvedova AA, Kisin ER, Mercer R, Murray AR, Johnson VJ, Potapovich AI, Tyurina YY, Gorelik O, Arepalli S, Schwegler-Berry D, Hubbs AF, Antonini J, Evans DE, Ku BK, Ramsey D, Maynard A, Kagan VE, Castranova V, Baron P (2005) Unusual inflammatory and fibrogenic pulmonary responses to single-walled carbon nanotubes in mice. *Am. J. Physiol. Lung. Cell. Mol. Physiol.* 289: L698–L708.
- Simon F, Peterlik H, Pfeiffer R, Bernardi J, Kuzmany H (2007) Fullerene release from the inside of carbon nanotubes: A possible route toward drug delivery. *Chem. Phys. Lett.* 445: 288–292.
- Singh R, Pantarotto D, McCarthy D, Chaloin O, Hoebeke J, Partidos CD, Briand JP, Prato M, Bianco A, Kostarelos K (2005) Binding and condensation of plasmid DNA onto functionalized carbon nanotubes: Toward the construction of nanotube-based gene delivery vectors. *J. Am. Chem. Soc.* 127: 4388–4396.
- Singh R, Pantarotto D, Lacerda L, Pastorin G, Klumpp C, Prato M, Bianco A, Kostarelos K (2006) Tissue biodistribution and blood clearance rates of intravenously administered carbon nanotube radiotracers. *Proc. Natl. Acad. Sci. USA* 103: 3357–3362.
- Sirotnak FM, Moccio DM, Kelleher LE, Goutas LJ (1981) Relative frequency and kinetic properties of transport-defective phenotypes among methotrexate-resistant L1210 clonal cell lines derived in vivo. *Cancer Res.* 41: 4447–4452.
- Special issue on Carbon Nanotubes (2002) *Acc. Chem. Res.* 35: 997–1113.
- Star A, Steuerman DW, Heath JR, Stoddart JF (2002) Starched carbon nanotubes. *Angew. Chem. Int. Ed.* 41: 2508–2512.
- Szlinder-Richert J, Cybulska B, Grzybowska J, Bolard J, Borowski E (2004) Interaction of amphotericin B and its low toxic derivative, N-methyl-N-D-fructosyl amphotericin B methyl ester, with fungal, mammalian and bacterial cells measured by the energy transfer method. *Il Farmaco* 59: 289–296.
- Taft BJ, Lazarek AD, Withey GD, Yin AJ, Xu JM, Kelley SO (2004) Site-specific assembly of DNA and appended cargo on arrayed carbon nanotubes. *J. Am. Chem. Soc.* 126: 12750–12751.
- Tasis D, Tagmatarchis N, Bianco A, Prato M (2006) Chemistry of carbon nanotubes. *Chem. Rev.* 106: 1105–1136.
- Tasis D, Tagmatarchis N, Georgakilas V, Prato M (2003) Soluble carbon nanotubes. *Chem. Eur. J.* 9: 4001–4008.
- Tsang SC, Guo ZJ, Chen YK, Green MLH, Hill HAO, Hambley TW, Sadler PJ (1997) Immobilization of platinated and iodinated oligonucleotides on carbon nanotubes. *Angew. Chem. Int. Ed. Engl.* 36: 2198–2200.
- Tsuji JS, Maynard AD, Howard PC, James JT, Lam CW, Warheit DB, Santamaria AB (2006) Research strategies for safety evaluation of nanomaterials, part IV: Risk assessment of nanoparticles. *Toxicol. Sci.* 89: 42–50.
- Valenti LE, Fiorito PA, Garcia CD, Giacomelli CE (2007) The adsorption-desorption process of bovine serum albumin on carbon nanotubes. *J. Colloid Interface Sci.* 307: 349–356.
- Varde NK, Pack DW (2004) Microspheres for controlled release drug delivery. *Expert Opin. Biol. Ther.* 4: 35–51.
- Venkatesan N, Yoshimitsu J, Ito Y, Shibata N, Takada K (2005) Liquid filled nanoparticles as a drug delivery tool for protein therapeutics. *Biomaterials* 26: 7154–7163.
- Wang J, Liu GD, Jan MR (2004) Ultrasensitive electrical biosensing of proteins and DNA: Carbon-nanotube derived amplification of the recognition and transduction events. *J. Am. Chem. Soc.* 126: 3010–3011.

- Wang SQ, Humphreys ES, Chung SY, Delduco DF, Lustig SR, Wang H, Parker KN, Rizzo NW, Subramoney S, Chiang YM, Jagota A (2003) Peptides with selective affinity for carbon nanotubes. *Nature Mater.* 2: 196–200.
- Warheit DB, Laurence BR, Reed KL, Roach DH, Reynolds GAM, Webb TR (2004) Comparative pulmonary toxicity assessment of single-wall carbon nanotubes in rats. *Toxicol. Sci.* 77: 117–125.
- Wick P, Manser P, Limbach LK, tllaff-Weglikowska U, Krumeich F, Roth S, Stark WJ, Bruinink A (2007) The degree and kind of agglomeration affect carbon nanotube cytotoxicity. *Toxicol. Lett.* 168: 121–131.
- Williams KA, Veenhuizen PTM, de la Torre BG, Eritja R, Dekker C (2002) Nanotechnology – Carbon nanotubes with DNA recognition. *Nature* 420: 761.
- Wohlstader JN, Wilbur JL, Sigal GB, Biebuyck HA, Billadeau MA, Dong LW, Fischer AB, Gudibande SR, Jamieson SH, Kenten JH, Leginus J, Leland JK, Massey RJ, Wohlstader SJ (2003) Carbon nanotube-based biosensor. *Adv. Mater.* 15: 1184–1187.
- Wu W, Wieckowski S, Pastorin G, Benincasa M, Klumpp C, Briand JP, Gennaro R, Prato M, Bianco A (2005) Targeted delivery of amphotericin B to cells by using functionalized carbon nanotubes. *Angew. Chem. Int. Ed.* 44: 6358–6362.
- Xie SS, Chang BH, Li WZ, Pan ZW, Sun LF, Mao JM, Chen XH, Qian LX, Zhou WY (1999) Synthesis and characterization of aligned carbon nanotube arrays. *Adv. Mater.* 11: 1135.
- Xie YH, Soh AK (2005) Investigation of non-covalent association of single-walled carbon nanotube with amylose by molecular dynamics simulation. *Mater. Lett.* 59: 971–975.
- Yim TJ, Liu JW, Lu Y, Kane RS, Dordick JS (2005) Highly active and stable DNAzyme – Carbon nanotube hybrids. *J. Am. Chem. Soc.* 127: 12200–12201.
- Yinghuai Z, Peng AT, Carpenter K, Maguire JA, Hosmane NS, Takagaki M (2005) Substituted carborane-appended water-soluble single-wall carbon nanotubes: New approach to boron neutron capture therapy drug delivery. *J. Am. Chem. Soc.* 127: 9875–9880.
- Zhang MG, Smith A, Gorski W (2004) Carbon nanotube-chitosan system for electrochemical sensing based on dehydrogenase enzymes. *Anal. Chem.* 76: 5045–5050.
- Zhang Q, Zhang L, Li JH (2007) DNA-hemoglobin-multiwalls carbon nanotube hybrid material with sandwich structure: Preparation, characterization, and application in bioelectrochemistry. *J. Phys. Chem. C* 111: 8655–8660.
- Zhang ZH, Yang XY, Zhang Y, Zeng B, Wang ZJ, Zhu TH, Roden RBS, Chen YS, Yang RC (2006) Delivery of telomerase reverse transcriptase small interfering RNA in complex with positively charged single-walled carbon nanotubes suppresses tumor growth. *Clin. Cancer Res.* 12: 4933–4939.
- Zheng M, Jagota A, Semke ED, Diner BA, Mclean RS, Lustig SR, Richardson RE, Tassi NG (2003a) DNA-assisted dispersion and separation of carbon nanotubes. *Nature Mater.* 2: 338–342.
- Zheng M, Jagota A, Strano MS, Santos AP, Barone P, Chou SG, Diner BA, Dresselhaus MS, Mclean RS, Onoa GB, Samsonidze GG, Semke ED, Usrey M, Walls DJ (2003b) Structure-based carbon nanotube sorting by sequence-dependent DNA assembly. *Science* 302: 1545–1548.
- Zorbas V, Ortiz-Acevedo A, Dalton AB, Yoshida MM, Dieckmann GR, Draper RK, Baughman RH, Jose-Yacaman M, Musselman IH (2004) Preparation and characterization of individual peptide-wrapped single-walled carbon nanotubes. *J. Am. Chem. Soc.* 126: 7222–7227.
- Zotchev SB (2003) Polyene macrolide antibiotics and their applications in human therapy. *Curr. Med. Chem.* 10: 211–223.

Chapter 3

Antioxidant Properties of Water-Soluble Fullerene Derivatives

Florian Beuerle¹, Russell Lebovitz², and Andreas Hirsch^{1,2}

Abstract Due to their inherent electronic properties, fullerenes are considered as radical sponges being capable of effectively quenching reactive oxygen species (ROS). The most promising candidates for potential pharmaceutical applications are therefore water-soluble fullerene derivatives, since they provide reasonable biological availability. In light of these considerations, we give an overview over the most recent concepts for designing and synthesizing real water-soluble fullerene compounds. Several studies concerning the quenching activities against ROS-like superoxide radical anion of some of these novel compounds are reviewed. We finally present first promising investigations about cytoprotective and neuroprotective activities of several carboxyfullerenes in zebrafish embryos as a mammalian model system. By comparing the activities for different addition patterns and other structural changes some first conclusions concerning a structure–function relationship can be drawn.

Keywords Fullerene, water-solubility, antioxidant, cytoprotection

3.1 Introduction

Shortly after the discovery of the fullerenes in 1985 (Kroto et al., 1985) and especially after their accessibility in macroscopic quantities (Kraetschmer et al., 1990) these new carbon allotropes raised great interest in the chemical world due to their unique structural and electronic properties. As a direct consequence of the curved conjugated π -system fullerenes were predicted to be fairly electronegative with the

¹Department for Chemistry and Pharmacy & Interdisciplinary Center for Molecular Materials, Lehrstuhl für Organische Chemie II, Universität Erlangen-Nürnberg, Henkestrasse 42, D-91054 Erlangen, Germany

²Tego Biosciences, 201 South Lake Avenue, Pasadena, CA 91101, USA

ability to undergo multiple reversible reduction steps. Indeed this was demonstrated by the fully reversible reduction up to the hexaanion for C_{60} , the most prominent and abundant fullerene (Echegoyen and Echegoyen, 1998). As another important chemical property their pronounced affinity towards radicals was pointed out, shortly thereafter (Hirsch and Brettreich, 2005). Upon addition of a large variety of radicals quite stable diamagnetic or paramagnetic adducts were observed and intensively studied.

Summarizing these facts, fullerenes can be considered as very effective ‘radical sponges’ (Krusic et al., 1991; McEwen et al., 1992) being capable of taking part in reversible redox processes. These properties make fullerenes very interesting with respect to potential applications in the field of biomedical or pharmaceutical chemistry. It is widely believed that reactive oxygen species (ROS) like hydroxyl radicals, peroxides and predominantly the superoxide radicals cause significant cell death and are important factors in aging as well as in chronic neurodegenerative diseases like ALS, *Alzheimer’s* and *Parkinson’s*. Due to their inherent structural properties and their ability to act as radical sponges, fullerenes and their derivatives were proposed to have potent antioxidant and neuroprotective activities in biomedical applications. In general, two different mechanisms for the quenching of ROS by fullerenes can be considered. The first involves a stoichiometric addition of ROS to the fullerene surface, probably followed by subsequent elimination or addition steps in order to regenerate the parent fullerene and resulting in a catalytic ROS cleavage. The second proposed mechanism is based on several outer sphere electron transfer processes involving reduction and reoxidation steps between the fullerene and radical species.

For successful clinical applications, it is necessary to demonstrate the specific mode of action, the pharmacokinetics and the distribution in various tissues after administration. One severe drawback for fullerenes in this context is the almost complete insolubility of these *all*-carbon allotropes in water. To overcome these impediments, one of the first goals in fullerene chemistry was to design and synthesize water-soluble derivatives, which retain the unique inherent fullerene properties while achieving reasonable biological availability. Subsequent antioxidant and protective studies using these novel water-soluble fullerenes produced promising results. Studies carried out with antibodies against fullerenes suggested that water-soluble fullerenes can readily pass cell membranes and are preferentially located at or near mitochondria (Foley et al., 2002) – the cellular organelle responsible for aerobic respiration and the site where most of the biological processes concerning ROS take place. These initial studies demonstrated substantial antioxidant activity both *in vitro* and *in vivo*, encouraging a flurry of new work in this area.

In this contribution we want to provide a short overview addressing the current state-of-the-art of water-soluble fullerene derivatives and their potential applications as antioxidant or neuroprotective drug candidates. After summarizing the most prominent concepts of designing water-soluble fullerenes in the first chapter we will present some more recent achievements with respect to biological activities of antioxidant fullerenes, with emphasis on our own results.

3.2 Water Solubility of Fullerene Derivatives

3.2.1 Dissolving Hydrophobic Fullerenes in Water

In principle, there are four basic strategies to compensate for the repulsive effects between the hydrophobic fullerene surface and water: (a) encapsulation in the internal hydrophobic moiety of water-soluble hosts like cyclodextrins (Andersson et al., 1992; Murthy and Geckeler, 2001), calixarenes (Kunsagi-Mate et al., 2004) or cyclotrimeratrylenes (Rio and Nierengarten, 2002); (b) supramolecular or covalent incorporation of fullerenes or derivatives into water-soluble polymers (Giacalone and Martin, 2006) or biomolecules like proteins (Pellarini et al., 2001; Yang et al., 2007); (c) suspension with the aid of appropriate surfactants; and (d) direct exohedral functionalization in order to introduce hydrophilic moieties.

From a pharmacological point of view the first two strategies raise several distinct disadvantages. First, the exact structures of these fullerene-based systems in solution are usually unknown and, especially for polymeric materials inhomogeneous samples are frequently obtained. Furthermore, in many cases the amount of incorporated fullerene is not clearly determined. In addition, the presence of other molecules like the hosts or polymeric residues can cause unpredictable side effects and in no case the mode of action or activity can doubtlessly be associated with the fullerenes. However, for systematic investigations on structure–function relationships or extensive testings of toxicological or human availability properties, the use of structurally well-defined and characterized materials is mandatory.

In recent years, a great diversity of structurally well-defined functionalized fullerenes has been designed and synthesized for that purpose. Some of them exhibit pronounced solubility in water (*vide infra*). But even for compounds being virtually insoluble in water, stable aqueous phases can be obtained in plenty of cases by diluting stock solutions of the compounds in polar organic solvents with various amounts of water. Notably, dimethyl sulfoxide (DMSO) and tetrahydrofuran (THF) have turned out to be excellent surfactants for preparing stable aqueous fullerene solutions (Angelini et al., 2005; Cassell et al., 1999; Da Ros et al., 1996; Gun'kin et al., 2006; Illescas et al., 2003). Also cosolvents such as dimethylformamide (DMF) and methanol can be used to promote water solubility. After subsequent dilution of a saturated solution of C₆₀ in benzene with THF, acetone and finally water, actually stable aqueous suspensions of pristine fullerene can be obtained (Scrivens et al., 1994).

In order to increase fullerene solubility in either non-aromatic solvents or polar phases like water, a large number of functionalized fullerenes have been synthesized (Da Ros and Prato, 1999; Nakamura and Isobe, 2003). The first examples of water-soluble derivatives were obtained after the addition of either several hydroxyl groups, leading to fullerlenols (Chiang et al., 1995, 1996), or the addition of six sulfobutyl groups to the fullerene surface, leading to hexasulfobutyl fullerenes (Chi et al., 1998; Huang et al., 2001; Jeng et al., 2001; Lee et al., 2000). Both substance classes exhibit good water solubility and show surprisingly potent antioxidant and

neuroprotective activities. However, both classes featured highly heterogeneous structures concerning their number of addends (for fullerenols) and especially their regiochemistry on the fullerene surface: this heterogeneity would almost certainly hamper their use as potential drug candidates. Over the course of time, various novel nucleophilic and cycloaddition reactions suitable for exohedral modification were developed that demonstrate excellent control over the regioselectivity of subsequent additions (Hirsch and Brettreich, 2005).

The two most commonly used derivatization methods for exohedral functionalization are the nucleophilic cyclopropanation with malonates (Bingel, 1993) and the formation of fulleropyrrolidines (Maggini et al., 1993). Both of these protocols have been used extensively to produce water-soluble fullerenes for biomedical applications. Other stable water-soluble fullerene adducts have also been reported (Hirsch and Brettreich, 2005). Sections 3.2.2–3.2.5 will give a short overview on the state-of-the-art of water-soluble fullerene derivatives and outline some general trends for designing such molecular structures.

3.2.2 Water-Soluble Malonate Adducts

One of the most common exohedral functionalization methods for fullerenes is the cyclopropanation of malonates and related 1,3-dicarbonyl compounds, the so-called BINGEL reaction. The easiest way to introduce polar groups in malonate adducts is the deprotection of appropriate precursors in order to generate the corresponding free malonic acids (Lamparth and Hirsch, 1994; Reuther et al., 2002). With an increasing number of acid groups, the water solubility increases. Whereas the deprotected monoadduct is only slightly soluble in strong basic solutions, several regioisomeric bisadducts are highly soluble in weakly basic media ($\text{pH} > 8$) and trisadducts like C_3 (*e,e,e*- $C_{63}(\text{COOH})_6$) **1** and D_3 (*trans3,trans3,trans3*- $C_{63}(\text{COOH})_6$) **2** are actually well soluble even in neutral water (Lamparth and Hirsch, 1994) (Figs. 3.1 and 3.2). Currently, **1** and **2** are the most extensively studied fullerene derivatives with respect to antioxidant and neuroprotective activity *in vitro* and *in vivo*, and have consistently shown very promising results as potential candidates for a variety of biomedical applications (Ali et al., 2004; Bisaglia et al., 2000; Bosi et al., 2000; Dugan et al., 1997, 2001; Foley et al., 2002; Fumelli et al., 2000; Huang et al., 1998; Kiritoshi et al., 2003; Lin et al., 1999, 2002, 2001; Lotharius et al., 1999; Mashino et al., 1999; Monti et al., 2000; Rieger et al., 2002; Straface et al., 1999; Tsao et al., 2001, 2002; Tzeng et al., 2002).

Yet hands-on experience with **1** and other related compounds showed that free malonic acid groups on fullerenes are rather unstable even under physiological conditions and readily decarboxylate into side products, some of which may show toxicity under certain circumstances (Beuerle et al., 2007). To avoid these potential side effects new polar derivatives of **1** like **3**, **4** and **5** have been synthesized (Beuerle et al., 2005; Witte et al., 2007). In these trisadducts the polar endgroups are attached *via* alkyl spacers to the fullerene core and thus no unwanted decarboxylation

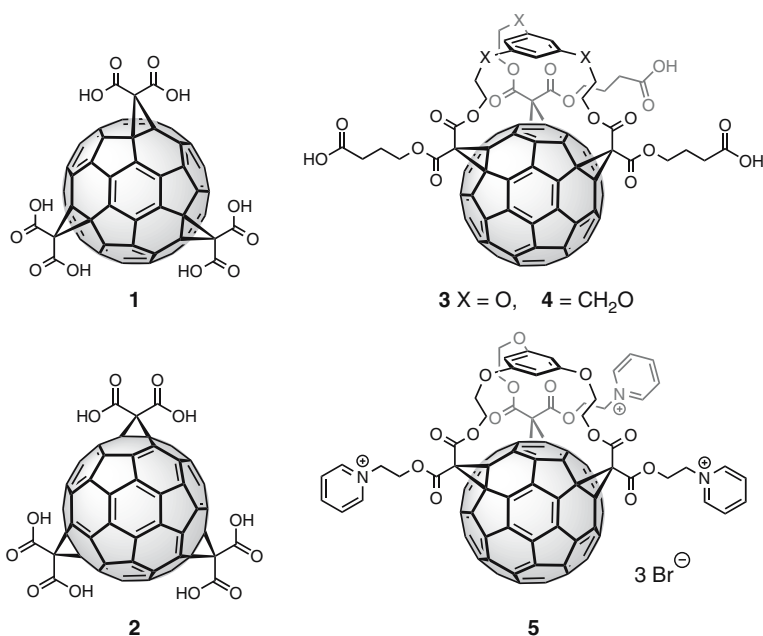


Fig. 3.1 Water-soluble fullerene trisadducts

processes are observed. Whereas the pyridinium fullerene **5** with three permanent positive charges shows a high and pH-independent water solubility, carboxyfullerenes **3** and **4** are only solubilized in basic media (pH > 8), probably due to incomplete deprotonation of all three acid groups under neutral conditions.

One drawback of multiple exohedral functionalization is a stronger disruption of the fullerene π -system with increasing number of addends. As a direct consequence, antioxidant or neuroprotective activities should decrease with a greater number of addends by virtue of a lower electron or radical affinity (de La Vaissiere et al., 2001). To enhance water solubility of less-functionalized fullerene derivatives, however, dendritic polar moieties can be introduced to enhance the number of charges. The most prominent example of a monoadduct of this kind is dendrofullerene **6** containing two second-generation NEWKOME-type dendritic branches (Brettreich and Hirsch, 1998). It is soluble in phosphate-buffered water in concentrations up to 1.2×10^{-2} M, which is one of the highest values for fullerene derivatives observed so far. Titration experiments revealed that at pH 7 on an average 16 of 18 acid groups are deprotonated (Brettreich, 2003). UV/Vis spectroscopic and small angle neutron scattering experiments indicated that dendrofullerene **6** is dispersed

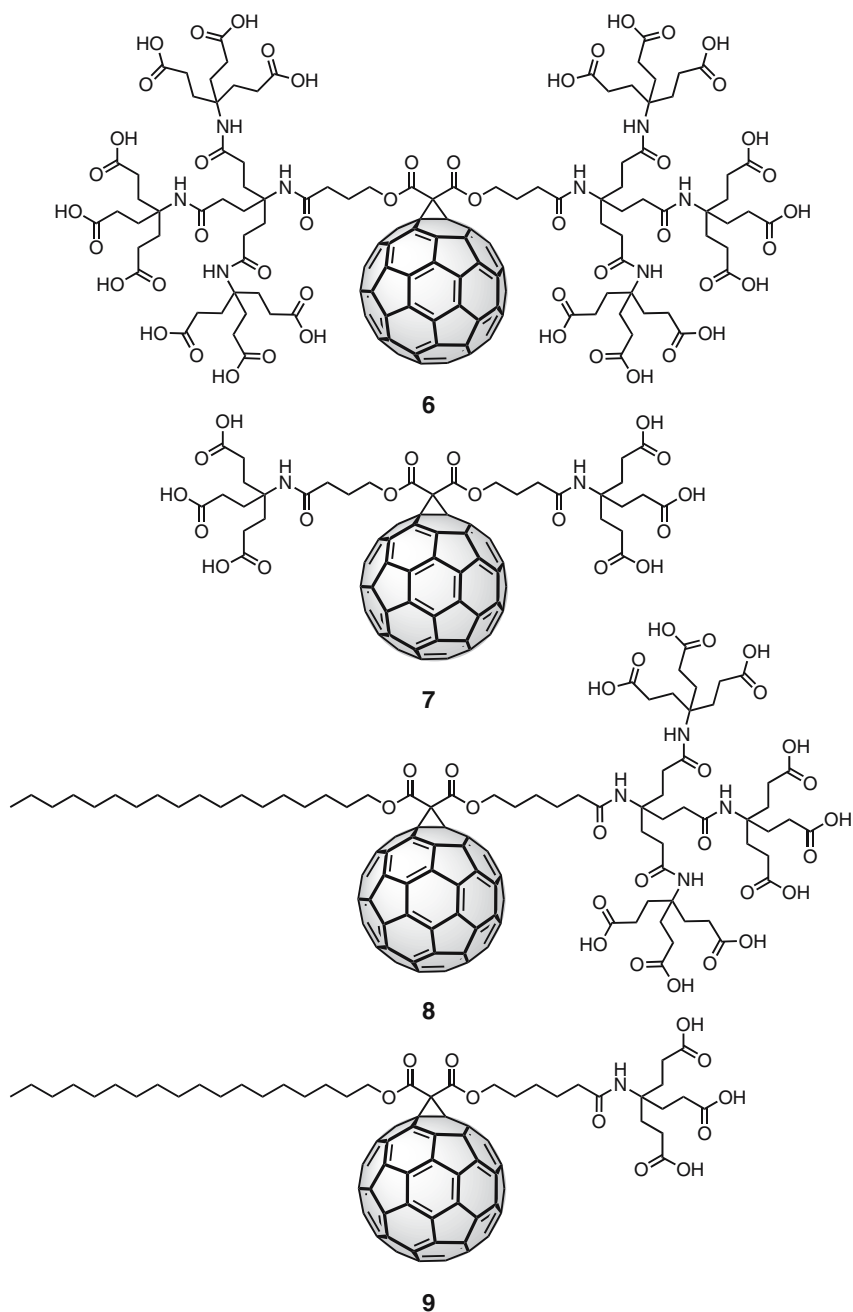


Fig. 3.2 Water-soluble monoadducts

in monomeric form at neutral pH due to the very effective shielding of the fullerene surface by the bulky dendritic branches (Brettreich, 2003). These observations make **6** an ideal candidate for kinetic studies of fullerenes in water, because no clustering phenomena are likely to complicate the measurements. For example,

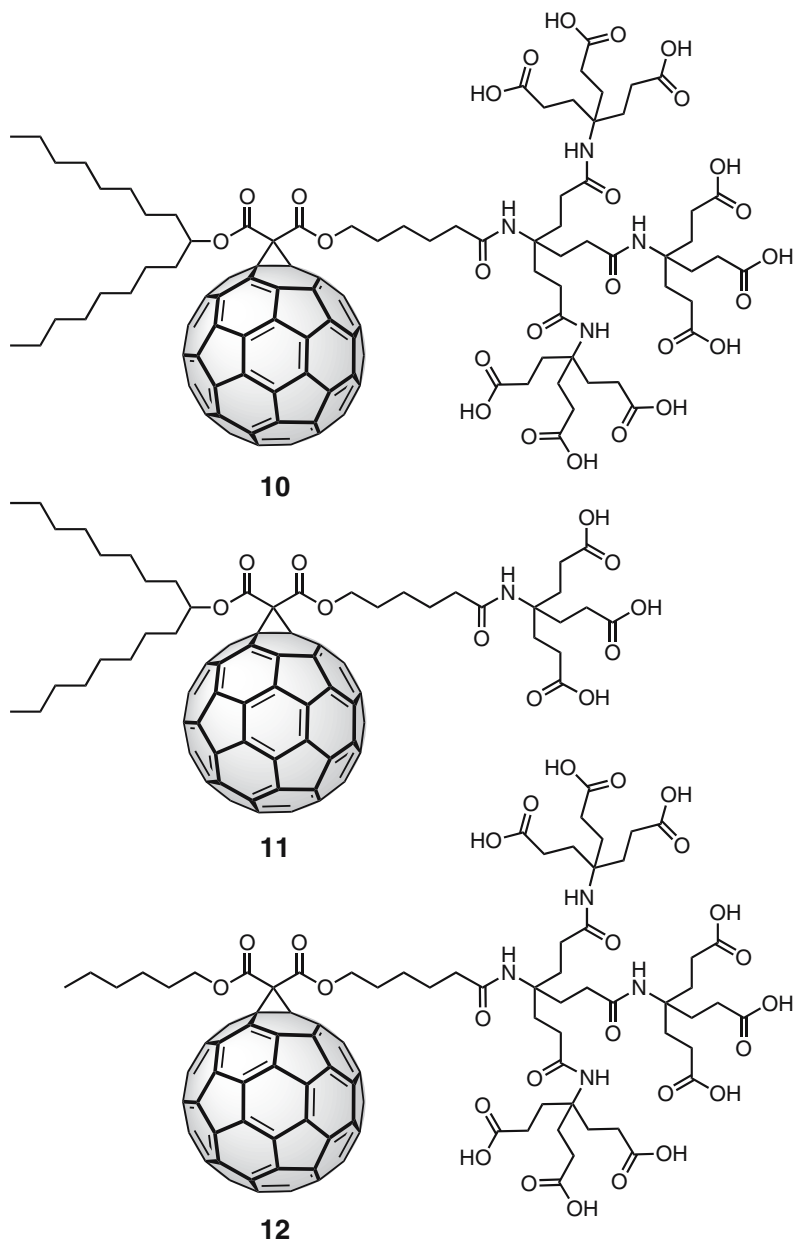


Fig. 3.3 Water-soluble amphiphilic monoadducts

reactions of photochemical-generated radicals with **6** and **1** have been investigated in detail (Bensasson et al., 2000).

As structural analogues of **6**, we have recently published the first-generation dendrofullerene **7** and a novel series of amphiphilic dendrofullerenes **8–12** (Witte et al., 2007) (Fig. 3.3). The hexaacid **7** exhibits a comparable but remarkably lower solubility in water than **6**. In the case of amphiphilic dendrofullerenes with only one hydrophilic dendron and one long alkyl chain as lipophilic moiety, the second-generation derivatives **8**, **10** and **12** are soluble in buffered water at pH 7 or in basic solution, whereas the first-generation analogues **9** and **11** are virtually insoluble even under basic conditions. Water-diluted stock solutions in DMSO though are stable for weeks. Because of their strong amphiphilic character, dendrofullerenes like **8** tend to aggregate in larger clusters in aqueous solutions indicated by line broadening in the UV/Vis spectra (Guldi and Prato, 2000). Nevertheless, their lipophilic side chains are expected to promote increased tissue accessibility and biodistribution within lipid-rich regions or easier crossing of the blood–brain barrier.

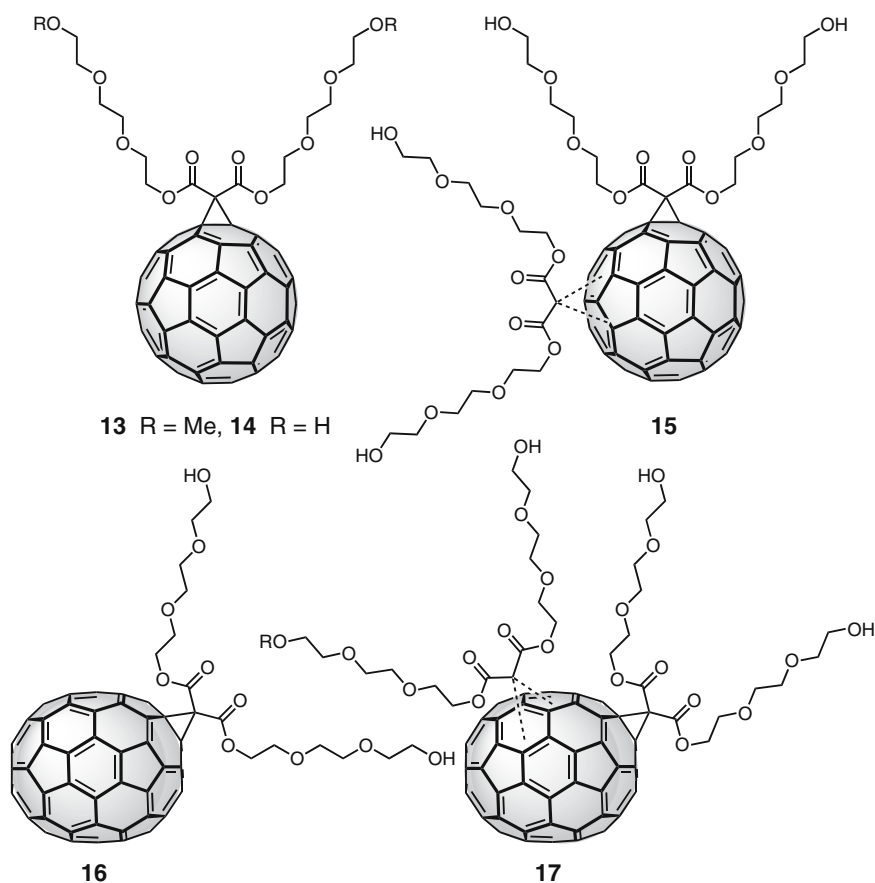


Fig. 3.4 Monoadducts and bisadducts of C₆₀- and C₇₀-containing ethylene glycol chains

We have also designed novel monoadducts and bisadducts of either C_{60} and C_{70} without any charged addends in order to obtain hydrophilic, but neutral fullerene derivatives and to make other addition patterns than those yielding monoadducts and certain trisadducts accessible for biological and medicinal applications. As depicted in Fig. 3.4, we synthesized both the monoadducts **13** and **14** of C_{60} , as well as **16** of C_{70} and two regioisomeric series of bisadducts **15** (*trans-2, trans-3, trans-4, e*) (Hirsch et al., 1994) and **17** (*2 o'clock, 3 o'clock, 12 o'clock*) (Herrmann et al., 1995) containing two and four polyethylene glycol chains, respectively.

Unfortunately, these nonionic but polar fullerene adducts exhibit virtually no water solubility over the whole pH range, indicating that even four polyethylene units are not sufficient to provide true water solubility. However, as mentioned before for other fullerenes, by diluting DMSO solutions with various amounts of water stable aqueous phases containing dispersed fullerenes can be obtained.

3.2.3 Water-Soluble Fulleropyrrolidines

Another important method for preparation for exohedrally functionalized fullerenes is the 1,3-dipolar cycloaddition of *in situ*-generated azomethine ylides to C_{60} yielding fulleropyrrolidines (Maggini et al., 1993). Further functionalization is facilitated either by the use of adequate aldehydes for the azomethine ylide formation or quaternization of the pyrrolidine nitrogen atom. Both bisaddition (Kordatos et al., 2001) and trisaddition (Marchesan et al., 2005) can be achieved regioselectively.

Monoadduct **18** with three positive charges and three ethylene glycol chains is soluble in aqueous solutions at concentrations around 10^{-5} M and in water/DMF and water/methanol mixtures at concentrations up to 10^{-3} M, but shows considerable formation of aggregates as demonstrated by UV/Vis spectroscopy (Cusan et al., 2002). In order to increase solubility and to diminish any tendencies to aggregate in polar media a series of bisadducts have been synthesized (Bosi et al., 2003). Three sets of bis-fulleropyrrolidines containing (i) two ethylene glycol chains and two positive charges (**20**); (ii) two ethylene glycol chains and four positive charges (**21**); (iii) two ethylene glycol chains and four negative charges (**22**); and (iv) mixed malonate/pyrrolidine adducts containing three ethylene glycol chains and one positive charge (**19**), have been investigated in isomerically pure form with *trans-2, trans-3, trans-4* and *e*-addition patterns, respectively.

Depending on their particular structures, these bisadducts show differing degrees of water solubility (Fig. 3.5). Whereas compounds **20** with a net charge of plus two are soluble in concentrations up to 10^{-4} M, the two additional charges in **21** increase the maximum concentration in water to 10^{-2} M. Regioisomers **19** and **22** nicely mirror the effect of pH, since the solubilities of **19** significantly decrease from 10^{-2} to 10^{-4} M by going from pure water to phosphate-buffered solution at pH 7.4 and vice versa for **22**. These differences are due to increased formation of the unprotonated amines for **19** and carboxylate anions for **22** in more basic aqueous solutions.

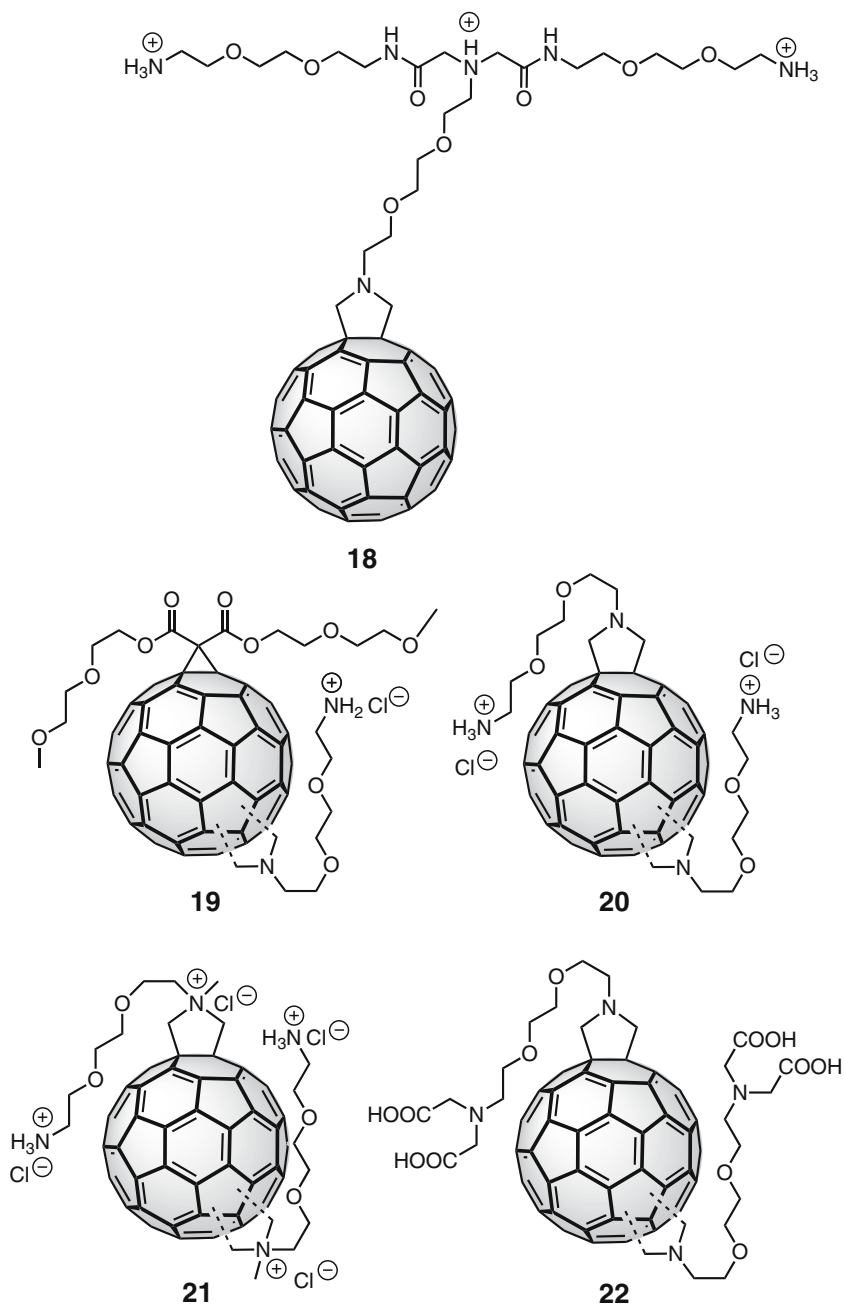


Fig. 3.5 Water-soluble fulleropyrrolidines

3.2.4 Miscellaneous Water-Soluble Fullerenes

Beside fulleropyrrolidines and malonate adducts, a variety of other water-soluble fullerene derivatives with entirely different addition patterns have been synthesized within the past years (Fig. 3.6). These investigations have enhanced the available

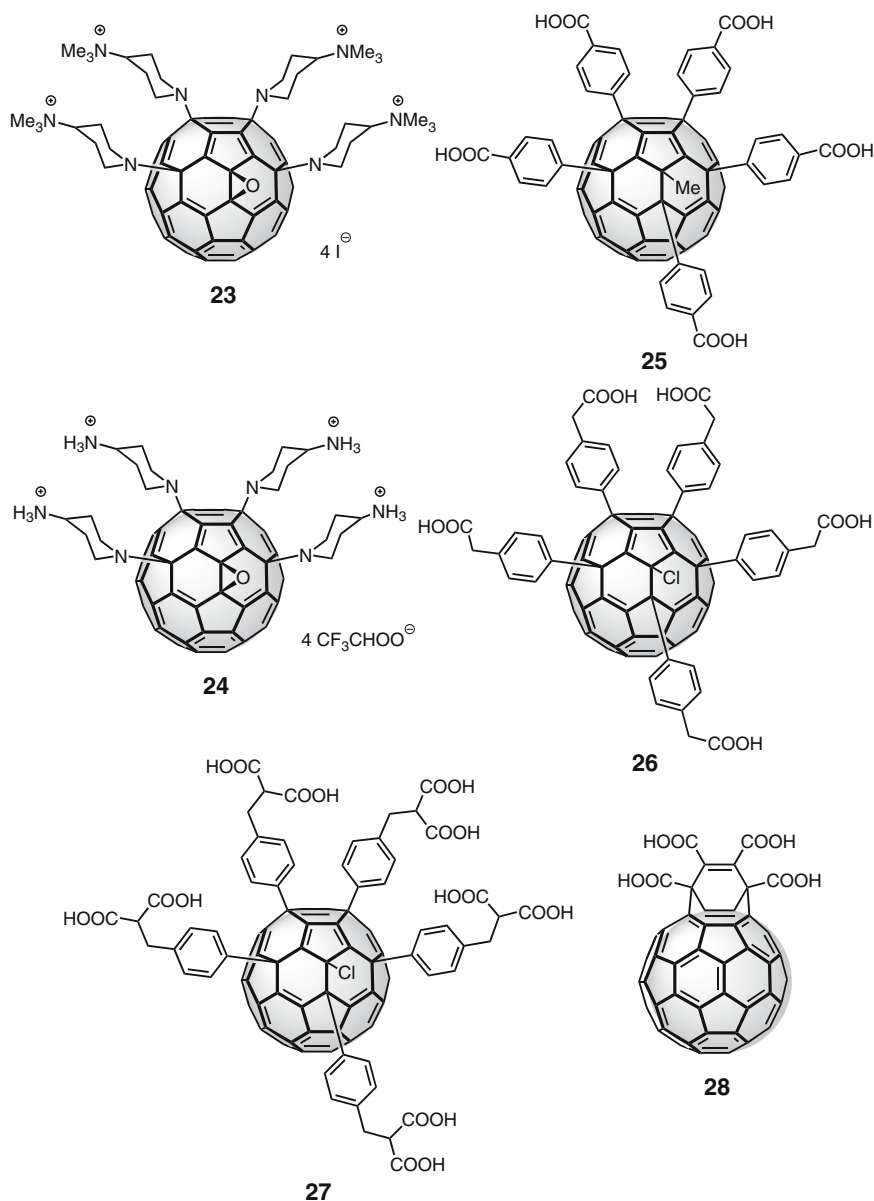


Fig. 3.6 Miscellaneous water-soluble fullerene derivatives

library of potential antioxidants and will allow deeper insights into the effects of the electronic structure of fullerenes on biomedical and pharmacological activities.

Among these less well-known addition patterns are oxo-tetraamino-[60]fullerenes like **23** and **24** containing four permanent or pH-dependent positive charges (Witte et al., 2007). Compound **23** is very well soluble in water over a wide pH range by virtue of its four permanent trimethyl ammonium groups, whereas **24** is only slightly soluble in acidic solutions (pH 4) but well dissolvable in polar solvents like methanol or ethanol.

A comparable addition pattern with as many as five attached groups allowing further functionalization is represented in pentaaryl-fullerenes like **25–27** (Troshina et al., 2007; Zhong et al., 2006). Whereas the free acids are virtually insoluble in pure water, the use of basic water in the case of **25** (Zhong et al., 2006) and conversion of the polyacids **26** and **27** to the corresponding potassium salts leads to stable aqueous solutions with high fullerene concentrations.

Another very interesting addition pattern is realized in bisfulleroids like **28**, as within this kind of fullerene derivative the original 60-electron π -system of pristine C_{60} remains almost unchanged rendering these water-soluble derivatives excellent probes for the behaviour of unmodified fullerene surfaces in aqueous solutions. The tetraacid **28** as a simple example is insoluble in neutral water, but highly soluble in basic aqueous media such as 0.01 M K_2CO_3 (Periya et al., 2004). Another very interesting molecule based on a related addition pattern is the so-called sugar ball **29** we presented recently containing six α -D-mannose units and also an unchanged fullerene π -system (Fig. 3.7). This molecule is well soluble in water and forms only small micellar aggregates (Kato et al., 2007). It is a very rare example of true water solubility for uncharged fullerenes creating a foundation for very interesting biological applications.

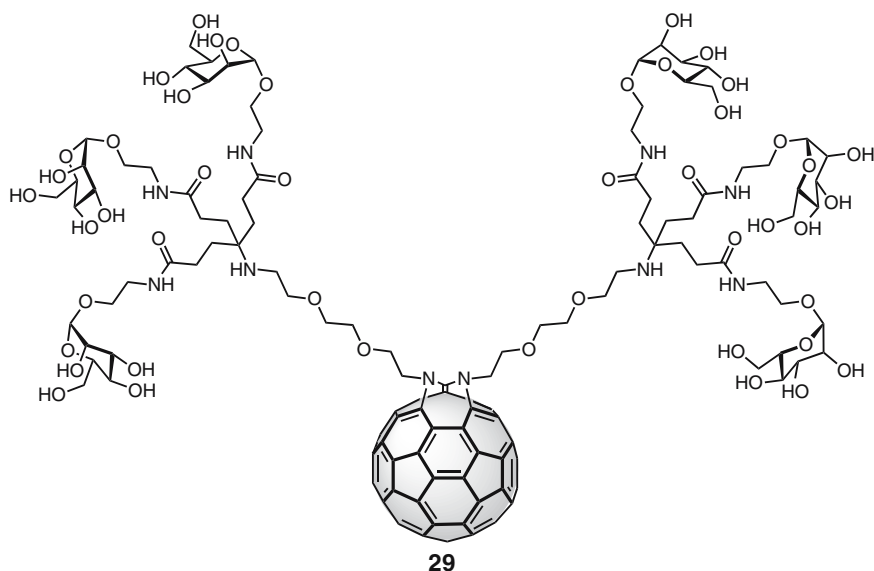


Fig. 3.7 Water-soluble fullerene sugar derivative containing a 60 electron π -system

3.2.5 *General Trends for Water Solubility of Fullerene Derivatives*

In summarizing these various approaches for promoting water solubility for fullerene derivatives, it can be generalized that at least three ionic charges with an appropriate arrangement at the fullerene surface or some combination of net charging and other polar moieties is required. A rare exception is the nonionic sugar derivative **29** with six α -D-mannose units exhibiting a surprisingly high solubility in water. Less hydrophilic addends such as those involving ethylene glycol chains (for example, in **13–17**) were shown to be not potent enough to provide water solubility without the aid of surfactants. Nevertheless, polar side chains like these can effectively enhance water solubility facilitated by several ionic charges as demonstrated, for example, with the adducts **19–22**. In addition, polar fullerenes with pH-dependently charged systems instead allow switching the solubility as it was mentioned for **19** and **22**. Especially for carboxy fullerenes such as **3**, **4** and **25–27** full deprotection is required to achieve water solubility.

Concerning the spherical arrangement of charged or hydrophilic moieties on the fullerene surface it appears that reducing the inherent amphiphilic structure of fullerene derivatives by going from mono to higher addition patterns effectively enhances water solubility. Whereas bisadducts **19–22** and trisadduct **5** are highly soluble, the amphiphilic monoadducts **9** and **11** are virtually insoluble even in their fully deprotected form. Significantly, the six negative charges in **7** provide only poor solubility, whereas higher generation dendritic moieties as realized in **8**, **10** and **12** lead to the formation of stable solubilized fullerene clusters in water. Water solubility of monoadducts in the almost monomeric form can be achieved by introducing two second-generation anionic dendritic branches as shown by compound **6**.

In conclusion, by varying the number and kind of the attached substructures for exohedrally functionalized fullerenes the solubility in water can be fine-tuned. From a pharmacological point of view, a well-balanced arrangement of both hydrophilic and lipophilic behaviour is required in order to achieve favourable bio-distribution. Amphiphilic monoadducts containing long lipophilic alkyl chains like **8** are promising candidates for potential medical applications.

3.3 ROS Quenching Activities of Water-Soluble Fullerene

It is widely accepted that the superoxide radical anion plays a very important role in neuronal degeneration (Dugan et al., 1995; Lafon-Cazal et al., 1993; Reynolds and Hastings, 1995) and is thought to be one of the predominant species responsible for ROS toxicity. Other small molecules including hydroxyl or nitric oxide radicals may also play important roles in triggering oxidative stress in animals and humans. In order to determine whether fullerenes can generally trap or quench ROS and to gain insights in possible structure–activity relationships some water-soluble

fullerene derivatives have been tested in standardized assays that evaluate their ability to quench the free-radical activities of these active oxygen species.

3.3.1 Superoxide Quenching Activities of Fullerenes

Given that oxidative injury plays an important role in central nervous system (CNS) degenerative diseases, novel drugs that protect cells from cytopathic effects of ROS could conceivably be used to treat some of these devastating illnesses. To screen for possible neuroprotective drugs, a variety of standardized test systems have been designed mostly based on the *in situ* generation of superoxide by xanthine/xanthine oxidase. Superoxide decomposition may be followed photometrically by the reduction of ferricytochrome *c*, as it was reported by McCord and Fridovich (McCord and Fridovich, 1969).

Fullerenols (Chiang et al., 1995; Mirkov et al., 2004) and hexasulfobutyl fullerenes (Chi et al., 1998, 2002) were among the earliest water-soluble fullerene derivatives to be examined for superoxide scavenging activities. Whereas the latter show excellent quenching properties with 60% and 95% suppression efficiency at 50 and 100 μM fullerene concentration, the scavenging activities for the hydroxy-functionalized fullerenols are significantly lower in the range of 40% efficiency at 1 mM fullerene concentration. Since the most probable explanation is a greater disruption of the spherical π -system in fullerenols rather than in hexasulfobutyl fullerenes due to a higher degree of functionalization on the fullerene surface, it was postulated that derivatives with less distorted π -systems would exhibit even higher antioxidant activities.

Around the same time, carboxy fullerenes with free malonic acid groups attached to the fullerene core were examined with respect to their antioxidant properties as an outstanding substance class given that control of both the number and spherical arrangement of the malonic groups is very well possible (Hirsch et al., 1994). In the case of bisadducts fullerene-induced scavenging of superoxide was observed for the *e*-isomer (Okuda et al., 1996) and enhanced superoxide dismutase (SOD) activity in LDS-activated microglia was reported for the *trans*-2- and *trans*-3-isomer (Tzeng et al., 2002). The first major breakthrough for fullerenes as antioxidants was the application of the trismalonic acids **1** and **2** as radical scavenging agents. Both isomers were able to completely eliminate *in situ*-generated superoxide radicals in concentrations of 40–50 μM mapped by electron paramagnetic resonance (EPR) spectroscopy (Dugan et al., 1997). More detailed experiments with **1** showed that this compound is indeed capable of removing superoxide radical anion in a catalytic reaction with a rate constant of $2 \times 10^6 \text{ mol}^{-1} \text{ s}^{-1}$ (Ali et al., 2004). There was no stoichiometric scavenging, but rather a catalytic dismutation of superoxide observed without any noticeable structural modification of **1**. The rate constant is approximately 100-fold lower compared with enzymatic SODs, but is within the range reported for manganese-containing SOD mimetics (Faulkner et al., 1994; Riley, 1999). Subsequently, intensive *in vitro* and *in vivo* studies of the

antioxidant and neuroprotective properties of **1** and **2** have been carried out (Bisaglia et al., 2000; Bosi et al., 2000; Dugan et al., 2001; Fumelli et al., 2000; Huang et al., 1998; Kiritoshi et al., 2003; Lin et al., 1999, 2002, 2001; Lotharius et al., 1999; Mashino et al., 1999; Monti et al., 2000; Rieger et al., 2002; Straface et al., 1999; Tsao et al., 2001, 2002; Tzeng et al., 2002) establishing **1** in particular as *the* reference compound for fullerene-based antioxidants and a lead compound for potential drug development.

In order to gain more insight into structure–impact relationships and to achieve a better understanding of the mechanisms involved in active oxygen quenching by fullerene derivatives, we recently published the syntheses of compounds **3–17**, **23** and **24** (Beuerle et al., 2005; Brettreich and Hirsch, 1998; Witte et al., 2007) and compared their superoxide scavenging activities with the reference compounds **1** and **2** (Witte et al., 2007). In Table 3.1 the IC₅₀ values measured according the protocol developed by McCord and Fridovich (McCord and Fridovich, 1969) are listed.

Careful analysis of this data leads to interesting conclusions concerning structure–function relationships. Generally, anionic monoadducts seem to be the best antioxidants; this is quite reasonable because of the lower reduction potentials and greater radical affinity of these derivatives due to a more intact π -system. Within the class of dendritic polycarboxylates **6–12** the best activities were reached for the dendrofullerenes **6** and **7** with IC₅₀ values of 11 and 6.2 μ M, respectively. For the amphiphilic monoadducts the second-generation compounds **8**, **10** and **12** exhibit significantly lower inhibition concentrations with IC₅₀ between 13.3 and 15.5 μ M than the first-generation ones **9** and **11** possessing values of 24 and 26.1 μ M.

One possible explanation for these observations may be the different aggregation states of these molecules in aqueous solutions due to their intrinsic structures.

Table 3.1 IC₅₀ values for superoxide quenching of fullerene derivatives (Witte, 2007)

Compound	IC ₅₀ (μ mol)	Compound	IC ₅₀ (μ mol)
e,e,e-Trisadducts		Monoadducts	
1	18.5	6	11.0
2	16.8	7	6.2
3	36.5	8	15.4
4	56.0	9	24.0
5	202.0	10	14.7
Bisadducts		11	26.1
15-trans-2	789.0	12	13.3
15-trans-3	139.6	13	289.0
15-trans-4	55.5	14	64.0
15-e	62.5	16	32.0
17-2 o'clock	50.0	Oxotetraamino fullerenes	
17-12 o'clock	76.9	23	45.4
		24 (pH 7.4)	35.0
		24 (pH 6.0)	45.4

Whereas the dendrofullerenes are water-soluble in an almost monomeric form, the amphiphilic structures **8–12** have a strong tendency to form aggregates in water as it is detected by line broadening in UV/Vis spectra.

Formation of such clusters decreases the actual concentration of active fullerene species in solution presumably leading to lower quenching activities compared with monomers. Comparing the first- and second-generation derivatives, the former exhibit a considerable lower net charge and smaller hydrophilic head group together with a comparably lipophilic moiety. Together with the essential presence of polar surfactants like DMSO, these differences in monomer structures may perhaps lead to greater supramolecular superstructures of the first-generation fullerenes, resulting in lower fullerene availability compared with the second-generation derivatives. These considerations might be a possible explanation for the different superoxide scavenging activities. For the nonionic C_{60} derivatives **14** ($IC_{50} = 64 \mu\text{M}$) and especially **13** ($IC_{50} = 289 \mu\text{M}$) an effective shielding of the quite unpolar fullerenes through strong clustering might also be a possible explanation for inferior quenching. The C_{70} analogon **16** however shows with $IC_{50} = 32 \mu\text{M}$ a higher activity, probably due to a more favourable electronic structure of C_{70} compared with C_{60} . In this context it is quite remarkable that for the fulleropyrrolidine monoadduct **18**, actually no superoxide quenching activity was observed (Cusan et al., 2002).

The series of regioisomeric bisadducts **15** and **17** meanwhile, nicely demonstrate the effect of an increasing distortion of the fullerene π -system on the quenching properties. With an increased distance of the addends on the fullerene surface, the rupture of the spherical π -system is enforced, attenuating the intrinsic electronic and radical scavenging properties of the accordant fullerene derivative. For example, the very remote *trans-2* addition pattern causes very low activity ($IC_{50} = 789 \mu\text{M}$) whereas for the *trans-4* and *e* binding quite low values ($IC_{50} = 55.5$ and $62.5 \mu\text{M}$) were obtained.

Trisadducts however were shown to be very good superoxide scavengers as demonstrated with **1** and **2** ($IC_{50} = 18.5$ and $16.8 \mu\text{M}$). Whether this enhancement in activity comparing to the bisadducts is due to the specific addition patterns or related with the fact that **1** and **2** possess real negative charges instead of nonionic side chains is still unclear. Also the differences in activity between **1** and **3–5** are not obvious and require further investigations, but one possible explanation might be the effective blocking of the surface region between the cyclopropane rings by the capped benzene moiety. This region was predicted to play an important role for superoxide quenching of **1** demonstrated by semi-empirical calculations (Ali et al., 2004). A quite surprising result is the very low activity of cationic fullerene derivatives such as **5**, **23** and **24** because favourable attractions between positively charged fullerenes and anionic superoxides were expected to enhance quenching activities as it was reported for other fullerene derivatives (Okuda et al., 2000). We still have no explanation for this behaviour.

In this context, one has to consider that these types of indirect assays are subjected to many variables that are difficult to control and interpretation of results is somewhat limited. Artefacts due to biological components like enzymes or cytochrome *c* within these assays may falsify the observed activities, and other possible

matrix effects due to aggregation behaviour among fullerenes and other components have to be taken into account as well. Notably, our observations that anionic fullerenes build up complexes with cytochrome *c* (Braun et al., 2003; Witte et al., 2007) show that there might be severe interference of unwanted side effects on the measured activities. This has to be always kept in mind upon the evaluation of antioxidant properties and in the near future more detailed investigations concerning the reaction of superoxide radical anions with certain fullerene derivatives have to be accomplished in order to get more funded kinetic data and a deeper insight into the quenching mechanisms.

3.3.2 Quenching of Other Reactive Oxygen Species

Beside superoxide, other small oxygen radicals such as hydroxyl radical or nitric oxide have also been implicated in inducing oxidative stress in mammals and humans. In this context, several papers addressing the scavenging abilities of fullerene derivatives for ROS other than superoxide have been published recently. It was pointed out that fullerenes are excellent quenchers for hydroxyl radicals under physiological conditions, exhibiting scavenging activities being in most cases about two orders of magnitude higher compared with quenching of superoxide (Bensasson et al., 2000; Chen et al., 2004; Hu et al., 2007; Sun et al., 2001; Sun and Xu, 2006; Wang et al., 1999; Xiao et al., 2005). This is probably due to the efficient formation of polyhydroxylated addition products. Also, nitric oxide radical quenching has been reported for fullerlenols (Mirkov et al., 2004) and several malonate adducts (Wolff et al., 2001), suggesting that antioxidant and neuroprotective effects of fullerene-based materials are due to different modes of action, greatly enhancing their potential for medicinal applications.

3.4 Neuroprotective Activities of Fullerene Derivatives *In Vivo*

Shortly after the first very promising results showing that various water-soluble fullerene derivatives exhibit high scavenging activities for several reactive oxygen species *in vitro*, first *in vivo* studies in appropriate mammals have been accomplished to evaluate the potential quenching effects of fullerene-based drug systems in living organisms. Although the data observed until now are still limited some promising observations have been made nevertheless. Thus, effective free radical scavenging activities for fullerlenols have been reported in several animal models including intestinal ischemia-reperfusion intestine in dogs (Lai et al., 2000a) and in grafts after small bowel transplantation (Lai et al., 2000b). Hexasulfobutyl fullerenes were further shown to be good neuroprotectants against focal cerebral ischemia in rats (Huang et al., 2001; Yang et al., 2001). As another antioxidant fullerene derivative, dendrofullerene **6** exhibits radioprotective effects on zebrafish

embryos comparable to the FDA-approved radioprotector amifostine (Daroczi et al., 2006). Recently, liver-protecting effects of aqueous suspensions of pristine C_{60} for acute carbon tetrachloride intoxication have been reported (Gharbi et al., 2005).

The most intensively studied fullerene compounds are the carboxyfullerenes **1** and **2**. Dugan et al. showed that systemic administration of **1** delayed motor deterioration and death in a mouse model of familial amyotrophic lateral sclerosis (FALS) (Dugan et al., 1997) and increased life span in SOD2 knockout mice lacking expression of mitochondrial manganese superoxide dismutase (Ali et al., 2004). In addition, prevention of iron-induced oxidative stress in rat brains has also been presented (Lin et al., 1999). In order to obtain more insight into the toxicity and antioxidant activities *in vivo* and the effects of various structural changes of exohedrally functionalized fullerenes, we tested compounds **1**, **3–11**, **23** and **24** in various zebrafish assays to evaluate both toxicity as well as protecting abilities against several chemical cytotoxins (Beuerle et al., 2007).

3.4.1 Toxicity of Water-Soluble Fullerenes

To check biological compatibility of the tested fullerenes, overall toxicities in zebrafish embryos were measured and body morphology and any changes to inner organs were inspected visually by light microscopy. The obtained LC_{50} values are summarized in Table 3.2. With respect to overall toxicity, the data indicate that cationic fullerenes **5**, **23** and **24** are considerably more toxic with LC_{50} values less than $120\mu\text{M}$. If this increased toxicity is due to the specific nature of the ammonium and pyridinium groups or related to a general effect of cationic fullerenes is still unclear. Anionic fullerenes exhibit significantly lower toxicity reaching up to 0% lethality at $250\mu\text{M}$ for **3**, **4** and **9**, and 20% and 30% lethality for **6** and **7**, respectively. As an important exception the decarboxylation products of **1** (referred to as **1-penta**, **1-tetra** and **1-tris** regarding to the number of acid groups) show greatly enhanced toxicity with decreasing number of acid groups.

Table 3.2 LC_{50} values of fullerenes in zebrafish embryos (Beuerle, 2007)

Compound	LC_{50} (μM)	Compound	LC_{50} (μM)
Monoadducts		e,e,e-Trisadducts	
6	20% at $500\mu\text{M}$	1	596
7	30% at $500\mu\text{M}$	1-penta	373
8	ND	1-tetra	134
9	0% at $250\mu\text{M}$	1-tris	10
10	ND	3	0% at $250\mu\text{M}$
11	ND	4	0% at $250\mu\text{M}$
Oxotetraamino fullerenes		5	117
23	30		
24	104		

By going from **1** to **1-penta**, **1-tetra** and **1-tris** the LC_{50} values decreased significantly from 596 down to $10\mu\text{M}$. This toxicity mostly effects the cardiac conduction system in the fish and may be due to binding of the decarboxylation products to the ZERG potassium channel in zebrafish as was reported for native unmodified fullerenes. Most anionic water-soluble fullerenes have bulky adducts on their surface, which block any significant binding to the ZERG channel.

In a few cases, water-soluble fullerenes at high doses induced abnormal morphologies like shortened body length and abnormal body curvature, and in several cases slightly abnormal cardiac chambers or enlarged or underdeveloped livers and intestines were observed at concentrations around the LC_{50} . These results suggest that anionic fullerene derivatives are generally nontoxic, but may exhibit teratogenic effects at higher concentrations. In general, few, if any, toxic effects have been observed when animals have been exposed to water-soluble fullerenes at therapeutic concentrations.

3.4.2 CNS Injury Protection

In order to test whether water-soluble fullerenes could be potential agents against the treatment of *Parkinson's* disease and other CNS degenerative diseases related to neuronal apoptosis, the protective effects of water-soluble fullerene derivatives **1** and **6–8** on 6-hydroxydopamine-induced apoptosis of CNS dopaminergic neurons (Silva et al., 2005) in developing zebrafish were investigated. It was demonstrated that **1**, **6** and **7** were able to protect 42%, 47% and 23%, respectively of total CNS neurons, whereas **1**, **6** and **8** blocked each with 60%, 100% and 60% of specific dopaminergic neuronal death in the diencephalon as it is exemplarily shown for **8** in Fig. 3.8.

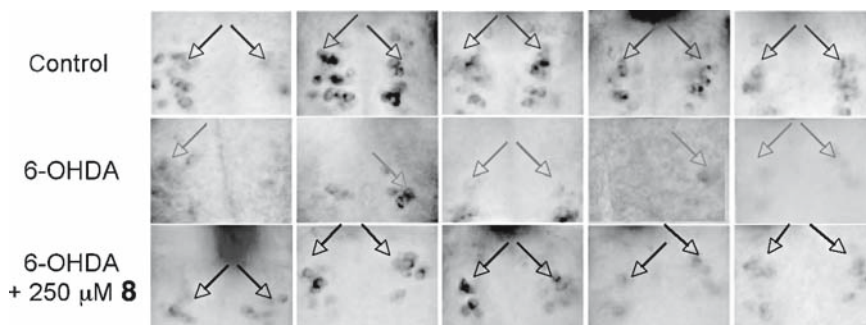


Fig. 3.8 Protection of central nervous system (CNS) dopaminergic neurons from 6-OHDA-induced apoptosis by **8**. Untreated (*top*), 6-OHDA plus vehicle treatment (*middle*) and 6-OHDA plus $250\mu\text{M}$ **8** (*down*) were stained with anti-tyrosine hydroxylase antibody. The number of TH-immunoreactive cells clustered in diencephalons was examined (*arrows*). After $250\mu\text{M}$ **8** treatment, three of five animals showed a normal number of TH-immunoreactive cells with normal morphology (Reprinted from Beuerle, 2007. With friendly permission of Taylor & Francis, <http://www.informaworld.com>)

3.4.3 Blocking Developmental Apoptosis

Fullerene derivatives appear to act both *in vitro* and *in vivo* by effectively blocking apoptotic cell death in the presence of known chemical, biological and physical toxins, and it would be interesting to evaluate if these derivatives can also block apoptosis occurring during embryonic development. For verification zebrafish embryos were exposed to **1**, **1-tris**, **6** and **7** for 5 days post-fertilization and after staining with acridine orange apoptotic cells were detected. As depicted in Fig. 3.9, **1** and **7** showed

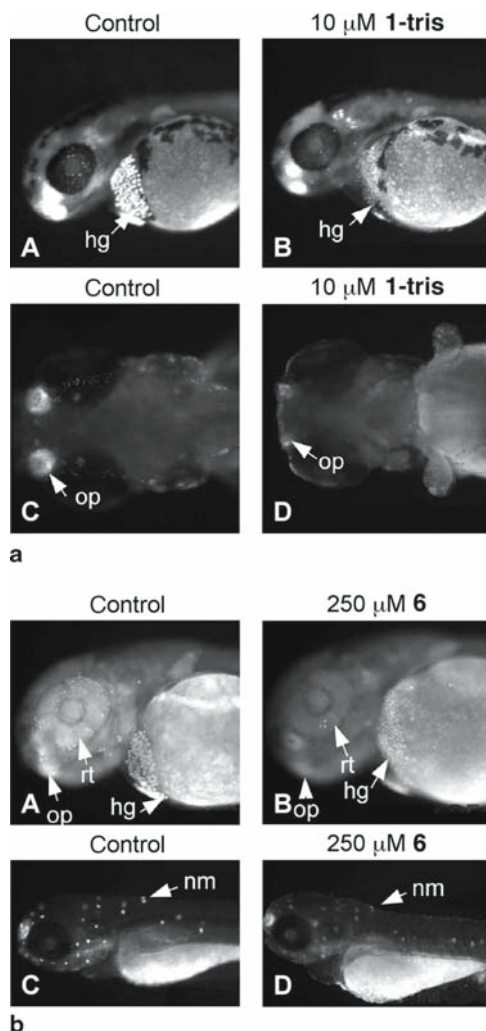


Fig. 3.9 Inhibition of normal apoptosis by **1-tris** and **6** in zebrafish embryos. (a) 10 μM **1-tris** caused decreased apoptosis in the hg at 2 dpf (B) and op at 4 dpf (D). (b) 250 μM **6** decreased apoptosis in the hg, op and rt at 2 dpf (B) and nm at 5 dpf (D) (Reprinted from Beuerle, 2007. With friendly permission of Taylor & Francis, <http://www.informaworld.com>)

little or no blocking effects on embryogenesis-associated apoptosis, whereas **1-tris** and **6** reduced the number of positively stained cells in hatching glands (hg) and olfactory pits (op) (**1-tris** and **6**) as well as retina (rt) and neuromast cells (nm) (**6** only).

3.4.4 Mechanoreceptor Hair Cell Protection

Because of their morphological similarity to outer hair cells of the inner ear in mammals, the dorsal mechanoreceptor hair cells of zebrafish embryos are excellent model systems for investigations on protective effects of drug candidates on multiple factor-induced hair cell apoptosis. Through specific staining using (2-(4-dimethyl-aminostyryl)-*N*-ethyl pyridinium iodide (DASPEI) the number of viable hair cells in the transparent zebrafish embryos can be tracked visually. As chemical toxins causing apoptotic cell death cisplatin, an effective chemotherapy agent inducing cell death most likely by direct DNA damage and gentamicin as a well-known aminoglycoside antibiotic were used.

Figure 3.10 shows the protection of zebrafish embryo hair cells by various water-soluble fullerene derivatives. The data for both gentamicin- and cisplatin-induced apoptotic cell death are summarized in Table 3.3. Comparing the data for

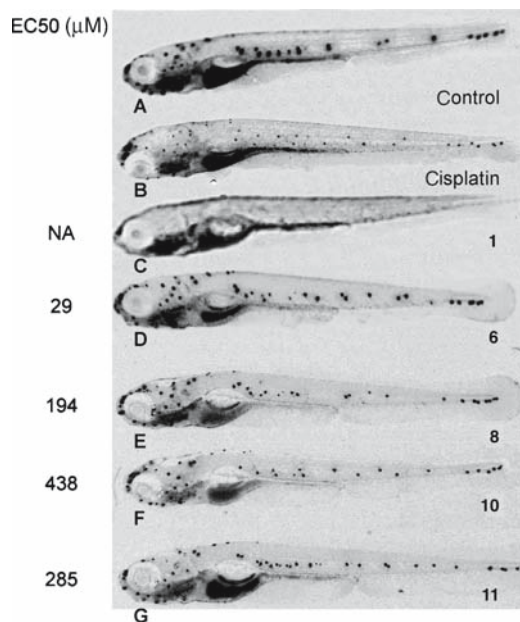


Fig. 3.10 Protection of hair cells from cisplatin damage by **1**, **6**, **8**, **10** and **11** (Reprinted from Beuerle, 2007. With friendly permission of Taylor & Francis, <http://www.informaworld.com>)

Table 3.3 EC₅₀ values for hair cell protection against cisplatin and gentamicin (Beuerle, 2007)

Compound	EC ₅₀ (μM) gentamicin	EC ₅₀ (μM) cisplatin
1	34	5% at 500 μM
3	78	ND
4	61	ND
6	128	29
7	98	ND
8	29	194
9	35	ND
10	124	438
11	47	285
Glutathione	438	ND

both chemical toxins, compounds **1** and **6** show surprisingly high differences in protection activity against cisplatin or gentamicin causing morphologically indistinguishable hair cell damage in zebrafish embryos. Compounds **1**, **3**, **4** and **8**, **9** and **11** are most effective in protecting against gentamicin-induced hair cell apoptosis with EC₅₀ values of 34, 78, 61, 29, 35 and 47 μM, respectively, but exhibit only moderate to poor protecting activity against cisplatin-induced cell death like **8** (EC₅₀ = 194 μM), **10** (EC₅₀ = 438 μM) and **11** (EC₅₀ = 285 μM) or even no activity in the case of **1** (less than 5% protection at 500 μM). Significantly higher EC₅₀ values in the gentamicin assays were instead observed for **6**, **7** and **10** with 128, 98 and 124 μM, respectively, but **6** shows excellent protection against cisplatin-induced hair cell damage with an IC₅₀ value of 29 μM.

Compared to glutathione (EC₅₀ = 438 μM), a reliable antioxidant, which has been successfully used in animal models to protect against aminoglycoside-induced hearing loss, all tested fullerene derivatives are at least three- to fourfold more effective in blocking the gentamicin-induced hair cell loss.

Summarizing these observations, there is some evidence that neuroprotective activity of derivatized fullerenes may occur via multiple quenching mechanisms and do not follow a monolithic pathway. Because of the undeniable differences in binding sites and chemical reactivities between gentamicin and cisplatin the differential activities of fullerenes for protecting against these two chemical toxins may reflect the inherent structural differences between the various fullerenes. Factors as intracellular localization, aggregation behaviour, chemical reactivity or possible interactions with cellular biomolecules may greatly influence any neuroprotective activity of these diverse fullerene structures. Especially, compounds such as **8**, which tend to protect in different ways against oxidative stress are very promising candidates for anti-apoptosis drugs.

3.5 Conclusion and Outlook

Within the first years of fullerene chemistry scientists working on this fascinating and fast developing field were mainly focusing on the development of new reactions and investigations of the unique structural and chemical properties of this kind of new *all*-carbon allotropes. It was soon recognized that these novel molecular structures may offer promising candidates for a plurality of applications in various fields ranging from material sciences to biomedicine. So in recent years the attention has more and more shifted to the design and optimization of suitable molecular architectures in order to promote fullerenes and their derivatives from subjects of pure academic interest to auspicious candidates for profitable applications. In this context up to now a great variety of most diverse water-soluble fullerene structures have been synthesized allowing an auspicious combination of the unique structural properties of fullerenes and all aspects of aqueous chemistry as, for example, bioavailability. To date, a huge library of water-soluble fullerene derivatives with a great structural diversity has been synthesized and characterized allowing a fine-tuning of different structural attributes like net charge, aggregation behaviour, hydrophilic–lipophilic balance, electronic structure, redox activity and more. Through specific modification of these inherent properties new materials and lead compounds will be tailored for specified applications.

Many of these water-soluble fullerene-based architectures have been assessed in both *in vitro* and *in vivo* studies to investigate their antioxidant activities and their potential use as neuroprotective agents in pharmacological applications. Most of these novel fullerene derivatives show excellent scavenging activities against a number of reactive oxygen species, which are known to be the predominant elicitors for oxidative stress within mammals and humans. Although there is strong evidence that antioxidant activity is an intrinsic property of fullerenes and related structures, the actual mechanisms of radical scavenging and neuroprotection are still unclear and need further evaluation using more precisely defined model systems.

More recent *in vivo* investigations suggest that fullerene structures may act on multiple pathways in protecting living systems against oxidative stress. Even though, understanding these complex and incompletely understood processes is just in its infancy. In the near future, both the design and the synthesis of new water-soluble fullerene derivatives are likely to focus on specific antioxidant and cytoprotective activities. At this point, it is not completely clear how the cytoprotective activities of various fullerenes relate to their antioxidant activities, if at all. Even 20 years after their discovery, the chemistry of these unique carbon nanomaterials is a still very fascinating and challenging task.

References

- Ali SS, Hardt JI, Quick KL, Sook Kim-Han J, Erlanger BF, Huang T-T, Epstein CJ, Dugan LL (2004) A biologically effective fullerene (C₆₀) derivative with superoxide dismutase mimetic properties. *Free Radic. Biol. Med.* 37: 1191–1202.

- Andersson T, Nilsson K, Sundahl M, Westman G, Wennerstroem O (1992) C₆₀ embedded in gamma-cyclodextrin: a water-soluble fullerene. *Chem. Commun.* 604–606.
- Angelini G, Cusan C, De Maria P, Fontana A, Maggini M, Pierini M, Prato M, Schergna S, Villani C (2005) The associative properties of some amphiphilic fullerene derivatives. *Eur. J. Org. Chem.* 1884–1891.
- Bensasson RV, Brettreich M, Frederiksen J, Gottinger H, Hirsch A, Land EJ, Leach S, McGarvey DJ, Schonberger H (2000) Reactions of e_{aq}⁻, CO₂^{•-}, HO[•], O₂^{•-} and O₂(¹Δ_g) with a dendro[60]fullerene and C₆₀[C(COOH)₂]_n (n = 2–6). *Free Radic. Biol. Med.* 29: 26–33.
- Beuerle F, Chronakis N, Hirsch A (2005) Regioselective synthesis and zone selective deprotection of [60]fullerene tris-adducts with an e,e,e addition pattern. *Chem. Commun.* 3676–3678.
- Beuerle F, Witte P, Hartnagel U, Lebovitz R, Parnig C, Hirsch A (2007) Cytoprotective activities of water-soluble fullerenes in zebrafish models. *J. Exp. Nanosci.* 2: 147–170.
- Bingel C (1993) Cyclopropanation of fullerenes. *Chem. Ber.* 126: 1957–1959.
- Bisaglia M, Natalini B, Pellicciari R, Straface E, Malorni W, Monti D, Franceschi C, Schettini G (2000) C₃-fullero-tris-methanodicarboxylic acid protects cerebellar granule cells from apoptosis. *J. Neurochem.* 74: 1197–1204.
- Bosi S, Da Ros T, Castellano S, Banfi E, Prato M (2000) Antimycobacterial activity of ionic fullerene derivatives. *Bioorg. Med. Chem. Lett.* 10: 1043–1045.
- Bosi S, Feruglio L, Milic D, Prato M (2003) Synthesis and water solubility of novel fullerene bisadduct derivatives. *Eur. J. Org. Chem.* 4741–4747.
- Braun M, Atalick S, Galdi Dirk M, Lanig H, Brettreich M, Burghardt S, Hatzimarinaki M, Ravanelli E, Prato M, Van Eldik R, Hirsch A (2003) Electrostatic Complexation and Photoinduced Electron Transfer between Zn-Cytochrome c and Polyanionic Fullerene Dendrimers. *Chem. Eur. J.* 9: 3867–3875.
- Brettreich M, Hirsch A (1998) A highly water-soluble dendro[60]fullerene. *Tetrahedron Lett.* 39: 2731–2734.
- Brettreich M (2003) 2000 Ph.D. thesis, Friedrich Alexander University Erlangen Nuremberg.
- Cassell AM, Asplund CL, Tour JM (1999) Self-assembling supramolecular nanostructures from a C₆₀ derivative: Nanorods and vesicles. *Angew. Chem. Int. Ed.* 38: 2403–2405.
- Chen Y-W, Hwang KC, Yen C-C, Lai Y-L (2004) Fullerene derivatives protect against oxidative stress in RAW 264.7 cells and ischemia-reperfused lungs. *Am. J. Physiol.* 287: R21–R26.
- Chi Y, Bhonsle JB, Canteenwala T, Huang J-P, Shiea J, Chen B-J, Chiang LY (1998) Novel water-soluble hexakis(4-sulfobutyl)fullerenes as potent free radical scavengers. *Chem. Lett.* 465–466.
- Chi Y, Canteenwala T, Chen HHC, Jeng US, Lin T-L, Chiang LY (2002) Free radical scavenging and photodynamic functions of micelle-like hydrophilic hexa(sulfobutyl)fullerene (FC4S). *Perspect. Fullerene Nanotechnol.* 165–183.
- Chiang LY, Lu F-J, Lin J-T (1995) Free radical scavenging activity of water-soluble fullerenols. *Chem. Commun.* 1: 1283–1284.
- Chiang LY, Bhonsle JB, Wang L, Shu SF, Chang TM, Hwu JR (1996) Efficient one-flask synthesis of water-soluble [60]fullerenols. *Tetrahedron* 52: 4963–4972.
- Cusan C, Da Ros T, Spalluto G, Foley S, Janot J-M, Seta P, Larroque C, Tomasini MC, Antonelli T, Ferraro L, Prato M (2002) A new multi-charged C₆₀ derivative: synthesis and biological properties. *Eur. J. Org. Chem.* 2928–2934.
- Da Ros T, Prato M, Novello F, Maggini M, Banfi E (1996) Easy Access to Water Soluble Fullerene Derivatives via 1,3-Dipolar Cycloadditions of Azomethine Ylides to C₆₀. *J. Org. Chem.* 61: 9070–9072.
- Da Ros T, Prato M (1999) Medicinal chemistry with fullerenes and fullerene derivatives. *Chem. Commun.* 663–669.
- Daroczi B, Kari G, McAleer MF, Wolf JC, Rodeck U, Dicker AP (2006) In vivo radioprotection by the fullerene nanoparticle DF-1 as assessed in a zebrafish model. *Clin. Cancer Res.* 12: 7086–7091.
- de La Vaissiere B, Sandall JPB, Fowler PW, de Oliveira P, Bensasson RV (2001) Regioselectivity in radical reactions of C₆₀ derivatives. *J. Chem. Soc. Perkin Trans.* 2: 821–823.

- Dugan LL, Sensi SL, Canzoniero LMT, Handran SD, Rothman SM, Lin TS, Goldberg MP, Choi DW (1995) Mitochondrial production of reactive oxygen species in cortical neurons following exposure to N-methyl-D-aspartate. *J. Neurosci.* 15: 6377–6388.
- Dugan LL, Turetsky DM, Du C, Lobner D, Wheeler M, Almlri CR, Shen CK, Luh TY, Choi DW, Lin TS (1997) Carboxyfullerenes as neuroprotective agents. *Proc. Natl. Acad. Sci. USA* 94: 9434–9439.
- Dugan LL, Lovett EG, Quick KL, Lotharius J, Lin TT, O'Malley KL (2001) Fullerene-based antioxidants and neurodegenerative disorders. *Parkinsonism Relat. Disord.* 7: 243–246.
- Echegoyen L, Echegoyen LE (1998) Electrochemistry of Fullerenes and Their Derivatives. *Acc. Chem. Res.* 31: 593–601.
- Faulkner KM, Liochev SI, Fridovich I (1994) Stable Mn(III) porphyrins mimic superoxide dismutase in vitro and substitute for it in vivo. *J. Biol. Chem.* 269: 23471–23476.
- Foley S, Crowley C, Smaih M, Bonfils C, Erlanger BF, Seta P, Larroque C (2002) Cellular localization of a water-soluble fullerene derivative. *Biochem. Biophys. Res. Commun.* 294: 116–119.
- Fumelli C, Marconi A, Salvioli S, Straface E, Malorni W, Offidani AM, Pellicciari R, Schettini G, Giannetti A, Monti D, Franceschi C, Pincelli C (2000) Carboxyfullerenes protect human keratinocytes from ultraviolet-B-induced apoptosis. *J. Invest. Dermatol.* 115: 835–841.
- Gharbi N, Pressac M, Hadchouel M, Szwarc H, Wilson SR, Moussa F (2005) [60]Fullerene is a Powerful Antioxidant in Vivo with No Acute or Subacute Toxicity. *Nano Lett.* 5: 2578–2585.
- Giacalone F, Martin N (2006) Fullerene Polymers: Synthesis and Properties. *Chem. Rev.* 106: 5136–5190.
- Guldi DM, Prato M (2000) Excited-State Properties of C_{60} Fullerene Derivatives. *Acc. Chem. Res.* 33: 695–703.
- Gun'kin IF, Tseluikin VN, Loginova NY (2006) Synthesis and properties of water-soluble derivatives of fullerene C_{60} . *Russ. J. Appl. Chem.* 79: 1001–1004.
- Herrmann A, Ruettimann M, Thilgen C, Diederich F (1995) Multiple cyclopropanations of C_{70} . Synthesis and characterization of bis-, tris-, and tetrakis-adducts and chiroptical properties of bis-adducts with chiral addends, including a recommendation for the configurational description of fullerene derivatives with a chiral addition pattern. *Helv. Chim. Acta* 78: 1673–1704.
- Hirsch A, Lamparth I, Karfunkel HR (1994) Fullerene chemistry in three dimensions: isolation of seven regioisomeric bisadducts and chiral trisadducts from C_{60} and bis(ethoxycarbonyl)methylene. *Angew. Chem. Int. Ed. Engl.* 33: 437–438.
- Hirsch A, Brettreich M (2005) Fullerenes – Chemistry and Reactions. Wiley-VCH Verlag, Weinheim.
- Hu Z, Guan WC, Tang XY, Huang LZ, Xu H (2007) Synthesis of water-soluble cystine C_{60} derivative with catalyst and its active oxygen radical scavenging ability. *Chin. Chem. Lett.* 18: 51–54.
- Huang SS, Tsai SK, Chih CL, Chiang LY, Hsieh HM, Teng CM, Tsai MC (2001) Neuroprotective effect of hexasulfobutylated C_{60} on rats subjected to focal cerebral ischemia. *Free Radic. Biol. Med.* 30: 643–649.
- Huang YL, Shen CK, Luh TY, Yang HC, Hwang KC, Chou CK (1998) Blockage of apoptotic signaling of transforming growth factor-beta in human hepatoma cells by carboxyfullerene. *Eur. J. Biochem.* 254: 38–43.
- Illscas BM, Martinez-Alvarez R, Fernandez-Gadea J, Martin N (2003) Synthesis of water soluble fulleropyrrolidines bearing biologically active arylpiperazines. *Tetrahedron* 59: 6569–6577.
- Jeng US, Lin TL, Chang TS, Lee HY, Hsu CH, Hsieh YW, Canteenwala T, Chiang LY (2001) Comparison of the aggregation behavior of water-soluble hexa(sulfobutyl)fullerenes and polyhydroxylated fullerenes for their free-radical scavenging activity. *Prog. Colloid Polym. Sci.* 118: 232–237.
- Kato H, Boettcher C, Hirsch A (2007) Sugar balls: synthesis and supramolecular assembly of [60]fullerene. *Eur. J. Org. Chem.* 2659–2666.

- Kiritoshi S, Nishikawa T, Sonoda K, Kukidome D, Senokuchi T, Matsuo T, Matsumura T, Tokunaga H, Brownlee M, Araki E (2003) Reactive oxygen species from mitochondria induce cyclooxygenase-2 gene expression in human mesangial cells: potential role in diabetic nephropathy. *Diabetes* 52: 2570–2577.
- Kordatos K, Bosi S, Da Ros T, Zambon A, Lucchini V, Prato M (2001) Isolation and characterization of all eight bisadducts of fulleropyrrolidine derivatives. *J. Org. Chem.* 66: 2802–2808.
- Kraetschmer W, Lamb LD, Fostiropoulos K, Huffman DR (1990) Solid C_{60} : a new form of carbon. *Nature* 347: 354–358.
- Kroto HW, Heath JR, O'Brien SC, Curl RF, Smalley RE (1985) C_{60} : buckminsterfullerene. *Nature* 318: 162–163.
- Krusic PJ, Wasserman E, Keizer PN, Morton JR, Preston KF (1991) Radical reactions of C_{60} . *Science* 254: 1183–1185.
- Kunsagi-Mate S, Szabo K, Bitter I, Nagy G, Kollar L (2004) Complex formation between water-soluble sulfonated calixarenes and C_{60} fullerene. *Tetrahedron Lett.* 45: 1387–1390.
- Lafon-Cazal M, Pietri S, Culcasi M, Bockaert J (1993) NMDA-dependent superoxide production and neurotoxicity. *Nature* 364: 535–537.
- Lai HS, Chen WJ, Chiang LY (2000a) Free radical scavenging activity of fullerol on the ischemia-reperfusion intestine in dogs. *World J. Surg.* 24: 450–454.
- Lai HS, Chen Y, Chen WJ, Chang KJ, Chiang LY (2000b) Free radical scavenging activity of fullerol on grafts after small bowel transplantation in dogs. *Transplantation Proc.* 32: 1272–1274.
- Lamparth I, Hirsch A (1994) Water-soluble malonic acid derivatives of C_{60} with a defined three-dimensional structure. *Chem. Commun.* 1727–1728.
- Lee YT, Chiang LY, Chen WJ, Hsu HC (2000) Water-soluble Hexasulfobutyl[60]fullerene inhibit low-density lipoprotein oxidation in aqueous and lipophilic phases. *C. Proc. Soc. Exp. Biol. Med.* 224: 69–75.
- Lin AM, Chyi BY, Wang SD, Yu HH, Kanakamma PP, Luh TY, Chou CK, Ho LT (1999) Carboxyfullerene prevents iron-induced oxidative stress in rat brain. *J. Neurochem.* 72: 1634–1640.
- Lin AM, Fang SF, Lin SZ, Chou CK, Luh TY, Ho LT (2002) Local carboxyfullerene protects cortical infarction in rat brain. *Neurosci. Res.* 43: 317–321.
- Lin HS, Lin TS, Lai RS, D'Rosario T, Luh TY (2001) Fullerenes as a new class of radioprotectors. *Int. J. Radiat. Biol.* 77: 235–239.
- Lotharius J, Dugan LL, O'Malley KL (1999) Distinct mechanisms underlie neurotoxin-mediated cell death in cultured dopaminergic neurons. *J. Neurosci.* 19: 1284–1293.
- Maggini M, Scorrano G, Prato M (1993) Addition of azomethine ylides to C_{60} : synthesis, characterization, and functionalization of fullerene pyrrolidines. *J. Am. Chem. Soc.* 115: 9798–9799.
- Marchesan S, Da Ros T, Prato M (2005) Isolation and characterization of nine tris-adducts of N-methylfulleropyrrolidine derivatives. *J. Org. Chem.* 70: 4706–4713.
- Mashino T, Okuda K, Hirota T, Hirobe M, Nagano T, Mochizuki M (1999) Inhibition of *E. coli* growth by fullerene derivatives and inhibition mechanism. *Bioorg. Med. Chem. Lett.* 9: 2959–2962.
- McCord JM, Fridovich I (1969) Superoxide dismutase. Enzymic function for erythrocyte (hemocuprein). *J. Biol. Chem.* 244: 6049–6055.
- McEwen CN, McKay RG, Larsen BS (1992) C_{60} as a radical sponge. *J. Am. Chem. Soc.* 114: 4412–4414.
- Mirkov SM, Djordjevic AN, Andric NL, Andric SA, Kostic TS, Bogdanovic GM, Vojinovic-Miloradov MB, Kovacevic RZ (2004) Nitric oxide-scavenging activity of polyhydroxylated fullerol, $C_{60}(OH)_{24}$. *Nitric Oxide* 11: 201–207.
- Monti D, Moretti L, Salvioi S, Straface E, Malorni W, Pellicciari R, Schettini G, Bisaglia M, Pincelli C, Fumelli C, Bonafe M, Franceschi C (2000) C_{60} carboxyfullerene exerts a protective

- activity against oxidative stress-induced apoptosis in human peripheral blood mononuclear cells. *Biochem. Biophys. Res. Commun.* 277: 711–717.
- Murthy CN, Geckeler KE (2001) The water-soluble beta-cyclodextrin-[60]fullerene complex. *Chem. Commun.* 1194–1195.
- Nakamura E, Isobe H (2003) Functionalized Fullerenes in Water. The First 10 Years of Their Chemistry, Biology, and Nanoscience. *Acc. Chem. Res.* 36: 807–815.
- Okuda K, Mashino T, Hirobe M (1996) Superoxide radical quenching and cytochrome C peroxidase-like activity of C_{60} -dimalonic acid, $C_{62}(\text{COOH})_4$. *Bioorg. Med. Chem. Lett.* 6: 539–542.
- Okuda K, Hirota T, Hirobe M, Nagano T, Mochizuki M, Mashino T (2000) Synthesis of various water-soluble C_{60} derivatives and their superoxide-quenching activity. *Fullerene Sci. Technol.* 8: 89–104.
- Pellarini F, Pantarotto D, Da Ros T, Giangaspero A, Tossi A, Prato M (2001) A novel [60]fullerene amino acid for use in solid-phase peptide synthesis. *Org. Lett.* 3: 1845–1848.
- Periya VK, Koike I, Kitamura Y, Iwamatsu S-I, Murata S (2004) Hydrophilic [60]fullerene carboxylic acid derivatives retaining the original 60 π electronic system. *Tetrahedron Lett.* 45: 8311–8313.
- Reuther U, Brandmüller T, Donaubaue W, Hampel F, Hirsch A (2002) A highly regioselective approach to multiple adducts of C_{60} governed by strain minimization of macrocyclic malonate addends. *Chem. Eur. J.* 8: 2261–2273.
- Reynolds JJ, Hastings TG (1995) Glutamate induces the production of reactive oxygen species in cultured forebrain neurons following NMDA receptor activation. *J. Neurosci.* 15: 3318–3327.
- Rieger JM, Shah AR, Gidday JM (2002) Ischemia-reperfusion injury of retinal endothelium by cyclooxygenase- and xanthine oxidase-derived superoxide. *Exp. Eye Res.* 74: 493–501.
- Riley DP (1999) Functional mimics of superoxide dismutase enzymes as therapeutic agents. *Chem. Rev.* 99: 2573–2587.
- Rio Y, Nierengarten J-F (2002) Water soluble supramolecular cyclotrimeratrylene-[60]fullerene complexes with potential for biological applications. *Tetrahedron Lett.* 43: 4321–4324.
- Scrivens WA, Tour JM, Creek KE, Pirisi L (1994) Synthesis of ^{14}C -Labeled C_{60} , Its Suspension in Water, and Its Uptake by Human Keratinocytes. *J. Am. Chem. Soc.* 116: 4517–4518.
- Silva RM, Ries V, Oo TF, Yarygina O, Jackson-Lewis V, Ryu EJ, Lu PD, Marciniak SJ, Ron D, Przedborski S, Kholodilov N, Greene LA, Burke RE (2005) CHOP/GADD153 is a mediator of apoptotic death in substantia nigra dopamine neurons in an in vivo neurotoxin model of parkinsonism. *J. Neurochem.* 95: 974–986.
- Straface E, Natalini B, Monti D, Franceschi C, Schettini G, Bisaglia M, Fumelli C, Pincelli C, Pellicciari R, Malorni W (1999) C_3 -fullero-tris-methanodicarboxylic acid protects epithelial cells from radiation-induced anoikia by influencing cell adhesion ability. *FEBS Lett.* 454: 335–340.
- Sun T, Jia ZS, Chen WX, Jin YX, Zhu DX (2001) Active oxygen radical scavenging ability of water-soluble beta-alanine C_{60} adducts. *Chin. Chem. Lett.* 12: 997–1000.
- Sun T, Xu Z (2006) Radical scavenging activities of alpha-alanine C_{60} adduct. *Bioorg. Med. Chem. Lett.* 16: 3731–3734.
- Troshina OA, Troshin PA, Peregudov AS, Kozlovskiy VI, Balzarini J, Lyubovskaya RN (2007) Chlorofullerene $C_{60}\text{Cl}_6$: a precursor for straightforward preparation of highly water-soluble polycarboxylic fullerene derivatives active against HIV. *Org. Biomol. Chem.* 5: 2783–2791.
- Tsao N, Luh TY, Chou CK, Wu JJ, Lin YS, Lei HY (2001) Inhibition of group A streptococcus infection by carboxyfullerene. *Antimicrob. Agents Chemother.* 45: 1788–1793.
- Tsao N, Luh TY, Chou CK, Chang TY, Wu JJ, Liu CC, Lei HY (2002) In vitro action of carboxyfullerene. *J. Antimicrob. Chemother.* 49: 641–649.
- Tzeng SF, Lee JL, Kuo JS, Yang CS, Murugan P, Ai Tai L, Chu Hwang K (2002) Effects of malonate C_{60} derivatives on activated microglia. *Brain Res.* 940: 61–68.

- Wang IC, Tai LA, Lee DD, Kanakamma PP, Shen CK, Luh TY, Cheng CH, Hwang KC (1999) C₆₀ and water-soluble fullerene derivatives as antioxidants against radical-initiated lipid peroxidation. *J. Med. Chem.* 42: 4614–4620.
- Witte P, Beuerle F, Hartnagel U, Lebovitz R, Savouchkina A, Sali S, Guldi D, Chronakis N, Hirsch A (2007) Water solubility, antioxidant activity and cytochrome C binding of four families of exohedral adducts of C(60) and C(70). *Org. Biomol. Chem.* 5: 3599–3613.
- Wolff DJ, Mialkowski K, Richardson CF, Wilson SR (2001) C₆₀-fullerene monomalonate adducts selectively inactivate neuronal nitric oxide synthase by uncoupling the formation of reactive oxygen intermediates from nitric oxide production. *Biochemistry* 40: 37–45.
- Xiao L, Takada H, Maeda K, Haramoto M, Miwa N (2005) Antioxidant effects of water-soluble fullerene derivatives against ultraviolet ray or peroxy lipid through their action of scavenging the reactive oxygen species in human skin keratinocytes. *Biomed. Pharmacother.* 59: 351–358.
- Yang DY, Wang MF, Chen IL, Chan YC, Lee MS, Cheng FC (2001) Systemic administration of a water-soluble hexasulfonated C₆₀ reduces cerebral ischemia-induced infarct volume in gerbils. *Neurosci. Lett.* 311: 121–124.
- Yang J, Alemany LB, Driver J, Hartgerink JD, Barron AR (2007) Fullerene-derivatized amino acids: synthesis, characterization, antioxidant properties, and solid-phase peptide synthesis. *Chem. Eur. J.* 13: 2530–2545.
- Zhong Y-W, Matsuo Y, Nakamura E (2006) Convergent synthesis of a polyfunctionalized fullerene by regioselective five-fold addition of a functionalized organocopper reagent to C₆₀. *Org. Lett.* 8: 1463–1466.

Chapter 4

Fullerenes as Photosensitizers in Photodynamic Therapy

Pawel Mroz^{1,2}, George P. Tegos^{1,2}, Hariprasad Gali³, Timothy Wharton³, Tadeusz Sarna⁴, and Michael R. Hamblin^{1,2,5*}

Abstract Fullerenes are a class of closed-cage nanomaterials made exclusively from carbon atoms. A great deal of attention has been focused on developing medical uses of these unique molecules especially when they are derivatized with functional groups to make them soluble and therefore able to interact with biological systems. Due to their extended π -conjugation they absorb visible light, have a high triplet yield and can generate reactive oxygen species (ROS) upon illumination, suggesting a possible role of fullerenes in photodynamic therapy (PDT). Depending on the functional groups introduced into the molecule, fullerenes can effectively photoinactivate either or both pathogenic microbial cells and malignant cancer cells. The mechanism appears to involve superoxide anion as well as singlet oxygen, and under the right conditions fullerenes may have advantages over clinically applied photosensitizers (PSs) for mediating photodynamic therapy of certain diseases.

Keywords Photodynamic therapy; Photosensitizer; Photochemistry; Reactive oxygen species; Cancer; Microorganism; Infection

4.1 Introduction

Fullerenes (originally buckminsterfullerenes) are a new class of carbon-only molecules; the first example discovered in 1985 (Kroto et al., 1985), being composed of 60 carbon atoms arranged in a soccer ball structure (C₆₀). The condensed aromatic

¹ Wellman Center for Photomedicine, Massachusetts General Hospital, Boston, MA, USA

² Department of Dermatology, Harvard Medical School, Boston, MA, USA

³ Lynntech Inc, College Station, TX, USA

⁴ Department of Biophysics, Jagiellonian University, Krakow, Poland

⁵ Harvard-MIT Division of Health Sciences and Technology, Cambridge, MA, USA

* Correspondence to: BAR 414, Wellman Center for Photomedicine, Massachusetts General Hospital, 40 Blossom Street, Boston, MA 02114, USA
Email: hamblin@helix.mgh.harvard.edu

rings present in the compound lead to an extended π -conjugated system of molecular orbitals and therefore to significant absorption of visible light. In recent years there has been much interest in studying possible biological activities of fullerenes (and other nanostructures produced in the nanotechnology revolution) with a view to using them in medicine (Bosi et al., 2003; Jensen et al., 1996; Tagmatarchis and Shinohara, 2001). Although pristine C_{60} can form nanocrystalline preparations that have been reported to have biological activity (Belgorodsky et al., 2006; Gharbi et al., 2005; Levi et al., 2006; Sayes et al., 2005), most workers have studied chemically modified or functionalized fullerenes that acquire solubility in water or biologically compatible solvents and thereby have increased versatility (Bagno et al., 2002; Martin et al., 2000; Nakamura and Isobe, 2003; Pantarotto et al., 2004).

Photodynamic therapy (PDT) is a rapidly advancing treatment for multiple diseases. It is based on the administration of a nontoxic drug or dye known as a photosensitizer (PS) either systemically, locally, or topically to a patient bearing a lesion (frequently, but not always cancer [Dolmans et al., 2003]), followed after some time by the illumination of the lesion with visible light, which activates the PS and, in the presence of oxygen, leads to the generation of cytotoxic reactive oxygen species (ROS) and consequently to cell death and tissue destruction (Castano et al., 2004, 2005). The light is absorbed by the PS molecule, and an electron is excited to the first excited singlet state. In addition to losing energy by fluorescence or internal conversion, the excited singlet can undergo the process known as intersystem crossing (*isc*) to the long-lived triplet state. The excited triplet state can then interact with ground-state molecular oxygen to form reactive oxygen species (ROS). This process may occur by

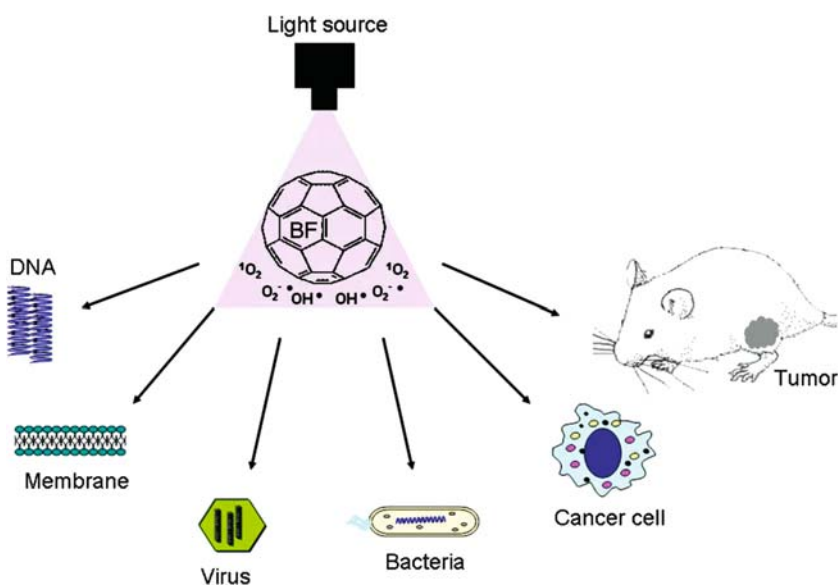


Fig. 4.1 Schematic outline of the possible applications of fullerenes as PDT sensitizers covered in this review (See Color Plates)

energy transfer from the triplet to produce singlet oxygen or by electron transfer to form superoxide anion (Castano et al., 2004). Reaction of singlet oxygen with biological molecules, such as proteins, unsaturated lipids and nucleic acids causing oxidative damage, is thought to be responsible for cell death, frequently occurring via the apoptosis pathway initiated by mitochondrial damage (Agostinis et al., 2004).

In this chapter we will cover the existing literature on fullerenes for PDT, summarize results from our laboratory and outline future possibilities concerning applications of fullerenes as PS for PDT. Figure 4.1 gives a schematic outline of the PDT applications that have been reported for fullerenes either pristine or functionalized with various solubilizing groups.

4.2 Photosensitizers

4.2.1 *Traditional Photosensitizers*

The majority of PS used, both clinically and experimentally, are derived from the tetrapyrrole aromatic nucleus found in many naturally occurring pigments such as heme (red), chlorophyll (green) and bacteriochlorophyll (blue) (Castano et al., 2004). Tetrapyrroles usually have a relatively large absorption band in the region of 400 nm known as the Soret band, and a set of progressively smaller absorption bands as the spectrum moves into the red wavelengths known as the Q-bands. Naturally occurring porphyrins are fully conjugated (non-reduced) tetrapyrroles and vary in the number and type of side groups particularly carboxylic acid groups (uroporphyrin has eight, coproporphyrin has four and protoporphyrin has two). Porphyrins have the longest wavelength absorption band in the region of 630 nm and it tends to be small. Chlorins are tetrapyrroles with the double bond in one pyrrole ring reduced. This means that the longest wavelength absorption band shifts to the region of 650–690 nm and increases severalfold in height; both these factors are highly desirable for PDT. Bacteriochlorins have two pyrrole rings with reduced double bonds, and this leads to the absorption band shifting even further into the red, and increasing even further in magnitude. Bacteriochlorins may turn out to be even more effective PS than chlorins, but with relatively few candidate molecules and some questions about the stability of these molecules upon storage this remains to be seen. There are a set of classical chemical derivatives generally obtained from naturally occurring porphyrins and chlorins that include such structures as purpurins, pheophorbides, pyropheophorbides, pheophytins, and phorbins, some of which have been studied (a few extensively) as PS for PDT.

Hematoporphyrin derivative or Photofrin was the first PS to be studied in detail. However, it proved highly frustrating for scientists who attempted to determine its chemical structure and to identify its components (Kessel, 1986, 1989b; Kessel and Thompson, 1987; Kessel et al., 1987a, b). There was significant variation between batches and attempts to fractionate it into its individual component molecules frequently yielded mixtures as complicated as the starting material (Kessel, 1982, 1989a).

Although there is good evidence for the presence of hematoporphyrin oligomers, it is uncertain whether they are predominantly ethers or esters, and whether the side chains are predominantly vinyl or hydroxy ethyl groups (Kessel, 1986). When these uncertainties were combined with other significant deficiencies of the preparation, enthusiasm for its widespread use was decreased. These deficiencies include a long-lasting skin photosensitivity so that patients may have to avoid sunlight for as long as 8 weeks, the lack of a reasonably sized absorption band $>650\text{ nm}$, and the fact that its tumor-localizing properties were not as pronounced or as predictable as first thought. These considerations spurred a large effort amongst organic chemists to develop novel PS that could in theory be candidates for mediating PDT. The net results of this effort are publications describing hundreds of compounds and it can be bewildering to try to choose among them.

A second widely studied structural group of PS is the phthalocyanines (PC), and to a lesser extent, their related cousins, the naphthalocyanines. Again, their longest absorption band is in $>650\text{ nm}$ and usually has a respectable magnitude. As can be imagined the presence of four phenyl groups (or even worse four naphthyl groups) causes solubility and aggregation problems. PCs are frequently prepared with sulfonic acid groups to provide water solubility and with centrally coordinated metal atoms. It was found that the asymmetrically substituted di-sulfonic acids acted as the best PS (compared to mono-, symmetrically di-, tri-, and tetra-substituted sulfonic acids) in both the zinc (Fingar et al., 1993) and aluminum (Peng et al., 1990) series of PC derivatives.

Another broad class of potential PS includes completely synthetic, non-naturally occurring, conjugated pyrrolic ring systems. These comprise such structures as texaphyrins (Detty et al., 2004), porphycenes (Szeimies et al., 1996), and sapphyrins (Kral et al., 2002). A last class of compounds that have been studied as PS are non-tetrapyrrole-derived naturally occurring pigments or synthetic dyes. Examples of the first group are hypericin (from St Johns wort) (Agostinis et al., 2002) and from the second group are toluidine blue O (Stockert et al., 1996) and Rose Bengal (Bottiroli et al., 1997). As yet these compounds have perhaps been more often studied as agents to mediate antimicrobial photoinactivation (Hamblin and Hasan, 2004) rather than as PS designed to kill mammalian cells for applications such as cancer.

The tetrapyrrole nucleus frequently holds a co-coordinated metal atom, but it has been found that only diamagnetic metals such as Zn, Pd, In, Sn, and Lu allow the tetrapyrrole to retain its photosensitizing ability, while paramagnetic metals such as Fe, Cu, and Gd do not (Rosenthal et al., 1986). Many of these compounds are lipophilic and some are even insoluble in water. These compounds must either be delivered in an emulsion or else incorporated in liposomes.

4.2.2 Fullerene C_{60} as a Photosensitizer

The discovery of fullerenes (Kroto et al., 1985) in 1985, and the subsequent development of synthetic methods for the preparation of large-scale quantities of the allotropes of carbon (Krätschmer et al., 1990), has generated considerable interest

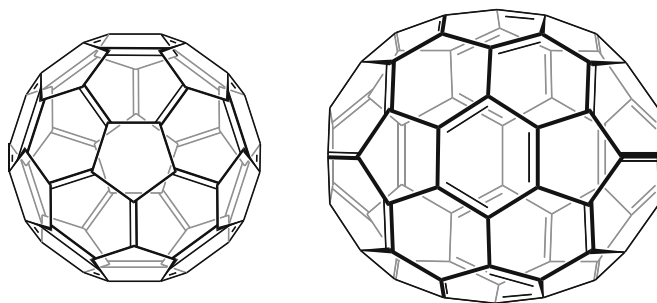


Fig. 4.2 Structures of typical fullerenes C_{60} (2A) and C_{70} (2B)

and opened a whole new field of carbon chemistry. Fullerenes are defined as closed-cage polyhedrons made up entirely of sp^2 -hybridized carbon atoms that contain exactly 12 pentagonal faces (known as Euler's theorem) and $(n/2-10)$ hexagonal faces where n is the number of carbon atoms (n must be even and greater than 20). The soccer ball-shaped fullerene C_{60} is shown in Fig. 4.2A. It is the most abundant fullerene that is produced during the graphite combustion production of the materials, followed by C_{70} (Fig. 4.2B). Among the interesting properties exhibited by C_{60} is its ability to form a long-lived excited triplet state after light excitation of the ground state that can then generate reactive oxygen species from molecular oxygen.

C_{60} is also a highly versatile synthetic scaffold that can easily be functionalized by the methods of synthetic organic chemistry. The formation of C_{60} derivatives (i.e., covalently modified C_{60}) nearly always involves the addition of a functional group (addend) across one or more of its 30 double bonds. When only one addend is attached, the fullerene derivative is called a monoadduct, with two, a bisadduct, etc. The ability to sensitize molecular oxygen in the presence of visible light is retained in the simple derivatives of C_{60} (i.e., mono-, bis-, and trisadducts).

Although it has been suggested for some time that fullerenes could potentially be useful as PS in PDT, relatively little research has appeared in the literature. Most of the articles are either purely theoretical or involve only photochemical studies (no biological studies on cells) (Belousova et al., 2005; Burlaka et al., 2004; Davydenko et al., 2006; Yu et al., 2005a, b).

4.3 Photophysics of PS

Figure 4.3 graphically illustrates the processes of light absorption and energy transfer that are at the heart of PDT in a depiction that has become to be known as a Jablonsky diagram. The ground-state PS has two electrons with opposite spins (this is known as singlet state) in the low-energy molecular orbital. Following the absorption of light (photons), one of these electrons is boosted into a high-energy orbital but keeps its spin (first excited singlet state). This is a short-lived (nanoseconds) species

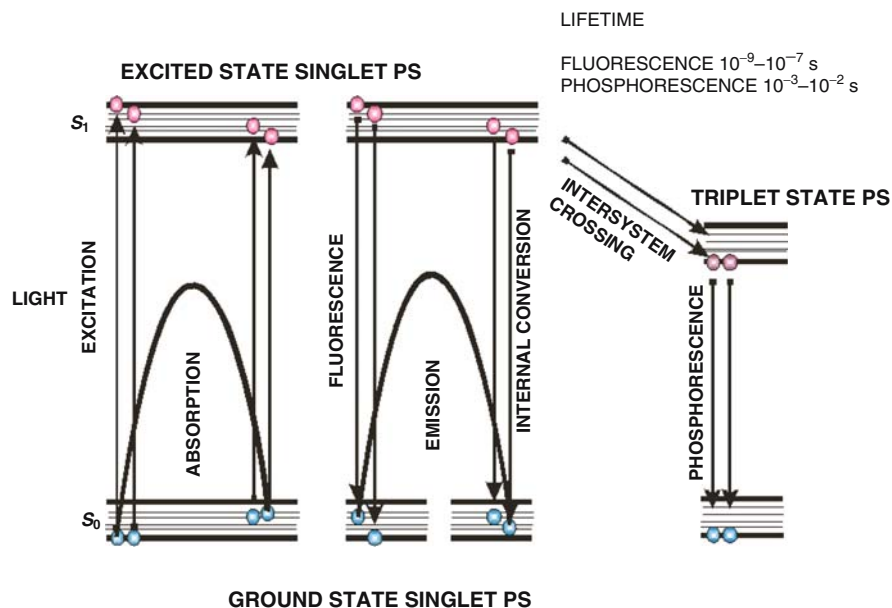


Fig. 4.3 Jablonsky diagram illustrating absorption of a photon by the ground-state singlet photo-sensitizer that gives rise to the short-lived excited singlet state. This can lose energy by fluorescence (negligible in case of fullerenes), internal conversion to heat, or by intersystem crossing the long-lived triplet state. The triplet state can undergo photochemistry as shown in Fig. 4.4 (See Color Plates)

and can lose its energy by emitting light (fluorescence) or by internal conversion into heat. The fact that most PS are fluorescent has led to the development of sensitive assays to quantify the amount of PS in cells or tissues, and allows *in vivo* fluorescence imaging in living animals or patients to measure the pharmacokinetics and distribution of the PS. The excited singlet state PS may also undergo the process known as intersystem crossing, whereby the spin of the excited electron inverts to form the relatively long-lived (microseconds to milliseconds) excited triplet state that has electron spins parallel. The long lifetime of the PS triplet state is explained by the fact that the loss of energy by emission of light (phosphorescence) is a “spin-forbidden” process as the PS would move directly from a triplet to a singlet state.

4.3.1 Photophysics of C_{60}

When C_{60} is irradiated with visible light, it is excited from the S_0 ground state to a short-lived (~ 1.3 ns) S_1 -excited state (E_S 46.1 kcal/mol). The S_1 state rapidly decays at a rate of 5.0×10^8 s $^{-1}$ and a triplet quantum yield (ϕ_T) of 1.0 to a lower lying triplet state T_1 (E_T 37.5 kcal/mol) with a long lifetime of 50–100 μ s. The $S_1 \rightarrow T_1$ decay is

formally a spin-forbidden intersystem crossing (*isc*), but is driven by an efficient spin-orbit coupling. In the presence of dissolved molecular oxygen ($^3\text{O}_2$), which exists as a triplet in its ground state, the fullerene T_1 state is quenched (as a consequence of the quenching, its lifetime is reduced to ~ 330 ns) to generate singlet oxygen ($^1\text{O}_2^*$) by energy transfer at a rate of $2 \times 10^9 \text{ M}^{-1}\text{s}^{-1}$. The singlet oxygen quantum yield, ϕ_Δ , for this process (at 532 nm excitation) has been reported to be near theoretical maximum, 1.0 (Yu et al., 2005b).

However, all these early photophysical studies with C_{60} were carried out in nonpolar organic solvents. Indeed, C_{60} is a remarkable singlet oxygen sensitizer under these conditions. However, as we have shown and as has been previously suggested (Yamakoshi et al., 2003), under biological conditions where mild reducing agents are ubiquitous (and the environment is polar and aqueous), fullerenes do not produce any singlet oxygen whatsoever. They only produce superoxide having switched from a Type II to a Type I mechanism. It is likely that this fact has hampered the development of PS based on fullerenes as early researchers would likely have been looking for singlet oxygen in detection assays. With the lack of observation of $^1\text{O}_2^*$, it would have been concluded that fullerenes are not PS in polar aqueous environments. To the best of our knowledge, nearly all PDT papers involving fullerenes have referred exclusively to $^1\text{O}_2^*$ as the ROS responsible for photoinduced events. We have shown that it is superoxide that is largely responsible for these events (Mroz et al., 2007a).

4.4 Photochemistry of PS

The PS-excited triplet can undergo three broad kinds of reactions that are usually known as Type I, Type II, and Type III (Fig. 4.4). Firstly, in a Type I reaction, the triplet PS can gain an electron from a neighboring reducing agent. In cells, these reducing agents are commonly either NADH or NADPH. The PS is now a radical anion bearing an additional unpaired electron. Alternatively, two triplet PS molecules can react together involving electron transfer to produce a pair consisting of a radical cation and a radical anion. Radical anions may further react with oxygen with electron transfer to produce reactive oxygen species in particular superoxide anion. In a Type II reaction, the triplet PS can transfer its energy directly to molecular oxygen (itself a triplet in the ground state), to form excited-state singlet oxygen. Both Type I and Type II reactions can occur simultaneously, and the ratio between these processes depends on the type of PS used, the concentrations of substrate and oxygen. A less common pathway is known as Type III and here the triplet-state PS reacts directly with a biomolecule, thus destroying the PS and damaging the biomolecules. Type III is likely to be oxygen-independent in nature. Type II processes are thought to best conserve the PS molecular structure in a photoactive state and in some circumstances a single PS molecule can generate 10,000 molecules of singlet oxygen. The PS can in some circumstances also react with the singlet oxygen it produces in a process known as oxygen-dependent photobleaching.

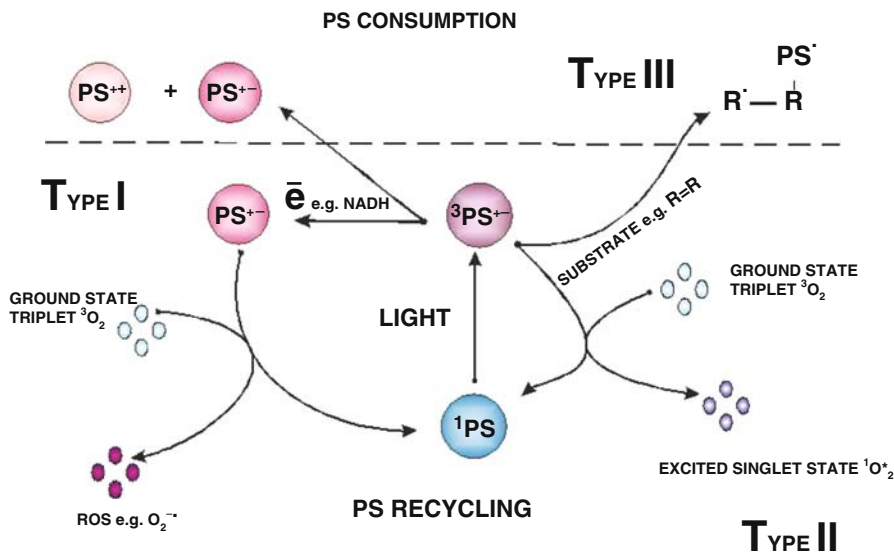


Fig. 4.4 Schematic representation of Type I, Type II, and Type III photochemical mechanisms thought to operate in PDT (See Color Plates)

Type I pathways frequently involve initial production of superoxide anion by electron transfer from the triplet PS to molecular oxygen (monovalent reduction) (Bilski et al., 1993; Ma and Jiang, 2001). Superoxide is not particularly reactive in biological systems and does not by itself cause much oxidative damage, but can react with itself to produce hydrogen peroxide (H_2O_2) and oxygen, a reaction known as “dismutation” that can be catalyzed by the enzyme superoxide dismutase (SOD). Hydrogen peroxide is important in biological systems because it can pass readily through cell membranes and cannot be excluded from the cells. It is actually necessary for the function of many enzymes, and thus is required (like oxygen itself) for health. Superoxide is also important in the production of the highly reactive hydroxyl radical (HO^\bullet). In this process, superoxide actually acts as a reducing agent, not as an oxidizing agent. This is because superoxide donates one electron to reduce the metal ions (such as ferric iron or Fe^{3+}) that act as the catalyst to convert hydrogen peroxide (H_2O_2) into the hydroxyl radical (HO^\bullet). This reaction is called the Fenton reaction, and was discovered over a hundred years ago. It is important in biological systems because most cells have some level of iron, copper, or other metals, which can catalyze this reaction. The reduced metal (ferrous iron or Fe^{2+}) then catalyzes the breaking of the oxygen–oxygen bond of hydrogen peroxide to produce a hydroxyl radical (HO^\bullet) and a hydroxide ion (HO^-). Superoxide can react with the hydroxyl radical (HO^\bullet) to form singlet oxygen, or with nitric oxide (NO^\bullet) (also a radical) to produce peroxynitrite ($OONO^-$), another highly reactive oxidizing molecule.

Like H_2O_2 , HO^\bullet passes easily through membranes and cannot be kept out of cells. Hydroxyl radical damage is “diffusion rate-limited”. This highly reactive radical can

add to an organic (carbon-containing) substrate (represented by R below); this could be, for example, a fatty acid, which would form a hydroxylated adduct that is itself a radical. The hydroxyl radical can also oxidize the organic substrate by “stealing” or abstracting an electron from it. The resulting oxidized substrate is again itself a radical, and can react with other molecules in a chain reaction. For example, it could react with ground-state oxygen to produce a peroxy radical (ROO^{*}). The peroxy radical again is highly reactive, and can react with another organic substrate in a chain reaction. This type of chain reaction is common in the oxidative damage of fatty acids and other lipids, and demonstrates why radicals such as the hydroxyl radical can cause so much more damage than one might have expected.

These ROS, together with singlet oxygen produced via Type II pathway, are oxidizing agents that can directly react with many biological molecules. Amino acid residues in proteins are important targets that include cysteine, methionine, tyrosine, histidine, and tryptophan (Grune et al., 2001; Midden and Dahl, 1992). Due to their reactivity, these amino acids are the primary target of an oxidative attack on proteins. The reaction mechanisms are rather complex and as a rule lead to a number of final products. Cysteine and methionine are oxidized mainly to sulfoxides, histidine yields a thermally unstable endoperoxide, tryptophan reacts by a complicated mechanism to give *N*-formylkynurenine, and tyrosine can undergo phenolic oxidative coupling. Unsaturated lipids typically undergo ene-type reactions to give lipid hydroperoxides (LOOHs derived from phospholipids and cholesterol) (Bachowski et al., 1991, 1994; Girotti, 1985; Girotti, 1983).

Because of the high reactivity and short half-life of singlet oxygen and hydroxyl radicals, only molecules and structures that are proximal to the area of its production (areas of PS localization) are directly affected by PDT. The half-life of singlet oxygen in biological systems is <40 ns, and, therefore, the radius of the action of singlet oxygen is of the order of 20 nm (Moan and Berg, 1991).

4.4.1 Photochemical Mechanisms of Fullerenes

It has been known since shortly after the discovery of fullerenes that these compounds will catalyze the formation of ROS after illumination of both pristine and functionalized C₆₀ (Foote, 1994). In a similar fashion to the tetrapyrrole PS used for photodynamic therapy (Greer, 2006; Schmidt, 2006), illumination of fullerenes dissolved in organic solvents in the presence of oxygen leads to the efficient generation of highly reactive singlet oxygen via energy transfer from the excited triplet state of the fullerene (Arbogast et al., 1991a, b). However, some recent reports have shown that in polar solvents, especially those containing reducing agents (such as NADH at concentrations found in cells), illumination of various fullerenes will generate different reactive oxygen derivatives, such as superoxide anion (Yamakoshi et al., 2003). These two pathways (singlet oxygen and superoxide anion) are analogous to the Type II and Type I photochemical mechanisms frequently discussed in PDT with tetrapyrroles (Foote, 1991; Ochsner, 1997).

Fullerenes with their triply degenerate, low-lying LUMO are excellent electron acceptors capable of accepting as many as six electrons (Koeppel and Sariciftci, 2006). There is some evidence that fullerene excited states (in particular the triplet) are even better electron acceptors than the ground state (Arbogast et al., 1992; Guldi and Prato, 2000). It is thought that the reduced fullerene triplet or radical anion can transfer an electron to molecular oxygen forming superoxide anion radical $O_2^{\cdot-}$.

Yamakoshi et al. (2003) carried out a photochemical study comparing energy transfer processes (singlet oxygen 1O_2) and electron transfer (reduced active oxygen radicals such as superoxide anion radical $O_2^{\cdot-}$), using various scavengers of ROS, physicochemical (electron paramagnetic resonance [EPR] radical trapping and near-infrared [near-IR] spectrometry), and chemical methods (nitro blue tetrazolium reaction with superoxide). Whereas 1O_2 was generated effectively by photoexcited C_{60} in nonpolar solvents such as benzene and benzonitrile, they found that $O_2^{\cdot-}$ and OH^{\cdot} were produced instead of 1O_2 in polar solvents such as water, especially in the presence of a physiological concentration of reductants including NADH.

Miyata et al. (2000) solubilized fullerenes into water with polyvinylpyrrolidone (PVP) as a detergent. Visible-light irradiation of PVP-solubilized C_{60} in water in the presence of NADH as a reductant and molecular oxygen resulted in the formation of $O_2^{\cdot-}$, which was detected by the EPR spin-trapping method. Formation of $O_2^{\cdot-}$ was also evidenced by the direct observation of a characteristic signal of $O_2^{\cdot-}$ by the use of a low-temperature EPR technique at 77 K. On the other hand, no formation of 1O_2 was observed by the use of TEMP as a 1O_2 trapping agent. No near-IR luminescence of 1O_2 was also observed in the aqueous C_{60} /PVP/ O_2 system. These results suggest that photoinduced bioactivities of the PVP-solubilized fullerene are caused not by 1O_2 , but by reduced oxygen species such as $O_2^{\cdot-}$, which are generated by the electron-transfer reaction of $C_{60}^{\cdot-}$ with molecular oxygen.

Highly water-soluble hexa(sulfobutyl)fullerenes (FC4S) were synthesized by the treatment of C_{60} in dimethoxyethane with sodium naphthalide followed by reacting the resulting hexa-anionic fullerene intermediates with an excess of 1,4-butanedisulfone (Yu et al., 2005b). Direct detection of 1O_2 production after irradiation at 500–600 nm of FC4S self-assembled nanospheres, was obtained by the measurement of its near-infrared luminescence at 1,270 nm. Despite having a relatively low optical absorption of FC4S at 600 nm, appreciable 1O_2 signal was detected comparable to that of Photofrin at the same molar concentration, but less than sulfonated aluminum phthalocyanine, AlS_4Pc . The quantum yield of FC4S for the generation of 1O_2 in H_2O was roughly estimated to be 0.36 using the relative correlation to that of C_{60} encapsulated in γ -cyclodextrin. These results demonstrated efficient energy transfer from 3FC4S triplet state to molecular oxygen in the nanosphere structure.

In two recent reports (Mroz et al., 2007b; Tegos et al., 2005) we studied the photosensitizer properties of two series of three functionalized fullerene compounds, one series with polar diserinol groups (**BF1–BF3**), and a second series of three compounds with quaternary pyrrolidinium groups (**BF4–BF6**) (Fig. 4.5). The bis-substituted and tris-substituted fullerenes are actually mixtures of regioisomers of the same molecular formula due to reaction with different double bonds. We asked the question whether the photodynamic effects displayed by these compounds operated

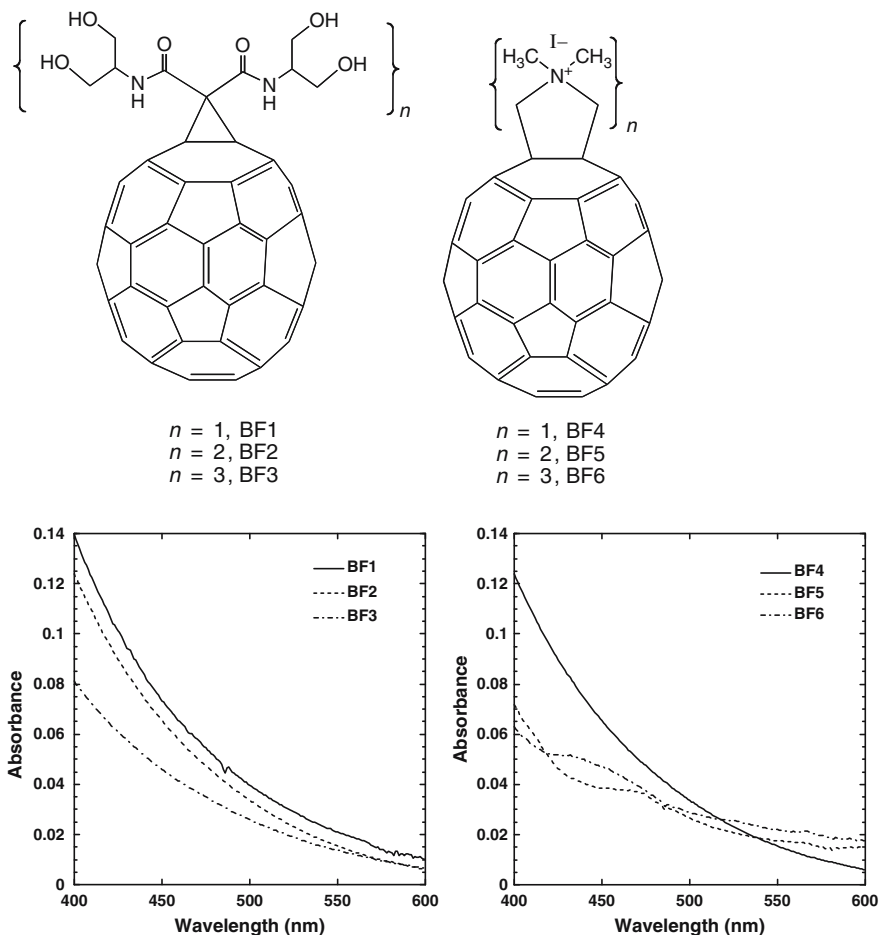


Fig. 4.5 Structures and visible absorption spectra recorded in DMSO of **BF1–BF3** and **BF4–BF6**

primarily by Type I mechanisms (superoxide) or Type II mechanisms (singlet oxygen) or a mixture of both and whether there was any difference between a fullerene (**BF4**) that was highly effective in killing cancer cells and a fullerene (**BF6**) that was highly effective in killing pathogenic microorganisms (see later).

The photochemical mechanism studies confirmed that depending on the precise conditions of the experiment, illuminated fullerenes can produce both superoxide and singlet oxygen. The singlet oxygen production of the more hydrophobic **BF4** dropped to almost zero when the solvent was changed from organic to aqueous. This is consistent with the aggregation of the compound in aqueous media, while the more polar **BF6** remained completely in solution. The production of superoxide as measured by specific EPR spin-trapping was as expected much higher in the presence of a reducing agent (NADH) than in the presence of a singlet oxygen trap

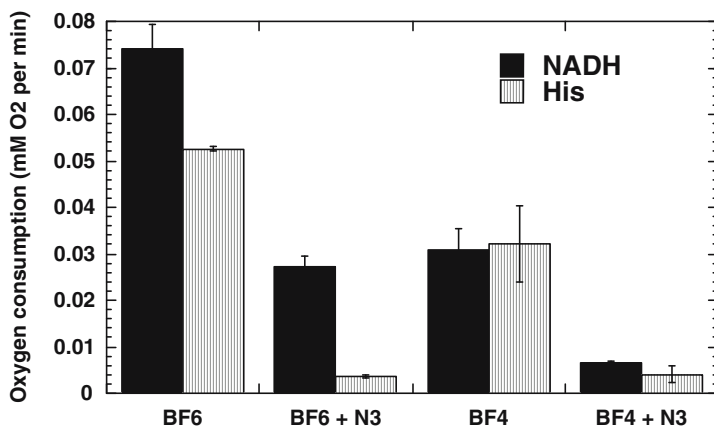


Fig. 4.6 Oxygen consumption rates for **BF4** or **BF6** (35 μ M) in presence of 1 mM NADH or 2 mM histidine with or without 5 mM sodium azide in 1:3H₂O/DMSO determined by ESR oximetry

(histidine). In both cases, **BF6** gave more superoxide than **BF4**, and the difference was significant in the presence of NADH. The fact that the reduction of oxygen consumption by both **BF4** and **BF6** was almost completely inhibited by azide in the presence of histidine confirmed that in the absence of an electron donor and in the presence of a singlet oxygen substrate the mechanism is almost all Type II for both fullerenes (Fig. 4.6). However, in the presence of NADH the relative reduction of oxygen consumption by azide was much less, and proportionately lower for **BF6** than for **BF4** suggesting that about 40% of the oxygen was transformed into superoxide, and the overall production was higher for **BF6** than for **BF4**.

4.5 Applications of Fullerenes for PDT

4.5.1 DNA Cleavage and Mutagenicity

DNA can be oxidatively damaged at both the nucleic bases (the individual molecules that make up the genetic code) and at the sugars that link the DNA strands by oxidation of the sugar linkages, or cross-linking of DNA to protein (a form of damage particularly difficult for the cell to repair). Although all cells have some capability of repairing oxidative damage to proteins and DNA, excess damage can cause mutations or cell death. Of the four bases in nucleic acids guanine is the most susceptible to oxidation by ¹O₂. The reaction mechanism has been extensively studied in connection with oxidative cleavage of DNA (Buchko et al., 1995). The first step is a [4 + 2] cycloaddition to the C-4 and C-8 carbons of the purine ring leading to an unstable endoperoxide (Buchko et al., 1993). The subsequent complicated sequence of reactions and the final products depend on whether the guanine moiety is bound in an oligonucleotide or a double-stranded DNA (Ravanat and Cadet, 1995).

One of the first biological applications of photoactivated fullerenes was to produce cleavage of DNA strands after illumination. Cleavage of supercoiled pBR322 DNA was observed after incubation with a fullerene carboxylic acid under visible-light irradiation but not in the dark (Tokuyama et al., 1993). Both nicked circular and linear duplex form DNA were observed and there was considerable selectivity for cleavage at guanine bases. The photoinduced action was more pronounced in D_2O in which singlet oxygen has a longer lifetime.

An and coworkers prepared (An et al., 1996) a covalent conjugate between an oligodeoxynucleotide and either a fullerene or eosin. Cleavage of target complementary 285-base single-stranded DNA was observed at guanosine residues in both cases upon illumination. However, the fullerene conjugate was more efficient in cleavage than the eosin conjugate. Moreover, the cleavage was not quenched by azide or increased by deuterium oxide as was found for the eosin conjugate suggesting the mechanism followed a Type I pathway.

Boutorine et al. (1994) described a fullerene-oligonucleotide that can bind single- or double-stranded DNA, and which also cleaves the strand(s) proximal to the fullerene moiety upon exposure to light. Nakanishi et al. (2001) also observed DNA cleavage by functionalized C_{60} . Yamakoshi et al. (1999) studied biological activities of fullerenes under illumination including DNA cleavage, hemolysis, mutagenicity, and cell toxicity. They prepared a conjugate between a fullerene and an acridine molecule as a DNA-intercalating agent and compared its DNA photocleavage capacity on pBR322 supercoiled plasmid with pristine fullerene both solubilized in PVP. This compound showed much more effective DNA-cleaving activity in the presence of NADH than pure C_{60} (Yamakoshi et al., 1996). Liu and coworkers (Liu et al., 2005) used a water-soluble conjugate between anthryl-cyclodextrin and C_{60} to carry out photocleavage of pGEX5X2 DNA. Ikeda et al. (2007a) used functionalized liposomes incorporating both C_{60} and C_{70} fullerenes into the lipid bilayer to carry out photocleavage of ColE1 supercoiled plasmid DNA using $\lambda > 350$ nm light. Interestingly, C_{70} was significantly better (3.5 times) than C_{60} in photocleaving DNA.

It has also been shown that fullerene-mediated-PDT may lead to mutagenic effects. PVP-solubilized fullerene was found to be mutagenic for *Salmonella* strains TA102, TA104, and YG3003 in the presence of rat liver microsomes when it was irradiated by visible light (Sera et al., 1996). The mutagenicity was elevated in strain YG3003, a repair enzyme-deficient mutant of TA102. The mutation was reduced in the presence of beta-carotene and parabromophenacyl bromide, a scavenger and an inhibitor, respectively, of phospholipase. The results suggested that singlet oxygen was generated by irradiating the C_{60} by visible light and that the mutagenicity was due to oxidized phospholipids in rat liver microsomes. The linoleate fraction isolated by high-performance liquid chromatography was a major component, and played an important role in mutagenicity. The results of electron spin resonance (ESR) spectrum analysis suggested generation of radicals at the guanine base but not thymine, cytosine, and adenine bases and formation of 8-hydroxydeoxyguanosine (8-OH-dG). The mechanism was proposed to involve indirect action of singlet oxygen due to lipid peroxidation of linoleate that causes oxidative DNA damage.

4.5.2 Membrane Damage by Photoactivated Fullerenes

A group from India has studied the ability of fullerenes to produce oxidative damage to lipids in microsomal preparations. Cyclodextrin encapsulated C_{60} added to rat liver microsomes followed by exposure to UV or visible light produced lipid peroxidation as assayed by thiobarbituric acid reactive substances, lipid hydroperoxides, damage to proteins as assessed by protein carbonyls, and loss of the membrane-bound enzymes (Kamat et al., 1998). Quenchers of singlet oxygen (beta-carotene and sodium azide) inhibited peroxidation, and deuteration of the buffer enhanced peroxidation, indicating that the photochemical mechanism is predominantly due to Type II (1O_2). In a subsequent study (Kamat et al., 2000) they compared pristine C_{60} with a polyhydroxylated derivative $C_{60}(OH)_{18}$ and found that the latter produced more pronounced peroxidative damage and the mechanism was different and was mediated primarily by radical species. Lipid peroxidation was also shown in sarcoma 180 ascites microsomes.

Yang et al. (2007) used human erythrocyte membranes (EMs) as a model system, to examine photoinduced lipid peroxidation by a bis-methanophosphonate fullerene (BMPF) and four other fullerene derivatives including a mono-methanophosphonic acid fullerene (MMPF), a dimalonic acid C_{60} (DMA C_{60}), a trimalonic acid C_{60} (TMAC $_{60}$), and a polyhydroxylated fullerene (fullerol). Lipid peroxidation was assessed as the malondialdehyde (MDA) level measured by the thiobarbituric acid assay. It was observed that BMPF increased the MDA level of EMs after irradiation in both time- and dose-dependent manners. The photoinduced activity became very significant ($P < 0.01$) under the conditions of either the concentration of $10\mu\text{M}$ and irradiation time of 30 min or the concentration of $5\mu\text{M}$ and irradiation time of 60 min. Involvement of reactive oxygen species (ROS) in the activity was also examined by specific inhibitors of singlet oxygen, superoxide anions and hydroxyl radicals, respectively. While all three kinds were found responsible for the activity, the former two might play more important roles than the last one.

4.5.3 Photoinactivation of Viruses

Photodynamic reactions induced by photoactivated fullerenes have been shown to inactivate enveloped viruses (Kasermann and Kempf, 1997). Buffered solutions containing pristine C_{60} and Semliki Forest virus (*Togaviridae*) or vesicular stomatitis virus (VSV) (*Rhabdoviridae*), when illuminated with visible light for up to 5 h, resulted in up to seven logs of loss of infectivity. Viral inactivation was oxygen-dependent and equally efficient in solutions containing protein (Kasermann and Kempf, 1998). Hirayama et al. (1999) used a methoxy-polyethylene glycol (PEG)-conjugated fullerene at $400\mu\text{M}$ in combination with $120\text{J}/\text{cm}^2$ white light to destroy more than five logs of plaque forming units of VSV. VSV inactivation was inhibited by oxygen removal or by the addition of sodium azide, a known singlet oxygen quencher. The substitution of H_2O by D_2O , which is known to prolong the

lifetime of singlet oxygen, promoted the virucidal activity. These results indicate that singlet oxygen may play a major role in VSV photoinactivation by the water-soluble fullerene derivative. The concentration needed for virus inactivation was higher than that of other sensitizers such as methylene blue.

Lin and coworkers (Lin et al., 2000) compared light-dependent and light-independent inactivation of dengue-2 and other enveloped viruses by the two regioisomers of carboxyfullerene, and found that asymmetric isomer had greater dark activity (albeit at much higher concentrations than needed for its PDT effect) due to its interaction with the lipid envelope of the virus.

4.5.4 Fullerenes for Antimicrobial Photoinactivation

The effectiveness of various PS proposed for antimicrobial PDT can be judged on several criteria. These PS should be able to kill multiple classes of microbes at relatively low concentrations and low fluences of light. PS should be reasonably nontoxic in the dark and should demonstrate selectivity for microbial cells over mammalian cells. PS should ideally have large extinction coefficients in the red part of the spectrum and demonstrate high triplet and singlet oxygen quantum yields.

We have shown, in a series of reported experiments that cationic fullerenes fulfill many, but not all the aforementioned criteria. Our laboratory was the first to demonstrate that the soluble functionalized fullerenes described above, especially the cationic compounds **BF4–BF6**, were efficient antimicrobial PS and could mediate photodynamic inactivation (PDI) of various classes of microbial cells (Tegos et al., 2005). We used a broadband-pass filter giving an output of the entire visible spectrum (400–700 nm) to excite the fullerenes that maximized the absorption.

Our initial screening experiment carried out against *Staphylococcus aureus* at 100 μM concentrations showed that the C_{60} substituted with pyrrolidinium groups behaved very differently than the series substituted by di-serinol groups. The cationic fullerenes gave high levels of dark toxicity (except for **BF4**) while the di-serinol-functionalized C_{60} had no dark toxicity, but showed a typical light dose-dependent loss of colony-forming ability. However, it needed concentrations as high as 100 μM and white-light fluences as high as 120 J/cm^2 to achieve significant killing (two to three logs or up to 99.9%) of the Gram-positive *S. aureus* (Fig. 4.7A). Even with these relatively high doses of both PS and light, the Gram-negative *Escherichia coli* was only slightly killed (less than 1 log or 90%). In sharp contrast the cationic fullerenes were highly effective PS at much lower concentrations and much lower light doses (Fig. 4.7B). **BF4–BF6** were all surprisingly effective in causing light-mediated killing of *S. aureus*. **BF5** and **BF6** needed only 1 μM concentration and 1 or 2 J/cm^2 of white light to kill four to five logs. **BF4–BF6** were tested against *E. coli* at 10 μM , and **BF5** and **BF6** showed similar high levels of activity (up to six logs). These findings agree with numerous reports in the literature that demonstrate that PS with one (or preferably more cationic groups) are efficient antimicrobial PS (Demidova and Hamblin, 2004, 2005; Hamblin and

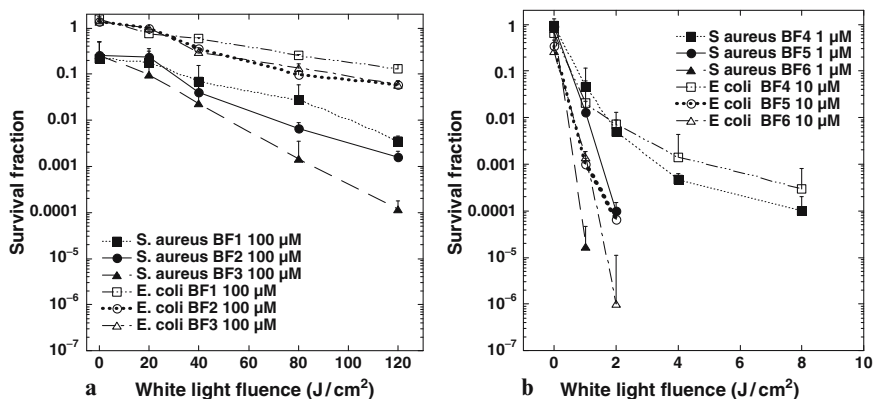


Fig. 4.7 (a) *Staphylococcus aureus* or *Escherichia coli* (10^8 cells per mL) was incubated for 10 min with **BF1–BF3** at 100 μM concentration in PBS followed by illumination with 400–700-nm light at an irradiance of 200 mW/cm^2 . Aliquots were removed from the suspensions after the various fluences of light had been delivered and CFU determined. Values are means of six independent experiments and bars are SEM. * $P < 0.05$, ** $P < 0.01$; two-tailed unpaired t -test. (b) *S. aureus* was incubated with 1 μM concentration of **BF4–BF6** and *E. coli* (both 10^8 cells per mL) was incubated with **BF4–BF6** at 10 μM concentrations for 10 min followed by a wash and illumination with white light. Values are means of six independent experiments and bars are SEM. * $P < 0.05$, ** $P < 0.01$, *** $P < 0.001$; two-tailed unpaired t -test

Hasan, 2004; Merchat et al., 1996; Minnock et al., 1996). Quaternary nitrogen-based groups are superior to primary, secondary, or tertiary amino groups as the positive charge is less dependent on the pH of the surrounding media, or the pKa of the molecules that the PS is interacting with. Microbial cells possess overall negative charges and it is thought that cationic PS bind to these groups on the outer layers of the cell surface. Gram-positive cells have relatively permeable outer layers of peptidoglycan and lipoteichoic acid or beta-glucan, respectively. This allows cationic and a lesser extent non-cationic PS to diffuse inwards to the plasma membrane where the generation of reactive oxygen species under illumination can damage the membrane structure allowing leakage of essential components and cause cell death. Cationic compounds are able to displace divalent cations (Ca^{2+} and Mg^{2+}) that play a role in the attachment of lipopolysaccharide to the outer membrane (Lambrechts et al., 2004). This displacement weakens the structure of the outer permeability allowing the PS to penetrate further in a process that has been termed “self promoted uptake” (Hancock and Bell, 1988). The fact that this mechanism requires cationic compounds explains why **BF1–BF3** were relatively noneffective against the Gram-negative *E. coli* and such findings have been reported with numerous other non-cationic PS (Hamblin and Hasan, 2004).

A recent study by Spesia et al. (2008) reported that a novel *N,N*-dimethyl-2-(4'-*N,N,N*-trimethylaminophenyl)fulleropyrrolidinium iodide (DTC_{60}^{2+}) was synthesized by 1,3-dipolar cycloaddition using 4-(*N,N*-dimethylamino)benzaldehyde,

N-methylglycine, and fullerene C₆₀ and quaternization with methyl iodide. The photodynamic properties of the DTC₆₀²⁺ were compared with a non-charged *N*-methyl-2-(4'-acetamidophenyl)fulleropyrrolidine (MAC₆₀) and a monocationic *N,N*-dimethyl-2-(4'-acetamidophenyl)fulleropyrrolidinium iodide (DAC₆₀⁺). The photodynamic effect was strongly dependent on the medium, and diminished when the sensitizer aggregated and increased in an appropriately surrounded microenvironment. The photodynamic inactivation produced by these fullerene derivatives was investigated *in vitro* in *E. coli*. Photosensitized inactivation of *E. coli* cellular suspensions by DTC₆₀²⁺ exhibited a approximately 3.5 log decrease of cell survival when the cultures are treated with 1 μM of sensitizer and irradiated for 30 min. This photosensitized inactivation remains high even after one washing step. Also, the photodynamic activity was confirmed by growth delay of *E. coli* cultures. The growth was arrested when *E. coli* was exposed to 2 μM of cationic fullerene and irradiated, whereas a negligible effect was found for the non-charged MAC₆₀.

4.5.5 Fullerenes and PDT of Mammalian Cells Including Cancer Cells

It is thought that one requirement for any PS to produce cell killing after illumination is that the PS should actually be taken up inside the cell, and that the generation of ROS outside the cell (unless in very large quantities) will not be sufficient to produce efficient cell death. Because fullerenes (in contrast to the vast majority of PS) are nonfluorescent, it is impossible to use the common technique of fluorescence microscopy to examine the intracellular uptake and subcellular localization of fullerenes. Taking these considerations into account, Scrivens et al. (1994) were the first to prepare a radiolabeled fullerene and demonstrate its uptake by human keratinocytes in tissue culture. In serum-free medium they found a time (up to 6 h) and concentration-dependent uptake so that 50% of added fullerene was taken up. Foley et al. (2002) used indirect immunofluorescence staining with antibodies that recognize fullerenes and other organelle probes to show that a dicarboxylic acid derivative is localized in mitochondria and other intracellular membranes. A recent report (Levi et al., 2006) has in fact used a pristine C₆₀ preparation obtained by sonication in methanol (different from the more commonly used toluene) and giving uniformly sized particles with a mean size of 32.7 nm together, with photoluminescence detection at 750 nm after excitation at 488 nm, to demonstrate cell uptake in normal and malignant breast cells after culturing them on fullerene-coated dishes. Another recent paper (Porter et al., 2007) describes the use of the related techniques of energy-filtered transmission electron microscopy and electron tomography to visualize the cellular uptake of pristine C₆₀ nanoparticulate clusters. When human monocyte derived macrophages were examined C₆₀ was found in the plasma membrane, lysosomes, and in the nucleus.

The first demonstration of phototoxicity in cancer cells mediated by fullerenes was in 1993 when Tokuyama et al. (1993) used carboxylic acid functionalized

fullerenes at $6\mu\text{M}$ and white light to produce growth inhibition in human HeLa cancer cells. However, these same authors later reported that other carboxylic acid derivatives of C_{60} and C_{70} were completely without any photoactivity as PDT agents at $50\mu\text{M}$ (Irie et al., 1996).

Burlaka et al. (2004) used pristine C_{60} at $10\mu\text{M}$ with visible light from a mercury lamp to produce some phototoxicity in Ehrlich carcinoma cells or rat thymocytes and used EPR spin-trapping techniques to demonstrate the formation of ROS.

The cytotoxic and photocytotoxic effects of two water-soluble fullerene derivatives, a dendritic C_{60} mono-adduct and the malonic acid C_{60} tris-adduct were tested on Jurkat cells when irradiated with UVA or UVB light (Rancan et al., 2002). The cell death was mainly caused by membrane damage and it was UV dose-dependent. Tris-malonic acid fullerene was found to be more phototoxic than the dendritic derivative. This result is in contrast to the singlet oxygen quantum yields determined for the two compounds.

Three C_{60} derivatives with two to four malonic acid groups (DMA C_{60} , TMA C_{60} , and QMA C_{60}) were prepared and the phototoxicity of these compounds against HeLa cells was determined by MTT assay and cell cycle analysis (Yang et al., 2002). The relative phototoxicity of these compounds was DMA C_{60} > TMA C_{60} > QMA C_{60} . Hydroxyl radical quencher mannitol (10mM) was not able to prevent cells from the damage induced by irradiated DMA C_{60} . DMA C_{60} , together with irradiation, was found to decrease the number of G(1) cells from 63% to 42% and increase G(2) + M cells from 6% to 26%.

Rancan et al. (2005) used the following approach to overcome the necessity to use UV or short-wavelength visible light to photoactivate fullerenes. They synthesized two new fullerene-bis-pyropheophorbide a derivatives: a mono-(FP1) and a hexa-adduct (FHP1). The photophysical characterization of the compounds revealed significantly different parameters related to the number of addends at the fullerene core. In this study, the derivatives were tested with regard to their intracellular uptake and photosensitizing activity towards Jurkat cells in comparison with the free sensitizer, pyropheophorbide a. The C_{60} -hexa-adduct FHP1 had a significant phototoxic activity (58% cell death, after a dose of $400\text{mJ}/\text{cm}^2$ of 688 nm light), but the mono-adduct FP1 had a very low phototoxicity and only at higher light doses. Nevertheless, the activity of both adducts was less than that of pure pyropheophorbide a, probably due to the lower cellular uptake of the adducts.

A group from Argentina has also studied the phototoxicity produced by tetrapyrrole-fullerene conjugates. Milanesio et al. (2005) compared PDT with a porphyrin- C_{60} dyad (P- C_{60}) and its metal complex with Zn(II) (ZnP- C_{60}) were compared with 5-(4-acetamidophenyl)-10,15,20-tris(4-methoxyphenyl)porphyrin (P), both in homogeneous medium containing photooxidizable substrates and *in vitro* on the Hep-2 human larynx carcinoma cell line. $^1\text{O}_2$ yields (Φ_{Δ}) were determined using 9,10-dimethylanthracene (DMA). The values of Φ_{Δ} were strongly dependent on the solvent polarity. Comparable Φ_{Δ} values were found for dyads and P in toluene, while $^1\text{O}_2$ production was significantly diminished for the dyads in DMF. In more polar solvent, the stabilization of charge-transfer state takes place, decreasing the efficiency of porphyrin triplet-state formation. Also, both dyads photosensitize

the decomposition of L-tryptophan in DMF. In biological medium, no dark cytotoxicity was observed using sensitizer concentrations $\leq 1 \mu\text{M}$ and 24 h of incubation. The uptake of sensitizers into Hep-2 was studied using $1 \mu\text{M}$ of sensitizer and different times of incubation. Under these conditions, a value of approximately $1.5 \text{ nmol}/10^6$ cells was found between 4 and 24 h of incubation. The cell survival after irradiation of the cells with visible light was dependent upon light-exposure level. A higher phototoxic effect was observed for P-C₆₀, which inactivates 80% of cells after 15 min of irradiation. Moreover, both dyads keep a high photoactivity even under argon atmosphere. In a subsequent paper (Alvarez et al., 2006) they showed the cells died by apoptosis by analysis using Hoechst-33258, toluidine blue staining, TUNEL, and DNA fragmentation. Changes in cell morphology were analyzed using fluorescence microscopy with Hoechst-33258 under low oxygen concentration. Under this anaerobic condition, necrotic cellular death predominated over the apoptotic pathway. It was found that P-C₆₀-induced apoptosis by a caspase-3-dependent pathway.

Ikeda and coworkers (Ikeda et al., 2007b) used a series of liposomal preparations containing cationic or anionic lipids together with dimyristoylphosphatidylcholine and introduced C₆₀ into the lipid bilayer by exchange from cyclodextrin. By adding a phospholipid with an additional fluorochrome they were able to use fluorescence microscopy to demonstrate uptake of the liposomes by HeLa cells after 24-h incubation. Illumination with $136 \text{ J}/\text{cm}^2$ at 350–500-nm light gave 85% cell killing in the case of cationic liposomes and apoptosis was demonstrated.

In our laboratory we have tested the hypothesis that fullerenes would be able to kill cancer cells by PDT *in vitro* (Mroz et al., 2007c). We studied the same group of fullerene derivatives described above, **BF1–BF3** and **BF4–BF6** (Mroz et al., 2007a). We showed that the C₆₀ molecule mono-substituted with a single pyrrolidinium group (**BF4**) is a remarkably efficient PS and can mediate killing of a panel of mouse cancer cells at the low concentration of $2 \mu\text{M}$ with very modest ($5 \text{ J}/\text{cm}^2$) exposure to white light as shown in Fig. 4.8A. The cells were all cancer cells; lung (LLC) and colon (CT26) adenocarcinoma and reticulum cell sarcoma (J774) and the latter showed much higher susceptibility perhaps due to an increased uptake of fullerene because J774 cells behave like macrophages (Liang-Takasaki et al., 1982). In Fig. 4.8B we show the comparative phototoxicity of all six fullerenes against J774 cells. Besides the exceptionally active **BF4**, the next group of compounds has only moderate activity (**BF2**, **BF5**, and **BF6**) against J774 cells showing some killing at high fluences. The last two compounds (**BF1** and **BF3**) had no detectable PDT killing up to $80 \text{ J}/\text{cm}^2$. For the first time we indirectly demonstrated that photoactive fullerenes are taken up into cells by measuring the increase in fluorescence of an intracellular probe (H₂DCFDA) that is specific for the formation of ROS (in particular hydrogen peroxide).

We also demonstrated the induction of apoptosis by PDT mediated by **BF4** and by **BF6** in CT26 cells at 4–6 h after illumination. The relatively rapid induction of apoptosis after illumination might suggest the fullerenes are localized in subcellular organelles such as mitochondria, as has been previously shown for PS such as benzoporphyrin derivative (Granville et al., 1998; Gupta et al., 1998; Li et al., 2003).

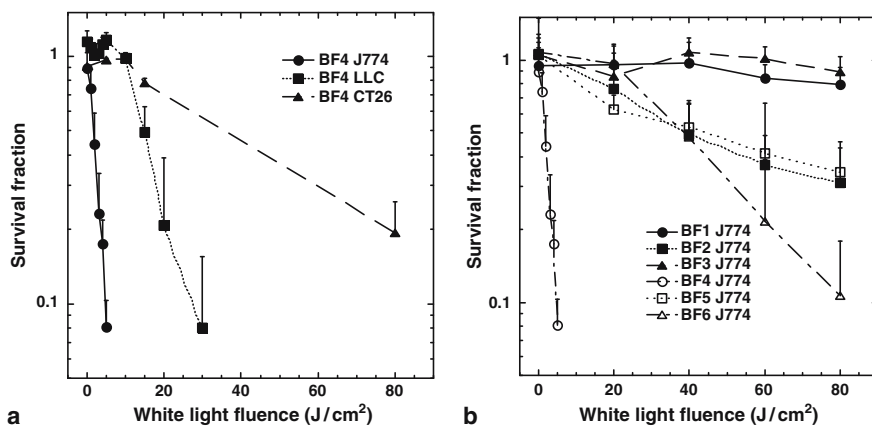


Fig. 4.8 Survival curves of (A) LLC, J774, CT26 cells after 24h incubation with 2 μ M **BF4** and (B) J774 cells after 24h incubation with 2 μ M **BF1–BF6**, in both cases followed by a wash and illumination with white light. An MTT assay was carried out after 24h incubation. Values are means of nine separate wells and bars are SD. Experiments were repeated at least twice

PS that localize in lysosomes tend to produce apoptosis more slowly after illumination than mitochondrial PS, due to the release of lysosomal enzymes that subsequently activate cytoplasmic caspases (Kessel et al., 2000).

We have also performed preliminary experiments comparing effectiveness of **BF4** to Photofrin[®], one of the clinically approved photosensitizers for cancer therapy (Hahn et al., 2006). Figure 4.9 shows that **BF4** was far superior at PDT-mediated killing of human ovarian cancer cells *in vitro* than Photofrin. Both compounds, **BF4** and Photofrin, show very little dark toxicity as evidenced by the survival fraction at zero fluence, which was after 24h incubation of the cells with each PS. Also, both show a light-dose-dependent response. However, the response of **BF4** at the light fluences used was much more pronounced than that of Photofrin, demonstrating that **BF4** is a significantly better photosensitizer than Photofrin against ovarian cancer cells *in vitro*.

4.5.6 Photodynamic Therapy of Tumors

Fullerenes should have a photodynamic effect on tumors, if (a) the compound is accumulated in the tumor tissue, (b) a reasonably efficient way to administer the compound to tumor bearing animals is found, and (c) enough excitation light can be delivered to the photosensitized tumors. The first report of fullerenes being used to carry out PDT of actual tumors was by Tabata in 1997 (Tabata et al., 1997). They chemically modified the water-insoluble C₆₀ with polyethylene glycol (PEG), not only to make it soluble in water, but also to enlarge its molecular size. When injected intravenously into mice carrying a subcutaneous tumor on the back, the

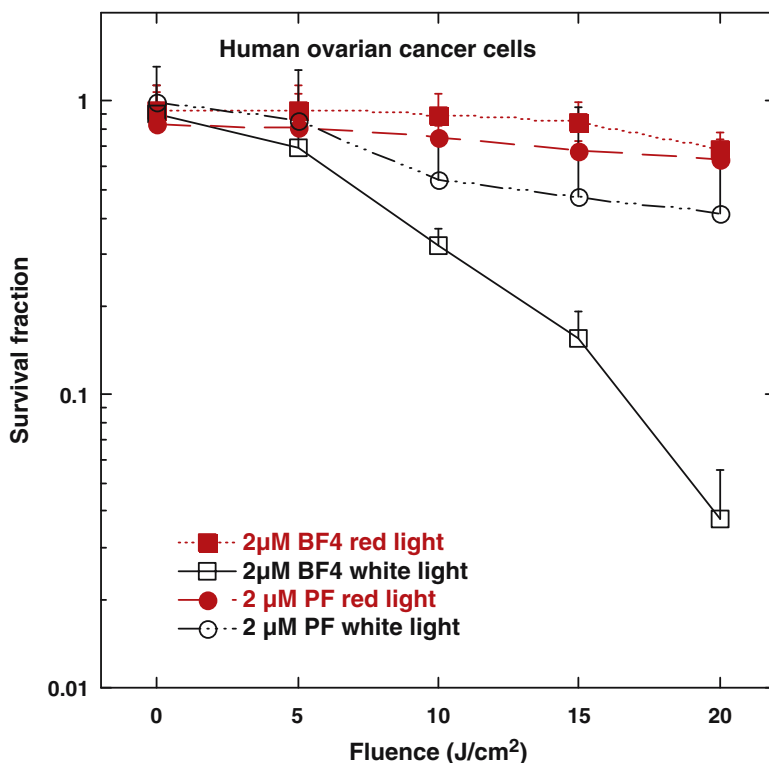


Fig. 4.9 Comparison of PDT-induced killing in human ovarian cancer cells by **BF4** or Photofrin both incubated for 24 h at 2 μ M concentration and illuminated with red (630 nm) or white light (400–700 nm) (See Color Plates)

C_{60} -PEG conjugate exhibited higher accumulation and more prolonged retention in the tumor tissue than in normal tissue. The conjugate was excreted without being accumulated in any specific organ. Following intravenous injection of C_{60} -PEG conjugate or Photofrin (a recognized PS) to tumor-bearing mice, coupled with exposure of the tumor site to visible light, the volume increase of the tumor mass was suppressed and the C_{60} conjugate exhibited a stronger suppressive effect than Photofrin. Histological examination revealed that conjugate injection plus light irradiation strongly induced tumor necrosis without any damage to the overlying normal skin. The antitumor effect of the conjugate increased with increasing fluence delivered and C_{60} dose, and cures were achieved by treatment with a low dose of 424 μ g/kg at a (very high) fluence of 10^7 J/cm².

Liu and others (Liu et al., 2007) conjugated polyethylene glycol (PEG) to C_{60} (C_{60} -PEG), and diethylenetriaminepentaacetic acid (DTPA) was subsequently introduced to the terminal group of PEG to prepare C_{60} -PEG-DTPA that was mixed with gadolinium acetate solution to obtain Gd^{3+} -chelated C_{60} -PEG-DTPA-Gd. Following intravenous injection of C_{60} -PEG-DTPA-Gd into tumor-bearing mice, the PDT

antitumor effect and MRI tumor imaging were evaluated. Similar generation of superoxide upon illumination was observed with or without Gd^{3+} chelation. Intravenous injection of C_{60} -PEG-DTPA-Gd into tumor-bearing mice plus light (400–500 nm, $53.5 J/cm^2$) showed significant antitumor PDT effect and the effect depended on the timing of light irradiation that correlated with tumor accumulation as detected by the enhanced intensity of MRI signal.

The FC4S nanostructures described in Section 4.1 (Yu et al., 2005b) have also been tested as PS *in vivo* (Yu et al., 1999). The median lethal dose (LD_{50}) of FC4S was defined as approximately 600 mg/kg in acute toxicity studies. No adverse effects were noted in the animals when the FC4S was administered orally. ICR mice subcutaneously implanted with sarcoma 180 tumor cells were given FC4S (15 mg/kg) by intraperitoneal injection, and PDT on tumor-bearing mice using argon laser irradiation at 514.5 nm with a total light dose of $100 J/cm^2$ delivered at $200 mW/cm^2$. Mean tumor size was found to decrease significantly to only 10% of the untreated tumor control at 30 days after laser irradiation. Mice treated with FC4S and no laser irradiation had a slight nonsignificant reduction in tumor size.

These data summarized above suggest that PDT with fullerenes is not only possible in animal tumor models, but demonstrate the potential use of these compounds as PS for PDT of cancer.

4.6 Conclusions and Future Outlook

At the end of this review we must ask ourselves whether in all reality it is likely that fullerenes will ever be accepted as viable PS for PDT of any disease. As discussed previously these compounds have certain unique features that could make them favorable candidates and at the same time other unique features that would argue against them as PS for PDT. The most important favorable property is their rather unusual photochemical mechanism. As shown by us and by others, in aqueous solutions and particularly in the presence of reducing agents, these compounds produce a substantial amount of superoxide anion in a Type I photochemical process involving electron transfer from the excited triplet state to molecular oxygen. Although many workers in the PDT field think that the product of the Type II photochemical process, singlet oxygen, is the major cytotoxic species operating in PDT-induced cell killing, there have been reports that Type I mechanisms may be equally effective or even more effective than Type II. This is because hydroxyl radicals are the most reactive and potentially the most cytotoxic of all ROS. It is assumed that hydroxyl radicals are formed from hydrogen peroxide by Fenton chemistry reactions catalyzed by Fe^{2+} or Cu^+ ions, and that the hydrogen peroxide is produced by dismutation of superoxide anion either by enzyme catalysis or naturally. Another possible mechanism of cytotoxicity is the diffusion-controlled reaction between superoxide and nitric oxide to form the highly toxic species, peroxynitrite. Elevated levels of nitric oxide are present both in cancers and infections, thus giving the possibility of additional levels of selectivity for target-specific damage.

The chief disadvantage of fullerenes is likely to be their optical absorption properties. The absorption spectrum of fullerenes is highest in the UVA and blue regions of the spectrum where the tissue penetration depth of illumination is shortest due to a combination of light absorption by cellular chromophores and light scattering by cellular structures. However, the molar absorption coefficients of fullerenes are relatively high and the tail of absorption does stretch out into the red regions of the visible spectrum. Fullerenes have been proposed as carrier vehicles for drug delivery of molecules such as taxol (Zakharian et al., 2005) and nonviral DNA (Isobe et al., 2006) so some knowledge about their pharmaceutical properties has been gathered. The cationic modifications described in this chapter demonstrate that with the correct functionalities present on the fullerene cage these molecules could have real applications in biomedicine as antimicrobial photosensitizers and possibly also in cancer treatment.

Acknowledgments This work was supported by the US National Institutes of Health (grants R43CA103268 and R44AI68400 to Lynntech Inc. and R01CA/AI838801 and R01AI050875 to MRH), and in Poland by Ministry of Science and Higher Education (DS/WBBB/16/06).

References

- Agostinis P, Vantieghem A, Merlevede W, de Witte PA (2002) Hypericin in cancer treatment: more light on the way. *Int J Biochem Cell Biol* 34:221–41.
- Agostinis P, Buytaert E, Breysens H, Hendrickx N (2004) Regulatory pathways in photodynamic therapy induced apoptosis. *Photochem Photobiol Sci* 3:721–729.
- Alvarez MG, Pucca C, Milanesio ME, Durantini EN, Rivarola V (2006) Photodynamic activity of a new sensitizer derived from porphyrin-C60 dyad and its biological consequences in a human carcinoma cell line. *Int J Biochem Cell Biol* 38:2092–2101.
- An YZ, Chen CB, Anderson JL, Sigman DS, Foote CS, Rubin Y (1996) Sequence-specific modification of guanosine in DNA by a C60-linked deoxyoligonucleotide: evidence for a non-singlet oxygen mechanism. *Tetrahedron* 52:5179–5189.
- Arbogast JW, Darmanyan AP, Foote CS, Rubin Y, Diederich FN, Alvarez MM, Anz SJ, Whetten RL (1991a) Photophysical properties of C60. *J Phys Chem A* 95:11–12.
- Arbogast JW, Darmanyan AP, Foote CS, Rubin Y, Diederich FN, Alvarez MM, Anz SJ, Whetten RL (1991b) Photophysical properties of C60. *J Phys Chem A Mol Spectrosc Kinet Environ Gen Theory* 95:11–12.
- Arbogast JW, Foote CS, Kao M (1992) Electron-transfer to triplet C-60. *J Am Chem Soc* 114:2277–2279.
- Bachowski GJ, Pintar TJ, Girotti AW (1991) Photosensitized lipid peroxidation and enzyme inactivation by membrane-bound merocyanine 540: reaction mechanisms in the absence and presence of ascorbate. *Photochem Photobiol* 53:481–491.
- Bachowski GJ, Korytowski W, Girotti AW (1994) Characterization of lipid hydroperoxides generated by photodynamic treatment of leukemia cells. *Lipids* 29:449–459.
- Bagno A, Claeson S, Maggini M, Martini ML, Prato M, Scorrano G (2002) [60]Fullerene as a substituent. *Chemistry* 8:1015–1023.
- Belgorodsky B, Fadeev L, Kolsenik J, Gozin M (2006) Formation of a soluble stable complex between pristine C60-fullerene and a native blood protein. *Chembiochem* 7:1783–1789.
- Belousova IM, Mironova NG, Yur'ev MS (2005) A mathematical model of the photodynamic fullerene-oxygen action on biological tissues. *Optic Spectrosc* 98:349–356.

- Bilski P, Motten AG, Bilka M, Chignell CF (1993) The photooxidation of diethylhydroxylamine by rose bengal in micellar and nonmicellar aqueous solutions. *Photochem Photobiol* 58:11–18.
- Bosi S, Da Ros T, Spalluto G, Prato M (2003) Fullerene derivatives: an attractive tool for biological applications. *Eur J Med Chem* 38:913–923.
- Bottioli G, Croce AC, Balzarini P, Locatelli D, Baglioni P, Lo Nostro P, Monici M, Pratesi R (1997) Enzyme-assisted cell photosensitization: a proposal for an efficient approach to tumor therapy and diagnosis. The rose bengal fluorogenic substrate. *Photochem Photobiol* 66:374–383.
- Boutorine AS, Tokuyama H, Takasugi, M, Isobe, H, Nkamura, E, Helene C (1994) Fullerene-oligonucleotide conjugates: photo-induced sequence-specific DNA cleavage. *Angew Chem Int Ed Engl* 33:2462–2465.
- Buchko GW, Cadet J, Ravanat JL, Labataille P (1993) Isolation and characterization of a new product produced by ionizing irradiation and type I photosensitization of 2'-deoxyguanosine in oxygen-saturated aqueous solution: (2S)-2,5'-ANHYDRO-1-(2'-deoxy-beta-D-erythro-pentofuranosyl)-5-guanidin ylidene- 2-hydroxy-4-oxoimidazolidine. *Int J Radiat Biol* 63:669–76.
- Buchko GW, Wagner JR, Cadet J, Raoul S, Weinfeld M (1995) Methylene blue-mediated photo-oxidation of 7,8-dihydro-8-oxo-2'-deoxyguanosine. *Biochim Biophys Acta* 1263:17–24.
- Burlaka AP, Sidorik YP, Prylutska SV, Matyshevska OP, Golub OA, Prylutsky YI, Scharff P (2004) Catalytic system of the reactive oxygen species on the C60 fullerene basis. *Exp Oncol* 26:326–327.
- Castano AP, Demidova TN, Hamblin MR (2004) Mechanisms in photodynamic therapy: part one – photosensitizers, photochemistry and cellular localization. *Photodiagn Photodyn Ther* 1:279–293.
- Castano AP, Demidova TN, Hamblin MR (2005) Mechanisms in photodynamic therapy: part two – cellular signalling, cell metabolism and modes of cell death. *Photodiagn Photodyn Ther* 2:1–23.
- Davydenko MO, Radchenko EO, Yashchuk VM, Dmitruk IM, Prylutsky YI, Matishevska OP, Golub AA (2006) Sensibilization of fullerene C60 immobilized at silica nanoparticles for cancer photodynamic therapy. *J Molec Liq* 127:145–147.
- Demidova TN, Hamblin MR (2004) Photodynamic therapy targeted to pathogens. *Int J Immunopathol Pharmacol* 17:245–254.
- Demidova TN, Hamblin MR (2005) Effect of cell-photosensitizer binding and cell density on microbial photoinactivation. *Antimicrob Agents Chemother* 49:2329–2335.
- Detty MR, Gibson SL, Wagner SJ (2004) Current clinical and preclinical photosensitizers for use in photodynamic therapy. *J Med Chem* 47:3897–3915.
- Dolmans DE, Fukumura D, Jain RK (2003) Photodynamic therapy for cancer. *Nat Rev Cancer* 3:380–387.
- Fingar VH, Wieman TJ, Karavolos PS, Doak KW, Ouellet R, van Lier JE (1993) The effects of photodynamic therapy using differently substituted zinc phthalocyanines on vessel constriction, vessel leakage and tumor response. *Photochem Photobiol* 58:251–258.
- Foley S, Crowley C, Smaih M, Bonfils C, Erlanger BF, Seta P, Larroque C (2002) Cellular localization of a water-soluble fullerene derivative. *Biochem Biophys Res Commun* 294:116–119.
- Foote CS (1991) Definition of Type-I and Type-II photosensitized oxidation. *Photochem Photobiol* 54:659–659.
- Foote CS (1994) Photophysical and photochemical properties of fullerenes. *Top Curr Chem* 169:347–363.
- Gharbi N, Pressac M, Hadchouel M, Szwarc H, Wilson SR, Moussa F (2005) [60]fullerene is a powerful antioxidant in vivo with no acute or subacute toxicity. *Nano Lett* 5:2578–2585.
- Girotti AW (1983) Mechanisms of photosensitization. *Photochem Photobiol* 38:745–51.
- Girotti AW (1985) Mechanisms of lipid peroxidation. *J Free Radic Biol Med* 1:87–95.
- Granville DJ, Carthy CM, Jiang H, Shore GC, McManus BM, Hunt DW (1998) Rapid cytochrome c release, activation of caspases 3, 6, 7 and 8 followed by Bap31 cleavage in HeLa cells treated with photodynamic therapy. *FEBS Lett* 437:5–10.

- Greer A (2006) Christopher Foote's discovery of the role of singlet oxygen [1O_2 ($^1\Delta_g$)] in photosensitized oxidation reactions. *Acc Chem Res* 39:797–804.
- Grune T, Klotz LO, Gieche J, Rudeck M, Sies H (2001) Protein oxidation and proteolysis by the nonradical oxidants singlet oxygen or peroxynitrite. *Free Radic Biol Med* 30:1243–1253.
- Guldi DM, Prato M (2000) Excited-state properties of C(60) fullerene derivatives. *Acc Chem Res* 33:695–703.
- Gupta S, Ahmad N, Mukhtar H (1998) Involvement of nitric oxide during phthalocyanine (Pc4) photodynamic therapy-mediated apoptosis. *Cancer Res* 58:1785–1788.
- Hahn SM, Putt ME, Metz J, Shin DB, Rickter E, Menon C, Smith D, Glatstein E, Fraker DL, Busch TM (2006) Photofrin uptake in the tumor and normal tissues of patients receiving intraperitoneal photodynamic therapy. *Clin Cancer Res* 12:5464–5470.
- Hamblin MR, Hasan T (2004) Photodynamic therapy: a new antimicrobial approach to infectious disease? 3:436–450.
- Hancock RE, Bell A (1988) Antibiotic uptake into gram-negative bacteria. *Eur J Clin Microbiol Infect Dis* 7:713–720.
- Hirayama J, Abe H, Kamo N, Shinbo T, Ohnishi-Yamada Y, Kurosawa S, Ikebuchi K, Sekiguchi S (1999) Photoinactivation of vesicular stomatitis virus with fullerene conjugated with methoxy polyethylene glycol amine. *Biol Pharm Bull* 22:1106–1109.
- Ikeda A, Doi Y, Hashizume M, Kikuchi J, Konishi T (2007a) An extremely effective DNA photocleavage utilizing functionalized liposomes with a fullerene-enriched lipid bilayer. *J Am Chem Soc* 129:4140–4141.
- Ikeda A, Doi Y, Nishiguchi K, Kitamura K, Hashizume M, Kikuchi J, Yogo K, Ogawa T, Takeya T (2007b) Induction of cell death by photodynamic therapy with water-soluble lipid-membrane-incorporated [60]fullerene. *Org Biomol Chem* 5:1158–1160.
- Irie K, Nakamura Y, Ohigashi H, Tokuyama H, Yamago S, Nakamura E (1996) Photocytotoxicity of water-soluble fullerene derivatives. *Biosci Biotechnol Biochem* 60:1359–1361.
- Isobe H, Nakanishi W, Tomita N, Jinno S, Okayama H, Nakamura E (2006) Nonviral gene delivery by tetraamino fullerene. *Mol Pharm* 3:124–34.
- Jensen AW, Wilson SR, Schuster DI (1996) Biological applications of fullerenes. *Bioorg Med Chem* 4:767–779.
- Kamat JP, Devasagayam TP, Priyadarsini KI, Mohan H, Mittal JP (1998) Oxidative damage induced by the fullerene C60 on photosensitization in rat liver microsomes. *Chem Biol Interact* 114:145–159.
- Kamat JP, Devasagayam TP, Priyadarsini KI, Mohan H (2000) Reactive oxygen species mediated membrane damage induced by fullerene derivatives and its possible biological implications. *Toxicol* 155:55–61.
- Kasermann F, Kempf C (1997) Photodynamic inactivation of enveloped viruses by buckminsterfullerene. *Antiviral Res* 34:65–70.
- Kasermann F, Kempf C (1998) Buckminsterfullerene and photodynamic inactivation of viruses. *Rev Med Virol* 8:143–151.
- Kessel D (1982) Components of hematoporphyrin derivatives and their tumor-localizing capacity. *Cancer Res* 42:1703–1706.
- Kessel D (1986) Photosensitization with derivatives of haematoporphyrin. [Review]. *Int J Radiat Biol Relat Stud Phys Chem Med* 49:901–907.
- Kessel D (1989a) On the purity and definition of oligomeric HPD formulations. *J Photochem Photobiol B* 3:637–638.
- Kessel D (1989b) Probing the structure of HPD by fluorescence spectroscopy. *Photochem Photobiol* 50:345–350.
- Kessel D, Thompson P (1987) Purification and analysis of hematoporphyrin and hematoporphyrin derivative by gel exclusion and reverse-phase chromatography. *Photochem Photobiol* 46:1023–1025.
- Kessel D, Thompson P, Musselman B, Chang CK (1987a) Chemistry of hematoporphyrin-derived photosensitizers. *Photochem Photobiol* 46:563–568.

- Kessel D, Thompson P, Musselman B, Chang CK (1987b) Probing the structure and stability of the tumor-localizing derivative of hematoporphyrin by reductive cleavage with LiAlH_4 . *Cancer Res* 47:4642–4645.
- Kessel D, Luo Y, Mathieu P, Reiners JJ (2000) Determinants of the apoptotic response to lysosomal photodamage. *Photochem Photobiol* 71:196–200.
- Koeppel R, Sariciftci NS (2006) Photoinduced charge and energy transfer involving fullerene derivatives. *Photochem Photobiol Sci* 5:1122–1131.
- Kral V, Davis J, Andrievsky A, Kralova J, Synytsya A, Pouckova P, Sessler JL (2002) Synthesis and biolocalization of water-soluble sapphyrins. *J Med Chem* 45:1073–1078.
- Krätschmer W, Lamb LD, Fostiropoulos K, Huffman DR (1990) Solid C60: a new form of carbon. *Nature* 347:354–356.
- Kroto HW, Heath JR, O'Brien SC, Curl RF, Smalley RE (1985) C60: Buckminsterfullerene. *Nature* 318:162–163.
- Lambrechts SA, Aalders MC, Langeveld-Klerks DH, Khayali Y, Lagerberg JW (2004) Effect of monovalent and divalent cations on the photoinactivation of bacteria with meso-substituted cationic porphyrins. *Photochem Photobiol* 79:297–302.
- Levi N, Hantgan RR, Lively MO, Carroll DL, Prasad GL (2006) C60-Fullerenes: detection of intracellular photoluminescence and lack of cytotoxic effects. *J Nanobiotechnology* 4:14.
- Li R, Bounds DJ, Granville D, Ip SH, Jiang H, Margaron P, Hunt DW (2003) Rapid induction of apoptosis in human keratinocytes with the photosensitizer QLT0074 via a direct mitochondrial action. *Apoptosis* 8:269–275.
- Liang-Takasaki CJ, Makela PH, Leive L (1982) Phagocytosis of bacteria by macrophages: changing the carbohydrate of lipopolysaccharide alters interaction with complement and macrophages. *J Immunol* 128:1229–35.
- Lin YL, Lei HY, Wen YY, Luh TY, Chou CK, Liu HS (2000) Light-independent inactivation of dengue-2 virus by carboxyfullerene C3 isomer. *Virology* 275:258–262.
- Liu J, Ohta S, Sonoda A, Yamada M, Yamamoto M, Nitta N, Murata K, Tabata Y (2007) Preparation of PEG-conjugated fullerene containing Gd(3+) ions for photodynamic therapy. *J Control Rel* 117:104–10.
- Liu Y, Zhao YL, Chen Y, Liang P, Li L (2005) A water-soluble beta cyclodextrin derivative possessing a fullerene tether as an efficient photodriven DNA-cleavage reagent. *Tetrahedron Lett* 46:2507–2511.
- Ma J, Jiang L (2001) Photogeneration of singlet oxygen (O_2) and free radicals ($\text{Sen}^{\cdot-}$, $\text{O}_2^{\cdot-}$) by tetra-brominated hypocrellin B derivative. *Free Radic Res* 35:767–777.
- Martin N, Maggini M, Guldi DM (2000) Functionalized Fullerenes. Proceedings of the International Symposium, Vol. 9, The Electrochemical Society, Toronto, Canada.
- Merchat M, Bertolini G, Giacomini P, Villanueva A, Jori G (1996) Meso-substituted cationic porphyrins as efficient photosensitizers of gram-positive and gram-negative bacteria. *J Photochem Photobiol B* 32:153–157.
- Midden WR, Dahl TA (1992) Biological inactivation by singlet oxygen: distinguishing $\text{O}_2(1 \text{ delta } g)$ and $\text{O}_2(1 \text{ sigma } g^+)$. *Biochim Biophys Acta* 1117:216–222.
- Milanesio ME, Alvarez MG, Rivarola V, Silber JJ, Durantini EN (2005) Porphyrin-fullerene C60 dyads with high ability to form photoinduced charge-separated state as novel sensitizers for photodynamic therapy. *Photochem Photobiol* 81:891–897.
- Minnock A, Vernon DI, Schofield J, Griffiths J, Parish JH, Brown SB (1996) Photoinactivation of bacteria. Use of a cationic water-soluble zinc phthalocyanine to photoinactivate both gram-negative and gram-positive bacteria. *J. Photochem. Photobiol. B* 32:159–164.
- Miyata N, Yamakoshi Y, Nakanishi I (2000) Reactive species responsible for biological actions of photoexcited fullerenes. *J Pharm Soc Jpn* 120:1007–1016.
- Moan J, Berg K (1991) The photodegradation of porphyrins in cells can be used to estimate the lifetime of singlet oxygen. *Photochem Photobiol* 53:549–553.
- Mroz P, Pawlak A, Satti M, Lee H, Wharton T, Gali H, Sarna T, Hamblin MR (2007a) Functionalized fullerenes mediate photodynamic killing of cancer cells: Type I versus Type II photochemical mechanism. *Free Radic Biol Med* 43:711–9.

- Mroz P, Pawlak A, Satti M, Lee H, Wharton T, Gali H, Sarna T, Hamblin MR (2007b) Functionalized fullerenes mediate photodynamic killing of cancer cells: Type I versus Type II photochemical mechanism. *Free Radical Biol Med* 43:711–719.
- Mroz P, Tegos GP, Gali H, Wharton T, Sarna T, Hamblin MR (2007c) Photodynamic therapy with fullerenes. *Photochem Photobiol Sci* 6:1139–1149.
- Nakamura E, Isobe H (2003) Functionalized fullerenes in water. The first 10 years of their chemistry, biology, and nanoscience. *Acc Chem Res* 36:807–815.
- Nakanishi I, Fukuzumi S, Konishi T, Ohkubo K, Fujitsuka M, Ito O, Miyata N (2001) In: Kamat PV, Guldi DM, and Kadish DM (eds.) Fullerenes for the new millennium, The Electrochemical Society, Pennigton, NJ, X1, Toronto, Canada, pp. 138–151.
- Ochsner M (1997) Photophysical and photobiological processes in the photodynamic therapy of tumours. *J Photochem Photobiol B* 39:1–18.
- Pantarotto D, Tagmatarchis N, Bianco A, Prato M (2004) Synthesis and biological properties of fullerene-containing amino acids and peptides. *Mini Rev Med Chem* 4:805–814.
- Peng Q, Moan J, Nesland JM, Rimington C (1990) Aluminum phthalocyanines with asymmetrical lower sulfonation and with symmetrical higher sulfonation: a comparison of localizing and photosensitizing mechanism in human tumor LOX xenografts. *Int J Cancer* 46:719–26.
- Porter AE, Gass M, Muller K, Skepper JN, Midgley P, Welland M (2007) Visualizing the uptake of C60 to the cytoplasm and nucleus of human monocyte-derived macrophage cells using energy-filtered transmission electron microscopy and electron tomography. *Environ Sci Technol* 41:3012–7.
- Rancan F, Rosan S, Boehm F, Cantrell A, Brellreich M, Schoenberger H, Hirsch A, Moussa F (2002) Cytotoxicity and photocytotoxicity of a dendritic C(60) mono-adduct and a malonic acid C(60) tris-adduct on Jurkat cells. *J Photochem Photobiol B* 67:157–162.
- Rancan F, Helmreich M, Molich A, Jux N, Hirsch A, Roder B, Witt C, Bohm F (2005) Fullerene-porphyrin complexes as sensitizer for photodynamic therapy: uptake and photo-induced cytotoxicity on Jurkat cells. *J Photochem Photobiol B* 80:1–7.
- Ravanat JL, Cadet J (1995) Reaction of singlet oxygen with 2'-deoxyguanosine and DNA. Isolation and characterization of the main oxidation products. *Chem Res Toxicol* 8:379–388.
- Rosenthal I, Murali Krishna C, Riesz P, Ben-Hur E (1986) The role of molecular oxygen in the photodynamic effect of phthalocyanines. *Radiat Res* 107:136–142.
- Sayes CM, Gobin AM, Ausman KD, Mendez J, West JL, Colvin VL (2005) Nano-C60 cytotoxicity is due to lipid peroxidation. *Biomaterials* 26:7587–7595.
- Schmidt R (2006) Photosensitized generation of singlet oxygen. *Photochem Photobiol* 82:1161–1177
- Scrivens WA, Tour JM, Creek KE, Pirisi L (1994) Synthesis of C-14-labeled C-60, its suspension in water, and its uptake by human keratinocytes. *J Am Chem Soc* 116:4517–4518.
- Sera N, Tokiwa H, Miyata N (1996) Mutagenicity of the fullerene C60-generated singlet oxygen dependent formation of lipid peroxides. *Carcinogenesis* 17:2163–2169.
- Spesia MB, Milanesio ME, Durantini EN (2008) Synthesis, properties and photodynamic inactivation of *Escherichia coli* by novel cationic fullerene C(60) derivatives. *Eur J Med Chem* 43(4):853–861.
- Stockert JC, Juarranz A, Villanueva A, Canete M (1996) Photodynamic damage to HeLa cell microtubules induced by thiazine dyes. *Cancer Chemother Pharmacol* 39:167–169.
- Szeimies RM, Karrer S, Abels C, Steinbach P, Fickweiler S, Messmann H, Baumler W, Landthaler M (1996) 9-Acetoxy-2,7,12,17-tetrakis-(beta-methoxyethyl)-porphycene (ATMPn), a novel photosensitizer for photodynamic therapy: uptake kinetics and intracellular localization. *J Photochem Photobiol B* 34:67–72.
- Tabata Y, Murakami Y, Ikada Y (1997) Photodynamic effect of polyethylene glycol-modified fullerene on tumor. *Jpn J Cancer Res* 88:1108–1116.
- Tagmatarchis N, Shinohara H (2001) Fullerenes in medicinal chemistry and their biological applications. *Mini Rev Med Chem* 1:339–348.
- Tegos GP, Demidova TN, Arcila-Lopez D, Lee H, Wharton T, Gali H, Hamblin MR (2005) Cationic fullerenes are effective and selective antimicrobial photosensitizers. *Chem Biol* 12:1127–1135.

- Tokuyama H, Yamago S, Nakamura E (1993) Photoinduced biochemical activity of fullerene carboxylic acid. *J Am Chem Soc* 115:7918–7919.
- Yamakoshi Y, Sueyoshi S, Miyata N (1999) Biological activity of photoexcited fullerene. *Bull Natl Inst Health Sci* 117:50–60.
- Yamakoshi Y, Umezawa N, Ryu A, Arakane K, Miyata N, Goda Y, Masumizu T, Nagano T (2003) Active oxygen species generated from photoexcited fullerene (C60) as potential medicines: O₂^{-•} versus 1O₂. *J Am Chem Soc* 125:12803–12809.
- Yamakoshi YN, Yagami T, Sueyoshi S, Miyata N (1996) Acridine Adduct of [60]Fullerene with Enhanced DNA-Cleaving Activity. *J Org Chem* 61:7236–7237.
- Yang XL, Fan CH, Zhu HS (2002) Photo-induced cytotoxicity of malonic acid [C(60)]fullerene derivatives and its mechanism. *Toxicol In Vitro* 16:41–46.
- Yang XL, Huang C, Qiao XG, Yao L, Zhao DX, Tan X (2007) Photo-induced lipid peroxidation of erythrocyte membranes by a bis-methanophosphonate fullerene. *Toxicol In Vitro* 21(8): 1493–1498.
- Yu C, Canteenwala T, Chen HH, Chen BJ, Canteenwala M, Chiang LY (1999) Hexa(sulfobutyl) fullerene-induced photodynamic effect on tumors in vivo and toxicity study in rats. *Proc Electrochem Soc* 99:234–249.
- Yu C, Canteenwala T, Chiang LY, Wilson BC, Pritzker K (2005a) Photodynamic effect of hydrophilic C60-derived nanostructures for catalytic antitumoral antibacterial applications. *Synth Metals* 153:37–40.
- Yu C, Canteenwala T, El-Khouly ME, Araki Y, Pritzker K, Ito O, Wilson BC, Chiang LY (2005b) Efficiency of singlet oxygen production from self-assembled nanospheres of molecular micelle-like photosensitizers FC4S. *J Mater Chem* 15:1857–1864.
- Zakharian TY, Seryshev A, Sitharaman B, Gilbert BE, Knight V, Wilson LJ (2005) A fullerene-paclitaxel chemotherapeutic: synthesis, characterization, and study of biological activity in tissue culture. *J Am Chem Soc* 127:12508–12509.

Chapter 5

Photodynamic Inactivation of Enveloped Viruses by Fullerene: Study of Efficacy and Safety

Vladimir V. Zarubaev, Inna Belousova, Vladimir Rylkov, Alexander Slita, Alexey Sirotkin, Pavel Anfimov, Tatyana Muraviova, and Andrey Starodubtsev

Abstract Viruses are the most dangerous contaminants of human blood and blood products. The purpose of this study was to investigate the light-mediated virus-inactivating properties of fullerene and its effect on the intactness of biological fluids. Influenza virus was propagated in chicken embryos, and a water suspension of C₆₀ fullerene was added to the allantoic fluid. The fluid was light-irradiated with a constant flow of oxygen through the specimen, and the dynamics of the virus titer were studied in Madin-Darby canine kidney (MDCK) cells. The morphology of the virions was studied by electron microscopy (EM). The electrophoretic pattern of the proteins in the allantoic fluid and blood plasma, as well as the growth properties of the calf serum were compared before and after 6 h of irradiation. A dramatic drop of infectious titer (from 6 to 0 log₁₀ EID₅₀) in the virus was observed within 2 h after the start of irradiation. No change in the titers was observed in control specimens without the fullerene, or light, or oxygen. EM revealed numerous defects in the morphology of the virions (destruction of the outer membrane) leading to the loss of infectious properties in the virus. Based on comparison of proteins and growth properties of the serum, no differences were revealed between intact and irradiated biological fluids. Water-insoluble fullerenes may therefore be considered an effective and safe way to inactivate enveloped viruses in biological materials including blood products.

Keywords Virus inactivation; fullerene; decontamination; blood serum

5.1 Introduction

The problem of quality control in donor blood and blood products is of great importance for a health service in practice. Among infectious agents that contaminate blood, mention should be made of human immunodeficiency virus, hepatitis B and C viruses, and human cytomegalovirus (Ender, 2004; Mohr, 2000). In the past decade, the role of

Influenza Research Institute, 15/17 Prof. Popova St., St. Petersburg 197376,
Russian Federation State Optical Institute, 199034, St. Petersburg, Russian Federation
Email: zarubaev@influenza.spb.ru

these agents has dramatically increased due to changes in ecology, human behavior, and the process of the evolution of natural viruses in the human population.

Currently, all donors and blood preparations undergo multistage and expensive control to ensure the absence of viral contamination. In this respect, the development of affordable methods of inactivation of viruses could be an important step toward safety in hemotransfusion. Currently used treatments such as UV irradiation damage therapeutic components of the blood (Williamson and Cardigan, 2003), so alternative selective approaches are needed for this purpose. Among them, chemotherapy, photochemotherapy (PCT), and photodynamic antibacterial therapy should be noted (Mohr, 2000).

Previously, enveloped viruses have been shown to be effectively inactivated by compounds generating singlet oxygen. The most widely used are water-soluble dyes. Virus-inactivating properties have been reported for dyes belonging to various chemical classes, in particular, phthalocyanins, merocyanins, derivatives of porphyrin, oxazines, and some others. Currently, the dye in clinical use is a compound from the class of phenothiazines – methylene blue, which demonstrates an optimal combination of toxicity/activity properties. The disadvantage of all these compounds is the difficulty or impossibility of removing from the solution the compounds themselves and/or their products of photodestruction. This step is necessary because some derivatives are supposed to be toxic (Käsermann and Kempf, 1997; Wainwright, 2002).

In this connection, the use of insoluble agents as photosensitizers seems promising. This approach, in particular, has been realized in respect to the suspension of crystal fullerene C_{60} (Käsermann and Kempf, 1997, 1998). Its marked advantage is that there are no byproducts of the destruction of fullerene and the compound can be easily removed from the solution by centrifugation. The high efficiency of C_{60} in viral inactivation has been demonstrated for specific enveloped viruses such as Semliki forest virus (SFV) and vesicular stomatitis virus (VSV) (Käsermann and Kempf, 1997, 1998). The inactivation was achieved in a model system where the virus was suspended in a saline buffer solution. The addition of 2% bovine serum albumin did not affect the kinetics of the photoinactivation of the virus.

The purpose of the present study was to investigate a photodynamic inactivation of influenza virus in the allantoic fluid of chicken embryos. Further, we have evaluated nonspecific effects of photodynamic treatment on the components of biological fluids.

5.2 Materials and Methods

5.2.1 Fullerene Preparation

A suspension of crystal fullerene C_{60} (1 mg/ml) in 0.15 M NaCl was used in experiments. To prepare the suspension, 60 mg of crystal fullerene was homogenized with a pestle, followed by sonication in 50 ml of saline for 60 min (5 min sonication/10 min interval). A freshly prepared suspension was used in experiments.

In a separate set of experiments, fullerene was used without preliminary homogenization.

5.2.2 Virus Propagation

Influenza virus A/Puerto Rico/8/34 (H1N1) was propagated in the allantoic cavity of chicken embryos for 48 h at 36 °C followed by overnight cooling at + 4 °C (Mahy, 1985). Allantoic fluid containing virus was harvested and centrifuged for 10 min at 3,000 rpm. To determine hemagglutinating activity, serial dual dilutions were prepared from the initial fluid, mixed with an equal volume of 1% chicken erythrocytes in saline in the wells of round-bottom plates and incubated at room temperature for 1 h. Hemagglutinating titer was considered as reciprocal to the final dilution of the initial fluid able to cause positive hemagglutination (HA) in the wells. Viruses with HA titer 64 or more were used in experiments.

In a separate set of experiments, in order to remove soluble components of allantoic fluid, the fluid was centrifuged for 1 h at 200,000 g. Supernatant was removed and virus was resuspended in saline in a volume equal to the initial volume of allantoic fluid.

5.2.3 Inactivation Assay

For photoinactivation, 25 ml of suspension of fullerene was added to an equal volume of virus-containing allantoic fluid. The mixture was placed in a cooled vessel and irradiated by visual light (the wavelengths in the resulting spectrum were 400–850 nm) under constant stirring and with constant access to oxygen. One milliliter aliquots were taken from the mixture at different time points followed by 10 min centrifugation of each specimen at 5,000 rpm. Both supernatant and pellets were then studied for viral infectious activity and morphology of virions, by virus titration and EM, respectively.

5.2.4 Determination of Viral Titer

A confluent monolayer of Madin-Darby canine kidney (MDCK) cells was grown in 96-well plates. Serial tenfold dilutions in minimal essential medium were prepared from the aliquots of allantoic fluid taken from the irradiated specimen. These dilutions were applied to MDCK cells and incubated for 48 h at 36 °C in 5% CO₂. The cells were then washed two times for 5 min with phosphate buffered saline (PBS) and incubated for 1 h with 100 µl of 0.5 mg/ml solution of 3-(4,5-dimethylthiazolyl-2) 2,5-diphenyltetrazolium bromide (MTT, ICN Biochemicals Inc., Aurora, Ohio). After 1 h, the colored deposit was dissolved in 100 µl DMSO, and optical density in the wells was measured on plate reader Victor 1420 (Perkin Elmer, Finland). Based on the data obtained, the infectious titer of the virus was determined as a decimal logarithm of reciprocal to the dilution of the specimen causing destruction of 50% of cells. The inhibiting action of irradiation was evaluated by decreasing the virus' titer.

5.2.5 *Electron Microscopy*

A copper disc with a carbon cover was placed onto a drop of the sample for 15–20 s, then the support was washed with distilled water and contrasted using a 1.5% sodium salt of phosphotungstic acid, pH 7.1. Preparations were dried at room temperature and studied under a JEM-100S electron microscope (JEOL, Tokyo) at instrumental magnification 5,000–50,000.

5.2.6 *Study of Growth Activity of Serum*

Cell lines U937 (human lymphoblastoid cells) and T-98G (human astrocytoma) were obtained from the collection of cell lines at the Influenza Research Institute. T-98G cells were grown on a DMEM medium with the addition of 10% calf serum, and U937 cells on RPMI1640 (Biolog, St. Petersburg) with 10% calf serum.

Calf serum was added to the medium for cell culture to 10% concentration. T98G or U937 cells were seeded onto 25 cm² flasks for cell culture (Nunc, Denmark). Cells were cultivated for 72 h without serum, with 10% of intact serum or 10% serum after 6 h of photodynamic treatment. After the incubation period cells were harvested with chymotrypsine and their number was calculated in a hemocytometer chamber.

The proliferative index of the culture was estimated as the ratio of number of cells per 1 ml of medium after 72 h of cultivation to the initial number of cells per 1 ml of medium.

5.2.7 *Denaturing Electrophoresis*

Sample preparation. All allantoic fluid of chicken embryos or calf serum used in experiments contained influenza virus (10^4 – 10^6 EID₅₀/ml). The samples of biological fluids underwent photodynamic treatment as described above. One milliliter aliquots were taken before treatment and at 3 and 6 h after the start of experiment. To analyze the effect of photodynamic treatment on proteins we used alkaline denaturing electrophoresis in the presence of sodium dodecylsulfate (SDS) and β -mercaptoethanol (β -ME).

Separation of proteins. Aliquots of biological fluids (blood serum or allantoic fluid) were mixed with the Laemmli buffer for the samples. For proteins denaturation samples were boiled for 5 min. Samples were loaded in and separated in the gel by Miniprotein II unit (BioRad). The voltage was 80 V when samples were in concentrating gel and 100 V when in separating gel. The movement of the proteins was tracked by bromophenol blue.

After completion of electrophoresis, the gel was stained with Coomassie blue. To prepare the staining solution, 40 mg Coomassie blue R-250 was dissolved in 25 ml isopropanol and 10 ml glacial acetic acid. The solution was filtered and the volume was increased to 100 ml with distilled water. The gel was placed in staining solution for 1 h, followed by washing with 10% acetic acid/2.5% isopropanol.

In order to quantitatively analyze the protein patterns, the gels were scanned, and the relative optical density of the bands was plotted against the distance from the start of the gel.

5.3 Results

5.3.1 *Viral Inactivation*

The infectious titers of influenza virus were determined in the irradiated specimen at different time points. The kinetics of the virus' activity in saline and allantoic fluid in the presence of fullerene and oxygen are presented in Fig. 5.1.

As can be seen from the data presented, the suspension of crystal C_{60} did not itself affect the influenza virus. In all control experiments without oxygen and irradiation the infectious activity of the virus remained on the same level throughout the experiment (Fig. 5.1). This was true for both virus in original allantoic fluid and virus resuspended in saline. Exposure of the virus to oxygen without irradiation did not affect the viral titer either.

Using the C_{60} suspension prepared from non-homogenized fullerene, the efficacy of inactivation of the virus was much lower compared to the fine suspension. The viral titer in this case decreased by one to two times, suggesting that the efficacy of inhibition of the virus strongly depends on the total surface of the fullerene exposed to oxygen and liquid.

When exposure to oxygen and light irradiation were commenced simultaneously, the infectious activity of the virus remained on the initial level for 30–50 min. This period of induction was observed both in the allantoic fluid and saline.

The kinetics of viral photoinactivation in the allantoic fluid differs substantially from that in saline (Fig. 5.1). Irrespective of the time of primary saturation with oxygen, the 15–20 min period of induction was always observed after the start of irradiation. The virus was then inactivated during the next 1.5–2 h, followed by a constant value for the viral titer up to 6 h of the experiment. The addition of a new portion of fullerene suspension resulted in a new stage of viral inactivation. We also observed the formation of fullerene-colored agglomerates in the cuvettes. Their size by the end of the experiment was 0.1–0.3 mm. Based on data resulting from EM, these agglomerates represent the aggregates of protein and other components of allantoic fluid (Fig. 5.2). The formation of these particles becomes visible approximately 1 h after the start of irradiation, as their number and size increase during the course of irradiation. These conglomerates could bind the fullerene particles, thus

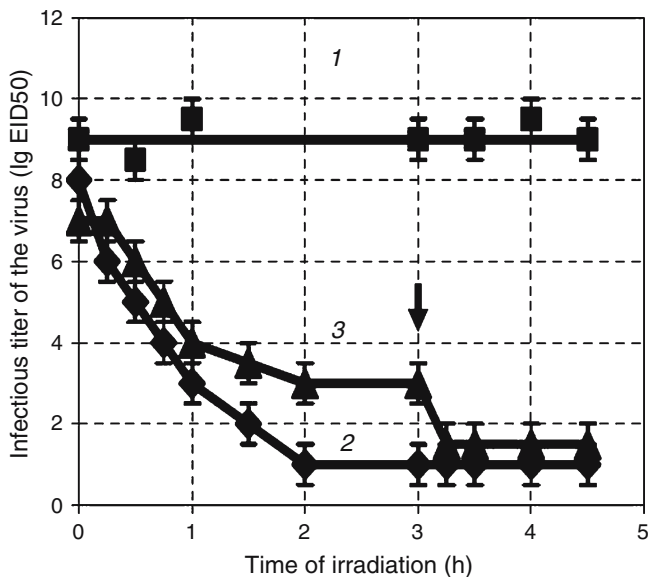


Fig. 5.1 Inactivation of influenza virus in allantoic fluid by fullerene. 1: virus in allantoic fluid, no illumination; 2: virus in saline, specific illumination 85 mW/cm^2 ; and 3: virus in allantoic fluid, specific illumination 85 mW/cm^2 . The moment of addition of fresh fullerene suspension is indicated by an arrow

restricting their active surface and decreasing the rate of viral inactivation. Probably for this reason the addition of a fresh portion of fullerene, not bound with proteins, leads to acceleration in inactivation of the virus.

5.3.2 Morphological Study

As was shown by EM, application of a water suspension of C_{60} fullerene combined with the presence of light and exposure to oxygen resulted in gradual destruction of influenza virions in the allantoic fluid. The intact virions prior to treatment looked like round-shaped particles with surface glycoproteins protruding from the envelope (Fig. 5.3a). In specimens treated with light in the presence of C_{60} and with oxygen exposure for 0.3–0.5 h no substantial changes of structure were observed. Nevertheless, the same treatment for 6 h resulted in destruction of most (~95%) of the virions. This was morphologically reflected in fragmentation of the surface membrane and loss of surface glycoproteins that serve as receptor-binding components of the virion and are responsible for their attachment to the surface of the target cells (Fig. 5.3b).

The relative number of intact and morphologically defective virions has been calculated. The kinetics of this parameter in the specimens is summarized in Fig. 5.4. As this diagram makes clear, the number of intact virions steadily decreases during the course of photodynamic therapy.

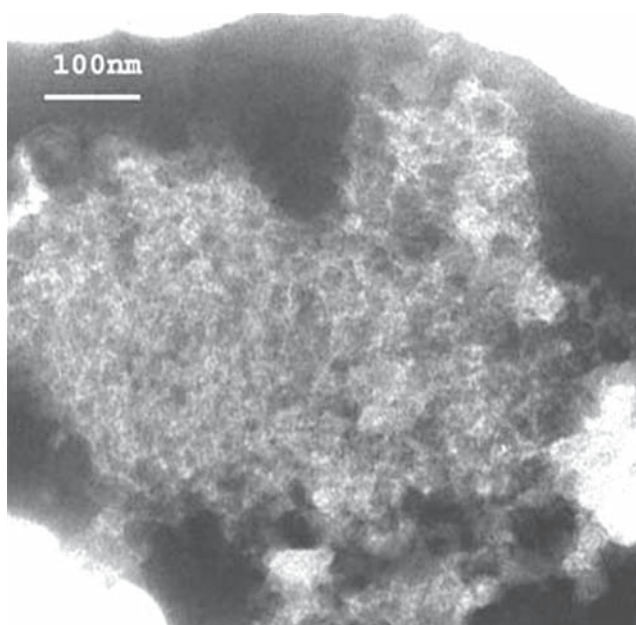


Fig. 5.2 Protein conglomerates in allantoic fluid after 5 h of irradiation in the presence of C_{60} and oxygen. Bar 100 nm. Negative contrast

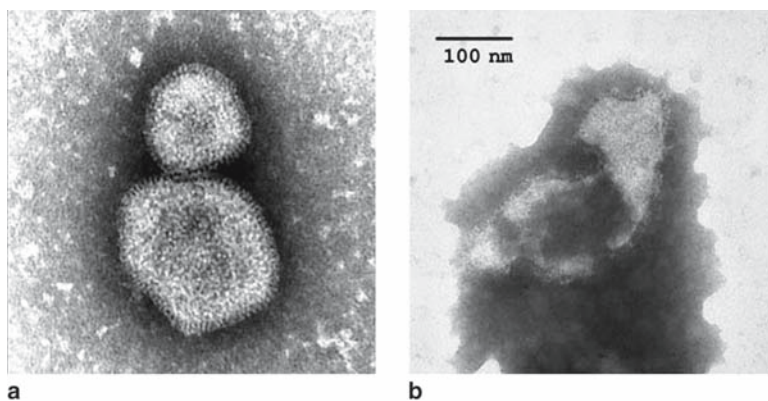


Fig. 5.3 Destruction of virions of influenza under irradiation in the presence of C_{60} suspension and O_2 . (a) Intact virions in allantoic fluid; and (b) virions after 5 h of irradiation in presence of oxygen. Note the fragmentation of the outer membrane of the virions and the loss of a significant part of surface glycoproteins. Negative contrast, bar 100 nm

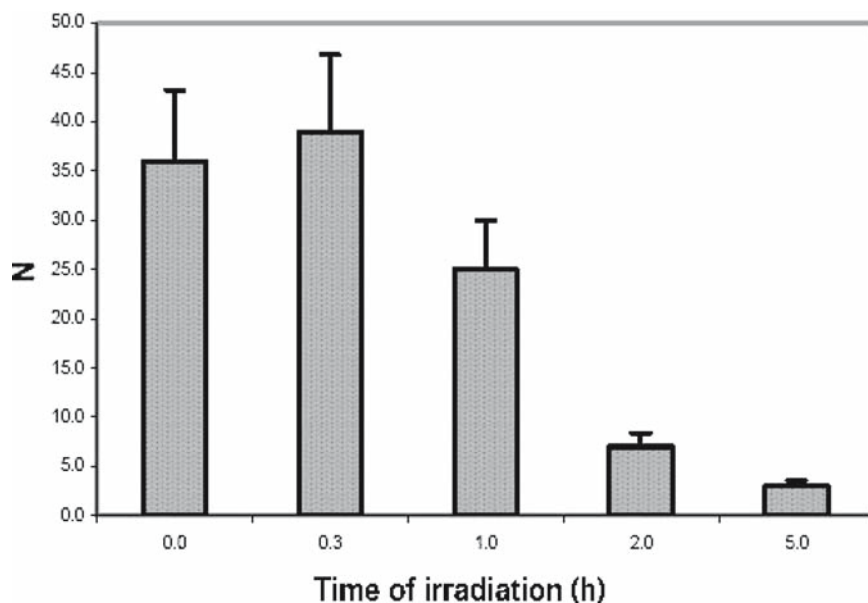


Fig. 5.4 Destruction of influenza virions after treatment with C_{60} in the presence of light and oxygen. N is the number of intact virions for one field of vision

5.3.3 Electrophoresis Study

In the version we used, electrophoresis of proteins makes it possible to separate proteins and evaluate molecular weight and relative amount of each fraction. Analysis of this data, therefore, has permitted us to detect the following types of modification of proteins resulting from photodynamic treatment:

- Destruction of protein molecules. In this case one can expect a decrease in the molecular weight of components of the protein mixture, reflected in a decrease in the intensity of bands in the high-molecular zone (closer to the start) and an increase in the relative amount of low-molecular weight components (in the proximal zone of the gel).
- Aggregation of proteins into oligo- and poly-globular complexes. In this case the opposite situation will occur, i.e., a shift of the density of bands towards the high-molecular weight zone (start).

Results of electrophoretic analysis of proteins in the allantoic fluid and blood serum before and after photodynamic treatment are presented in Figs. 5.5 and 5.6. Visually, we did not detect any changes in the position and intensity of protein bands. In order to quantitatively analyze these parameters we scanned the gels and measured the relative optical density of the bands (Figs. 5.7 and 5.8).

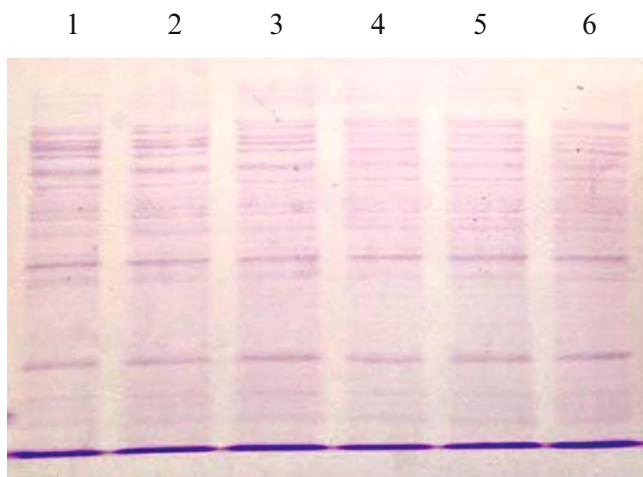


Fig. 5.5 Electrophoresis pattern of proteins in the allantoic fluid of chicken embryos. Lanes 1–3: intact fluid; lanes 4–6: fluid after 6 h of irradiation

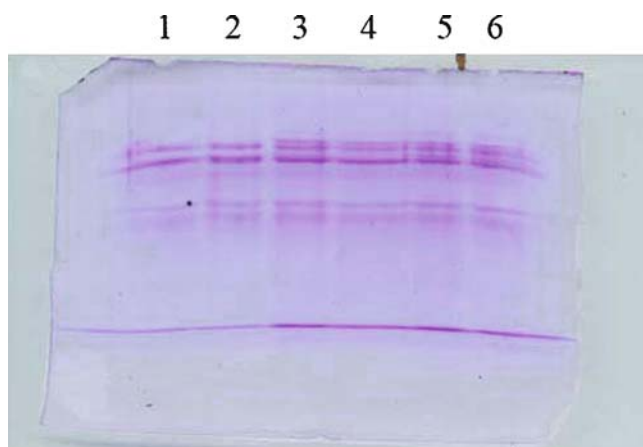


Fig. 5.6 Electrophoresis pattern of proteins of blood serum. Lanes 1–3: intact serum, lanes 4–6: serum after 6 h of irradiation (*See Color Plates*)

As can be seen from the figures, there are no visual differences between intact and irradiated specimens, independently of duration of irradiation. This suggests that the molecular weights of protein components neither increase (due to oxygen-induced aggregation of protein molecules into oligomers) nor decrease (due to nonspecific cleavage of the molecules) during the course of the treatment.

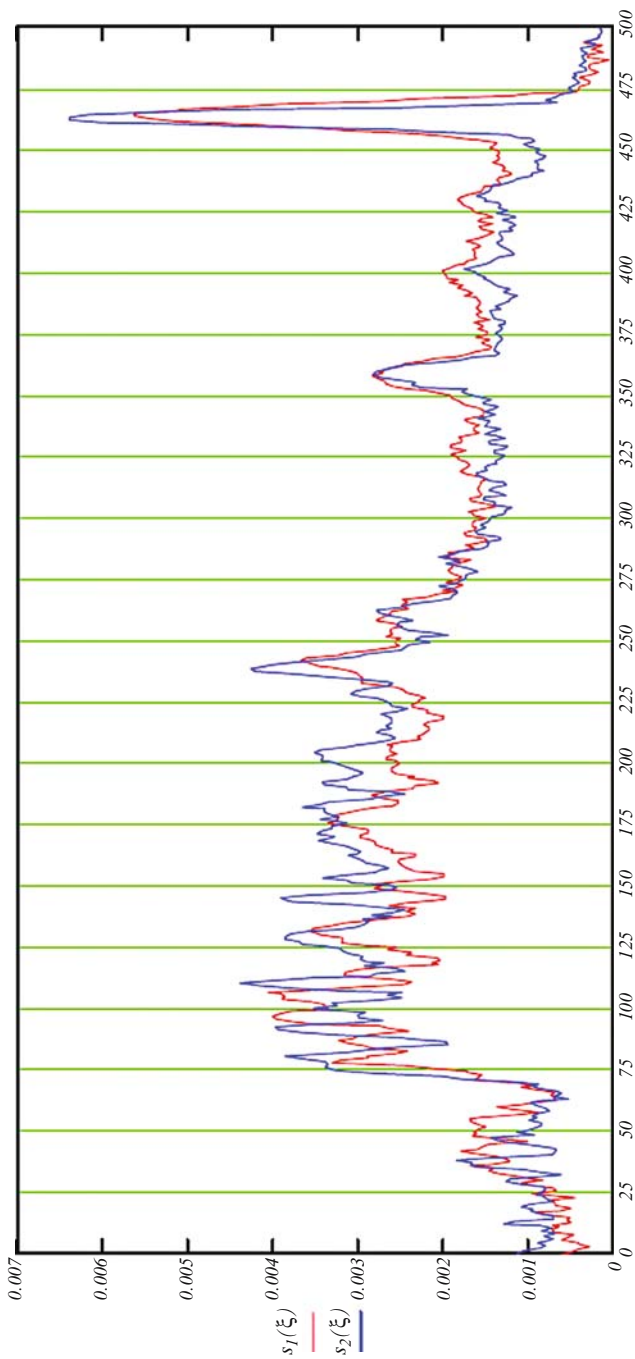


Fig. 5.7 Photometric representation of electrophoresis results. Allantoic fluid before (red) and after (blue) 6h of irradiation (See Color Plates)

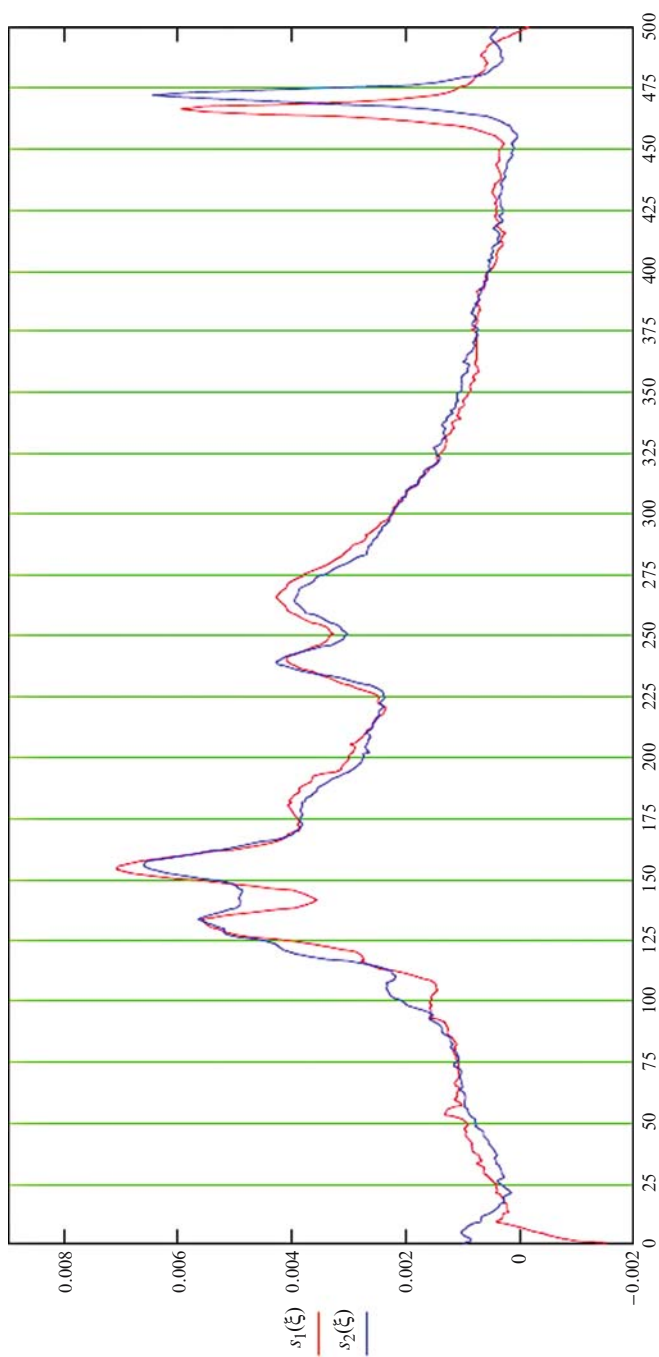


Fig. 5.8 Photometric representation of electrophoresis results. Blood serum before (red) and after (blue) 6 h of irradiation (See Color Plates)

From the data presented it can be concluded that the processes of both destruction and aggregation of proteins do not contribute significantly to the photodynamic treatment.

5.3.4 Study of Growth Activity of Cells in the Presence of Irradiated Serum

In order to compare the biological properties of the serum before and after treatment, its effect on the rate of proliferation of cells in the culture was studied. The results are presented in Table 5.1. As can be seen from these data, the proliferative activity of cells in the presence of the serum is significantly greater than that for serum-free medium. At the same time, 6 h of preliminary treatment of serum does not affect the proliferative activity of the cells. Therefore, the growth properties of the serum do not change after photodynamic treatment.

5.4 Discussion

In the present study we have investigated the process of photodynamic inactivation of influenza virus in the allantoic fluid of chicken embryos. This inactivation has been realized by C_{60} water suspension used as a photosensitizer. Similar studies have been carried out previously by Käserman and Kempf (1997, 1998). Unlike the latter studies, in which viruses were inactivated in salt solutions (buffer), our experiments were performed in a natural biological fluid that contains all typical components (proteins, lipids, salts, etc.). Comparing the viral inactivation over time in our experiments with previous results we conclude that the process described by Käserman and Kempf (1997, 1998) was more time-consuming, a fact that may significantly restrict its practical use.

Table 5.1 Growth properties of calf serum under photodynamic influence

Cell line	Seed dose (cells per ml)	Characteristics of proliferation					
		No serum		Intact (non-irradiated) serum		Irradiated serum	
		Number of cells	Proliferation index	Number of cells	Proliferation index	Number of cells	Proliferation index
U937	2×10^5	2.4×10^5	1.20	5.4×10^5	2.70	5.2×10^5	2.60
T98G	2×10^5	2.2×10^5	1.10	5.7×10^5	2.85	5.4×10^5	2.70

The course of viral photodynamic inactivation in allantoic fluid is probably directed by the following process: the initial period of induction is a result of the quenching of singlet oxygen (or other reactive forms of oxygen) by natural antioxidants present in the fluid (Kolb, 1991). Subsequently, a dramatic drop in the viral titer was observed. This then reached a plateau due to the consumption of the active fraction of the fullerene. This may be indirectly confirmed by the results of viral titration after the addition of a new portion of fullerene when the process of inactivation was observed again.

EM investigation of the C_{60} deposit did not reveal any increase in virions over the number of virions in supernatant. This suggests that the C_{60} used in the experiments does not possess a specific affinity to the virions (e.g., due to membrane tropism or other specific mechanism).

The particles of C_{60} are, therefore, uniformly distributed in the suspension and the interaction between fullerene-produced reactive oxygen species and components of allantoic fluid (including virions) is of a stochastic character. This may lead to photochemical modification of the biological components of the allantoic fluid, as was indirectly confirmed by visual and EM observation of aggregates (Fig. 5.2) and differences in foam formation between irradiated and non-irradiated specimens. This fact raises the question of the degree and significance of photomodification of components of the biological fluid during the course of inactivation of the viruses it contains. In other words, the action of singlet oxygen may be non-selective, i.e., following the procedure of photoinactivation infectious virions might be destroyed along with therapeutic components of the blood (red blood cells, leukocytes, etc.) or blood products (platelets, proteins, etc.), thus making them useless. Taking into account the relatively large size of the blood cells compared with the virions, these cells are supposed to be more vulnerable to the damage caused by singlet oxygen. The method we describe is, therefore, more appropriate for decontaminating cell-free blood products, above all, plasma. Plasma proteins can also serve, nevertheless, as a target for singlet oxygen destruction, so to apply this approach for clinical purposes the tests have been performed for clinical value of the plasma, namely, the intactness of its components. In addition, the growth properties of the serum have not been shown to change after photodynamic treatment. These two facts indirectly confirm that therapeutic properties of blood plasma will remain at the initial level or decrease slightly despite substantial inactivation of the virus.

It should be noted that the same problem exists for both other photosensitizers and other methods for decontamination of the blood and its components (e.g. absorption) (Mohr, 2000). The use of fullerenes is to be preferred to the use of photoactive dyes because the former are water-soluble components. Due to its insolubility in water, fullerene may be easily removed from the liquid phase after the procedure of decontamination.

As a result of our experiments, it was shown that the growth properties of the serum do not change after photodynamic treatment. Nevertheless, the infectious titer of influenza virus both in blood serum and allantoic fluid decreased from 6 to 0 \log_{10} EID₅₀ after the treatment. This fact suggests a selectivity of photodynamic treatment regarding the virions. In our opinion, this can be explained by the following.

Photodynamic treatment equally affects viral particles and protein components in biological fluid, but virions, being large supramolecular structures, are more vulnerable compared to protein molecules. For this reason, damage to one of the components of a virion leads to inactivation of the entire viral particle without affecting the growth properties of serum or the electrophoretic pattern of the proteins.

On the other hand, this procedure does not remove virus-specific components from the liquid. Even in cases where virions are destroyed completely following treatment, the product will remain immunogenic to the same extent as before the treatment. Nevertheless, no infectious virions able to reproduce, multiply, and cause an infectious disease will be found in the product.

5.5 Conclusion

1. Units and methods are developed to study the effect of active forms of oxygen on fullerene-based photosensitizers. The kinetics of the inactivation of influenza virus in saline and allantoic fluid during the course of photodynamic treatment using fullerene preparations is studied. Optimization of conditions has been conducted for viral inactivation (irradiation, doses, concentration of fullerene, and intensity of oxygen flow). Experiments are performed for inactivation of virus in blood serum.
2. Based on optimized conditions, complete inactivation of influenza virus is achieved in allantoic fluid (resulting in a decrease in the infectious titer of the virus from $>4-5 \log_{10} \text{EID}_{50}$ to 0) using separable fullerene-based photosensitizer.
3. Studies have been conducted for the intactness of biological fluids after photochemical treatment, in particular, proteins of allantoic fluid and blood serum, by methods of spectrophotometry and gel electrophoresis. The growth properties of serum were evaluated in cell culture. The protein composition of biological fluid was shown not to undergo dramatic changes during the course of photodynamic inactivation of viruses.

Acknowledgments This work was supported partially by an International Scientific Technical Center grant (ISTC #2593).

References

- Ender A et al. (2004) Screening of blood donations for HIV-1 and HCV RNA by transcription-mediated amplification assay: one year experience. *Transfus Med Hemother.* 31: 10–15.
- Käsermann F, Kempf C (1997) Photodynamic inactivation of enveloped viruses by buckminsterfullerene. *Antiviral Res.* 34: 65–70.
- Käsermann F, Kempf C (1998) Buckminsterfullerene and photodynamic inactivation of viruses. *Rev Med Virol.* 8: 143–151.

- Kolb E et al. (1991) Ascorbic acid concentration in plasma, in amniotic and allantoic fluids, in the placenta and in 13 tissues of sheep fetuses and newborn lambs. *Dtsch Tierarztl Wochenschr.* 98(11): 424–427.
- Mahy BWJ (1985) *Virology: a practical approach*. IRL Oxford Press, Washington, DC.
- Mohr H (2000) Inactivation of viruses in human plasma. *Methods Enzymol.* 319: 207–216.
- Wainwright M (2002) The emerging chemistry of blood product disinfection. *Chem Soc Rev.* 31: 128–136.
- Williamson LM, Cardigan R (2003) Methylene blue-treated fresh-frozen plasma: what is its contribution to blood safety? *Transfusion.* 43: 1322–1329.

Chapter 6

Effects of Photoexcited Fullerene C₆₀-Composites in Normal and Transformed Cells

S.V. Prylutska¹, I.I. Grynyuk¹, O.P. Matyshevska¹, A.A. Golub²,
A.P. Burlaka⁴, Yu.I. Prylutsky³, U. Ritter⁵, and P. Scharff⁵

Abstract The supramolecular composites containing fullerenes C₆₀ immobilized at nanosilica were used for the design of the molecular systems that can be an effective agent in cancer photodynamic therapy (PDT). In particular, it was shown that photoexcited fullerene C₆₀-containing composites decrease viability of transformed cells, intensify the process of lipid peroxidation (LPO) in cell membranes and accumulation of low-molecular weight DNA fragments, and also decrease the activity of electron-transport chain of mitochondria.

Keywords C₆₀ fullerene composites; normal and transformed cells; photoexcitation; reactive oxygen species

6.1 Introduction

Presently photodynamic therapy (PDT) is considered as a perspective way for therapy of different diseases, including cancer. PDT is a method based on the local light-induced activation of photosensitizers able to accumulate selectively in energy-deficient cells (malignant or dysplastic ones) not influencing the remaining normal cells of the body (Pass, 1993). Upon the action of irradiation of certain wavelength characteristic for individual photosensitizer, photochemical reaction occurs

¹Kyiv National Shevchenko University, Departments of Biochemistry, Volodymyrska Str., 64, 01033 Kyiv, Ukraine
Email: prylut@biocc.univ.kiev.ua

²Kyiv National Shevchenko University, Departments of Chemistry, Volodymyrska Str., 64, 01033 Kyiv, Ukraine

³Kyiv National Shevchenko University, Departments of Biophysics, Volodymyrska Str., 64, 01033 Kyiv, Ukraine

⁴R.E. Kavetsky Institute of Experimental Pathology, Oncology, and Radiobiology, Vasylykivska Str., 45, Kyiv, Ukraine

⁵Institute of Physics, Technical University of Ilmenau, D-98684 Ilmenau, Germany

that leads to selective destruction of malignant cells. Mechanism of PDT action consists in the fact that the molecule of photosensitizer after absorption of quantum of light switches to excited triplet state and enters into two types of reactions (Grossweiner et al., 1982). In the first type, interaction directly with the molecules of biological substrate occurs, thus leading to generation of free radicals. In the second type, interaction of the excited photosensitizer takes place with generation of singlet oxygen that is cytotoxic for vital cells due to the properties of potent oxidizer of biomolecules. At the final stage, photochemical reactions of both types lead to destructive changes of important structures of malignant cells and their death.

Fullerenes C_{60} are considered as perspective compounds for PDT. They are inert compounds that do not reveal toxic properties in low concentration range. Due to small size and hydrophobicity, fullerenes C_{60} are able to interact with biologic molecules, be embedded in membranes, and cause biologic effects (Foley et al., 2002; Kamat et al., 2000; Wilson, 2000). They are characterized by significant reducing potential and are able to absorb free radicals (Kamat et al., 2000; Tabata and Ikada, 1999). From the other side, cytotoxic effects of fullerenes C_{60} upon their photoexcitation has been revealed. Upon the action of ultraviolet or visible light irradiation, C_{60} molecule switches to triplet state. As a result of energy transfer (its efficacy reaches nearly 100%) from the excited fullerene C_{60} to molecular oxygen, intense generation of singlet oxygen takes place. Also the excited C_{60} molecule may be an acceptor of electrons. In the presence of donors of electrons in the medium (e.g., $NADH \rightarrow NAD^+$, H^+) the excited fullerene C_{60} may be reduced due to electron transfer and be converted to anion radical $C_{60}^{\bullet-}$, that in turn transfer electrons to molecular oxygen with generation of superoxide anion $O_2^{\bullet-}$ (Kamat et al., 2000; Guldi and Asmus, 1999; Hamano et al., 1997).

For potentiation of photosensitizing properties of fullerenes C_{60} to the composition of their molecules antenna is being introduced, for example, porphyrine, and anthracenal (Arbogast and Foote, 1991).

Apart from this, among the means to promote accumulation and retention of preparations applied in PDT, in tumor tissue, the increase in their molecular size via conjugation with inert carrier could be used. For example, upon intravenous introduction of fullerene C_{60} -polyethylene glycol (PEG) conjugate to mice it has been shown that this conjugate was accumulated in tumor tissue in large amount and was retained longer than in healthy tissue. This conjugate was not accumulated in other organs. The histology has proved that administration of irradiated C_{60} -PEG conjugate is causing notable necrosis of tumor without affecting healthy tissues (Tabata and Ikada, 1999).

So, fullerenes C_{60} and their derivatives may be potential damaging agents of biologic systems upon PDT, because upon irradiation C_{60} molecule is able to generate singlet oxygen, selectively penetrate tumor cells, and be accumulated there and could be easily removed from biologic medium.

Low affinity to polar solvents and fullerenes aggregation in water limit their use in biologic systems. To increase water solubility of fullerenes, few ways are used: solubilization with the use of some water-soluble polymers like PDT or polyvinylpyrrolidone, generation of complexes with cyclodextrines or calixarenes, and

covalent modification of surface with polar substitutes (Isaacs et al., 1997; Yamakoshi et al., 1994; Yoshida et al., 1994). However, the presence of large functional groups protecting spheroid of fullerene from water as well and numerous substitutes on its surface are influencing the properties of the molecule and may decrease its photosensitizing potential as well as ability to interact with biologic molecules (Da Ros et al., 2001).

For optimization of introduction of fullerenes in aqueous medium, prevention of aggregation, elevation of contact area, and for providing equable placement and specific interaction of fullerenes C₆₀ in the zone of contact with biologic material, we have carried out immobilization of C₆₀ molecules on the spheric particles of silicon oxide – aerosyl (the mean diameter of about 9nm), which is a highly dispersed chemically inert material with hydrophilic surface (Chuyiko, 2003). Generation of such composites is a perspective approach, because their content could be enriched by introduction of different components, in particular, the structures able to entrap light (porphyrines and anthracenal) and elevate photosensitizing effect of fullerenes.

The other way to introduce fullerenes C₆₀ to biomedium, that we have used, was based on the transfer of these molecules from organic solvent (e.g., toluene) to the water using ultrasound sonication (Scharff et al., 2004).

The aim of the work was evaluation of the ability of photoexcited fullerene C₆₀ and synthesized fullerene C₆₀-containing composites to generate reactive oxygen species (ROS) and to perform comparative analysis of the state of the cells of two types (normal ones – thymocytes, and malignant ones – the cells of ascite Erlich carcinoma [EAC] and leucosis L1210) by such indexes as viability, content of LPO products, MTT test, and DNA fragmentation upon incubation in the presence of photoexcited fullerene C₆₀.

6.2 Materials and Methods

Thymocytes were obtained by grinding thymus of rats of Wistar line weighing 120–150g through nylon lattice in the buffer A (3mM Na₂HPO₄, 5mM KCl, 120mM NaCl, 1mM CaCl₂, 10mM glucose, 1mM MgSO₄, 4mM NaHCO₃, 10mM HEPES, pH 7.4). Malignantly transformed cells were obtained at days 8–12 after intraperitoneal transplantation of ascitic Erlich's carcinoma cells to inbred mice (weighing 20g), and leucosis L1210 cells – to hybrid mice of F₁ line (DBA2 × C57Bl/6). Animals were maintained on the standard chow diet.

Water colloid solutions of fullerenes C₆₀ (10⁻⁴ M) were prepared as described in Scharff et al. (2004). Fullerene-aminopropylaerosyl (fullerene C₆₀-composite-1) was synthesized (Golub et al., 2003) by the introduction of aminopropyl chains oriented ad extra by amine groups (0.9mM/g), to the surface layer of silicon dioxide nanoparticles that were bound to fullerene C₆₀ (0.12mM/g) (Fig. 6.1). Fullerene-anthracenaliminopropylaerosyl (fullerene C₆₀-composite-2) was composed also from anthracenalimine (0.2mM/g) that was introduced via azomethine condensation of aldehyde group of anthracenal with surface amino group.

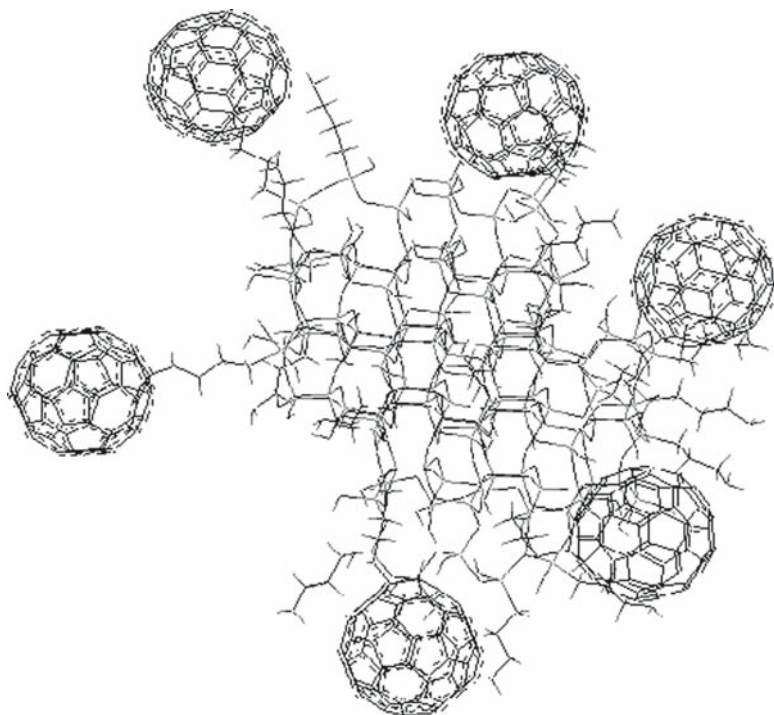


Fig. 6.1 Molecular model of C_{60} fullereneaminopropylaerosyl

Registration of ROS was carried out by electron paramagnetic resonance (EPR) technique using spin trap 1-hydroxy-2,2,6,6-tetramethyl-piperidine-4-OH (2×10^{-3} M). EPR spectra in the samples were registered at room temperature in quartz cuvette with the volume of 200 μ l (Burlaka et al., 1994).

The cells ($1-3 \times 10^6$ cells/ml) were incubated for 24h at 37°C in RPMI 1640 medium supplemented with 8mM NaHCO_3 , 20mM HEPES, 5% FCS, 10 μ g streptomycin, and 10U/ml penicillin without agents or in the presence of fullerenes C_{60} . The number of viable cells was counted in hemocytometer using 0.4% solution of trypan blue.

After addition of solutions of fullerenes C_{60} or fullerene C_{60} -containing composites to the cell medium, the concentration of silicon dioxide was 0.02%, and that of fullerenes C_{60} – 10^{-5} M. Samples were placed in a glass tube and irradiated for 2 min by mercury-vapor lamp (power 24 W) at the distance of 5 cm.

The content of the products of lipid peroxidation (LPO) was determined after 1 h of incubation of the cells in a buffer A at 37°C . Aliquot of cell suspension (100 μ g protein) was treated with heptane/isopropyl alcohol mixture at the ratio of 1:1. The content of Schiff bases in heptane phase was analyzed on fluorimeter RF-510, Shimadzu (Japan) at $\lambda_{\text{exit}} = 360$ nm and $\lambda_{\text{emis}} = 420$ nm (Kolesova et al., 1984). The content of diene conjugates was determined by spectrophotometry (Gavrillov et al., 1988) at the wavelength of $\lambda = 245$ nm using spectrophotometer Scinco (Germany).

The content of low-molecular weight DNA fragments – polydesoxyribonucleotides (PDN) – in the cells after 5 and 20 h of incubation in the presence or absence of fullerenes C₆₀ was evaluated after treatment with lyzing buffer (10 mM EDTA, 10 mM Tris-HCl (pH 7.4), 0.5% Triton X-100), and centrifugation (15,000 g, 20 min). PDN content in supernatant was determined using reaction with diphenylamine (Burton, 1956).

Reaction with MTT (3-[4,5-dimethylthiazol-2-yl]-2,5-diphenyltetrazolium bromide, “Sigma”) was carried out in 96-well plate at 37 °C in thermostat (Carmichael et al., 1987). The cells were incubated for 0.5, 2, and 5 h in RPMI 1640 medium in the presence or absence of fullerenes C₆₀ samples, then MTT was added, and incubation continued for 2 h. The content of generated formazane was evaluated by spectrophotometry at the wavelength of $\lambda = 570$ nm at the digital spectrophotometer IFCO-2 (ABOTEK, Russia).

Statistical analysis of the results was performed using applied program “Microsoft Excel 98”.

6.3 Results and Discussion

Biologic effects of non-excited fullerenes C₆₀, that are revealed at the concentration range lower than 10⁻⁴ M, are mostly positive, but depend on the type of cells and the way of modification of fullerene C₆₀ (Yamakoshi et al., 1994). As we have shown earlier, upon the presence of 10⁻⁶ M fullerenes C₆₀ in incubation medium, resistance of erythrocytes to hemolysis is not altered, whilst at the concentration of 10⁻⁵ M fullerenes C₆₀ the hemolysis rate is accelerated. Hemolytic effect was not revealed if fullerene C₆₀ at the concentration of 10⁻⁵ M was introduced to the content of aminopropylaerosyl (i.e., upon the presence of fullerene C₆₀-composite-1). Cytotoxic influence was not found if thymocytes and EAC cells were incubated with fullerenes C₆₀ (10⁻⁵ M) or fullerene C₆₀-containing composites for 24 h (Prylutska et al., 2006). That is why the study of the influence of irradiation on biologic activity of fullerenes C₆₀ was carried out at their concentration of 10⁻⁵ M.

It is known that fullerene C₆₀ molecule maximally absorbs light at the range of $\lambda = 220$ –345 nm, and is low at $\lambda = 450$ nm (Scharff et al., 2004). The rate of ROS generation upon irradiation of fullerenes C₆₀ with visible light that deeper penetrates tissues and possesses lower damaging effect compared to ultraviolet is studied insufficiently. That is why we have studied the effects of fullerene C₆₀ and fullerene C₆₀-containing composites irradiated in the range of $\lambda = 320$ –580 nm.

After irradiation of fullerenes C₆₀ in the cell medium, ROS production has been detected, and this index increased as follow: fullerene C₆₀ < fullerene C₆₀-composite-1 < fullerene C₆₀-composite-2. As one may see from the data presented in Table 6.1, the rate of ROS generation elevated nearly twice after absorption of light in predetermined range by fullerenes C₆₀, if fullerene C₆₀ was bound to the surface of aminopropylaerosyl, and threefold, if anthracenal that absorbs at $\lambda = 357$ nm was introduced to the content of composite.

Table 6.1 The rate of generation of reactive oxygen species (ROS) and cell viability after irradiation of samples of fullerenes in incubation medium

Experimental conditions	nmole ROS/ min.10 ⁶ cells	Viability cells in 24h incubation (%) (M ± m, n = 7)
Samples of fullerenes		
C ₆₀	2.9 ± 0.2	
C ₆₀ -composites-1	6.3 ± 0.2	
C ₆₀ -composites-2	11.0 ± 0.4	
Suspension of thymocytes	2.3 ± 0.2	97 ± 6
+C ₆₀	4.3 ± 0.3	100 ± 3
+C ₆₀ -composite-1	5.4 ± 0.3	90 ± 5
+C ₆₀ -composite-2	7.8 ± 0.4	88 ± 3
Suspension of ascitic		
Erlich's carcinoma cells	1.4 ± 0.1	100 ± 5
+C ₆₀	3.0 ± 0.2	80 ± 6
+C ₆₀ -composite-1	6.1 ± 0.4	71 ± 5*
+C ₆₀ -composite-2	7.2 ± 0.2	66 ± 7*
Suspension of leucosis		
L1210 cells	1.2 ± 0.1	98.0 ± 2.0
+10 ⁻⁵ M C ₆₀	2.6 ± 0.2	88.0 ± 3.0
C ₆₀ -composite-1	5.5 ± 0.6*	77.0 ± 6.0*
C ₆₀ -composite-1	6.7 ± 0.7*	71.0 ± 4.0*

* $P \leq 0.05$ compared to the control.

Upon the absence of fullerenes C₆₀, insignificant level of ROS generation in the suspensions of thymocytes, EAC, and L1210 cells has been registered (Table 6.1). After irradiation of fullerenes C₆₀ in the cell suspension, elevation of ROS generation rate was observed, but by absolute value the indexes were lower than it could be expected accounting the mentioned data on the rate of ROS generation in water solutions. Certainly, it may be explained by the fact that viscosity of cell suspension is higher than that of water solutions, thus determining the period of existence of fullerenes C₆₀ in triplet state (Irie et al., 1996). Upon the presence of photoexcited fullerene C₆₀, the rate of ROS generation in the suspensions of thymocytes, EAC, and L1210 cells increased equally – twice compared to the control. After irradiation of fullerene C₆₀-composite-1 and fullerene C₆₀-composite-2 in the cell medium, the rate of ROS generation increases by 2.3- and threefold in the suspension of thymocytes, and by 4.4- and 5.1-fold in the suspensions of tumor cells, respectively. The higher effect in both cases was observed for fullerene C₆₀-composite-2 that contains anthracenal.

The influence of photoexcited fullerene C₆₀ on viability of thymocytes, EAC, and L1210 cells was studied after 24h of incubation, considering the content of viable cells at incubation as 100% (Table 6.1). After irradiation of fullerenes C₆₀ in the cell medium, significant decrease in the content of viable cells in the suspension of thymocytes was not registered, whilst the number of viable malignant cells decreased. Upon the presence of photoexcited fullerene C₆₀ in incubation medium, the number of viable EAC cells decreased by 20%, and L1210 by 12%, while in the

presence of photoexcited fullerene C₆₀-composite-1 by 29% and 23%, respectively, and photoexcited fullerene C₆₀-composite-2 by 34% and 29%, respectively compared to the samples without addition of fullerenes C₆₀.

Taking into account that ROS produced by irradiated fullerenes C₆₀ may act only in the radius of their short diffusion existence, one may suppose that cytotoxic effect is determined by the interaction of fullerene C₆₀ with the surface of cells and initiation of chain reactions of free radical peroxidation in membranes. That is why the influence of photoexcited fullerene C₆₀ on the course of LPO process was studied and evaluated by the content of generated primary (diene conjugates) and final (Schiff bases) products. The content of diene conjugates in thymocytes was 17.7 ± 4.2 , in EAC cells was 21.1 ± 1.3 , and in L1210 was 12.8 ± 3.1 nM/mg protein, and Schiff bases -56 ± 7.9 , 46.5 ± 4.5 , and 36.6 ± 4.6 rel. units/mg protein, respectively, and did not alter during 1 h incubation of the cells.

In the case of photoexcited fullerenes C₆₀ and fullerene C₆₀-containing composites in incubation medium of thymocytes, the indexes of LPO did not alter compared to the control too (Fig. 6.2A). Upon incubation of EAC cells in the presence of photoexcited samples of fullerenes, the decrease in the content of diene conjugates by 35% in the presence of fullerene C₆₀ and by 20% in the presence of fullerene C₆₀-composite-1 and fullerene C₆₀-composite-2 was observed (Fig. 6.2B). The presence of photoexcited samples of fullerenes in the suspension of L1210 cells influenced LPO indexes only in the presence of fullerene C₆₀-composite-2, when the content of diene conjugates increased by 35% (Fig 6.2C).

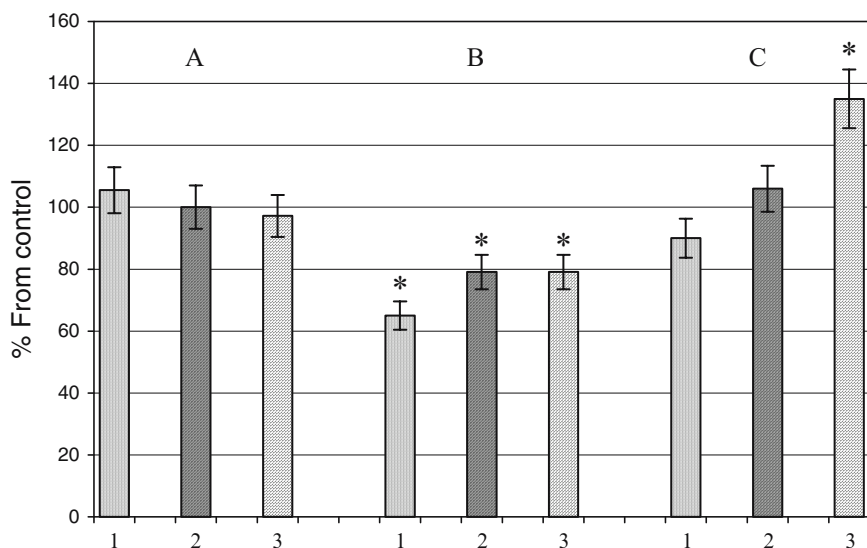


Fig. 6.2 Content of diene conjugates (% from control) in thymocytes (A), EAC (B), and L1210 cells (C) after 1 h of incubation in the presence of photoexcited samples of fullerenes (1 – fullerene C₆₀, 2 – C₆₀-composite-1, 3 – C₆₀-composite-2). * $P \leq 0.05$ compared to the control

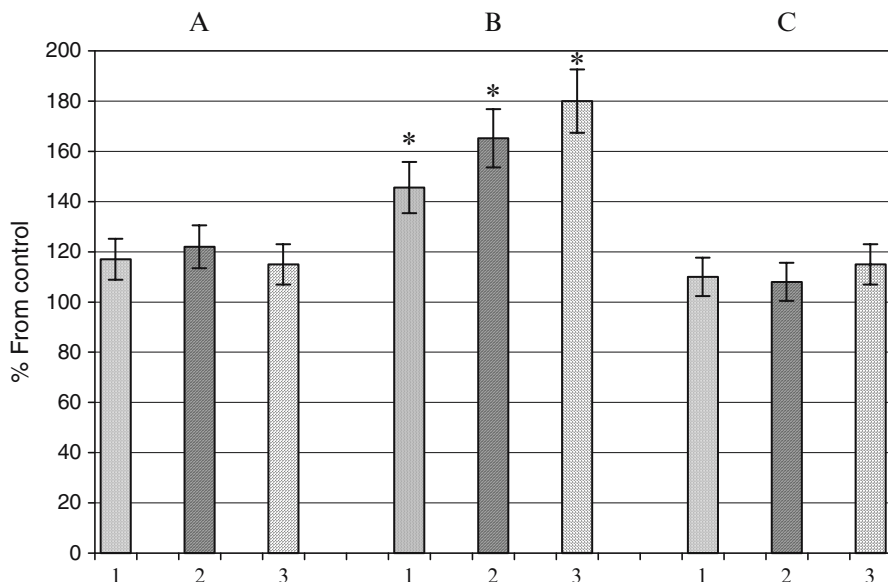


Fig. 6.3 Content of Schiff bases (% from control) in thymocytes (A), EAC (B), and L1210 cells (C) after 1h of incubation in the presence of photoexcited samples of fullerenes (1 – fullerene C₆₀, 2 – C₆₀-composite-1, 3 – C₆₀-composite-2). **P* ≤ 0.05 compared to the control

Upon the presence of the fullerenes C₆₀ in incubation medium of thymocytes and L1210 cells, the content of Schiff bases did not alter compared to the control (Fig. 6.3A, C – 1, 2, 3).

However, upon incubation of EAC cells in the presence of photoexcited samples of fullerenes the increase in the content of Schiff bases was observed by 46% in the presence of photoexcited fullerene C₆₀, by 65% – in the presence of photoexcited fullerene C₆₀-composite-1, and by 80% – in the presence of photoexcited fullerene C₆₀-composite-2 (Fig. 6.3B).

Simultaneous decrease in the content of diene conjugates and increase in the content of Schiff bases evidence the quick shift of pro-/antioxidant equilibrium, generation of reactive radicals, and damage of cell membranes in EAC cells, because Schiff bases, generated as a consequence of interaction of malonic dialdehyde with aminogroups of phospholipids and proteins, are highly reactive compounds causing polycondensation of molecules and formation of intermolecular bonds.

It has been shown that the influence of photoexcited fullerene C₆₀ on the processes of free-radical oxidation depends on the type of the cell and on the composition of composite. So, in thymocytes in the presence of photoexcited fullerene C₆₀ as well as fullerene C₆₀-containing composites, the content of primary and final LPO products did not alter compared to the control. In malignant cells the intensification of LPO processes was registered, and its level depends on the type of cells. So, in thymocytes in the presence of photoexcited fullerene C₆₀ in suspension of EAC cells the decrease in the content of diene conjugates simultaneously with the increase in the

final LPO products – Schiff bases – was observed. Pro-oxidant effect was more pronounced upon the use of photoexcited fullerene C₆₀-composite-2. In the presence of photoexcited fullerene C₆₀ composite-2 in L1210 cells the increase in the content of primary LPO products was registered, but the increase in the content of final LPO products was not detected.

Literature data on cytotoxic effects of photoexcited fullerene C₆₀ are controversial. In the studies on transformed B-lymphocytes of Raji line, phototoxic action of water-soluble carboxy-C₆₀ was not revealed even upon its concentration of 5×10^{-5} M (Irie et al., 1996). In the study (Kamat et al., 2000) damaging effect of fullerenes C₆₀ in dependence on intensity of irradiation toward CHO cells has been demonstrated. Using microsomal fraction of rat liver that was treated with C₆₀-cyclodextrin complex, it was shown that already in 5–30 min after UV-irradiation the accumulation of LPO products occurs that is suppressed by antioxidants like ascorbic acid and α -tocopherol. Similar effect of fullerenes C₆₀ has been revealed in microsomal fraction of the cells of ascitic sarcoma 180 (Kamat et al., 2000).

As a consequence of accelerated generation of oxygen-containing radicals and intensification of LPO reactions the alteration of the structural state of DNA may appear. To perform quantitative biochemical evaluation of the state of DNA of thymocytes, EAC, and L1210 cells upon the presence of photoexcited fullerene C₆₀, the content of the products of DNA degradation – low-molecular weight polydesoxyribonucleotides (PDN) after 5 and 20 h of incubation – has been analyzed. The portion of degraded DNA in the control cells after 5 and 20 h of incubation in the thymocytes is composed of 8 ± 2 and $10 \pm 2\%$, correspondingly, in the EAC cells – 5 ± 1 and $8 \pm 1\%$, correspondingly, in L1210 cells – 5 ± 1 and $7 \pm 1\%$, correspondingly, from the general DNA content. It turned out that the thymocytes are characterized by the high degree of DNA degradation in comparison with the tumor cells. This effect can be explained by the fact that the thymocytes are the incompletely differentiated cells with the unstable genome and possess the low activity of the reparation systems of the single-stranded breaks of DNA. The level of PDN generated upon incubation of cells in the absence of C₆₀ fullerenes (control) was considered as 100%.

Upon 20 h of incubation of thymocyte suspension in the presence of photoexcited fullerene C₆₀, the part of the degraded DNA increased insignificantly. As one may see from Fig. 6.4a, upon the presence of fullerenes C₆₀, the content of PDN increased by 10%, fullerene C₆₀-composite-1 by 14%, and fullerene C₆₀-composite-2 by 13% compared to the control.

Irradiation of fullerene C₆₀-containing composites (1 and 2) in the suspension of L1210 cells caused more significant damage of the structural state of DNA compared to that in thymocytes, while fullerene C₆₀ did not affect this index in L1210 cells, also. Upon 5 h of incubation of L1210 cells in the presence of photoexcited fullerene C₆₀, the content of PDN increased by 12% in the presence of fullerene C₆₀, by 18% in the presence of fullerene C₆₀-composite-1, and by 24% in the presence of fullerene C₆₀-composite-2 compared to the control. During 20 h of incubation of L1210 cells, insignificant increase in the content of generated PDN was observed: by 14% in the presence of fullerene C₆₀, by 20% in the presence of fullerene

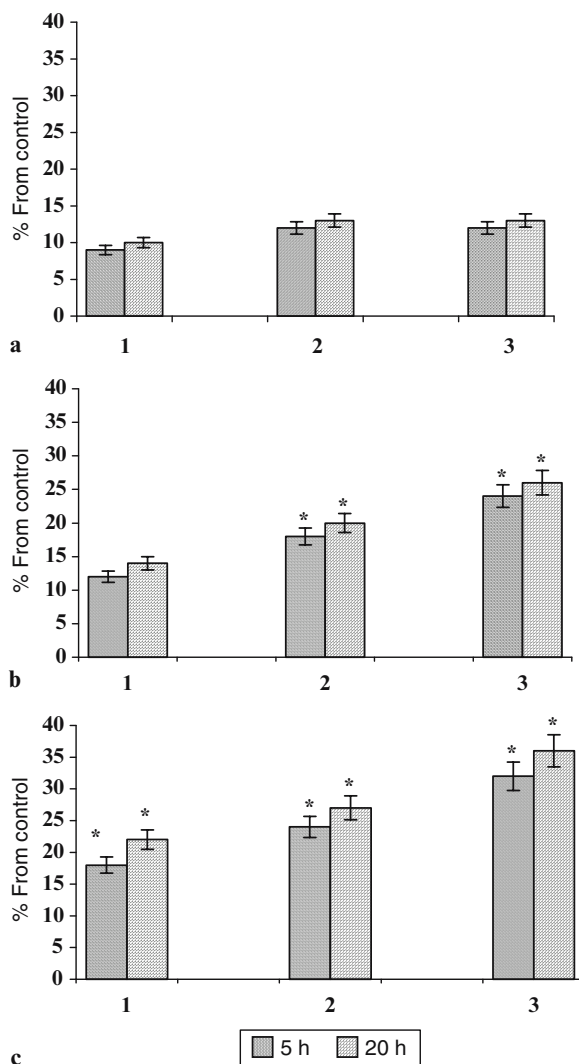


Fig. 6.4 DNA fragmentation (% from control) in thymocytes (a), L1210 (b), and EAC cells (c) incubated for 5 and 20h in the presence of photoexcited samples of fullerenes (1 – fullerene C_{60} ; 2 – C_{60} -composite-1; 3 – C_{60} -composite-2). * $P \leq 0.05$ compared to the control

C_{60} -composite-1, and by 26% in the presence of fullerene C_{60} -composite-2 compared to suspension of L1210 cells incubated without addition of the samples of fullerenes (Fig. 6.4b).

The most intense alteration of the structural state of DNA in the presence of photoexcited fullerene C_{60} was observed in EAC cells. As one may see from Fig. 6.4c, during 5h the increase in the content of DNA degradation products was observed:

by 18% in the presence of fullerenes C₆₀, by 24% in the presence of fullerene C₆₀-composite-1, and by 32% in the presence of fullerene C₆₀-composite-2 compared to the cells without samples of fullerenes. In the case of 20h of incubation of EAC cells in the presence of photoexcited fullerene C₆₀ the accumulation of DNA degradation products continued to rise: in the presence of fullerenes C₆₀ by 22%, fullerene C₆₀-composite-1 by 27%, and fullerene C₆₀-composite-2 by 36% compared to the cells without addition of the samples of fullerenes.

Thus, photoexcited samples of fullerenes are able to promote degradation of DNA and accumulation of low-molecular weight DNA fragments in L1210 and EAC cells already after 5h of incubation, but more intense DNA damage is observed upon the presence of C₆₀-containing composites, evidencing the promotion of damaging effects of fullerenes C₆₀ due to introduction of anthracenal to the content of composite.

From the literature reports it is known that some derivatives of fullerenes C₆₀ upon light irradiation are able to alter the structural state of DNA (Samal and Geckeler, 2001). There are the data on specific damage of DNA structure by guanine by irradiated derivatives of fullerenes, and on electron transfer from guanosine to photoexcited fullerene C₆₀ derivative that occurs with the involvement of singlet oxygen. For example, fullerene C₆₀ solubilized in polyvinylpyrrolidone, upon irradiation caused damage of DNA with the formation of 8-OH-dG (Boutorine et al., 1994). Photoexcited C₆₀-PEG conjugate damaged DNA structure in C₈ position of guanine (Chi et al., 2002).

It is proposed that the cleavage of oligonucleotides occurs as a consequence of photoexcitation of fullerene C₆₀ via its transfer in triplet state ³C₆₀ and generation of singlet oxygen ¹O₂, which interacts with oligonucleotide. However, apart from oxygen, acceptors of electrons may also be aromatic rings of tertiary amines, including those of guanine in the content of nucleotide chain (Tokuyama et al., 1993).

For evaluation of influence of the samples of fullerenes C₆₀ on total metabolic state of thymocytes, EAC, and L1210 cells we have used MTT test based on the reduction of MTT by reductase system that consists, in particular, of mitochondrial succinate dehydrogenase.

From the data of literature it is known that water-soluble derivatives of fullerenes are able to be localized in mitochondria and influence their state as well as enzyme system (Foley et al., 2002). Such intracellular localization of fullerenes C₆₀ could explain biologic effects under irradiation, because generation of free oxygen radicals in the cells occurs during emission of electrons from electron-transport chain of mitochondria.

The rate of MTT reduction was determined adding the agent to cell incubation medium on 0.5, 2, and 5h after irradiation of samples. In the case of non-irradiation of fullerenes C₆₀ in incubation medium, the indexes of total metabolic state of thymocytes, EAC, and L1210 cells did not alter compared to the control.

As one may see from the data presented in Fig. 6.5a, upon the presence of photoexcited samples of fullerenes in incubation medium of thymocytes, no significant changes in the rate of MTT reduction were observed during 5h. Upon the presence of photoexcited fullerene C₆₀ in incubation medium of suspension of L1210 cells,

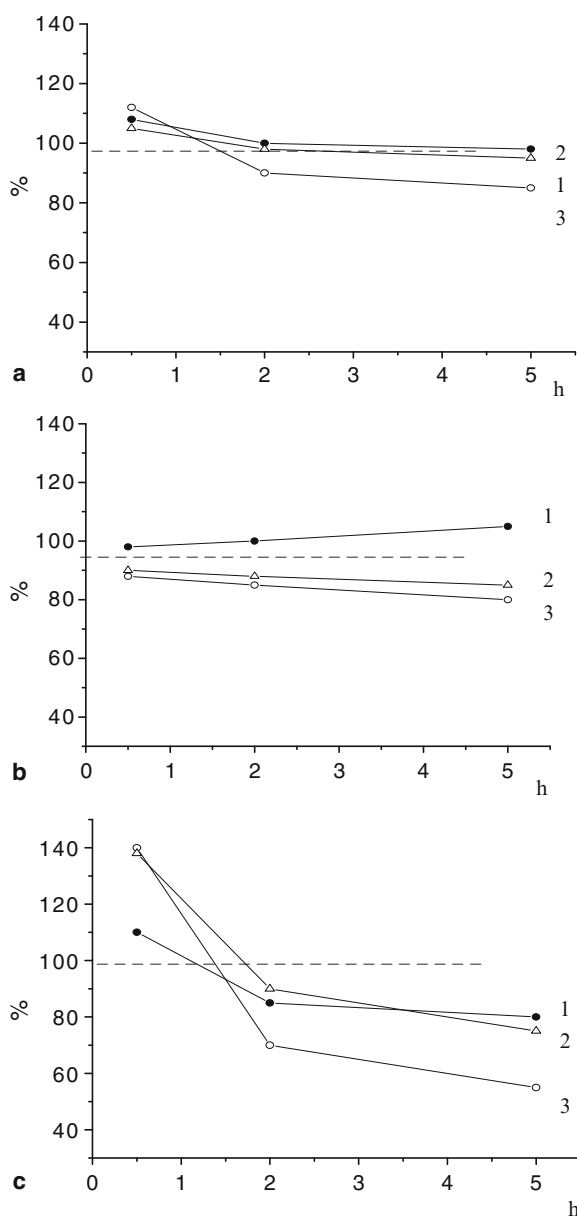


Fig. 6.5 Dependence of the level of MTT reduction (% from control) in thymocytes (a), L1210 (b), and EAC cells (c) incubated in the presence of photoexcited samples of fullerenes (1 – fullerene C_{60} ; 2 – C_{60} -composite-1; 3 – C_{60} -composite-2). $P \leq 0.05$ compared to the control

no change in the rate of MTT reduction during 5 h of incubation was revealed (Fig. 6.5b, curve 1). But in the case of incubation of L1210 cells in the presence of fullerene-containing composites insignificant decrease in the rate of MTT reduction was observed already during the early stage of incubation (0.5 h) (in the presence of fullerene C₆₀-composite-1 and 2 by 10%) (Fig. 6.5b, curves 2, 3) that further continued to decrease. During 5 h of incubation of L1210 cells in the presence of fullerene-containing composites-1 and 2 the rate of MTT reduction decreased by 18% and 20%, respectively compared to the control. So, during 5 h of incubation irradiated samples of fullerene C₆₀-containing composites decrease the rate of MTT reduction in L1210 cells.

As one may see from the data presented in Fig. 6.5c, in the case of 0.5 h incubation of EAC cells elevation of the rate of MTT reduction was observed upon the presence of fullerenes C₆₀ by 10%, fullerene C₆₀-composite-1 by 38%, and fullerene C₆₀-composite-2 by 40% compared to the control. After 2 h of incubation of EAC cells after irradiation of samples, the rate of MTT reduction decreased (in the presence of fullerenes C₆₀ by 15%, fullerene C₆₀-composite-1 by 10%, and C₆₀-composite-2 by 25% compared to the control). In the case of 5 h of incubation of EAC cells after irradiation of samples, the rate of MTT reduction decreased at higher degree (in the presence of fullerenes C₆₀ by 12%, fullerene C₆₀-composite-1 by 20%, and fullerene C₆₀-composite-2 by 42% compared to the control). One should pay attention to the fact that the rate of MTT reduction markedly elevated at early period after irradiation of fullerene C₆₀-containing composites in the culture medium (by 38% and 40% compared to the control). Such effect could be determined by elevation of electron-transport activity of fullerene C₆₀ after irradiation. There are the data showing that fullerene C₆₀ accelerates electron transfer from oxidized compounds, in particular, from such physiologic substrate as NADH (Yamakoshi et al., 1994), thus influencing the rate of redox processes. At this moment fullerene C₆₀ transforms to anion radical C₆₀^{-•}, that in turn transfer electrons to molecular oxygen with generation of superoxide anion O₂^{-•}. In the case of large production of superoxide its toxic effect may be exerted, what is supported by the data on the fall of the rate of MTT reduction along with the increase in the period of incubation of EAC cells with irradiated composites. It is known that mitochondria are most sensitive to the action of superoxide radicals, where upon the development of oxidative stress the destruction of the barrier function of membranes and the damage of respiratory chain are taking place (Vladimirov, 2002). Lipophylic nature of fullerene C₆₀ promotes its penetration in membrane structures. For example, using fluorescent probes (erythrosine and pyrene) incorporated in bilayer of phosphatidylcholine liposomes, it has been shown that upon interaction of membranes of liposome the complex of C₆₀-polyvinylpyrrolidone is broken, and fullerene C₆₀ penetrates the membrane. During this process, the polymeric matrix remains outside, whilst fullerene C₆₀ diffuses in membrane. The study of subcellular distribution of water-soluble derivative of fullerene C₆₁(COOH)₂ by the method of fluorescent microscopy using monoclonal antibodies against fullerene C₆₀ and labeled ¹⁴C analog has shown that this compound may penetrate plasma membrane and enter the cells where it is bound mainly by mitochondria (Foley et al., 2002).

6.4 Conclusion

So, in this work it has been shown that after irradiation of 10^{-5} M fullerene C_{60} and fullerene C_{60} -containing composites ($\lambda = 320\text{--}580$ nm) in aqueous solutions and cell suspensions, the generation of reactive oxygen species is observed, and the rate of their generation increases in the case of introduction of fullerenes C_{60} to the content of aminopropylaerosyl and anthracenaliminopropylaerosyl.

It has been shown that the influence of photoexcited fullerene C_{60} on the indexes of metabolic processes depends on the type of the cells and on the content of composite. The specificity of the effects of photoexcited fullerene C_{60} -containing composites is not observed in normal cells (thymocytes), but appear in malignantly transformed cells – Erlich ascite carcinoma (breast cancer) and L1210 (leucosis). It is shown that photoexcited fullerene C_{60} -containing composites decrease viability of transformed cells, intensify the process of lipid peroxidation in cell membranes and accumulation of low-molecular weight DNA fragments, and decrease the activity of electron-transport chain of mitochondria. The presented data point out the possibility of application of fullerene C_{60} -containing composites for photodynamic therapy.

Acknowledgments This work was partly supported by the BMBF grant (Ukr 04-008) and joint Ukrainian-Hungarian project. S.V. Prylutska is grateful to the INTAS (Grant N 05-109-4328) for the support too.

References

- Arbogast J, Foote Y (1991) Photophysical properties of C_{70} . *J Am Chem Soc.* 113: 8886–8889.
- Boutorine AS, Tokuyama H, Takasugi M et al. (1994) Singlet oxygen production from fullerene derivatives. *Angew Chem Int Ed.* 33: 2462–2465.
- Burlaka AP, Danko MI, Sidorik EP (1994) Kinetic patterns of the rate of generation and content of oxygen radicals in EPR membranes upon chemical carcinogenesis of liver and breast. *Ukrainian DAN Ukr.* 10: 141–145.
- Burton K (1956) A study of the conditions and mechanism of the diphenylamine reaction for the colorimetric estimation of deoxyribonucleic acid. *Biochem.* 62: 315–323.
- Carmichael J, DeGraff WG, Gazdar AF et al. (1987) Evaluation of a tetrazolium-based semiautomated colorimetric assay: assessment of chemosensitivity testing. *Cancer Res.* 47: 936–942.
- Chi Y, Canteenwala T, Chen H et al. (2002) Free radicals scavenging and photodynamic functions of micelle-like hydrophilic hexa(sulfobutyl)fullerene (FC_4S). *Perspect Fullerene Nanobiotechnol.* 15: 165–183.
- Chuyiko AA (2003) Medical chemistry and clinic application of silicon dioxide. *Russian Naukova Dumka, Kiev.*
- Da Ros T, Spalluto G, Prato M (2001) Biological applications of fullerene derivatives: a brief overview. *Croatica Chemica Acta.* 74: 743–755.
- Foley S, Crowley C, Smaih M et al. (2002) Cellular localization of a water-soluble fullerene derivative. *Biochem Biophys Res Commun.* 294: 116–119.

- Gavrilov VB, Gavrilova AR, Khmara NF (1988) Measurement of diene conjugants in the plasma blood by UV absorption of heptane and isopropanole extracts. *Russian Laboratornoe Delo*. 2: 60–63.
- Golub A, Matyshevska O, Prylutska S et al. (2003) Fullerenes immobilized at silica surface: topology, structure and bioactivity. *J Mol Liq*. 105: 141–147.
- Grossweiner LI, Patel AS, Grossweiner JB (1982) Type I and type II mechanisms in the photosensitizing lyses of phosphatidylcholine liposomes by hematoporphyrin. *Photochem Photobiol*. 36: 159–167.
- Guldi DM, Asmus KD (1999) Activity of water-soluble fullerenes towards OH-radicals and molecular oxygen. *Radiat Phys Chem*. 56: 449–456.
- Hamano T, Okuda K, Mashino T, et al. (1997) Singlet oxygen production from fullerene derivatives: effect of sequential functionalization of the fullerene core. *Chem Commun*. 1: 21–22.
- Irie K, Nakamura Y, Ohigashi H et al. (1996) Photocytotoxicity of water-soluble fullerene derivatives. *Biosci Biotechnol Biochem*. 60: 1359–1361.
- Isaacs N, Nichols P, Raston C et al. (1997) Solution volume studies of a deep cavity inclusion complex of C₆₀: p-benzyl calyx[5]arene. *Chem Commun*. 19: 1839–1840.
- Kamat J, Devasagayam T, Priyadarsini K, Mohan H (2000) Reactive oxygen species mediated membrane damage induced by fullerene derivatives and its possible biological implications. *Toxicology*. 155: 55–61.
- Kolesova OE, Markin AA, Fedorova TN (1984) Peroxide oxidation of lipids and the methods for determination of lipid peroxidation products in the biological mediums. *Russian Laboratornoe Delo*. 9: 540–546.
- Pass HI (1993) Photodynamic therapy in oncology: mechanisms and clinical use. *J. Natl Cancer Inst*. 85: 443–456.
- Prylutska SV, Grynyuk II, Golub OA, Matyshevska OP (2006) Estimation of cytotoxicity parameters of C₆₀ fullerenes and C₆₀-containing composites in vitro. *Ukrainian DAN Ukr*. 1: 163–167.
- Samal S, Geckeler K (2001) DNA-cleavage by Fullerene-Based Synzymes. *Macromolecular Bioscience*. 1: 329–331.
- Scharff P, Risch K, Carta-Abelmann L et al. (2004) Structure of C₆₀ fullerene in water: spectroscopic data. *Carbon*. 42: 1203–1206.
- Tabata Y, Ikada Y (1999) Biological functions of fullerene. *Pure Appl Chem*. 71: 2047–2053.
- Tokuyama H, Yamago S, Nakamura E, et al. (1993) Photoinduced biochemical activity of fullerene carbocyclic acid. *J Am Chem Soc*. 115: 7918–7919.
- Vladimirov YuA (2002) Breach of barrier properties for internal and external mitochondrion membranes, necrosis and apoptosis. *Russian Biol Membr*. 19: 356–377.
- Wilson SR (2000) Fullerenes: chemistry, physics and technology. Wiley, New York.
- Yamakoshi Y, Yagami T, Fukuhara K, et al. (1994) Solubilisation of fullerenes into water with polyvinylpyrrolidone applicable to biological test. *J Chem Soc Chem Commun*. 4: 517–518.
- Yoshida Z, Takekuma H, Takekuma S, Matsubara Y (1994) Molecular recognition of C₆₀ with γ -cyclodextrin. *Angew Chem Int Ed*. 33: 1597–1599.

Chapter 7

Biological Effects in Cell Cultures of Fullerene C₆₀: Dependence on Aggregation State

Levon B. Piotrovsky¹, Mikhail Yu. Eropkin², Elena M. Eropkina²,
Marina A. Dumpis¹, and Oleg I. Kiselev²

Abstract The mechanisms of biological action of various fullerene preparations – water-soluble C₆₀/polyvinylpyrrolidone (C₆₀/PVP) complex and solid-state pristine fullerene C₆₀ (fullerene on the surfaces [FoS]), in cell-free system and in different cell cultures were studied. In the cell-free system the C₆₀/PVP complex showed the pro-oxidant activity. On the other hand, FoS in the darkness proved to be antioxidant (AO) and was nontoxic for different cell lines. But under visible-light illumination cell viability dropped in time- and light-dose-dependent way. Moreover, photodynamic damage of cells of tumor origin was greater than normal. The effect of illumination was reversed by some antioxidants. Therefore, redox properties in cell-free system and biological activity of pristine fullerene *in vitro*, in particular, phototoxicity, depend on its aggregation state.

Keywords pristine fullerene, C₆₀/PVP complex, cell culture, antioxidant, prooxidant

7.1 Introduction

Fullerenes are very attractive compounds not the least extent because of their aesthetics beauty (Hoffmann, 2003). At first sight, it seems that the structure of their molecules, which are geodesic, is nonbiological and is the play of human imagination. Nevertheless, their size, physical, and chemical properties make them real candidates for lead compounds in drug design. Biological activity of fullerenes is determined by their physical and chemical properties: under illumination they can manifest the oxidant properties though in the darkness they can be active antioxidants because of their capacity to scavenge free radicals. One also should take into consideration high lipophilic properties of fullerenes, which determine their capacity to interact with biological membranes (Piotrovsky, 2006).

¹Institute of Experimental Medicine Russian Academy of Medical Sciences, Saint Petersburg, Russia

²Institute of Influenza Russian Academy of Medical Sciences, Saint Petersburg, Russia

Therefore, the interest in the investigations of the biological activity of fullerenes appeared practically after they became available in real amounts (Kratschmer et al., 1990). The first works for the use of fullerene C_{60} in medicinal chemistry appeared as early as in 1993 (Tokuyama et al., 1993; Sijbesma et al., 1993). These quickly developing studies were brought out in many reviews devoted to the investigations of the fullerenes biological activity (Jensen et al., 1996; Da Ros and Prato, 1999; Bosi et al., 2003; Bianco et al., 2001; Da Ros et al., 2001). However, owing to the well-known insolubility of fullerenes in polar media, most parts of these works were done using water-soluble derivatives of fullerenes, mostly fullerene C_{60} . It should be mentioned that sometimes the literature data on biological properties obtained with the application of functionalized derivatives of fullerene C_{60} were transferred on the pristine fullerene itself. The brightest example could be the well-known paper (Foley et al., 2002), which is often cited as a study where a cellular distribution of C_{60} is described. However, this work is dedicated to the study of distribution of fullerenemalonic acid $C_{60}C(COOH)_2$ and it is quite evident that the penetration of the acid and a neutral compound, as well as their distribution inside the cells will not be identical.

However, from the theoretical point of view it is necessary at first to clear up the properties of the parent compound. These data would help to elucidate the role of fullerene core itself and the input of substituents into different biological properties, which in turn can help to plan the design of new biologically active compounds of these series in a more rational way.

It should be emphasized that mankind has come and still comes into contact with fullerene in everyday life. Pristine fullerene C_{60} itself can be found in our environment, e.g., in the soot produced by free burning of hydrocarbons like benzene and cyclohexane, as well as in charcoal, though in very small amounts (Shibuya et al., 1999) and in "the kitchen" (in natural gas combustion streams) (Bang et al., 2004; Murr and Soto, 2005). The impact of these natural sources is rather negligible though with the growth of production of fullerenes it could lead to much more serious environment pollution and be (or could not?) of a hazard to some extent.

Another problem, which makes the studies of fullerenes and their functionalized derivatives properties complicated is their high ability to aggregation. The fullerene core strive to self-aggregation is so great that even functionalized derivatives of fullerene C_{60} , with charged groups as well as bisfullerene derivatives of calyx[4]arene aggregate (Guldi et al., 2005; Ikeda et al., 2006). Aggregation notably influences photophysical and chemical properties of fullerene core (Guldi et al., 1995; Guldi, 1997).

Needless to say, the abovementioned is important while considering biological properties in physiological media. In case of pristine fullerene the aggregation can be compared with the introduction of substituents by decreasing the accessible surface square (Guldi and Asmus, 1999; Prat et al., 1999; Cheng et al., 2000). However, there is a different and important one, as the introduction of substituent in the fullerene core is irreversible, while the aggregation is reversible (unfortunately frequently not obvious). It is also important for biological properties studies that the distribution of aggregates and monomer molecules in biological systems can differ to a great extent.

On the other hand, the sample standardization is one of the main demands considered in biological studies. In case of pristine fullerene various preparations are used; these are the complexes with low-weight organic compounds and polymers (Piotrovsky, 2006), water suspensions (Moussa et al., 1995; Chiron et al., 2000), and water colloidal dispersions (nanoC₆₀) prepared by various methods (Scrivens et al., 1994; Andrievsky et al., 1995; Deguchi et al., 2001; Brant et al., 2006). Thus, the biological activity of one compound (pristine fullerene C₆₀) is examined in conditions, which cannot be compared. Probably, this is the reason why the literature data for biological activity of C₆₀ are quite various.

Practically, all works on toxicity (or nontoxicity) of pristine fullerene have been carried out using nanoC₆₀. But this is only one of the possible forms with which fullerene C₆₀ can be introduced into biological systems. The specific qualities of nanoC₆₀ here are not only that the hydrated are negatively charged, but they became hydrophilic (Brant et al., 2005a, b, 2006).¹ Secondly, the most important thing is that the clusters are not stable at the physiological values of ionic power – they destroyed forming “usual” crystalline fullerene. Consequently, the effects of nanoC₆₀ and crystalline fullerene can be the same. Thus, while investigating the biological properties of pristine fullerene everything can be principally brought to two types of preparations: crystalline form or water-soluble supramolecular complexes with low-weight organic compounds or polymers. In the first case, the high degree of association of fullerene molecules is obvious, while in the case of complexes “monomer” molecules or low associated clusters of fullerene C₆₀ can interact with biological objects.

One of the examples of the complex containing isolated molecules of fullerene is the complex of fullerene C₆₀ with γ -cyclodextrin (C₆₀/ γ -CD) (Andersson et al., 1992; Buvari-Barcza et al., 2001; Braun, 1997). As we know, this inclusion complex is a rare example when it was undoubtedly shown that fullerene molecule is in an isolated nonaggregated state. Therefore, the fullerene molecules can transfer into other media, because the intermolecular forces, stabilizing this complex, are weak. For example, lipid-membrane-incorporated fullerenes (LMIC_x) can be easily prepared by mixing of the solution of C₆₀/ γ -CD_x complexes with liposomes (Ikeda et al., 2005, 2007), and incubating native bovine serum albumin (BSA) with C₆₀/ γ -CD₂ complex at a physiological pH range resulted in the formation of a water-soluble BSA–C₆₀ hybrid (Belgorodsky et al., 2006). These data point out the peculiar behavior of the isolated molecules of fullerene in biological systems.

This is the reason why in our investigation we studied the influence of pristine fullerene C₆₀ to different biological objects in order to evaluate, first of all, the general biological properties of pristine fullerene (Kiselev et al., 1998a, b; Sushko et al., 1999; Piotrovsky et al., 2000; Podol'skii et al., 2002; Podolski

¹Moreover, some samples of nanoC₆₀ can contain the organic solvents or product of their degradation, capable of revealing pronounced toxic action (Oberdörster 2004; Fortner et al. 2005; Henry et al. 2007).

et al., 2004; Piotrovsky and Kiselev, 2004; Piotrovsky, 2006). Previously, we have shown that water-soluble preparations of pristine fullerene, namely C_{60} /polyvinylpyrrolidone (C_{60} /PVP) complex and molecular-colloidal water solutions of C_{60} , prepared accordingly (Andrievsky et al., 1995), exhibit virucidal activity due to different mechanisms: C_{60} /PVP complexes act mainly on the lipid component of virus membranes, while the mechanism of virucidal action of molecular-colloidal water solutions of C_{60} is mainly connected with the ability of fullerene to generate singlet oxygen under illumination. In the first case, fullerene acts as a membranotropic agent, whereas in the second case it acts as a photosensibilizer (Sirotkin et al., 2006).

To continue this investigation we studied the influence and mechanism of action of two preparations of pristine fullerene C_{60} , namely, the C_{60} /PVP complex and fullerene on the surface (FoS) on the cells in the culture.

7.2 C_{60} /Polyvinylpyrrolidone Complexes

One of the examples of inclusion complexes formed by intermolecular forces is the C_{60} /PVP complex for the first time described by Yamakoshi et al. (1994). The non-covalent intermolecular nature of forces that stabilizes this complex confirms the fact that fullerene can be quantitatively extracted from its water solution by toluene.

The method of preparation of this complex is simple enough and consists of mixing of fullerene solution in toluene with solution of PVP in chloroform with the following evaporation of organic solvents and dissolution of the residue in water. It was shown that the complex formation caused the bathochromic and hypochromic shifts of the fullerene absorption bands in UV–VIS spectra (Yamakoshi et al., 1994).

The change of the spectral characteristics, as well as the fact of the dissolution of fullerene C_{60} in water with PVP itself, confirms the formation of interaction between the fullerene and PVP, most probably of a donor–acceptor type. According to the NMR ^{13}C data in D_2O the electronic state of carbon atoms $\text{C}^{(1)}$ and $\text{C}^{(4)}$ of pyrrolidone cycle and $\text{C}^{(5)}$ of monomer unit of PVP, nearest to nitrogen atom, cardinally changes in the complex (Vinogradova et al., 1998).

In the more detailed mechanism of the formation of water-soluble fullerene-containing system of the donor–acceptor type and their structure are studied in the work (Krakovjak et al., 2006). It has been shown that during the gradual concentrating of solutions of PVP and C_{60} in organic solvents the noncovalent intermolecular contacts are appeared and primary fullerene-containing complex (“complex 1”) is formed. The origins of the intermolecular contacts that appeared in the reaction system are the donor–acceptor interactions of fullerene molecules with amide carbonyl groups of polymer units, which are confirmed by NMR data.

The water solutions of “complex 1” are not stable and other supramolecular structures are formed during the storage. The modification of the properties, including the increase of their water solutions stability can be achieved by evaporation of water solution of “complex 1” and dissolution of the residue in water. “Complex 2”

formed by this procedure contains the same quantity of fullerene cores as the initial “complex 1”, and is much more stable in water.

The polymer chains of PVP in “complex 2” in comparison with chains of both the pure PVP and the PVP in “complex 1” change their functional characteristics, e.g., they bind the organic ions in water more effectively. Such changes can be caused by the structural reorganization of PVP macromolecules at the final stage of the “complex 2” formation: destroying of the elements of internal structure of PVP chains during their interaction with C₆₀ (Krakovjak et al., 2006).

In accordance with this data the methods of preparation of C₆₀/PVP complexes containing up to 3% of fullerene (Krakovjak et al., 2005b) and water-soluble C₆₀-fullerene complexes with *N*-vinylcaprolactam homopolymers and copolymers with 0.75–3.3% of C₆₀-fullerene (Krakovjak et al., 2005a) were worked out.

The most convenient method for the evaluation of fullerene molecules aggregation is the comparison of UV–VIS absorption spectra in various solvents and for Langmuir–Blodgett films (Bensasson et al., 1994). Some preliminary conclusions about the state of aggregation can be made basing only the absorption maximum of fullerene C₆₀ in the region of 330–340 nm concern.

As our investigation shows, the properties of the obtained complexes depend on the PVP molecular mass. For example, at PVP with molecular mass 10,000 in the region of 330–340 nm the increase in fullerene C₆₀ content results in the bathochromic shift of the absorption band from 332 (0.3% C₆₀) to 340 nm (0.6–0.7% C₆₀). Hypochromic shift happens as well – from ~100,000 to 50,000 M⁻¹ cm⁻¹ at $\lambda = 332$ and 340 nm correspondingly. If PVP with molecular mass 25,000 was used for complex preparation, maximum of absorption is in the region of 338–340 nm and does not depend on the concentration (0.5–0.7% C₆₀). In the samples with PVP 40,000 and higher in UV–VIS spectra absorption band was always found at 340 nm or more.

Thus, if mentioned above is to be taken into consideration that absorption band in the region of 330–340 nm reflects to a certain extent the degree of fullerene molecules association in solution, we can come to the conclusion that the less the PVP molecular mass and the less the fullerene contents is the more fullerene molecules are in low associated state. It is quite probable that the increase of the fullerene contents in the complex brings to the formation of adducts, where not single fullerene C₆₀ molecules are bonded with PVP but their associates. It can be one of the reasons of the observed fact of the difference of UV–VIS spectra of C₆₀/PVP complex with PVP of different molecular mass (up to spectra crossover, which is a singular evidence that these compounds are nonidentical).

The abovementioned data show that the spectral characteristics of C₆₀/PVP complexes vary depending on the PVP molecular mass and fullerene content in the complex. Therefore, the quantitative determination of fullerene concentration in such complexes by measuring their absorbance at 336 nm without extraction (Lyon et al., 2006) can give non-reliable results. For quantitative analysis of fullerene in such complexes we used the “heterophase” and “homophase” methods, based on destruction and isolation of pure fullerene C₆₀ (Krakovjak et al., 2006). The choice of the method was determined by fullerene concentration – at concentration less

than 0.5% the “heterophase” method was used, while at concentration more than 0.5% the “homophase” method was convenient.

In order to prepare the complexes with low association of fullerene molecules it is necessary to start with diluted solutions of C_{60} (in toluene) and PVP (in $CHCl_3$), but the goal can be achieved only at relatively low content of fullerene in the complex. Thus, the degree of association of C_{60} molecules depends also on the molecular mass of PVP, and “low associated” complexes can be obtained only with PVP 10,000 and fullerene low concentration. It must be mentioned however that such complexes are relatively unstable – during their storage for about several months the association of fullerene molecules changes what can be seen from the shift of the band in UV–VIS spectra between 330 and 340nm (bathochromic and hypochromic shifts).

Certainly, it is not very good when fullerene concentration in C_{60} /PVP complexes is rather low, but let us keep in mind that the acting antiviral dose of fullerene itself in this complex is not high. The active quantity of fullerene, calculated with the neglecting of the polymer vehicle, against the influenza virus is about 7 μ M (Piotrovskii et al., 2001).

For the further investigations C_{60} /PVP complex was prepared by the modified method (Piotrovskii et al., 2001). Fullerene C_{60} (99.5%) was purchased from NeoTechProduct (Saint Petersburg, Russia). As polymer vehicles PVP with molecular mass 25,000 (“Merck”) or PVP pharmacopoeia grades were used. The fullerene C_{60} content in the investigated complexes was 0.50–0.66%.

A possible pro-/antioxidant effect of C_{60} was tested in the presence of fluorescence probe 2',7'-dichlorofluorescein. This compound is oxidized by reactive oxygen species (ROS), primarily by hydrogen peroxide (H_2O_2) with the transformation into the fluorescent oxidized form ($\lambda_{ex} = 385$ nm; $\lambda_{em} = 535$ nm). The method is supposed to be one of the most direct techniques of ROS indication (Bass et al., 1983; Clothier et al., 2002; Lautraite et al., 2003).

In the cell-free system (phosphate-buffered saline, pH 7.4) the C_{60} /PVP complex (C_{60} 0.66%, PVP with molecular mass 25,000) under illumination increased the fluorescence level significantly compared to control values (pure PVP at the same concentration), which indicates the presence of pro-oxidant activity in C_{60} under the given conditions. This effect augmented significantly at increasing time of illumination, which could be judged as another evidence in favor of pro-oxidant activity of the C_{60} /PVP complex (Fig. 7.1).

However, at the introduction of C_{60} /PVP complex (up to 5 μ g/ml) into the cultivating media during cell growth no effects were observed. In the cell MA-104 (cell line derived of green monkey kidney epithelium) grown normally within 3–6 days, no morphological changes and cell metabolism intensiveness were observed (Table 7.1).

The most reasonable explanation for the observed differences in fullerene behavior as a part of complex C_{60} /PVP in chemical and biological systems is the fact that the complex itself is stable in the pure water media. Dissolution in the saline causes the formation of fullerene precipitate, which, naturally reveals the photodynamic properties. But a basic difference between water-soluble C_{60} complexes with organic compounds (PVP, γ -CD, etc.) from other forms used for biological investigations is the low degree of fullerene molecules association

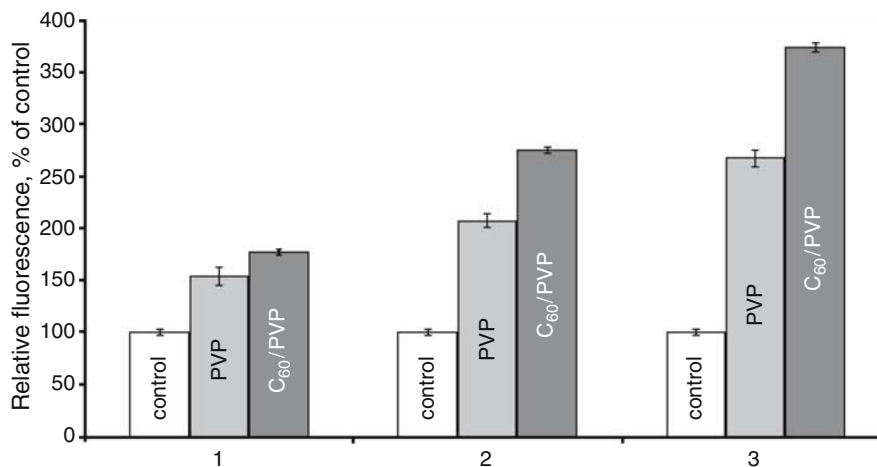


Fig. 7.1 Pro-oxidant effect of C₆₀/polyvinylpyrrolidone (C₆₀/PVP) complex (1 – in the darkness, 2 – illumination with visible light 15 min, 3 – illumination with visible light 30 min). Test method – fluorescence of 2',7'-dichlorofluorescein

Table 7.1 Absence of C₆₀/polyvinylpyrrolidone (C₆₀/PVP) complex influence (5 mg/ml) on cellular viability in cell culture MA-104. Endpoint – resazurin reduction

Sample	Time of incubation (days)		
	3	5	6
Control	4.00 ± 0.29	4.51 ± 0.20	3.89 ± 0.18
PVP	3.86 ± 0.17	4.51 ± 0.23	3.91 ± 0.23
C ₆₀ /PVP	3.87 ± 0.21	4.54 ± 0.20	4.01 ± 0.17

(Piotrovsky and Kiselev, 2006). It was shown that after dissolving these complexes in the liposome solutions fullerene molecules pass on to a lipid phase (Piotrovsky, 2006; Ikeda et al., 2005). It has also been shown that the zero-charged tetradecyltrimethylammonium laurate vesicle-phase tends to be more fluid after fullerenes are incorporated into the hydrophobic microdomains of aggregates (Li and Hao, 2007). In our case the cell membranes act as lipophilic structures. The comparison of the UV–VIS spectra of cultural media during the cell cultivation with C₆₀/PVP complex showed that fullerene absorption in 320–340 nm region was decreased, which can be explained as the pass of fullerene molecules from this media into the cells (or cell membranes). The transition of fullerene molecules into lipid bilayer causes the loss of their ability to convert triplet oxygen into singlet form under illumination. Although it necessary to mention that lipid-membrane-incorporated fullerenes (LMIC₆₀ and LMIC₇₀), prepared by transferring fullerenes from water-soluble host–guest complexes to lipid membranes, showed a distinct DNA cleaving activity under visible-light illumination ($\lambda_{\text{ex}} > 350 \text{ nm}$), but not in darkness (Ikeda et al., 2007). At the same time in the work of Janot et al. (2000) it is stated that in phospholipid membrane the quantum yield of triplet ¹C₆₀ decreases.

It is necessary to emphasize one more important property of fullerene C_{60} in the complex with PVP – it not just nontoxic, but prevents toxic (or other undesirable action) from PVP itself. It was first described by Tsuchiya et al. (1996) that PVP itself inhibits cell differentiation and proliferation, however, this effect diminishes to a great extent when C_{60} /PVP complex is used. The injection of C_{60} /PVP complex in dorsal region of hippocampus in rats prevents the disturbance of long-term memory consolidation induced by cycloheximide, however, the PVP itself influences negatively (Podol'skii et al., 2002; Podolski et al., 2004). It has also been shown that if PVP itself causes at least minor but visible morphological changes in some internal organ tissues (brain, myocardium, lungs, liver, spleen, and kidney), the C_{60} /PVP complex injection reduces these negative phenomena (Popov et al., 2007).

7.3 Fullerene on the Surface

Continuing the investigations of biological properties of different pristine fullerene preparations, we have studied the biological effects of fullerene immobilized on the surface. Several methods for preparations of fullerene thin films are known (Prato, 1999). For the first time a surface with fullerene, obtained by evaporation of solution of C_{60} in benzene, was proposed in 1994 to be used in the methods of growing cells as a substrate for cell growth, and for immobilizing biological materials including cells, macromolecules, drugs, aromatic molecules, and aliphatic substances (Richmond and Gibson, 1994).

The application of fullerene on the surfaces has an essential advantage in the studies with cell cultures as in this case we can obtain the maximum contact of cells with fullerene – cells adhere on the surface and colonize it as a confluent monolayer. That is the basic difference from the water-soluble complexes and micro-dispersed suspensions of fullerene C_{60} . The pro-/antioxidant activities of fullerene were tested in chemical and biological systems.

In order to control the quantity of fullerene, contacting biological objects, FoS were obtained by evaporation of saturated solution of C_{60} in hexane introduced in the wells of 96-well culture plates (“Sarstedt”). Twenty-five microliters of solution was applied to each well and evaporated at 20–25 °C, after which the procedure was repeated several times to obtain a desirable concentration of fullerene (10, 20, and 30 $\mu\text{g}/\text{cm}^2$). Application of such volume allows obtaining a surface, covered with fullerene on the bottom and partly on the walls of a well at a high less than 2 mm. Microscopic investigations (optical and electronic microscopy) have shown that the surface was covered irregularly: fullerene formed the isolated clusters, so that obtained “fullerene films” were not the real films, but rather isolated clusters of fullerene molecules (data not shown). However, it should be noted that their dimensions were smaller than those of cells and each cell covered several such clusters.

The possible pro-/antioxidant actions of FoS on cells were tested with 2',7'-dichlorofluorescein (see above).

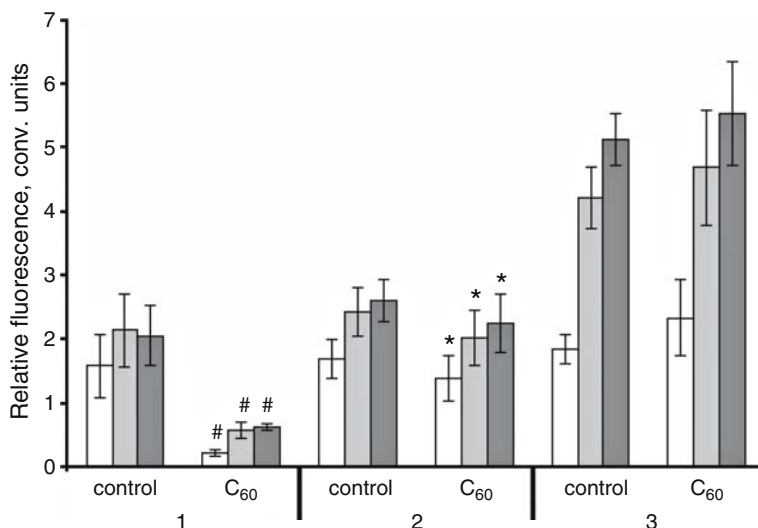


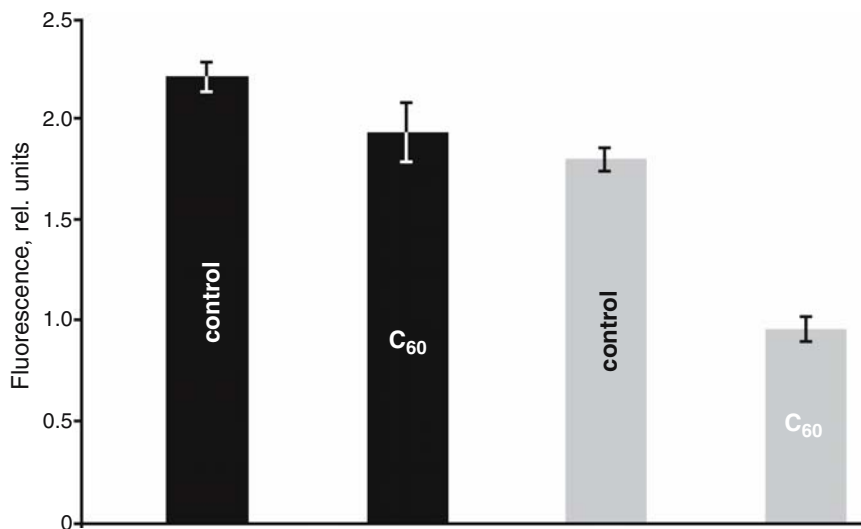
Fig. 7.2 Effect of fullerene on the surfaces (FoS) ($10 \mu\text{g}/\text{cm}^2$ of C₆₀) on the fluorescence of 2',7'-dichlorofluorescein in the presence of different concentrations of H₂O₂. (Incubation time: □ – 10 min, ■ – 20 min, ■ – 30 min; 1, 2, 3 – concentration of H₂O₂ 97, 194, and 970 μM). * $p < 0.05$; # $p < 0.001$

FoS had obvious antioxidant effect. In cell-free system after the addition of hydrogen peroxide solution the extinguishing of fluorescence of 2',7'-dichlorofluorescein was evident with H₂O₂ concentrations at 97 and 194 μM . At the substantially higher concentration of the latter (970 μM) a slight nonsignificant overlap of control level was evident (Fig. 7.2). These data confirm the antioxidant activity of pristine C₆₀. On the other hand, they indicate that it is limited to a certain “antioxidant capacity” (Fig. 7.2).

However, fullerene C₆₀-modified surface is adequate for the adhesion and normal growth of cells in culture. Cells of the line MA-104 in the Eagle-MEM medium formed on “fullerene film” a normal monolayer. Cellular viability was assessed with the resazurin (Alamar Blue) reduction test. The dye resazurin is reduced by mitochondrial dehydrogenases of viable cells into the fluorescent product resorufin (maximum $\lambda_{\text{exc}} = 530 \text{ nm}$, max $\lambda_{\text{emis}} = 590 \text{ nm}$). The intensity of fluorescence was registered on the multiwell plate analyzer “Chameleon” (Hydrex, Finland). This method is one of the most widely used in toxicity assessment *in vitro* (Andrews et al., 1997; Clothier et al., 2002). Our data have shown that C₆₀ applied on the propylene surface of culture plates in the chosen range of concentrations (10–30 $\mu\text{g}/\text{cm}^2$ of C₆₀) practically had no effect on the growth properties for cultured cells (Table 7.2). A slight nonsignificant diminishment of resazurin reduction can be interpreted in our opinion in view of simple change of hydrophobicity of a surface by fullerene. Furthermore, a possible damage of surface by solvent (hexane) should not be neglected. It should be emphasized that in any case

Table 7.2 Cellular viability of MA-104 culture grown on fullerene on the surfaces (FoS) during 72 h. (resazurin reduction test)

Concentration of C_{60} ($\mu\text{g}/\text{cm}^2$)	Relative fluorescence (conv. Units)
0	3.93 ± 0.17
10	3.83 ± 0.19
20	3.84 ± 0.18
30	3.84 ± 0.10

**Fig. 7.3** Photodynamic action of fullerene C_{60} on cells MA-104, grown on fullerene on the surfaces (FoS) ($10\mu\text{g}/\text{cm}^2$ C_{60}). Black columns – in the darkness; grey – under illumination

the observed differences were insignificant. Taking into consideration the absence of influence of fullerene C_{60} quantity on cell culture growth only plates with $10\mu\text{g}/\text{cm}^2$ of fullerene C_{60} were used.

As a result we could assume that fullerene C_{60} in the crystalline form in normal conditions of cellular cultivation (in the absence of intensive light) has no toxic effect on cellular cultures.

The picture was absolutely different when cells grown on FoS ($10\mu\text{g}/\text{cm}^2$) were irradiated 30 min with intensive visible light. In this condition fullerene C_{60} has revealed a powerful phototoxic action: a relative fluorescence of irradiated control cells (MA-104) was 1.80 ± 0.05 and of the cells, grown on fullerene surface – 0.96 ± 0.06 ($p < 0.001$), so the intensity of cellular metabolism has dropped to the level of cell-free control (1.0). It means that practically all cells were dead (Fig. 7.3).

It follows that toxic action of solid-phase fullerene on biological objects is revealed only under illumination.

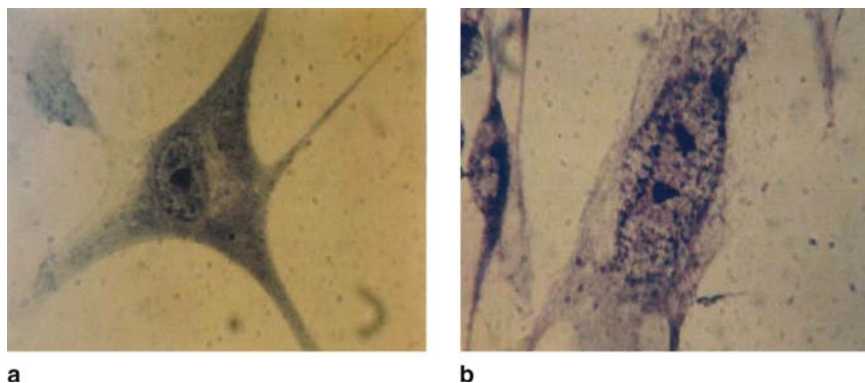


Fig. 7.4 Normal human embryonic fibroblasts grown on fullerene on the surfaces (FoS) before (A) and after 30 min illumination with halogen lamp 45 mW/cm² (B). Magnification 1,200× (See Color Plates)

The morphological structure of irradiated cells was also significantly injured: all membrane structures “melted” and became less contrast, organelles, especially nuclei, were round off, condensed, and fragmented – a typical picture of toxic stress (Fig. 7.4).

In order to demonstrate that phototoxicity of C₆₀ is in fact associated to ROS generation, we have studied photodynamic effect of fullerene in the presence of various antioxidants (AO).

As the AO with a direct nonspecific mechanism of action we have chosen Hypoxene® – sodium poly(2,5-dihydroxyphenyl)-4-thiosulfonate. Besides a direct AO effect as a scavenger of free radicals it exerts an anti-hypoxic effect shunting I and II complexes of mitochondrial respiratory chain, which are inhibited as a consequence of hypoxia (Eropkin et al., 2007). Hypoxene was introduced into cell incubation media before illumination and left during cells further incubation. Hypoxene in the concentration of 40 μg/ml, comparable to doses applied *in vivo*, completely blocked C₆₀-induced phototoxicity (Table 7.3). Cellular viability has completely recovered to control level, which is a convincing evidence of free radical nature of cellular damage in photodynamic effect of fullerene.

Phototoxic effect of C₆₀ was partly blocked by sodium azide, which is known to be a specific scavenger of singlet oxygen *in vivo* (Andrews et al., 1997; Hirayama et al., 1999; Lin et al., 2000). At the same time, we did not observe in our experimental conditions a protective effects of superoxide dismutase (SOD) from human red blood cells (10 μg/ml, 0.338 μM) and reduced glutathione (100 μg/ml, 325 μM), which supports a suggestion that the damaging agent in photodynamic effect of C₆₀ is exactly the singlet oxygen but not other ROS (hydroxyl or superoxide radicals) (Table 7.3).

As a conclusion we can deduce that solid-phase fullerene C₆₀ being in contact with polar medium can manifest antioxidant as well as pro-oxidant properties, the latter only under illumination.

Table 7.3 Photodynamic action of fullerene on the surfaces (FoS) ($10\mu\text{g}/\text{cm}^2$ of C_{60}) on cell culture MA-104 under effect of some antioxidants and Na-azide

Control	Control + preparation		C_{60}	C_{60} + preparation
		Hypoxene ^a		
100.0 ± 3.3	100.0 ± 1.7		51.7 ± 2.0*	96.8 ± 2.1**
		Na-azide ^b		
100.0 ± 3.7	80.0 ± 2.8*		36.7 ± 0.35*	62.1 ± 1.3*,**
		SOD ^c		
100.0 ± 2.7	108.8 ± 3.4*		89.4 ± 3.1*	87.4 ± 3.0*
		SOD + glutathione-SH ^d		
100.0 ± 3.2	–		45.5 ± 1.8*	45.2 ± 2.5*

Cells were grown for 24 h, growth medium was replaced for serum-free medium and the appropriate preparations were introduced, plates were illuminated with halogen lamp (about $45\text{ mW}/\text{cm}^2$) and further incubated for 18 h in the darkness. Viability was assessed by Alamar Blue reduction. Results are presented as percent of control.

*Significant difference of control ($p < 0.01$).

**Significant difference of C_{60} without preparations ($p < 0.01$).

^aHypoxene (oliphene) $40\mu\text{g}/\text{ml}$, illumination 10 min.

^bNa-azide, 25 mM, illumination 15 min.

^cRecombinant human SOD from yeasts (Recsod) $10\mu\text{g}/\text{ml}$ (about $0.34\mu\text{M}$), illumination 10 min.

^dHuman SOD extracted from red blood cells (Erysod) $10\mu\text{g}/\text{ml}$ plus the reduced glutathione $100\mu\text{g}/\text{ml}$ ($325\mu\text{M}$), illumination 30 min.

Our further studies were devoted to the C_{60} phototoxic effect on the different cell lines. Earlier we have got preliminary data on the opposite effect of a C_{60} /PVP complex on some cell lines of tumor and non-tumor origin: the life span of the former in the presence of $5\text{ mg}/\text{ml}$ of the complex ($30\text{--}40\mu\text{g}/\text{ml}$ of C_{60}) diminished during three consecutive passages while of the later – slightly augmented (data not published).

We investigated the kinetic of photodynamic action of FoS ($10\mu\text{g}/\text{cm}^2$) on the cell lines of malignant tumor origin (HeLa, A-549) and non-tumor origin (normal diploid embryonic fibroblasts and spontaneously transformed line MA-104). In these experiments a half of 96-well plate (four upper lines) was seeded with one cell culture and the other half with second culture. The experiments of phototoxicity assessment of C_{60} were designed as mentioned above. The results were subjected to liner regression analysis. Linear regression coefficients (b) in the pairs of tumor/non-tumor lines were always statistically significantly different (Table 7.4). Consequently, the cell lines of malignant tumor origin were more sensitive to photodynamic action of fullerene C_{60} , than cells of non-tumor origin (Table 7.4).

The obtained results have shown that cell cultures of tumor origin are more sensitive to phototoxic damage induced by solid-phase C_{60} than the cultures of non-tumor origin (normal or spontaneously transformed ones) – the effect that could be interesting for the perspective of possible fullerene usage in photodynamic therapy of tumors.

Table 7.4 Time-dependence of phototoxicity of fullerene on the surfaces (FoS) for cell lines of tumor and non-tumor origin

No of experiment	Cell line	Origin and degree of transformation	Coefficient of linear regression	Significance of difference between two cell lines
1*	MA-104	Kidney epithelium of green monkey (spontaneously transformed, non-tumor origin)	-0.062 ± 0.0034	$p < 0.001$
	A-549	Human lung carcinoma (malignant)	-0.087 ± 0.005	
2**	Human lung embryonic fibroblasts	Normal diploid cells of human lung, non-transformed	-0.177 ± 0.028	$p < 0.001$
	HeLa	Human cervical carcinoma (malignant)	-0.21 ± 0.017	
3**	Human lung embryonic fibroblasts	Normal diploid cells of human lung, non-transformed	-0.114 ± 0.009	$p < 0.001$
	A-549	Human lung carcinoma (malignant)	-0.176 ± 0.012	

*Exposition 30 min at 38 mW/cm².**Exposition 30 min at 45 mW/cm².

7.4 Conclusion

Fullerene and its derivatives have a wide spectrum of biological activity (photodynamic action, antioxidant activity, enzyme inhibition etc., [Da Ros and Prato, 1999]). However, not only fullerene derivatives are highly “narcissistic” and undergo self-assembly even at low concentrations (Sessler et al., 2006), the same is true for pristine fullerene itself especially in polar media. Therefore, the action of fullerenes and first of all of fullerene C₆₀ on biological objects depends both on conditions in which the experiment is carried out (in darkness or illumination), and the way it is introduced into a biological system. In the latter case the mode of water-soluble form preparation and precisely the degree of association (dissociation) of fullerene molecules in the polar medium or in biological object play an important role. It is difficult to imagine the efficient penetration into biological membranes of fullerene molecules from the negatively charged clusters with the dimensions of 20 nm and more. However, in water-soluble complexes with the organic compounds, in contrast to molecular-colloidal solutions or fullerene-modified surfaces, the degree of association of fullerene molecules is much lower (in the complex with γ -CD we are dealing with practically “isolated” molecules) (Ikeda et al., 2005), and that allows the fullerene molecules to penetrate into membrane having the thickness of about 5–7 nm. Thus, in a low aggregate state fullerene has a membranotropic activity as well (Piotrovsky and Kiselev, 2004).

As mentioned earlier, fullerene molecules can destroy the virions, but do not affect living cells. It is possible to suppose that the differences of the structures of virion envelope and cell membrane are the main reason for this phenomenon: the outer side of virion envelope is enriched with protein molecules, whereas the outer side of cell membranes is more lipophylic. On the one hand, fullerene molecules can interact with proteins (Belgorodsky et al., 2006), and on the other hand, their penetration into a lipid bilayer does not destroy them (Ikeda et al., 2005; Piotrovsky, 2006). So it is not unlikely that the difference in the structure of outer side is the main driving force of the observed differences in the response of virions and cells in the presence of C_{60} .

The toxicity of fullerene is at present one of the most widely discussed subjects. Though commonplace, it should be noted that toxicity is an extreme manifestation of biological activity leading to the death of biological object. One can conclude that the mechanisms of toxicity of any substance reflect the mechanisms of its biological activity.

In the case of pristine fullerene, these mechanisms are photodynamic action (the ability of excited state $^*C_{60}$ to transfer energy to the molecule of triplet oxygen turning it into the singlet state), antioxidant activity (due to electron deficiency of the core), and membranotropic properties (as a consequence of the high lipophylicity of the molecule). As the introduction of substituents into the fullerene core can diminish these properties, the pristine fullerene C_{60} itself is in our opinion a very significant object for the studies of biological activities of fullerenes in particular as well as carbon nanostructures in general.

With all this, considering every above-mentioned data, it becomes obvious that investigations of any fullerene effect demand to consider the state of the substance while under investigation strictly. Fullerene is whimsical as a real beauty.

References

- Andersson T, Nilsson K, Sundahl M et al. (1992) C60 embedded in γ -cyclodextrin: a water-soluble fullerene. *J Chem Soc Chem Commun.* 604–605.
- Andrews MJ, Garle MJ, Clothier RH et al. (1997) Reduction of the new tetrazolium dye, Alamar Blue™, in cultured rat hepatocytes and liver fractions. *ATLA.* 25: 641–653.
- Andrievsky GV, Kosevich MV, Vovk OM et al. (1995) On the production of an aqueous colloidal solution of fullerene. *J Chem Soc Chem Commun.* 1281–1282.
- Andrievsky G, Klochkov V, Derevyanchenko L (2005) Is C60 fullerene molecule toxic? *Full Nanotubes Carb Nanostruct.* 13: 363–376.
- Bang J, Guerrero P, Lopez D et al. (2004) Carbon nanotubes and other fullerene nanocrystals in domestic propane and natural gas combustion streams. *J Nanosci Nanotechnol.* 4: 716–718.
- Bass DA, Parce JW, Dechatelet LR et al. (1983) Flow cytometric studies of oxidative product formation by neutrophils: a graded response to membrane stimulation. *J Immunol.* 130: 1910–1918.
- Belgorodsky B, Fadeev L, Kolsenik J, Gozin M (2006) Formation of a soluble stable complex between pristine C60-fullerene and a native blood protein. *ChemBioChem.* 7: 1783–1789.
- Bensasson RV, Bienvenue E, Dellinger M et al. (1994) C60 in model biological systems. A visible-UV absorption study of solvent dependent parameters and solute aggregation. *J Phys Chem.* 98: 492–3500.

- Bianco A, Da Ros T, Prato M et al. (2001) Fullerene-based amino acids and peptides. *J Pept Sci.* 7: 208–219.
- Bosi S, Da Ros T, Spalluto G et al. (2003) Fullerene derivatives: an attractive tool for biological applications. *Eur J Med Chem.* 38: 913–923.
- Brant J, Lecoanet H, Hotze M et al. (2005a) Comparison of electrokinetic properties of colloidal fullerenes (n-C60) formed using two procedures. *Environ Sci Technol.* 39: 6343–6351.
- Brant J, Lecoanet H, Wiesner MR (2005b) Aggregation and deposition characteristics of fullerene nanoparticles in aqueous systems. *J Nanopart Res.* 7: 545–553.
- Brant JA, Labille J, Bottero JY et al. (2006) Characterizing the impact of preparation method on fullerene cluster structure and chemistry. *Langmuir.* 22: 3878–3885.
- Braun T (1997) Water soluble fullerene-cyclodextrin supramolecular assemblies. Preparation, structure, properties (an annotated bibliography). *Full Sci Technol.* 5: 615–626.
- Buvari-Barcza A, Rohonczy J, Rozlosnik N et al. (2001) Aqueous solubilization of [60]fullerene via inclusion complex formation and the hydration of C60. *J Chem Soc Perkin Trans.* 2: 191–196.
- Chiron J, Lamande J, Moussa F, et al. (2000) Effect of “micronized” C60 fullerene on the microbial growth *in vitro*. *Ann Pharm Fr.* 58: 170–175 (French).
- Cheng F, Yang X, Zhu H et al. (2000) Synthesis of oligoadducts of malonic acid C60 and their scavenging effects on hydroxyl radical. *J Phys Chem Solids.* 61: 1145–1148.
- Clothier R, Starzec G, Pradel L et al. (2002) The prediction of human skin responses by using the combined *in vitro* fluorescein leakage/Alamar Blue (Resazurin) assay. *ATLA.* 30: 493–504.
- Da Ros T, Prato M (1999) Medicinal chemistry with fullerenes and fullerene derivatives. *J Chem Soc Chem Commun.* 663–669.
- Da Ros T, Spalluto G, Prato M et al. (2001) Biological applications of fullerene derivatives: a brief overview. *Croatica Chemica Acta.* 74: 743–755.
- Deguchi S, Alargova RG, Tsujii K (2001) Stable dispersions of fullerenes, C60 and C70, in water. preparation and characteristics. *Langmuir.* 17: 6013–6017.
- Eropkin MYu, Eropkina EM, Kiselev OI (2007) Studying the effect of antioxidants and/or anti-hypoxants on cell cultures under conditions of cytotoxic action of rimantadine. *Exp Clin Pharmacol.* 70: 56–61 (Russian).
- Foley S, Crowley C, Smaih M et al. (2002) Cellular localisation of a water-soluble fullerene derivative. *Biochem Biophys Res Commun.* 294: 116–119.
- Fortner ID, Lyon DY, Sayes CM et al. (2005) C60 in water: nanocrystal formation and microbial response. *Environ Sci Technol.* 39: 4307–4316.
- Guldi DM (1997) Capped fullerenes: stabilization of water-soluble fullerene monomers as studied by flash photolysis and pulse radiolysis. *J Phys Chem A.* 101: 3895–3900.
- Guldi DM, Asmus KD (1999) Activity of water-soluble fullerenes towards •OH-radicals and molecular oxygen. *Radiation Phys Chem.* 56: 449–456.
- Guldi DM, Hungerbuhler H, Asmus KD (1995) Stable monolayers and Langmuir-Blodgett films of functionalized fullerenes. *J Phys Chem.* 99: 17673–17676.
- Guldi DM, Zerbetto F, Georgakilas V et al. (2005) Ordering fullerene materials at nanometer dimensions. *Acc Chem Res.* 38: 38–43.
- Henry TB, Menn FM, Fleming JT et al. (2007) Attributing effects of aqueous C60 nano-aggregates to tetrahydrofuran decomposition products in larval zebrafish by assessment of gene expression. *Environ. Health Perspect.* 115: 1059–1065.
- Hirayama J, Abe H, Kamo N et al. (1999) Photoinactivation of vesicular stomatitis virus with fullerene conjugated with methoxy polyethylene glycol amine. *Biol Pharm Bull.* 22: 1106–1109.
- Hoffmann R (2003) Thoughts on aesthetics and visualization in chemistry. *HYLE.* 9: 7–10.
- Ikeda A, Sato T, Kitamura K et al. (2005) Efficient photocleavage of DNA utilising water-soluble lipid membrane-incorporated [60]fullerenes prepared using a [60]fullerene exchange method. *Org Biomol Chem.* 3: 2907–2909.

- Ikeda A, Irisa T, Hamano T et al. (2006) Control of self-aggregation of fullerenes by connection with calyx[4]arene: solvent and guest effects to particle size. *Org Biomol Chem*. 4: 519–523.
- Ikeda A, Doi Y, Hashizume M et al. (2007) An extremely effective DNA photocleavage utilizing functionalized liposomes with a fullerene-enriched lipid bilayer. *J Am Chem Soc*. 129: 4140–4141.
- Janot JM, Bienvenüe E, Seta P et al. (2000) [60]Fullerene and three [60]fullerene derivatives in membrane model environments. *J Chem Soc Perkin Tran*. 2: 301–306.
- Jensen AW, Wilson SR, Schuster DI (1996) Biological applications of fullerenes. *Bioorg Med Chem*. 4: 767–779.
- Kiselev O, Kozeletskaia K, Melenevskaya E et al. (1998a) The antiviral activity of the complex of fullerene C60 with poly(N-vinyl-pyrrolidone). *Mol Mat*. 11: 121–124.
- Kiselev O, Kozeletskaia KN, Melenevskaya EYu et al. (1998b) Antiviral activity of fullerene (60)C complexed with poly(N-vinylpyrrolidone). *Dokl Akad Nauk*. 361: 547–549 (Russian).
- Krakovjak MG, Anufrieva EV, Anan'eva TD, Nekrasova TN (2005a) Water-soluble fullerene complexes with n-vinylcaprolactam homo- and copolymers and a method for preparation of these complexes. Russian patent RU 2 264 415 10.02.2005
- Krakovjak MG, Anufrieva EV, Piotrovskij LB et al. (2005b) Water-soluble complex of fullerene with poly-N-vinylpyrrolidone and method for preparing these complexes. Russian patent RU 2 255 942 20.02.2005.
- Krakovjak MG, Anufrieva EV, Anan'eva TD et al. (2006) Water-soluble complexes of poly(N-vinylamides) of various structures with C60 and C70 fullerenes. *Polym Sci Ser A*. 48: 590–595.
- Kratschmer W, Lamb LD, Fostiropoulos K et al. (1990) Solid C60: a new form of carbon. *Nature*. 347: 354–358.
- Lautraite S, Bigot-Lasserre D, Bars R et al. (2003) Optimization of cell-based assays for medium throughput screening of oxidative stress. *Toxicol In Vitro*. 17: 207–220.
- Li H, Hao J (2007) Phase behavior of salt-free cationic surfactant aqueous solutions with fullerene C60 solubilized. *J Phys Chem B*. 111: 7719–7724.
- Lin YL, Lei HY, Luh TY et al. (2000) Light-independent inactivation of dengue-2 virus by carboxyfullerene C3 isomer. *Virology*. 275: 258–262.
- Lyon D, Adams LK, Falkner JC, Alvarez PJJ (2006) Antibacterial activity of fullerene water suspensions: effects of preparation method and particle size. *Environ Sci Technol*. 40: 4360–4366.
- Moussa F, Chretien P, Dubois P et al. (1995) The influence of C60 powders on cultured human leukocytes. *Full Sci Technol*. 3: 333–342.
- Murr LE, Soto KF (2005) A TEM study of soot, carbon nanotubes, and related fullerene nanopolyhedra in common fuel-gas combustion sources. *Mater Characteriz*. 55: 50–65.
- Oberdörster E (2004) Manufactured nanomaterials (fullerenes, C60) induce oxidative stress in brain of juvenile largemouth bass. *Environ Health Perspect*. 112: 1058–1062.
- Piotrovsky LB (2006) Biological activity of pristine fullerene C60. In: Dai L (ed) *Carbon Nanotechnology*. Elsevier, Amsterdam.
- Piotrovsky LB, Kiselev OI (2004) Fullerenes and viruses. *Full Nanotubes Carb Nanostruct*. 12: 397–403.
- Piotrovsky LB, Kiselev OI (2006) Fullerenes in Biology. Rostok, St. Petersburg, Russia.
- Piotrovsky LB, Dumpis MA, Poznyakova LN et al. (2000) Study of the biological activity of the adducts of fullerenes with poly(N-vinylpyrrolidone). *Mol Mat*. 13: 41–50.
- Piotrovskii LB, Kozeletskaia KN, Medvedeva NA et al. (2001) Effect of fullerene C60-polyvinylpyrrolidone complexes on influenza virus reproduction. *Voprosy Virusologii*. 46(3): 38–42 (Russian).
- Podol'skii IYa, Kondrat'eva EV, Shcheglov IV et al. (2002) Fullerene C60 complexed with poly(N-vinylpyrrolidone) prevents the disturbance of long-term memory consolidation. *Phys Solid States*. 44: 552–554.

- Podolski IYa, Kondratjeva EV, Gurin SS et al. (2004) Fullerene C₆₀ complexed with poly(N-vinylpyrrolidone) prevents the disturbance of long-term memory consolidation induced by cycloheximide. *Full Nanotubes Carb Nanostruct.* 12: 421–424.
- Popov VA, Tyumin MA, Zaitseva OB et al. (2007) Influence of C₆₀/PVP complex on the healing of wounds and the toxicity in the experiments in vivo. In: *Book of abstracts 8th Biennial International Workshop Fullerenes and Atomic Clusters*, July 2–6, St. Peterburg, Russia P173.
- Prat F, Stackow R, Bernstein R et al. (1999) Triplet-state properties and singlet oxygen generation in a homologous series of functionalized fullerene derivatives. *J Phys Chem.* 103: 7230–7235.
- Prato M (1999) Fullerene materials. *Top Curr Chem.* 199: 173–186.
- Richmond RC, Gibson UJ (1994) Fullerene coated surfaces and uses thereof. US Patent 5,310,669 May 10, 1994.
- Scrivens WA, Tour JM, Creek KE et al. (1994) Synthesis of ¹⁴C-labeled C₆₀, its suspension in water and its uptake by human keratinocytes. *J Am Chem Soc.* 116: 4517–4518.
- Sessler JL, Jayawickramarajah J, Gouloumis A et al. (2006) Guanosine and fullerene derived deaggregation of a new phthalocyanine-linked cytidine derivative. *Tetrahedron.* 62: 2123–2131.
- Shibuya M, Kato M, Ozawa M et al. (1999) Detection of buckminsterfullerene in usual soot and commercial charcoals. *Full Sci Technol.* 7: 181–193.
- Sijbesma R, Srdanov G, Wudl F et al. (1993) Synthesis of fullerene derivative for the inhibition of HIV enzymes. *J Am Chem Soc.* 115: 6510–6512.
- Sirotkin AK, Zarubaev VV, Poznyakova LN et al. (2006) Pristine fullerene C₆₀: different water soluble forms – different mechanisms of biological action. *Full Nanotubes Carb Nanostruct.* 43: 327–333.
- Sushko ML, Klenin SI, Dumpis MA et al. (1999) Light scattering in water solutions of fullerene-containing polymers: Part 2. Effect of the molecular weight of the carrier molecule. *Tech Phys Lett.* 25: 778–779.
- Tokuyama H, Yamago S, Nakamura E et al. (1993) Photoinduced biochemical activity of fullerene carbocyclic acid. *J Am Chem Soc.* 115: 7918–7919.
- Tsuchiya T, Oguri I, Yamakoshi YN et al. (1996) Novel harmful effects of [60]fullerene on mouse embryos in vitro and in vivo. *FEBS Lett.* 393: 139–145.
- Vinogradova LV, Melenevskaya EYu, Khachaturov AS et al. (1998) Water soluble complexes of fullerene C₆₀ with poly-N-vinylpyrrolidone. *Vysokomol Soed.* 40: 1854–1862 (Russian).
- Yamakoshi YN, Yagami T, Fukuhara K et al. (1994) Solubilization of fullerenes into water with polyvinylpyrrolidone applicable to biological tests. *J Chem Soc Chem Commun.* 517–518.

Chapter 8

Gadolinium Endohedral Metallofullerene-Based MRI Contrast Agents

Robert D. Bolskar

Abstract With the ability to encapsulate and carry the highly paramagnetic Gd^{3+} ion, gadolinium endohedral metallofullerenes or “gadofullerenes” are being explored as alternatives to the chelate complexes that are currently used for contrast-enhanced magnetic resonance imaging (MRI). Reviewed here are the various water-soluble derivatives of the gadofullerenes $Gd@C_{82}$, $Gd@C_{60}$, and $Gd_3N@C_{80}$ that have been investigated as MRI contrast agents. The water proton r_1 relaxivities of gadofullerenes can be more than an order of magnitude higher than those of clinically used chelate agents. Gadofullerene relaxivity mechanisms have been studied, and multiple factors are found to contribute to their high relaxivities. *In vitro* and *in vivo* T_1 -weighted MRI tests of gadofullerene derivatives have shown their utility as bright image-enhancing agents. The gadofullerene MRI contrast agents are a promising new and unique style of gadolinium carrier for advanced imaging applications, including cellular and molecular imaging.

Keywords Metallofullerene, endohedral, gadolinium, magnetic resonance imaging, contrast agent, relaxivity, cellular imaging, molecular imaging

8.1 Introduction

Endohedral metallofullerenes are those fullerene cages containing a metal atom or atoms entrapped in their otherwise hollow interior spaces. The promise for using these fascinating new materials in biomedical applications was realized soon after their discovery, as noted by Prof. Richard Smalley and others (Edelson, 1991). One of the most promising early biomedical applications that has distinctly progressed since the discovery of fullerenes is the use of gadolinium metallofullerenes as paramagnetic agents to increase contrast in magnetic resonance imaging (MRI). In MRI, the nuclear magnetic resonance (NMR) signals from biological protons are

TDA Research Inc., 12345 West 52nd Avenue, Wheat Ridge, CO 80033, USA
Email: bolskar@tda.com

used to create images of tissue, organs, and disease *in vivo*. The information derived from inherent differences in the longitudinal (spin-lattice) relaxation times (T_1) and/or transverse (spin-spin) relaxation times (T_2) of water protons in the tissues of interest are used to create the anatomical MR images. A major advantage of MRI is that it is a noninvasive procedure, which means that surgical procedures are not needed and ionizing radiation, such as x-rays, is not required for its operation. Proton MRI has not only a high spatial resolution, but also a high background signal that comes from endogenous protons, and a relatively low sensitivity.

To increase the low sensitivity of the MRI technique and improve delineation between tissues, paramagnetic contrast-enhancing agents are used in approximately 35% of clinical MRI procedures. Current clinically approved agents are chelates of the Gd^{3+} ion, which is selected because of its high paramagnetic moment (Gd^{3+} has seven unpaired 4f electrons) and favorably long electron-spin relaxation time. Free Gd^{3+} is toxic, and cannot be administered directly to patients. Instead, clinical Gd contrast agents use chelating molecules to securely coordinate the Gd^{3+} ion, while providing at least one open coordination site for solvent water molecules to reversibly coordinate to the metal center. The chelate molecules also provide potential chemical scaffolds for modifying the agent's properties. As discussed below, even with many years of success with the first clinical Gd chelate contrast agents, room remains to improve on their chelation stabilities, potency, and function. This is where gadolinium endohedral metallofullerenes, also called gadofullerenes, present a new opportunity. Gadofullerenes offer a combination of unique properties that make them potentially superior to standard coordinative chelates for Gd^{3+} entrapment and delivery in use as MRI contrast agents. Since the initial discovery of fullerenes and metallofullerenes, the understanding of the many fundamentals behind the use of gadofullerenes as paramagnetic MRI contrast agents has greatly improved. The primary focus of this chapter is a review of current progress in the study and use of gadolinium metallofullerenes as paramagnetic MRI contrast agents. Derivatives of $Gd@C_{82}$, $Gd@C_{60}$, and $Gd_3N@C_{80}$ gadofullerenes are covered in sequence. Their respective relaxivity properties and MRI tests performed with the agents are discussed. In addition, brief discussions of other biomedical applications of metallofullerenes and related systems are included when warranted.

8.2 MRI Contrast-Enhancing Agents

Paramagnetic MRI contrast agents function by decreasing the spin relaxation times of water protons. In principle, any paramagnetic ion can perform this function, but the high magnetic moment of Gd^{3+} has led to its prominence, and the contrast agents approved for clinical use employ Gd^{3+} chelates. There are two primary ways paramagnetic ions shorten the relaxation times of surrounding water protons. The first is by the inner-sphere mechanism, which involves water molecule(s) directly coordinated to the metal and in exchange with solvent water, and outer sphere mechanisms, which involves water molecule(s) not coordinated to the metal, but

located in the vicinity of the paramagnetic center. Delineation of tissues is obtained by the relative difference in water proton relaxation times in the tissues containing the relaxation agent versus those lacking the agent; T_1 agents serve to increase the detectable MR signal.

“Relaxivity” is the term given to a contrast agent’s characteristic potency to decrease the nuclear spin relaxation times of water protons. Relaxivity is defined by the following relationship:

$$(1/T_x)_{\text{obsd}} = (1/T_x)_d + r_x[\text{agent}]$$

where $(1/T_x)_{\text{obsd}}$ is the solvent proton relaxation rate in the presence of agent; $(1/T_x)_d$ is water proton diamagnetic relaxation rate in the absence of agent, and r_x is the characteristic “relaxivity” of agent. T_x is linearly dependent on MRI contrast agent concentration [agent], and r_x is the slope of the line calculated from regression analysis of $(1/T_x)_{\text{obsd}}$ vs. [agent]. The relaxivity r_x ($x = 1, 2$) is expressed in reciprocal millimolar-second ($\text{mM}^{-1}\text{s}^{-1}$), which reflects the agent’s ability to increase the respective relaxation rates ($1/T_1$ and/or $1/T_2$) on a millimolar basis. The higher a contrast agent’s relaxivity is, the greater the relative contrast offered, which potentially lowers the dosage of agent required for imaging. In practice, proton MRIs can be obtained using T_1 - or T_2 -weighted imaging sequences, with T_1 agents providing positive contrast (image brightening) and T_2 agents providing negative contrast (image darkening).

The clinically approved linear and macrocyclic Gd^{3+} chelate complexes are designed to tightly hold the metal ion and prevent its release *in vivo*, and the reader is directed to the widely available review articles and books that have already detailed the chemistry of chelate contrast agents and their relaxivity properties (e.g., see Lauffer, 1987; Caravan et al., 1999; Tóth et al., 2001). Highly modified coordination complexes are being synthesized to increase relaxivities and impart special functions to these contrast agents. Improved Gd^{3+} chelation stability is an ever-present goal to prevent possible exposure to free Gd^{3+} . When a chelate agent has a very long residence time in the body (either by intentional design or otherwise) transmetallation of Gd^{3+} by endogenous ions is a particular concern (Idée et al., 2006). A recently recognized debilitating condition, nephrogenic systemic fibrosis (NSF), appears to be related to these issues. This disease, found in renally compromised patients that had been administered clinically approved Gd chelate MRI agents, can cause severe skin and organ damage and even death (Grobner, 2006; Grobner and Prischl, 2007). Currently, NSF is not entirely understood, as the symptoms vary widely in severity as well as in their timing after Gd chelate agent exposure. Research on how Gd^{3+} may trigger NSF is ongoing, but a causal correlation between NSF and Gd chelate exposure is documented (Collidge et al., 2007). The risk of NSF precludes use of clinically approved Gd chelates in end-stage renal patients, and causes potential concern with patients having more moderate renal dysfunction. Clearly, any new style of Gd-based MRI contrast agents (chelate or nanoparticle-based, etc.) will be required to be highly resistant to transmetallation and Gd^{3+} loss.

8.3 Fullerenes and Metallofullerenes

Endohedral fullerenes have an atom or atoms entrapped in their hollow interior spaces (Heath et al., 1985; Weiss et al., 1988; Chai et al., 1991). Metallofullerenes are endohedrals that trap a metal atom or atoms, and are trivially written as “M@C_{2n}” with the encapsulated nature of the metal denoted by the “@” symbol. Metallofullerenes of the lanthanide elements are the most prevalent type, with the carbon arc process (used first to produce empty fullerenes on gram-scales [Krätschmer et al., 1990]) being the most common method used to produce metallofullerenes. Substituting lanthanide-doped graphite rods in place of pure graphite rods in the arc process produces lanthanide-containing metallofullerenes mixed in with empty fullerenes and amorphous carbon soot. Metallofullerenes are made with a wide variety of fullerene cage sizes and isomers, just as non-endohedral fullerenes are. The lanthanides are electropositive metal elements, and fullerenes are in general electronegative. As a natural consequence three electrons (in most, but not all cases) are transferred from the lanthanide to the fullerene cage, resulting in a trivalent metal cation inside a triply reduced anionic fullerene, i.e., “M³⁺@C_{2n}³⁻” (Nagase et al., 2000; Shinohara, 2000).

Metallofullerenes physically encase the metal ion inside the closed fullerene shell. This feature endows them with a unique and advantageous way to entrap and hold metal ions in a manner quite unlike the chelates, in which classic coordination chemistry clutches the metal ion. Fullerene cages in general are comprised of stable closed networks of carbon atoms that do not open up with exposure to typical physiological conditions. The endohedral metal ion is thus not susceptible to transmetalation and is not in exchange with exterior solvated cations. This special resistance to metal ion loss is a distinct advantage that metallofullerenes have over traditional chelates used in biomedicine. It is no surprise that researchers rapidly recognized the potential metallofullerenes had as carriers of otherwise toxic metal ions for applications including gadolinium-containing MRI contrast agents, lanthanide x-ray imaging contrast agents, and radioisotope carriers for nuclear medicine.

One area in which gadofullerene-based MRI contrast agents could provide particular benefits over chelate agents is with long-circulating agents. For example, MR angiography and *in vivo* targeted agents require long circulation times for the agents to be effective, but long residency *in vivo* could present a Gd³⁺ ion-release safety issue. This is even more an issue in light of the earlier discussed NSF, which appears to be related to Gd³⁺ exposure. Further study on the safety of individual metallofullerene drug and imaging agent candidates will of course need to be completed before their study in humans and eventual drug regulatory agency approval.

While there are no studies of the toxicity of endohedral fullerenes in general, or gadofullerenes in particular, there are several preliminary studies regarding empty fullerenes and their derivatives. In initial steps toward characterizing the safety of water-soluble fullerene derivatives, a cytotoxicity study of various fullerene materials, including underivatized C₆₀, C₆₀[C(COOH)₂]₃, and two C₆₀(OH)_x species, was conducted (Sayes et al., 2004). The results clearly showed that water-soluble derivatives were significantly less toxic than underivatized C₆₀, and the trend was one of

decreasing cytotoxicity with an increasing degree of functionalization. A similar effect was seen with comparisons of derivatized and water-solubilized carbon nanotubes (CNTs) and underivatized carbon nanotubes (Sayes et al., 2006). Furthermore, *in vivo* comparison of the toxicity of $C_{60}(OH)_{24}$ to underivatized C_{60} in embryonic zebra fish showed $C_{60}(OH)_{24}$ to be significantly less toxic (Usenko et al., 2007). These results are highly promising for the fullerene drug development enterprise, as any practical fullerene-based drug or imaging agent will almost certainly be rationally derivatized for biocompatibility, since underivatized fullerenes are virtually insoluble in water.

The potential disadvantages of metallofullerenes are their somewhat exotic production methods, the need for separating the metallofullerenes from empty fullerenes, and their relatively low abundances (Nagase et al., 2000; Shinohara, 2000). It follows that maximizing their availability has been a major research focus. Fortunately for gadofullerene-based MRI contrast agent development, metallofullerenes made with gadolinium by the arc process have relatively higher yields in comparison to most of the other lanthanides. The product obtained by arcing metal-doped graphite rods is dominated by carbonaceous soot, which contains varying amounts of empty fullerenes and metallofullerenes mixed in. Fullerenes and metallofullerenes are most commonly separated from the arc soot using solvent extraction or washing with solvents, such as toluene, that are good fullerene solvents (Ruoff et al., 1993). Further separation of the metallofullerenes from the empty fullerenes typically follows. Among the soluble species, $M@C_{82}$ metallofullerenes can be routinely extracted and isolated using chromatographic techniques, particularly multistage high-performance liquid chromatography (HPLC). Chemical and electrochemical methods can also be used to enrich and separate $M@C_{82}$ metallofullerenes from fullerene arc product mixtures (Diener et al., 2002; Sun and Gu, 2002; Tsuchiya et al., 2004; Lu et al., 2005; Tsuchiya et al., 2006a, b). HPLC reliably generates isomerically pure samples of $M@C_{82}$, but it requires a large resource expenditure (in terms of effort and solvents) to obtain only milligram samples of purified metallofullerenes. While it is not unusual for high-value biomedical agents to be needed in only small quantities in the early stages, eventually much larger amounts will be needed for proper development and testing of gadofullerene contrast agents. Drug development will require moving beyond use of just the minority, soluble $M@C_{82}$ content of the arc metallofullerenes.

To surpass the above limitations, new developments have recently enabled access to all of the metallofullerenes generated by the arc process, not just $M@C_{82}$ (Bolskar and Alford, 2003; Bolskar et al., 2003). Other metallofullerenes such as $M@C_{60}$, $M@C_{70}$, and $M@C_{74}$ are more prevalent in the arc products, but are not as soluble as $M@C_{82}$ (Diener and Alford, 1998). A recent study of arc-generated Gd metallofullerenes found that soluble $Gd@C_{82}$ comprises only about 10% of the total metallofullerene product, with the majority, 90%, being other insoluble $Gd@C_{2n}$ (Raebiger and Bolskar, 2008). To access the total Gd metallofullerene content, processes other than just arc soot extraction with solvents were implemented. Sublimation effectively removed all fullerenes and metallofullerenes from the arc soot, leaving the non-fullerene amorphous carbon behind. Direct solvent extraction

of the soot as practiced before leaves behind about 90% of the Gd metallofullerenes in the soot. Next, the different Gd metallofullerenes in the sublimate were separated into fractions having different chemical properties, following their responses to combinations of oxidative treatments and solvent extractions of the resulting cationic species. Separate fractions highly enriched in the Gd@C₆₀ class of metallofullerenes as well as Gd@C₈₂ were obtained. This access to the Gd@C₆₀ class of metallofullerenes has effectively increased by about a factor of 10 the yield of Gd metallofullerenes that can be studied and used as contrast agents and in other applications.

Gd metallofullerene MRI contrast agents have emerged as a classic example of a biomedical application with a metal in which direct access to the ion's coordination sphere is not required, yet the ion(s) still exhibits its desired activity. With the metallofullerenes containing a trivalent lanthanide, three electrons are donated to the fullerene (as reflected in the "M³⁺@C_{2n}³⁻" formalism), and thus the fullerene cage itself is paramagnetic with an odd number of electrons (Funasaka et al., 1995; Kato et al., 2000). The seven unpaired 4*f* electrons of Gd³⁺ also contribute significant paramagnetism to the metallofullerene. Based on their magnetic properties, it was reasonable to expect that gadofullerenes could function as water proton relaxation agents, even without direct water-to-Gd³⁺ coordination. For gadofullerenes to be practical contrast agents, water solubility is needed at some level because native fullerenes and metallofullerenes are fully hydrophobic. The best way to water-solubilize fullerenes and metallofullerenes is to derivatize their all-carbon surfaces with hydrophilic functional groups, and there are now a variety of creative synthetic strategies to accomplish this (Nakamura and Isobe, 2003).

8.4 Gd@C₈₂ Compounds as MRI Contrast Agents

Gd@C₈₂, being the first accessible Gd metallofullerene due to its organic-soluble nature, was the first gadofullerene investigated as an MRI contrast agent. Gd@C₈₂ is most commonly converted to a water-soluble derivative with surface polyhydroxylation. One of the first water proton relaxivity measurements on a gadofullerene was reported by Zhang et al. (1997) for Gd@C₈₂(OH)_x mixed with polyhydroxylated empty fullerenes. The r_1 for this mixture was reported to be 47 mM⁻¹s⁻¹ (9.4 T, temperature unspecified) as calculated on a per-Gd³⁺ basis. This result was significant for demonstrating that a gadofullerene derivative can function as water proton relaxation agent, and the authors speculated that the high r_1 resulted from the fullerene essentially "enlarging" the surface area of the Gd³⁺ ion (for hydrogen bonding to waters) as compared to standard chelates. Several other early studies also reported high but different r_1 values for Gd@C₈₂(OH)_x, including 47 mM⁻¹s⁻¹ (9.4 T, 25 °C) (Shukla et al., 1997) and 20 mM⁻¹s⁻¹ (0.47 T, 40 °C) (Wilson, 1999). For Gd@C₈₂(OH)₄₀ (pH = 7.5, 25 °C), Shinohara and coworkers reported r_1 values of 67, 81, and 31 mM⁻¹s⁻¹ at 0.47, 1.0, and 4.7 T, respectively, and r_2 values of 79, 108, and 131 mM⁻¹s⁻¹ at 0.47, 1.0, and 4.7 T, respectively (Mikawa et al., 2001). A second

report by the same group noted that for $\text{Gd}@C_{82}(\text{OH})_{40}$ at 0.47 T and 37 °C, $r_1 = 62 \text{ mM}^{-1}\text{s}^{-1}$ and $r_2 = 69 \text{ mM}^{-1}\text{s}^{-1}$ (Okumura et al., 2002). Relaxivities of a gadofullerene mixture containing $\text{Gd}@C_{82}(\text{OH})_{22}$, $\text{Gd}@C_{80}(\text{OH})_{22}$, and $\text{Gd}_2@C_{80}(\text{OH})_{22}$ were also tested at 0.47 T and 37 °C, with $r_1 = 56 \text{ mM}^{-1}\text{s}^{-1}$ and $r_2 = 67 \text{ mM}^{-1}\text{s}^{-1}$. A nuclear magnetic relaxation dispersion (NMRD) profile (NMRD is measurement of nuclear magnetic resonance dispersion, i.e., measurement of proton relaxivities as a function of magnetic field, and are generally obtained with a field cycling relaxometer) of this gadofullerene mixture at 30 °C revealed r_1 to remain nearly flat at 45–35 $\text{mM}^{-1}\text{s}^{-1}$ from very low field up to approximately 0.23 T (about 10 MHz proton Larmor frequency), but a distinct increase and a peak r_1 of about 70 $\text{mM}^{-1}\text{s}^{-1}$ at near 1 T follows (Okumura et al., 2002).

There are several conspicuous features in the above-reported $\text{Gd}@C_{82}(\text{OH})_x$ gadofullerene relaxivities. Most prominent are the high r_1 relaxivity values of these gadofullerenes. The r_1 values of the clinically used Gd chelates are much lower, being generally about 3–6 $\text{mM}^{-1}\text{s}^{-1}$ under similar measurement conditions (Laufer, 1987; Caravan et al., 1999). The order of magnitude elevation of gadofullerene relaxivities is striking, and immediately raises the prospect that gadofullerenes are inherently more potent paramagnetic contrast agents than the clinical chelates. Another conspicuous feature is the high variation in the reported gadofullerene relaxivities, as the reported r_1 values vary from 20 to 81 $\text{mM}^{-1}\text{s}^{-1}$. Variation of relaxivity is normally very modest or negligible with the Gd chelates. Some degree of the gadofullerene relaxivity variation is due to obtaining the data at different magnetic field strengths (i.e., different proton Larmor frequencies), concentrations, and temperatures, which are well known to affect r_1 and r_2 values (Laufer, 1987; Caravan et al., 1999; Tóth et al., 2001). Furthermore, there is variation in the value of x in polyhydroxylated $\text{Gd}@C_{2n}(\text{OH})_x$ species because the synthetic processes are not especially selective for a given value of x . It is also challenging to analytically determine the value of x to a high degree of accuracy, as varying waters of hydration potentially complicate matters. It is also possible that the polyhydroxylated products are mixtures of different structural isomers with some variation in x . Nonetheless, at these relatively high levels of fullerene surface coverage by hydroxyl groups, these variations are not expected to have a large influence on relaxivity. Rather, the influence of other factors such as solution pH may be influencing the measured relaxivities of gadofullerenes. This was hinted at by the preliminary results of Shinohara and coworkers with $\text{Gd}@C_{82}(\text{OH})_{40}$, who noted a maximum r_1 between pH 3 and 8, and a 6 $\text{mM}^{-1}\text{s}^{-1}$ decrease in r_1 units (from 67 to 61 $\text{mM}^{-1}\text{s}^{-1}$) when changing from an aqueous NaCl solution concentration of 0–1.0 M (Mikawa et al., 2001).

In another interesting study, Shinohara and coworkers compared the water proton relaxivity properties of $\text{M}@C_{2n}(\text{OH})_x$ containing lanthanides other than Gd (including $\text{M} = \text{La}, \text{Ce}, \text{Dy}, \text{and Er}$), to the gadofullerene compound $\text{Gd}@C_{82}(\text{OH})_x$ (Kato et al., 2003). For these polyhydroxylated metallofullerenes, r_1 and r_2 ranged from 0.8 to 73 $\text{mM}^{-1}\text{s}^{-1}$ and from 1.2 to 80 $\text{mM}^{-1}\text{s}^{-1}$, respectively (with the gadofullerene presenting the highest r_1 and r_2 values). This survey of relaxivities with different metals inside the polyhydroxylated C_{82} fullerene cage demonstrated several important

points. For one, the relaxivities are all higher than the corresponding relaxivities of each of the given metal's DTPA chelate complex, illustrating that the derivatized fullerene cage itself imparts a special effect that boosts relaxivity. While La^{3+} has no $4f$ electrons, $\text{La}@C_{82}(\text{OH})_x$ is paramagnetic by virtue of the unpaired fullerene cage electron and does exhibit modest nonzero relaxivity. All the other metals have varying magnetic moments and less favorable electron-spin relaxation times than Gd^{3+} does for water proton relaxation, but their polyhydroxylated metallofullerene species all exhibit nonzero relaxivities as well. As these materials lack direct metal to water coordination, direct contact interactions can be disregarded in analysis of their relaxivities. In accord with these observations and other data, it was proposed that the high relaxivities of polyhydroxylated metallofullerene compounds are due to several contributing factors, including the metal-centered spin from unpaired $4f$ electrons (when present with a given metal), the unpaired spin on the fullerene cage (from electron transfer from the metal to the cage), and attendant dipole–dipole relaxation of water protons. Also serving an important role is the relatively slow molecular rotational motion (τ_r). Higher τ_r values are known to raise relaxivities of chelate complexes, and polyhydroxylated metallofullerenes may have relatively slower rotational motion due to their increased hydrodynamic radius (via hydrogen bonding to water) and/or intermolecular aggregation. Finally, the many hydroxyl groups attached to the fullerene surface present a large surface area for hydrogen bonding of the metallofullerene to many solvent waters. *In vitro* phantom imaging results obtained with the different polyhydroxylated $\text{M}@C_{82}$ metallofullerenes were consistent with the above observations (Kato et al., 2003). Table 8.1 summarizes selected relaxivity data for examples of clinically used chelate agents and $\text{M}@C_{82}$ derivatives.

Shinohara and coworkers also tested various lanthanide $\text{M}@C_{82}(\text{OH})_{40}$ compounds ($\text{M} = \text{Dy}, \text{Er}, \text{Gd}, \text{Eu}, (\text{Lu})_2$) as x-ray contrast agents, due to their heavy metal x-ray absorbing contents (Miyamoto et al., 2006). Computed tomography (CT) number analysis of the metallofullerene derivatives in water did not rate the metallofullerenes as high as currently used iodinated contrast agents, and it was suggested that metallofullerene performance may be improved by increasing the number of metals per agent and/or raising their water solubilities with more derivatization.

A differently modified $\text{Gd}@C_{82}$ derivative bearing a mixture of hydrophilic functional groups was recently reported by Wang and coworkers, $[\text{Gd}@C_{82}\text{O}_6(\text{OH})_{16}(\text{NHCH}_2\text{CH}_2\text{COOH})_8]_x$ (Shu et al., 2006a). At pH 7, the r_1 of this water-soluble $\text{Gd}@C_{82}$ compound was reported to be $9.1 \text{ mM}^{-1}\text{s}^{-1}$ at 1.5 T, and the hydrodynamic radius was measured as 73 nm by dynamic light scattering (DLS). A second more detailed study of the pH-dependent aggregation properties of this derivative found that nanocluster size and r_1 varied with pH (Shu et al., 2006b). Measured at the high field of 14.1 T, r_1 decreased with increasing pH (at pH = 2, 7, and 9, $r_1 = 7.68, 3.83,$ and $2.52 \text{ mM}^{-1}\text{s}^{-1}$, respectively). At pH 2, 30 nm clusters form, which in turn associate to form clusters of clusters, and it was proposed that at lower pH values, intermolecular aggregation is governed by hydrogen bonding effects. Also in this second study, at pH 7 the clusters are 30 nm, but form some dimers and/or trimers

Table 8.1 r_1 relaxivities of three clinically used Gd^{3+} chelate MRI contrast agents and selected water-soluble $M@C_{82}$ derivatives

Contrast Agent	r_1 ($mM^{-1}s^{-1}$)	Measurement conditions	Reference
Gd-DTPA (gadopentate dimeglumine)	3.4	0.47 T, 37 °C	Idée et al. (2006)
Gd-DTPA-BMA (gadodiamide)	3.5	0.47 T, 37 °C	Idée et al. (2006)
Gd-HP-DO3A (gadoteridol)	3.1	0.47 T, 37 °C	Idée et al. (2006)
$Gd@C_{82}(OH)_x$	47	9.4 T	Zhang et al. (1997)
$Gd@C_{82}(OH)_x$	47	9.4 T, 25 °C	Shukla et al. (1997)
$Gd@C_{82}(OH)_x$	20	0.47 T, 40 °C	Wilson (1999)
$Gd@C_{82}(OH)_{40}$	67	0.47 T, 25 °C	Mikawa et al. (2001)
$Gd@C_{82}(OH)_{40}$	81	1.0 T, 25 °C	Mikawa et al. (2001)
$Gd@C_{82}(OH)_{40}$	31	4.7 T, 25 °C	Mikawa et al., 2001
$Gd@C_{82}(OH)_{40}$	62	0.47 T, 37 °C	Okumura et al. (2002)
$Gd@C_{82}(OH)_x$	73	0.47 T, 19 °C	Kato et al. (2003)
$La@C_{82}(OH)_x$	0.8	0.47 T, 19 °C	Kato et al. (2003)
$Ce@C_{82}(OH)_x$	1.2	0.47 T, 19 °C	Kato et al. (2003)
$Dy@C_{82}(OH)_x$	1.1	0.47 T, 19 °C	Kato et al. (2003)
$Er@C_{82}(OH)_x$	1.3	0.47 T, 19 °C	Kato et al. (2003)
$[Gd@C_{82}O_6(OH)_{16}(NHCH_2CH_2COOH)_8]_x$	9.1	1.5 T, pH = 7	Shu et al. (2006a)
$[Gd@C_{82}O_6(OH)_{16}(NHCH_2CH_2COOH)_8]_x$	7.68	14.1 T, pH = 2	Shu et al. (2006b)
$[Gd@C_{82}O_6(OH)_{16}(NHCH_2CH_2COOH)_8]_x$	3.83	14.1 T, pH = 7	Shu et al. (2006b)
$[Gd@C_{82}O_6(OH)_{16}(NHCH_2CH_2COOH)_8]_x$	2.52	14.1 T, pH = 9	Shu et al. (2006b)
$Gd@C_{82}(OH)_{16}$	19.3	4.7 T, 25 °C	Zhang et al. (2007)

of the 30 nm subclusters. At alkaline pH (pH = 9), taking into account the derivative group structures, cluster formation dominated by dipole–dipole interactions and a crystal-growth mechanism was proposed to explain the formation of large particles. Increased content of larger clusters for samples stored in aqueous solution for 1 month as compared to fresh samples was seen by DLS. Scanning electron microscopy (SEM) and atomic force microscopy (AFM) were also used to characterize sizes of clusters deposited on wafers. The differences in relaxivity and nanoclustering (aggregation) of this $Gd@C_{82}$ derivative to other gadofullerenes (above, and in the following section) highlight the need for detailed

characterization of their relaxivity properties, and the distinct behavior of gadofullerenes as compared to the clinically used chelate agents.

The first *in vivo* MRI study of a gadofullerene was conducted by Shinohara and coworkers with $\text{Gd}@C_{82}(\text{OH})_{40}$ (Mikawa et al., 2001). The agent was intravenously administered to mice at 1/20 of the typical dosage of a clinical Gd chelate agent. T_1 -weighted MRI showed localization of this gadofullerene after 30 min in the organs of the reticuloendothelial system (RES), including the lung, liver, and spleen, but also some image enhancement in the kidneys. The biodistribution of $\text{Gd}@C_{82}(\text{OH})_{40}$ was also determined by obtaining the agent's concentration in dissected organs, and it matched the RES uptake seen by imaging. Interestingly, these biodistribution results for $\text{Gd}@C_{82}(\text{OH})_{40}$ were similar to those seen in a radiotracing study by Cagle et al. (1999) with the holmium metallofullerene analogue $\text{Ho}@C_{82}(\text{OH})_x$. The latter study with $\text{Ho}@C_{82}(\text{OH})_x$ showed RES uptake similar to that of $\text{Gd}@C_{82}(\text{OH})_{40}$, as well as some bone localization. This type of biodistribution may be a general property of polyhydroxylated fullerene materials (Qingnuan et al., 2002; Xu et al., 2007), but may be modifiable via further, secondary derivatization.

Qu et al. (2006) prepared $\text{Gd}@C_{82}(\text{OH})_{22}$ in order to compare its properties to the previously studied more highly polyhydroxylated $\text{Gd}@C_{82}(\text{OH})_x$ species. The relaxivity of $\text{Gd}@C_{82}(\text{OH})_{22}$ was qualitatively lower than that of the $\text{Gd}@C_{82}(\text{OH})_x$ species, but still higher than the chelate Gd-DTPA, as determined by an *in vivo* MRI test in which mice were administered the $\text{Gd}@C_{82}(\text{OH})_{22}$ agent intravenously. An *in vivo* test was next conducted with the slightly less hydroxylated derivative $\text{Gd}@C_{82}(\text{OH})_{16}$ (Zhang et al., 2007). A claim was made in this work that, based on a separate study of empty polyhydroxylated $C_{60}(\text{OH})_x$ (Xing et al., 2004), $\text{Gd}@C_{82}(\text{OH})_x$ with x higher than about 36 may be vulnerable to Gd^{3+} ion loss. However, no data to substantiate this claim with gadofullerenes polyhydroxylated at high (or low) levels was presented. The r_1 and r_2 relaxivities of $\text{Gd}@C_{82}(\text{OH})_{16}$ were 19.3 and $44.9 \text{ mM}^{-1}\text{s}^{-1}$, respectively (4.7 T, 25 °C). *In vivo* MRI of mice injected with $\text{Gd}@C_{82}(\text{OH})_{16}$ showed localization of the agent in both the liver and the kidneys at 1/20 of the usual clinical dosage of a Gd chelate agent.

In addition to *in vivo* imaging with polyhydroxylated $\text{Gd}@C_{82}$ contrast agents, *in vitro* cellular imaging has been performed. Anderson and coworkers have shown that $\text{Gd}@C_{82}(\text{OH})_{40}$ is a promising high-relaxivity intracellular imaging agent for T_1 -weighted cellular MRI (Anderson et al., 2006). In an *in vitro* study, HeLa cells, mesenchymal stem cells (MSC), and macrophages were labeled with $\text{Gd}@C_{82}(\text{OH})_{40}$ and subsequently examined with MRI. Protamine sulfate was required as a transfection agent to effectively label the cells to a level suitable for MRI, in this case reaching up to 4×10^7 Gd atoms per cell. Very high intracellular T_1 -weighted MR signal intensity was found with MRI of gadofullerene-labeled live cells, which were relatively maintained even after the application of magnetic fields higher than the fields routinely used in the clinic (i.e., greater than 3 T). These results emphasize the utility of this gadofullerene compound as a T_1 -weighted MRI agent. Electron microscopy imaging of labeled cells revealed that the agents are localized in the cells' cytoplasmic endosomes. Importantly, cell viability remained very high after exposure to the polyhydroxylated gadofullerene agent, which

supports a lack of Gd^{3+} release once the agent is localized inside the cell. This study is an exciting demonstration of the potential that gadofullerenes have to contribute to emerging applications in cellular and molecular imaging, in particular, for the labeling and tracking of stem cells with *in vivo* stem cell therapy.

8.5 $\text{Gd}@C_{60}$ Compounds as MRI Contrast Agents

Recently, other gadofullerenes, besides $\text{Gd}@C_{82}$, have become available due to advances in the processing of the normally insoluble metallofullerene fractions. Bolskar and coworkers reported methods to use and fractionate all of the arc-produced Gd metallofullerenes. By accessing the $\text{Gd}@C_{60}$ class of metallofullerenes, the useable amount of Gd mono-metallofullerenes was raised by a factor of more than 10 overall as compared to extraction-based processes that access $\text{Gd}@C_{82}$ (Bolskar and Alford, 2003; Raebiger and Bolskar, 2008). This increased access is important for the development of metallofullerenes in biomedicine, for which larger amounts of the raw materials will eventually be needed for preclinical and clinical testing.

Covalent derivatization of these metallofullerenes' surfaces is used to overcome the native insolubility of the $\text{Gd}@C_{60}$ class of gadofullerenes in the usual fullerene solvents. Hydroxyl and carboxyl groups are the two main functional groups that have been attached to make $\text{Gd}@C_{60}$ materials aqueous-soluble for water proton relaxivity investigation. The $\text{Gd}@C_{60}$ materials still contain varied amounts of empty fullerenes, but lacking paramagnetism, these will not affect relaxivity measurements. Similar to the earlier described situation with $\text{Gd}@C_{82}(\text{OH})_x$ species, a distribution of r_1 values have been found for water-soluble $\text{Gd}@C_{60}$ -class derivatives, although they have been synthesized with the same synthetic processes each time. For example, r_1 values reported for $\text{Gd}@C_{60}(\text{OH})_x$ (average $x \approx 27$ [Sitharaman et al., 2004]) include $83.2 \text{ mM}^{-1}\text{s}^{-1}$ (Laus et al., 2005) and $97.7 \text{ mM}^{-1}\text{s}^{-1}$ (Laus et al., 2007); r_1 values reported for $\text{Gd}@C_{60}[\text{C}(\text{COOH})_2]_{10}$ include $24.0 \text{ mM}^{-1}\text{s}^{-1}$ (Laus et al., 2005) and $14.8 \text{ mM}^{-1}\text{s}^{-1}$ (1.4 T, 37 °C) (Laus et al., 2007). For comparison, the compound $\text{La}@C_{60}[\text{C}(\text{COOH})_2]_x$ ($x \approx 10$) was prepared, and its r_1 was measured to be $0.3 \text{ mM}^{-1}\text{s}^{-1}$ (0.47 T, 40 °C) (Bolskar et al., 2003). This small but nonzero r_1 value for cage-paramagnetic-only carboxylated metallofullerene is similar to that seen for $\text{La}@C_{82}(\text{OH})_x$ (Kato et al., 2003). This underscores the importance of endohedral Gd^{3+} to the relaxivity of metallofullerene contrast agents, as seen earlier for $\text{M}@C_{82}(\text{OH})_x$ species.

To help unravel reasons behind the r_1 variability seen for different batches of polyhydroxylated and polycarboxylated $\text{Gd}@C_{60}$ (and to give insight into the related r_1 variation of $\text{Gd}@C_{82}(\text{OH})_x$ species), Tóth et al. obtained NMRD profiles for $\text{Gd}@C_{60}(\text{OH})_x$ and $\text{Gd}@C_{60}[\text{C}(\text{COOH})_2]_{10}$ over a broad magnetic field range (Tóth et al., 2005). This relaxometry study revealed a distinct peak or hump in both agents' relaxivity profiles between approximately 0.7 and 1.4 T. This type of peak is characteristic of large, slow-rotating Gd^{3+} agents, and is often associated with

species such as dendrimer and nanoparticle MRI contrast agents (Tóth et al., 2001). Analysis of the data for $\text{Gd}@C_{60}[\text{C}(\text{COOH})_2]_{10}$ revealed that this slow-tumbling gadofullerene has a rotational correlation time τ_R^{298} of 2.6 ns and a proton exchange rate k_{ex}^{298} of $1.4 \times 10^7 \text{ s}^{-1}$ (consistent with the rate for malonic acid). The gadofullerenes' relaxation mechanism is exclusively outer sphere, as revealed by ^{17}O NMR measurements.

Next, Tóth et al. investigated the effects of changing pH on the relaxivities of $\text{Gd}@C_{60}(\text{OH})_x$ and $\text{Gd}@C_{60}[\text{C}(\text{COOH})_2]_{10}$ (Tóth et al., 2005). At 1.4 T and 26.1 °C, both derivatives displayed strong changes in r_1 over the pH range 2–12. Relaxivity was lower at high pH values, with large relaxivity increases as pH was lowered. When pH decreased from 12 to 3, the r_1 of $\text{Gd}@C_{60}(\text{OH})_x$ increased 2.6 times, and the r_1 of $\text{Gd}@C_{60}[\text{C}(\text{COOH})_2]_{10}$ increased 3.8 times (note that the precipitation of the derivatives begins to occur below approximately pH 3). Changes in pH may influence relaxivity by affecting the rotational motion of the gadofullerenes and/or the proton exchange rate. The latter is not likely, as evidenced by the decrease in relaxivity seen for $\text{Gd}@C_{60}[\text{C}(\text{COOH})_2]_{10}$ when sample temperature was increased.

Sitharaman et al. next conducted a detailed study of the intermolecular aggregation of the $\text{Gd}@C_{60}$ gadofullerene agents as a function of pH by laser light scattering (dynamic light scattering [DLS] and static light scattering [SLS]), transmission electron microscopy (TEM), and cryo-TEM (Sitharaman et al., 2004). The hydrodynamic diameters (D_H) of both $\text{Gd}@C_{60}(\text{OH})_x$ and $\text{Gd}@C_{60}[\text{C}(\text{COOH})_2]_{10}$ were both significantly larger than expected for individual molecules, and varied strongly between pH 4 and 9. At pH 9, average D_H values were 50 and 70 nm for $\text{Gd}@C_{60}(\text{OH})_x$ and $\text{Gd}@C_{60}[\text{C}(\text{COOH})_2]_{10}$, respectively. Near pH 7, both derivatives were approximately 450–500 nm in average D_H . At pH 4.5, average D_H values were 1,200 and 700 nm for $\text{Gd}@C_{60}(\text{OH})_x$ and $\text{Gd}@C_{60}[\text{C}(\text{COOH})_2]_{10}$, respectively. D_H values for both derivatives were only modestly temperature- and concentration-dependent at pH 9. Debye plot analyses of SLS data indicated that the intermolecular forces that aggregate $\text{Gd}@C_{60}[\text{C}(\text{COOH})_2]_{10}$ into nanoclusters are weaker than those of $\text{Gd}@C_{60}(\text{OH})_x$. This conclusion was also supported by variable-temperature TEM measurements showing that $\text{Gd}@C_{60}(\text{OH})_x$ aggregates maintained crystallinity when warmed to room temperature, while $\text{Gd}@C_{60}[\text{C}(\text{COOH})_2]_{10}$ aggregates did not.

The above-described studies (Sitharaman et al., 2004; Tóth et al., 2005) together reveal the importance of gadofullerene intermolecular aggregation or nanoclustering to their relaxivity properties. Light scattering and TEM analyses have shown the gadofullerenes to have pH-dependent hydrodynamic diameters, which correlates well with their pH-dependent r_1 relaxivities. At low pH, the gadofullerenes are aggregated into larger clusters that tumble relatively slowly (increasing their rotational correlation times), which consequently increases relative r_1 . At high pH, the clusters are smaller, and with relatively faster tumbling, present lower relative r_1 relaxivities. Gadofullerenes thus might function as pH-sensitive MRI contrast agents for selective T_1 -weighted enhancement of diseased tissues having low pH, such as tumors, since gadofullerene relaxivities are elevated at lower pH.

Using relaxivity as an indicator of aggregation state, and DLS characterization, Laus et al. (2005) next determined that aqueous gadofullerene aggregates can be disrupted (broken apart) by high concentrations of dissolved salts. Salt addition breaks up the aggregates into smaller and more rapidly tumbling units, which have much lower relaxivities and smaller hydrodynamic diameters. Phosphate salts were found to be more effective at disaggregating gadofullerenes in solution than sodium halide salts. For example, without added dissolved salts, $\text{Gd}@C_{60}(\text{OH})_x$ had $r_1 = 83.2 \text{ mM}^{-1}\text{s}^{-1}$ and $D_H = 810 \text{ nm}$ (1.4 T, 37 °C). After adding a respective salt solution to $\text{Gd}@C_{60}(\text{OH})_x$, $r_1 = 14.1 \text{ mM}^{-1}\text{s}^{-1}$ and $D_H = 91 \text{ nm}$ in 10 mM phosphate, while $r_1 = 31.6 \text{ mM}^{-1}\text{s}^{-1}$ and $D_H = 121 \text{ nm}$ in 150 mM NaCl solution. While disaggregation certainly decreases gadofullerene rotational correlation times, it may also decrease relaxivity via influences on proton exchange and electronic relaxation. The salt-induced disaggregation process is relatively slow, with *in vitro* aggregation half-lives in 100 mM phosphate-buffered saline (PBS) and in mouse serum (both at 37 °C) being 30 and 45 min for $\text{Gd}@C_{60}(\text{OH})_x$, and 25 min in both media for $\text{Gd}@C_{60}[\text{C}(\text{COOH})_2]_{10}$. These results indicate that these two gadofullerenes will be present in high-relaxivity (aggregated) form during the time for a typical MRI examination, followed by disaggregation and clearance. The aggregation half-lives may be even longer *in vivo* because the phosphate concentration in human blood plasma is about 250 times lower than the concentration used in the disaggregation half-life study. The effects that added salt concentration have on gadofullerene relaxivity goes a long way in explaining the discrepancies between different reports of gadofullerene relaxivities (for both $\text{Gd}@C_{82}$ and $\text{Gd}@C_{60}$ compounds) because their derivatization methods all involve or produce aqueous salts, varying amounts of which likely remain in samples after product isolation unless special effort is taken to eliminate them.

Relaxivity characterization was then conducted by Laus et al. (2007) on the two $\text{Gd}@C_{60}$ gadofullerenes under aggregate-free conditions. Sodium phosphate was used to disrupt the hydrogen-bonded intermolecular gadofullerene nanoclusters, so that the relaxivity properties of the completely disaggregated molecules could be characterized. It was determined that 75–100 equivalents of phosphate were adequate to disaggregate the agents by plotting relaxivity versus phosphate concentration and noting where the relaxivities plateau to minimum values. ^{17}O NMR measurements of the longitudinal and transverse relaxation rates were conducted on both aggregated and disaggregated $\text{Gd}@C_{60}(\text{OH})_x$ and $\text{Gd}@C_{60}[\text{C}(\text{COOH})_2]_{10}$. Large differences were seen between $1/T_1$ and $1/T_2$ values for the aggregated forms of the gadofullerenes. However, after disaggregation, these differences diminished strongly. This behavior is characteristic of water molecules confined to interstitial spaces between gadofullerenes in an intermolecular aggregate. Furthermore, the difference between $1/T_1$ and $1/T_2$ values was greater for $\text{Gd}@C_{60}(\text{OH})_x$ than for $\text{Gd}@C_{60}[\text{C}(\text{COOH})_2]_{10}$, indicating that the intermolecular forces in $\text{Gd}@C_{60}(\text{OH})_x$ aggregates are greater than those holding together $\text{Gd}@C_{60}[\text{C}(\text{COOH})_2]_{10}$ aggregates, and was consistent with data from earlier light scattering results (Sitharaman et al., 2004). Exchange of confined and bulk water molecules was found to be much faster than the corresponding exchange of the first-sphere water molecule(s) of

Table 8.2 r_1 relaxivities of water-soluble Gd@C₆₀ derivatives at 1.4 T

Contrast agent	r_1 (mM ⁻¹ s ⁻¹)	Aqueous conditions	Reference
Gd@C ₆₀ (OH) _x	83.2	pH = 7.4	Laus et al. (2005)
Gd@C ₆₀ (OH) _x	97.7	pH = 7.4	Laus et al. (2007)
Gd@C ₆₀ (OH) _x	74.9	pH = 4.12	Tóth et al. (2005)
Gd@C ₆₀ (OH) _x	28.9	pH = 12.35	Tóth et al. (2005)
Gd@C ₆₀ (OH) _x	31.6	150 mM NaCl, pH = 7.4	Laus et al. (2005)
Gd@C ₆₀ (OH) _x	14.1	10 mM phosphate, pH = 7.4	Laus et al. (2005)
Gd@C ₆₀ (OH) _x	13.0	100 mM phosphate, pH = 7.4	Laus et al. (2007)
Gd@C ₆₀ [C(COOH) ₂] ₁₀	24.0	pH = 7.4	Laus et al. (2005)
Gd@C ₆₀ [C(COOH) ₂] ₁₀	14.8	pH = 7.4	Laus et al. (2007)
Gd@C ₆₀ [C(COOH) ₂] ₁₀	21.4	pH = 2.91	Tóth et al. (2005)
Gd@C ₆₀ [C(COOH) ₂] ₁₀	5.7	pH = 12.51	Tóth et al. (2005)
Gd@C ₆₀ [C(COOH) ₂] ₁₀	16.0	150 mM NaCl, pH = 7.4	Laus et al. (2005)
Gd@C ₆₀ [C(COOH) ₂] ₁₀	6.8	10 mM phosphate, pH = 7.4	Laus et al. (2005)
Gd@C ₆₀ [C(COOH) ₂] ₁₀	4.6	100 mM phosphate, pH = 7.4	Laus et al. (2007)

Gd³⁺ chelate compounds with bulk solvent waters. Table 8.2 lists r_1 relaxivity data for the two Gd@C₆₀ derivatives under a variety of aqueous solution conditions.

Laus et al. (2007) also obtained NMRD profiles of the gadofullerenes while disaggregated at several different temperatures. When disaggregated, the overall relaxivities of both gadofullerenes are much lower than while aggregated, but both agents retained a broad peak or hump in relaxivity at higher magnetic fields (approximately 0.7–1.4 T). The high-field r_1 maximum for Gd@C₆₀(OH)_x was greater than that of Gd@C₆₀[C(COOH)₂]₁₀, consistent with the polyhydroxylated derivative's greater number of protonatable sites. However, at lower fields, the two derivatives had similar relaxivities, consistent with Gd@C₆₀(OH)_x possessing a faster electronic relaxation than Gd@C₆₀[C(COOH)₂]₁₀ that at the lower fields otherwise mitigates the advantage of having more protonatable sites. Contributions from both an "inner-sphere-like" mechanism and an outer sphere mechanism were deduced for both derivatives. The inner-sphere-like mechanism does not arise from direct water-to-Gd³⁺ coordination (which is absent in gadofullerenes), but instead reflects the chemical proton exchange between protonated derivative groups on the gadofullerene (COOH or OH groups) and bulk water molecules. Both gadofullerene derivatives had nearly identical rotational correlation times ($\tau_R = 1.2$ ns) when disaggregated, and interestingly are only slightly shorter than the τ_R of 2.6 ns determined previously for aggregates of Gd@C₆₀[C(COOH)₂]₁₀ (Tóth et al., 2005). This indicates that while slow rotational correlation is a factor in the high relaxivities of the gadofullerenes, the interstitial confinement of water molecules between gadofullerene molecular units in an aggregate plays a more important role in elevating their relaxivities.

Based on the above studies of water-soluble Gd@C₈₂ and Gd@C₆₀ derivatives, it appears that once Gd³⁺ is inside the fullerene cage, the relaxivity properties are largely directed by the nature, number, and disposition of derivative groups. The particulars of intermolecular aggregation (nanoclustering) that result from the chemical composition of derivative groups seems to exert a major influence on

gadofullerene relaxivity properties. This is evidenced by the differences seen when the properties of charged carboxylated gadofullerenes are compared with uncharged hydroxylated gadofullerenes, as well as the mixed amino-hydroxy derivatized Gd@C_{82} compound. Varying the geometrical disposition and number of derivative groups may influence gadofullerene relaxivity. The effects of fullerene cage size and cage symmetry on gadofullerene relaxivity, while not rigorously investigated, do not seem to play a significant role. The above studies of gadofullerene relaxivity suggest that careful design of derivative makeup can be used to manipulate their relaxivity properties.

The high stability of Gd^{3+} encapsulation offered by $\text{Gd@C}_{60}[\text{C}(\text{COOH})_2]_{10}$ and $\text{Gd@C}_{60}(\text{OH})_x$ was verified using a relaxivity measurement-based method (Laus et al., 2005, 2007; Tóth et al., 2005). At 1.4 T, gadofullerene r_1 were measured in aqueous solution before and after the addition of the ligand TTHA^{6-} (in a 1:1 TTHA^{6-} to gadofullerene molar ratio; H_6TTHA = triethylenetetramine- N,N,N',N',N',N' -hexacetic acid). The TTHA^{6-} ligand forms a highly stable complex with Gd^{3+} that lacks inner-sphere water molecules; any such complex (having only an outer sphere relaxation mechanism) would have a much lower relaxivity than free Gd^{3+} . Any relaxivity decrease after adding TTHA^{6-} would signal that free Gd^{3+} ion was present in solution before ligand addition. With the gadofullerene samples, the relaxivities with and without added TTHA^{6-} were identical, proving the absence of free Gd^{3+} ion. The lack of free Gd^{3+} is also consistent with the reversible nature of the relaxivity response to changes in pH for the gadofullerenes. The total encapsulation of Gd^{3+} is a very important feature that gadofullerenes offer to avoid Gd^{3+} -based toxicity in contrast agents for *in vivo* MRI applications.

An *in vivo* MRI test was conducted by Bolskar et al. (2003) with the polycarboxylated Gd@C_{60} compound $\text{Gd@C}_{60}[\text{C}(\text{COOH})_2]_{10}$. This gadofullerene was intravenously administered to a rat at a dosage of 35 mg/kg, after which the agent's *in vivo* progress was monitored in a series of T_1 -weighted MRI scans. This agent's biodistribution was more similar to those of clinically used Gd chelate compounds and less similar to the previously *in vivo* tested $\text{Gd@C}_{82}(\text{OH})_x$ agents. Unlike the case with polyhydroxylated metallofullerenes, polycarboxylated Gd@C_{60} did not specifically target the organs of the RES. MR images showed the $\text{Gd@C}_{60}[\text{C}(\text{COOH})_2]_{10}$ agent reached the kidneys, with excretion via the bladder within 1 h of the agent's injection. Uptake by the liver was much less than had been the case with $\text{Gd@C}_{82}(\text{OH})_x$ agents. The rat tolerated the agent well and completed the imaging procedure without complications. This preliminary *in vivo* test demonstrated that $\text{Gd@C}_{60}[\text{C}(\text{COOH})_2]_{10}$ is an effective contrast agent for T_1 -weighted MRI and that its basic biodistribution, with ready renal excretion, is quite different from the RES-targeting polyhydroxylated fullerenes. The lack of major RES uptake by the polycarboxylated derivative is consistent with the earlier findings that the aggregates (nanoclusters) of polycarboxylated Gd@C_{60} are weaker than the aggregates of the polyhydroxylated derivative.

In vitro cellular MRI was also recently conducted with $\text{Gd@C}_{60}[\text{C}(\text{COOH})_2]_{10}$ (Sitharaman et al., 2007). In this study, marrow stromal cells (MSC) and NIH 3T3 stem cells were efficiently labeled with the polycarboxylated gadofullerene and

imaged with T_1 -weighted MRI. Without the need for an externally added transfection agent, the cells were efficiently labeled nonspecifically, with an average of 10^{11} Gd^{3+} ions per cell. The labeling process did not adversely affect cell viability, as shown by comparison with unlabeled control cells. The gadofullerenes were located either intracellularly, or deep in the cellular membranes, as shown by an acid strip test. The $Gd@C_{60}[C(COOH)_2]_{10}$ -labeled cells were imaged at 1.5 T and their T_1 -weighted signal intensities were almost 250% greater than for corresponding unlabeled cells. This level of gadofullerene-induced MR signal enhancement and cellular internalization is potentially enough for cellular imaging of small numbers of cells, noninvasive cell tracking *in vivo* using MRI, and with further design, development of a specifically targeted intracellular $Gd@C_{60}[C(COOH)_2]_{10}$ -based contrast agent.

Lanthanide metallofullerene-based compounds have also been proposed as candidates for controlled delivery of radioisotopes in nuclear medicine (Wilson, 1999; Cagle et al., 1999; Thrash et al., 1999; Wilson et al., 1999). Similar to the advantages conferred by holding Gd^{3+} inside gadofullerenes for MRI contrast agents, metallofullerenes that encapsulate radioisotopes may offer certain advantages over chelate compounds. For example, for many desirable radioisotopes, the known chelate structures do not stably contain the radionuclide for as long as is needed to accomplish *in vivo* targeting. Toward demonstrating this, an evaluation of $^{212}Pb@C_{60}$ as a radioisotope carrier was recently conducted (Diener et al., 2007). This study suggested that $M@C_{60}$ species containing α -particle-emitting radioisotopes could be effective isotope carriers for radioimmunotherapy, as the higher energies of α -decay are particularly lethal towards cells. With antibody targeting of radioisotopes having appropriate half-lives, radiofullerenes may lead to more effective treatment of diseases including cancer.

8.6 $Gd_3N@C_{80}$ Compounds as MRI Contrast Agents

A new class of endohedrals different from the mono-metal $M@C_{2n}$ type of metallofullerene was recently discovered, the trimetallic nitride metallofullerenes (sometime abbreviated “TNTs”) (Stevenson et al., 1999). This new variant has three metal atoms bonded to a central nitrogen atom inside a fullerene cage, denoted as “ $M_3N@C_{2n}$ ”. Their synthesis is similar to arc production of $M@C_{2n}$ metallofullerenes, except that a nitrogen source is included during arcing. As with the $M@C_{2n}$ species, the arc method produces a mixture of carbonaceous soot, empty C_{2n} fullerenes of different sizes and isomers, assorted cage sizes, and isomers of $M_3N@C_{2n}$, as well as $M@C_{2n}$ species. Several cage isomers of C_{80} and C_{78} have been the most common fullerene cages associated with $M_3N@C_{2n}$ species. The $M_3N@C_{2n}$ can contain most of the lanthanides, including gadolinium, and certain mixed-metal species with more than one type of lanthanide can also be prepared (Krause and Dunsch, 2005; Dunsch and Yang, 2007). The $M_3N@C_{2n}$ are similar to the $M@C_{82}$ metallofullerenes in that they are soluble

in organic solvents in which they are extractable from arc soot, and are usually purified using chromatography. Alternate means to separate and isolate $M_3N@C_{2n}$ metallofullerenes are being investigated (Elliott et al., 2005; Ge et al., 2005; Stevenson et al., 2006).

Different from the lanthanide $M@C_{2n}$ metallofullerenes, the $M_3N@C_{2n}$ metallofullerenes have no unpaired fullerene cage-centered electrons. The endohedral M_3N unit is formally hexa-cationic (i.e., a central N^{3-} with three M^{3+} bonded to it), and thus the even number of six electrons is donated to the fullerene cage. Paramagnetism must therefore come exclusively from the Gd^{3+} ions. As $Gd@C_{82}$ and $Gd@C_{60}$ were for $Gd@C_{2n}$ metallofullerenes, $Gd_3N@C_{80}$ was the first trimetallic nitride gadofullerene investigated as an MRI contrast agent. Dorn and coworkers prepared the water-soluble derivative $Gd_3N@C_{80}[DiPEG5000(OH)_x]$ having ester-linked poly(ethylene glycol) chains (DiPEG5000 is $[COO(CH_2CH_2O)_{114}CH_3]_2$) and hydroxyl functionalities independently attached to the gadofullerene surface (Fatouros et al., 2006). At magnetic fields of 0.35, 2.4, and 9.4 T the r_1 relaxivities were 102, 143, and $32 \text{ mM}^{-1}\text{s}^{-1}$ respectively, and the r_2 relaxivities were 144, 222, and $137 \text{ mM}^{-1}\text{s}^{-1}$ at the same respective fields. The relaxivities were concentration-dependent, with higher relaxivities at lower gadofullerene concentrations. A slight increase in r_1 with increasing temperature was observed up to 60°C . It was stated that the non-polyhydroxylated derivative $Gd_3N@C_{80}[DiPEG5000]$ had much lower relaxivities than the version with polyhydroxyl groups, but relaxivity data were not given. The r_1 and r_2 relaxivities of the similarly derivatized $Lu_3N@C_{80}$ analogue were also measured, and in comparison were nearly zero. This result was expected because this Lu_3N analogue has no unpaired f electrons and no unpaired fullerene cage electrons, thus rendering it diamagnetic. Interestingly, the above results show that even though there are several prominent differences between the $Gd@C_{2n}$ and $Gd_3N@C_{2n}$ metallofullerenes, including the number of entrapped metal ions and the presence or lack of fullerene-cage-centered paramagnetism, their basic relaxivity features including the relaxivity magnitudes are very similar. Differences such as that seen for the concentration dependence of r_1 are likely due to differences in exterior derivatization chemistry and how the chemical functionalities influence solution structure and intermolecular clustering. The relaxivity characteristics of gadofullerenes are complex, with many factors contributing to a given derivative's overall behavior.

T_1 -weighted *in vitro* MR images of $Gd_3N@C_{80}[DiPEG5000(OH)_x]$ phantom solutions reflected the high r_1 relaxivities (Fatouros et al., 2006). Comparative imaging with the clinical Gd chelate agent gadodiamide revealed the gadofullerene to be approximately 30 times more effective than the chelate on a concentration basis. *In vivo* MRI tests were also conducted with $Gd_3N@C_{80}[DiPEG5000(OH)_x]$ after infusing the derivative directly into a rat brain bearing a glioma tumor model. T_1 -weighted MRI showed the agent to offer high contrast in both normal brain tissue and in the tumor at relatively low agent concentration. Compared to MRI with intravenously injected gadodiamide (Gd-DTPA-BMA) in the animal, the gadofullerene provided improved tumor margin differentiation. The $Gd_3N@C_{80}$ agent also diffused in tissue slower, and cleared slower, than did gadodiamide.

In addition to the above-described examples, there are several other groups investigating $\text{Gd}_3\text{N}@C_{2n}$ -based materials for MRI contrast agents (Wilson et al., 2007), as well as the fundamental chemistry of $\text{Gd}_3\text{N}@C_{2n}$ and other $\text{M}_3\text{N}@C_{2n}$ species, including separation technology and surface derivatizations (Stevenson et al., 2005). Besides function as paramagnetic MRI contrast agents, similar other biomedical applications have also been proposed for $\text{M}_3\text{N}@C_{2n}$ species as with the $\text{M}@C_{2n}$ metallofullerenes. For example, a preliminary demonstration of x-ray contrast agents using “heavy atom” x-ray absorbing lanthanides in metallofullerenes such as $\text{Lu}_3\text{N}@C_{80}$ has been reported, and $\text{M}_3\text{N}@C_{2n}$ metallofullerenes have also been proposed as potential carriers of radionuclides (Iezzi et al., 2002). These are all topics that will likely to promote new biomedical applications of the TNT-style metallofullerenes. These $\text{M}_3\text{N}@C_{2n}$ systems, both with one type of metal and the mixed-metal variants, are poised to join the $\text{M}@C_{2n}$ species as innovative carriers of metals for biomedical imaging and other uses.

8.7 Shortened Carbon Nanotube MRI Contrast Agents

A new type of nanomaterial that is conceptually related to endohedral fullerenes has recently emerged, internally gadolinium-loaded “ultrashort” single-walled carbon nanotubes. Also termed US tubes, they are segments of carbon nanotubes (CNTs) shortened from their microns-long spans into much shorter lengths of approximately 50 nm, using a fluorination-based cutting procedure (Gu et al., 2002). The interior spaces of US tubes can be filled with elements and compounds, just as full-length single- and multiwalled carbon nanotubes can. Once inside, the contents are quite robust; washing studies on full-length nanotubes filled with salts showed very high resistance to loss of contents (Chen et al., 1997; Sloan et al., 1997; Brown et al., 2003). The encapsulation stability that CNTs offer is further demonstrated in studies where filled CNTs were subjected to very high temperatures without leakage.

For US tubes, a detailed study of NaI filling convincingly demonstrated their high encapsulation stability (Mackeyev et al., 2005). In this study, a very small amount (~0.1 mg) of aqueous NaI (entirely labeled with radioactive ^{125}I) was added to a suspension of empty US tubes in water and vigorously stirred. The mixture was periodically centrifuged and both the US tubes and the aqueous decantate were tested for radioactivity. Remarkably, within 10 min, all of the ^{125}I activity was associated with the solid US tubes (with none remaining in the water), showing how quickly US tubes take up ions from water, a solvent in which the US tubes themselves are not soluble. More detailed wash-off experiments showed that ^{125}I very slowly comes out of the US tubes with a half-life of over 113 days. Conversion of encapsulated iodide to iodine by in situ oxidation with hydrogen peroxide increased the encapsulation half-life to over 1.5 years. Separately, thermogravimetric analysis on iodide-filled US tubes performed under helium showed no weight loss up to 1,000 °C. As NaI melts at 660 °C, the

US tubes are thus protecting their contents from the normal effects of heating and melting; this would not be the case when NaI is located outside the tubes, either adsorbed or bound in between bundled tubes (Kissell et al., 2006). These results demonstrated the robustness of the encapsulation by US tubes, and that the interior contents are not in rapid exchange with the exterior. Importantly, this indicates that filled US tubes will not release their contents under normal, physiological conditions, imperative for safety reasons in biomedical applications of metal-filled US tubes.

With confidence in the encapsulating stability of the US tubes, Wilson and coworkers were the first to investigate US tubes filled with gadolinium salts as MRI contrast-enhancing agents. US tubes loaded with GdCl_3 were found to contain superparamagnetic nanoclusters of the Gd^{3+} salt, while displaying r_1 and r_2 relaxivities orders of magnitude higher than clinically used Gd^{3+} chelates (Sitharaman et al., 2005; Sitharaman and Wilson, 2006). For example, the r_1 of surfactant-suspended gadolinium-containing US tubes at 60 MHz and 40 °C is approximately $170 \text{ mM}^{-1}\text{s}^{-1}$. Note that this relaxivity was calculated on a per- Gd^{3+} ion basis, *not* on a per-nanoparticle (or per-tube) basis. The r_2 relaxivities are even greater than their r_1 values, being as high as $600 \text{ mM}^{-1}\text{s}^{-1}$ over the range of 40–200 MHz. Relaxivities of Gd-filled US tube samples can have maxima at low fields, suggesting their application as millitesla imaging agents. Also discovered with Gd-filled US tubes was an intriguing variation of r_1 with changing pH. Below pH 7, r_1 is above $140 \text{ mM}^{-1}\text{s}^{-1}$, and near pH 7 is a steep inflection-like decrease of r_1 down to about $40 \text{ mM}^{-1}\text{s}^{-1}$ near pH 10 (Hartman et al., 2008). Unlike with polyhydroxy and polycarboxylate Gd metallofullerene derivatives, there is no significant dependence of nanoparticle size with changing pH. This indicates that inter-tube clustering (aggregation) does not operate as it does with aqueous fullerene and metallofullerene derivatives and thus has no aggregation-triggered influence on relaxivity. This sharp relaxivity increase below pH 7 may very well be useful for selective high-relaxivity imaging of the lower-pH extracellular environments, such as those of cancerous cells and lysosomes. High-relaxivity Gd-filled US tube materials are likely to have applications as both T_1 - and T_2 -weighted MRI agents.

Towards developing US tubes' applications, exterior covalent derivatization of US tubes is commencing (Ashcroft et al., 2007). Besides US tube-based MRI contrast agents, other biomedical applications are being investigated with US tubes as the nanocarrier. A prominent example is the use of US tubes as radioisotope carriers, such as recently demonstrated by Wilson with US tubes containing ^{211}At , an α -particle-emitting radioisotope of interest for radiotherapeutic cancer treatment (Hartman et al., 2007). The wide potential of filled carbon nanotubes as carriers of biomedically useful metal ions and compounds is clear. In this sense US tubes offer several potentially important advantages, including not only their robust containment of desired compounds, but also potentially easier preparation than endohedral metallofullerenes, as well as much shorter lengths than full-length carbon nanotubes, for improved RES avoidance and biological compatibility.

8.8 Conclusions

MRI has become increasingly important over the past several decades as an imaging modality used in diagnosis and treatment of disease. Paramagnetic contrast agents have contributed significantly to the utility of MRI, and there is continued need for new and improved contrast agents. This is underscored by the recent emergence of NSF, a serious condition in renally compromised patients associated with exposure to approved Gd chelate contrast agents. For applications of lanthanides in biomedicine, including Gd^{3+} , endohedral metallofullerenes offer a new type of metal sequestration different from and potentially superior to chelate compounds. Gadolinium-containing metallofullerenes, or gadofullerenes, are a new type of paramagnetic MRI contrast agent offering high T_1 -weighted relaxivities and safe encapsulation of Gd^{3+} ions in their carbon shells. Water-soluble derivatives of $Gd@C_{82}$, $Gd@C_{60}$, and $Gd_3N@C_{80}$ have been examined in both *in vitro* and *in vivo* MRI contexts.

The r_1 relaxivity values reported for gadofullerene derivatives vary. To illuminate the reasons for this variation, detailed examinations of the relaxivity properties of polyhydroxylated and polycarboxylated $Gd@C_{60}$ compounds were performed. These studies showed that several different factors contribute to and modify the relaxivities of gadofullerenes. Intermolecular aggregation or nanoclustering operates as a function of pH, and the resultant slow tumbling plays some role in relaxivity elevation. Another substantial factor behind the gadofullerenes' unusually large r_1 relaxivities is the interstitial confinement of water molecules between gadofullerene molecular units in an aggregate, and proton exchange between the many protonated derivative surface groups on the gadofullerene surface with bulk water molecules. It is apparent that the derivative group composition, disposition, and numbers are relaxivity-driving features of the gadofullerenes, which indicates that gadofullerene contrast agent relaxivities and imaging performance can be tuned by control of exterior chemical derivatization. This feature should be useful for maximizing gadofullerene relaxivities and for the development of their advanced imaging applications. Finally, new nanomaterials such as those based on gadolinium-loaded US carbon nanotubes have r_1 and r_2 relaxivities even higher than gadofullerenes on a per- Gd^{3+} ion basis. With these high relaxivities and aqueous phase behavior differing from gadofullerenes, the Gd-filled US tubes show great promise for enabling highly sought after goals in cellular and molecular MRI.

Acknowledgments Valuable collaboration with my colleagues on studies of gadofullerene MRI contrast agents, including Professor Lon Wilson of Rice University (Houston, Texas, USA) and his students, and Professor André Merbach and Professor Lothar Helm of the École Polytechnique Fédérale de Lausanne (Lausanne, Switzerland) and their students, is sincerely appreciated. Support of biomedical metallofullerene research and contrast agent development at TDA Research by the US National Institutes of Health (NIH), including grants R01EB000703 and R43EB005857 from the National Institute of Biomedical Imaging and BioEngineering (NIBIB), is gratefully acknowledged.

References

- Anderson SA, Lee KK, Frank JA (2006) Gadolinium-fullerenol as a paramagnetic contrast agent for cellular imaging. *Invest. Radiol.* 41: 332–338.
- Ashcroft JM, Hartman KB, Kissell KR, Mackeyev Y, Pheasant S, Young S, Van der Heide PAW, Mikos AG, Wilson LJ (2007) Single-molecule $I_2@US$ -tube nanocapsules: a new X-ray contrast-agent design. *Adv. Mater.* 19: 573–576.
- Bolskar RD Alford JM (2003) Chemical oxidation of endohedral metallofullerenes: identification and separation of distinct classes. *Chem. Commun.* 11: 1292–1293.
- Bolskar RD, Benedetto AF, Husebo LO, Price RE, Jackson EF, Wallace S, Wilson LJ, Alford JM (2003) First soluble $M@C_{60}$ derivatives provide enhanced access to metallofullerenes and permit *in vivo* evaluation of $Gd@C_{60}[C(COOH)_2]_{10}$ as a MRI contrast agent. *J. Am. Chem. Soc.* 125: 5471–5478.
- Brown G, Bailey SR, Novotny M, Carter R, Flahaut E, Coleman KS, Hutchison JL, Green MLH, Sloan J (2003) High yield incorporation and washing properties of halides incorporated into single walled carbon nanotubes. *Appl. Phys. A* 76: 457–462.
- Cagle DW, Kennel SJ, Mirzadeh S, Alford JM, Wilson LJ (1999) *In vivo* studies of fullerene-based materials using endohedral metallofullerene radiotracers. *Proc. Natl. Acad. Sci. USA* 96: 5182–5187.
- Caravan P, Ellison JJ, McMurry TJ, Lauffer RB (1999) Gadolinium(III) chelates as MRI contrast agents: structure, dynamics, and applications. *Chem. Rev.* 99: 2293–2352.
- Chai Y, Guo T, Jin C, Haufler RE, Chibante LPF, Fure J, Wang L, Alford JM, Smalley RE (1991) Fullerenes with metals inside. *J. Phys. Chem.* 95: 7564–7568.
- Chen YK, Chu A, Cook J, Green MLH, Harris PJF, Heesom R, Humphries M, Sloan J, Tsang SC, Turner JFC (1997) Synthesis of carbon nanotubes containing metal oxides and metals of the d-block and f-block transition metals and related studies. *J. Mater. Chem.* 7: 545–549.
- Collidge TA, Thomson PC, Mark PB, Traynor JP, Jardine AG, Morris ST, Simpson K, Roditi GH (2007) Gadolinium-enhanced MR imaging and nephrogenic systemic fibrosis: retrospective study of a renal replacement therapy cohort. *Radiology* 245: 168–175.
- Diener MD, Alford JM (1998) Isolation and properties of small-bandgap fullerenes. *Nature* 393: 668–671.
- Diener MD, Bolskar RD, Alford JM (2002) Redox properties and purification of endohedral metallofullerenes. In: Akasaka T, Nagase S (eds.) *Endofullerenes: a new family of carbon clusters*. Kluwer, Dordrecht, pp. 133–151.
- Diener MD, Alford JM, Kennel SJ, Mirzadeh S (2007) $^{212}Pb@C_{60}$ and its water-soluble derivatives: synthesis, stability, and suitability for radioimmunotherapy. *J. Am. Chem. Soc.* 129: 5131–5138.
- Dunsch L, Yang S (2007) Metal nitride cluster fullerenes: their current state and future prospects. *Small* 3: 1298–1320.
- Edelson E (1991) Buckyball: the magic molecule. *Pop. Sci.* 239(August): 52–57, 87.
- Elliott B, Yu L, Echegoyen L (2005) A simple isomeric separation of D_{5h} and $I_h Sc_3N@C_{80}$ by selective chemical oxidation. *J. Am. Chem. Soc.* 127: 10885–10888.
- Fatouros PP, Corwin FD, Chen ZJ, Broaddus WC, Tatum JL, Kettenmann B, Ge Z, Gibson HW, Russ JL, Leonard AP, Duchamp JC, Dorn HC (2006) *In vitro* and *in vivo* imaging studies of a new endohedral metallofullerene nanoparticle. *Radiology* 240: 756–764.
- Funasaka H, Sakurai K, Oda Y, Yamamoto K, Takahashi T (1995) Magnetic properties of $Gd@C_{82}$ metallofullerene. *Chem. Phys. Lett.* 232: 273–277.
- Ge Z, Duchamp JC, Cai T, Gibson HW, Dorn HC (2005) Purification of endohedral trimetallic nitride fullerenes in a single, facile step. *J. Am. Chem. Soc.* 127: 16292–16298.
- Grobner T (2006) Gadolinium – a specific trigger for the development of nephrogenic fibrosing dermopathy and nephrogenic systemic fibrosis? *Nephrol. Dial. Transplant.* 21: 1104–1108.

- Grobner T, Prischl FC (2007) Gadolinium and nephrogenic systemic fibrosis. *Kidney Int.* 72: 260–264.
- Gu Z, Peng H, Hauge RH, Smalley RE, Margrave JL (2002) Cutting single-wall carbon nanotubes through fluorination. *Nano Lett.* 2: 1009–1013.
- Hartman KB, Hamlin DK, Wilbur DS, Wilson LJ (2007) $^{211}\text{AtCl}$ @US-tube nanocapsules: a new concept in radiotherapeutic-agent design. *Small* 3: 1496–1499.
- Hartman KB, Laus S, Bolskar RD, Muthupillai R, Helm L, Tóth E, Merbach AE, Wilson LJ (2008) Gadonanotubes as ultra-sensitive pH-smart probes for magnetic resonance imaging. *Nano Lett.* 8: 415–419.
- Heath JR, O'Brien SC, Zhang Q, Liu Y, Curl RF, Tittel FK, Smalley RE (1985) Lanthanum complexes of spheroidal carbon shells. *J. Am. Chem. Soc.* 107: 7779–7780.
- Idée JM, Port M, Raynal I, Schaefer M, Le Greneur S, Corot C (2006) Clinical and biological consequences of transmetallation induced by contrast agents for magnetic resonance imaging: a review. *Fundam. Clin. Pharmacol.* 20: 563–576.
- Iezzi EB, Duchamp JC, Fletcher KR, Glass TE, Dom HC (2002) Lutetium-based trimetallic nitride endohedral metallofullerenes: new contrast agents. *Nano Lett.* 2: 1187–1190.
- Kato H, Suenaga K, Mikawa M, Okumura M, Miwa N, Yashiro A, Fujimura H, Mizuno A, Nishida Y, Kobayashi K, Shinohara H (2000) Syntheses and EELS characterization of water-soluble multi-hydroxyl $\text{Gd}@C_{82}$ fullereneols. *Chem. Phys. Lett.* 324: 255–259.
- Kato H, Kanazawa Y, Okumura M, Taninaka A, Yokawa T, Shinohara H (2003) Lanthanoid endohedral metallofullerenols for MRI contrast agents. *J. Am. Chem. Soc.* 125: 4391–4397.
- Kissell KR, Hartman KB, Van der Heide PA, Wilson LJ (2006) Preparation of I_2 @SWNTs: synthesis and spectroscopic characterization of I_2 -loaded SWNTs. *J. Phys. Chem. B* 110: 17425–17429.
- Krätschmer W, Lamb LD, Fostiropoulos K, Huffman DR (1990) Solid C_{60} : a new form of carbon. *Nature* 347: 354–358.
- Krause M, Dunsch L (2005) Gadolinium nitride Gd_3N in carbon cages: the influence of cluster size and bond strength. *Angew. Chem. Int. Ed. Engl.* 44: 1557–1560.
- Lauffer RB (1987) Paramagnetic metal complexes as water proton relaxation agents for NMR imaging: theory and design. *Chem. Rev.* 87: 901–927.
- Laus S, Sitharaman B, Tóth É, Bolskar RD, Helm L, Asokan S, Wong MS, Wilson LJ, Merbach AE (2005) Destroying gadofullerene aggregates by salt addition in aqueous solution of $\text{Gd}@C_{60}(\text{OH})_x$ and $\text{Gd}@C_{60}[\text{C}(\text{COOH}_2)]_{10}$. *J. Am. Chem. Soc.* 127: 9368–9369.
- Laus S, Sitharaman B, Tóth É, Bolskar RD, Helm L, Wilson LJ, Merbach AE (2007) Understanding paramagnetic relaxation phenomena for water-soluble gadofullerenes. *J. Phys. Chem. C* 111: 5633–5639.
- Lu X, Li H, Sun B, Shi Z, Gu Z (2005) Selective reduction and extraction of $\text{Gd}@C_{82}$ and $\text{Gd}_2@C_{80}$ from soot and the chemical reaction of their anions. *Carbon* 43: 1546–1549.
- Mackeyev YA, Marks JW, Rosenblum MG, Wilson LJ (2005) Stable containment of radionuclides on the nanoscale by cut single-wall carbon nanotubes. *J. Phys. Chem. B* 109: 5482–5484.
- Mikawa M, Kato H, Okumura M, Narazaki M, Kanazawa Y, Miwa N, Shinohara H (2001) Paramagnetic water-soluble metallofullerene having the highest relaxivity for MRI contrast agents. *Bioconj. Chem.* 12: 510–514.
- Miyamoto A, Okimoto H, Shinohara H, Shibamoto Y (2006) Development of water-soluble metallofullerenes as X-ray contrast media. *Eur. Radiol.* 16: 1050–1053.
- Nagase S, Kobayashi K, Akasaka T, Wakahara T (2000) Endohedral metallofullerenes: theory, electrochemistry, and chemical reactions. In: Kadish KM, Ruoff RS (eds.) *Fullerenes: chemistry, physics, and technology*. Wiley, New York, pp. 395–436.
- Nakamura E, Isobe H (2003) Functionalized fullerenes in water. The first 10 years of their chemistry, biology, and nanoscience. *Acc. Chem. Res.* 36: 807–815.
- Okumura M, Mikawa M, Yokawa T, Kanazawa Y, Kato H, Shinohara H (2002) Evaluation of water-soluble metallofullerenes as MRI contrast agents. *Acad. Radiol.* 9: S495–S497.
- Qingnuan L, Yan X, Xiaodong Z, Ruili L, Gieqie D, Xiaoguang S, Shaoliang C, Wenxin L (2002) Preparation of $^{99\text{m}}\text{Tc}-C_{60}(\text{OH})_x$ and its biodistribution studies. *Nucl. Med. Biol.* 29: 707–710.

- Qu L, Cao W, Xing G, Zhang J, Yuan H, Tang J, Cheng Y, Zhang B, Zhao Y, Lei H (2006) Study of rare earth encapsulated carbon nanomolecules for biomedical uses. *J. Alloys Compd.* 408–412: 400–404.
- Raebiger JW, Bolskar RD (2008) Improved production and separation processes for gadolinium metallofullerenes. *J. Phys. Chem. C* 112: 6605–6612.
- Ruoff RS, Tse DS, Malhotra R, Lorents DC (1993) Solubility of fullerene (C_{60}) in a variety of solvents. *J. Phys. Chem.* 97: 3379–3383.
- Sayes CM, Fortner JD, Guo W, Lyon D, Boyd AM, Ausman KD, Tao YJ, Sitharaman B, Wilson LJ, Hughes JB, West JL, Colvin VL (2004) The differential cytotoxicity of water-soluble fullerenes. *Nano Lett.* 4: 1881–1887.
- Sayes CM, Liang F, Hudson JL, Mendez J, Guo W, Beach JM, Moore VC, Doyle CD, West JL, Billups WE, Ausman KD, Colvin VL (2006) Functionalization density dependence of single-walled carbon nanotubes cytotoxicity *in vitro*. *Toxicol Lett.* 161: 135–142.
- Shinohara H (2000) Endohedral metallofullerenes. *Rep. Prog. Phys.* 63: 843–892.
- Shu CY, Gan LH, Wang CR, Pei XL, Han HB (2006) Synthesis and characterization of a new water-soluble endohedral metallofullerene for MRI contrast agents. *Carbon* 44: 496–500.
- Shu CY, Zhang EY, Xiang JF et al. (2006) Aggregation studies of the water-soluble gadofullerene magnetic resonance imaging contrast agent: $[Gd@C_{82}O_6(OH)_{16}(NHCH_2CH_2COOH)_8]_x$. *J. Phys. Chem. B* 110: 15597–15601.
- Shukla RB, Kumar K, Weber R, Zhang X, Tweedle M (1997) Alteration of electronic relaxation in MR contrast agents through de-novo ligand design. *Acta Radiol Suppl.* 38(S412): 121–123.
- Sitharaman B, Bolskar RD, Rusakova I, Wilson LJ (2004) $Gd@C_{60}[C(COOH)_2]_{10}$ and $Gd@C_{60}(OH)_x$: Nanoscale aggregation studies of two metallofullerene MRI contrast agents in aqueous solution. *Nano Lett.* 4: 2373–2378.
- Sitharaman B, Kissell KR, Hartman KB, Tran LA, Baikov A, Rusakova I, Sun Y, Khant HA, Ludtke SJ, Chiu W, Laus S, Tóth É, Helm L, Merbach AE, Wilson LJ (2005) Superparamagnetic gadonanotubes are high-performance MRI contrast agents. *Chem. Commun.* 31: 3915–3917.
- Sitharaman B, Wilson LJ (2006) Gadonanotubes as new high-performance MRI contrast agents. *Int. J. Nanomed.* 1: 291–295.
- Sitharaman B, Tran LA, Pham QP, Bolskar RD, Muthupillai R, Flamm SD, Mikos AG, Wilson LJ (2007) Gadofullerenes as nanoscale magnetic labels for cellular MRI. *Contrast Media Mol. Imag.* 2: 139–146.
- Sloan J, Cook J, Green MLH, Hutchison JL, Tenne R (1997) Crystallization inside fullerene related structures. *J. Mater. Chem.* 7: 1089–1095.
- Stevenson S, Rice G, Glass T, Harich K, Cromer F, Jordan MR, Craft J, Hadju E, Bible R, Olmstead MM, Maitra K, Fisher AJ, Balch AL, Dorn HC (1999) Small-bandgap endohedral metallofullerenes in high yield and purity. *Nature* 401: 55–57.
- Stevenson S, Stephen RR, Amos TM, Cadorette VR, Reid JE, Phillips JP (2005) Synthesis and purification of a metallic nitride fullerene bisadduct: exploring the reactivity of $Gd_3N@C_{80}$. *J. Am. Chem. Soc.* 127: 12776–12777.
- Stevenson S, Harich K, Yu H, Stephen RR, Heaps D, Coumbe C, Phillips JP (2006) Nonchromatographic “Stir and Filter Approach” (SAFA) for Isolating $Sc_3N@C_{80}$ metallofullerenes. *J. Am. Chem. Soc.* 128: 8829–8835.
- Sun B, Gu Z (2002) Solvent-dependent anion studies on enrichment of metallofullerene. *Chem. Lett.* 31: 1164–1165.
- Thrash TP, Cagle DW, Alford JM, Wright K, Ehrhardt GJ, Mirzadeh S, Wilson LJ (1999) Toward fullerene-based radiopharmaceuticals: high-yield neutron activation of endohedral ^{165}Ho metallofullerenes. *Chem. Phys. Lett.* 308: 329–336.
- Tóth É, Helm L, Merbach AE (2001) Relaxivity of Gadolinium(III) Complexes: theory and mechanism. In: Tóth É, Merbach AE (eds.) *The chemistry of contrast agents in medical magnetic resonance imaging*. Wiley, Chichester, pp. 45–119.
- Tóth É, Bolskar RD, Borel A, González G, Helm L, Merbach AE, Sitharaman B, Wilson LJ (2005) Water-soluble gadofullerenes: toward high-relaxivity, pH-responsive MRI contrast agents. *J. Am. Chem. Soc.* 127: 799–805.

- Tsuchiya T, Wakahara T, Shirakura S, Maeda Y, Akasaka T, Kobayashi K, Nagase S, Kato T, Kadish KM (2004) Reduction of endohedral metallofullerenes: a convenient method for isolation. *Chem. Mater.* 16: 4343–4346.
- Tsuchiya T, Wakahara T, Lian Y, Maeda Y, Akasaka T, Kato T, Mizorogi N, Nagase S (2006) Selective extraction and purification of endohedral metallofullerene from carbon soot. *J. Phys. Chem. B* 110: 22517–22520.
- Tsuchiya T, Sato K, Kurihara H, Wakahara T, Nakahodo T, Maeda Y, Akasaka T, Ohkubo K, Fukuzumi S, Kato T, Mizorogi N, Kobayashi K, Nagase S (2006) Host-guest complexation of endohedral metallofullerene with azacrown ether and its application. *J. Am. Chem. Soc.* 128: 6699–6703.
- Usenko CY, Harper SL, Tanguay RL (2007) *In vivo* evaluation of carbon fullerene toxicity using embryonic zebrafish. *Carbon* 45: 1891–1898.
- Weiss FD, Elkind JL, O'Brien SC, Curl RF, Smalley RE (1988) Photophysics of metal complexes of spheroidal carbon shells. *J. Am. Chem. Soc.* 110: 4464–4465.
- Wilson LJ (1999) Medical applications of fullerenes and metallofullerenes. *Electrochem. Soc. Interface* 8: 24–28.
- Wilson LJ, Cagle DW, Thrash TP, Kennel SJ, Mirzadeh S, Alford JM, Ehrhardt GJ (1999) Metallofullerene drug design. *Coord. Chem. Rev.* 190–192: 199–207.
- Wilson SR, MacFarland D, Zhou Z, Zhang J, Shukla R (2007) Commercial development of trimetasphere metallofullerene MRI contrast agents. Abstract 1127: 211th Meeting of The Electrochemical Society, Chicago, IL, May 6–10.
- Xing G, Zhang J, Zhao Y, Tang J, Zhang B, Gao X, Yuan H, Qu L, Cao W, Chai Z, Ibrahim K, Su R (2004) Influences of structural properties on stability of fullerlenols. *J. Phys. Chem. B* 108: 11473–11479.
- Xu JY, Li QN, Li JG, Ran TC, Wu SW, Song WM, Chen SL, Li WX (2007) Biodistribution of $^{99m}\text{Tc}-\text{C}_{60}(\text{OH})_x$ in Sprague–Dawley rats after intratracheal instillation. *Carbon* 45: 1865–1870.
- Zhang S, Sun D, Li X, Pei F, Liu S (1997) Synthesis and solvent enhanced relaxation property of water-soluble endohedral metallofullerenes. *Fullerene Sci. Tech.* 5: 1635–1643.
- Zhang J, Liu K, Xing G, Ren T, Wang S (2007) Synthesis and *in vivo* study of metallofullerene based MRI contrast agent. *J. Radioanal. Nucl. Chem.* 272: 605–609.

Chapter 9

Biomolecules Functionalized Carbon Nanotubes and Their Applications

Daxiang Cui

Abstract In recent years, functionalization of carbon nanotubes (CNTs) with biomolecules such as nucleotide acids, proteins, and artificial polymers have emerged as a new exciting field. Theoretical and experimental studies of structure and function of bio-inspired CNT composites have made great advances. The importance of nucleic acids, proteins, and synthesized polymers to the fundamental developments in CNT-based bio-nano-composites or devices has been recognized. In particular, biomechanics, biochemistry, thermodynamics, electronic, optical and magnetic properties, and biocompatibility and toxicology of the bio-inspired CNT composites have become a new interdisciplinary frontier in life science and nanomaterial science. Bio-inspired CNT composites have been actively exploited potentials in applications such as gene/drug delivery system, tissue engineering scaffolds, hydrogen storage, molecular imaging, biocatalyst systems, biosensors, and antifouling films. Here we review the main advances in this field over the past few years, explore their application prospects, and discuss the issues, approaches, and challenges, with the aim of improving and developing CNT-based bio-nanotechnology.

Keywords Carbon nanotubes, biomolecules, nanocomposites, functionalization, applications

9.1 Introduction

Since Iijima discovered the carbon nanotubes (CNTs) in 1991 (Iijima, 1991), many unique properties of CNTs such as excellent mechanical, electrical, magnetic, optical, and chemical properties, have been gradually uncovered (Dresselhaus et al.,

Department of Bio-Nano Science and Engineering, National Key Laboratory of Nano/Micro Fabrication Technology, Key laboratory for thin film and microfabrication of Ministry of Education, Institute of Micro and Nano Science and Technology, Shanghai Jiaotong University, Dongchuan Road 800, Shanghai 200240, P. R. China,
Email: dxcui@sjtu.edu.cn or daxiangcui@yahoo.com

1996, 2000; Ajayan et al., 2003). Both single- and multi-walled carbon nanotubes have become ideal nanoscale-building blocks for nanoengineering. A lot of studies suggest that CNTs have extensive commercial application potential in medical chemistry and biomedical engineering.

Biomolecules such as DNA, RNA, proteins, and synthesized polymers are multifunctional nanomaterials, which can be employed in applications such as self-assembly of nanosystems and devices, gene/drug delivery system, and functional molecular imaging (Yan et al., 2003; Salem et al., 2003). DNA, RNA, proteins, and artificial polymers have been demonstrated to self-assemble into linear or more sophisticated topological structures (Seeman, 2005); which can also be used as templates for nanofabrication; their shape and chemical properties can be employed to fabricate ordered arrangements of inorganic substances (Bashir, 2004; Um et al., 2006). Such nanostructures possess unique physical and chemical properties and could serve as a basis for nanoscale devices or nano-machinery in bio-nanotechnology. Integration of biomolecules and carbon nanotubes provide a novel functional platform for bioanalytical sciences and biomedical engineering.

Up to date, functionalization of CNTs with biomolecules such as nucleic acids, proteins, and artificial polymers is currently a developing area of nano-biotechnology, which can achieve improved properties and functions such as good biocompatibility and biological molecular recognition capabilities (Hafner et al., 2001; Shim et al., 2002). Especially the biomolecules-CNT composites, with novel mechanical, biological, optical, electronic, and magnetic properties have been actively investigated, and are being continually exploited to harness the potential applications in various fields including molecular electronics, medical chemistry, and biomedical engineering (Martin and Kohli, 2002; Odom et al., 2002; Keren et al., 2003; Nalwa, 2000). The broad range of increasing nanotechnology applications for CNTs results in the increased chance for both human and environmental exposures to this kind of nanomaterials. Evaluation of biocompatibility and possible adverse effects of CNTs has also been very imperative and urgent (Weiss et al., 2001; Kuempel et al., 2006; Shvedova et al., 2003; Barnard, 2006). Here, we review the main advances of functionalization of CNTs with biological molecules such as nucleic acids, peptides, and artificial polymers as well as cells, and explore their potential applications and prospects, and discuss the issues, approaches, and challenges, with the aim of improving and developing the CNT-based bio-nanotechnology.

9.2 Advances of Biomolecules Functionalized CNTs

In the last 10 years, CNTs are successfully functionalized via end terminal or sidewall modification or filling with biomolecules, or conjugating with polymers; the resulting biomolecules-CNTs nanocomposites own special properties such as optimized mechanical, optical, electronic, and magnetic, and have great potential application in industry, agriculture, defense, and bio-medicine. Effects of CNTs on the cells, human health, and environment also attract more and more attention; CNTs' potential hazards

are being actively investigated, the possible measurements to improve CNTs' biocompatibility and reduce their potential risks are being actively explored; all these advances would lay foundation for CNTs' application in the near future.

9.2.1 Functionalization of CNTs with DNA Molecules

CNTs own excellent materials properties. DNA is an excellent molecule to construct macromolecular networks because it is easy to synthesize, with a high specificity of interaction, and is conformationally flexible. The complementary base-pairing properties of DNA molecules have been used to make two-dimensional crystals and prototypes of DNA computers and electronic circuits (Yan et al., 2002; Batalia et al., 2002). Therefore functionalization of CNTs with DNA molecules has great potential for applications such as developing nanodevices or nanosystems, biosensors, electronic sequencing, and gene transporters.

CNTs can conjugate with nucleic acids via non-covalent bond. ssDNA, short double-stranded DNA and total RNA molecules can attach to the surface of CNTs and can disperse CNTs in aqueous environment. The poly(30T) has the highest dispersion efficiency (Zheng et al., 2003). For example, 1 mg DNA molecules mix with 1 mg CNTs in 1 ml water, yield at most 4 mg/ml CNT solution. DNA-CNT complexes can be purified or isolated by electronic properties such as agarose gel electrophoresis and centrifuge method (Cui et al., 2004a; Karajanagi et al., 2004).

CNTs can also conjugate with nucleic acids via covalent bond. They can be functionalized via covalently bonded adducts. For example, COOH or NH₂ group can be formed on the terminal or sidewall of CNTs (Bahr and Tour, 2002). Antisense-myc can be conjugated with CNTs via covalent bond and can be delivered into HL-60 cells to achieve killing human leukemia cells (Cui et al., 2007).

CNTs can also be encapsulated with DNA molecules. As shown in Fig. 9.1, a DNA molecule could be spontaneously inserted into a SWNT in a water solution via molecular dynamics simulation (Gao et al., 2003). The van der Waals and hydrophobic forces were very key factors for the insertion process, with the former playing a more dominant role in the course of DNA entering into the hole of CNT. Experiment also confirmed that Pt-labeled DNA molecules can be encapsulated into multi-walled carbon nanotubes in water solution at 400 K and 3 Bar as shown in Fig. 9.2 (Cui et al., 2004). The CNTs filled with DNA molecules have potential in applications such as gene delivery system, and electronic sequencing, nanomotor, etc.

SWCNTs can regulate the efficiency of polymerase chain reaction (PCR) (Cui et al., 2004). Adding SWCNTs into the PCR reagents increases the amount of PCR yields at lower SWCNT concentrations, but this effect is reversed at higher SWCNT concentrations. As shown in Fig. 9.3, the XPS result showed that the C1s binding energy intensity of PCR products increased after the reaction. A new C 1s peak appeared to the left of the main peak. The peak width increased and the binding energy spectrum moved towards the left compared with the results before reaction.

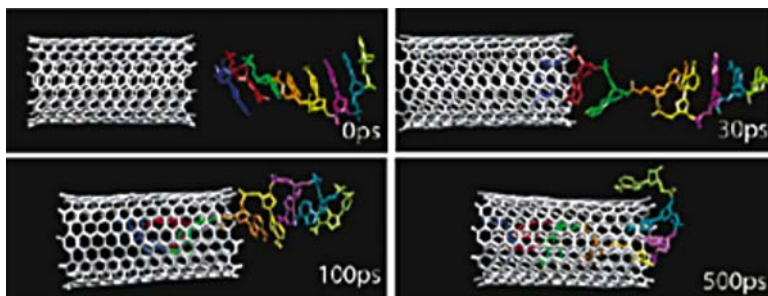


Fig. 9.1 Simulation snapshots of a DNA oligonucleotide (8 adenine bases) interacting with a (10,10) carbon nanotube at 0, 30, 100, and 500 ps. Water molecules are not displayed for clarity (Chaudhary et al., 2006. With permission from American Chemical Society) (*See Color Plates*)

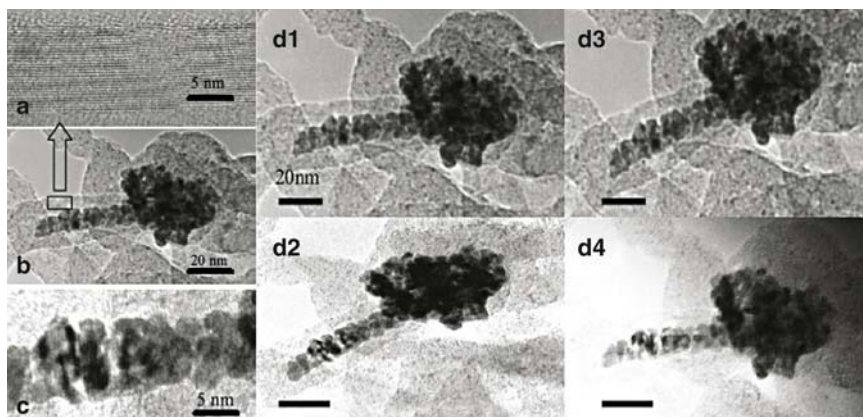


Fig. 9.2 HR-TEM images of carbon nanotubes with partially encapsulated nucleic acid fragments labeled with platinum nanoparticles. (A) A local HR-TEM image of the MWCNT shell structure. (B) An image of a Pt-labeled DNA fragment partially drawn into a linear strand inside a MWCNT. The part of the DNA outside the MWCNT is folded into a globular conformation. The TEM image was obtained at an accelerating voltage of 200 KV. (C) HR-TEM image of a partially inserted Pt-labeled DNA fragment inside a MWCNT, showing that the lattice fringe lines of the MWCNT cross over the encapsulated DNA strand. (D) HR-TEM images of the partially inserted Pt-labeled DNA strand under different tilting angles and different focus conditions. D1–3 showed that the Pt-labeled DNA strand is observed to align along the nanotube axis under different tilting angles, D4 showed the image of Pt-labeled DNA strand under the de-focus condition. Bar: 20 nm (Correa-Duarte et al., 2001. With permission from Tech Science Press)

These observations confirmed that strong interactions happened among SWCNTs, DNA templates, and Taq enzyme in the course of the PCR. SWCNTs could improve the PCR efficiency, which indirectly demonstrate that CNTs could improve the bio-activity of Taq enzyme, and may own bio-catalytic function in a variety of biochemical reactions.

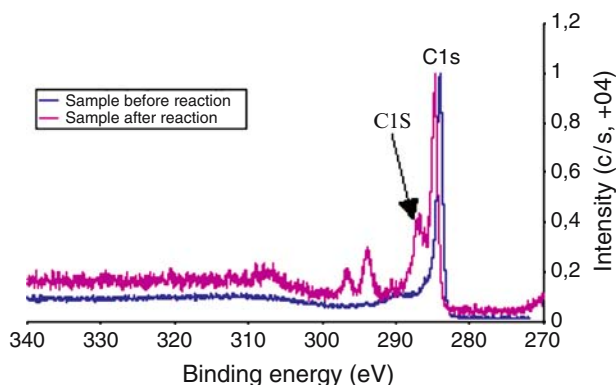


Fig. 9.3 The result of C1s binding energy intensity of samples before (lower curve) and after (upper curve) PCR reaction. The left peaks represent the binding energy intensity of C 1s of SWCNTs after PCR reaction; the right-most peak represents the binding energy intensity of C 1s of SWCNTs before reaction. The graph shows that the C 1s peak of SWCNTs moves towards the left with the emergence of two C 1s peaks, indicating enhanced binding energy after PCR reaction (Chen et al., 2001. With permission from IOP Publishing) (*See Color Plates*)

9.2.2 Functionalization of CNTs with Proteins

Protein is an excellent natural nanomaterial for molecular machines. Protein-based molecular machines, often driven by an energy source such as ATP, are abundant in biology. Surfactant peptide molecules undergo self-assembly in solution to form a variety of supermolecular structures at the nanoscale such as micelles, vesicles, unilamellar membranes, and tubules (Maslov and Sneppen, 2002). These assemblies can be engineered to perform a broad spectrum of functions, including delivery systems for therapeutics and templates for nanoscale wires in the case of tubules, and to create and manipulate different structures from the same peptide for many different nanomaterials and nanoengineering applications.

The studies of recognitive proteins and protein-binding domains reveal molecular architectures with specific chemical moieties that provide a framework for selective recognition of a target analyte in aqueous environment. Since proteins are heteropolymers of amino acids, proper matching and positioning of chemical residues can lead to artificial macromolecular structures capable of specific recognition. By analyzing binding proteins, scientists have been successful in designing biomimetic polymer networks that specifically bind biologically significant molecules (Huynh et al., 2002).

Peptides directing assembly can be designed using motifs found in natural proteins (Ikkala and Brinke, 2002). After conjugation with hydrophilic polymers, these peptides can keep biological activity. The peptides not only alter the mechanical properties of fibrin but also allow a mechanism for creating a self-assembling network. Furthermore, these biomaterials can be designed with physiologically relevant

enzymatic degradation sites and can support the release of bioactive factors such as adhesion molecules, growth factors, and extracellular matrix proteins.

Synthetically lipidated peptides possess the self-assembly character of amphiphilic molecules and biological activity of the peptide headgroups. This enables interfaces to be assembled that deliver biofunctionality in a controllable way. Incorporation of peptide amphiphiles in liposomes greatly increases the uptake of synthetic dyes by cells, indicating their potential utility in targeted drug delivery.

CNTs have recently received extensive attention due to their nanoscale dimensions and outstanding materials properties. Integration of CNTs and proteins can gain more advantages over CNTs or proteins and can realize novel, specific functions. Therefore, functionalization of CNTs with proteins own broad application prospects.

9.2.2.1 Functionalization of CNTs with Proteins via Covalent or Non-Covalent Bond

CNTs can be functionalized with protein via non-covalent bond (Li et al., 2005; Kim et al., 2003; Mitchell et al., 2002). For example, (beta-lactamase I, that can be immobilized inside or outside CNTs, doesn't change enzyme's activity (Vinueza and Goodnow, 2002). Taq enzyme can attach to the outside of CNT, and doesn't change its activity (Cui et al., 2004). Peptide with Histidine and Tryptophan can have selective affinity for CNT(Guo et al., 1998). Monoclonal antibody can attach to SWNTs. Protein-modified CNTs can be used to improve its biocompatibility and biomolecular recognition capabilities (Um et al., 2006). For example, CNTs functionalized with PEG and Triton X-100 can prevent nonspecific binding of protein and CNTs. Biotin moiety is attached to the PEG chains; Streptavidin can bind specifically with biotin-CNT (Shim et al., 2002).

CNTs can also be employed for protein immobilization via covalent sidewall functionalization (Wang et al., 2003). A bifunctional molecule, 1-pyrenebutanoic acid, succinimidyl ester irreversibly adsorbed onto the hydrophobic surface of SWNTs in methanol, succinimidyl ester groups on the surface of SWCNTs can react with amine on the surface of proteins and result in the formation of an amide bond decorated SWNT (Georgakilas et al., 2002). For example, SWCNTs-streptavidin conjugates can enter into human leukemia cells and human T cells via the endocytosis pathway (Chen et al., 2001; Kam et al., 2006), which highly hint that SWCNTs should be a good gene/drug transporters.

CNTs can also be filled with amino acids or short peptides. For example, molecular dynamics simulation showed that the three polypeptides such as strong hydrophobic phenylalanine (Phe), moderate hydrophobic leucine (Leu), and strong hydrophilic asparagines (Arg) can be encapsulated inside the nanotube but with different encapsulation velocity as shown in Fig. 9.4 (Kong et al., 2003). The encapsulation of protein inside a CNT depends on the free energy change of the whole complex system. The larger the encapsulation-induced free energy reduction the faster is the encapsulation process.

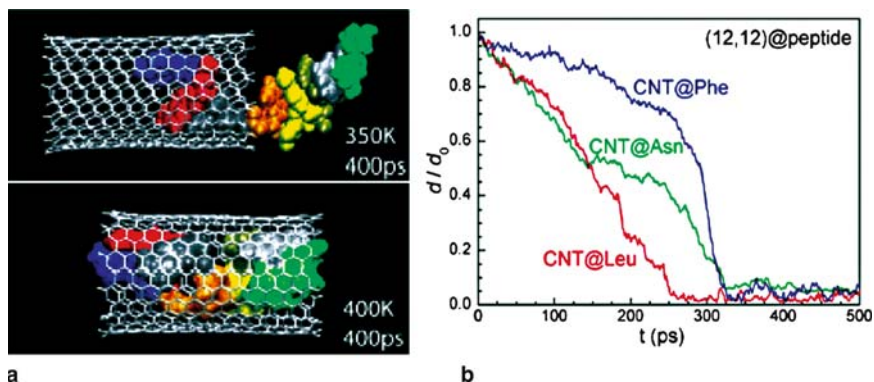


Fig. 9.4 (a) Snapshot of peptide being filled into CNT; (b) normalized COM distances between polypeptide and CNT as function of simulation time (d_0 is the initial COM distance) (Dillon et al., 1997. With permission from American Materials Research Society) (*See Color Plates*)

Bioactive-peptide-functionalized CNTs can cause strong anti-peptide immunological responses in mice, no cross-reactivity against CNTs was detected (Pantarotto et al., 2003; Salvatat et al., 2006). Employing fully the advantages of CNTs and proteins may fabricate a lot of nanomotor or nanoscale machinery with unique function.

9.2.2.2 Interaction Between CNTs and Enzyme Molecules

CNTs have been used as supports for the enzymes (Rege et al., 2004; Yim et al., 2005). The higher surface area of CNTs can support a much higher density of enzymes than previous approaches such as thin films. Their high aspect ratio aids in the retention of enzyme-CNT conjugates in the matrix. CNTs also enhance the stability of adsorbed proteins relative to micro- or macro-scale supports, thereby helping to preserve or enhance enzyme bioactivity in the nanocomposites (Wang, 2006). For example, Asuri and his co-workers (Asuri et al., 2007) reported that the proteases attached to the surface of SWCNTs can create self-cleaning surfaces that resist protein adsorption. This kind of SWCNT-enzyme composite exhibited 30 times higher overall catalytic activity than control composites where the proteases were conjugated to a non-nanoscale graphite support. Importantly, the enzymes preserved more than 90% of their initial activity over 30% days in the liquid buffer, with only negligible amounts of enzymes leaching out. The result demonstrates that the nanocomposites of SWCNTs and polymers can act as hosts for enzymes and can prevent protein contamination on the surface of medical devices. We consider that SWCNTs may have the function as biocatalyst to improve the enzyme activity attached to the surface of CNTs. Our previous work also indirectly hints that CNTs could improve the bioactivity of enzymes such as Taq enzyme Cui et al. (2004). However, there are also adverse reports. CNTs can

change the conformation of enzyme protein molecules, and reduce the bioactivity of enzyme molecules.

9.2.3 Biocompatibility and Toxicology of CNTs

The biocompatibility and toxicological studies of CNTs have become a controversial hotspot. Although several reports showed that CNTs are non-toxic and could be used as *in vivo* multifunctional biological transporters (Kam et al., 2005), there is no doubt that the possible hazards associated with CNTs are significant, and that concern is valid; the key to address the challenge is to clarify the range and mechanism of nanohazards of CNTs, and possible measurements to reduce CNTs' toxicity.

A lot of animal experiments showed that CNTs are toxic to living organisms (Pantarotto et al., 2004a; Singh et al., 2005; Lovat et al., 2005; Foley et al., 2002; Goho, 2004; Hoet et al., 2004; Lam et al., 2004). For example, CNTs could damage mouse lung, skin, and cause mouse death, CNTs also can damage fish brain (Raloff, 2005; Oberdorster et al., 2004; Maynard et al., 2004).

CNTs also showed toxic sign to cells. For example, Pantarotto and his colleagues (Pantarotto et al., 2004) reported that CNT-conjugated bioactive peptides can cross cell membranes, can accumulate in the cytoplasm, or reach the nucleus; this kind of peptides-functionalized CNTs may exhibit cytotoxicity when the concentration inside the cells exceed 10 μM .

Length and size of CNTs seriously affect their cytotoxicities (Sato et al., 2005; Cui et al., 2007). CNTs of 825 nm in length caused stronger inflammation in human acute monocytic leukemia cell line THP-1 than CNTs of 220 nm in length, as shown in Fig. 9.5. However, histological observation as shown in Fig. 9.6, showed that no severe inflammatory response such as necrosis, white cells aggregates, etc. This result indirectly shows that CNTs can cause noninflammatory damage to local tissues.

Degeneration or neutrophil infiltration *in vivo* were exhibited around CNTs examined throughout the experimental period. Different sizes of CNTs cause different cell reaction (Goh et al., 2003). For example, SWCNTs inhibit HEK293 cell proliferation, decrease cell adhesive ability in a dose- and time-dependent manner (Grunlan et al., 2004) as shown in Fig. 9.7 and Fig. 9.8.

Our previous studies showed that CNTs exhibit marked cytotoxicity (Cui et al., 2005; Tian et al., 2006). For example, SWCNTs can inhibit HEK293 cell proliferation, decrease cell adhesive ability in a dose- and time-dependent manner as shown in Fig. 9.7. HEK293 cells also exhibit active responses to SWCNTs such as secretion of some 20–30 kD proteins to wrap SWCNTs, aggregation of cells attached by SWCNTs and formation of nodular structures as shown in Fig. 9.8. Cell cycle analysis showed that 25 $\mu\text{g}/\text{ml}$ SWCNTs in medium induced G_1 arrest and cell apoptosis in HEK293 cells as shown in Fig. 9.9. Biochip analysis showed that SWCNTs can induce up-regulation expression of cell cycle-associated genes such

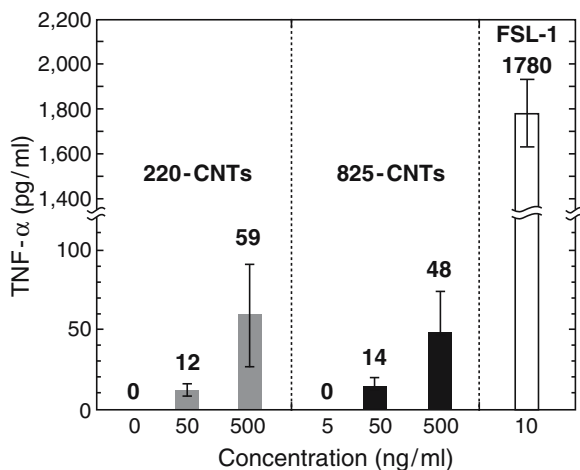


Fig. 9.5 Induction of THP-1 cells by 220-CNTs and 825-CNTs. The diacylated lipopeptide FSL-1 was used as a positive control (Gong et al., 2000. With permission from The Royal Society of Chemistry)

as *p16*, *bax*, *p57*, *hrk*, *cdc42* and *cdc37*, down-regulation expression of cell cycle genes such as *cdk2*, *cdk4*, *cdk6*, and *cyclin D3*, and down-regulation expression of signal transduction-associated genes such as *mad2*, *jak1*, *ttk*, *pcdha9*, and *erk*. Western blot analysis showed that SWCNTs can induce down-regulation expression of adhesion-associated proteins such as laminin, fibronectin, cadherin, FAK, and collagen IV. SWCNTs inhibit HEK293 cells growth by inducing cell apoptosis and decreasing cellular adhesion ability. It is also observed that SWCNTs stimulate human osteoblast cells and human fibroblast cells to produce many protuberances on the surface compared with the control, as shown in Fig. 9.9, which is one kind of active protective reaction of stimulated cells. Some new reports also support that CNTs own the cytotoxicity. For example, Terrones and his colleagues (Jares-Erijman EA, and Jovin, 2003) reported that when MWCNTs were injected into the mice's trachea, the mice could die by dyspnea depending on the MWCNTs doses. CNTs can induce serious oxidative stress injury within cells (Joshi et al., 2005).

Some reports showed that pure CNTs can cross cell membrane with high efficiency (Kam et al., 2005; Pantarotto et al., 2004). Some reports showed that CNTs could not be found in cells by HR-TEM (Carrero-Sánchez et al., 2006; Stone and Donaldson, 2006). In our previous studies, we also found that pure CNTs were very difficult to enter into cells such as human fibroblast cells (Tian et al., 2006) and HEK293 cells (Cui et al., 2005), and stem cells, we spent almost 6 months on sectioning these cells and looking for CNTs within cells by HR-TEM, finally we could not find CNTs within cells, we only observed that a lot of CNTs attached to the surface of cells (Fig. 9.10a), and some tubers appeared on the surface of CNTs (Fig. 9.10c). That is to say, non-modified CNTs enter into cells via low-efficient means. However, biomolecules-modified CNTs can efficiently enter into almost all

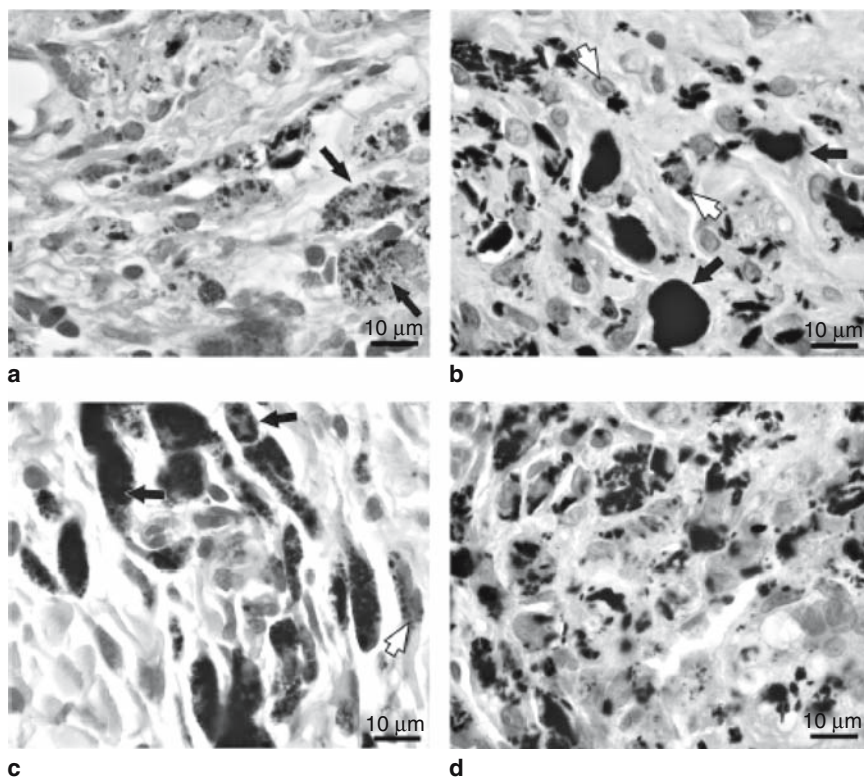


Fig. 9.6 Histology of 220-CNTs and 825-CNTs implanted in the subcutaneous tissue. 1 week: Clusters of both of 220-CNTs and 825-CNTs were surrounded by granulation tissue. (a) Many of the 220-CNTs were enveloped by macrophages (arrows). (b) Some of the 825-CNTs were observed in the intercellular space (arrows), while others were observed in macrophages (white arrows), 4 weeks: (c) Most of the 220-CNTs were observed in macrophages (arrows) and fibroblasts (white arrows). (d) There was a negligible difference in the degree of inflammation around 825-CNTs 4 weeks following surgery, compared to 1 week. All scale bars are 10 μm (Gong et al., 2000. With permission from The Royal Society of Chemistry)

cells including tumor cells, normal primary cultured cells as well as stem cells. For example, we observed that biomolecules-modified CNTs located in the cytoplasm of HL-60 cells, MCF-7, and HepG2 cells by HR-TEM (Cui et al., 2007; Tian et al., 2006), as shown in Fig. 9.10b, cy3-modified SWCNTs located inside HL-60 cells. Dai and his colleagues (Kam et al., 2005) reported that PL-PEG-FA-modified SWCNTs can efficiently enter into HeLa cells, and can be used as near-infrared agents for selective cancer cell destruction because SWCNTs have the ability of the strong optical absorbance in the range of 700–1,100 nm. Different biomolecules such as nitrogen (Carrero-Sánchez et al., 2006), peptides (Pantarotto et al., 2004), dyes (Cui et al., 2007; Maynard et al., 2004), and dendrimers (Pan et al., 2006, 2007) can markedly enhance cellular uptake of CNTs, and also markedly decrease CNTs' cytotoxicity; interaction between dyes and CNTs are also reported (Casey et al., 2007).

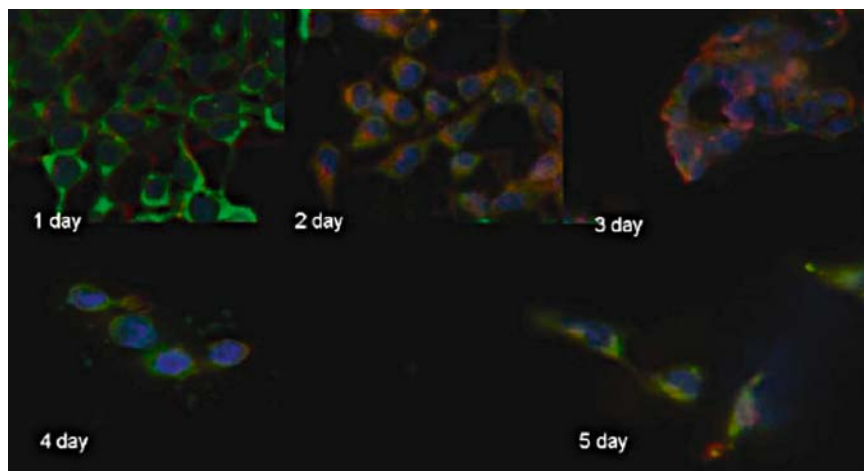


Fig. 9.7 Indirect immunofluorescent staining of SWCNTs-treated HEK293 cells for day 1–5 by fluorescent microscopy ($\times 630$). Green: cadherin; red: collagen; blue: cellular nucleus staining with DAPI. The expression levels of cadherin and collagen IV in cells decreased gradually as the culture days increased; HEK293 cells gradually detached from the cell populations as the culture days increased (Grunlan et al., 2004. With permission from Elsevier) (*See Color Plates*)

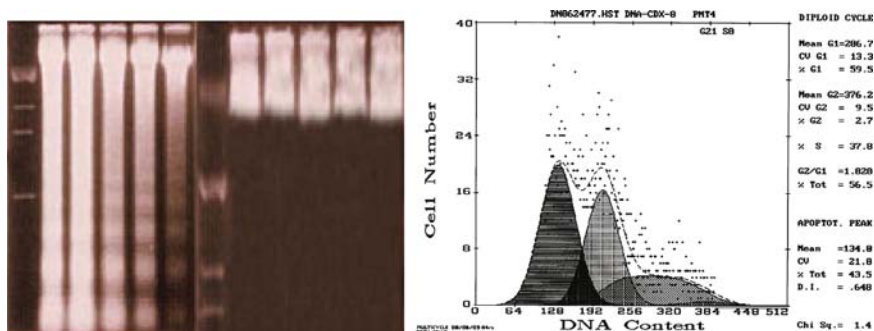


Fig. 9.8 Apoptosis of HEK293 cells induced by SWCNTs. B1: DNA electrophoresis of cells cultured with 25 μ g/ml SWCNTs for 1–5 days, *M* molecular marker, no. 1–5 denote the results of cells cultured for day 1–5, respectively; B2: DNA electrophoresis results of control cells cultured for day 1–5; C: the cell cycle distribution of HEK293 cells cultured with 25 μ g/ml SWCNTs for 4 days, the percentage of sub-G1 cells (apoptosis cells) was 43.5%. (Grunlan et al., 2000. With permission from Elsevier) (*See Color Plates*)

We also confirmed that CNTs-based materials endocytosis behavior was highly dependent on surface characteristics. Under the condition of less than 4°C, it is difficult for biomolecules-modified CNTs to enter into cells, whereas at 37°C, biomolecules-modified CNTs easily enter into cells, the phenomena demonstrates that endocytosis of biomolecules-modified CNTs into cells is an active course with energy consumption.

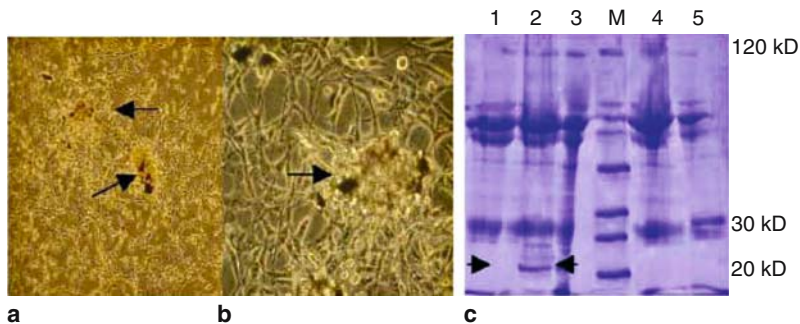


Fig. 9.9 Responses of HEK293 to single-walled carbon nanotubes. (a) SWCNTs were aggregated together and surrounded by HEK293 cells ($\times 200$). (b) The aggregated SWCNTs were surrounded by secretion from HEK293 cells ($\times 400$). (c) SDS-PAGE result showed that some 20–30 kD proteins existed in the supernatants of HEK293 cells with 25 g/ml SWCNTs. *M* is protein marker; the no. 1–5 denote the results for HEK293 cells cultured with SWCNTs for 1–5 days, respectively, showing some small secreted proteins were only detected on the day 2 and day 3 after SWCNTs were added inside the cell culture (Grunlan et al., 2000. With permission from Elsevier) (*See Color Plates*)

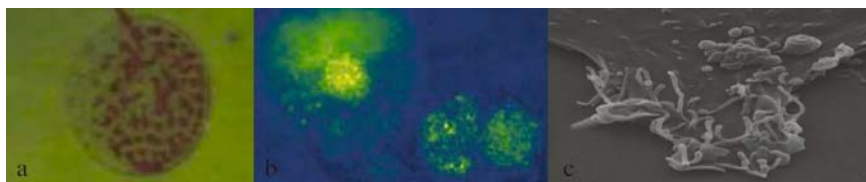


Fig. 9.10 SWCNTs attached to the surface of cells and located within cells **a.** SWCNTs attached to the surface of cells; **b.** SWCNTs labeled with Cy3 located within cells; **c.** Some protuberances appeared on the cell surface after cells are stimulated by SWCNTs. Right picture is control. Bar is $10\mu\text{m}$ (With permission from American Scientific publisher) (*See Color Plates*)

Regarding the mechanism of biomolecules functionalized CNTs entering into cells, endocytosis mechanism may be responsible for the phenomena, a theory model is also suggested (Gao et al., 2005); the optimal size of particles entering into cells is between 20 nm and 700 nm or so, too small nanoparticles are very difficult to enter into cells because of cellular surface tension force and adhesion. The further mechanism of effects of CNTs on human healthcare and environment is being investigated from the following four scales such as molecular, cellular, animals, and environment levels.

In short, CNTs own potential nanohazards because we still do not know the concrete metabolism course of CNTs within cells and human body, and possible effects on heredity, gene transcriptional, and post-translational regulations, at present, we still do not have enough proofs to confirm CNTs are no toxic, thereby the key is to find these methods to reduce potential risk of CNTs by series of studies.

9.2.4 Interaction Between CNTs and Polymer Matrix

CNTs are excellent nanomaterials with outstanding high Young's modulus, stiffness, and flexibility (Treacy et al., 1996; Otten et al., 2002; Lourie et al., 1998; Yu et al., 2000), can be used as a filler in polymer composite systems to obtain ultralight structural materials with enhanced electrical, thermal, and optical properties. For example, CNTs can be dispersed and aligned in the polymer matrix. The resulting novel homologous multifunctional nanostructure materials exhibit excellent properties such as optimal mechanical, thermal, electrical, electrochemical, electromagnetic, optical, and super-hydrophobic properties.

9.2.4.1 Mechanical Properties of Polymer/CNTs Composites

Incorporation of CNTs into a polymer matrix can form the structural materials with dramatically increased modulus and strength. The composites' strength depends on two variables. Firstly, there should be a high degree of load transfer between the matrix and the CNTs. Secondly, CNTs should be well dispersed in matrix. Chemically functionalized MWCNTs incorporated into a polymer matrix can improve the transfer of mechanical load through a chemical bond (Velasco-Santos et al., 2003b). The resulting composite exhibits higher storage modulus (E') and tensile strength than the composites without added CNTs. For example, E' at 90°C is increased by 1135%.

CNT can markedly reinforce polystyrene rod and epoxy thin film by forming CNT/polystyrene (PS) and CNT/epoxy composites (Wong et al., 2003). Molecular mechanics simulations and elasticity calculations clearly showed that, in the absence of chemical bonding between CNT and the matrix, the non-covalent bond interactions including electrostatic and van der Waals forces result in CNT-polymer interfacial shear stress (at 0K) of about 138 and 186 MPa, respectively, for CNT/epoxy and CNT/PS, which are about an order of magnitude higher than microfiber-reinforced composites, the reason should attribute to intimate contact between the two solid phases at the molecular scale. Local non-uniformity of CNTs and mismatch of the coefficients of thermal expansions between CNT and polymer matrix may also promote the stress transfer between CNTs and polymer matrix.

The composites of polyamide-6 and CNTs showed an increase of 27% in the Young's modulus, as shown in Fig. 9.11, these selectively filled polyamide-6/ABS-blends exhibit a highly irregular, continuous morphology (Meincke et al., 2004). The CNT-filled composites show superior mechanical properties in the tensile tests. For example, in the composites of MWCNTs filled polyvinyl alcohol (PVA) and poly(9-vinyl carbazole) (PVC), adding various concentrations of CNTs into the composites, both Young's modulus and hardness increased by factors of 1.8 and 1.6 at 1 wt.% in PVA and 2.8 and 2.0 at 8 wt.% in PVC. CNTs act as nucleation sites in the matrix, their inclusion enhances polymer crystallization. This crystal growth enhanced matrix-CNT stress transfer.

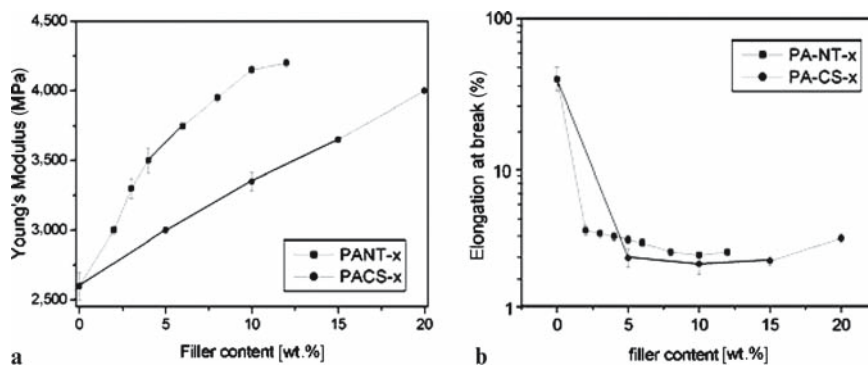


Fig. 9.11 Young's moduli (a) and elongation at break (b) of PA-Nt composites and PA-CB-composites plotted versus the filler content (Huang et al., 2006. With permission from Wiley-VCH)

The possible fatigue failure mechanisms of SWCNT in the composite were also reported (Ren et al., 2004). Possible failure modes mainly include three stages, that is, splitting of SWCNT bundles, kink formation, and subsequent failure in SWCNTs, and the fracture of SWCNT bundles. As shown in Fig. 9.12, for zigzag SWCNT, failure of defect-free tube and tubes with Stone–Wales defect of either A or B mode all resulted in brittle-like, flat fracture surface. A kinetic model for time-dependent fracture of CNTs is also reported (Satapathy et al., 2005). These simulation results are almost consistent with the observed fracture surfaces, which can be reproduced reasonably well, suggesting the possible mechanism should exist in CNT-polymer composites.

Crack toughness behavior of MWCNT/polycarbonate nanocomposites was also reported (Xiao et al., 2004; Foster et al., 2005). When 2 wt.% MWCNTs was added into the composites, the resistance to crack propagation was markedly increased compared to pure Polycarbonate. At 4 wt.% MWCNTs, a tough-to-brittle transition has been observed. The attack of crack initiation needs shorter time for nanocomposites with 4 wt.% MWCNT compared to the composites with 2 wt.% MWCNTs, which supports that a tough-to-brittle transition exists in these nanocomposites.

9.2.4.2 Water Solubility and Super-Hydrophobic Properties of CNTs

The solubility of CNTs in water or organic solvents can be improved via non-covalent or covalent interactions such as the straight dispersion in a single solvent (Peng et al., 2007), charge transfer between electron donor and acceptor, the wrapping effect of soluble polymers or cylindrical micelles, and the covalent modification including end-opening, chemical derivation, and side-walled chemical modification (Zhao et al., 2005; Panhuis et al., 2005; Li et al., 2001). For example, Poly(aminobenzene sulfonic acid) (PABS) and polyethylene glycol (PEG) were covalently attached to SWCNTs, the water-soluble graft copolymers of a fairly uniform length and diameter with a water solubility of about 5 mg/ml SWCNTs can

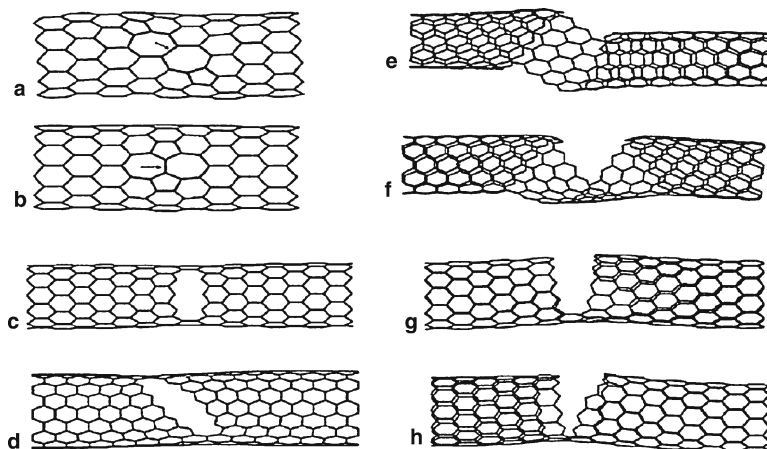


Fig. 9.12 Results of molecular mechanics simulations: (a) A Stone–Wales defect (A mode) in a zigzag SWCNT, (b) a Stone–Wales defect (B mode) in a zigzag SWCNT, the bonds with highest potential energy are indicated by arrows. Propagating cracks in: (c) A defect-free zigzag tube, and (d) defect-free armchair tube. Fracture mode of armchair tube with (e) Stone–Wales defect (A mode), and (f) Stone–Wales defect (B mode). Fracture mode of zigzag tube with (g) Stone–Wales defect (A mode), and (h) Stone–Wales defect (B mode) (Huynh et al., 2002. With permission from Wiley)

be formed, the loading of SWCNTs in the graft copolymers is almost 30% for SWNT-PABS and 71% for SWNT-PEG. This graft copolymer has a ground state, that is, a hybrid of the electronic structures of the isolated PABS and SWNT macromolecules.

CNTs own super-hydrophobic properties. The contact angle for water on an aligned CNT film by the pyrolysis of metal phthalocyanines is about 128° (Liang et al., 2002), as shown in Fig. 9.13. After the CNT film is modified through immersion in a methanol solution of hydrolyzed fluoroalkylsilane, the modified aligned CNT films show super-“hydrophobic” properties, the contact angles for water and rapeseed oil on the film are 171° and 161° , respectively. In general, the contact angle (θ) of a flat surface and that of a suitably rough surface (θ_r) is given by $\cos \theta_r = r f_1 \cos \theta - f_2$, where r is the surface roughness factor, f_1 and f_2 are fractions of CNTs and air on the aligned CNT films. The structure of aligned CNT films formed a rough surface, where the liquid may trap air and result in a composite surface effect. The very large fraction (f_1) of air and the very small fraction (f_2) of CNTs on the films are responsible for large contact angles for water and oil.

The lotus-like and honeycomb-like aligned CNT films with a combination of micro- and nanostructures were also reported (Sun et al., 2003; Choi et al., 2003). They all displayed super-hydrophobic properties as shown in Fig. 9.14. The well-aligned CNT-polymer films or coatings have potential on applications such as super-hydrophobic surfaces to textiles, coatings, gene delivery, micro-fluid channels, non-wetting liquid transfer, and so forth.

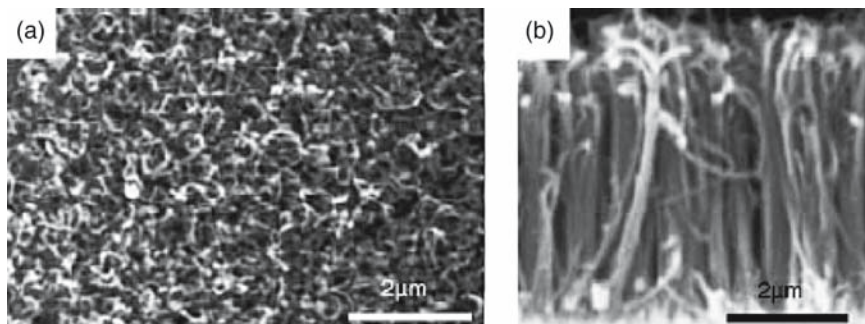


Fig. 9.13 SEM images of aligned CNT films by pyrolysis of metal phthalocyanines: (a) top view; and (b) cross-sectional view (Kam et al., 2005. With permission from all authors and Wiley)

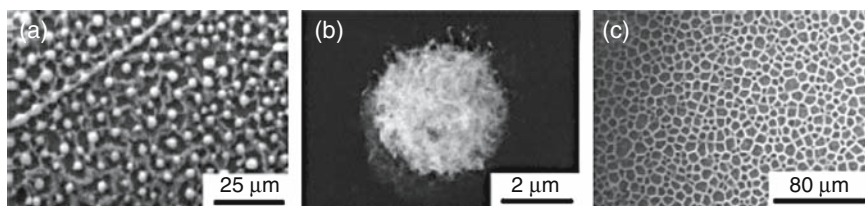


Fig. 9.14 SEM images of lotus-like and honeycomb-like aligned CNT films: (a) top view of lotus-like aligned CNT films; (b) enlarged view of single micro-papilla of the lotus-like aligned CNT films; and (c) top view of honeycomb-like aligned CNT films (Kashiwagi et al. 2002. With permission from all authors and Wiley)

9.2.4.3 Electrical and Electrochemical Properties of CNTs/Polymer Matrix

CNT-filled polymer composites own better electrical conductivity, which is closely associated with the amounts and alignment order of CNTs in polymer composites. For example, General Electric Company employed CNTs to replace conventional microscale conducting fillers, and add into the poly(phenylene oxide) (PPO)/polyamide (PA) blend for automotive mirror housings (Grunlan et al., 2004). In order to gain a satisfactory anti-static property, the loadings of CNTs is required as high as 15 wt.%. When the poly(*p*-phenylenevinylene-co-2,5-dioctoxy-*m*-phenylenevinylene) (PMPV) polymer includes 8 wt.% CNTs, its electric conductivity is dramatically increased by ten orders of magnitude. Similarly, the *in situ* polymerized polyimide (PI)/SWCNT composite films also exhibited significant conductivity enhancement by ten orders of magnitude at a very low loading (0.1 vol.%) without significantly sacrificing optical transmission.

Figure 9.15 shows how the electric conductivity of SWCNT-filled composites increases with SWCNT concentration (Park et al., 2002). The solid curve is the fit to the experimental data using the classical percolation power law. $\sigma = \sigma_0(V - V_c)^s$

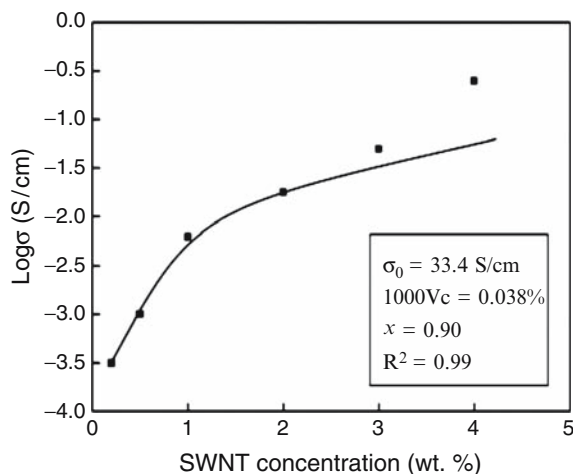


Fig. 9.15 Electrical conductivity as a function of SWNT concentration in PVAc emulsion-based matrix. The solid curve is the fit to the percolation power law (Eq. 9.1), whose parameters are shown on the graph (Keren et al., 2003. With permission from Wiley-VCH)

where σ is the composite conductivity in S cm^{-1} , σ_0 is a scaling factor related with the intrinsic conductivity of the filler, s is the power law exponent, and V_c is the volume fraction of filler at the percolation threshold. Figure 9.17 is schematics of the drying of an emulsion-based composite. Once a lot of water has evaporated, the polymer particles will assume a close-packed structure. If the drying temperature is above the minimum film formation temperature of the polymer, these particles will inter-diffuse to form a coherent film. In the presence of SWCNTs, a “segregated network” evolves because of the inability of the nanotubes to penetrate the polymer particles. This restricted organization of the conductive filler results in the low percolation threshold shown in Fig. 9.16. In the poly(vinyl acetate)(PVAc) emulsion-based CNT composite film, the CNTs almost existed in the chain of end to end shown in Fig. 9.17.

Alignment of CNTs markedly affects the electrical properties of polymer/CNT composites. For example, the nanocomposites of epoxy/MWCNTs with MWCNTs aligned under a 25 T magnetic field leads to a 35% increase in electric conductivity compared to those similar composites without magnetic aligned CNTs (Kilbride et al., 2002). Improvements on the dispersion and alignment of CNTs in a polymer matrix could markedly decrease the percolation threshold value.

Similar results are also obtained from the CNT-filled polymer blends such as CNT-filled polyethylene terephthalate (PET)/polyvinylidene fluoride, PET/nylon 6,6, PET/polypropylene, and PET/high-density polyethylene blends.

Kilbride et al. (2002; Andriotis et al., 2003) measured the alternating current (ac) and direct current (dc) conductivities of polymer-SWCNT composite thin films such as PMPV and polyvinylalcohol (PVA), the result showed that the ac conductivity

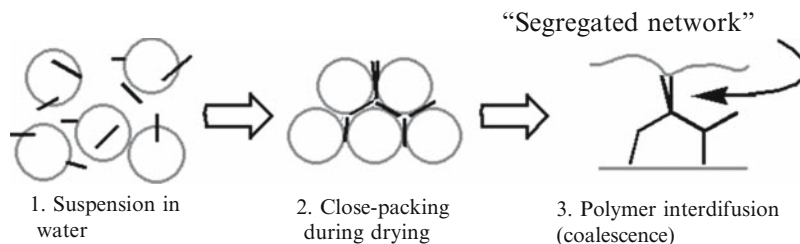


Fig. 9.16 Schematic illustration of drying process for SWNT-filled polymer emulsion. Initially the nanotubes and polymer particles are uniformly suspended in water (left). Once most of water has evaporated, the polymer particles assume a close-packed configuration with the nanotubes occupying interstitial space(center). Finally, the polymer particles will interdiffuse (i.e., coalesce) to form a coherent film, locking the SWNTs within a segregated network (right) (Keren et al., 2003. With permission from Wiley-VCH)

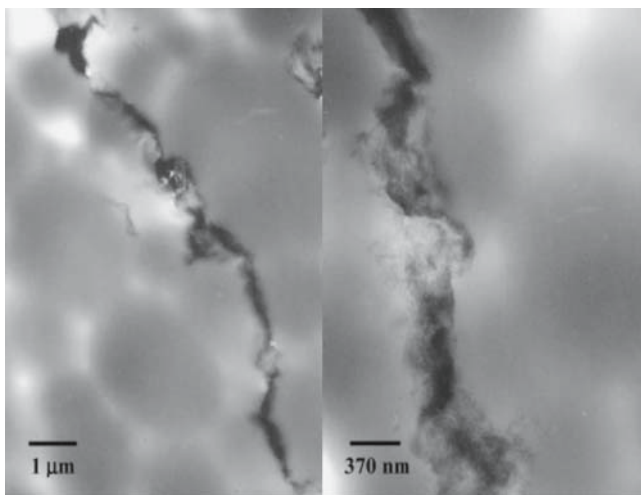


Fig. 9.17 TEM images of PVAc emulsion-based composite film, containing 3 wt.%-SWCNT, at 10,000 × (left) and 27,000 × (right) magnification (With permission from Wiley-VCH)

displayed two distinct regions, a frequency-independent region of magnitude $\sigma(0)$ at low frequency and a frequency-dependent region at higher frequency. When a thick polymer coating is wrapped around CNTs, poor electrical connection exists between CNTs, which clearly hints that charge transport is controlled by fluctuation-induced tunneling. In the high frequency regime, the CNTs' electrical conductivity increases with frequency, indicative of hopping transport. This result supports that the nonlinear resistance is dependent on the length of CNTs (Yang and Gupta, 2005).

The MWCNT-filled polystyrene composites have good electromagnetic interference shielding properties (Snow and Perkins, 2005). The shielding effectiveness of MWCNT-filled composites was frequency independent, and increased with the

increase of loaded MWCNTs. At the same filler loading, MWCNT-filled polystyrene composites exhibited higher shielding effectiveness compared to those filled with carbon nanofibers. CNTs were more effective than nanofibers in providing high EMI shielding at low filler loadings. For example, the shielding effectiveness of the composite including 7 wt.% MWCNTs may reach more than 26 dB.

In recent several years, super-capacitors are attracting more and more attention because of their high capacitance and potential applications in electronic devices. The performance of super-capacitors with MWCNTs deposited with conducting polymers as active materials is greatly enhanced compared to electric double-layer super-capacitors with CNTs due to the Faraday effect of the conducting polymer as shown in Fig. 9.18 (Valter et al., 2002). Besides those mentioned above, polymer/CNT nanocomposites own many potential applications (Breuer and Sundararaj, 2004) in electrochemical actuation, wave absorption, electronic packaging, self-regulating heater, and PTC resistors, etc. The conductivity results for polymer/CNT composites are summarized in Table 9.1 (Biercuk et al., 2002).

9.2.4.4 Optical and Photovoltaic Properties

In the polymer/CNT composites including n -conjugated polymers, the polymer becomes photo-excited under visible light and transfers electrons efficiently to CNTs, which allows the transfer of electrons into the CNTs while leaving the holes to be preferentially transported through the polymer. The interesting optical properties of CNT-based composite system arise from the low dimensionality and unique electronic band structure of CNTs (Lefebvre et al., 2004). For example, the optoelectronic properties occurred in the composites such as SWCNTs conjugated poly(3-octylthiophene) composites (Levitsky et al., 2006) and poly(*o*-anisidine) (POAS)-MWCNTs composites (Panhuis et al., 2005). The specific conductivity was markedly improved as the increment of monolayers of POAS-coated MWCNTs thin films, which showed their potentiality as a new class of materials for inorganic

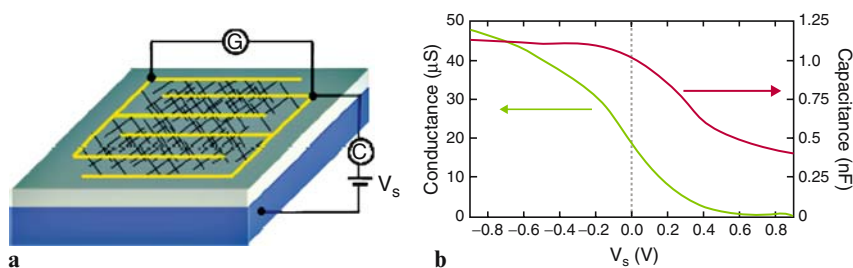


Fig. 9.18 (a) Schematic of the device, which was designed for simultaneous measurement of the SWNT network capacitance and conductance. (b) Dependence of the network capacitance (red) and conductance (green) on the substrate voltage, V_s . The network capacitance is approximately 1/4 the value of the capacitance for a parallel-plate capacitor with an equivalent area and oxide thickness (Kong et al., 2003. With the permission from American Chemical Society) (*See Color Plates*)

Table 9.1 Summary of conductivity results for polymer/CNT composites

Polymer	Filler type	Percolation threshold	Volume or surface reactivity	Processing method
PP	VGCF	9–19 wt. %	$10^0 \Omega\text{-cm}$	Melt mixing in internal mixer
PP	VGCF	5 vol. %	$10^1\text{--}10^2 \Omega\text{-cm}$	Melt mixing, injection molding
PP	VGCF	< 1 vol. %	$10^0 \Omega\text{-cm}$	Melt mixing in MiniMAX molder
PP Nylon	VGCF	< 9 vol. %	$0.15 \Omega\text{-cm}$	Melt mixing in MiniMAX molder
PP PS	MWNT	0.05 vol. %	$10^5\text{--}10^{12} \Omega/\text{square}$	Melt mixing in internal mixer
		0.25 vol. %	$10^5 \Omega/\text{square}$	
PS	MWNT	2.49 vol. %	$10^5 \Omega/\text{square}$	Film casting and spin casting
PC	PC/15% MWNT masterbatch	2 wt. %	$10^5 \Omega\text{-cm}$	Melt mixing in intermeshing co-rotating twin screw extruder
PMMA	MWNT	0.5 wt. %	$10^5 \Omega\text{-cm}$	Spin coating
	SWNT	0.4 wt. %		
PA	SWNT	3 vol. %	$10^{-1}\text{--}10^5 \Omega\text{-cm}$ at 6 vol. %	Powder technology methods

vapors detection for environmental applications. The completely soluble optically active polyaniline-MCNT composites retained the polymer's optical activity in the presence of CNTs (Goh et al., 2003, Kymakis and Amaratunga, 2002a).

Nonlinear optical organic materials such as porphyrins, dyes, and phthalocyanines provide optical limiting properties for photonic devices to control light frequency and intensity in a predictable manner. The optical limit of CNTs composites is saturated at CNTs exceeding 3.8 wt. % relative to the polymer mass (Chen et al., 2002). Polymer/CNT composites could also be used to protect human eyes, for example, optical elements, optical sensors, and optical switching (Cao et al., 2002).

So far CNTs are also widely used in organic photovoltaic devices. Doping with 6 wt. % chemical functionalized MWCNTs by grafting dodecylamine chains, the photosensitivity of oxotitanium phthalocyanine (TiOPc) is five-fold higher than that of un-doped TiOPc when exposed to 570 nm wavelength (Ago et al., 2000). It is beneficial to design photo-conductive devices with high efficiency of charge carrier generation. Clearly, the polymer/CNT nanocomposites represent an alternative class of organic semi-conducting materials promising for organic photovoltaic cells and devices with improved performance (Ago et al., 2000; Woo et al., 2000; Fournet et al., 2001; Kim et al., 2003; Kymakis and Amaratunga, 2002a and b, 2003; Hone et al., 2002).

9.2.4.5 Thermal Properties of CNT-Polymer Composites

CNTs own excellent thermal conductivity. Aligned bundles of SWCNTs show a thermal conductivity of $>200 \text{ W/m K}$ at room temperature (Biercuk et al., 2002).

Incorporation of CNTs into polymer matrix can improve the thermal properties of CNT-polymer composites. This is because CNTs could increase the glass transition, melting, and thermal decomposition temperatures of the polymer matrix. Three factors are closely associated with the thermal properties of CNT-polymer composites. One is the amount of CNTs in the composites. For example, 1 wt.% un-purified SWNTs in epoxy showed a 70% increase in thermal conductivity at 40K, rising to 125% at room temperature (Gong et al., 2000), 3 wt.% SWCNTs in epoxy showed a 300% increase in the thermal conductivity at 40K. Two is ordered dispersion of CNTs in the composites. Aligned CNTs in the composites will markedly improve the thermal conductivity more than randomly distributed CNTs in the composites. Three is additive or exterior magnetic field. For example, with a nonionic surfactant, adding 1 wt.% CNTs to epoxy increases the glass transition temperature from 63°C to 88°C (Velasco-Santos et al., 2003), in contrast, the addition of CNTs without the surfactant takes moderate effects on the glass transition temperature. Similarly, with 1 wt.% well-dispersed SWCNTs, the glass transition temperature of PMMA increased by 40°C or so (Cadek et al., 2002; Kashiwagi et al., 2002). CNTs markedly increased the thermal decomposition temperature of polymer composites. For example, the thermal decomposition temperature of polypropylene (PP) was increased by 12°C or so with 2 vol.% MWCNTs (Choi et al., 2003). Thermal and electrical properties of (CNT)-polymer composites are significantly enhanced by magnetic alignment during processing (Chen et al., 2002). Compared to the epoxy/MWCNT nanocomposites without an applied magnetic field, the alignment of MWCNTs under a 25T magnetic field has lead to a 10% increase in thermal conductivity (Wang et al., 2005). The incorporation of CNTs can improve the thermal transport properties of polymer composites, which offers an opportunity for polymer/CNT composites for usages as printed circuit boards, connectors, thermal interface materials, heat sinks, lids and housings, and high-performance thermal management from satellite structures down to electronic device packaging.

9.3 Advancement of Research Tools and Techniques

In recent years, great advance have been made in research tools and techniques. For example, the various processing methods such as melt mixing, solution processing, *in situ* polymerization, and plasma polymerization have been broadly used. Research tools, besides general tools such as high-resolution TEM, Atomic Force Microscopy, x-ray diffraction, soft lithography, total internal reflection fluorescence microscopy, laser-trapping ultra high-resolution single-molecule technique, and optical tweezer; techniques such as surface ion resonance, Nicolet Almega XR, Field Emission SEM, analytical high-resolution-TEM, three-dimensional electronic microscopy based on ultrasound wave and scanning electronic microscopy, as well as molecular dynamics simulation and modeling methods, have also been used to characterize the CNT-filled nanocomposites.

9.3.1 *Optimum Physical Blending*

To maximize the advantage of CNTs as effective reinforcements in high-strength composites, CNTs should not form aggregates and must be well dispersed in the composites. For polymer/CNT composites, the high-power dispersion methods such as ultrasound and high-speed shearing, are the simplest and most convenient to improve the dispersion of CNTs in a polymer matrix. For example, Wang et al. (2005; Xia et al., 2006; Feng et al., 2003; Deng et al., 2002) used a combined shear small-angle neutron scattering (shear-SANS) and rheo-optical method to study the dilute aqueous suspensions of SWCNT bundles dispersed using ionic surfactants. The result showed that weak shear force can induce the alignment of SWCNT bundles along the direction of flow, the degree of alignment increased with the shear rate; addition of a soluble polymer into the SWCNT suspensions may diminish shear-induced alignment.

Well-dispersed and long-term stable carbon nanotubes/polyol dispersions can also be prepared by a mechanochemical approach with the aid of a dispersing agent (Tang and Xu, 1999). Good dispersion of CNTs in polymer matrix can be achieved by means of high-power dispersion, compatibilizer, polymer-assisted blending, and surfactants (Cochet et al., 2001).

9.3.2 *In Situ Polymerization*

In situ polymerization is a method to improve dispersion and integration between the phases. The main advantage is to gain the enforcement at nanometer scale (Kong et al., 2004; Sung et al., 2004). To improve the processability, electrical, magnetic, and optical properties of CNTs, biomolecules can be attached to their surfaces by *in situ* polymerization. Lin et al. (2003) synthesized poly(phenylacetylene)-wrapped carbon nanotubes (PPA-CNTs), which were soluble in organic solvents. PPA-CNTs show strong photo-stabilization effect. The π - π bond between SWCNT and PPA backbone alters the local electric field at the surface of SWCNTs. Cochet et al. (2001; Li et al., 1996) synthesized polyaniline (PANI)/MWCNT composites by *in situ* polymerization. Their electric properties were improved markedly. High-performance structural composites based on CNTs and polymer have also been fabricated by *in situ* polymerization. For example, a core-shell hybrid nanostructure, possessing a hard backbone of MWCNTs and a soft shell of brush-like polystyrene (PS), was successfully fabricated by *in situ* atom transfer radical polymerization (ATRP), using Cu(I)Br/*N,N,N',N'',N'''*-pentamethyldiethylenetriamine (PMDETA) as the catalyst, at 100°C in diphenyl ether solution (Yoshida et al., 1995). The molecular weight of PS was well controlled. TEM images of the samples provided direct evidence for the formation of a core-shell structure, the MWCNT coated with polymer layer. To further establish the covalent linkage between PS and MWCNT moieties, the resulting PS-functionalized MWCNTs were defunctionalized by hydrolysis or by

thermal decomposition. These achieved hybrid products based on the simple grafting will pave the way for the design, fabrication, optimization, and eventual application of multifunctional CNTs-based nanomaterials.

9.3.3 Plasma Polymerization

Plasma polymerization is a technical method, in which gaseous monomers stimulated by a plasma condense on the surface of substrates as high cross-linked layers. Condition for this technological process is the presence of chain-producing atoms in the working gas. As the monomer molecules in plasma, for the most part, become shattered into reactive particles, there remain at most, only partially preserved chemical structures of the output gases in the product, which results in cross-linked and disordered structure. Structural preservation and cross-linking gradients can be controlled through process parameters, such as pressure, working gas-flow, and applied electrical output; so that one can also construct gradient layers; for example, with increasing degree of cross-linking over the thickness. This technology has also been used to functionalize CNTs. For example, rare-earth-doped Y_2O_3 was deposited on the surface of the MWCNTs by plasma polymerization (Shi et al., 2006), the resultant thin film on the surface of CNTs is less than 5 nm thick, and provide the carboxyl functional group, which can be used to conjugate with amine-functionalized quantum dots, more interesting, is that CNTs do not bleach the fluorescent signals of quantum dots on the surface of CNTs, this MWCNTs-QDs heterostructures may be used for cancer diagnosis and therapy (Shi et al., 2007). Plasma polymerization can also be used to functionalize CNTs and obtain these advantages such as hydrophobic and oleophobic surfaces with anti-soiling, self-cleaning surface, scratch-resistant coatings, corrosion protection, anti-bonding, and anti-soiling coatings.

9.3.4 Chemical Functionalization

CNTs can be chemically functionalized to achieve good dispersion in polymer/CNT composites and strong interface adhesion (Gao et al., 2004). CNTs can be assembled as ropes or bundles, and there are some catalyst residuals, bucky onions, spheroidal fullerenes, amorphous carbon, polyhedron graphite nanoparticles, and other forms of impurities during the growth process of CNTs.

CNTs can be processed such as purification based on oxidation, cutting, and activation by forming carboxylic acid and hydroxyl groups on the surface of CNTs, which can further be linked with other biomolecules to realize special function (Ajayan et al., 1994). As shown in Fig. 9.19, ferritin molecules attached to the surface of CNTs via covalent bond, the nanocomposites with ferritin molecules-functionalized CNTs own better mechanical, thermal, and electronic properties

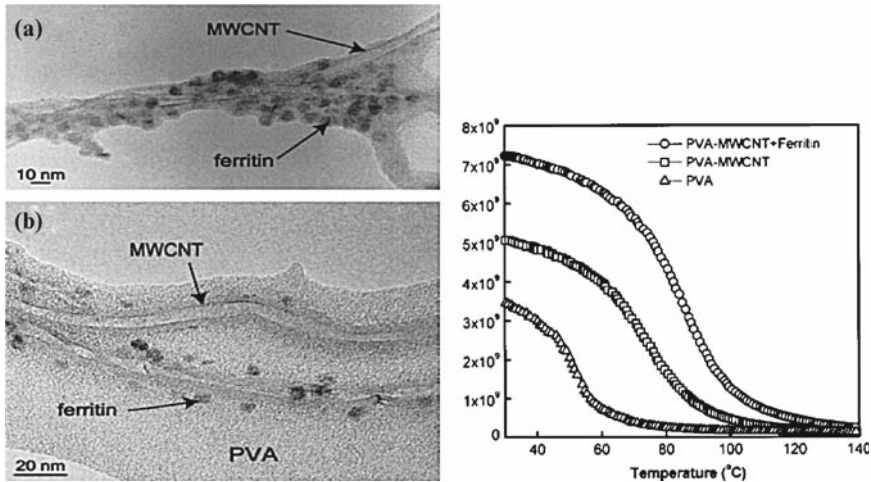


Fig. 9.19 (a) and (b) TEM micrograph of MWCNTs with attached ferritin molecules. (c) Temperature variation of storage modulus E' Published with permission from American Institute of Physics)

(Liu et al., 2005). Chemical functionalization can improve strength, thermal, electrical properties of polymer/CNT composites and will play a key role in future development and applications of CNT-based nanocomposites.

9.3.5 Alignment of CNTs

How to order CNTs in nanocomposites is a key technology challenge. The mechanical properties of polymer/CNTs composites such as stiffness and strength and functional properties such as electrical, magnetic, and their optical properties are linked directly to the alignment of carbon nanotubes in the matrix. *Ex situ* alignment of CNTs offers a general route for controlled assembly of organized nanocomposites and devices (Tang et al., 2002). The course includes three stages such as filtration, plasma-enhanced chemical vapor deposition, and template. The aligned CNTs pave a way for the development of novel nano-electronic applications. For example, CNT field effect transistors are fabricated by lithographically applying electrodes to CNTs that are either randomly distributed on a silicon substrate or orderly arranged on the substrate with the AFM (Cai et al., 2004). Integrated nano-electronic devices involve two or more CNT field effect transistors and provide the basis for large-scale integration circuits. Besides the above mentioned, there are also some methods such as force field-induced alignment of CNTs (Joshi et al., 2005), magnetic field-induced alignment of CNTs (Chaudhary

et al., 2006), electrospinning-induced alignment of CNTs (Camponeschi et al., 2007), and liquid crystalline phase-induced alignment of CNTs (Merkoci et al., 2005). PMMA and neuronal cells also can be grown on the surface of CNTs (Davoren et al., 2007; Hu et al., 2006). Highly ordered CNTs and well-aligned polymer/CNT composites own great potential on application such as field emission displays and sensors, data storage, and light-emitters, biomedical engineering.

9.3.6 Molecular Dynamics Simulation and Modeling

Molecular dynamics (MD) simulation has been broadly used for exploration of structure dynamics of biomolecules, protein/DNA interaction, and the effect of solvent as well as interaction between CNTs and biomolecules.

CNTs have extremely high stiffness and strength, and are regarded as perfect reinforcing fibers for developing a new class of nanocomposites. The use of atomistic or molecular dynamics (MD) simulations is inevitable for the analysis of such nanomaterials in order to study the local load transfers, interface properties, or failure modes at the nanoscale. Meanwhile, continuum models based on micromechanics have been shown in several recent studies to be useful in the global analysis for characterizing such nanomaterials at the micro- or macro-scale.

A fast multipole boundary element method (BEM) has been used for large-scale modeling of CNT composites (Lee et al., 2006). In this analysis, CNTs are treated as rigid fibers in the elastic matrix, the BEM is used to solve the boundary integral equations governing this rigid-inclusion problem. For example, the fast multipole BEM solved successfully the modeling of the CNT composites, with the number of CNT fibers considered reaching 16,000 and total degrees of freedom above 28.8 millions. This method is a very promising first-order tool for large-scale modeling and characterizations of CNT-based composites.

9.4 Some Major Challenges

In recent years, biomolecules functionalized CNTs technologies have made great advances. However, like any emerging field, they face many challenges. Biological molecules own special structure and function, how to fully use the structure and function of CNTs and biomolecules to fabricate novel multifunctional nanocomposites, is a great challenge. The mechanism of interaction between biomolecules and CNTs is still not clarified. How to use these laws and principles from an optimized biosystem for fabricating novel multifunctional or homogenous nanocomposites with CNTs, is also a great challenge. The processing, characterization, interface problems, nanotube availability, nanotube tailoring, and the mechanisms governing the behavior of these nanoscale composites is a great challenge for present existing techniques. For example, how to align CNTs in polymer matrix along identical direction is a great challenge.

CNTs show sign of toxicity. Although biomolecules functionalized CNTs can be cleaned from blood circulation system by renal secretion, so far the course of CNTs metabolism in cells or environment, and the potential measurements to reduce CNTs' toxicity, is still not clear. How to clarify those mechanisms and reduced risk measurements associated with CNTs toxicity is a great challenge.

9.5 Application of Biomolecules: CNTs Composites

Biomolecules-functionalized CNTs provide an exciting application prospects. CNTs can be employed to obtain low-weight nanocomposites with super mechanical, electrical, thermal, and multifunctional properties, which provide advantages in a variety of applications including electrostatic dissipative materials, advanced materials with combined stiffness, strength and impact for aerospace or sporting goods, composite mirrors, automotive parts that require electrostatic painting and automotive components with enhanced mechanical properties, antifouling interface, and own great potential on applications such as developing nanodevices, biosensors, electronic sequencing and delivery system, etc.

9.5.1 Gene/Drug Delivery System

Development of a safe and high-efficient nonviral delivery system is a very important goal in gene therapy. Despite many efforts that have been made, to date the delivery efficiencies of these nonviral vectors still need to be improved. For example, carbon nanotubes, including both single-walled and multi-walled, have been actively functionalized with different biological molecules and investigated as possible multifunctional biological transporters (Pantarotto et al., 2004). Previous reports show that single-walled carbon nanotubes can take antisense oligonucleotides (Cui et al., 2007), siRNA (Kam et al., 2005), and peptides (Pantarotto et al., 2004) across cell membrane and enter the cell nucleus, and can also be used as near-infrared agents for selective cancer cell destruction. However, in these reports, all single-walled carbon nanotubes were directly conjugated with biological molecules via covalent or disulfide bonds. These methods are feasible, but the number of molecules completely conjugated with carbon nanotubes is very small and it is very difficult to fabricate final pure products. Therefore, applications of these methods in clinical therapy are very limited. In addition, carbon nanotubes also have been confirmed to have potential risk for both the cells and the environment (Sato et al., 2005; Cui et al., 2005; Tian et al., 2006; Carrero-Sánchez et al., 2006; Stone and Donaldson, 2006). Therefore, as long as we use carbon nanotubes for biological and medical engineering, finding a way to enhance their safety is very important.

Dendrimers are a novel special class of organic molecules: they can take different functional groups through a series of chemical modifications, and their interior

cavities can serve as storage areas for a lot of genes or drugs (Lee et al., 2006; Hong et al., 2006). Dendrimers may be a good nonviral delivery vector because it has the advantages of safety, simplicity of use, and ease of mass production compared with viral vectors, which are inherently risky for clinical use (Majoros et al., 2006, 2005). Our previous work confirmed that the No. 5 generation of polyamidoamine (PAMAM) dendrimer-modified magnetic nanoparticles can markedly enhance the delivery efficiency for antisense oligonucleotides (Pan et al., 2007), dendrimer-modified single-walled carbon nanotubes can reduce cytotoxicity and enhance the cellular uptake of the nanoparticles (Pan et al., 2006, 2007).

Although CNTs show signs of toxicity to cells, biomolecules-modified CNTs show low or no toxicity to cells. Therefore, biomolecules-functionalized CNTs should be a better gene/drug delivery system. Singh and his colleagues (Singh et al., 2006) reported that, biomolecules-functionalized SWCNTs can be cleaned from blood circulation system by renal excretion route, and do not retain in any of the reticuloendothelial system organs including liver or spleen. These results fully demonstrated that the biomolecules-functionalized CNTs can be used as gene/drug delivery systems. Therefore, future work should concentrate on animal experiments to confirm bio-safety of use of CNTs as delivery system for disease therapy.

9.5.2 Luminescent CNTs and Molecular Imaging

Metal nanoparticles such as magnetic nanoparticles, quantum dots, etc. have potential application in disease diagnosis and therapy. Developing new hybrid materials consisting of metal nanoparticles and CNTs have great potential application in cancer diagnosis and therapy. For example, quantum dots have been used successfully in cellular imaging (Fig. 9.21) (Kaul et al., 2003; Dintz et al., 2005), immunoassays (Shino et al., 2005), DNA hybridization (Han et al., 2001), and optical barcoding (Jares-Erijman and Jovin, 2003). Quantum dots also have been used to study the interaction between protein molecules or detect the dynamic course of signal transduction in live cells by Fluorescence Resonance Energy Transfer (FRET) (Huang et al., 2006; Alivisato, 2004). CNTs own unique holes that can be used for gene or drug storage. CNTs binding with quantum dots together can provide one kind of novel nanomaterials – luminescent carbon nanotubes (Pan et al., 2006; Shi et al., 2006, 2007), have potential applications in molecular imaging and real-time detection. These synthesized luminescent CNTs (Fig. 9.20) provide a new functional platform for bioanalytical sciences and biomedical engineering.

9.5.3 Biocatalyst Systems

Since the large-scale application of immobilized enzymes in the 1960s, substantial research efforts have aimed to optimize the structure of carrier materials for better catalytic efficiency. To date, nanoscale materials may provide the upper limits in

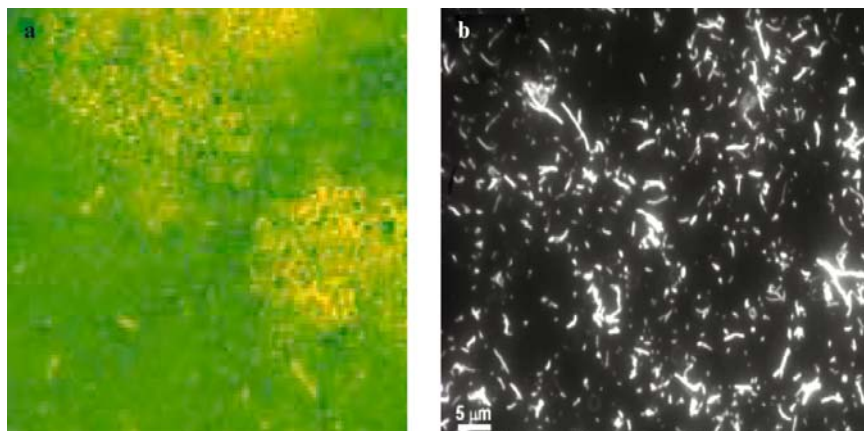


Fig. 9.20 Luminescent carbon nanotubes (a) Cy3 labeled antisense myc-modified SWCNTs; (b) quantum dots-modified MWCNTs (With permission from American Scientific publisher and Wiley-VCH) (*See Color Plates*)

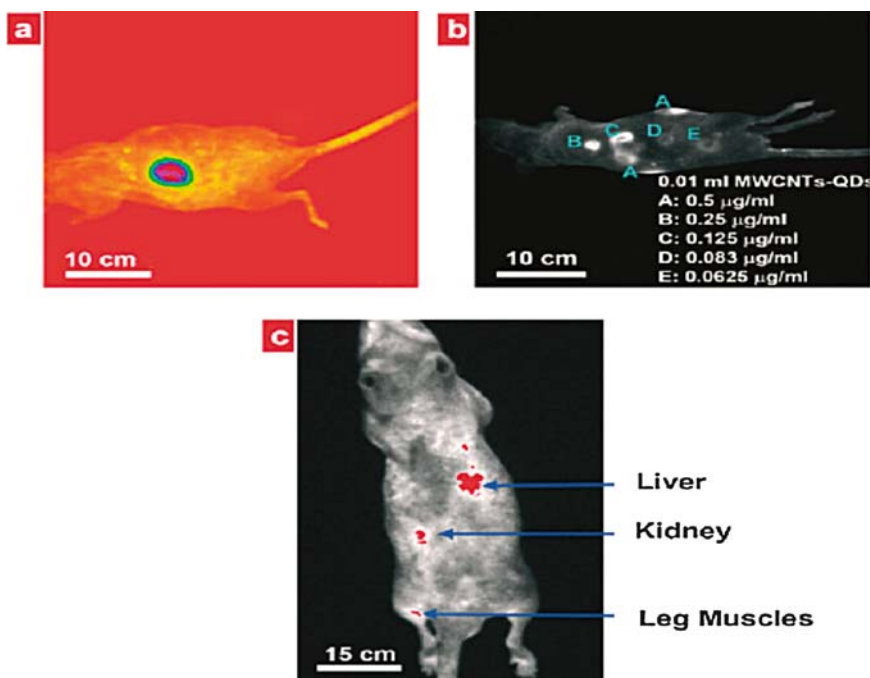


Fig. 9.21 *In vivo* images of MWCNTs-QDs ($0.5 \mu\text{g ml}^{-1}$ in PBS) in mice injected at different body regions: a) MWCNTs attached with CdSe/Zns quantum dots (emission of 600 nm) at middorsal location; b) MWCNTs attached with CdSe/Zns quantum dots at ventrolateral locations, the suspensions were diluted by PBS at various concentrations as indicated (A through E); c) MWCNTs attached with InGaP/ZnS quantum dots (emission of 680 nm, $0.25 \mu\text{g ml}^{-1}$ in PBS) in liver, kidney, and leg muscles. All images were taken successfully in 2 min under epi-UV illuminator with excitation of 435nm. (Shi et al. 2007). Published with permission from Wiley-VCH (*see Color Plates*)

balancing the key factors that determine the efficiency of biocatalysts, including surface area, mass transfer resistance, and effective enzyme loading. Various nanomaterials such as CNTs have shown potential for revolutionizing the preparation and use of biocatalysts (Rege et al., 2004; Yim et al., 2005; Wang, 2006; Asuri et al., 2007). Beyond high area/volume ratios, nanoscale biocatalyst systems exhibit unique behaviors that distinguish them from traditional immobilized systems. The Brownian motion of nanoparticles, confining effect of nanopores and self-assembling behaviors of discrete nanostructures are providing exciting opportunities in this field. The development of catalyst systems that are highly stable and efficient, capable of self-targeting or that function as molecular machines to catalyze multiple reactions is rapidly reshaping our vision of biocatalysts.

For example, Rege and his colleagues (Rege et al., 2006) reported that SWCNTs can reduce to leach out of enzyme from films, and improve the activity and stability of enzyme-containing polymer films. They also observed that the enzyme activity highly depends on time, polymer type, and the amount of SWCNTs. This possible mechanism is the chemical interaction of hydrophobic carbon with polymers and/or the high surface area of the SWCNTs, which reduces enzyme leaching from the film, yet provides effective pore sizes large enough to allow the enzymatic substrate to diffuse to the biocatalyst, thereby allowing the film to be biocatalytically active. As the amount of SWCNTs increases in the films, exposed hydrophobic and structured surface area of the SWCNTs incorporated into polymer film also increased, thus the film activity also increases. This phenomenon has potential use as selective biocatalysts for bioengineering, biotransformations, antifouling surfaces, and biosensors.

9.5.4 Active Antifouling Films

Protein fouling of surfaces has become a major problem in medical implants, diagnostic devices, and bio-membranes for downstream processing and water filtering. These proteins can help bacteria and cells attach to surfaces, resulting in the growth of biofilms that can significantly reduce the performance of devices or instruments. Thus, it is very necessary to design and fabricate non-fouling surfaces to resist adsorption of proteins. Except traditional methods, for example, functionalization surfaces with hydrophilic polymers such as PEG, the composites of SWCNTs and polymers can be used as hosts for proteases and can prevent 99% nonspecific protein adsorption contamination on the surface of medical instruments. This result also highly hint that we can use SWCNT-based enzyme composites to degrade other polymers such as bacterial polysaccharides and adhesive proteins attached to the surfaces of ship or other devices (Asuri et al., 2007). The other method is to use plasma polymerization to deposit a thin layer of specific film on the SWCNTs, and then use the modified film to realize antifouling function. Under realistic conditions, materials are susceptible to chemical degradation. How to fully use the advantages of SWCNTs to resist fouling is also a great challenge.

9.5.5 Biosensor

Polymer-CNTs composites can obtain high electrical conductivity and good mechanical properties, which offer the exciting chance of developing ultrasensitive, electrochemical biosensors. For example, the glucose biosensor (Chen et al., 2003; Luo et al., 2005; Dillon et al., 1997) was constructed by incorporation of SWCNTs modified with enzyme into redox polymer hydrogels. The glucose biosensor exhibited better sensitivity and specificity compared with traditional glucose biosensor.

Biomolecules-functionalized CNTs can result in characteristic electric conductivity changes of CNTs (Hou et al., 2003), which may be developed into specific biosensor for ultrasensitive detection of biomolecules such as DNA molecules, bacteria and virus, etc. We also observed that oligo DNA-filled SWCNTs appeared as characteristic Electric Resistance peaks as shown in Fig. 9.22, which also may be used as biosensor to detect biomolecules or sequence DNA sequences.

9.5.6 Hydrogen Storage

Carbon nanotubes can draw up liquids by capillarity. Yoo, et al. (2001; Valentini et al., 2005) reported that hydrogen gas can be condensed to high density inside

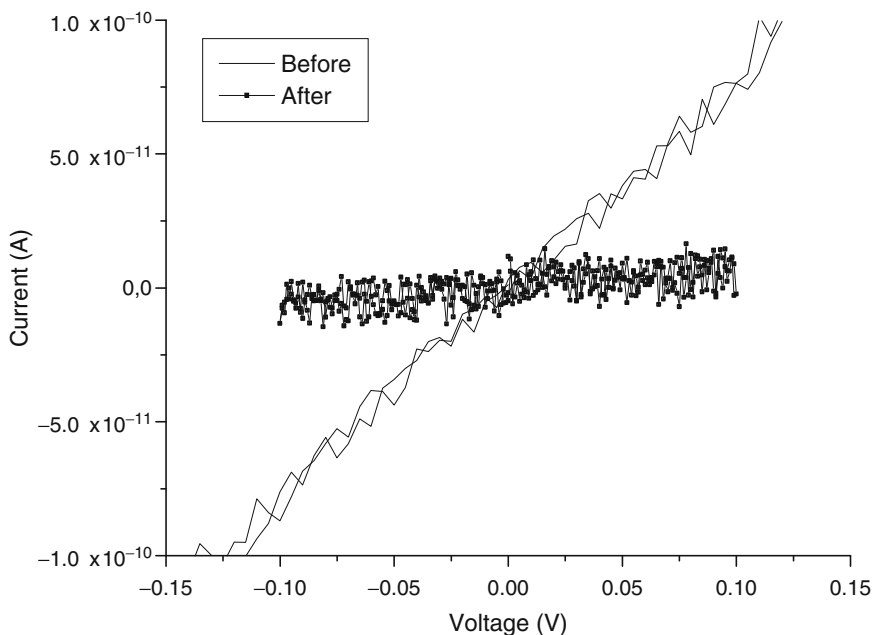


Fig. 9.22 ERs of single-walled carbon nanotubes before and after being filled with c-myc oligonucleotides (With permission from American Scientific publisher)

SWCNTs, which might be effective as a hydrogen-storage material for fuel-cell electric vehicles. Hou et al. (2003) reported that MWCNTs with different mean outer diameters in the range of 13–53 nm can be used for hydrogen storage. The hydrogen capacity of the purified and pretreated MWCNTs was proportional to their diameter, and the hydrogen in all types of MWCNTs could not be completely desorbed at room temperature and ambient pressure. These small “carbon islands” might be the main hydrogen adsorption site in MWCNTs. Yoo et al. (2001) employed CNTs and highly oriented pyrolytic graphite (HOPG) for atomic hydrogen storage. Defect sites on the surface of CNTs were the adsorption sites of atomic hydrogen. Pd catalysts are then deposited on CNT surfaces for dissociation of H₂ into atomic hydrogen, which spills over to the defect sites. In the best case, 1.5 wt.% of hydrogen is stored in the defective CNT with Pd particles at 1 atm and 573 K.

9.5.7 Scaffolds in Tissue Engineering

The polymer/SWCNT composites can be used as Scaffolds in tissue engineering. The donor–acceptor interactions can be used to assemble thin polymer/SWCNT films stepwise. This method also can be expended to more thermally and oxidatively stable polymer systems. For example, the P4VP/SWCNT films can be used as scaffolds for the synthesis of novel hybrid structures (Correa-Duarte et al., 2004). The polyethyl-enimine (PEI)-SWCNTs composites were used as a substrate for cultured neurons, and promoted neurite outgrowth and branching (Rouse et al., 2004). Correa-Duarte et al. (2004; Landi et al., 2005) reported that 3D-MWCNT-based networks are ideal candidates for scaffolds/matrices in tissue engineering.

9.5.8 Biocompatible Electrode Arrays

The polyimide-CNT composites have good biocompatibility and conductive properties, which can be used to fabricate the electrode arrays, and enhance their biocompatibility. For example, they can be used as the stimulator embedded in the blind eyes, and can be used for the electrode arrays transplanted in the human body without damaging human organs and tissues (Tulevski et al., 2007).

9.5.9 The Polymeric Solar Cells

The QD-MWNT hybrid structures were formed via the assembly of quantum dot (QD) on the surface of MWNTs in aqueous solution (Jares-Erijman and Jovin, 2003), which shows an excellent solubility in aqueous solution, and owns potential application in bioassay, bio-conjugation, and biosensors as well as solar cell. For example, incorporation of QDs and SWNTs into the poly(3-octylthiophene)-(P₃OT)

composites, facilitated exciton dissociation and carrier transport in a properly structured device (Breuer and Sundararaj, 2004). The polymer composites including QDs, SWCNTs and the P_3OT complexes have been employed to fabricate solar cells, showing limited efficiency due to recombination and surface effects. However, the optical absorption spectra for these nanomaterial–polymeric composites showed a marked enhancement in capturing the available irradiance of the air mass zero (AM_0) spectrum.

9.5.10 Thermal Stability Materials

CNTs can enhance the thermal properties of CNT–polymer nanocomposites. The reinforcing function is closely associated with the amount and alignment of CNTs in the composites. Well-dispersed and long-term stable carbon nanotubes/polymer composites own higher modulus and better thermal property as well as better electronic conductivity (Valter et al., 2002; Biercuk et al., 2002). Both SWNT and MWNT can improve the thermal stability and thermal conductivity of polymer, the polymer–CNT composites can be used for fabricating resistant-heat materials.

9.5.11 Optically Driven Nanotube Actuators

Optically driven actuators have been successfully fabricated from SWCNT–polymer composite sheets (Lu et al., 2005; Cui, 2007; Kymakis et al., 2002; Peng et al., 2007). Like natural muscles, the micrometer scale actuators are composed of the millions of individual nanotube actuators, which were processed into macroscopic length scales and bonded to an acrylic elastomer sheet and finally form an actuator, which can generate higher stress than natural muscles and higher strains than high-modulus piezoelectric materials. An optically actuated nanotube gripper can manipulate small objects. This actuation technology overcomes some fundamental limitations such as the use of high voltages or electrochemical solutions for actuation, opening up the door for developing the remote light-induced actuation technologies. As shown in Fig. 9.23, the actuator owns the good optical reaction properties.

9.6 Concluding Remarks

Functionalization of CNTs with biomolecules provides novel opportunities for developing the CNT-based bio-nanotechnology. CNTs in the Polymer/CNT composites can improve mechanical, electric, thermal, electrochemical, optical,

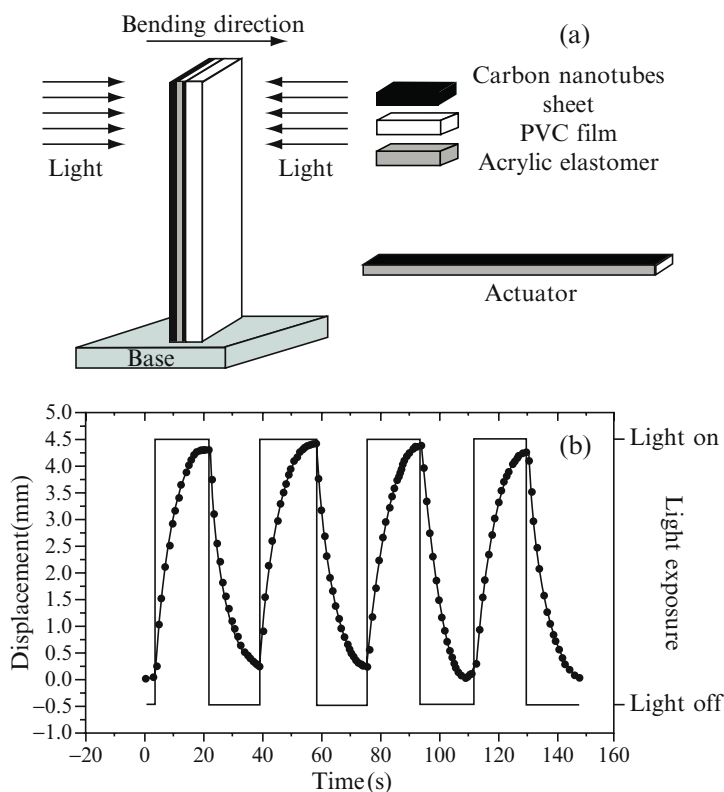


Fig. 9.23 (a) A cantilever vertically anchored on a base. The cantilever is composed of an actuator (shown in the right lower part) and a 100 μm thick PVC film. (b) The displacement of the cantilever measured when light was turned on and off (Snow and Perkins, 2005. With permission from IOP Publishing)

magnetic and super-hydrophobic properties, and own potential application in industry, defense and biomedical engineering. Effects of CNTs on human health and environment also have attracted extensive attentions, as CNTs show the sign of toxicity. However, biomolecules-functionalized carbon nanotubes exhibit low toxicity and can be cleaned from blood circulation system by renal secretion, suggesting biomolecules functionalized CNTs have potential as gene/drug delivery system. Studies these measurements to further reduce toxicity or risk of CNTs have become very urgent. How to fully use the advantages of CNTs and biomolecules to fabricate novel multifunctional composites or nanodevices are of great challenge. Future work should concentrate on furtherly clarifying the mechanism of interaction between CNTs and biomolecules and discovering novel potential properties as well as using those novel properties to exploit potential applications.

Acknowledgments This work is supported by 863 Project (No.2007AA022003), Shanghai Pujian Plan Project (No.06PJ14049), and Shanghai Municipal Commission for Science and Technology (Grant No.03DZ14025 and No.054119527).

References

- Ago JERH, Shaffer MSP, Ginger DS, Windle AH, Friend RH (2000). Electronic interaction between photoexcited poly(p-phenylene vinylene) and carbon nanotubes. *Phys. Rev. B* 61: 2286–2290.
- Ago G, Guo Z, Carroll DL, Sun YP (2000). Strong luminescence of solubilized carbon nanotubes. *J. Am. Chem. Soc.* 122: 5879–5880.
- Alivisato P (2004). The use of nanocrystals in biological detection. *Nature Biotechnol.* 22: 47–52.
- Ajayan PM, Stephen O, Colliex C, Trauth D (1994). Aligned carbon nanotube arrays formed by cutting a polymer resin–nanotube composite. *Science* 265: 1212–1214.
- Ajayan PM, Schadler LS, Braun PV (2003). *Nanocomposite science and technology*. Wiley-VCH/Verlag GmbH & Co. KGaA, Weinheim, Germany.
- Andriotis AN, Menon M, Chernozatonskii L (2003). Nonlinear resistance dependence on length in single-wall carbon nanotubes. *Nano Lett.* 3: 131–134.
- Asuri P, Karajanagi SS, Kane RS, Dordick JS (2007). Polymer-nanotube –enzyme composites as active antifouling films. *Small* 3: 50–53.
- Bahr JL, Tour JM (2002). Covalent chemistry of single-wall carbon nanotubes. *J. Mater. Chem.* 12: 1952–1958.
- Barnard AS (2006). Nanohazards: knowledge is our first defence. *Nature Mater.* 5: 245–248.
- Bashir R (2004). BioMEMS: state-of-the-art in detection, opportunities and prospects. *Adv Drug Deliv Rev.* 56: 1565–1586.
- Batalia M, Protozanova E, Macgregor R, Erie D (2002). Self-assembly of frayed wires and frayed-wire networks: nanoconstruction with multistranded DNA. *Nano Lett.* 2: 269–274.
- Biercuk MJ, Llaguno MC, Radosavljevic M, Hyun JK, Johnson AT (2002). Morphological and mechanical properties of carbon-nanotube-reinforced semicrystalline and amorphous polymer composites. *Appl. Phys. Lett.* 80: 2767–2769.
- Breuer O, Sundararaj U (2004). Big returns from small fibers: a review of polymer/carbon nanotube composites. *Polymer Composites* 25: 630–645.
- Cadek M, Coleman JN, Barron V, Hedicke K, Blau WJ (2002). Morphological and mechanical properties of carbon-nanotube-reinforced semicrystalline and amorphous polymer composites. *Appl. Phys. Lett.* 81: 5123–5125.
- Cai H, Bashar MT, Picot JJC (2004). Thermal and mechanical anisotropy in compression molded carbon fiber/resin composites. *Polymer Composites* 26: 684–688.
- Camponeschi E, Vance R, Al-Haik M, Garmestani H, Tannenbaum R (2007). Properties of carbon nanotube-polymer composites aligned in a magnetic field. *Carbon* 45: 2037–2046.
- Cao L, Chen HZ, Wang M, Sun JZ (2002). Photoconductivity study of modified carbon nanotube/xotitanium phthalocyanine composites. *J. Phys. Chem. B* 6: 8971–8975.
- Carrero-Sánchez JC, Eliás AL, Mancilla R, Arrellín G, Terrones H, Laclette JP, Terrones M (2006). Biocompatibility and toxicological studies of carbon nanotubes doped with nitrogen. *Nano Lett.* 6: 1609–1616.
- Casey A, Davoren M, Herzog E, Lyng FM, Byrne HJ, Chambers G (2007). Spectroscopic analysis confirms the interaction s between single-walled carbon nanotubes and various dyes commonly used to assess cytotoxicity. *Carbon* (in press).
- Casey A, Davoren M, Herzog E, Lyng FM, Byrne HJ, Chambers G (2007). Probing the interaction of single walled carbon nanotubes within cell culture medium as a precursor to toxicity testing. *Carbon* 45: 34–40.

- Correa-Duarte MA, Wagner N, Rojas-Chapana J, Morsczech C, Thie M, Giersig M (2004). Fabrication and biocompatibility of carbon nanotube-based 3D networks as scaffolds for cell seeding and growth. *Nano Lett.* 4: 2233–2236.
- Chen RJ, Bangsaruntip S, Drouvalakis KA, Kam NWS, Shim M, Li Y, Kim W, Utz PJ, Dai HJ (2003). Noncovalent functionalization of carbon nanotubes for highly specific electronic biosensors. *Proc. Natl. Acad. Sci. USA.* 100: 4984–4989.
- Chaudhary S, Kim JH, Ozkan M (2006). Controlled electron-beam-induced large-scale alignment of carbon nanotubes at metal electrodes. *J. Nanoelectron. Optoelectron.* 1: 211–214.
- Chen RJ, Zhang Y, Wang D, Dai H (2001). Noncovalent sidewall functionalization of single-walled carbon nanotubes for protein immobilization. *J. Am. Chem. Soc.* 123: 3838–3839.
- Chen YC, Ravivakar NR, Schadler LS, Ajayan PM, Zhao YP, Lu TM, Wang GC, Zhang XC (2002). Ultrafast optical switching properties of single-wall carbon nanotube polymer composites at 1.55 μm . *Appl. Phys. Lett.* 81: 975–977.
- Chen J, Tao ZL, Li SL, Fan XB, Chou S-L (2002). Synthesis of TiSe_2 Nanotubes/Nanowires. *Adv. Mater.* 14: 1379–1382.
- Choi ES, Brooks JS, Eaton DL, Al-Haik MS, Hussaini MY, Garmestani H, Li D, Dahmen K (2003). Enhancement of thermal and electrical properties of carbon nanotube polymer composites by magnetic field processing. *J. Appl. Phys.* 94: 6034–6039.
- Cochet M, Maser WK, Benitor A, Callejas A, Martinez MT, Benoit JM, Schreiber J, Chauvet O (2001). Synthesis of a new polyaniline/nanotube composite: “*in-situ*” polymerisation and charge transfer through site-selective interaction. *Chem. Commun.* 16: 1450–1451.
- Cui D, Tian F, Coyer SR, Wang J, Pan B, Gao F, He R and Zhang Y (2007). Effects of antisense-myc-conjugated single-walled carbon nanotubes on HL-60 cells. *J. Nanosci. Nanotech.* 7: 1639–1641.
- Cui D, Ozkan CS, Ravindran S, Yong K, Gao H (2004a). Encapsulation of Pt-labelled DNA molecules inside carbon nanotubes. *MCB* 1: 113–121.
- Cui D, Tian F, Kong Y, Titushikin I, Gao H (2004b). Effects of single-walled carbon nanotubes on Polymerase Chain Reaction (2004). *Nanotechnology* 15: 154–157.
- Cui D, Tian F, Ozkan CS, Wang M, Gao H (2005). Effect of single-walled carbon nanotubes. *Toxicol. Lett.* 155: 73–85.
- Cui D (2007). Advances and prospects of biomolecules functionalized carbon nanotubes. *J. Nanosci Nanotech* 7: 1298–1314.
- Davoren M, Herzog E, Casey A, Cottineau B, Chambers G, Byrne HJ, Lyng FM (2007). In vitro toxicity evaluation of single walled carbon nanotubes on human A549 lung cells. *Toxicology in Vitro* 21: 438–448.
- Deng JG, Ding XB, Zhang WC, Peng YX, Wang JH, Long XP, Li P, Chan AS (2002). Carbon nanotube–polyaniline hybrid materials. *European Polymer Journal* 38: 2497–2501.
- Dillon A, Jones KM, Bekkedahl TA, Kiang CH, Bethune DS, Heben MJ (1997). Storage of hydrogen in single-walled carbon nanotubes. *Nature* 386: 377–379.
- Dintz IL, Uyeda HT, Goldman ER, Mattoussi H (2005). Quantum dot bioconjugates for imaging, labelling and sensing. *Nature Mater.* 4: 435–446.
- Dresselhaus MS, Dresselhaus G, Avouris P (2000). In carbon nanotubes: synthesis, structure, properties and application, Chap. 13. Springer, Berlin, Germany.
- Dresselhaus MS, Dresselhaus G, Eklund PC (1996). Science of fullerenes and carbon nanotubes. Academic Press, San Diego, USA.
- Feng W, Bai XD, Lian YQ, Liang J, Wang XG, Yoshino K (2003). Well-aligned polyaniline/carbon-nanotube composite films grown by in-situ aniline polymerization. *Carbon* 41: 1551–1557.
- Foley S, Crowley C, Smaih M, Bonfils C, Erlanger BF, Seta P, Larroque C (2002). Cellular localization of a water-soluble fullerene derivative. *Biochem. Biophys. Res. Commun.* 294: 116–119.
- Foster J, Singamaneni S, Kattumenu R, Bliznyuk V (2005). Dispersion and phase separation of carbon nanotubes in ultrathin polymer films. *J. Colloid and Interface Science* 287: 167–172.

- Fournet P, Coleman JN, Lahr B, Drury A, Blau WJ, O'Brien DF, Hörhold HH (2001). Enhanced brightness in organic light-emitting diodes using a carbon nanotube composite as an electron-transport layer. *J. Appl. Phys.* 90: 969–975.
- Gao JB, Yu AP, Itkis ME, Bekyarova E, Zhao B, Niyogi S, Haddon RC (2004). Large-scale fabrication of aligned single-walled carbon nanotube array and hierarchical single-walled carbon nanotube assembly. *J. Am. Chem. Soc.* 126: 16698–16699.
- Gao H, Kong Y, Cui D, Ozkan CS (2003). Spontaneous insertion of DNA oligonucleotides into carbon nanotubes. *Nano. Lett.* 3: 471–473.
- Gao H, Shi W, Fraund LB (2005). Mechanics of receptor-mediated endocytosis. *Proc. Natl. Acad. Sci. USA.* 102: 5469–5474.
- Georgakilas V, Pellarini F, Prato M, Guldi DM, Melle-Franco M, Zerbetto F (2002). Supramolecular self-assembled fullerene nanostructures. *Proc. Natl. Acad. Sci. USA.* 99: 5075–5080.
- Goho A (2004). Tiny trouble: nanoscale materials damage fish brains. *Science News Online* 165: 211.
- Gong XY, Liu J, Baskaran S, Voise RD, Young JS (2000). Surfactant-assisted processing of carbon nanotube/polymer composites. *Chem. Mater.* 12: 1049–1052.
- Goh HW, Goh SH, Xu GQ, Lee KY, Yang GY, Lee YW, Zhang WD (2003). Optical limiting properties of double-C₆₀-end-capped poly(ethylene oxide), double-C₆₀-end-capped poly(ethylene oxide)/poly(ethylene oxide) blend, and double-C₆₀-end-capped poly(ethylene oxide)/multiwalled carbon nanotube composite. *J. Phys. Chem. B* 107: 6056–6062.
- Grunlan JC, Mehrabi AR, Bannon MV, Bahr JL (2004). Water-based single-walled-nanotube-filled polymer composite with an exceptionally low percolation threshold. *Adv. Mater.* 16: 150–154.
- Guo ZJ, Sadler PJ, Tsang SC (1998). Immobilization and visualization of DNA and proteins on carbon nanotubes. *Adv. Mater.* 10: 701–703.
- Hafner JH, Cheung CL, Woolley AT, Lieber CM (2001). Structural and functional imaging with carbon nanotube AFM probes. *Progress in Biophysics & Molecular Biology* 77: 73–110.
- Han M, Gao X, Su JZ, Nie SM (2001). Quantum-dot-tagged microbeads for multiplexed optical coding of biomolecules. *Nature Biotechnol.* 19: 631–635.
- Hong S, Leroueil PR, Janus EK, et al. (2006). Interaction of polycationic polymers with supported lipid bilayers and cells: nanoscale hole formation and enhanced membrane permeability. *Bioconjug. Chem.* 17: 728–34.
- Hone J, Llaguno MC, Biercuk MJ, Johnson AT, Batlogg B, Benes Z, Fischer JE (2002). Thermal properties of carbon nanotubes and nanotube-based materials. *Applied Physics A-Materials Science & Processing* 74: 339–343.
- Hoet PH, Bruske-Hohlfeld I, Salata OV (2004). Nanoparticles - known and unknown health risks. *J. Nanobiotechnol.* 2: 12
- Hou PX, Xu ST, Yang QH, Liu C, Cheng HM (2003). Hydrogen adsorption/desorption behavior of multi-walled carbon nanotubes with different diameters. *Carbon* 41: 2471–2476.
- Huang XY, Li L, Qian HF, Dong CQ, Ren CJ (2006). A resonance energy transfer between chemiluminescent donors and luminescent quantum-dots as acceptors (CRET). *Angew. Chem. Int. Ed.* 45: 5140–5143.
- Hu H, Ni YC, Mandal SK, Montana V, Zhao N, Haddon RC, Parpura V (2005). Polyethyleneimine functionalized single-walled carbon nanotubes as a substrate for Neuronal Growth. *J. Phys. Chem. B* 109: 4285–4289.
- Huynh U, Dittmer J, Alivisatos A (2002). Hybrid nanorod polymer solar cells. *Science* 295: 2425–2427.
- Ikkala O, Brinke G (2002). Functional materials based on self-assembly of polymeric supramolecules. *Science* 295: 2407–2413.
- Iijima S (1991). Helical microtubules of graphitic carbon. *Nature* 354: 56–58.
- Jares-Erijman EA, Jovin TM (2003). FRET imaging. *Nature Biotechnol.* 21: 1387–1395.
- Joshi PP, Merchant SA, Wang YD, Schmidtke DW (2005). MEMS sensor material based on polypyrrole-carbon nanotube nanocomposite: film deposition and characterization. *J. Micromech. Microengin.* 5: 2019–2027.

- Kam NWS, Liu Z, Dai H (2006). Carbon nanotubes as intracellular transporters for proteins and DNA: an investigation of the uptake mechanism and pathway. *Angew. Chem. Int. Ed. Engl.* 45: 577–581.
- Kam NWS, O'Connell M, Wisdom JA, Dai H (2005). Carbon nanotubes as multifunctional biological transporters and near-infrared agents for selective cancer destruction. *Proc. Natl. Acad. Sci. USA.* 102: 11600–11605.
- Karajanagi SS, Vertegel AA, Kane RS, Dordick JS (2004). Structure and function of enzymes adsorbed onto single-walled carbon nanotubes. *Langmuir.* 22: 211–213.
- Kashiwagi T, Grulke E, Hilding J, Harris R, Awad W, Douglas J (2002). Thermal degradation and flammability properties of poly(propylene)/carbon nanotube composites. *Macromol. Rapid Commun.* 23: 761–765.
- Kaul Z, Yaguchi T, Kaul SC, Hirano T, Wadhwa R, Mortalin TK (2003). Imaging in normal and cancer cells with quantum dot immuno-conjugates. *Cell Research* 13: 503–507.
- Keren K, Berman RS, Buchstab E, Sivan U, Braun E (2003). DNA-templated carbon nanotube field-effect transistor. *Science* 302: 1380–1382.
- Kilbride BE, Coleman JN, Fournet P, Cadek A, Hutzler S, Roth S, Blau WJ (2002). Experimental observation of scaling laws for alternating current and direct current conductivity in polymer-carbon nanotube composite thin films. *J. Appl. Phys.* 92: 4024–4030.
- Kim J, Grate JW (2003). Single-enzyme nanoparticles armored by a nanometer-scale organic/inorganic network. *Nano Lett.* 3: 1219–1222.
- Kim JY, Kim M, Kim H, Joo J, Choi JH (2003). Electrical and optical studies of organic light emitting devices using SWCNTs-polymer nanocomposites. *Opt. Mater.* 21: 147–151.
- Kong H, Gao C, Yan DY (2004). Functionalization of multiwalled carbon nanotubes by atom transfer radical polymerization and defunctionalization of the products. *Macromolecules* 37: 4022–4030.
- Kong Y, Cui D, Ozkan CS, Gao H (2003). American Materials Research Society Symposium Proceeding-Biomicroelectromechanical Systems (BIOMEMS) 773: 111–116
- Kuempel ED, Tran CL, Castranova V, Bailer AJ (2006). Lung dosimetry and risk assessment of nanoparticles: evaluating and extending current models in rats and humans. *Inhal. Toxicol.* 18: 717–24.
- Kymakis E, Amaratunga GAJ (2002a). Polymer-nanotube composites: burying nanotubes improves their field emission properties. *Appl. Phys. Lett.* 80: 1435–1437.
- Kymakis E and Amaratunga GAJ (2002b). Single-wall carbon nanotube/conjugated polymer photovoltaic devices. *Appl. Phys. Lett.* 80: 112–114.
- Kymakis E, Amaratunga GAJ (2003). Photovoltaic cells based on dye-sensitisation of single-wall carbon nanotubes in a polymer matrix. *Solar Ener. Mater. Solar Cells* 80: 465–472.
- Kymakis E, Alexandrou I, Amaratunga GAJ (2003). High open-circuit voltage photovoltaic devices from carbon-nanotube-polymer composites. *J. Appl. Phys.* 93: 1764–1768.
- Lam CW, James JT, McCluskey R, Hunter RL (2004). Pulmonary toxicity of single-wall carbon nanotubes in mice 7 and 90 days after intracheal instillation. *Toxicol. Sci.* 77: 126–134.
- Landi BJ, Castro SL, Ruf HJ, Evans CM, Bailey SG, Raffaele RP (2005). CdSe quantum dot-single wall carbon nanotube complexes for polymeric solar cells. *Solar Energy Mater And Solar Cells* 87: 733–746.
- Lee JW, Kim BK, Kim H, Han SC, Shin WS, Jin SH (2006). Convergent synthesis of symmetrical and unsymmetrical PAMAM dendrimers. *Macromolecules* 39: 2418–2422.
- Lefebvre J, Fraser JM, Homma Y, Finnie P (2004). Photoluminescence from single-walled carbon nanotubes: a comparison between suspended and micelle-encapsulated nanotubes. *Appl. Phys. A* 78: 1107–1110.
- Levitsky IA, Kanelos PT, Woodbury DS, Euler WB (2006). Photoactuation from a carbon nanotube-nafion bilayer composite. *J. Phys. Chem. B.* 110: 9421–9425.
- Li HJ, Wang XB, Song YL, Liu YQ, Li QS, Jiang L, Zhu BD (2001). Super-“amphiphobic” aligned carbon nanotube films. *Angew. Chem. Int. Ed.* 40: 1743–1746.
- Liang Z, Susha AS, Yu A, Caruso F (2002). Nanotubes prepared by layer-by-layer coating of porous membrane templates. *Adv. Mater.* 14: 1849–1853.

- Liu YJ, Nishimura N, Otani Y (2005). Large-scale modeling of carbon-nanotube composites by a fast multipole boundary element method. *Comput. Mater. Sci.* 34: 173–187.
- Lin T, Bajpai V, Ji T, Dai LM (2003). Chemistry of carbon nanotubes. *Australian J. Chem.* 56: 635–651.
- Li WZ, Xie SS, Qian LX, Chang BH, Zou BS, Zhou WY, Zhao RA, Wang G (1996). Large-scale synthesis of aligned carbon nanotubes. *Science* 274: 1701–1703.
- Li H, Huang J, Lv J, An H., Zhang X, Zhang Z, Fan C, Hu J (2005). Nanoparticle-PCR: Nanogold-assisted PCR with enhanced specificity. *Angew. Chem. Int. Ed.* 44: 5100–5103.
- Lovat V, Pantarotto D, Lagostena L, Cacciari B, Grandolfo M, Righi M, Spalluto G, Prato M, Ballerini (2005). Carbon nanotube substrates boost neuronal electrical signaling. *Nano Lett.* 5: 1107–1110.
- Lourie O, Cox DM, Wagner HD (1998). Buckling and collapse of embedded carbon nanotubes. *Phys. Rev. Lett.* 81: 1638–1641.
- Lu SX, Panchapakesan B (2005). Optically driven nanotube actuators. *Nanotechnology* 16: 2548–2554.
- Luo XL, Xu JJ, Wang JL, Chen HY (2005). Electrochemically deposited nanocomposite of chitosan and carbon nanotubes for biosensor application. *Chem. Commun.* 16: 2169–2171.
- Majoros IJ, Myc A, Thomas T, Mehta CB, Baker JR (2005). Poly(amidoamine) dendrimer-based multifunctional engineered nanodevice for cancer therapy. *J. Med Chem.* 48: 5892–5899.
- Majoros IJ, Myc A, Thomas T, Mehta CB, Baker JR (2006). PAMAM dendrimer-based multifunctional conjugate for cancer therapy: synthesis, characterization, and functionality. *Biomacromolecules* 7: 572–579.
- Merkoci A, Pumera M, Llopis X, Perez B, Valle M del, Alegret S (2005). New materials for electrochemical sensing VI: Carbon nanotubes. *Trac-Trends in Anal. Chem.* 24: 826–838.
- Mitchell DT, Lee SB, Trofin L, Li N, Nevanen TK, Suerlund H, Martin CR (2002). Smart nanotubes for bioseparations and biocatalysis. *J. Am. Chem. Soc.* 124: 11864–11865.
- Martin CR, Kohli P (2002). The emerging field of nanotube biotechnology. *Nature Rev. Drug Discov.* 2: 29–37.
- Maslov S, Sneppen K (2002). Specificity and stability in topology of protein networks. *Science* 296: 910–913.
- Maynard AD, Baron PA, Foley M, Shvedova AA, Kisin ER, Castranova V (2004). Exposure to carbon nanotube material: aerosol release during the handling of unrefined single-walled carbon nanotube material. *J. Toxicol. Environ. Health A* 67: 87–107.
- Meincke O, Kaempfer D, Weickmann H, Friedrich C, Vathauer M, Warth H (2004). Mechanical properties and electrical conductivity of carbon-nanotube filled polyamide-6 and its blends with acrylonitrile/butadiene/styrene. *Polymer* 45: 739–748.
- Nalwa HS (2000). *Handbook of Nanostructured Materials and Nanotechnology*, vol. 5, Academic Press, New York.
- Oberdorster G, Sharp Z, Atudorei V, Elder A, Gelein R, Kreyling W, Cox C (2004). Translocation of inhaled ultrafine particles to the brain. *Inhal. Toxicol.* 16: 437–445.
- Odom TW, Huang JL, Lieber CM (2002). Single-walled carbon nanotubes: from fundamental studies to new device concepts. *Ann. N Y Acad. Sci.* 960: 203–15.
- Otten CJ, Lourie OR, Yu MF, Cowley JM, Dyer MJ, Ruoff RS, Buhro WE (2002). Crystalline boron nanowires. *J. Am. Chem. Soc.* 124: 4564–4565.
- Pan B, Cui D, Xu P, Huang T, Li Q, He R, Gao F (2007). Cellular uptake enhancement of polyamidoamine dendrimer modified single walled carbon nanotubes. *J. Biomed. Pharmaceut. Eng.* 1: 1–4.
- Pan B, Cui D, Gao F, He R (2006). Growth of multi-amine terminated poly(amidoamine)dendrimers on the surface of carbon nanotubes. *Nanotechnology* 17: 2483–2489.
- Pan B, Cui D, He R, Gao F, Zhang Y (2006). Covalent attachment of quantum dot on carbon nanotubes. *Chem. Phys. Phys. Lett.* 417: 419–424.
- Pan B, Cui D, Sheng Y, Ozkan CS, Gao F, et al. (2007). Dendrimer-modified magnetic nanoparticles enhance efficiency of gene delivery system. *Cancer Res.* 67: 8156–8163.

- Panhuis MIH, Sainz R, Innis PC, Kane-Maguire LAP, Benito AM, Martinez MT, Moulton SE, Wallace GG, Maser WK (2005). Optically active polymer carbon nanotube composite. *J. Phys. Chem. B* 109: 22725–22729.
- Pantarotto D, Partidos CD, Graff R, Hoebeke J, Briand JP, Prato M, Bianco A (2003). Synthesis, structural characterization, and immunological properties of carbon nanotubes functionalized with peptides. *J. Am. Chem. Soc.* 125: 6160–6164.
- Pantarotto D, Briand JP, Prato M, Bianco A (2004a). Translocation of bioactive peptides across cell membranes by carbon nanotubes. *Chem. Commun.* 16–17.
- Pantarotto D, Singh R, McCarthy D, Erhardt M, Briand JP, Prato M, Kostarelos K, Bianco A (2004b). Functionalized carbon nanotubes for plasmid DNA gene delivery. *Angew. Chem. Int. Ed.* 43: 5242–5246.
- Park C, Ounaies Z, Watson KA, Crooks RE, Smith J, Lowther SE, Connell JW, Siochi EJ, Harrison JS, Clair TL (2002). Dispersion of single wall carbon nanotubes by in situ polymerization under sonication. *Chem. Phys. Lett.* 364: 303–308.
- Peng F, Fu X, Yu H, Wang H (2007). Preparation of carbon nanotube-supported Fe_2O_3 catalysts and their catalytic activities for ethylbenzene dehydrogenation. *New Carbon Mater.* 22: 213–217.
- Pengfei QF, Vermesh Q, Grecu M, Javey A, Wang O, Dai HJ, Peng S, Cho KJ (2003). Synthesis of p-type gallium nitride nanowires for electronic and photonic nanodevices. *Nano Lett.* 3: 347–351.
- Raloff J (2005). Nano hazards: exposure to minute particles harms lungs, circulatory system. *Sci. News Online* 167:179.
- Rege K, Raravikar NR, Kim D-Y, Schadler LS, Ajayan PM, Dordick JS (2004). Enzyme-polymer-single walled carbon nanotube composites as biocatalytic films. *Nano Lett.* 3: 829–832.
- Ren Y, Fu YQ, Liao K, Li F, Cheng HM (2004). Fatigue failure mechanisms of single-walled carbon nanotube ropes embedded in epoxy. *Appl. Phys. Lett.* 84: 2811–2813.
- Rouse JH, Lillehei PT, Sanderson J, Siochi EJ (2004). Polymer/Single-walled carbon nanotube films assembled via donor-acceptor interactions and their use as scaffolds for silica deposition. *Chem. Mat.* 16: 3904–3910.
- Salvetat JP, Bhattacharyya S, Pipes RB (2006). Progress on mechanics of carbon nanotubes and derived materials. *J. Nanosci. Nanotechnol.* 6: 1857–1882.
- Salem AK, Searson PC, Leong KW (2003). Multifunctional nanorods for gene delivery. *Nat. Mater.* 2: 668–671.
- Seeman NC (2005). From genes to machines: DNA nanomechanical devices. *Trends Biochem. Sci.* 30: 119–125.
- Shi D, Guo Y, Dong Z, Lian J, Wang W, Liu G, Wang L, Ewing RC (2006). Luminescent carbon nanotubes by surface functionalization. *Adv. Mater.* 18: 189–193.
- Shi D, Guo Y, Dong Z, Lian J, Wang W, Liu G, Wang L, Ewing RC (2007). Quantum-dot-activated luminescent carbon nanotubes via a nanoscale surface functionalization for in vivo imaging. *Adv. Mater* 19(23): 4033–4037.
- Shim M, Kam NMS, Chen RJ, Li R, Dai H (2002). Functionalization of carbon nanotubes for biocompatibility and biomolecular recognition. *Nano Lett.* 2: 285–288.
- Shino A, Fujioka K, Manabe N, Yamaya S, Goto Y, Yasuhara M, Yamamoto K (2005). Simultaneous multicolor detection system of the single-molecular microbial antigen with total internal reflection fluorescence microscopy. *Microbiol. Immunol.* 49: 461–470.
- Shvedova AA, Castranova V, Kisin ER, Schwegler-Berry D, Murray AR, Gandelsman VZ, Maynard A, Baron P (2003). Exposure to carbon nanotube material: assessment of nanotube cytotoxicity using human keratinocyte cells. *J. Toxicol. Environ. Health A* 66: 1909–1926.
- Singh R, Pantarotto D, McCarthy D, Chaloin O, Hoebeke J, Partidos CD, Briand JP, Prato M, Bianco A, Kostarelos K (2005). Binding and condensation of plasmid DNA onto functionalized carbon nanotubes: toward the construction of nanotube-based gene delivery vectors. *J. Am. Chem. Soc.* 127: 4388–4396.

- Singh R, Pantarotto D, Lacerda L, Pastorin G, Klumpp C, Prato M, Bianco A, Kostarelos K (2006). Tissue biodistribution and blood clearance rates of intravenously administered carbon nanotube radiotracers. *Proc. Natl. Acad. Sci. USA.* 103: 3357–3362.
- Snow ES, Perkins FK (2005). Capacitance and conductance of single-walled carbon nanotubes in the presence of chemical vapors. *Nano Lett.* 5: 2414–2417.
- Satapathy BK, Weidisch R, Potschke P, Janke A (2005). Crack toughness behaviour of multi-walled carbon nanotube (MWNT)/polycarbonate nanocomposites. *Macromol. Rapid Commun.* 26: 1246–1252.
- Sato Y, Yokoyama A, Ken-ichiro S, Akimoto Y, Shin-ichi Ogino, Nodasaka Y, Kohgo T, Tamura K, Akasaka T, Uo M, Motomiya K, Jeyadevan B, Ishiguro M, Hatakeyama R, Watari F, Tohji K (2005). Influence of length on cytotoxicity of multi-walled carbon nanotubes against human acute monocytic leukemia cell line THP-I in vitro and subcutaneous tissue of rats in vivo. *Mol. BioSyst.* 1: 176–182.
- Stone V, Donaldson K (2006). Signs of stress. *Nature Nanotechnology* 1: 23–24.
- Sun TL, Wang GJ, Liu H, Feng L, Jiang L, Zhu DB (2003). Control over the wettability of an aligned carbon nanotube film. *J. Am. Chem. Soc.* 125: 14996–14997.
- Sung JH, Kim HS, Jin HJ, Choi HJ, Chin IJ (2004). Nanofibrous membranes prepared by multi-walled carbon nanotube/poly(methyl methacrylate) composites. *Macromolecules* 37: 9899–9902.
- Tang CY, Xie XL, Wu XC, Li RK, Mai YW (2002). Enhanced wear performance of ultra high molecular weight polyethylene crosslinked by organosilane. *J. Mater. Sci. Mater. Med.* 13: 1065–1069.
- Tang BZ, Xu HY (1999). Preparation, alignment, and optical properties of soluble poly(phenylacetylene)-wrapped carbon nanotubes. *Macromolecules* 32: 2569–2576.
- Tian F, Cui D, Schwarz H, Estrada GG, Kabayashi H (2006). Cytotoxicity of single-wall carbon nanotubes on human fibroblasts. *Toxicol. In Vitro* 20: 1202–1212.
- Treacy MMJ, Ebbesen TW, Gibson JM (1996). Exceptionally high Young's modulus observed for individual carbon nanotubes. *Nature* 381: 678–681.
- Tulevski GS, Hannon J, Afzali A, Chen Z, Avouris P, Kagan CR (2007). Chemically assisted directed assembly of carbon nanotubes for the fabrication of large-scale device arrays. *J. Am. Chem. Soc.* 129: 11964–11968.
- Um SH, Lee JB, Park N, Kwon SY, Umbach CC, Luo D (2006). Enzyme-catalysed assembly of DNA hydrogel. *Nature Mater.* 5: 797–801.
- Valter B, Ram MK, Nicolini C (2002). Thermal desorption high-resolution mass spectrometry of mixed self-assembled monolayers on gold. *Langmuir.* 18: 1535–1541.
- Valentini L, Kenny JM (2005). Novel approaches to developing carbon nanotube-based polymer composites: fundamental studies and nanotech applications. *Polymer* 46: 6715–6718.
- Velasco-Santos C, Martı́nez-Hernández AL, Fisher FT, Ruoff R, Castaño VM (2003a). Dynamical mechanical and thermal analysis of carbon nanotube-methyl methacrylate nanocomposites. *J. Phys. D-Applied Phys.* 36: 1423–1428.
- Velasco-Santos C, Martı́nez-Hernández AL, Fisher FT, Ruoff R, Castaño V M (2003b). Improvement of thermal and mechanical properties of carbon nanotube composites through chemical functionalization. *Chem. Mater.* 15: 4470–4475.
- Vinuesa C, Goodnow C (2002). Immunology: DNA drives autoimmunity. *Nature* 416: 595.
- Wang H, Christopherson GT, Xu ZY, Porcar L, Ho DL, Fry D, Hobbie EK (2005). Shear-SANS study of single-walled carbon nanotube suspensions. *Chem. Phys. Lett.* 416: 182–186.
- Wang P (2006). Nanoscale biocatalyst systems. *Curr. Opin. Biotechnol.* 17: 574–579
- Wang SQ, Humphreys ES, Chung SY, Delduco DF, Lustig SR, Wang H, Parker KN, Rizzo NW, Subramoney S, Chiang YM, Jaqota A (2003). Peptides with selective affinity for carbon nanotubes. *Nature Mater.* 2: 196–200.
- Weiss N, Kind H, Stockli T, Forro L, Kern K, Chatelain A (2001). Tuning the field emission properties of patterned carbon nanotube films. *Adv. Mater.* 13: 184–188.
- Wong M, Paramsothy M, Xu XJ, Ren Y, Li S, Liao K (2003). Physical interactions at carbon nanotube-polymer interface. *Polymer* 44: 7757–7764.

- Woo HS, Czerw R, Webster S, Carroll DL, Ballato J, Strevens AE, O'Brien D, Blau WJ (2000). Hole blocking in carbon nanotube-polymer composite organic light-emitting diodes based on poly (*m*-phenylene vinylene-co-2, 5-dioctoxy-*p*-phenylene vinylene). *Appl. Phys. Lett.* 77: 1393–1395.
- Xia H, Cheng D, Xiao C, Chan HS (2006). Controlled synthesis of Y-junction polyaniline nanorods and nanotubes using in situ self-assembly of magnetic nanoparticles. *J. Nanosci. Nanotechnol.* 6: 3950–3954.
- Xiao T, Fang N, Chan V, Liao K (2004). A kinetic model for time-dependent fracture of carbon nanotubes. *Nano Lett.* 4: 1139–1142.
- Yang YL, Gupta MC (2005). Novel carbon nanotube-polystyrene foam composites for electromagnetic interference shielding. *Nano Lett.* 5: 2131–2134.
- Yan H, Park SH, Finkelstein G, Reif JH, LaBean TH (2003). DNA-templated self-assembly of protein arrays and highly conductive nanowires. *Science* 301: 1882–1884.
- Yan H, Zhang X, Shen Z, Seeman C (2002). A robust DNA mechanical device controlled by hybridization topology. *Nature* 415: 62–65.
- Yim T-J, Liu J, Lu Y, Kane RS, Dordick JS (2005). Highly active and stable DNA zyme-carbon nanotube hybrids. *J. Am. Chem. Soc.* 127: 12200–12201.
- Yoo E, Habe T, Nakamura J (2005). Possibilities of atomic hydrogen storage by carbon nanotubes or graphite materials. *Sci. Technol. Adv. Mater.* 6: 615–619.
- Yoshida Y, Okano M, Wang S, Kobayashi M, Kawasumi M, Hagiwara H, Mitsumata M (1995). Hemodynamic-force-induced difference of interendothelial junctional complexes. *Ann. N Y. Acad. Sci.* 748: 104–120.
- Yu MF, Lourie O, Dyer MJ, Moloni K, Kelly TF, Ruoff RS (2000). Strength and breaking mechanism of multiwalled carbon nanotubes under tensile load. *Science* 287: 637–640.
- Zhao B, Hu H, Yu AP, Perea D, Haddon RC (2005). Synthesis and characterization of water soluble single-walled carbon nanotube graft copolymers. *J. Am. Chem. Soc.* 127: 8197–8203.
- Zheng M, Jagota A, Semke ED, Diner BA, Mclean RS, Lustig SR, Richardson RE, Tassi NG (2003). DNA-assisted dispersion and separation of carbon nanotubes. *Nature Mater.* 2: 338–342.

Chapter 10

Applications of Carbon-Based Nanomaterials for Drug Delivery in Oncology

Nicole H. Levi-Polyachenko^{1*}, David L. Carroll², and John H. Stewart, IV³

Abstract The goal of this chapter is to introduce carbon nanomaterials and highlight research focused on their use as cancer therapeutics. The physical properties of fullerenes and carbon nanotubes, including their spectral characteristics are described. Current oncology treatment regimes are described to provide an overview of where carbon nanomaterials may have significant value in further development of the established standards of care procedures. Photodynamic therapy and drug delivery using fullerene C₆₀ is explored. Thermal ablation techniques using carbon nanotubes are explained and alternate hyperthermic methods using carbon nanotubes are described. Specifically, carbon nanotubes are examined for their potential contribution to the currently practiced clinical therapy intraperitoneal hyperthermic chemoperfusion. Nanotubes and nanohorns filled with chemotherapeutic agents are examined as are different methods for filling and containment of drug moieties. The attachment of active molecules to fullerenes is described with examples for use in oncology. Toxicity issues are explored and the future directions and potential for carbon nanomaterial types concludes the chapter.

Keywords Carbon Nanotubes, Fullerenes, Hyperthermic, Chemoperfusion, Cancer

Abbreviations PDT, Photodynamic therapy; EPR, Enhanced permeability and retention; THF, Tetrahydrofuran; UV, Ultraviolet; DNA, Deoxyribonucleic acid; PL, Photoluminescence; SWNT, Single-walled nanotube; DWNT, Double-walled nanotube; MWNT, Multi-walled nanotube; IV, Intravenous; HSP, Heat shock protein;

^{1*}Department of Plastic and Reconstructive Surgery, Wake Forest University Health Sciences, Medical Center Blvd., Winston-Salem, NC 27157, USA
E-mail: nlevi@wfubmc.edu

²Director of the Center for Nanotechnology and Molecular Materials, Department of Physics, 100 Olin Physical Laboratory, Wake Forest University, Winston-Salem, NC 27109, USA
E-mail: carroldl@wfu.edu

³Department of General Surgery, Section on Surgical Oncology, Wake Forest University Health Sciences, Medical Center Blvd., Winston-Salem, NC 27157, USA
E-mail: jhstewart@wfubmc.edu

IPHC, Intraperitoneal hyperthermic chemoperfusion/chemotherapy; MMC, Mitomycin C; IP, Intraperitoneal; SOD, Superoxide dismutase; Nd:YAG, Neodymium-doped yttrium aluminium garnet; Nd:Y₃Al₅O₁₂; NIR, Near infrared; FITC, Fluorescein isothiocyanate; PEG, Polyethylene glycol; FA, Folic acid; CDDP, Cisplatin; TEM, Transmission electron microscopy

10.1 Introduction

Many improvements in diagnosis and treatment of cancer phenotypes have been made in recent years; however, this disease still afflicts many individuals worldwide and impacts their livelihood, families, and communities. Nano-therapeutics, especially carbon-based, have the potential to more effectively localize drug delivery, to increase drug efficiency, and to reduce the amount of chemotherapeutic agent required. Statistics from the International Agency for Research on Cancer cite that 10.9 million cases of cancer are diagnosed every year, with a 61.9% incidence of death (International Agency for Research on Cancer, 2002). Unfortunately, the more underdeveloped regions of the world suffer the highest mortality rates, as high as 77.9%, whereas societies with more economic resources have mortality rates around 40% (International Agency for Research on Cancer, 2002). The most frequently occurring cancers are of the prostate, breast, lung, stomach, cervical/uterine, liver, and skin (International Agency for Research on Cancer, 2002). Treatment options are designed based on location of the primary lesions, possible metastasis, and genetic factors. Refinements in treatment regimes are made according to patient tolerance and therapeutic effectiveness, referred to as cancer response. Novel treatments are more likely to progress from currently accepted oncology (cancer) regimes including radiation therapy, chemotherapy, surgery, and, more recently, photodynamic therapy (PDT) and hyperthermic chemotherapy.

Nanotechnology refers to particles sized 1–100 nm, although particles 100–500 nm in size may also be referred to as nanoparticles and may be composed of a multitude of material types. As a comparison a red blood cell is approximately 5 μ m in diameter, making it 5,000 times larger than a 1 nm-sized particle of C₆₀, as shown in Fig. 10.1.

Current trends in nanotechnology have developed from inorganic devices for optics and energy storage and transport towards novel techniques in medicine, including ventures into novel cancer therapies. Why should nano-sized particles be helpful in medicine? Materials in the nano regime have different properties from their macroscopic counterparts, even when they are composed of the same elemental composition. For instance, they may have increased heat capacity values due to specific gravity, or increased energy storage and transport due to the dimensionality of nano-sized materials (Blank et al., 2001). Or, they may couple to radiation differently than macroscopic materials (Hanson, 2005; Wang et al., 2004a). Also, due to their size, composition, or morphology, they may travel through the body

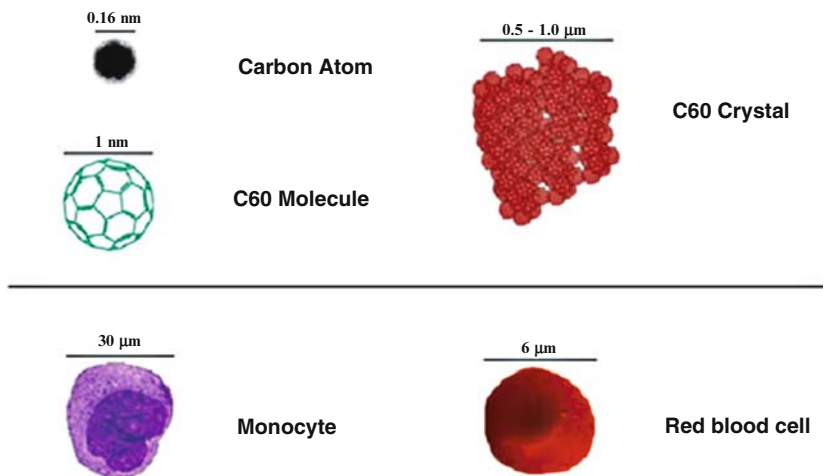


Fig. 10.1 Comparative sizes of one carbon atom, one molecule of C_{60} fullerene, a typically sized aggregate of C_{60} fullerene, a red blood cell, and a large immune system cell, a monocyte (*See Color Plates*)

unimpeded by the immune system, thus gaining access to various parts of the body, or individual cells that may be inaccessible otherwise. Furthermore, there is such a wide variety of nanomaterials that may be used so multiple functional components may be added for site-specific targeting. An alternative to tumor-destructive therapies is the use of nanoparticles to reduce unwanted side-effects from currently used chemotherapeutics. In addition, some nanomaterials have anti-bacterial and anti-viral properties which might be used to offset chronic infections that can lead to cancer development in sensitive tissues, or aid in the reduction of secondary infections following reduced immune response due to chemotherapy (Bosi et al., 2000; Yu et al., 2005). In addition to their use as beneficial agents, some nanoparticles can also serve a dual purpose of acting as contrast agents for tracking progress to a tumor site (Bolskar et al., 2003; Brusentsov et al., 2007; Sitharaman et al., 2005; Wang et al., 2004b). There are a wide variety of nano-sized materials that may be useful in cancer therapies. These include carbon-based materials, liposomal carrying molecules, dendrimers, aptamers, metallics, ceramics, and a multitude of polymeric materials, all of which have a variety of sizes and morphologies that can impact their internal effects and clearance.

Common ideas about dimensionality include that three-dimensional objects have all three-dimensional parameters (length, width, depth) in the same macroscopic size range. Two-dimensional objects have one length which is considerably smaller than the other two (consider a line such that the length and thickness of the line may be determined but the depth is so much smaller that it may essentially be considered as a two-dimensional object). A one-dimensional object has two dimensions much smaller than the third. An example of this is the carbon nanotube, which has a length much longer than the tube diameter. Dimensionality essentially adds

confinement to the electrons of the nano-system, and this can alter the quantum mechanically allowed states of the system. That is why nano-systems are important and unique, and hence why they might be beneficial to medicinal applications in the same way they are in other fields such as optics, semiconductors, and material science. Nanoparticles exist in many applications that have not been previously labeled as nanotechnology; for example, nanoparticles in cements and ceramic composites such as bone (Brunner et al., 2007; Jonsson et al., 2005). Nano-sized particles, especially carbon, exhibit unique properties due to dimensionality and atomic arrangement.

Phenomenon in this size regime obey quantum principles more readily than classical principles. The C_{60} fullerene is composed of carbon atoms joined by π bonds and although each atom is bound to four other carbon atoms and therefore has filled electron orbitals, quantum statistics explains how the C_{60} molecule can be an acceptor of electrons by electron localization probabilities. Dimensionality plays a role in nanotubes' exceptional electrical conduction: resistivity and conduction values of $10^{-7} \Omega/m$ and $10^6 S/m$ compared to copper, $10^{-8} \Omega/m$ and $10^7 S/m$ (Dalmás et al., 2006; Dresselhaus et al., 1996). Dimensionality leads to quantum confinement, essentially allowing only certain modes for electrons along the length of the one-dimensional nanotube. The phenomenon is ballistic conduction which is quite different from the diffusive conduction that generates heat, and has slower electrical transport down the length of the material (see Fig. 10.2) (Berger et al., 2003; Brown et al., 2005; Poncharal et al., 2002; Schonberger and Forro 2000). Diffusive transport allows electrons to have multiple interactions with other electrons in a three-dimensional system where there are layers above, below, and next to a specific electron situated somewhere in the bulk material. During ballistic conduction, one electron can only interact with nearest neighbor electrons which exist only in the thin "sheet" of nanotube wall. Therefore, all energy from one electron is transferred to the next electron down the line. Since the graphite walls of the nanotubes are only one atomic layer thick the electrons will only interact with other electrons in the tube wall, essentially propagating conduction down the tube length. Thus electrical conduction by carbon nanotubes is very efficient. So, dimensionality in nanoscale materials enhances specific properties of the material.

Dimensionality has been exploited in medicine to increase circulation times in the body. Nano-sized particles have been shown able to avoid immune system detection and clearance and therefore become more localized in tumors (Bibby et al., 2005; Di Paolo 2004; Zhang et al., 2006). This means that nano-sized particles will linger in the body longer before they are cleared. Longer circulation times means more drug can be circulated thus reducing need for delivery of more drug. Another effect that nanoparticle size influences is where the drugs, delivered by the small particles, can go in the body. Enhanced permeability and retention (EPR) is an important characteristic of nanoparticles, especially for applications in oncology (Hirsch et al., 2006; Portney and Ozkan, 2006; Reddy, 2005; Shenoy and Amiji, 2005). The vascular (blood supply) of developing tumors tends to be more porous as there are larger gaps between endothelial cells of these underdeveloped vessels. Nano-sized particles can easily pass through the

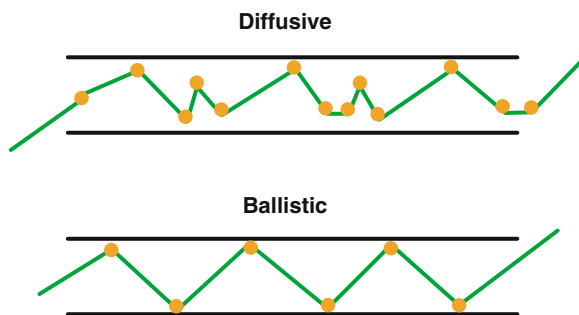


Fig. 10.2 Diffusive versus ballistic transport of electrons (*See Color Plates*)

leaky vasculature and therefore can more readily access tumors than can larger-sized particles. Particles that circulate for longer times with higher potential for retention in tumors offer exceptional promise for new drug delivery options in oncology. Non-carbon-based nanomaterials utilizing the EPR effect are under development and some are already in mainstream use; for example, the chemotherapeutic doxorubicin contained in liposomes (fatty acid micelle molecules) (Brigger et al., 2004; Gabizon et al., 1998).

10.2 Carbon Nanomaterials

Carbon was known to exist in two allotropes, graphite and diamond, prior to the discovery of the fullerene in 1986 by Smalley, Curl, and Kroto (Kroto et al., 1985). Modified forms of graphite such as carbon black and pyrolytic carbon were also used, with biological implications. Pyrolytic carbon is used as a coating for cardiac valve replacements (Ely et al., 1998; Goodman et al., 1996). Carbon black is widely used in tire manufacturing but has been shown to induce lung fibrosis (scarring), thus it is viewed as a toxic material (Driscoll et al., 1996; Ernst et al., 2002). Fullerenes' geodesic shape garnered them the name buckminsterfullerene after the architect, Buckminster Fuller, who designed dome structures (Kroto et al., 1985). Fullerenes are now classified into two forms: the more spherically shaped molecules are called fullerenes or bucky balls and the more tubular-shaped molecules called carbon nanotubes. Nanotubes were not mainstream in research and applications until S. Iijima's famous publication describing them in 1991 (Iijima 1991). Carbon is now found in three forms: graphite, diamond, and fullerene. Fullerenes have very special electrical, optical, and thermal characteristics based on the specific arrangement of the carbon atoms (Brown et al., 2005; Dresselhaus et al., 1996; Dresselhaus et al., 2004; Hepplestone et al., 2006; Kroto et al., 1985; Mittal, 1995).

10.2.1 Fullerenes

Fullerenes can be grown using arc deposition in a Kratschmer generator which uses a chamber pressurized with an inert gas such as argon (Lamb and Huffman, 1993; Scott and Majetich, 1995). Within the vessel are two graphite rods at the radial center of the vessel with a slight gap between their ends. An electrical discharge between the ends of the rods forms carbon nanotubes as well as the smaller spherical fullerenes (Lamb and Huffman, 1993). Although the icosahedron C_{60} is commonly discussed, there are many other types of fullerene with more or fewer carbon atoms; for example, C_{48} , C_{70} , C_{86} , and C_{108} (Dresselhaus et al., 1996). Although fullerenes with numbers of carbon atoms other than 60 are generated in the arc process, since C_{60} forms the most spherical molecule, it is thus the most stable, and therefore, the most abundant (Dresselhaus et al., 1996). Fullerenes with variable number of carbon atoms are typically differentiated by solvent extraction techniques as C_{60} is readily dissolved in toluene leading to a color change of the solution from clear to bright purple. C_{70} on the other hand, changes the solution to a vivid red color.

A major dilemma in using fullerenes (and other carbon nanomaterials) in medical applications, is their hydrophobic nature. Fullerenes are solubilized in aqueous suspensions by one of two mechanisms: solvent phase separation or functionalization of the molecular cage. Solvent phase separation involves dispersal of the fullerenes in an organic solvent such as toluene or tetrahydrofuran (THF) (Avdeev et al., 2004; Deguchi et al., 2001; Fortner et al., 2005; Sayes et al., 2004; Scharff et al., 2004; Scrivens et al., 1994). Interaction of the organic phase with water and subsequent evaporation of the organic solvent leaves no where else for the fullerene molecules to go except into the water, thus forming a water stable suspension. Depending upon the organic solvent used, removal of the organic phase may affect toxicity of the fullerene end product (Gharbi et al., 2005). An example is between the use of toluene and THF for phase separation into an aqueous media. Toluene is immiscible with water and is easily removed from the aqueous phase by sonication, leaving no organic within fullerene nano-clusters. THF on the other hand, is miscible with water and by numerous aqueous dilutions and organic solvent evaporation can be removed from the system. However, since THF is miscible with water, there is potential for interaction of the THF with fullerenes during the organic solvent evaporation leaving residue within fullerene clusters. Any residual solvent may lead to erroneous toxicity results to be pinned on the fullerene. Nuclear magnetic resonance is used to evaluate water soluble materials for residual solvent, but it may still be difficult to remove all the THF (trace amounts may be left) from the system. Prior experience indicates that the use of THF in lieu of toluene makes preparation of a water soluble fullerene more difficult and has more potential for residual solvent effects.

The second way to prepare water soluble fullerenes is by adding functional groups to the molecules' exterior (Brettreich and Hirsch, 1998; Foley et al., 2002b; Guldi et al., 1999; Nakajima et al., 1996; Rajagopalan et al., 1996; Sayes et al., 2004; Wang et al., 1999). Numerous efforts have pushed for fullerene functionalization to be the most useful way to make water soluble fullerenes. Fullerene functionalization

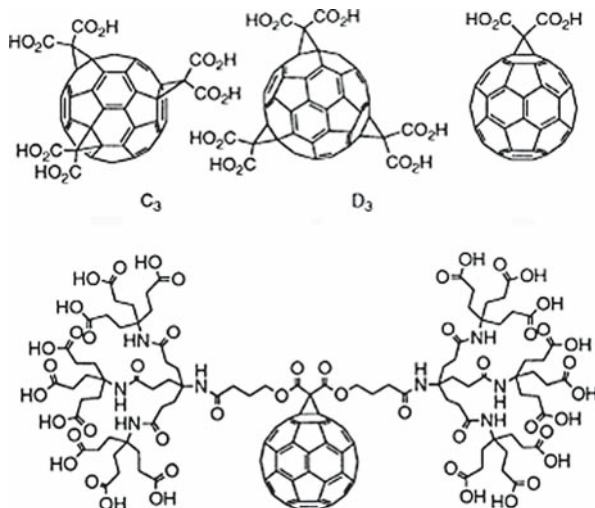


Fig. 10.3 Examples of water-soluble derivatized fullerenes with 1, 3, and 18 carboxyl groups attached (Reprinted from Bosi et al., 2003. With permission from Elsevier)

frequently begins with addition of carboxyl groups attached to the outside of the fullerene cage and subsequent addition of hydrophilic molecules. Diserinol, quaternary pyrrolidinium, hydroxyl, carboxyl groups, and drug compounds have been attached to fullerenes, some examples are shown in Fig. 10.3 (Bisaglia et al., 2000; Bosi et al., 2003; Lin et al., 2000; Monti et al., 2000; Mroz et al., 2007; Scharff et al., 2005; Tsao et al., 2002). In addition to making the fullerenes more water soluble, attached molecules such as drug compounds can be delivered upon endocytosis of the nanoparticle (Isobe et al., 2006). However, there remains the implication that by functionalizing the fullerene, it may no longer behave like the pristine material and is not an appropriate analogue for toxicity assays unless pristine material is compared. There is also potential for fullerenes to negate the effects of an attached drug molecule. For example, if a drug moiety functions primarily by production of radical oxygen species, the fullerene may readily scavenge these radicals and thus negate effectiveness of the drug (Bogdanovic et al., 2004).

The lack of true spherical symmetry provides some of its unique properties such as free radical scavenging ability. C_{60} is electronegative and has the ability to accept up to six more electrons (Dresselhaus et al., 1996; Wang et al., 1999). In this respect many people want to employ it as an antioxidant and there are numerous studies showing its effectiveness in such capacity (Alvarez et al., 2003; Bosi et al., 2003; Chen et al., 2004; Da Ros et al., 2001; Jensen et al., 1996; Lin et al., 2000; Marchesan et al., 2005; Monti et al., 2000; Wang et al., 1999). So the molecule may be protective or detrimental depending upon the situation. Specifically C_{60} has absorption peaks at 280 and 360 nm (Fig. 10.4) with a long Rayleigh tail out to the infrared (Levi et al., 2006). Studies involving singlet oxygen species of functionalized C_{60} use ultraviolet

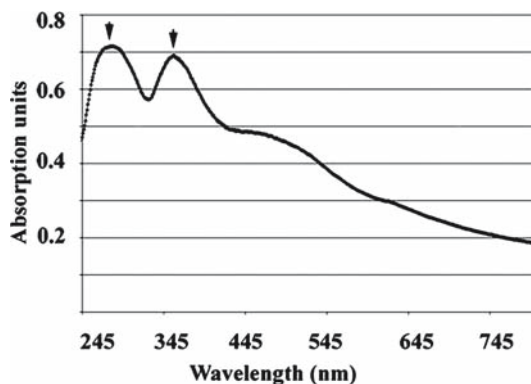


Fig. 10.4 Absorption spectra of dissolved C_{60} . The main absorbance peaks are clearly in the blue although the long absorption tail allows longer wavelength light to be used to stimulate C_{60} (Levi et al., 2006)

light (Kamat et al., 1998), but white light from a halogen source (without a UV filter) has also been used effectively (Bashkin et al., 1997; Kasermann and Kempf, 1998). Although fullerenes can be vacuum annealed, sealed, and stored under an inert gas such as nitrogen, they are most likely to interact with an oxygen environment, especially for biological applications. Therefore, oxygen molecules can localize at the interstitial spaces between fullerene molecules and the amount of diffused oxygen affects the photophysical properties of crystalline C_{60} . In organic solvents C_{60} is easily dispersed into aggregates containing just a few C_{60} molecules; however, water soluble molecules usually contain larger C_{60} aggregates with greater potential for more interstitial oxygen (Levi et al., 2006). For example, C_{60} aggregates held under vacuum had a decrease in the emitted photoluminescence (Ohno et al., 1997). When oxygen is present, C_{60} can aid in the generation of singlet oxygen species which are very reactive in biological systems and lead to DNA damage and membrane disruptions (Foley et al., 2001; Foley et al., 2002a; Nakamura et al., 1996; Yang et al., 2007).

C_{60} naturally forms clusters due to its inherent hydrophobicity and it has been found that in cluster form when exposed to white light or the components of white light it will produce photoluminescence (PL) in the near infrared extending its PL into the red and orange (Capozzi et al., 1997; Levi et al., 2006; Li and Mianami, 2003; Ma et al., 1998; Ma et al., 2000). The photoluminescence spectra and photoluminescent C_{60} clusters within a cancer cell are shown in Fig. 10.5. It is known that the presence of PL is associated with the singlet oxygen release. The atoms that make the C_{60} molecule are covalently bound to one another. Each atom is bound to three atoms creating two single bonds and one double bond. Molecules of C_{60} are then bound together through the molecular van der Waals forces which are not as strong as the covalent bonds of the C_{60} molecule. The weaker bonds between molecules allow for vibrational modes of the crystal. These modes affect the energies which can be imparted to a crystal thus causing the energy cascade (Belin and Epron, 2005; Berger et al., 2003). Results from optics experiments have shown that C_{60} aggregates will photoluminescence in the red and near infrared (emission peaks at 685 and

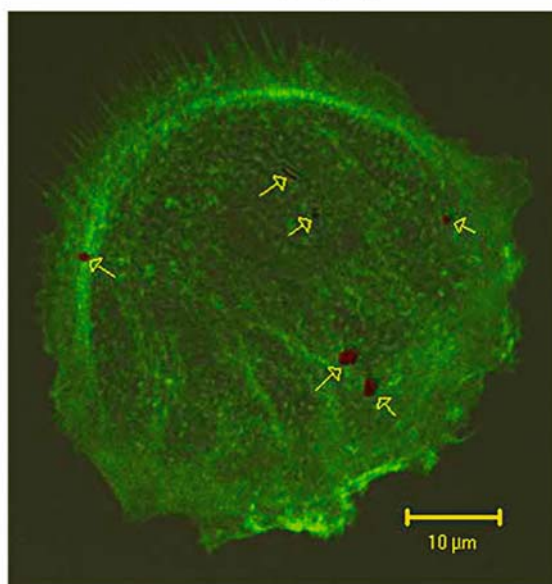
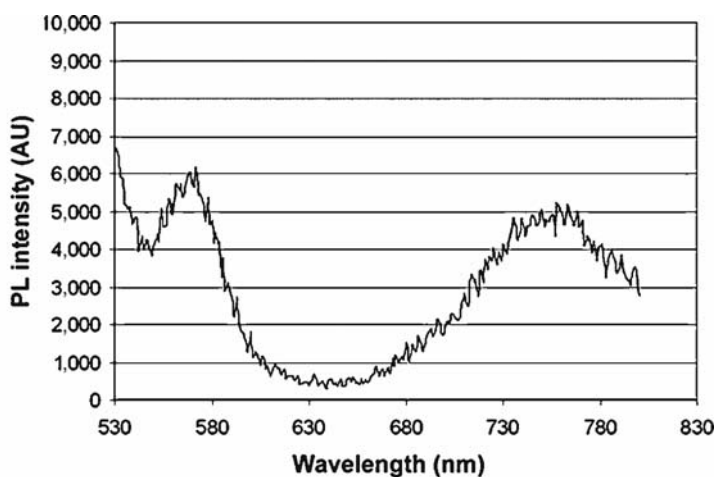


Fig. 10.5 Photoluminescence spectra of dissolved C_{60} . The peak at 750 nm is the photoluminescence signature of the material. Photoluminescent C_{60} aggregates can be visualized within cells and exhibit a vivid red signature which is easily detectable (Levi et al., 2006) (See Color Plates)

730 nm) following absorption of white light (Capozzi et al., 1997; Levi et al., 2006; Ma et al., 1998; Tachibana et al., 1996). Defects in the crystalline structure of C_{60} aggregates give rise to this phenomenon and scratch tests have shown that annealed aggregates do not exhibit as strong a PL signature as aggregates with significant scratching to induce Frenkel defects in the molecular lattice (Capozzi et al., 1997).

Excited singlet oxygen has one electron promoted to a higher valence orbital making an unpaired electron and a highly reactive molecule. Excited singlet oxygen will

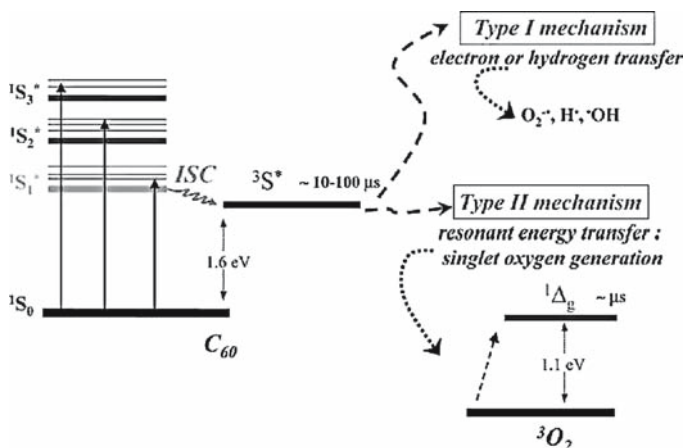


Fig. 10.6 Energy schematic of excited C₆₀ leading to the formation of reactive oxygen species via the reaction one pathway, or leading to the formation of singlet oxygen via the type two mechanism (Reprinted from, Vilenko et al., 2005. With permission from Elsevier)

relax back to the ground state (triplet) upon interaction with stabilizing molecules (electron acceptors) (Danilov et al., 2003; Mroz et al., 2007; Vilenko et al., 2005). C₆₀ fullerene, in the presence of white light and oxygen can form singlet oxygen species, or radical oxygen species like superoxide or hydroxyls (Danilov et al., 2003; Vilenko et al., 2005; Yu et al., 2005). Upon absorption of white light, C₆₀ in its singlet ground state will promote an electron and achieve an excited singlet state which will further decay to a triplet state. When oxygen is present, the C₆₀ triplet state will de-excite by imparting energy to nearby oxygen in its ground state to generate singlet oxygen molecules (Vilenko et al., 2005). This is known as a type II photodynamic pathway. The reaction I pathway involves transfer of an excited electron from C₆₀ to molecular oxygen leading to superoxide and/or hydroxyl radical generation (Castano et al., 2005). Either pathway may be utilized by C₆₀ to impart damage to the surrounding media, polymers, or biological systems. The Jablonski diagram for electron excitations within the C₆₀ cluster is shown in Fig. 10.6. Excitation of C₆₀ is due to phonon modes of the aggregate upon absorption of light (Capozzi et al., 1997).

10.2.2 Nanotubes and Nanohorns

Carbon nanotubes can have one, two, or many sidewalls and are referred to as single-, double-, or multi-walled nanotubes (SWNT, DWNT, or MWNT). Nanotubes can be metallic, or semi-conducting depending on the chirality of the tube. Single-walled nanotubes (SWNT) are about 1 nm in diameter, and hundreds of nanometers long, whereas multi-walled nanotubes (MWNT) are like nested

SWNTs with increasing diameters up to about 20–30 nm and lengths into the multiple micron range. Dimensionality essentially adds confinement of the electrons to the nano-system, and this can alter the quantum mechanically allowed modes of the system as determined using tight-binding approximations in a one-dimensional system (Dresselhaus et al., 1996). Depending on the chirality of the nanotubes (how it is rolled), they can be metallic or semiconducting, and therefore have improved electrical and thermal properties as compared to bulk graphitic carbon (Dresselhaus et al., 1996). Nanotubes are generally classified as armchair, zig-zag, or chiral dependent upon the axis about which the graphite sheet rolls up. Nanotubes can be grown by a number of different mechanisms and variations in the amount of nanotubes produced, residual catalyst, and graphite abound (Charlier and Iijima, 2001). SWNT are plentiful using an arc chamber method, whereas various amounts of metallic catalyst can be imparted using chemical vapor deposition techniques, or laser ablation growth. An interesting carbon nanomaterial, also developed by S. Iijima, is the carbon nanohorns which consists of SWNT bundled to form a spherical ball with closed tube ends at the inside of the aggregate (Ajima et al., 2006). Usually nanotubes have closed ends, and if a metal catalyst was used for growth, the ends contain small amounts of the metal seed. Furthermore, carbon nanotubes can be doped with alternative atoms distributed throughout the tube lattice; for example, nitrogen or boron doping of carbon nanotubes (Liu et al., 2005a, b; Misra et al., 2006; Xu et al., 2004). Currently, doped nanotubes are being explored for medicinal applications since they may have reduced toxicological potential (Carrero-Sanchez et al., 2006). As stated earlier, dimensionality gives special properties to carbon nanotubes, and they not only have high electrical conductivity but also high thermal conductivity, heat capacity, excellent mechanical strength along the tube axis, and resiliency radially upon bending of the nanotube (Dresselhaus et al., 2004; Hepplestone et al., 2006; Iijima, 1991; Mittal, 1995; Sears and Batra, 2006; Wang et al., 2006). Experimental confirmation has shown that SWNT have low resistivity (10^{-7} Ω /m), and high conductivity (10^6 S/m) (Dalmás et al., 2006; Dresselhaus et al., 1996) as compared to copper (10^{-8} Ω /m and 10^7 S/m). For medicinal applications, nanotubes absorb infrared light strongly, although exact absorption peaks depend upon the length and processing of the tube (Kouklin et al., 2004). Following nanotubes growth, there is a need for cleaning of the tubes to remove graphitic carbon and excess catalyst. Cleaning is commonly done by oxidative treatments by sonicating them in acids or by annealing the tubes under a pressurized oxygen environment (Kam et al., 2005; Menna et al., 2003; Sinani et al., 2005; Tkac and Ruzgas 2006; Torti et al., 2007). Cleaning can also remove the caps at the ends of the tubes thus leaving the hollow core open for filling. Filled nanotubes offer exciting potential for medicinal applications and have already proved their promise in materials science when filled with liquid metals or metallic salts to improve electronic devices made with carbon nanotubes (Huang et al., 2004; Kumar et al., 2004; Tessonnier et al., 2005; Toh et al., 2004).

The inherent metallic or semi-conducting properties of nanotubes are defined by the way the graphite sheets roll up during formation. Figure 10.7a shows the

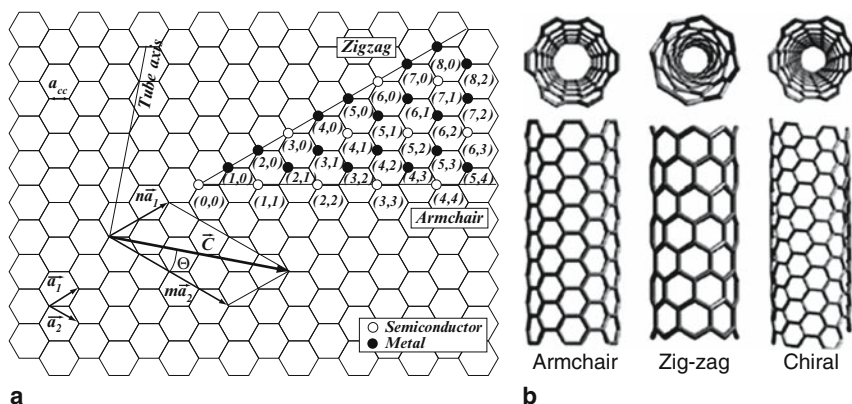


Fig. 10.7 Chirality vector and folding scheme for semiconducting and metallic nanotube (a). Zig-zag, armchair, and chiral nanotubes by rolling-up of the graphite lattice (b) (Reprinted from Terrones 2003. With permission from Annual Reviews)

two-dimensional graphite lattice and the chiral vector, $C = na_1 + ma_2$, which describes how the nanotube rolls. The values in parenthesis are integral values, denoted (n, m) , are the chiral coefficients, and describe the electronic structure of the nanotube: $m = n$, armchair; $m, n = 0$, zig-zag; $m \neq n$, chiral (Fig. 10.7b), and whether the folded points will produce a metallic or semi-conducting nanotube (Bandow et al., 1998; Belin and Epron, 2005).

10.3 Oncology Standards of Care and Drug Delivery

Malignancies are therapeutically handled depending upon the location, and overall physical health of the patient. Radiation, chemotherapy, and surgical techniques may be employed. There are subsets for treatment regimes within each of these categories, and they are often delivered as adjuvant therapies to maximize removal of the malignancies and to minimize recurrence. Surgical resection of solid tumors can be quite complicated if they are significantly involved with organs such as the liver, bowel, or lungs; therefore access to all tumors may not be possible by resection. Techniques such as radiofrequency ablation and focused ultrasound can be used to deliver intense hyperthermia (temperatures above 45°C) in an area to eliminate solid tumors and are commonly used for tumors involved in the liver and kidney (Bastide et al., 2006; Hanajiri et al., 2006; Janzen et al., 2005; Zhou et al., 2007). Recently, magnetic nanoparticles have been developed for use with radiofrequency to localize in a specific region and induce hyperthermia (Jiang et al., 2004; Neuberger et al., 2005; Sonvico et al., 2005; Zhang et al., 2006). Nanoparticles do not even need to be directly at the tumor site, but if they can localize in tumor vasculature and impede blood flow, that may be sufficient for tumor regression. Chemotherapeutic agents are commonly used

as systemic therapies to tackle malignancies at multiple locations, but they can be delivered to specific locations by perfusion techniques. Chemotherapy remains a first line of defense to inhibit primary lesion metastasis by systemic delivery and to aid in elimination of cancer metastasis in regions by perfusion.

Examination of chemotherapy delivery aids in understanding patient preference and cancer response which is beneficial for developing patient friendly and highly successful nano-therapies. Although many cancers will go into remission and lives saved, a secondary effect of cancer is the decrease in the quality of life and the disruption that time and cost of treatments have on patients and their families. When given a choice between intravenous (IV) and oral chemotherapy most patients prefer oral therapy for a few reasons: oral delivery can be administered at home and there are no needle sticks involved (Hirsh et al., 2007). Unfortunately, many chemotherapeutics cannot be delivered orally due to dosing constraints and potential emesis (Bourgeois et al., 2007; Lush et al., 2005). Chemotherapeutic agents are less likely to be degraded by IV delivery and they reach target areas more rapidly and at higher doses, thus making them more effective. Chemotherapy delivered by IV though requires patients to travel to hospitals or treatment facilities 3–5 days a week for 1–6 months. Cost for travel can add up and patients often cannot travel alone for treatments due to side effects, thus leading to disruption of family routines, work schedules, and income potential. Therefore, use of nanoparticles will be more beneficial if they could be given orally without degradation or intravenously with a few treatments.

10.3.1 Photodynamic Therapy

Localized chemotherapy certainly has advantages including potential for high-dose delivery at the target site. Another therapeutic alternative involves the use of relatively benign agents made active at a target site by stimulation with light; this is called photodynamic therapy (PDT) (Dougherty and Marcus, 1992) The photosensitizer molecules absorb light and an electron is excited into a singlet state which is more energetic than the singlet ground state (Castano et al., 2005; Fuchs and Thiele 1998; Harrod-Kim 2006; Sharman et al., 1999). The photosensitizer can relax into an excited triplet state and further energetically relax by transferring energy or an electron to surrounding molecules. If the neighboring molecule is oxygen, reactive oxygen species such as superoxide anions and hydroxyl radicals can be formed (type I reaction) by transfer of an electron from the photosensitizer (Sharman et al., 1999). Alternatively, energy transfer from the triplet excited state photosensitizer can generate singlet oxygen in a type II reaction (Sharman et al., 1999). Fullerenes have already been discussed for their ability to undergo either reaction mechanism although they are not yet used clinically. There is a wide range of photosensitizers, mostly based on tetrapyrrole structures like chlorophyll. The main clinically used photosensitizer is Photofrin, although other agents such as foscan, 5-aminolevulinic acid, and naphthalocyanines are under clinical trials (Babilas et al., 2005; Brewis et al., 1998; Chen et al., 2006; Fotinos et al., 2006; Kubler et al., 2001; Li et al.,

2006; Pech et al., 2005). Regions of the body where light can be externally or endoscopically applied are options for PDT and they include skin, lungs, esophagus, colon, liver, bladder, and prostate (Corti et al., 2000; Harrod-Kim 2006; Pinthus et al., 2006). Typical drug delivery doses are from 0.1 to 7 mg/kg delivered topically or intravenously 3–72 h prior to light exposure (Pinthus et al., 2006; Sharman et al., 1999). Light doses have wide variability from 10 to 200 J/cm² applied for minutes to hours (Pinthus et al., 2006; Sharman et al., 1999). Two drawbacks of PDT are inaccessibility to various tumor locations which make application of light impossible and hypersensitivity to sunlight following delivery of the photosensitizing agents. PDT can be a very effective therapy dependent upon the tumor type, photosensitizer used, and light dose applied. Cancer response rates vary between 20% for low light dose using Photofrin against bladder cancer, and 100% using Haematoporphyrin against lung cancer (Harrod-Kim 2006; Pinthus et al., 2006). PDT deterministically effects biological systems by inducing cell death through cell and reactive oxygen species interactions, by vascular damage or by stimulating immune response at the tumor site (Castano et al., 2005). Although there are multiple photosensitizers currently available, there is potential to use carbon nanomaterials as photosensitizer agents. The lifetime of singlet oxygen species is approximately 0.1 μ s depending on the tissue type and since free radicals interact readily they only travel about 15 nm in a biological environment (Castano et al., 2005). An example of a commonly used sensitizing agent is Photofrin, which to date is the only FDA approved photosensitizing agent (Sharman et al., 1999). However, there are drawbacks to PDT using systemically injected Photofrin. The agent is not delivered to only the cancerous tumor, and after injection a patient's skin and eyes may be sensitive to light for up to 6 weeks post-treatment (Sharman et al., 1999).

10.3.2 Intraperitoneal Hyperthermic Chemotherapy

Chemotherapeutic agents are most commonly delivered systemically but they can be localized to a specific region to aid in cancer cell destruction of micrometastasis that cannot be easily discovered using imaging analysis or during surgical resection of larger lesions. Perfusion has been used on whole limbs, within the pleural lining of the lungs, and is extensively used in to treat disseminations in the peritoneal cavity (abdomen) (Abe et al., 2005; Dang et al., 2007; Pearce and Thomsen, 1999; Reingruber et al., 2007). Addition of hyperthermia with chemotherapeutic agents is beneficial on the cellular and vascular levels; however, not all chemotherapeutic agents respond to hyperthermia. Hyperthermic ranges used with drugs is critical for maximizing treatment effectiveness; appropriate ranges are between 40°C and 43°C. Above 45°C there is coagulation of proteins, and irreversible cell damage. Colorectal cancer cell response to hyperthermia can be seen in Fig. 10.8. There are families of heat shock proteins (HSP) that can be induced at hyperthermic temperatures, especially above 45°C and HSPs can modify oncology outcomes (Hildebrandt et al., 2002). HSPs are upregulated in response to cell stress like hyperthermia but

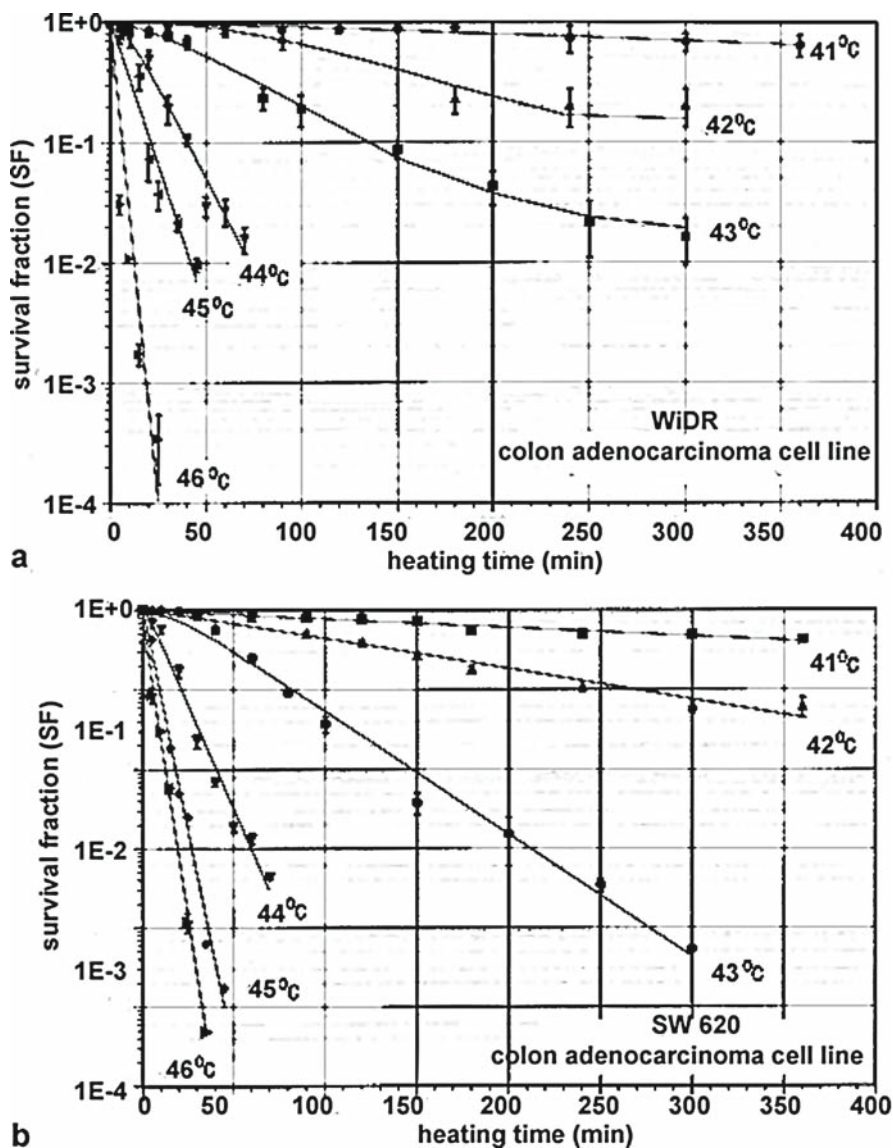


Fig. 10.8 Effect of various hyperthermic temperatures on colorectal cancer cells. Temperatures above 42°C are the most effective for cell killing (Reprinted from Hildebrandt et al., 2002. With permission from Elsevier)

also in response to hypoxia and some therapeutic agents. Upregulation of HSPs protects cells and makes them more resistant to chemotherapy, hyperthermia, and radiation treatments and thus imparts the potential for disastrous malignancies (Hildebrandt et al., 2002). Temperatures above 45°C which produce irreversible

cell damage are referred to as thermal ablation techniques. Figure 10.8 provides plots for how different hyperthermic temperatures affect cell survival in two different colorectal carcinoma cell lines. Great care is required when thermal ablation techniques are to be used around the borders of tumors since there is potential for insufficient heating for cell kill, but high enough temperatures to upregulate HSPs. If not all cells are killed there is potential for aggressive recurrences. Use of nanoparticles to highlight tumor border edges via ultrasound, infrared, or fluorescent imaging is helpful to surgeons and some nanoparticles such as fluorescently labeled nanoparticles are under development to aid in this area (Trehin et al., 2006). An alternate version of hyperthermic chemotherapy involves systemic delivery of the agent and warming of the target region to aid in vascular flow to the tumor and cellular uptake of the drug (Dewhirst 1994; Ponce et al., 2006).

Large tumors that can be visualized during open peritoneal surgery can be removed but micrometastasis may not be visible or detectable by imaging techniques. Unfortunately, chemotherapeutic agents delivered systemically do not reach the peritoneum in high enough doses to be very effective; therefore regional dose delivery is preferred (Levine et al., 2007). To attain more thorough removal of metastatic lesions, perfusion of hyperthermic chemotherapy is used. Certain primary cancers tend to metastasize to the organs and walls of the peritoneal cavity; specifically colorectal, gastric, and breast cancers in addition to primary intraperitoneal cancers of the pancreas and liver. Intraperitoneal hyperthermic chemoperfusion (IPHC) delivers drugs up to 3mm into the tissue of the peritoneum which is adequate for micrometastatic lesions unless they are covered by adipose tissue or scars from previous surgeries (Sugarbaker et al., 2005). Current IPHC regimes require a perfusion of warm (40–43°C) chemotherapeutic agent into the peritoneal cavity for a few hours following debulking of the larger tumor lesions (Levine et al., 2007; Shen et al., 2004; Stewart et al., 2005; Stewart et al., 2006). During perfusion, the abdomen is gently palpated to aid in distribution of the chemotherapeutic agent. A schematic of the perfusion set-up is shown in Fig. 10.9. Although survival rates have dramatically improved using IPHC in combination with surgical resection (Levine et al., 2007), there are drawbacks to the method. The time to setup, flush a saline solution to pre-warm the abdomen, run the perfusion, and complete flushes of the cavity to remove residual drug adds about 3h of additional time that the patient must be anesthetized; it is optimal for the patient to reduce the time under anesthesia. Also, liters of the high-dose chemotherapeutic agent are used during treatment and thus cost for the drugs is quite high, as is disposal for a large amount of toxic material. Although flow rates are modified to promote adequate circulation of agents throughout the peritoneal cavity and palpating the abdomen also aids in circulation there can still be problems with inhomogeneous drug and heat delivery.

Chemotherapeutic agents that have significant cancer response when combined with hyperthermia (up to 43°C) include doxorubicin, melphalan, mitomycin C (MMC), mitoxantrone, gemcitabine, etoposide, and especially the platinum-based agents carboplatin and oxaliplatin (Mohamed et al., 2003; Sugarbaker et al., 2005). Agents that do not work well with hyperthermia include irinotecan, paclitaxel, docetaxel, 5-fluorouracil, and floxuridine (Mohamed et al., 2003; Sugarbaker et al., 2005).

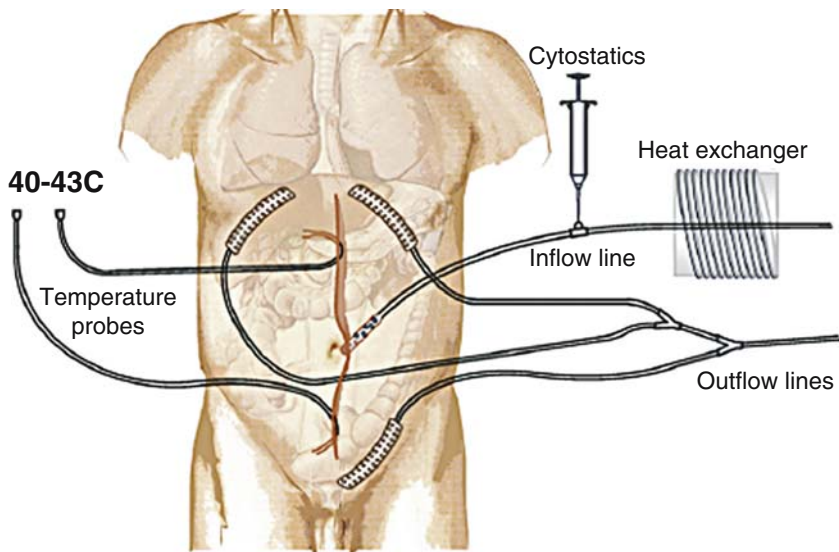


Fig. 10.9 Circuit diagram for intraperitoneal hyperthermic chemoperfusion. Warmed chemotherapeutic agents are circulated through the abdomen and temperature at the inflow and outflow ports are continuously monitored (Reprinted from Reingruber et al., 2007. With permission from Elsevier) (See Color Plates)

In particular, chemotherapeutic agents that require enzymatic activation, such as cyclophosphamide, are not acceptable choices for IP administration (Sugarbaker et al., 2005). All chemotherapeutic agents are delivered at 43°C or below to minimize complications such as upregulated HSPs and damage to non-malignant cells in the region of perfusion. However, it is theorized that anti-neoplastic effect can be enhanced if temperatures over 43°C can be used in a very localized region, as shown in Fig. 10.8 (Hildebrandt et al., 2002).

Hyperthermic chemotherapy aids in drug delivery by a few mechanisms. Increased temperature leads to increased blood flow and tumors are generally able to recruit a good blood supply; thus more drugs will be localized to a tumor if the surrounding area is warmed. On a cellular level, hyperthermia increases permeability of cell membranes. The cell membrane will therefore allow passage of more chemotherapeutic agent, the nuclear membrane will allow more of agent to access DNA, and the mitochondrial machinery will be more susceptible to disruption by drugs targeting mitochondria. In addition, hyperthermia increases cellular metabolism and potentially drug efflux out of the cell. Hyperthermia is advantageous on multiple levels and is therefore a superior adjunct for combinatorial drug delivery. Since IPHC delivers higher doses of chemotherapeutic agents to a local region without much leakage into systemic circulation, another chemotherapeutic can be given systemically to add additional anti-neoplastic capacity without the risk of overdosing.

10.4 Carbon Nanoparticles for Cancer Therapies

Some of the currently used therapeutics, and pitfalls associated with them, have been outlined above. Carbon nanomaterials may be beneficial in oncology to deliver chemotherapeutic agents or begin cascades of damaging molecules like radical oxygen species. Although C_{60} fullerenes and carbon nanotubes are closely related, they have very different pathways as potential therapeutics in oncology.

10.4.1 Fullerenes for Use in Photodynamic Therapy and Drug Delivery

C_{60} fullerenes have been shown to have protective or detrimental effects on biological systems that can be exploited for medicinal use. Due to rearrangement of electrons and statistical probabilities, they can accept up to six electrons and may therefore be used to scavenge damaging reactive oxygen species (Krusic et al., 1991). This phenomenon has been explored and fullerenes were found to be beneficial against neuronal damage (Dugan et al., 2001). Figure 10.10 shows the effectiveness for C_{60} to scavenge superoxide species. A similar opportunity exists in oncology to use the scavenging potential of C_{60} fullerenes to mediate undesirable secondary effects from some chemotherapeutic agents. For example, doxorubicin is a routinely used agent whose primary cell killing mechanism is DNA strand breakage. However, doxorubicin also generates radical oxygen species and tends to

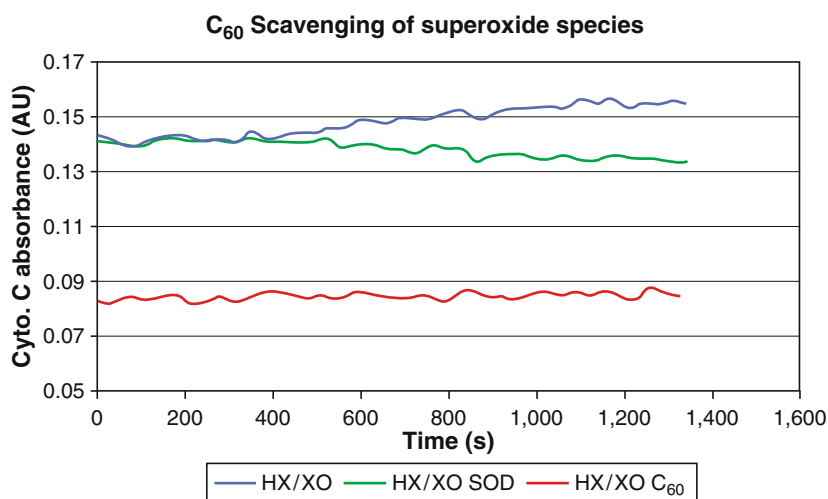


Fig. 10.10 C_{60} is a very effective scavenger of superoxide species. The standard superoxide scavenger, superoxide dismutase, is not nearly as effective (See Color Plates)

localize to mitochondria as well as in the nucleus (Green and Leeuwenburgh 2002). Systemically delivered doxorubicin has been shown to induce irreversible cardiac damage due to the potential of the drug to target mitochondria (Kluza et al., 2004). If C_{60} could be localized near doxorubicin, then perhaps it could reduce damage from the radicals produced by the drug, and there is evidence that functionalized C_{60} fullerenes localize to the nucleus, lysosomes, and mitochondria (Chen et al., 1998; Mroz et al., 2007; Porter et al., 2006; Ueng et al., 1997).

Alternatively, C_{60} can be used as a photosensitizing agent for use in photodynamic therapies. The majority of fullerenes explored as photosensitizing agents are functionalized to aid in water solubility; however, functionalization modifies the photodynamic properties of C_{60} (Koeppel and Sariciftci, 2006; So et al., 2006; Yang et al., 2002). The greater the number of functional molecules attached to the fullerene, the more reduced the yield of singlet oxygen or radical species produced. But there can also be a decrease in quantum yield for fullerenes with fewer numbers of functional moieties due to the greater potential for these molecules to aggregate in aqueous solution (Mroz et al., 2007). Some examples of functionalized fullerenes that have been explored for use as photosensitizer molecules include cyclodextrin C_{60} , tris-malonic acid C_{60} , fullerenes with eighteen carboxylic acid groups, with one to three diserinol groups and one to three quaternary pyrrolidinium groups (Bisaglia et al., 2000; Brettreich and Hirsch, 1998; Foley et al., 2002a; Mroz et al., 2007; Sayes et al., 2004; Wang et al., 1999; Yang et al., 2002). All these molecules exhibit cell killing upon exposure to white (400–700 nm) light, and molecules with fewer functional groups were most effective. The quantum yield of singlet oxygen that can be produced utilizing C_{60} fullerenes functionalized with three quaternary pyrrolidinium groups can be as high as 0.97 (Foley et al., 2001); by comparison, the clinically used Photofrin has a quantum yield of singlet oxygen from 0.11 to 0.89 depending upon the state of aggregation of the molecule (Fernandez et al., 1997; Tanielian et al., 2001). Possibilities exist to use C_{60} fullerenes as photosensitizers but this molecule, like any other, has some limitations. Functionalization of C_{60} is a sufficient way to prepare a material that will not aggregate in aqueous solution upon delivery in the body, but there is a decrease in light absorption with functionalization, leading to less efficient quantum yields (Mroz et al., 2007). The main absorption peaks for pristine fullerene are 280 and 360 nm and for functionalized fullerenes only absorption shoulders are seen above 400 nm (Levi et al., 2006; Mroz et al., 2007). The best wavelengths for PDT though are the longer wavelengths since deeper light penetration will occur at longer wavelengths. However absorption of long wavelengths is not energetically favorable for promotion from the ground state to the first excited state of the photosensitizer (Castano et al., 2005).

Fullerenes can be grown with molecules within their interior, which can be useful in imaging applications but not really for drug delivery. Breaking of the fullerene cage is not easily done, and would be even more difficult to do in the body. Since many chemotherapeutic agents are larger than the interior of a C_{60} fullerene, filled fullerenes are not an acceptable choice for drug delivery. Molecules can be attached to the outside of the fullerene and by exploiting fullerenes' tendency to localize in the nucleus and mitochondria might be useful. However, since addition to the outside

of the fullerene can dramatically affect the resultant molecules' size and charge, drug delivery using fullerenes may not be an effective option in oncology.

10.4.2 Thermal Ablation Using Carbon Nanotubes

Carbon nanotubes (either SWNT, DWNT, or MWNT) strongly absorb electromagnetic radiation throughout the infrared due to transitions between the first and second van Hove singularities, as shown in the absorption spectra in Fig. 10.11 (Bachilo et al., 2002; Kouklin et al., 2004; O'Connell et al., 2002; Saito et al., 2004). Nanotubes generate heat by absorbing incident light which induces phonon and plasmon resonances along the tube length (Dresselhaus and Eklund, 2000; Hepplestone and Srivastava, 2006; Maksimenko et al., 2007). It has been shown that both metallic and semi-conducting nanotubes exhibit this phenomenon, with metallic tubes being the most efficient (Maksimenko et al., 2007). Decreases in the surface plasmon resonances of nanotubes strongly affect the ability of the nanotube to behave as a classical dipole antenna. Plasmon resonances correspond with the geometrical resonance of a metallic nanotube and lead to very specific peaks of thermal intensity that correspond to the length of the nanotube (Maksimenko et al., 2007). Thus, the length of nanotubes can be chosen to match a specific incident frequency of light and will be most efficient when the nanotubes have lengths that are multiples of half the wavelength of the incident light (Burke et al., 2006; Hanson, 2005; Kempa et al., 2007; Wang et al., 2004a). Specific wavelengths within the optical transmission region where body tissues are most transparent can be used to stimulate

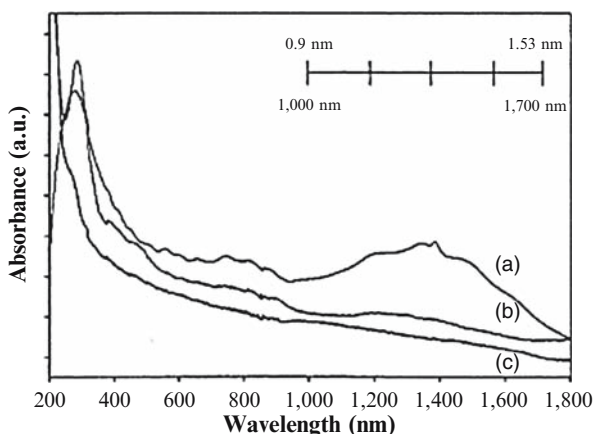


Fig. 10.11 Carbon nanotubes have an absorption peak between 1,000 and 1,500nm as defined by line (a) in this figure. A decrease in absorption is seen in lines (b) and (c) due to wrapping of polysaccharides around the tubes for water solubilization (Reprinted from Casey et al., 2005. With permission from Elsevier)

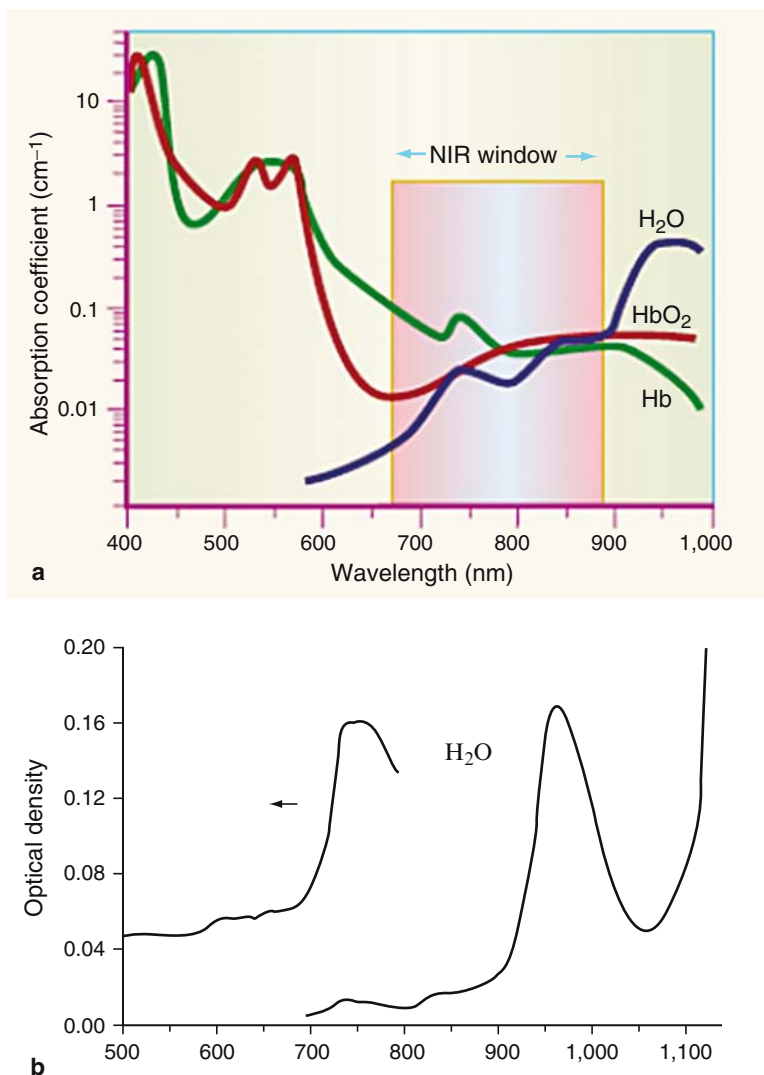


Fig. 10.12 The most efficient regions for nanotube absorption lie where water and hemoglobin have absorption minima: between 700 and 900 nm and around 1,100 nm (Braun and Smirnov 1993; Reprinted from Weissleder, 2001. With permission from Elsevier) (See Color Plates)

nanotubes. The spectral region where water, and hemoglobin absorb the least in between 700–900 nm and near 1,100 nm (see Fig. 10.12); making use of light sources in this range acceptable for nanotube stimulation (Weissleder, 2001). There are lasers with emission near 800 nm (diode lasers) and 1064 nm (Nd:YAG lasers) that are clinically used, especially for applications in dermatology and plastic surgery. To most efficiently couple to incident radiation they should be longer than half the wavelength of the incident light. So for the clinically relevant lasers operating

at 800 and 1064 nm, maximum absorption should occur for nanotubes longer than 400 or 532 nm. Length may contribute to efficiency of nanotube infrared absorption but if the nanotubes were grown with metallic catalyst, residual catalyst material will affect thermal efficiency. Nanotubes with minimal catalyst are superior since there are more nanotubes per unit mass if there is little or no catalyst adding to the mass. Furthermore, MWNT might be more efficient than SWNT due to their additional mass which adds to the heat transfer effect from nanotubes contained in a media surrounding the tissue to be ablated. This concept stems from experiments designed to whisk away heat from a mechanical system by incorporating MWNT into the flowing water system (Launay et al., 2006; Park and Jung, 2007). MWNT can be used not only to induce the thermal precedent of the biosystem, but can also efficiently transfer heat from a surrounding fluid to generate larger hyperthermic regions. Transfer of heat from a nanoparticle to the surrounding media is a limiting factor of thermal therapies but carbon nanotubes can overcome this limitation more effectively than metallic nanoparticles.

“Nanobombs” have recently been discovered to generate even more powerful anti-tumor effects. “Nanobombs” have been explained as tight bundles of carbon nanotubes, such that when incident radiation excites them the energy/heat has nowhere to go so a microscopic explosion occurs (Panchapakesan et al., 2005). However, this explosion of tumor matter may be potentially hazardous since if not all the cancerous material is thermally destroyed, the material could become mobile due to the induced force. Another avenue for nanotubes is to act as carrier molecules, since they can be functionalized to carry molecules like DNA (Xin and Woolley, 2005; Xu et al., 2003). As an example of current technique researchers have piggy-backed a DNzyme to a nanotube to get it across cell membranes (Yim et al., 2005). The DNzyme are sequences of single-stranded DNA capable of interrupting RNA activity in a tumor cell, and thereby activating apoptosis (Yim et al., 2005). Although it is unknown how much heat is generated at the surface of nanotubes, they can be used to rapidly (within minutes) heat a bulk solution above 45°C, leading to thermal ablation and cell death (Kam et al., 2005; Torti et al., 2007). Both SWNT and MWNT have been shown to be effective for thermal ablation, as shown in Fig. 10.13.

As with fullerenes, carbon nanotubes are also hydrophobic and must be made soluble for suspension in aqueous media. Nanotubes are commonly functionalized to make them water soluble although they can also be non-covalently wrapped with polymers, polysaccharides, surfactants, and DNA to aid in solubilization (Casey et al., 2005; Kam et al., 2005; Sinani et al., 2005; Torti et al., 2007). Functionalization usually begins by formation of carboxylic acid groups on the exterior of the nanotubes by oxidative treatments such as sonication in acids, followed by secondary chemical reactions to attach functional molecules to the carboxyl groups. For example, polyethylene glycol has been attached to SWNT to aid in solubility (Zhao et al., 2005). DNA has also been added onto SWNT for efficient delivery into cells (Kam et al., 2005).

Thermal ablation using carbon nanotubes is a definite option for use in oncology, especially since nanotubes can be functionalized with targeting modalities like folic acid. Some cancer cell types express large numbers of folic acid receptors on

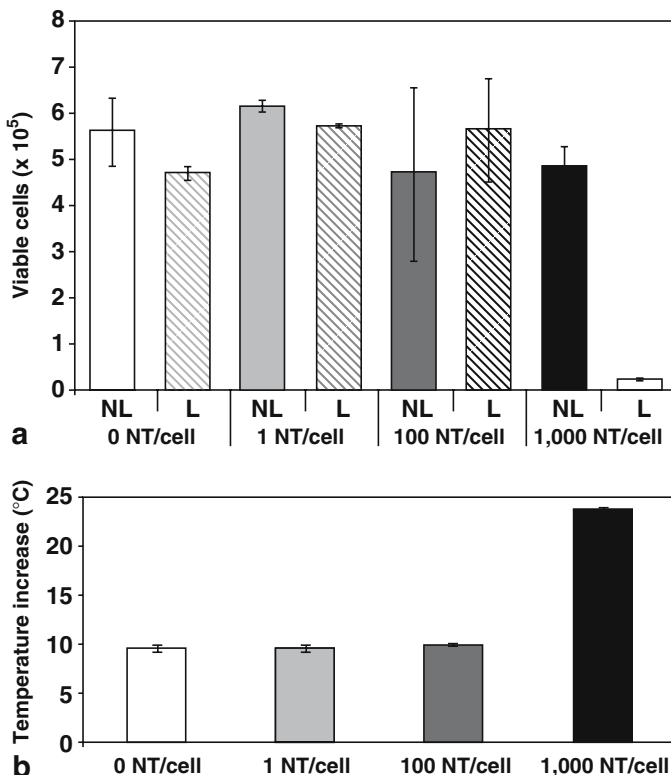


Fig. 10.13 MWNT, 1,100nm in length are efficient generators of heat in a bulk solution leading to cell death. Within 60s of exposure temperature increases of almost 25°C over the baseline, or up to almost 60°C can be achieved. Kidney cancer cells exposed to such a high temperature undergo irreversible cell damage leading to death. The number of nanotubes needed for efficient cell killing was found to be 1,000 nanotubes per cell with exposure to 1,064nm light (L). With no light exposure (NL) the amount of cells killed was statistically the same as control cells without nanotubes or light exposure (Reprinted from Torti et al., 2007. With permission from Dove Medical Press Ltd.)

their surfaces and thus will bind readily to folic acid attached to nanotube sidewalls (Kam et al., 2005). This is just one example and is shown in Fig. 10.14, for cell targeting by functionalizing nanotubes but there are many more, making nanotubes potentially very valuable since they can be targeted directly to tumors and the tumors then ablated using heat generated by infrared stimulation of the nanotubes (Kam et al., 2005). Using infrared radiation to pass through tissues and target tumors loaded with nanotubes is the ideal situation, but there are complicating factors. Infrared radiation can only penetrate a short distance within tissue; less than 2 cm for 1,064 nm light. It is very likely that thermal ablation techniques will need to be applied to malignancies on the skin or to those that be reached using endoscopes or during open surgical operations. This may limit thermal ablation using

nanotubes to the same cancer types that could be targeted using photodynamic therapy. Functionalized nanotubes can lose their functional molecules due to breakage of the bonds by the heat generated at the nanotube sidewall following infrared exposure. Release of functional molecules may be a useful delivery mechanism, but since functional molecules also tend to aid in water solubility of the nanotubes, such release may result in reaggregation of the nanotubes and potential blockage.

Recently single-walled carbon nanotubes have been used for thermal ablation of hepatic and pancreatic tumors by a very different heating mechanism. SWNT generated hyperthermic temperatures rapidly via stimulation with radiofrequency at 13 MHz, 600 W for 2 min with excellent cell death in both the *in vitro* and *in vivo* studies. Radiofrequency ablation is commonly employed clinically for ablation of kidney, bone, liver, and pancreatic cancers. Researchers have been investigating the use of magnetic nanoparticles to more effectively target tumors through the use of radiofrequency. The novel use of SWNT coupled with radiofrequency was not attributed to any magnetic effects but rather alignment of the nanotubes with the magnetic field to create long antennae and the electrical resistance in nanotubes with high aspect ratios. The result of the study further indicates the importance that the length of nanotubes has upon interaction with the incident electromagnetic field to generate heat.

10.4.3 Filled Nanotubes and Nanohorns for Drug Delivery

Carbon nanomaterials can be used for delivery of drugs by attachment of molecules to the outside of fullerenes or nanotubes with release mechanisms such as thermal or enzymatic disengagement. However, either release mechanism might damage the drug moiety; a more efficient method is available by simply filling the hollow interiors of carbon nanotubes. Metals can fill the interior of nanotubes by thermal vaporization of the metal during nanotube growth or in the presence of open-ended nanotubes (Huang et al., 2004; Kumar et al., 2004). This method works well for stable particles like metals, but is not applicable for adding chemotherapeutic agents to nanotube interiors. The simplest way to fill nanotubes is by capillary action, especially since most chemotherapeutic agents can be dispersed in solvents that are compatible with this method. Capillary mechanisms and filled nanotubes are shown in Fig. 10.15. Important parameters for capillary filling include the viscosity and surface tension of the carrier solvent (Kim et al., 2005; Tessonnier et al., 2005); fluids with surface tension much higher than water will not flow all the way through the tubes (Monthioux, 2002). Also, the carrier solvent containing the drugs to fill the interior of the nanotubes must be supersaturated, so that the drug molecules will adhere to the interior of the tube sidewall (Monthioux, 2002). Nanotubes opened by oxidative methods not only have their ends removed but also have holes along the tube wall which can allow for increased permeability of the nanotube for drug filling (Sitharaman et al., 2005). Opened nanotubes (not functionalized or coated) usually

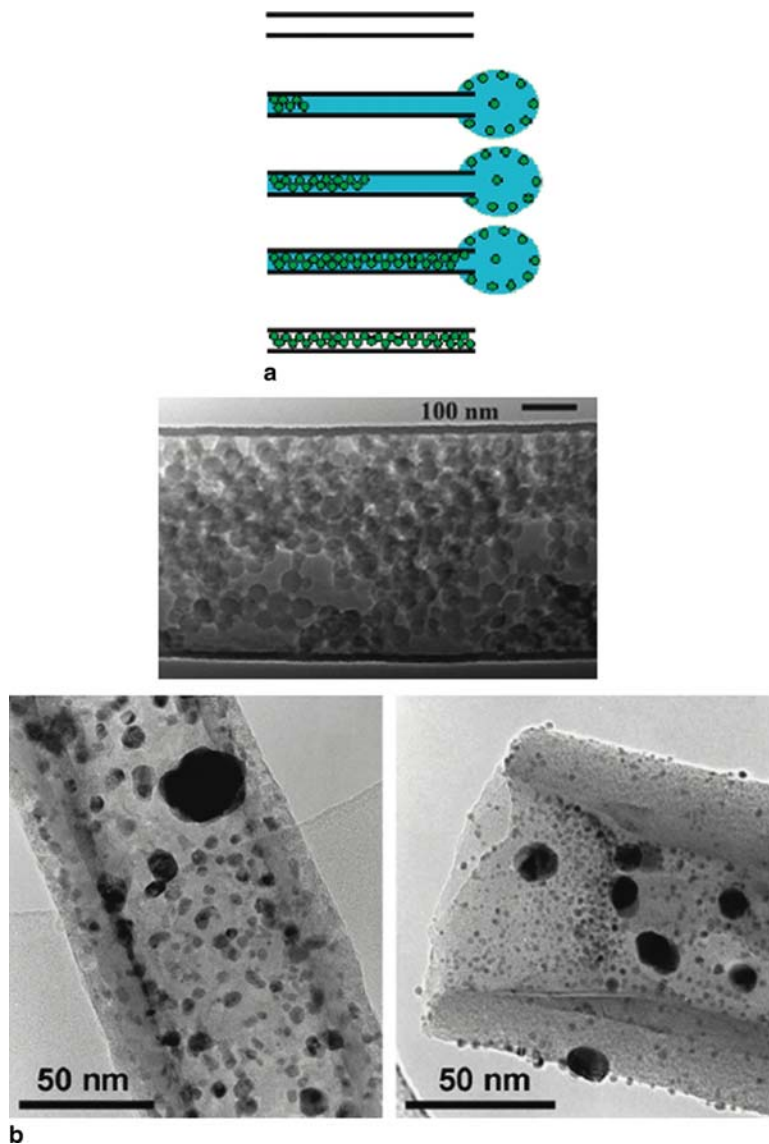


Fig. 10.15 The methods for capillary filling of nanotubes involves dispersal of the agent in a liquid capable of flowing into the nanotube followed by subsequent evaporation of the solvent to leave particles inside the tube. Nanotubes have been filled with polystyrene spheres and palladium nanocrystals using this method (Reprinted from Kim et al., 2005. With permission from American Chemical Society; Reprinted from Tessonnier et al., 2005. With permission from Elsevier) (*See Color Plates*)

have enough carboxyl groups to be slightly water soluble and when stirred with an aqueous drug, will allow for fluid transport down the length of the tube (Ajima et al., 2005; Matsumura et al., 2007; Murakami et al., 2004). Many chemotherapeutic agents are hydrophobic but there is no problem with using a non-aqueous carrier solvent, so long as the surface tension is comparable to that of water. Upon evaporation of the solvent, drug molecules will aggregate along the interior walls of the nanotubes. There is evidence for stronger binding potentials of N_2 and H_2 along the interior tube wall which may further aid in drug aggregation along the tube interiors (Ajima et al., 2006). The goal of drug-filled nanotubes or nanohorns is delivery of the drug at a specific site which requires that the drug be released slowly to account for the time needed to localize to a site, or that the drug is sealed within the tube. Once drug molecules are aggregated at the interior of the nanotubes, the tubes cannot simply be redispersed in the same solvent that was used for filling since the drug may solvate and fluid flow will leach the drug out of the tube. Another difficulty is that drug molecules will also adhere to the exterior of the nanotubes. Ideally, for release of the drug at a specific site, the drug would be encapsulated within the tube with minimal drug along the exterior which could induce negative consequences at sites other than the target location. However, it is difficult to remove drugs adhered to the outside of the tube without removing drug at the interior unless the nanotube ends are capped. Therefore, methods to enclose chemotherapeutic agents within the nanotubes while still allowing for drug release at a specific site are sought.

Viscous polymer solutions will not flow into the interiors of nanotubes by capillary mechanisms, but they can be forced into the tubes using centrifugal force. The polysaccharide sodium alginate is commonly used for drug delivery and food stuffs as a natural thickener. Alginate is easily and rapidly cross-linked with metal ions and biocompatible calcium chloride is commonly used. A clever technique for filling and sealing nanotubes has recently emerged using this sodium alginate. Sodium alginate polymer was loaded with fluorescent polystyrene nanoparticles or quantum dots and forced through hollow MWNT by centrifugation and filled tubes were cross-linked with calcium chloride, as shown in Fig. 10.16 (Nadarajan et al., 2007). Nanotubes filled with this method were found to be gradient loaded depending on the length of the nanotubes. Although the exteriors of the nanotubes are coated with alginate, sufficient washing removed alginate from the exterior, while leaving the tube ends capped and the fluorescent particles trapped inside (Nadarajan et al., 2007). A method using alginate for nanotube filling is an excellent choice since depending upon the molecular weight of the alginate, it will degrade within specific time intervals to release drugs over time. A problem with chemotherapeutic agents is their rapid clearance which requires more doses to be delivered. A nanoparticle that can be filled with a chemotherapeutic agent, targeted to a specific location, and releases the agent slowly is an ideal choice for successful drug delivery and patient comfort.

Although MWNT have large hollow interiors, SWNT aggregated into nanohorns, were the first tubular materials to be filled with drug agents. Nanohorns have the distinct advantage of having one closed end so there is outflow only from one end of the tube and possibly better retention within the nanotube. Nanohorns are spherical aggregates of SWNT with a diameter of 80–100 nm so they are no bigger than a large diameter MWNT (Ajima et al., 2005). The first drugs encapsulated

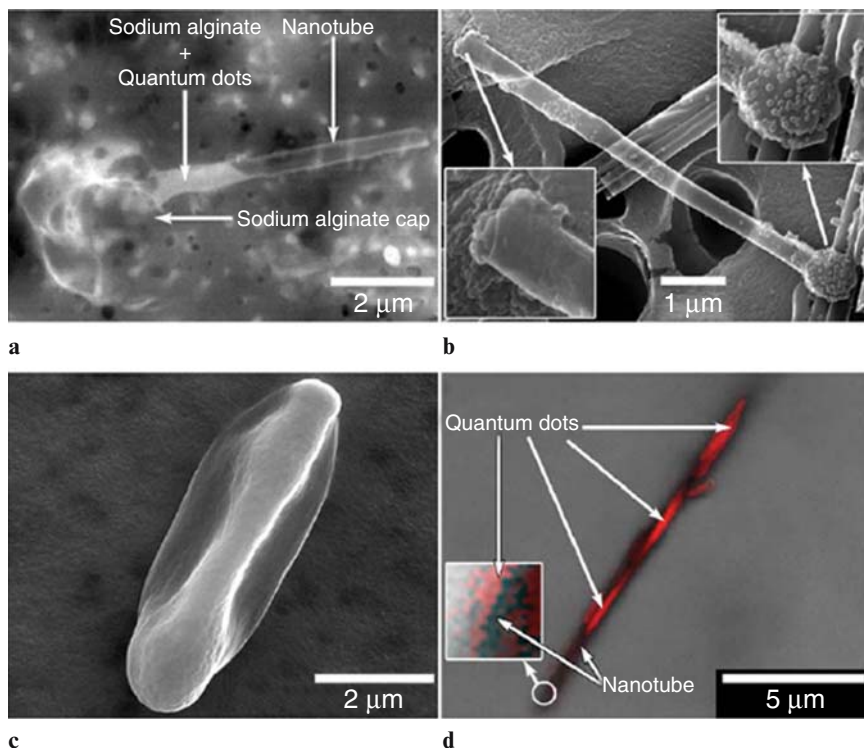


Fig. 10.16 Carbon nanotubes filled with quantum dots in a sodium alginate carrier solvent. The alginate encloses the dots into the tubes by sealing the tube ends. A large majority of excess alginate around the tubes was removed by repeated washing (Reprinted from Nadarajan et al., 2007. With permission from Elsevier) (*See Color Plates*)

within nanohorns were dexamethsone (an anti-inflammatory glucocorticoid) and cisplatin (CDDP) (a platinum-based chemotherapeutic), as shown in Fig. 10.17 (Ajima et al., 2005; Murakami et al., 2004). Using capillary filling methods a 12% loading of the nanotubes was possible using CDDP, and 80% of the CDDP was released with 50h soaking of the nanohorns in phosphate buffered saline (PBS) (Matsumura et al., 2007). Platinum-based chemotherapeutic agents (cisplatin, carboplatin, and oxaliplatin; see Fig. 10.18) are stable under standard laboratory conditions, and the platinum core remains intact upon delivery in the body. Therefore, it is easy to monitor the distribution of platinum-based chemotherapeutic agents throughout the lifespan of the drug (from bench to human to waste) by measuring platinum concentrations using elemental analysis or other techniques. These compounds are also small and will fit within SWNT and MWNT. Platinum-based chemotherapeutic agents are an ideal choice for use in conjunction with carbon nanotube drug delivery since they are stable, small, easy to quantify due to the metallic core, and furthermore illicit better cancer response when used in conjunction with hyperthermia.

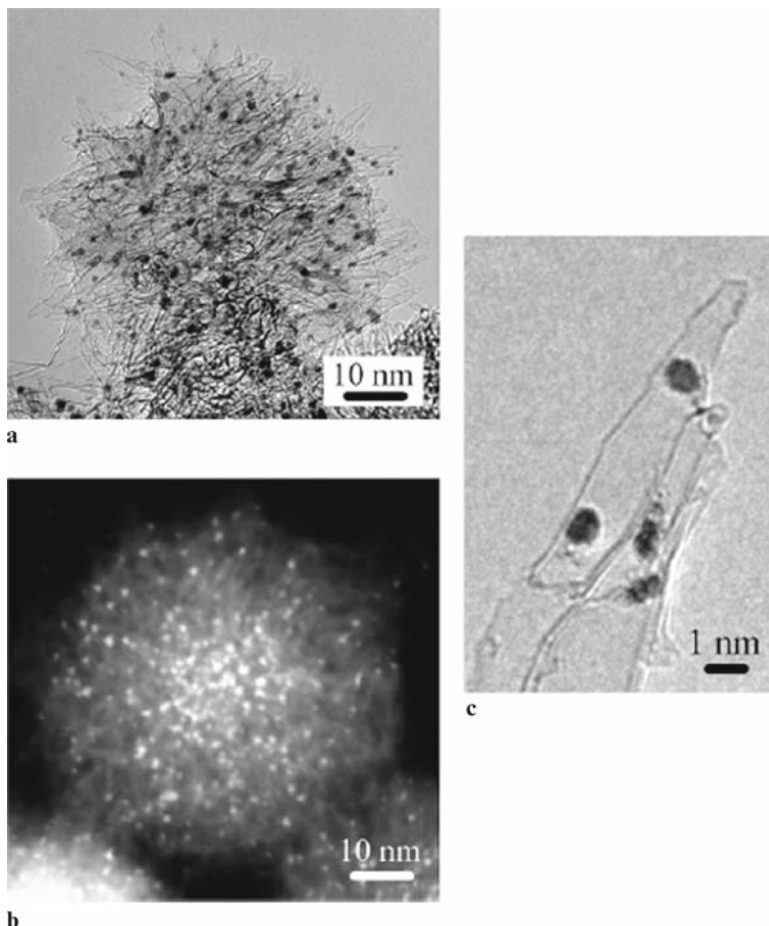


Fig. 10.17 Carbon nanohorns encapsulate the chemotherapeutic agent cisplatin. TEM image (a) and inverse contrast TEM image of cisplatin loaded into the nanohorns (b). The drug is held at the closed end of the nanotube according to the image in (c) (Ajima et al., 2006)

10.4.4 Toxicity of Carbon Nanomaterials

Without a doubt, one of the great concerns in the field of nanotechnology is the potential toxicity of carbon nanomaterials. Growth and processing techniques will strongly influence perceived toxic effects attributed to the carbon structures. Aggregation can affect clearance rates by the immune system. Lymphatic drainage is very important since one of the first drainage repositories is the lungs and inhaled carbon nanoparticles have been found to induce lung fibrosis (scarring) (Stoeger et al., 2006).

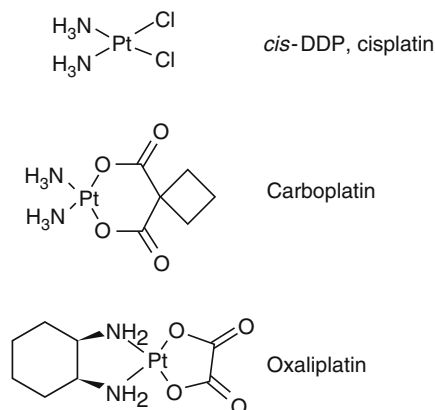


Fig. 10.18 The platinum based chemotherapeutic agents are stable and small enough to fit within the interior of an SWNT or MWNT

10.4.4.1 Fullerene Toxicity

C₆₀ fullerenes are still being evaluated for toxicity parameters. They have been found to induce lipid peroxidation with the addition of functional groups mediating the toxicity (Sayes et al., 2004). Preparations to make water-soluble fullerenes involves organic solvents which could be retained within the fullerene clusters leading to toxic effects; however, any amount of residual solvent would be miniscule and doubtful to illicit such response. Use of pristine nano-sized fullerene aggregates, most likely to be encountered in standard laboratory usage, have not shown toxic behavior on *in vitro* cell cultures, as shown in Fig. 10.19 (Levi et al., 2006). An alternative mechanism for potential toxicity of fullerenes is their interaction with light. Fullerenes have been repeatedly demonstrated to have the potential to act as photosensitizing agents capable of producing singlet oxygen and radical oxygen species, which can damage cell membranes by lipid peroxidation (Foote, 1995; Kasermann and Kempf, 1998; Mroz et al., 2007; Rancan et al., 2005; Tabata et al., 1997; Yang et al., 2007). Therefore, only very careful toxicity analysis of pristine fullerenes, protected from light exposure, can evaluate the true toxic nature of fullerenes for medicinal applications.

10.4.4.2 Carbon Nanotubes Toxicity

Very long nanotubes may not be able to be removed from the body by immune system cells like macrophages and hence may linger in the body for a long time. There is some data that radioactive-labeled water-soluble fullerenes are cleared

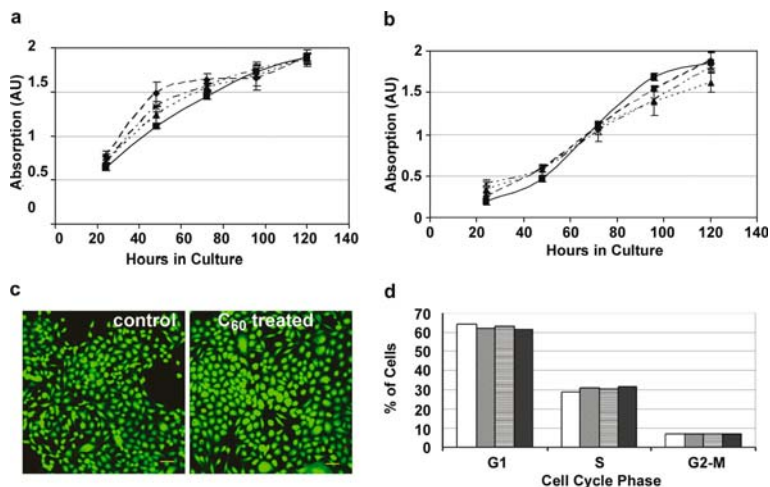


Fig. 10.19 Lack of toxic effects of C₆₀ fullerene on breast epithelial cells. C₆₀ does not inhibit cell proliferation. MCF 10A and (A) MDA MB 231 (B) breast cancer cell lines were cultured either in the absence or presence of methanol C₆₀ and cell proliferation was assayed by crystal violet staining. ♦ Control, no C₆₀, ■ 10 μg C₆₀, ▲ 50 μg C₆₀, X 250 μg C₆₀. (C). MDA MB 231 cells were simultaneously stained with calcein and ethidium using a live-dead assay kit. Lack of red-colored cells and the presence of cells stained in green indicate the lack of toxicity (D). MDA MB 231 cells were either untreated (open box) cultured with varying amounts 10 (gray ■), 50 (patterned ■) and 100 μg (filled ■) of C₆₀ for 48 h and analyzed for cell cycle progression by flow cytometry (Levi et al., 2006) (See Color Plates)

from the body (Singh et al., 2006), but the dilemma is that functionalized nanotubes may behave differently than pristine nanotubes and thus the immune response and clearance rates might be different. An unknown toxicity factor with nanotubes is the potential for fibrosis around nanotube deposits used for oncology applications. This would be a highly undesirable effect as it could lead to pain in the fibrotic area. It seems to depend upon the mechanism of exposure as to whether carbon nanotubes will be toxic or not. Instillation in the lungs has been shown to be detrimental but the delivered doses were also quite high. Keratinocytes (skin cells) exposed to nanotubes *in vitro* showed an immune response as has whole skin on laboratory animals exposed to nanotube dust (Monteiro-Riviere et al., 2005a, b). Unfunctionalized or uncoated nanotubes readily aggregate in aqueous solutions and are readily coated by proteins when placed in media containing serum (Meng et al., 2005). Coating by serum proteins occurs when nanotubes contact with blood and although such coating may aid in solubility of the nanotubes, any potential aggregation of the nanotubes in the bloodstream could impede blood flow with deadly consequences. A final point about toxicity which must be accounted for is residual metallic catalyst used to grow some types of nanotubes that may be available for biological interactions. Nanotubes grown without catalyst are the best choice to evaluate the true toxicity of nanotubes

alone. Since nanotubes may be doped, for example, with boron or nitrogen, these varieties must be evaluated separately to determine toxic effects due to the degree of added dopant. Nitrogen-doped nanotubes have been compared undoped MWNT and were found to illicit a decreased toxic in *in vitro* cell culture experiments (Carrero-Sanchez et al., 2006). To evaluate the toxicity of any carbon nanoparticles, the size, shape, surface charge, and any functionality need to be examined.

10.5 Future Pharmacological Potential of Carbon Nanomaterials

Carbon nanomaterials have been described according to reported results and based on published results there is great potential for the use of carbon nanoparticles in oncology applications. Although nanotubes have previously been explored for use in thermal ablation techniques and for drug delivery, combining the two techniques will be the next generation of techniques for potential clinical use. Filling of nanotubes, hyperthermic chemotherapy using nanotubes, and composites of chemotherapeutic agents, biopolymers, and nanotubes offer new fronts for future scientific exploration. C₆₀ fullerenes may not be the ideal choice for drug delivery but they could aid in development of more efficient photosensitizers for photodynamic therapy or to mediate free radical damage from chemotherapeutic agents.

10.5.1 Applications to Intraperitoneal Hyperthermic Chemotherapy

History has shown that peritoneal carcinomatosis is uniformly fatal with median survival in the range of approximately 6 months. For more than a decade, a handful of centers have pursued aggressive surgical management of peritoneal surface dissemination as an alternative approach to this disease. This chapter establishes the conceptual framework for understanding the role of carbon nanotubes in the treatment of patients with advanced malignancies. Intraperitoneal hyperthermic chemoperfusion (IPHC) is designed to deliver chemotherapeutic agents to a local area for delivery at higher doses than can be given systemically and also to increase uptake of the drug by malignant cells by increasing cell membrane permeability and cell metabolism. Carbon nanotubes especially may be able to further improve IPHC surgical techniques by localizing the area of applied heat during chemoperfusion. There are a few pathways through which this is possible, and an advantage of using carbon nanotubes with this technique is that it is an open surgical technique so the entire contents of the abdomen can be viewed and manipulated to provide the most effective treatment. Since many cancers that express folate receptors (ovarian, lung,

kidney, and colon) metastasize to the peritoneum, nanotubes functionalized with folic acid could be applied directly into the peritoneal cavity by perfusion techniques and/or via systemic delivery. The tubes would then label metastatic lesions, including micrometastasis and areas where nanotubes have attached appear black which will pinpoint locations where a small diameter beam of infrared light should be applied. If infrared stimulation is applied to targeted nanotubes when a chemotherapeutic agent is in fluid surrounding the target area then hyperthermic chemotherapy will be induced only in the specific location chosen by the surgeon. Although this may seem to be a tedious task, resection of micrometastasis would be far more labor-intensive, especially since they may be difficult to find. An easier alternative would be to apply a mixed solution of chemotherapeutic agent and nanotubes around suspicious areas where larger metastasis have been removed concurrent with application of infrared light. This method of delivery would ensure that residual nodules would be treated; however, it would not address micrometastasis that are undetectable to the surgeon. Perhaps the most efficient method to combine hyperthermia and chemotherapy in a nano-localized area is to target nanotubes, filled with the chemotherapeutic agent and apply infrared light to heat the nanotube and release the drug at the target site in the open peritoneum. Use of targeted nanotubes would make delivery of chemotherapeutic agents and hyperthermia potentially very easy since one large light source could also be used to stimulate all regions which have collected nanotubes and drug. There are some very grand benefits from using nanotube-induced hyperthermic chemotherapy, namely that the nanotubes will generate sufficient heat in a localized area to promote drug delivery, thus sparing surrounding tissues from receiving hyperthermic chemotherapy unnecessarily, and more effectively treating micrometastatic lesions. Nano-IPHC would be much faster since only seconds of light exposure are needed to generate hyperthermia, and the (untargeted) nanotube material could quickly be flushed from the peritoneum.

10.5.2 Composites

Combining carbon nanotubes with biopolymers may be an alternate pathway for drug delivery. Biopolymer delivery of chemotherapeutic agents is an established technique for delivery and mechanisms for drug release include diffusion and osmosis. Since nanotubes can be functionalized or wrapped with polymers to aid in solubility, or even to encapsulate drugs, a larger composite of nanotubes and biopolymers could be used for localized hyperthermic chemotherapy. Hydrogels are polymers that absorb water readily and release therapeutic agents slowly. Incorporation of nanotubes into the hydrogel and subsequent heating of the hydrogel complex would lead to rapid release of the drug by dissolving the hydrogel using heat from the nanotubes. Hydrogel materials that have been examined for medicinal applications include xanthan gum, guar gum, polyethylene oxide, polyvinyl alcohol, chitosan/polyethylene glycol blends, dextran, and gelatin (El Sherbiny et al., 2005; Jain et al.,

2006; Li et al., 2004; Novikova et al., 2006; Wu et al., 2007; Zhang et al., 2003). In fact, nanotubes have been shown to stabilize gelatin hydrogels for biological applications (Li et al., 2004). Perhaps small, round composites of nanotubes, chemotherapeutic agents, and polymers are envisioned but sheets of such a material could be made such that a surgeon would be able to wrap the material around an area of interest, shine infrared light and entire sections of tissue would be treated simultaneously. For afflictions where large portions of the bowel are involved this may reduce the total amount of bowel that must be resected.

C_{60} may not deliver agents as effectively as nanotubes, but the potential to act as a photosensitizer in photodynamic therapy applications is advantageous. An exciting opportunity is to couple C_{60} with a standard photodynamic agent such as Photofrin to maximize the amount of reactive oxygen species produced, and research is being pursued to explore synergistic behavior of C_{60} and porphyrins (Milanesio et al., 2005). It may be possible to make an effective therapy using such a combination since both photosensitizers absorb in the visible wavelengths so white light could be used.

10.5.3 Benefits of Carbon Nanomaterials in Medicine

Carbon nanomaterials will most likely be beneficial in medicine, specifically in oncology applications in the future. There are multiple possibilities for drug delivery using carbon nanotubes to directly release a drug at a specific site, or to increase cellular uptake and effectiveness of a chemotherapeutic by inducing hyperthermia at the cell membranes. Since IPHC is an open surgical technique nanotubes could be targeted to micrometastasis and then targeted areas could be visualized by the surgeon. Use of nanotubes in this application is an exciting first step towards clinical use of nanotubes in oncology. C_{60} fullerenes seem to offer the most potential as photosensitizer agents for use in photodynamic therapy, but their ability to scavenge damaging

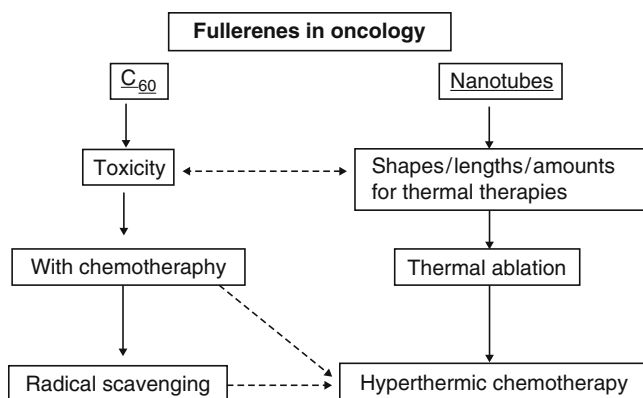


Fig. 10.20 A flow diagram for the potential applications of using fullerenes in oncology

secondary species produced by chemotherapeutic agents has not yet been determined. Thus C_{60} may be able to play a dual role in oncology by scavenging reactive species in a protective mechanism, or generating them to illicit cell damage and death.

10.6 Conclusion

A few of the current methods used in oncology have been described, as have some of the properties of carbon nanotubes and C_{60} fullerenes. There are applications in oncology where use of carbon nanomaterials can aid in drug delivery or potentiate reactive oxygen species to induce damage and cell death of malignancies. Applications using carbon nanomaterials which may proceed to clinical usage more rapidly than standard drug delivery are (1) the use of C_{60} as a photosensitizing agent or (2) the use of carbon nanotubes to induce localized hyperthermic chemotherapy. A schematic of the different pathways for pharmacological ventures incorporating carbon nanotubes in oncology is provided in Fig. 10.20. There is a long way to go to develop the applications fully, but the ideas may be more readily accepted by the medical community since they are based on modifying some of the current standards of care.

References

- Abe S, Tokizaki T, Miki Y, Tateishi A, Ogawa K, Nakano H, Matsushita T (2005) Hyperthermic isolated regional perfusion with CDDP for bone and soft-tissue sarcoma of the lower limb: pharmacokinetics, thermal dose, toxicity, and feasibility. *Cancer Chemotherapy and Pharmacology* 56: 55–62.
- Ajima K, Maigne A, Yudasaka M, Iijima S (2006) Optimum hole-opening condition for cisplatin incorporation in single-wall carbon nanohorns and its release. *Journal of Physical Chemistry B* 110: 19097–19099.
- Ajima K, Yudasaka M, Murakami T, Maigne A, Shiba K, Iijima S (2005) Carbon nanohorns as anticancer drug carriers. *Molecular Pharmacology* 2: 475–480.
- Alvarez SJ, Leon R, Hernandez B, Sampedro EA, Zhang LM, Castell AE (2003) Fullerene C_{60} protects against Langerhans cells depletion induced by DMBA. *Journal of Investigative Dermatology* 121: 1244.
- Avdeev MV, Khokhryakov AA, Tropin TV, Andrievsky GV, Klochkov VK, Derevyanchenko LI, Rosta L, Garamus VM, Priezhev VB, Korobov MV, Aksenov VL (2004) Structural features of molecular-colloidal solutions of C_{60} fullerenes in water by small-angle neutron scattering. *Langmuir* 20: 4363–4368.
- Babilas P, Karrer S, Sidoroff A, Landthaler M, Szeimies RM (2005) Photodynamic therapy in dermatology – an update. *Photodermatology Photoimmunology and Photomedicine* 21: 142–149.
- Bachilo SM, Strano MS, Kittrell C, Hauge RH, Smalley RE, Weisman RB (2002) Structure-assigned optical spectra of single-walled carbon nanotubes. *Science* 298: 2361–2366.
- Bandow S, Asaka S, Saito Y, Rao AM, Grigorian L, Richter E, Eklund PC (1998) Effect of the growth temperature on the diameter distribution and chirality of single-wall carbon nanotubes. *Physical Review Letters* 80: 3779–3782.
- Bashkin IO, Izotov AN, Moravsky AP, Negrii VD, Nikolaev RK, Ossipyan YA, Ponyatovsky EG, Steinman EA (1997) Photoluminescence of solid C_{60} polymerized under high pressure. *Chemical Physics Letters* 272: 32–37.

- Bastide C, Garcia S, Anfossi E, Ragni E, Rossi D (2006) Histologic evaluation of radiofrequency ablation in renal cancer. *European Journal of Surgical Oncology* 32: 980–983.
- Belin T, Epron R (2005) Characterization methods of carbon nanotubes: a review. *Materials Science and Engineering B-Solid State Materials for Advanced Technology* 119: 105–118.
- Berger C, Poncharal P, Yi Y, de Heer W (2003) Ballistic conduction in multiwalled carbon nanotubes. *Journal of Nanoscience and Nanotechnology* 3: 171–177.
- Bibby DC, Talmadge JE, Dalal MK, Kurz SG, Chytil KM, Barry SE, Shand DG, Steiert M (2005) Pharmacokinetics and biodistribution of RGD-targeted doxorubicin-loaded nanoparticles in tumor-bearing mice. *International Journal of Pharmaceutics* 293: 281–290.
- Bisaglia M, Natalini B, Pellicciari R, Straface E, Malorni W, Monti D, Franceschi C, Schettini G (2000) C-3-fullero-tris-methanodicarboxylic acid protects cerebellar granule cells from apoptosis. *Journal of Neurochemistry* 74: 1197–1204.
- Blank VD, Nuzdin AA, Bagramov RK, Prokhorov VM (2001) A comparison of some thermodynamic parameters between superhard fullerite, some metals and some covalent elements. *Carbon* 39: 905–908.
- Bogdanovic G, Kojic V, Dordevic A, Canadanovic-Brunet J, Vojinovic-Miloradov M, Baltic VV (2004) Modulating activity of fullerol C₆₀(OH)₂₂ on doxorubicin-induced cytotoxicity. *Toxicology In Vitro* 18: 629–637.
- Bolskar RD, Benedetto AF, Husebo LO, Price RE, Jackson EF, Wallace S, Wilson LJ, Alford JM (2003) First soluble M@C-60 derivatives provide enhanced access to metallofullerenes and permit in vivo evaluation of Gd@C-60[C(COOH)₂](10) as a MRI contrast agent. *Journal of the American Chemical Society* 125: 5471–5478.
- Bosi S, Da Ros T, Castellano S, Banfi E, Prato M (2000) Antimycobacterial activity of ionic fullerene derivatives. *Bioorganic and Medicinal Chemistry Letters* 10: 1043–1045.
- Bosi S, Da Ros T, Spalluto G, Prato M (2003) Fullerene derivatives: an attractive tool for biological applications. *European Journal of Medicinal Chemistry* 38: 913–923.
- Bourgeois H, Vermorken J, Dark G, Jones A, Fumoleau P, Stupp R, Tourani J, Brain E, Nguyen L, Lefresne F, Puozzo C (2007) Evaluation of oral versus intravenous dose of vinorelbine to achieve equivalent blood exposures in patients with solid tumours. *Cancer Chemotherapy and Pharmacology* 60: 407–413.
- Braun C, Smirnov S (1993) Why is water blue. *J. Chemical Education* 70: 612.
- Brettreich M, Hirsch A (1998) A highly water-soluble dendro[60]fullerene. *Tetrahedron Letters* 39: 2731–2734.
- Brewis M, Clarkson GJ, Humberstone P, Makhseed S, McKeown NB (1998) The synthesis of some phthalocyanines and naphthalocyanines derived from sterically hindered phenols. *Chemistry-A European Journal* 4: 1633–1640.
- Brigger I, Morizet J, Laudani L, Aubert G, Appel M, Velasco V, Terrier-Lacombe MJ, Desmæle D, d'Angelo J, Couvreur P, Vassal G (2004) Negative preclinical results with stealth((R)) nanospheres-encapsulated Doxorubicin in an orthotopic murine brain tumor model. *Journal of Controlled Release* 100: 29–40.
- Brown E, Hao L, Gallop JC, Macfarlane JC (2005) Ballistic thermal and electrical conductance measurements on individual multiwall carbon nanotubes. *Applied Physics Letters* 87: 2–3.
- Brunner TJ, Grass RN, Bohner M, Stark WJ (2007) Effect of particle size, crystal phase and crystallinity on the reactivity of tricalcium phosphate cements for bone reconstruction. *Journal of Materials Chemistry* 17: 4072–4078.
- Brusentsov NA, Brusentsova TN, Filinova EY, Jurchenko NY, Kupriyanov DA, Pirogov YA, Dubina AI, Shumskikh MN, Shumakov LI, Anashkina EN, Shevelev AA, Uchevatkin AA (2007) Magnetohydrodynamic thermochemotherapy and MRI of mouse tumors. *Journal of Magnetism and Magnetic Materials* 311: 176–180.
- Burke PJ, Li SD, Yu Z (2006) Quantitative theory of nanowire and nanotube antenna performance. *IEEE Transactions on Nanotechnology* 5: 314–334.
- Capozzi V, Trovato T, Berger H, Lorusso GF (1997) Photoluminescence spectra of C-60 thin films deposited on different substrates. *Carbon* 35: 763–766.

- Carrero-Sanchez JC, Elias AL, Mancilla R, Arrellin G, Terrones H, Lacleste JP, Terrones M (2006) Biocompatibility and toxicological studies of carbon nanotubes doped with nitrogen. *Nano Letters* 6: 1609–1616.
- Casey A, Farrell GF, McNamara M, Byrne HJ, Chambers G (2005) Interaction of Carbon Nanotubes with Sugar Complexes. *Synthetic Metals* 153: 357–360.
- Castano AP, Demidova TN, Hamblin MR (2005) Mechanisms in photodynamic therapy: Part three – Photosensitizer pharmacokinetics, biodistribution, tumor localization and modes of tumor destruction. *Photodiagnosis and Photodynamic Therapy* 2: 91–106.
- Charlier JC, Iijima S (2001) Growth mechanisms of carbon nanotubes. *Carbon Nanotubes* 80: 55–80.
- Chen B, Pogue BW, Hoopes PJ, Hasan T (2006) Vascular and cellular targeting for photodynamic therapy. *Critical Reviews in Eukaryotic Gene Expression* 16: 279–305.
- Chen HHC, Yu C, Ueng TH, Chen SD, Chen BJ, Huang KJ, Chiang LY (1998) Acute and subacute toxicity study of water-soluble polyalkylsulfonated C-60 in rats. *Toxicologic Pathology* 26: 143–151.
- Chen YW, Hwang KC, Yen CC, Lai YL (2004) Fullerene derivatives protect against oxidative stress in RAW 264.7 cells and ischemia-reperfused lungs. *American Journal of Physiology-Regulatory Integrative and Comparative Physiology* 287: R21–R26.
- Corti L, Skarlatos J, Boso C, Cardin F, Kosma L, Koukourakis MI, Giatromanolaki A, Norberto L, Shaffer M, Beroukas K (2000) Outcome of patients receiving photodynamic therapy for early esophageal cancer. *International Journal of Radiation Oncology*Biophysics* 47: 419–424.
- Da Ros T, Spalluto G, Prato M (2001) Biological applications of fullerene derivatives: a brief overview. *Croatica Chemica Acta* 74: 743–755.
- Dalmas F, Dendievel R, Chazeau L, Cavaille JY, Gauthier C (2006) Carbon nanotube-filled polymer of electrical conductivity in composites. Numerical simulation three-dimensional entangled fibrous networks. *Acta Materialia* 54: 2923–2931.
- Dang A, Mansfield P, Ilsin B, Hightower C, Aravindan N, Rice D, Riedel B (2007) Intraoperative Hyperthermic Intrathoracic Chemotherapy for Pleural Extension of Pseudomyxoma Peritonei. *Journal of Cardiothoracic and Vascular Anesthesia* 21: 265–268.
- Danilov OB, Belousova IM, Mak AA, Belousov VP, Grenishin AS, Kiselev VM, Kris'ko AV, Ponomarev AN, Sosnov EN (2003) Generation of singlet oxygen with the use of optically excited fullerenes and fullerene-like nanoparticles. *Optics and Spectroscopy* 95: 833–842.
- Deguchi S, Alargova RG, Tsujii K (2001) Stable dispersions of fullerenes, C-60 and C-70, in water. Preparation and characterization. *Langmuir* 17: 6013–6017.
- Dewhirst MW (1994) Future-Directions in Hyperthermia Biology. *International Journal of Hyperthermia* 10: 339–345.
- Di Paolo A (2004) Liposomal anticancer therapy: pharmacokinetic and clinical aspects. *J. Chemotherap.* 16: 90–93.
- Dougherty TJ, Marcus SL (1992) Photodynamic Therapy. *European Journal of Cancer* 28A: 1734–1742.
- Dresselhaus M, Dresselhaus G, Eklund PC (1996) *Science of Fullerenes and Carbon Nanotubes*. Academic Press,
- Dresselhaus MS, Dresselhaus G, Charlier JC, Hernandez E (2004) Electronic, thermal and mechanical properties of carbon nanotubes. *Philosophical Transactions of the Royal Society of London Series A-Mathematical Physical and Engineering Sciences* 362: 2065–2098.
- Dresselhaus MS, Eklund PC (2000) Phonons in carbon nanotubes. *Advances in Physics* 49: 705–814.
- Driscoll KE, Carter JM, Howard BW, Hassenbein DG, Pepelko W, Baggs RB, Oberdorster G (1996) Pulmonary inflammatory, chemokine, and mutagenic responses in rats after subchronic inhalation of carbon black. *Toxicology and Applied Pharmacology* 136: 372–380.
- Dugan LL, Lovett EG, Quick KL, Lotharius J, Lin TT, O'Malley KL (2001) Fullerene-based anti-oxidants and neurodegenerative disorders. *Parkinsonism and Related Disorders* 7: 243–246.

- El Sherbiny IM, Lins RJ, Abdel-Bary EM, Harding DRK (2005) Preparation, characterization, swelling and in vitro drug release behaviour of poly [N-acryloyl]glycine-chitosan interpolymeric pH and thermally-responsive hydrogels. *European Polymer Journal* 41: 2584–2591.
- Ely JL, Emken MR, Accuntius JA, Wilde DS, Haubold AD, More RB, Bokros JC (1998) Pure pyrolytic carbon: preparation and properties of a new material, On-X (R) carbon for mechanical heart valve prostheses. *Journal of Heart Valve Disease* 7: 626–632.
- Ernst H, Rittinghausen S, Bartsch W, Creutzenberg O, Dasenbrock C, Gorlitz BD, Hecht M, Kairies U, Muhle H, Muller M, Heinrich U, Pott F (2002) Pulmonary inflammation in rats after intratracheal instillation of quartz, amorphousSiO(2), carbon black, and coal dust and the influence of poly-2-vinylpyridine-N-oxide (PVNO). *Experimental and Toxicologic Pathology* 54: 109–126.
- Fernandez JM, Bilgin MD, Grossweiner LI (1997) Singlet oxygen generation by photodynamic agents. *Journal of Photochemistry and Photobiology B-Biology* 37: 131–140.
- Foley S, Bosi S, Larroque C, Prato M, Janot JM, Seta P (2001) Photophysical properties of novel water soluble fullerene derivatives. *Chemical Physics Letters* 350: 198–205.
- Foley S, Crowley C, Smahli M, Bonfils C, Erlanger BF, Seta P, Larroque C (2002a) Cellular localisation of a water-soluble fullerene derivative. *Biochemical and Biophysical Research Communications* 294: 116–119.
- Foley S, Curtis ADM, Hirsch A, Brettreich M, Pelegrin A, Seta P, Larroque C (2002b) Interaction of a water soluble fullerene derivative with reactive oxygen species and model enzymatic systems. *Fullerenes Nanotubes and Carbon Nanostructures* 10: 49–67.
- Foote CS (1995) Fullerenes as photosensitizers. *Light-Activated Pest Control* 616: 17–23.
- Fortner JD, Lyon DY, Sayes CM, Boyd AM, Falkner JC, Hotze EM, Alemany LB, Tao YJ, Guo W, Ausman KD, Colvin VL, Hughes JB (2005) C-60 in water: nanocrystal formation and microbial response. *Environmental Science and Technology* 39: 4307–4316.
- Fotinos N, Campo MA, Popowycz F, Gurny R, Lange N (2006) 5-Aminolevulinic acid derivatives in photomedicine: characteristics, application and perspectives. *Photochemistry and Photobiology* 82: 994–1015.
- Fuchs J, Thiele J (1998) The role of oxygen in cutaneous photodynamic therapy. *Free Radical Biology and Medicine* 24: 835–847.
- Gabizon A, Goren D, Cohen R, Barenholz Y (1998) Development of liposomal anthracyclines: from basics to clinical applications. *Journal of Controlled Release* 53: 275–279.
- Gharbi N, Pressac M, Hadchouel M, Szwarc H, Wilson SR, Moussa F (2005) [60]Fullerene is a powerful antioxidant in vivo with no acute or subacute toxicity. *Nano Letters* 5: 2578–2585.
- Goodman SL, Tweden KS, Albrecht RM (1996) Platelet interaction with pyrolytic carbon heart-valve leaflets. *Journal of Biomedical Materials Research* 32: 249–258.
- Green PS, Leeuwenburgh C (2002) Mitochondrial dysfunction is an early indicator of doxorubicin-induced apoptosis. *Biochimica et Biophysica Acta-Molecular Basis of Disease* 1588: 94–101.
- Guldi DM, Hungerbuhler H, Asmus KD (1999) Inhibition of cluster phenomena in truly water soluble fullerene derivatives: bimolecular electron and energy transfer processes. *Journal of Physical Chemistry B* 103: 1444–1453.
- Hanajiri K, Maruyama T, Kaneko Y, Mitsui H, Watanabe S, Sata M, Nagai R, Kashima T, Shibahara J, Omata M, Matsumoto Y (2006) Microbubble-induced increase in ablation of liver tumors by high-intensity focused ultrasound. *Hepatology Research* 36: 308–314.
- Hanson GW (2005) Fundamental transmitting properties of carbon nanotube antennas. *IEEE Transactions on Antennas and Propagation* 53: 3426–3435.
- Harrod-Kim P (2006) Tumor ablation with photodynamic therapy: introduction to mechanism and clinical applications. *Journal of Vascular and Interventional Radiology* 17: 1441–1448.
- Hepplestone SP, Ciavarella AM, Janke C, Srivastava GP (2006) Size and temperature dependence of the specific heat capacity of carbon nanotubes. *Surface Science* 600: 3633–3636.
- Hepplestone SP, Srivastava GP (2006) The intrinsic lifetime of low-frequency zone-centre phonon modes in silicon nanowires and carbon nanotubes. *Applied Surface Science* 252: 7726–7729.

- Hildebrandt B, Wust P, Ahlers O, Dieing A, Sreenivasa G, Kerner T, Felix R, Riess H (2002) The cellular and molecular basis of hyperthermia. *Critical Reviews in Oncology/Hematology* 43: 33–56.
- Hirsch LR, Gobin AM, Lowery AR, Tam F, Drezek RA, Halas NJ, West JL (2006) Metal nanoshells. *Annals of Biomedical Engineering* 34: 15–22.
- Hirsh V, Desjardins P, Needles BM, Rigas JR, Jahanzeb M, Nguyen L, Zembryki D, Leopold LH (2007) Oral versus intravenous administration of vinorelbine as a single agent for the first-line treatment of metastatic nonsmall cell lung carcinoma (NSCLC) – A randomized phase II trial. *American Journal of Clinical Oncology-Cancer Clinical Trials* 30: 245–251.
- Huang H, Zhang WK, Li MC, Gan YP, Ma CA, Zhang XB (2004) Electrochemical production of Sn-filled carbon nanotubes in molten salts. *Transactions of Nonferrous Metals Society of China* 14: 441–445.
- Iijima S (1991) Helical microtubules of graphitic carbon. *Nature* 354: 56–58.
- International Agency for Research on Cancer. 2002. www-dep.iarc.fr, Globocan 2002 Ref Type: Report
- Isobe H, Nakanishi W, Tomita N, Jinno S, Okayama H, Nakamura E (2006) Gene delivery by aminofullerenes: Structural requirements for efficient transfection. *Chemistry-An Asian Journal* 1: 167–175.
- Jain A, Kim YT, Mckeeon RJ, Bellamkonda RV (2006) In situ gelling hydrogels for conformal repair of spinal cord defects, and local delivery of BDNF after spinal cord injury. *Biomaterials* 27: 497–504.
- Janzen N, Perry K, Han K, Kristo B, Raman S, Said J, Belledegrun A, Schulam P (2005) The Effects of Intentional Cryoablation and Radio Frequency Ablation of Renal Tissue Involving the Collecting System in a Porcine Model. *The Journal of Urology* 173: 1368–1374.
- Jensen AW, Wilson SR, Schuster DI (1996) Biological applications of fullerenes. *Bioorganic and Medicinal Chemistry* 4: 767–779.
- Jiang W, Yang HC, Yang SY, Horng HE, Hung JC, Chen YC, Hong CY (2004) Preparation and properties of superparamagnetic nanoparticles with narrow size distribution and biocompatible. *Journal of Magnetism and Magnetic Materials* 283: 210–214.
- Jonsson B, Nonat A, Labbez C, Cabane B, Wennerstrom H (2005) Controlling the cohesion of cement paste. *Langmuir* 21: 9211–9221.
- Kam NWS, O'Connell M, Wisdom JA, Dai HJ (2005) Carbon nanotubes as multifunctional biological transporters and near-infrared agents for selective cancer cell destruction. *Proceedings of the National Academy of Sciences of the United States of America* 102: 11600–11605.
- Kamat JP, Devasagayam TPA, Priyadarsini KI, Mohan H, Mittal JP (1998) Oxidative damage induced by the fullerene C-60 on photosensitization in rat liver microsomes. *Chemico-Biological Interactions* 114: 145–159.
- Kasermann F, Kempf C (1998) Buckminsterfullerene and photodynamic inactivation of viruses. *Reviews in Medical Virology* 8: 143–151.
- Kempa K, Rybczynski J, Huang ZP, Gregorczyk K, Vidan A, Kimball B, Carlson J, Benham G, Wang Y, Herczynski A, Ren ZF (2007) Carbon nanotubes as optical antennae. *Advanced Materials* 19: 421.
- Kim BM, Qian S, Bau HH (2005) Filling carbon nanotubes with particles. *Nano Letters* 5: 873–878.
- Kluza J, Marchetti P, Gallego MA, Lancel S, Fournier C, Loyens A, Beauvillain JC, Bailly C (2004) Mitochondrial proliferation during apoptosis induced by anticancer agents: effects of doxorubicin and mitoxantrone on cancer and cardiac cells. *Oncogene* 23: 7018–7030.
- Koeppel R, Sariciftci NS (2006) Photoinduced charge and energy transfer involving fullerene derivatives. *Photochemical and Photobiological Sciences* 5: 1122–1131.
- Kouklin N, Tzolov M, Straus D, Yin A, Xu JM (2004) Infrared absorption properties of carbon nanotubes synthesized by chemical vapor deposition. *Applied Physics Letters* 85: 4463–4465.
- Kroto HW, Heath JR, O'Brien SC, Curl RF, Smalley RE (1985) C-60 – Buckminsterfullerene. *Nature* 318: 162–163.
- Krusic PJ, Wasserman E, Keizer PN, Morton JR, Preston KF (1991) Radical reactions of C₆₀. *Science* 254: 1183–1185.

- Kubler AC, de Carpentier J, Hopper C, Leonard AG, Putnam G (2001) Treatment of squamous cell carcinoma of the lip using Foscan-mediated photodynamic therapy. *International Journal of Oral and Maxillofacial Surgery* 30: 504–509.
- Kumar TP, Ramesh R, Lin YY, Fey GTK (2004) Tin-filled carbon nanotubes as insertion anode materials for lithium-ion batteries. *Electrochemistry Communications* 6: 520–525.
- Lamb LD, Huffman DR (1993) Fullerene production. *Journal of Physics and Chemistry of Solids* 54: 1635–1643.
- Launay S, Fedorov AG, Joshi Y, Cao A, Ajayan PM (2006) Hybrid micro-nano structured thermal interfaces for pool boiling heat transfer enhancement. *Microelectronics Journal* 37: 1158–1164.
- Levi N, Hantgan R, Lively M, Carroll D, Prasad G (2006) C60-Fullerenes: detection of intracellular photoluminescence and lack of cytotoxic effects. *Journal of Nanobiotechnology* 4: 14.
- Levine EA, Stewart JH, Russell GB, Geisinger KR, Loggie BL, Shen P (2007) Cyto-reductive surgery and intraperitoneal hyperthermic chemotherapy for peritoneal surface malignancy: experience with 501 procedures. *Journal of the American College of Surgeons* 204: 943–953.
- Li H, Wang DQ, Liu BL, Gao LZ (2004) Synthesis of a novel gelatin-carbon nanotubes hybrid hydrogel. *Colloids and Surfaces B-Biointerfaces* 33: 85–88.
- Li Lb, Luo Rc, Liao Wj, Zhang Mj, Luo Yl, Miao Jx (2006) Clinical study of Photofrin photodynamic therapy for the treatment of relapse nasopharyngeal carcinoma. *Photodiagnosis and Photodynamic Therapy* 3: 266–271.
- Li G, Mianami N (2003) Increase of photoluminescence from fullerenes-doped poly (alkyl methacrylate) under laser irradiation. *Journal of Photoluminescence* 104: 207.
- Lin YL, Lei HY, Wen YY, Luh TY, Chou CK, Liu HS (2000) Light-independent inactivation of dengue-2 virus by carboxyfullerene C3 isomer. *Virology* 275: 258–262.
- Liu J, Czerw R, Carroll DL (2005a) Large-scale synthesis of highly aligned nitrogen doped carbon nanotubes by injection chemical vapor deposition methods. *Journal of Materials Research* 20: 538–543.
- Liu JW, Webster S, Carroll DL (2005b) Temperature and flow rate of NH₃ effects on nitrogen content and doping environments of carbon nanotubes grown by injection CVD method. *Journal of Physical Chemistry B* 109: 15769–15774.
- Lush RM, Mccune JS, Tetteh L, Thompson JA, Mahany JJ, Garland L, Suttle AB, Sullivan DM (2005) The absolute bioavailability of oral vinorelbine in patients with solid tumors. *Cancer Chemotherapy and Pharmacology* 56: 578–584.
- Ma GB, Cheng WJ, Chen GH, Ming NB (2000) Orientation and photoluminescence of C-60 crystallites in C-60-polymethyl methacrylate films. *Thin Solid Films* 375: 292–295.
- Ma GB, Yang YH, Chen GH (1998) Anomalous photoluminescence from C-60 polymethyl methacrylate films. *Materials Letters* 34: 377–382.
- Maksimenko SA, Slepian GY, Nemilentsau AM, Shuba MV (2008) Carbon nanotube antenna: far-field, near-field and thermal-noise properties. *Physica E: Low-dimensional Systems and Nanostructures* 40: 2360–2364.
- Marchesan S, Da Ros T, Spalluto G, Balzarini J, Prato M (2005) Anti-HIV properties of cationic fullerene derivatives. *Bioorganic and Medicinal Chemistry Letters* 15: 3615–3618.
- Matsumura S, Ajima K, Yudasaka M, Iijima S, Shiba K (2007) Dispersion of cisplatin-loaded carbon nanohorns with a conjugate comprised of an artificial peptide aptamer and poly(ethylene glycol). *Molecular Pharmacology* 4: 723–729.
- Meng J, Kong H, Xu HY, Song L, Wang CY, Xie SS (2005) Improving the blood compatibility of polyurethane using carbon nanotubes as fillers and its implications to cardiovascular surgery. *Journal of Biomedical Materials Research Part A* 74A: 208–214.
- Menna E, Scorrano G, Maggini M, Cavallaro M, Della Negra F, Battagliarin M, Bozio R, Fantinel F, Meneghetti M (2003) Shortened single-walled nanotubes functionalized with poly(ethylene glycol): preparation and properties. *Arxiv* 64–73.
- Milanesio ME, Alvarez MG, Rivarola V, Silber JJ, Durantini EN (2005) Porphyrin-fullerene C-60 dyads with high ability to form photoinduced charge-separated state as novel sensitizers for photodynamic therapy. *Photochemistry and Photobiology* 81: 891–897.

- Misra A, Tyagi PK, Singh MK, Misra DS (2006) FTIR studies of nitrogen doped carbon nanotubes. *Diamond and Related Materials* 15: 385–388.
- Mittal JP (1995) Excited-States and Electron-Transfer Reactions of Fullerenes. *Pure and Applied Chemistry* 67: 103–110.
- Mohamed F, Marchettini P, Stuart OA, Urano M, Sugarbaker PH (2003) Thermal enhancement of new chemotherapeutic agents at moderate hyperthermia. *Annals of Surgical Oncology* 10: 463–468.
- Monteiro-Riviere NA, Inman AO, Wang YY, Nemanich RJ (2005a) Surfactant effects on carbon nanotube interactions with human keratinocytes. *Nanomedicine: Nanotechnology, Biology and Medicine* 1: 293–299.
- Monteiro-Riviere NA, Nemanich RJ, Inman AO, Wang YY, Riviere JE (2005b) Multi-walled carbon nanotube interactions with human epidermal keratinocytes. *Toxicology Letters* 155: 377–384.
- Monthioux M (2002) Filling single-wall carbon nanotubes. *Carbon* 40: 1809–1823.
- Monti D, Moretti L, Salvioli S, Straface E, Malorni W, Pellicciari R, Schettini G, Bisaglia M, Pincelli C, Fumelli C, Bonafe M, Franceschi C (2000) C₆₀ carboxyfullerene exerts a protective activity against oxidative stress-induced apoptosis in human peripheral blood mononuclear cells. *Biochemical and Biophysical Research Communications* 277: 711–717.
- Mroz P, Pawlak A, Satti M, Lee H, Wharton T, Gali H, Sarna T, Hamblin MR (2007) Functionalized fullerenes mediate photodynamic killing of cancer cells: Type I versus Type II photochemical mechanism. *Free Radical Biology and Medicine* 43: 711–719.
- Murakami T, Ajima K, Miyawaki J, Yudasaka M, Iijima S, Shiba K (2004) Drug-loaded carbon nanohorns: adsorption and release of dexamethasone in vitro. *Molecular Pharmacology* 1: 399–405.
- Nadarajan SB, Katsikis PD, Papazoglou ES (2007) Loading carbon nanotubes with viscous fluids and nanoparticles – a simpler approach. *Applied Physics A-Materials Science & Processing* 89: 437–442.
- Nakajima N, Nishi C, Li FM, Ikada Y (1996) Photo-induced cytotoxicity of water-soluble fullerene. *Fullerene Science and Technology* 4: 1–19.
- Nakamura E, Tokuyama H, Yamago S, Shiraki T, Sugiura Y (1996) Biological activity of water-soluble fullerenes. Structural dependence of DNA cleavage, cytotoxicity, and enzyme inhibitory activities including HIV-protease inhibition. *Bulletin of the Chemical Society of Japan* 69: 2143–2151.
- Neuberger T, Schopf B, Hofmann H, Hofmann M, von Rechenberg B (2005) Superparamagnetic nanoparticles for biomedical applications: possibilities and limitations of a new drug delivery system. *Journal of Magnetism and Magnetic Materials* 293: 483–496.
- Novikova LN, Mosahebi A, Wiberg M, Terenghi G, Kellerth JO, Novikov LN (2006) Alginate hydrogel and matrigel as potential cell carriers for neurotransplantation. *Journal of Biomedical Materials Research Part A* 77A: 242–252.
- O’Connell MJ, Bachilo SM, Huffman CB, Moore VC, Strano MS, Haroz EH, Rialon KL, Boul PJ, Noon WH, Kittrell C, Ma JP, Hauge RH, Weisman RB, Smalley RE (2002) Band gap fluorescence from individual single-walled carbon nanotubes. *Science* 297: 593–596.
- Ohno T, Matsuishi K, Onari S (1997) Effects of laser irradiation on photoluminescence of C-60 single crystal with/without air exposure. *Solid State Communications* 101: 785–789.
- Panchapakesan B, Lu S, Sivakumar K, Teker K, Cesarone G, Wickstrom E (2005) Single wall carbon nanotube nanobomb agents for killing breast cancer cells. *Nanobiotechnology* 1: 133–140.
- Park KJ, Jung D (2007) Enhancement of nucleate boiling heat transfer using carbon nanotubes. *International Journal of Heat and Mass Transfer* 50: 4499–4502.
- Pearce JA, Thomsen S (1999) Kinetic models of tissue perfusion processes. *Proceedings of Laser Surgery (SPIE): Advanced Characterization, Therapeutics, and Systems III* 1643: 251.
- Pech O, Gossner L, May A, Rabenstein T, Vieth M, Stolte M, Berres M, Ell C (2005) Long-term results of photodynamic therapy with 5-aminolevulinic acid for superficial Barrett’s cancer and high-grade intraepithelial neoplasia. *Gastrointestinal Endoscopy* 62: 24–30.

- Pinthus JH, Bogaards A, Weersink R, Wilson BC, Trachtenberg J (2006) Photodynamic therapy for urological malignancies: past to current approaches. *Journal of Urology* 175: 1201–1207.
- Ponce AM, Vujaskovic Z, Yuan F, Needham D, Dewhirst MW (2006) Hyperthermia mediated liposomal drug delivery. *International Journal of Hyperthermia* 22: 205–213.
- Poncharal P, Berger C, Yi Y, Wang ZL, de Heer WA (2002) Room temperature ballistic conduction in carbon nanotubes. *Journal of Physical Chemistry B* 106: 12104–12118.
- Porter AE, Muller K, Skepper J, Midgley P, Welland M (2006) Uptake of C-60 by human monocyte macrophages, its localization and implications for toxicity: studied by high resolution electron microscopy and electron tomography. *Acta Biomaterialia* 2: 409–419.
- Portney NG, Ozkan M (2006) Nano-oncology: drug delivery, imaging, and sensing. *Analytical and Bioanalytical Chemistry* 384: 620–630.
- Rajagopalan P, Wudl F, Schinazi RF, Boudinot FD (1996) Pharmacokinetics of a water-soluble fullerene in rats. *Antimicrobial Agents and Chemotherapy* 40: 2262–2265.
- Rancan F, Helmreich M, Molich A, Jux N, Hirsch A, Roder B, Witt C, Bohm F (2005) Fullerene-porphyrin complex as sensitizer for photodynamic therapy: uptake and photo-induced cytotoxicity on Jurkat cells. *Journal of Photochemistry and Photobiology B: Biology* 80: 1–7.
- Reddy LH (2005) Drug delivery to tumours: recent strategies. *Journal of Pharmacy and Pharmacology* 57: 1231–1242.
- Reingruber B, Boettcher MI, Klein P, Hohenberger W, Pelz JOW (2007) Hyperthermic intraperitoneal chemoperfusion is an option for treatment of peritoneal carcinomatosis in children. *Journal of Pediatric Surgery* 42: e17–e21.
- Saito R, Gruneis A, Samsonidze GG, Dresselhaus G, Dresselhaus MS, Jorio A, Cancado LG, Pimenta MA, Souza AG (2004) Optical absorption of graphite and single-wall carbon nanotubes. *Applied Physics A-Materials Science and Processing* 78: 1099–1105.
- Sayes CG, Fortner JD, Guo W, Lyon D, Boyd AM, Ausman KD, Tao YJ, Sitharaman B, Wilson LJ, Hughes JB, West JL, Colvin VL (2004) The differential cytotoxicity of water-soluble fullerenes. *Nano Letters* 4: 1881–1887.
- Scharff P, Risch K, Carta-Abelmann L, Dmytruk IM, Bilyi MM, Golub OA, Khavryuchenko AV, Buzaneva EV, Aksenov VL, Avdeev MV, Prylutskiy YI, Durov SS (2004) Structure of C-60 fullerene in water: spectroscopic data. *Carbon* 42: 1203–1206.
- Scharff P, Siegmund C, Risch K, Lysko I, Lysko O, Zhrebetskiy A, Ivanisik A, Gorchinskiy A, Buzaneva E (2005) Characterization of water-soluble fullerene C-60 oxygen and hydroxyl group derivatives for photosensitizers. *Fullerenes Nanotubes and Carbon Nanostructures* 13: 497–509.
- Schonenberger C, Forro L (2000) Multiwall carbon nanotubes. *Physics World* 13: 37–41.
- Scott JHJ, Majetich SA (1995) Morphology, Structure, and Growth of Nanoparticles Produced in A Carbon-Arc. *Physical Review B* 52: 12564–12571.
- Scrivens WA, Tour, J, Creek, K, Pirisi, L (1994) Synthesis of ¹⁴C-labeled C60, its suspensions in water. Preparation and Characterization. *J.American Chemical Society* 116, 4517–4518.
- Ref Type: Generic
- Sears A, Batra RC (2006) Buckling of multiwalled carbon nanotubes under axial compression. *Physical Review B* 73(8): 11.
- Sharman WM, Allen CM, van Lier JE (1999) Photodynamic therapeutics: basic principles and clinical applications. *Drug Discovery Today* 4: 507–517.
- Shen P, Hawksworth J, Lovato J, Loggie BW, Geisinger KR, Fleming RA, Levine EA (2004) Cyto-reductive surgery and intraperitoneal hyperthermic chemotherapy with mitomycin C for peritoneal carcinomatosis from non-appendiceal colorectal carcinoma. *Annals of Surgical Oncology* 11: 178–186.
- Shenoy DB, Amiji MA (2005) Poly(ethylene oxide)-modified poly(epsilon-caprolactone) nanoparticles for targeted delivery of tamoxifen in breast cancer. *International Journal of Pharmaceutics* 293: 261–270.
- Sinani VA, Gheith MK, Yaroslavov AA, Rakhnyanskaya AA, Sun K, Mamedov AA, Wicksted JP, Kotov NA (2005) Aqueous dispersions of single-wall and multiwall carbon nanotubes with designed amphiphilic polycations. *Journal of the American Chemical Society* 127: 3463–3472.

- Singh R, Pantarotto D, Lacerda L, Pastorin G, Klumpp C, Prato M, Bianco A, Kostarelos K (2006) Tissue biodistribution and blood clearance rates of intravenously administered carbon nanotube radiotracers. *Proceedings of the National Academy of Sciences of the United States of America* 103: 3357–3362.
- Sitharaman B, Kissell KR, Hartman KB, Tran LA, Baikov A, Rusakova I, Sun Y, Khant HA, Ludtke SJ, Chiu W, Laus S, Toth E, Helm L, Merbach AE, Wilson LJ (2005) Superparamagnetic gadonanotubes are high-performance MRI contrast agents. *Chemical Communications* 3915–3917.
- So G, Karotki A, Verma S, Pritzker K, Wilson B, Chiang LY (2006) Comparison of singlet oxygen generation efficiency between water-soluble C60-diphenylaminofluorene conjugates and molecular micelle-like FC4S. *Journal of Macromolecular Science Part A-Pure and Applied Chemistry* 43: 1955–1963.
- Sonvico F, Mornet S, Vasseur S, Dubernet C, Jaillard D, Degrouard J, Hoebeke J, Duguet E, Colombo P, Couvreur P (2005) Folate-conjugated iron oxide nanoparticles for solid tumor targeting as potential specific magnetic hyperthermia mediators: synthesis, physicochemical characterization, and in vitro experiments. *Bioconjugate Chemistry* 16: 1181–1188.
- Stewart JH, Shen P, Levine EA (2005) Intraperitoneal hyperthermic chemotherapy for peritoneal surface malignancy: current status and future directions. *Annals of Surgical Oncology* 12: 765–777.
- Stewart JH, Shen P, Russell GB, Bradley RF, Hundley JC, Loggie BL, Geisinger KR, Levine EA (2006) Appendiceal neoplasms with peritoneal dissemination: outcomes after cytoreductive surgery and intraperitoneal hyperthermic chemotherapy. *Annals of Surgical Oncology* 13: 624–634.
- Stoeger T, Reinhard C, Takenaka S, Schroepel A, Karg E, Ritter B, Heyder J, Schulz H (2006) Instillation of six different ultrafine carbon particles indicates a surface area threshold dose for acute lung inflammation in mice. *Environmental Health Perspectives* 114: 328–333.
- Sugarbaker PH, Mora JT, Carmignani P, Stuart OA, Yoo D (2005) Update on chemotherapeutic agents utilized for perioperative intraperitoneal chemotherapy. *Oncologist* 10: 112–122.
- Tabata Y, Murakami Y, Ikada Y (1997) Photodynamic effect of polyethylene glycol-modified fullerene on tumor. *Japanese Journal of Cancer Research* 88: 1108–1116.
- Tachibana M, et al. (1996) Photoluminescence and structural defects of C₆₀ crystals. *Journal of Photoluminescence* 66 & 67: 249.
- Tanielian C, Schweitzer C, Mechin R, Wolff C (2001) Quantum yield of singlet oxygen production by monomeric and aggregated forms of hematoporphyrin derivative. *Free Radical Biology and Medicine* 30: 208–212.
- Terrones M (2003) Science and technology of the twenty-first century: synthesis, properties and applications of carbon nanotubes. *Annual Review of Materials Research* 33: 419–501.
- Tessonnier JP, Pesant L, Ehret G, Ledoux MJ, Pham-Huu C (2005) Pd nanoparticles introduced inside multi-walled carbon nanotubes for selective hydrogenation of cinnamaldehyde into hydrocinnamaldehyde. *Applied Catalysis A: General* 288: 203–210.
- Tkac J, Ruzgas T (2006) Dispersion of single walled carbon nanotubes. Comparison of different dispersing strategies for preparation of modified electrodes toward hydrogen peroxide detection. *Electrochemistry Communications* 8: 899–903.
- Toh S, Kaneko K, Hayashi Y, Tokunaga T, Moon WJ (2004) Microstructure of metal-filled carbon nanotubes. *Journal of Electron Microscopy* 53: 149–155.
- Torti S, Byrne F, Whelan O, Levi N, Ucer B, Schmid M, Torti F, Akman S, Liu J, Ajayan P, Nalamasu O, Carroll D (2007) Thermal ablation therapeutics based on CN_x multi-walled nanotubes. *International Journal of Nanomedicine* 2(4): 707–714.
- Trehin R, Figueiredo JL, Pittet MJ, Weissleder R, Josephson L, Mahmood U (2006) Fluorescent nanoparticle uptake for brain tumor visualization. *Neoplasia* 8: 302–311.
- Tsao N, Luh TY, Chou CK, Chang TY, Wu JJ, Liu CC, Lei HY (2002) In vitro action of carboxyfullerene. *Journal of Antimicrobial Chemotherapy* 49: 641–649.
- Ueng TH, Kang JJ, Wang HW, Cheng YW, Chiang LY (1997) Suppression of microsomal cytochrome P450-dependent monooxygenases and mitochondrial oxidative phosphorylation by fullerene, a polyhydroxylated fullerene C60. *Toxicology Letters* 93: 29–37.

- Vileno B, Lekka M, Sienkiewicz A, Marcoux P, Kulik AJ, Kasas S, Catsicas S, Graczyk A, Forro L (2005) Singlet oxygen ($(^1\Delta(g))$)-mediated oxidation of cellular and subcellular components: ESR and AFM assays. *Journal of Physics-Condensed Matter* 17:S1471–S1482.
- Wang IC, Tai LA, Lee DD, Kanakamma PP, Shen CKF, Luh TY, Cheng CH, Hwang KC (1999) C-60 and water-soluble fullerene derivatives as antioxidants against radical-initiated lipid peroxidation. *Journal of Medicinal Chemistry* 42: 4614–4620.
- Wang X, Sun B, Yang HK (2006) Stability of multi-walled carbon nanotubes under combined bending and axial compression loading. *Nanotechnology* 17: 815–823.
- Wang Y, Kempa K, Kimball B, Carlson JB, Benham G, Li WZ, Kempa T, Rybczynski J, Herczynski A, Ren ZF (2004a) Receiving and transmitting light-like radio waves: antenna effect in arrays of aligned carbon nanotubes. *Applied Physics Letters* 85: 2607–2609.
- Wang YW, Xie XY, Wang XD, Ku G, Gill KL, O'Neal DP, Stoica G, Wang LV (2004b) Photoacoustic tomography of a nanoshell contrast agent in the in vivo rat brain. *Nano Letters* 4: 1689–1692.
- Weissleder R (2001) A clearer vision for in vivo imaging. *Nature Biotechnology* 19: 316–317.
- Wu J, Wei W, Wang LY, Su ZG, Ma GH (2007) A thermosensitive hydrogel based on quaternized chitosan and poly(ethylene glycol) for nasal drug delivery system. *Biomaterials* 28: 2220–2232.
- Xin HJ, Woolley AT (2005) High-yield DNA-templated assembly of surfactant-wrapped carbon nanotubes. *Nanotechnology* 16: 2238–2241.
- Xu JF, Xiao M, Czerw R, Carroll DL (2004) Optical limiting and enhanced optical nonlinearity in boron-doped carbon nanotubes. *Chemical Physics Letters* 389: 247–250.
- Xu JZ, Zhu JJ, Wu Q, Hu Z, Chen HY (2003) An amperometric biosensor based on the coimmobilization of horseradish peroxidase and methylene blue on a carbon nanotubes modified electrode. *Electroanalysis* 15: 219–224.
- Yang XL, Fan CH, Zhu HS (2002) Photo-induced cytotoxicity of malonic acid [C-60]fullerene derivatives and its mechanism. *Toxicology In Vitro* 16: 41–46.
- Yang XL, Huang C, Qiao XG, Yao L, Zhao DX, Tan X (2007) Photo-induced lipid peroxidation of erythrocyte membranes by a bis-methanophosphonate fullerene. *Toxicology In Vitro* 21: 1493–1498.
- Yim TJ, Liu JW, Lu Y, Kane RS, Dordick JS (2005) Highly active and stable DNAzyme – Carbon nanotube hybrids. *Journal of the American Chemical Society* 127: 12200–12201.
- Yu C, Canteenwala T, Chiang LY, Wilson B, Pritzker K (2005) Photodynamic effect of hydrophilic C60-derived nanostructures for catalytic antitumoral antibacterial applications. *Synthetic Metals* 153: 37–40.
- Zhang RY, Wang XM, Wu CH, Song M, Li JY, Lv G, Zhou J, Chen C, Dai YY, Gao F, Fu DG, Li XO, Guan ZQ, Chen BA (2006) Synergistic enhancement effect of magnetic nanoparticles on anticancer drug accumulation in cancer cells. *Nanotechnology* 17: 3622–3626.
- Zhang XZ, Wu DQ, Sun GM, Chu CC (2003) Novel biodegradable and thermosensitive Dex-AI/PNIPAAm hydrogel. *Macromolecular Bioscience* 3: 87–91.
- Zhao B, Hu H, Yu AP, Perea D, Haddon RC (2005) Synthesis and characterization of water soluble single-walled carbon nanotube graft copolymers. *Journal of the American Chemical Society* 127: 8197–8203.
- Zhou XD, Ren XL, Zhang J, He GB, Zheng MJ, Tian X, Li L, Zhu T, Zhang M, Wang L, Luo W (2007) Therapeutic response assessment of high intensity focused ultrasound therapy for uterine fibroid: utility of contrast-enhanced ultrasonography. *European Journal of Radiology* 62: 289–294.

Chapter 11

Visualization of Carbon Nanoparticles Within Cells and Implications for Toxicity

Alexandra Porter and Mhairi Gass

Abstract Carbon nanostructures (CNS), such as C_{60} , single-walled nanotubes (SWNTs) exhibit extraordinary properties and are one of the most commercially relevant class of NS. CNS have already found uses in high-performance sports equipment (nanotubes) and face cream (C_{60}), whilst potential applications include optical and electronic materials and superconductors. Following the huge growth in these nanotechnology-related industries, significant concerns have arisen about their potential toxicity and impact on the environment. A lack in understanding of the interaction of such small structures with cellular material has resulted in concerns over their impact on human health. The potential toxicity of CNS and safety to human health requires an understanding of their interaction with cells and this in turn relies on the measurement of the pathways by which they enter the cell, their spatial distribution within and whether the CNS are transformed by the action of the cell; visualization of intracellular CNS is therefore imperative. However visualizing unlabelled CNS within cells is demanding because it is difficult to distinguish CNS from carbon-rich organelles given their similarity in composition and dimensions. In particular, the challenge lies in translating analytical imaging tools developed for inorganic systems to organic systems. This chapter describes how the state-of-the-art transmission electron microscopy (TEM) techniques, such as low-loss energy-filtered TEM (EFTEM) can be employed to differentiate between unlabelled C_{60} , SWNTs and the cell. Further, we demonstrate how these techniques can be used to trace the uptake of CNS into the cell and to assess their localized effects on cell structure.

Keywords analytical electron microscopy, carbon nanoparticles, macrophage cell, toxicity

11.1 Introduction

There has been a vast increase in publications on carbon nanoparticles, such as Buckminster fullerene (C_{60}) and single-walled nanotubes (SWNTs), since the late 1990s in response to the successful mass production methods of manufacturers

The Nanoscience Centre, 11 JJ Thompson Av., The Madingley Road,
Cambridge, CB3 0FF, UK
E-mail: aep30@cam.ac.uk; a.porter@imperial.ac.uk

such as Carbon Nanotechnologies. Carbon-based nanoparticles have achieved a great deal of commercial interest due to their unique chemical and physical properties. Potential applications for carbon-based nanoparticles include optical and electronic materials and superconductors. In biological systems the use of these nanomaterials opens avenues for novel biosensing and imaging technologies. For example, C_{60} and their water soluble derivatives have been used as oxygen scavengers, anti-HIV drugs (Friedman et al., 1998), x-ray contrast agents (Ashcroft et al., 2006) and transporters for delivery of the murine anti-gp240 melanoma antibody (Ma and Sun, 1996). Surface-functionalized SWNTs also demonstrate great promise in clinical applications such as cancer diagnosis or as innovative gene delivery systems (Kam et al., 2005a; Pantarotto et al., 2004). Despite the extensive interest in carbon nanoparticles in commercial applications, concerns have recently been raised regarding the toxic potential of carbon nanoparticles to human health. Such concerns are becoming more significant as an increasing number of nanoparticles find their way into everyday use. This case is particularly relevant in the clinical setting, since the application of nanoparticles for clinical use will rely on the execution of systematic studies to assess their toxicological and pharmacological profiles. In response to these concerns there has been an increased output in the number of papers addressing the toxicity of carbon nanoparticles over the last few years, however, much of this data appears contradictory (Cherukuri et al., 2004; Chui et al., 2005; Kam et al., 2005; Lin et al., 2006; Manna et al., 2005; Nimmagadda et al., 2006; Sayes et al., 2006; Worle-Knirsch et al., 2006; Zhang et al., 2006). The requirement for alternative studies is now apparent in order to achieve an improved understanding of the uptake and cytotoxic effect of carbon nanoparticles within cells. Assessing the toxicity of carbon nanoparticles is imperative chiefly since the individual structures have a diameter of 0.7–1 nm: small enough to penetrate through ion channels or diffuse through pores in the nuclear membrane. Clearly an improved understanding of how the human body interacts with these nanostructures, i.e.: mechanisms of transport across the cell membrane, interactions with the membranes and organelles and their distribution within the cell will be essential to address any potential toxicity.

11.2 Toxicity of C_{60}

The toxicity of C_{60} has been found to be related to its ability to cause oxidative stress (Oberdorster, 2004 and Sayes et al., 2005, 2007). However, literature describing the toxicity of C_{60} is contradictory. The first report on C_{60} cytotoxicity originated from Tsuchiya et al. who found that C_{60} inhibited cell proliferation and differentiation dose-dependently in mouse midbrain cells treated at ~400 $\mu\text{g/ml}$ for six days. Tsuchiya et al. proposed that reactive oxygen species (ROS) contributed to C_{60} cytotoxicity. The ROS generation and embryo head abnormalities suggested that C_{60} may contribute to brain and neuronal diseases such as Down syndrome, Alzheimer's, and Parkinson's disease (Tsuchiya, 1996). The research that

prompted the carbon nanoparticle cytotoxicity scare was Oberdörster's experiment: a study that found C_{60} causing lipid peroxidation in the brain of largemouth Seabass fish. This experiment proposed that C_{60} enters the brain via the olfactory receptor cells, based on other nanoparticle studies. Interestingly, the gills and liver showed decreased lipid peroxidation; however, depletion in glutathione levels suggested that the antioxidant defence system in the gills and liver was being stressed to counter the C_{60} (Oberdorster, 2004). In water, uncoated C_{60} forms crystalline colloids, described as nano- C_{60} (Sayes et al., 2005). These colloids have a high electron affinity and a propensity for generating superoxide anions (Sayes et al., 2005). Sayes et al. found an inverse correlation between the number of hydroxyl and carbonyl attachments and cytotoxicity. Nano- C_{60} , with the fewest attachments, resulted in 50% cell death at 20 ppb in human dermal fibroblasts in comparison to at least 10,000 ppb for other water derivative forms of C_{60} . Nano- C_{60} was found to cause lipid peroxidation through ROS generation; however, damage to DNA, protein, and mitochondria was not observed (Sayes et al., 2005). Additionally, damage to lipid bilayer causes the membranes to become 'leaky', compromising ion homeostasis (Sayes et al., 2007). This mechanism of membrane damage by pore formation has been confirmed using molecular dynamic simulations (Qiao et al., 2007). In a rat model, nano- C_{60} also causes lipid peroxidation, however, only transient inflammatory and cell injury effects were observed, with little or no difference in toxicity to the lung compared to control samples (Sayes et al., 2005).

11.3 Toxicity of SWNTs

The toxicity of SWNTs is of particular concern, since this class of nanoparticle is routinely synthesized using a metal catalyst, and the toxic effect of the SWNTs could potentially be a combined effect of SWNTs and an oxidative stress response to the metal catalyst (Nimmagadda et al., 2006; Pulskamp et al., 2007). This complication renders unambiguous determination of the toxicity of pure SWNTs a challenge. *In vitro* reports on the toxicity of SWNT have presented conflicting evidence for their toxicity. For example, Worle-Knirsch et al. exposed lung epithelial-like cells to large SWNTs (2–5.6 nm diameter) and described different outcomes depending on which cell viability assay was used (Worle-Knirsch et al., 2006). The (3-(4,5-dimethylthiazol-2-yl)-2,5-diphenyltetrazolium bromide) [MTT] assay showed a significant reduction in cell viability but the (2-(4-iodophenyl)-3-(4-nitrophenyl)-5-(2,4-disulfophenyl)-2H-tetrazolium, monosodium salt) [WST] assay gave no reduction in viability for comparable concentrations and duration of exposure to SWNTs (Worle-Knirsch et al., 2006). The authors found no changes in mitochondrial activity or evidence of cell death by necrosis or apoptosis in comparison with control cells. Weisman et al. exposed human monocyte macrophage cells to SWNTs, coated with a surfactant, and found that the morphology and growth of cells were unaffected (Cherukuri et al., 2004). Exposure of cells to SWNTs with up to 30 wt.% iron and with a smaller diameter (0.9–1.2 nm), has been shown to induce acute toxicity,

i.e. decreased cell proliferation, reduced cell viability (Chui et al., 2005; Mann et al., 2005; Pulskamp et al., 2007; Shvedova, 2003), reduced cell adhesion (Shvedova, 2005), activation of necrosis factor (NF- κ B) (Worle-Knirsch et al., 2006) and the upregulation of genes associated with apoptosis (Chui et al., 2005).

11.4 Need for Imaging Studies

In recent years, the literature on toxicity of carbon nanoparticles has grown rapidly, however the findings are evidently contradictory. Much of this ambiguity arises from limitations of standard cell viability assays to give a true estimate of the effect of nanoparticle exposure on cell viability (Worle-Knirsch et al., 2006; Porter et al., 2007a), in particular the localized effect of the particles on cell ultrastructure. The potential human toxicity of carbon nanoparticles requires an understanding of their interaction with cells and this in turn relies on the measurement of their spatial distribution within exposed cells. Imaging distributions of carbon nanoparticles within cells are currently procured by tagging particles with a fluorochrome label and imaging the uptake using confocal microscopy. However, fluorochrome labelling alters the surface chemistry of the particles which may modify uptake (Kam et al., 2005). Imaging the cellular distribution of unlabelled carbon-based nanoparticles is challenging because of the difficulty in achieving high spatial resolution with sufficient image contrast to enable the nanoparticles to be clearly distinguished from the cell organelles. In particular, the challenge lies in translating analytical tools developed for inorganic systems to organic systems where sample preparation and stability of the sample under the electron beam become critical issues. In a recent set of studies we used a set of high-resolution electron microscopy techniques to visualize C₆₀ and SWNTs in human cells (Porter et al., 2006; Porter et al., 2007a, b). The following sections will describe techniques available to image carbon nanoparticles within the cell.

11.5 Transmission Electron Microscopy

Transmission electron microscopy (TEM) is an imaging technique where a beam of electrons of known energy, generally ranging from 60 to 400 kV, is transmitted through a thin specimen and the image formed. However, standard TEM techniques such as bright-field imaging of these cellular structures result in very weak contrast; traditionally, researchers have stained the cells with heavy metal stains to enhance the cellular structure, however this can lead to confusion when analyzing the samples at high resolution. Subsequently, alternative methods have been investigated to increase the contrast between carbonaceous nanoparticles and the cell. Furthermore, the preparation of the samples has been reviewed to optimize the data obtainable from different techniques and their suitability to 3-D tomography.

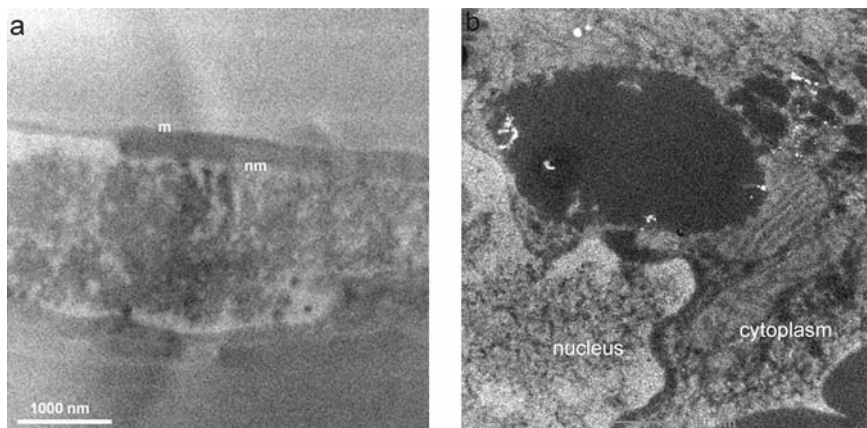


Fig. 11.1 (a) Low loss EFTEM image taken at 45 eV using a 3 eV slit of a non-stained cell section (70 nm thick) showing the nuclear membrane (nm) and plasma membrane (pm) (300 kV TEM). (b) HAADF-STEM image of a 40 nm thick cell section, showing improved contrast from cell organelles (200 kV TEM)

In general, there are several techniques available to enhance contrast from the cell without staining, these include working with small objective apertures, employing an energy filter with a small energy slit (Fig. 11.1a) and using ultrathin samples (Fig. 11.1b). Lowering the operating voltage of the microscope also significantly improves cell contrast; however, this increases damage to the cell by beam heating. For imaging carbon nanoparticles within the cell, one of the main challenges is to avoid damage to the graphitic structure of the nanoparticles. Operating at low voltages reduces damage to the graphitic structure via knock-on damage, so overall lower voltages are optimal for imaging fixed cell samples where the cell is relatively stable under the beam.

11.5.1 Sample Preparation

One of the greatest challenges for imaging nanoparticles within cells is in the sample preparation. When preparing samples for TEM it is essential to induce minimal alteration to cell ultrastructure and also to the distribution of nanoparticles within the cell. There are several techniques available to prepare TEM samples: freeze-drying of whole mounts on grids and fixation, dehydration and embedding followed by ultramicrotomy: sectioning with a glass or diamond knife and focused ion beam milling. Alternative methods have also been developed for specimen preparation as an alternative to the traditional dehydration and chemical fixation procedures, which can produce aggregation and/or changes in the spatial arrangement of the components. One procedure that has proved to be efficient in keeping the

components' intrinsic spatial distribution involves freezing the tissues, either by drastically decreasing the temperature (10,000 K) or by applying a high pressure (ca 2,100 bar) for 10–20 ms before cooling in liquid nitrogen. Future work should investigate application of these techniques for improved imaging of nanoparticles within cells.

To increase contrast from cell organelles, heavy metal stains are often employed. Stains such as Os, Pb and U leave heavy metals in specific regions of the structure (for example, osmium binds to lipids and stains membranes), thus allowing distinction of specific cell organelles. However, these stains obscure visualization and characterization of the carbon nanoparticles, therefore we have compared stained and unstained sections to correlate distributions of nanoparticles within cell structure. For ultramicrotomy, standard sample thicknesses for TEM sections can vary from 70 nm to several hundred nanometers. This results in the acquisition of a two-dimensional image containing three-dimensional information which can in turn result in the 'blurring' of data or lack of information. For electron energy loss (EEL)-based techniques or high-resolution imaging, optimum contrast can be achieved by sectioning ultra-thin sections of around 20 nm in thickness. By using these ultrathin sections, two-dimensional slices through cells are obtained, therefore minimizing the three-dimensional information and allowing for high-resolution imaging of nanoparticles within the cell. Contrast from cell organelles can also be significantly improved by sectioning at 20–40 nm (Fig. 11.1b). The limitation with ultra-thin sections, however, is durability of the section under the beam thus when energy or spatial resolution is not critical thicker sample thickness (~70 nm) will provide sufficient contrast. Here on, the challenge will be to improve the visualization of cell organelles whilst maintaining contrast from the carbon nanoparticles.

11.5.2 High-Angular Annular Dark-Field Scanning Transmission Electron Microscopy

The first technique to discuss regarding enhancement of carbonaceous nanoparticle/cellular contrast is high-angle annular dark-field scanning transmission electron microscopy (HAADF-STEM). HAADF-STEM uses an annular detector to collect electrons which have been scattered to high angles, where the intensity is proportional to Z^2 . This technique may be used to map distributions of SWNTs and C_{60} clusters with cells at medium resolution (Fig. 11.2a, b) (Porter et al., 2006, 2007a, b). Here the contrast arises as the cell, C_{60} and SWNTs have different carbon atom densities (crystalline C_{60} and SWNTs having a higher density compared to the amorphous cell), which scatter by differing amounts. This technique is particularly suited to imaging SWNTs within the cell since the surface iron catalyst particles, which are generally present unless the SWNTs have been purified via a lengthy process, scatter strongly due to their higher atomic number, producing enhanced contrast from the SWNTs (Porter et al., 2007). For these reasons, HAADF-STEM

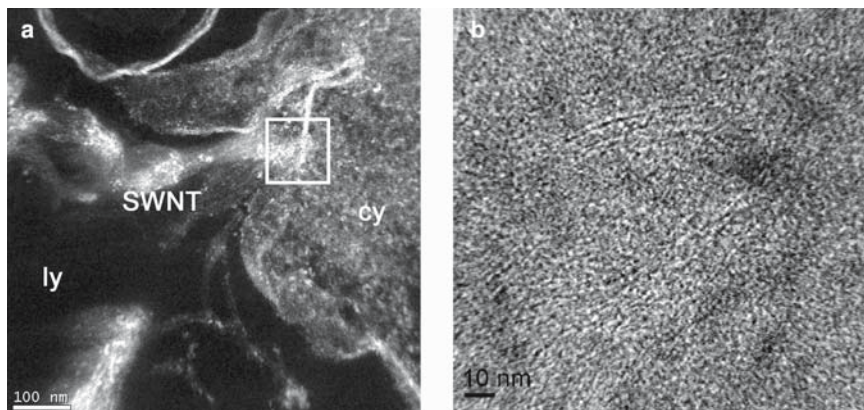


Fig. 11.2 (a) HAADF-STEM image of a stained cell section (40 nm thick). A SWNT cluster within a lysosome invading the lysosomal cell membrane. (b) Corresponding high-resolution lattice image of SWNTs at the lysosomal membrane from boxed area. Cytoplasm (cy) and secondary lysosomes (ly)

techniques offer the potential for improved imaging of carbon nanostructures within stained cells to further our understanding of how these structures interact with cell organelles. An additional advantage of using HAADF-STEM over TEM techniques is its ability to image thick samples, as this technique is not curbed by the chromatic aberration effects that limit TEM resolution. Consequently, this technique is ideal for 3-D imaging techniques such as electron tomography, in which volume information becomes critical (Fig. 11.3).

11.5.3 *Electron Energy Loss Microscopy*

In TEM, the incident electron beam has a known energy; as the electrons pass through the specimen they interact with the atomic electrons and scatter in one of two ways. The first is called elastic scattering; this is where the incident electron may be deflected as it passes through the specimen, but loses no energy. The second is inelastic scattering, an incident electron ionizes an atomic electron, and therefore the electron beam exits the specimen with a reduced energy. The energy required to ionize an electron is specific to both the element and shell in which the electron is sitting prior to ionization; thus elemental analysis can be carried out by studying the energy lost from the electron beam, this is known as electron energy loss spectroscopy (EELS). The energy loss spectrum consists of three main areas: firstly, the zero loss peak. This is the most intense component of the spectrum and consists of the elastically scattered electrons. The remainder of the spectrum is the result of inelastically scattered electrons and can be split into low loss and core loss. The low-loss region (0–100 eV) results from the interaction of

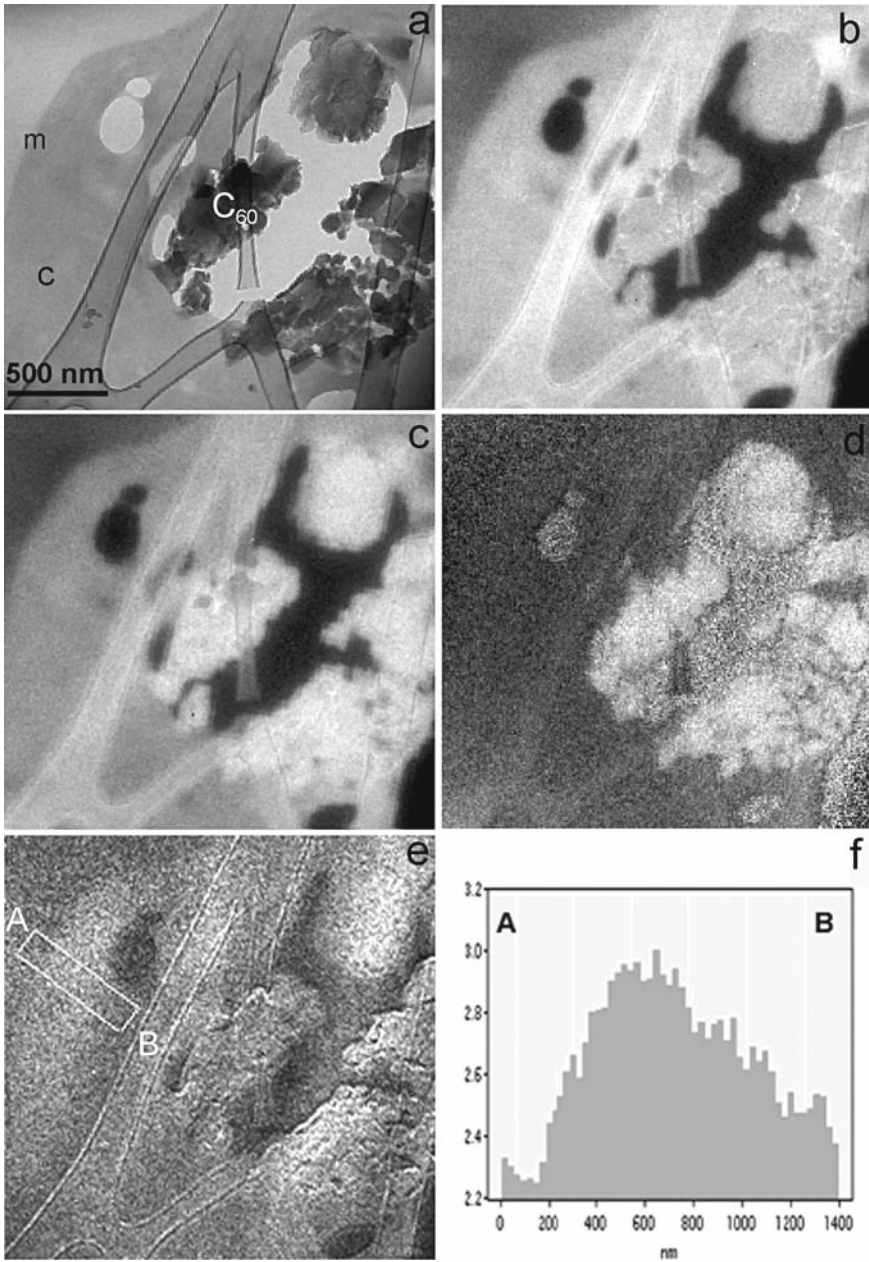


Fig. 11.3 (a) 0eV, (b) 20eV, (c) 26eV, (d) 26/20eV, and (e) 6/4eV images using a 2eV slit of crystals of C₆₀ within a lysosome. Clusters in the 26eV image have a higher intensity than the cell medium in the 26eV image than in the 20eV image, and this increase in intensity is confirmed in the ratio image (26/20eV) in part (d). In part (b) regions of lighter contrast are marked on the surface of the crystals which suggest the presence of surface plasmons (p). The histogram (Fig. 11.2f) across the plasma membrane in part (e) shows an increase in intensity at the plasma membrane which is indicative of a greater density of C₆₀ at this site. m – plasma membrane, c – cytoplasm

the incident electrons with the outer-shell atomic electrons, where the most prominent feature is the plasmon peak. Plasmon excitations are an important process and are a consequence of collective electron oscillations in extended arrays of atoms. Finally, the core loss section of the spectrum is the outcome of interactions between the incident electrons and the inner-shell atomic electrons. For energies above that of the plasmon, the spectrum consists of a gradually decreasing background caused by different interactions. Ionization edges from core-loss are superimposed onto it.

11.5.4 Energy Loss Microscopy of Intracellular Carbon Nanostructures

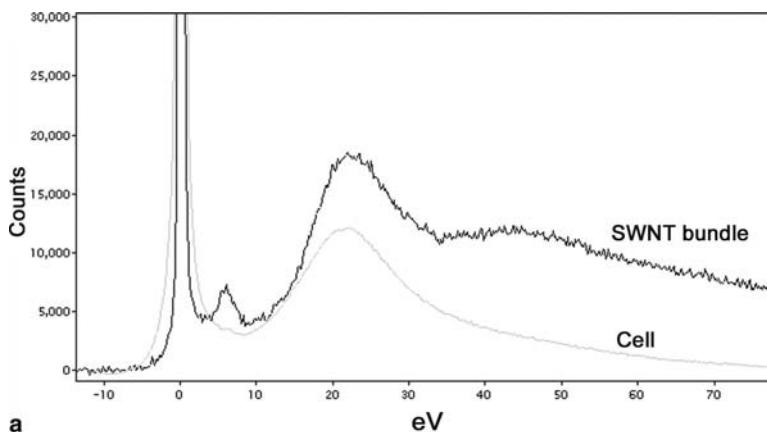
In a TEM, energy loss can either be measured in series, i.e. an image is acquired over a defined energy loss window, known as energy-filtered TEM (EFTEM); or in parallel, where an entire energy loss spectrum is acquired from a point in the specimen, known as electron energy loss spectroscopy (EELS). With EFTEM, an energy slit is used to select a region of the energy loss spectrum. Using this technique it is possible to acquire two-dimensional, elemental maps using electrons with an energy loss characteristic of a core level, interband transition or plasmon resonance energy. With EFTEM, the EELS spectrum may be extracted by acquiring a series of energy-filtered images, using a narrow energy window (1–3 eV). Image processing software may then be employed to extract the EELS spectra over a given energy range. In comparison to EFTEM, EELS spectrum imaging allows for a data set from a user-defined area and pixel density (x, y) to be collected, where each pixel contains an energy loss spectrum over a defined energy range (E). Using these techniques it is possible to utilize the low-loss region of the energy spectrum to map carbon nanoparticles within the cell. Both techniques have their advantages, and should be selected depending on the information required. Traditionally, EFTEM, which has a poor energy resolution compared to EELS, has been used for the study of core-loss excitations. This however requires substantial acquisition times to obtain sufficient counts and can result in specimen damage. The issue becomes critical when mapping distributions of carbon nanoparticles within the cell, as the graphitic carbon nanoparticles rapidly degrade under the beam by knock-on damage.

There are two energy regions available to map carbon in the energy loss spectrum: the K-shell carbon ionization edge and the low-loss region of the EELS spectrum. Both of these edges offers a means to map similar but distinct carbon species; however, in practice, mapping using the carbon K-edge will not succeed as the high electron dose necessary for this technique leads to rapid degradation of the graphitic carbon and subsequent amorphization.

The low-loss region of the electron energy loss spectrum (EELS) has two advantages for imaging carbonaceous species: (i) the scattering cross-sections are many orders of magnitude larger than for core-loss scattering, and thus

acquisition times and beam damage can be minimized, and (ii) the ($\sigma + \pi$) volume plasmon excitation which dominates the low-loss spectrum is sensitive to the electronic structure of the carbon species (Saito et al., 1991). In the low-loss spectrum, fullerenes and SWNTs exhibit a bulk plasmon energy, arising from oscillations of the σ and π electrons, of around 26 eV, whereas amorphous carbon exhibits a plasmon energy of ~ 23 eV (Porter et al., 2006, 2007a, b; Saito et al., 1991). Graphitic-like carbonaceous materials also exhibit an interband, $\pi \rightarrow \pi^*$, transition at 6 eV. This $\pi \rightarrow \pi^*$ transition results from the excitation of electrons in the π bond and is therefore very weak or missing in the amorphous material.

Using EFTEM and EEL-spectrum imaging techniques, we have been able to image the plasma membrane, nucleus and lysosomes by mapping these shifts in plasmon energy between the cell and the SWNT/ C_{60} (Sloan et al., 2007; Stöckli et al., 2000). We have shown that the difference in volume plasmon energies between the cell and fullerene C_{60} enables a ratio of energy-filtered images recorded at around 6, 20 and 26 eV, and can be used to differentiate the two carbonaceous materials in both two and three dimensions (Zhao, 2005). In this work we demonstrated the use of electron energy loss spectroscopy (EELS) to map disordered and crystalline at medium resolution, where no contrast is apparent in the conventional image (Fig. 11.3). Using these techniques we have been able to image C_{60} localizing at the plasma membrane, lysosomes, and more significantly, within the cell nucleus. More recently we have extended the work on C_{60} and used electron energy loss (EEL) spectrum imaging combined with EFTEM to map the distribution of SWNTs within the cell, where no contrast is apparent in conventional imaging (Porter et al., 2006, 2007a, b). For example, in Fig. 11.4, low-loss EELS from the SWNT bundle exhibits peaks at 6 and 22 eV, corresponding to the $\pi \rightarrow \pi^*$ transition and the $\sigma + \pi$ bulk plasmon from the graphitic nanotubes, respectively (see Fig. 11.4 spectrum), whilst the other spectra from the cell exhibits no $\pi \rightarrow \pi^*$ transition and a reduced $\sigma + \pi$ bulk plasmon energy. Figure 11.4d shows a plasmon map of SWNTs in the cell. This map was taken by applying a non-linear least squares (NLLS) fit to the ($\sigma + \pi$) bulk plasmon peak and extracting the peak energy position – the apparent lower plasmon energy observed in this work compared to previous results on C_{60} (Porter et al., 2007) was due to the introduction of the surface plasmon, resulting from the ultra-thin nature of the specimen. By mapping the plasmon energy (Fig. 11.4c), we were able to identify bright lines through the map, associated with a higher plasmon energy of the SWNTs. Figure 11.2 shows the corresponding BF image, which demonstrates the lack of information obtained from conventional BF imaging of unstained sections. Figure 11.2e is a high-resolution BF image of the boxed area defined in Fig. 11.2a: several SWNTs are visible running diagonally across the image, in accordance with the feature in the plasmon map. The resolution of low-loss EELS, in particular the bulk plasmon which is a delocalized event, is not sufficient to distinguish between the individual SWNTs. These studies demonstrate the potential of high-resolution TEM and STEM as techniques to probe interactions occurring at the interface between nanoscale and biological systems.



a

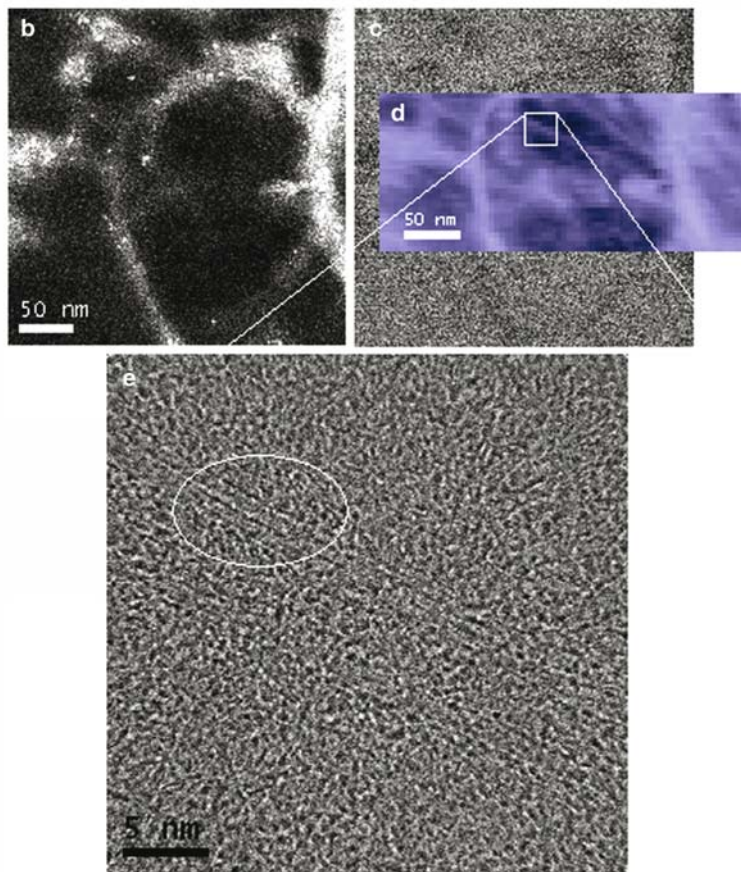


Fig. 11.4 (a) (c) Low-loss EELS spectra of SWNT bundles and the cell alone. The π - π^* transition at ~ 6 eV can be seen clearly only from the bulk of the SWNT bundle, it also exhibits a slightly higher bulk plasmon energy which is clearly visible when mapped as in (d). (b) HAADF image of SWNT bundles with Fe catalyst particles. Fe particles give bright contrast in HAADF image so allow SWNT bundles to be identified. (c) The corresponding bright field image showing no visible features in the same area. (d) Area of interest picked out with plasmon peak map from Fig. 11.1b. (e) High-resolution bright field imaging of the boxed area shows several SWNTs across the image (c). Diameter of SWNT indicated by arrows is 1.2 nm (See Color Plates)

11.6 3-D Techniques

It is not possible, using 2-D imaging, to obtain complete certainty as to whether the nanoparticles lie on the surface of the sections, or have actually penetrated the cell. It is therefore necessary to use 3-D microscopy techniques such as confocal microscopy or 3-D tomography to determine the 3-D distributions of the particles. In general a number of complementary techniques must be utilized to fully understand the 3-D distribution and structure of the nanoparticles/tubes within the cell.

11.6.1 Confocal Microscopy

The advantage of confocal microscopy is that it may be used to image live cells, where post-fixation and freeze-drying techniques for TEM may modify the distribution of the nanoparticles within the cell. SWNTs are commonly imaged within cells in the confocal microscope by tagging the SWNT with a fluorochrome label (Kam et al., 2005; Pantarotto et al., 2004), however the bulky fluorochrome tag may modify uptake of the SWNTs by cells. We have shown that SWNTs can be imaged in the confocal microscope without chemically modifying their surface by filling them with heavy metal halides or metal oxides such as AgI (Sloan et al., 2003) or PbO (Fig. 11.5). When the SWNTs are filled, the metal halide/oxide is fully encapsulated by the SWNTs (Hafner et al., 1998) and therefore has no contribution to the potential toxicity (Horak et al., 1998). We have developed a simple method for imaging intracellular SWNTs filled with AgI in live cells, in reflectance mode

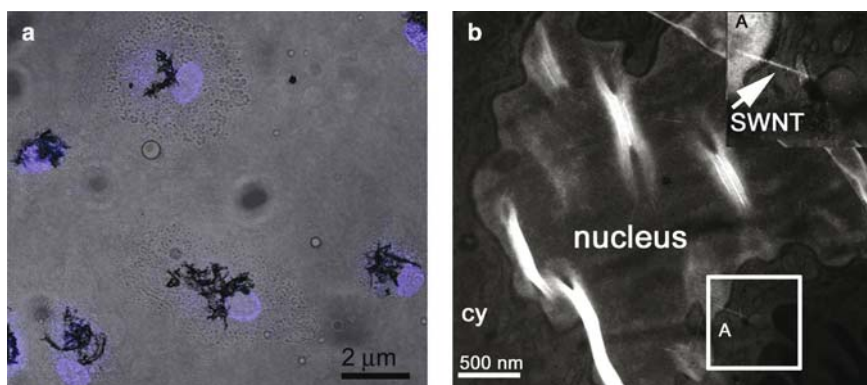


Fig. 11.5 (a) Confocal microscope image of HMMs exposed to AgI@SWNT at 3 days confirming inclusion of SWNT bundles inside the nucleus (blue). (b) HAADF-STEM image of PbO@SWNTs crossing the nuclear membrane into the nucleus (inset from boxed region A) (40 nm thick section, unstained) (See Color Plates)

using the confocal microscope. This technique can also be applied to facilitate imaging of the SWNTs in the cell using TEM (Fig. 11.5).

11.6.2 Electron Tomography

Electron tomography is a 3-D technique which is key for understanding the organization and structure of inorganic and biological materials (Midgley et al., 2007). For example, in the life sciences, cryotomography is commonly used to analyze cellular structures, viruses and bacteria; in physico-chemical sciences, there is a need to understand the functional and mechanical behaviour of materials in three dimensions at the nanoscale. For a detailed review of this technique the reader should refer to Midgley et al. (2007). The basis of the technique is the rotation of a specimen about a single axis, leading to the acquisition of an image every $1-2^\circ$, typically in a tilt range of $\pm 70^\circ$. A back-projection or SIRT algorithm is then used to compute a 3-D reconstruction of the specimen.

Electron tomography can be combined with either EFTEM or HAADF-STEM. The advantage of HAADF-STEM tomography is its suitability for imaging thick sections: the absence of a post-specimen imaging lens means the effects of chromatic aberration can be avoided, such that image contrast and resolution remain high (Fig. 11.6). Using HAADF-STEM tomography, it is possible to image sections of up to 300 nm thickness with good resolution, even freeze-dried whole cells cultured on a TEM grid. As described previously, energy-filtered transmission electron microscopy (EFTEM) tomography is based on acquiring two or three, or sometimes a large series, of energy-filtered images near an ionization edge of interest. With EFTEM the benefits consist in being able to acquire data at different energy losses for each tilt angle. By acquiring an extended series of images over the energy loss edges of interest, fully quantitative elemental maps can be generated; a technique called spectral tomography (Gass et al., 2006). The ability of spectral tomography to extract chemical information from specific volumes of material enables a far more accurate 3-D characterization of carbonaceous nanocomposites, and indeed of many other nanoscale structures, than has been previously possible (Gass et al, 2006). EFTEM tomography may also be applied to image carbon nanoparticles within cells by acquiring energy-filtered images near the ionization edge of $\sigma+\pi$ plasmon energy. For example, by reconstructing data from ratio images of 26/20 eV, it may be possible to gain contrast between the graphitic nanoparticles and the cell. However, the spectral tomography technique is limited for imaging carbon nanoparticles in cells, since long exposure times are required, with subsequent beam damage.

11.7 Relevance of Imaging Studies to Toxicology

Our imaging studies have demonstrated that it is possible to image C_{60} and SWNTs in both fixed and live cells using STEM, TEM and confocal microscopy techniques. We exposed human macrophage cells to C_{60} and SWNTs and found that both C_{60}

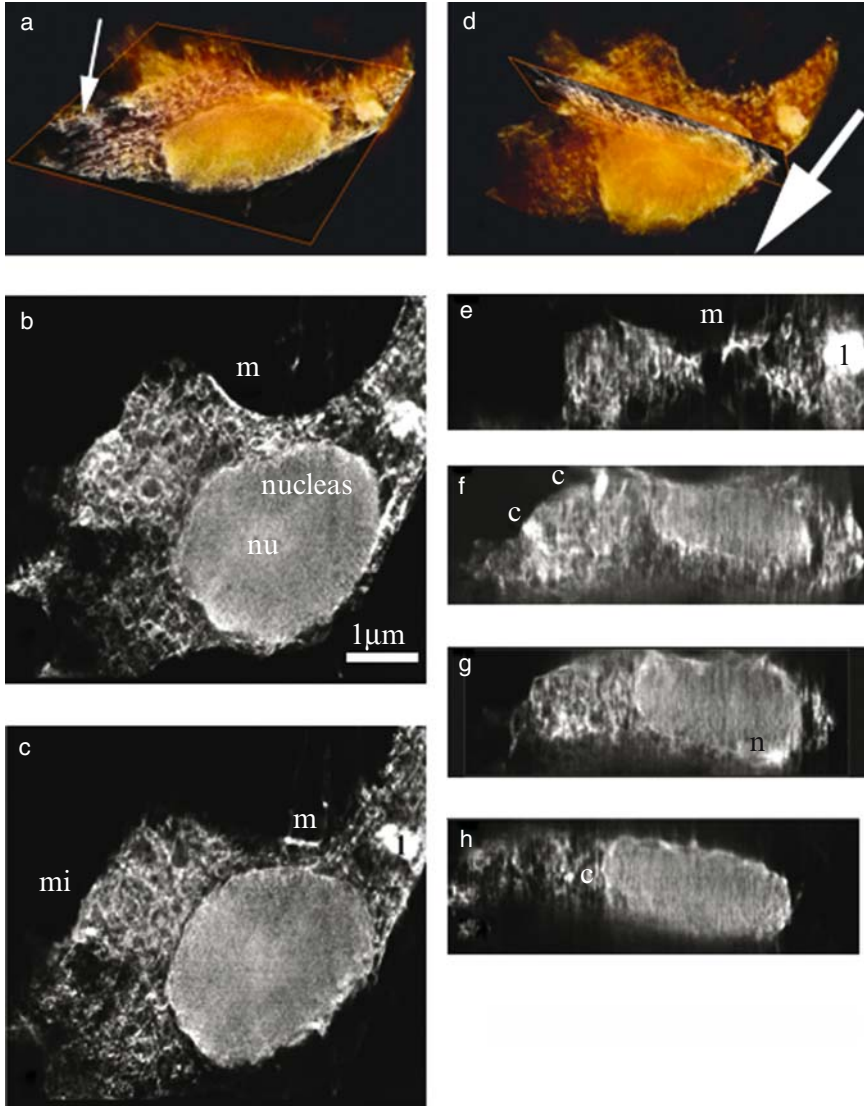


Fig. 11.6 A series of horizontal (b–c) slices and vertical slices (e–h) through a HAADF-STEM reconstruction of a freeze-dried whole cell exposed to C_{60} for 24 h. Slices are $\sim 0.15 \mu\text{m}$ apart. (a) Voltex reconstruction of the same cell showing a horizontal orthoslice through the 3-D reconstruction. (d) Vertical orthoslice through the Voltex reconstruction. Slices through the reconstruction illustrate membranes (m), the nucleus (n), the cytoplasm (c), and secondary lysosomes (l). Several distributions of particles with the cell are revealed at each height through the reconstructed cell (See Color Plates)

and SWNTs are predominantly discovered within lysosomes, suggesting that they enter cells by energy-dependent phagocytosis or endocytosis. More significantly, our work illustrated that C_{60} concentrates at the plasma membrane, where it has the potential to cause cell damage via lipid peroxidation and oxidative stress (Porter et al., 2006, 2007). Individual SWNTs were regularly found within lysosomes but also traversed lysosomal membranes to the cytoplasm of the cell. These findings suggest that passive diffusion across lipid bilayers is also a potential entry mechanism. Uptake to the nucleus implies that SWNTs and C_{60} may interact with intracellular proteins, organelles and DNA, which would greatly enhance their toxic potential. For example, Zhao et al. investigated C_{60} interaction with DNA and found that C_{60} tended to bind to the hydrophobic free ends and minor groove sites of DNA, due to its own hydrophobicity. Attachment to the minor grooves was of significant concern because the C_{60} disrupts the normal DNA structure by creating a 20° angle between the base pair stack plane (Zhao et al., 2005). Finally we have shown that imaging studies are essential to understand the localized effects of nanoparticles on cell viability. In a time course study, we compared localized effects of SWNTs on cell structure in the TEM with standard cell viability assays. In this work we showed that localization of SWNTs at these sites was correlated to an increase in cell death in both cell viability assays and TEM analysis (Porter et al., 2007). In conclusion our work has shown that imaging studies are essential to compliment traditional cell viability assays to understand the toxicity of carbon nanoparticles.

References

- Ashcroft JM, Tsybouski DA, Hartman KB, Zakharian TY, Marks JW, Weisman RB, Rosenblum MG, Wilson LJ (2006). Fullerene (C_{60}) immunoconjugates: interaction of water-soluble C_{60} derivatives with the murine anti-gp240 melanoma antibody. *Chem. Comm.* 28: 3004–3006.
- Cherukuri P, Bachilo SM, Liovsky SH, Weisman RB (2004). Near-infrared fluorescence microscopy of single-walled carbon nanotubes in phagocytic cells. *J. Am. Chem. Soc.* 126: 15638–15629.
- Chui D, Tian F, Ozkan CS, Want M, Gao H (2005). Effect of single wall carbon nanotubes on human HEK293 cells. *Toxicol. Lett.* 155: 73–85.
- Friedman SH, Ganapathi PS, Rubin Y, Kenyon GL (1998). Optimizing the binding of fullerene inhibitors of the HIV-1 protease through predicted binding of fullerene inhibitors of the HIV-1 protease through predicted increases in hydrophobic desolvation. *J. Med. Chem.* 41: 2424–2429.
- Gass MH, Koziol KK, Windle AH, Midgley PA (2006). Four-dimensional spectral tomography of carbonaceous nanocomposites. *Nano. Lett.* 6(3): 376–379.
- Hafner JH, Jason H et al. (1998). Catalytic growth of single-wall carbon nanotubes from metal particles. *Chem. Phys. Lett.* 296: 195–202.
- Horak D, Cervinka M, Puza V (1998). Radiopaque poly(2-hydroxyethyl methacrylate) particles containing silver iodide complexes tested on cell culture. *Biomaterials* 19(14): 1303–7.
- Kam NWS, Liu Z, Dai H (2005a). Carbon nanotubes as intracellular transporters for proteins and DNA: An investigation of the uptake mechanism and pathway. *Angew. Chem. Int.* 44: 1–6.
- Kam NWS, O'Connell M, Wisdom JA, Dai H (2005b). Carbon nanotubes as multifunctional biological transporters and near-infrared agents for selective cancer cell destruction. *Proc. Natl. Acad. Sci. USA* 102(33): 11600–11605.
- Lin M et al. (2006). Direct observation of single-walled carbon nanotube growth at the atomistic scale. *Nano. Lett.* 6(3): 449–452.

- Ma B, Sun YP (1996). Fluorescence spectra and quantum yields of 60–70 fullerenes under different solvent conditions. *J. Chem. Soc. Perkin. Trans. 12*: 2157.
- Manna SK et al. (2005). Single-walled carbon nanotube induces oxidative stress and activates nuclear transcription factor- κ B in human keratinocytes. *Nano. Lett.* 5(9): 1676–1684.
- Midgley PA, Ward EPWW, Hungria AB, Thomas JM (2007). Nanotomography in the chemical, biological and materials sciences. *Chem. Soc. Rev.* 36: 1477–1494.
- Nimmagadda A, Thurston K, Nollert MU, McFetridge PS (2006). Chemical modification of SWNT alters in vitro cell-SWNT interactions. *J. Biomed. Mater. Res.. A.* 1:76(3): 614–625.
- Oberdorster E (2004). Manufactured nanomaterials (fullerenes, C60) induce Oxidative stress in the brain of juvenile largemouth bass. *Environ. Health. Perspect.* 112(10): 1058–1062.
- Pantarotto D, Singh R, McCarthy D, Ehardt M, Briand JP, Prato M, Kostarelos K, Bianco A (2004). Functionalized carbon nanotubes for plasmid DNA gene delivery. *Angew. Chem. Int. Ed.* 43: 5242–5246.
- Porter AE, Muller K, Skepper J, Midgley P, Welland M (2006). Uptake of C₆₀ by human monocyte macrophages, its localization and implications for toxicity: studies by high resolution electron microscopy and electron tomography. *Acta. Biomater.* 2(4): 409–419.
- Porter AE, Gass M, Muller K, Skepper JN, Midgley PA, Welland M (2007a). Direct imaging of single-walled carbon nanotubes in cells. *Nature Nanotechnol.* 2: 713–717.
- Porter AE, Gass M, Muller K, Skepper JN, Midgley PA, Welland M (2007b). Visualizing the uptake of C₆₀ to the cytoplasm and nucleus of human monocyte-derived macrophage cells using energy-filtered transmission electron microscopy and electron tomography. *Environ. Sci. Tech.* 41(8): 3012–3017.
- Pulskamp K, Diabate S, Krug HF (2007). Carbon nanotubes show no sign of acute toxicity but induce intracellular reactive oxygen species in dependence on contaminants. *Toxicol. Lett.* 168(1): 58–74.
- Qiao R, Roberts AP, Mount AS, Klaine SJ, Ke PC (2007). Translocation of C₆₀ and its derivatives across a lipid bilayer. *Nano. Lett.* 7(3): 614–619.
- Saito Y, Shinoara H, Ohshita A (1991). Bulk plasmons in solid C₆₀. *Jpn J. Appl. Phys.* 30(6A): 1068–1070.
- Sayes CM, Goin AM, Ausman KD, Mendex J, West J, Colvin VL (2005). Nano-C(60) cytotoxicity is due to lipid peroxidation. *Biomaterials* 26(36): 7586–7595.
- Sayes CM et al. (2006). Functionalization density dependence of single-walled carbon nanotubes cytotoxicity in vitro. *Toxicol. Lett.* 161(2): 135–142.
- Sayes CM, Marchione AA, Reed KL, Warheit DB (2007). Comparative pulmonary toxicity assessments of C₆₀ water suspensions in rats: few differences in fullerene toxicity in vivo in contrast to in vitro profiles. *Nano. Lett.* 7(8): 2399–2406.
- Shvedova AA (2005). Unusual inflammatory and fibrogenic pulmonary responses to single-walled carbon nanotubes in mice. *Am J Physiol Lung Cell Mol Physiol* 289: L698–L708.
- Sloan J, Kirkland AI, Hutchinson JL, Green MLH (2003). Aspects of crystal growth within carbon nanotubes. *C.R. Phys.* 4: 1063–1074.
- Stöckli T, Bonard JM, Châtelain A (2000). Plasmon excitations in graphitic carbon spheres measured by EELS. *Phys. Rev. B.* 61: 5751–5759.
- Tsuchiayai T, Oguri I, Yamakoshi YN, Miyata N (2006). Novel harmful effects of [60]fullerene on mouse embryos in vitro and in vivo. *FEBS Lett.* 393(1): 139–145.
- Worle-Knirsch JM, Pulskamp K, Krug HF. (2006). Oops they did it again! Carbon nanotubes hoax scientists in viability assays. *Nano. Lett.* 6(6): 1261–1268.
- Zhao X, Striolo A, Cummings PT (2005). C₆₀ Binds to and deforms nucleotides. *Biophys. J.* 89: 3856–3862.
- Zhang Z et al. (2006). Delivery of telomerase reverse transcriptase small interfering RNA in complex with positively charged single-walled carbon nanotubes suppresses tumor growth. *Clin. Cancer Res.* 12(16): 4933–4939.

Chapter 12

Pharmacological Applications of Biocompatible Carbon Nanotubes and Their Emerging Toxicology Issues*

Tae-Joon Park¹, Jeffrey G. Martin^{2,3}, and Robert J. Linhardt^{1,2,3}

Abstract Since their discovery in 1991, carbon nanotubes (CNTs) have been studied for their application as diagnostic tools, chemical sensors, and vectors for drug delivery. Carbon nanotubes are of great interest because of their unique array of physical and chemical properties, including their high aspect ratio, ultralight weight, high mechanical strength, high electrical conductivity, high thermal conductivity, and high surface area. The unique properties of carbon nanotubes also raise substantial concern about their potentially toxic effects on the environment and human health. This review focuses on the current pharmacological applications and emerging toxicology issues of biocompatible carbon nanotubes. Carbon nanotubes as agents for drug delivery, cancer therapeutics, along with their *in vivo* challenges and potential toxicity are discussed.

Keywords carbon nanotubes, biomaterials, biocompatibility, toxicity, nanomaterials

12.1 Introduction

12.1.1 Historical Overview of Bio-Nanomaterials

Biomaterials can be defined as any nondrug material that can be used to treat, enhance, or replace any tissue, organ, or function in an organism. Biomaterials also

¹Department of Chemical and Biological Engineering, Center for Biotechnology and Interdisciplinary Studies Rensselaer Polytechnic Institute, Biotech Center 4005, 110 8th Street, Troy, NY 12180-3590, USA

²Department of Chemistry and Chemical Biology, Center for Biotechnology and Interdisciplinary Studies Rensselaer Polytechnic Institute, Biotech Center 4005, 110 8th Street, Troy, NY 12180-3590, USA

³Department of Biology, Center for Biotechnology and Interdisciplinary Studies Rensselaer Polytechnic Institute, Biotech Center 4005, 110 8th Street, Troy, NY 12180-3590, USA

* In *Medicinal Chemistry and Pharmacological Potential of Fullerenes and Carbon Nanotubes*, Franco Cataldo and Tatiana Da Ros (eds.), Springer Vol. 1, Topics in Carbon Materials Chemistry and Physics, 2007.

refer to biologically derived materials that are used for their structural rather than their biological properties. Collagen, the protein found in bones and connective tissues, is an example of a biologically derived biomaterial that can be used as a cosmetic ingredient. Even though the term “biomaterial” did not even exist until 50 years ago, crude biomaterials have been used since the earliest days of human civilization (Ratner et al., 2004). This historical overview touches on some highlights in biomaterials leading to the biomedical application of carbon nanotubes.

The first ever injectable crude biomaterial, that is a dental implant, appeared early in AD 600 (Fig. 12.1). During those times, Mayan people trimmed seashells into artificial teeth to replace missing teeth (Michael, 2006; Ratner et al., 2004). Early biomaterials also led to problems, including sterilization, toxicity, inflammation, and immunological issues. Since the Mayan’s initial use of artificial teeth, biomaterials have evolved to be used in modern artificial hearts, hip and knee prostheses, artificial kidneys, and breast implants. Materials used in these applications include titanium, silicons, polyurethanes, teflon, polybiodegradable polymers, and most recently bio-nanomaterials (Pearce et al., 2007)

The artificial hip has been used to replace the human hip because the hip is easily worn out over a lifetime of mechanical stress resulting from normal activity. The first artificial hip implant was made by Thernistokles Gluck in 1891 in Berlin. This implant made use of a femoral head of ivory fixed with plaster of paris and glue (Glück, 1890, 1891). The results were not good due to severe infection problems and adverse foreign body tissue reactions. To develop better hip replacement prosthesis, many materials and procedures were examined between 1925 and 1953.

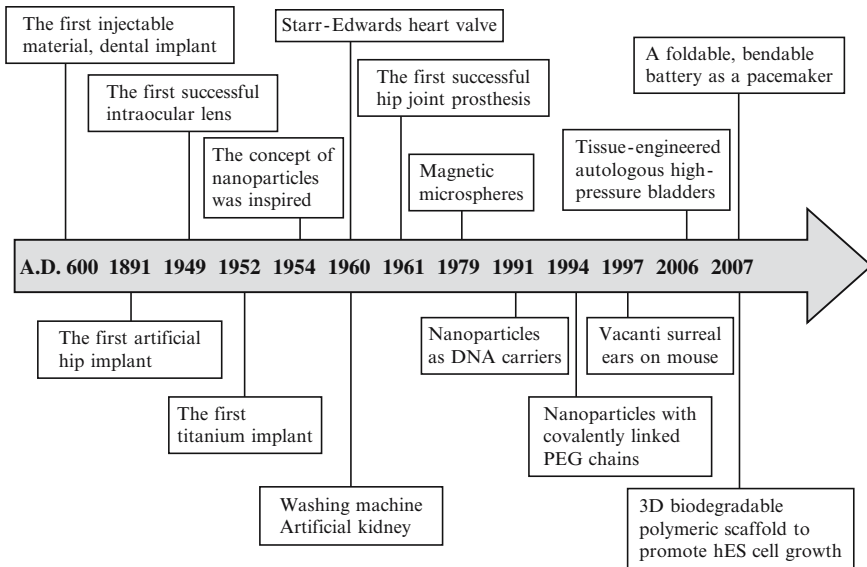


Fig. 12.1 Timeline of important events in biomaterial history

These include attempts by surgeon M.N. Smith-Petersen in 1925, Robert and Jean Judet in 1938, and Dr. Edward J. Haboush in 1953. However, the first successful hip prosthesis was not developed until 1961 when Dr. Charnley made a hip prosthesis out of a high molecular weight polyethylene cup. Today, artificial hip joints are implanted in over 200,000 people each year in the USA (Ratner, 2004).

The first titanium implant was developed by Per Ingvar Branemark, an orthopedic surgeon at the University of Lund, Sweden in 1952. After finishing an experiment with rabbit bone, Branemark observed that the titanium implant was tightly integrated into the bone (Branemark et al., 1964). This phenomenon, supported by Branemark's theory of osseointegration, is responsible for the use of modern titanium alloy in dental and orthopedic implants (Eriksson and Branemark, 1996).

Another example of a biomaterial is the intraocular lens, which have been commonly used to treat cataracts. They were traditionally made of inflexible materials, but more recently consist of poly(methyl methacrylate) and soft flexible materials such as silicone and acrylic. The first person to successfully implant an intraocular lens was Sir Harold Riley at the St Thomas' Hospital in London in 1949. The first lenses were made of glass, were heavy, and carried several risks including infection, inflammation, loosening of the lens, lens rotation, and night time halos (Thompson, 2007). These problems, now less frequent, still occur today in a small fraction of more than one million intraocular lenses that are implanted annually in the USA.

In 1960, the Starr-Edwards heart valve was invented by Albert Starr and Lowell Edwards. Before the invention of this heart valve, people had only survived for 3 months following the introduction of a prosthetic heart valve. The Starr-Edwards heart valve was a great success as it significantly extended patient survival. This was a particularly impressive invention because the replacement of a heart valve is highly challenging due to the continuous flow of blood.

An important development towards the artificial kidney was achieved by Dr. Belding Scribner in 1960, who devised a "U"-shaped shunt implanted through the skin between an artery and vein to access the blood stream to perform routine dialysis (Ratner, 2004). Dr. Scribner made use of Teflon tubes to access the vessels and provides a nonstick surface for the transport of blood. The Scribner shunt has allowed more than one million patients to survive from kidney failure.

In 1997, Joseph and Charles Vacanti made a nude mouse with a surreal, human-like, ear growing out of its back to create cartilage structures for transplantation into patients. The human ear is the one of the most difficult cartilaginous tissues to reconstruct and rebuild. The Vacanti brothers seeded cow cartilage cells into a biodegradable ear-shaped mold to grow an ear-shaped cartilage structure to construct this ear. The same method was used for a 12-year-old child, who had no bone or cartilage on his left chest to protect his heart and lungs. This was a necessary procedure because the child was a starting pitcher for a baseball team, and a single ball striking his chest might have killed him. The boy's own cartilage cells were used to grow a chest plate on a synthetic biodegradable polymer developed by the Vacanti brothers. This operation was a success and the implant was able to grow with the boy.

An important breakthrough in bioartificial organs was recently reported by Atala and coworkers (Atala et al., 2006). They were able to implant tissue-engineered autologous high-pressure bladders into seven patients. These implanted bladders grew successfully and were still functional 5 years after the surgery with no adverse effects (Atala et al., 2006; Becker and Jakse, 2007; Patel et al., 2007). This work emphasizes the remarkable relevance of stem cell tissue engineering, which is one of the most promising technologies in modern regenerative medicine. The two major drawbacks of using human embryonic stem cells (hESCs) in clinical applications are the lack of supply and the current inability to stimulate these cells to undergo tissue-specific differentiation (Becker and Jakse, 2007; Chai and Leong, 2007; Eberli and Atala, 2006; Frimberger et al., 2006; Gardner, 2007; Jan and Kotov, 2007; Karp et al., 2007; Patel, 2007; Yang et al., 2006).

Dr. Robert Langer, one of the pioneers in the field of biomedical engineering, has been responsible for the remarkable development of biomaterials in drug delivery systems and tissue engineering since the late 1970s (Langer, 1998, 2001, 2007; Langer and Vacanti, 1993). The Langer group focused primarily on drug delivery systems and their ability to treat cancer patients. This group also reported 3D biodegradable sponge-like scaffolds, hyaluronic acid hydrogels, and dextran-based hydrogels for promoting hESC growth and controllable vascular differentiation of hESCs (Gerecht, 2007; Levenberg, 2003).

Our laboratory has focused on the structure and activity of heparin and the pharmaceutical application of enzymology in the fields of glycobiology, glycochemistry, and glycoengineering since the 1980s. Recently, we have combined our laboratory skills in biocatalysis and carbohydrate-based therapeutics with bioprocessing, polymer chemistry, bioimaging, and nanotechnology to help develop new biocompatible materials (Capila and Linhardt, 2002; Folkman et al., 1983; Kumar et al., 2007; Linhardt et al., 1992; Lohse and Linhardt, 1992; Murugesan et al., 2006a, b; Langer et al., 1982; Pushparaj et al. 2007; Viswanathan et al., 2006).

Carbon nanotubes (CNTs) and other nanostructure biomaterials are currently being investigated in our laboratory for their use as building blocks to create artificial kidneys and other medical devices. A common cause of device failure occurs when blood components, both cells and proteins, stick to these artificial materials resulting in the formation of fibrin clot. Our laboratory is approaching this problem by coating materials such as CNTs with heparin, a commonly used anticoagulant (Murugesan et al., 2006a, b). Heparin-coated CNTs, for example, were shown to exhibit significantly less clotting and thus were much more biocompatible than uncoated CNTs (Dumortier et al., 2006; Ostomel et al., 2006). This significance of blood compatibility of nanodevices is extremely important if CNTs are to be used as novel drug carriers for therapeutic agents (Dumortier et al., 2006; Kam et al., 2005; Singh et al., 2006; Sugibayashi et al., 1977, 1979a, b).

We have recently turned our attention to cellulose-heparin, blood-compatible, nanoporous composite membranes for use in kidney dialysis (Murugesan et al., 2006a, b). Advanced kidney dialysis system contains heparin covalently bound to the surface of biomaterials to reduce clotting effects. Our new approach relies instead on composite materials. Unfortunately, no technology has been available to

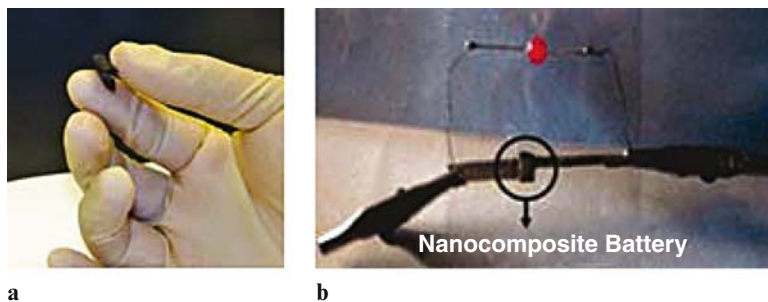


Fig. 12.2 A foldable, bendable battery; paper invention which can be inserted under the skin as a pacemaker and powered in part by bodily fluids. (a) A postage-stamp-sized battery as thin as paper, (b) the flexible nanocomposite film battery used to glow a red light-emitting diode (LED) (See Color Plates)

heparinize cellulose membranes without adversely impacting its properties as a dialysis membrane. Thus, for most patients undergoing kidney dialysis, the majority of the surface area of the dialyzer consists of uncoated cellulose fibers. These patients must receive heparin by injection to prevent their blood from clotting. A composite material containing heparin represents a novel approach for increasing the blood compatibility of biomaterials.

Recently, our laboratory produced a foldable, bendable, and cutable postage-stamp-sized battery (Fig. 12.2). The device looks like a simple sheet of black paper, but it could spell a revolution in implantable battery technology (Pushparaj et al., 2007). The paper battery, a one-piece-integrated device is made of cellulose with CNT and lithium electrodes. The device is flexible, rechargeable, and has the ability to function over a wide range of temperatures giving it a wide variety of potential biomedical applications. As a biomaterial, this paper battery may be useful as a pacemaker because it could easily be inserted under a patient's skin.

Most experts define nanotechnology as the design and engineering of objects (e.g., nanotubes, quantum dots, gold nanoparticles, fullerenes, and nanohorns) smaller than 100 nm. Nanotechnology has grown into an interdisciplinary area that shows potential to be effectively used to solve problems in cancer diagnosis, gene therapy, and drug delivery. Nanoparticles are so small (100 nm) that they are not visible because they are smaller than wavelengths of light (about 700 nm in the red to 400 nm in the violet). For size comparison, the diameter of a human hair is 50–100 μm , the size of a bacterium is 1 μm , and the size of a single sugar molecule is 1 nm (Bell, 2006; Bianco et al., 2005; Cai et al., 2005; Cuenca et al., 2006; Ferrari, 2005; Goldberg et al., 2007; Labhasetwar, 2005; Liu and Wang, 2007; Martin and Kohli, 2003; Nepal and Geckeler, 2007; Nie et al., 2007; Son et al., 2007a, b; Tasis et al., 2006).

Bio-nanomaterials are significantly different from traditional larger biomaterials (e.g., implants or microparticles as mentioned earlier) in terms of their physical and biological properties. Due to their new set of biological and physical properties, bio-nanomaterials also show potential for use as therapeutics and in drug delivery systems. For instance, Na and coworkers in 2007 used a bio-nanomaterial, heparin/

poly(L-lysine) nanoparticle-coated polymeric spheres, as an excellent substrate for stem cell therapy (Na et al., 2007). Nanomaterials introduced microscale and nanoscale features onto culture surfaces to enable stem cell responses. These topographical cues of bio-nanomaterials are currently being researched as they may play a significant role in minimizing host immunoreactivity towards transplanted cells or engineered grafts (Chai and Leong, 2007).

The first bio-nanomaterials were prepared during the pharmaceutical boom of the 1950s and 1960s. In 1954, Paul Ehrlich, whose work focused on the staining of bacteria and tissues, first motivated the development of nanoparticles for drug targeting. During the 1960s and 1970s, Peter Speiser and his group developed polyacrylic beads that were able to function as miniaturized drug delivery systems for oral administration, microcapsules, or nanocapsules that were able to circulate in the blood after *intravenous* injection, and the first nanoparticles for drug delivery (Birrenbach and Speiser, 1976; Kopf et al., 1976, 1977; Kreuter, 2007; Speiser and Khanna, 1970).

Since the concept of nanoparticles was first introduced, their biomedical applications have been investigated and their use has improved drug therapy. In 1973, albumin microspheres were one of the first drug delivery systems tested for targeting to the reticuloendothelial system study (Scheffel et al., 1972; Zolle et al., 1970). In 1977, researchers investigated albumin microspheres for their ability to carry bound 5-fluorouracil (Kramer, 1974). In 1979, the first rapidly biodegradable acrylic nanoparticles were introduced (Couvreur et al., 1979). Researchers also began to investigate the properties of magnetic particles and their response to an external magnetic field (Sugibayashi et al., 1977, 1979a, b; Widder et al., 1979). Four years later in 1983, magnetic albumin particles were used to selectively target in rats with tumors (Widder et al., 1983a, b).

The immobilization of protein to biodegradable poly(acryl-dextran) nanospheres and microspheres was demonstrated in the 1980s (Edman et al., 1980). Poly(lactic acid) nanoparticles were synthesized for the purpose of drug delivery (Gurny, 1981; Gurny et al., 1981). Poly(acryl-starch) microparticles were characterized (Arthursson et al., 1984) and antigens were entrapped in these particles for use as a vaccine (Arthursson et al., 1985). Researches also used nanoparticles to improve the oral bioavailability of drugs (Maincent et al., 1986) and antiinfective drugs (Henrymichelland et al., 1987) and DNA have been used in nanoparticle carriers (Bertling et al., 1991).

Over the past decade, nanoparticles have been covalently linked with poly(ethylene glycol) chains to prolong the blood circulation time and reduce their liver uptake (Bazile et al., 1995; Brigger et al., 2002; Gref et al., 1994; Maincent et al., 1986; Peracchia et al., 1997, 1999). Nanoparticles have been coated with polysorbate 80 to minimize their effects on the central nervous system (Alyautdin et al., 1995, 1997; Alyautdin et al., 1998; Gulyaev et al., 1999) and apolipoprotein E has been covalently linked to albumin nanoparticles to enhance drug transport into the brain (Michaelis et al., 2006).

Nanoscale materials have been categorized in different ways by many popular official sources. For instance, the National Academies categorized nanoscale materials

into four different groups: (1) the metal oxides such as zinc or titanium oxides, (2) nanoclays, (3) nanotubes, and (4) quantum dots (Goldman and Coussens, 2005). According to the US Environmental Protection Agency (EPA), nanomaterials can be classified as (1) carbon-based materials (CNTs, fullerenes), (2) metal-based materials (metal oxides, quantum dots), (3) dendrimers, and (4) composites (including nanoclays) (Bell, 2006).

CNTs in the field of biomaterials have been of major interest for medical applications (Feazell et al., 2007; Ke and Qiao, 2007; McDevitt et al., 2007; Regev et al., 2004). Carbon nanotubes were originally discovered by Iijima in 1991, who deposited nanotubules of graphite onto negative electrodes by arcing graphite for the preparation of fullerenes (Iijima, 1991). At that time, they were categorized as a cylinder-like material containing several layers in a coaxial manner, named multiwalled carbon nanotubes (MWNTs). Later CNTs that only contained one rolled sheet of graphite were discovered and named single-walled carbon nanotubes (SWNTs). Since CNTs were discovered, they have been biologically proposed as diagnostic tools, chemical sensors, and vectors for drug delivery. Due to the increasing biological application of CNTs, there is a concern about their effects on the environment and on human health. In this chapter, we discuss administration, uptake, distribution, metabolism, and elimination of CNTs and explore limitations of CNTs as drug delivery carriers, including toxicology issues.

12.1.2 Physical and Chemical Properties of CNTs

CNTs demonstrate a variety of unique physical–chemical properties. These properties include: high aspect ratio, ultralight weight, high mechanical strength, high electrical conductivity, high thermal conductivity, metallic or semimetallic behavior, and high surface area. Because of these properties, CNTs have been the focus of intense research during the past few decades (Lacerda et al., 2006). These hollow tubes were derived from fullerenes by direct current arcing (Iijima, 1991; Polizu et al., 2006). Kroto discovered that fullerenes afforded this closed-cage structure of CNTs as well as graphite, the well-known form of crystalline carbon having three-coordinate sp^2 carbons (Rao et al., 2001). The three-coordinate sp^2 carbons of graphite form planar sheets containing flat six-membered benzene rings. In the presence of five-membered rings, CNTs can close at either end and form concentric graphitic cylinders.

From an atomic configuration point of view, a nanotube can be divided into two parts that are generated by curvatures: the end caps and sidewall. The end caps are close to the hemispherical fullerene and are curved in 2D, and the sidewall contains less-distorted carbon atoms and is curved in 1D (Polizu et al., 2006). Owing to their specific curvatures, the chemical reactivity at the sidewall is significantly lower than that at the end caps. The sidewall is thought to be inert and highly reactive agents are required for the covalent functionalization of CNT sidewalls (Wei et al., 2007).

Chemical modification plays a significant role in determining the biological properties of CNTs. To increase CNT solubility, the end caps must be functionalized. The end functionalization procedure is composed of two steps: oxidation of the ends using HNO_3 , $\text{HNO}_3 + \text{H}_2\text{SO}_4$, HClO_4 , $\text{H}_2\text{SO}_4 + \text{K}_2\text{Cr}_2\text{O}_7$, and $\text{H}_2\text{SO}_4 + \text{KMnO}_4$ followed by the formation of the covalent linkages to surface functional groups including $-\text{OH}$, $-\text{COOH}$, $-\text{CO}$. Noncovalent interactions (π - π stacking, electrostatic forces, van der Waals forces, and hydrogen bonding) can also provide an important mechanism for absorption and self-assembly of molecules and polymers on CNTs.

CNTs are widely used as electrodes in electrochemical devices (Che et al., 1998; Endo et al., 2001; Frackowiak, 2007; Frackowiak et al., 1999, 2000; Niu et al., 1997; Wu et al., 1999). Since physical and chemical properties of CNTs come from graphite (e.g., the high electrical conductivity of graphite by π bonds), the delocalized electrons of CNTs result in high electrical conductivity. CNTs can individually demonstrate either conductivity or semiconductivity depending on the method used in their fabrication (Bandaru, 2007; Victor et al. 2007; Wei et al., 2007). Our laboratory introduced a foldable and bendable energy-storage device prepared from cellulose and CNTs (Fig. 12.3) (Pushparaj et al., 2007). Supercapacitor can be prepared using aqueous body fluids, and nonaqueous room temperature ionic liquid (RTIL) electrolytes. The CNT-cellulose-RTIL nanocomposite showed a higher operating voltage (~ 2.3 V) compared with those using KOH electrolyte (~ 0.9 V). The supercapacitor device operated through a wide range of temperatures (195–450 K). These flexible nanocomposite sheets were configured as energy-storage

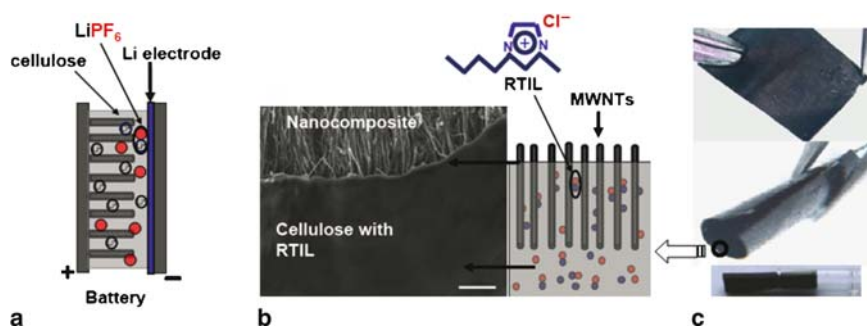


Fig. 12.3 Fabrication of the nanocomposite paper units for battery. (a) Schematic of the battery assembled by using nanocomposite film units. The nanocomposite unit comprises LiPF_6 electrolyte and multiwalled carbon nanotube (MWNT) embedded inside cellulose paper. A thin extra layer of cellulose covers the top of the MWNT array. Ti/Au thin film deposited on the exposed MWNT acts as a current collector. In the battery, a thin Li electrode film is added onto the nanocomposite. (b) Cross-sectional SEM image of the nanocomposite paper showing MWNT protruding from the cellulose-RTIL ($[\text{bmIm}] [\text{Cl}]$) thin films (scale bar, $2\mu\text{m}$). The schematic displays the partial exposure of MWNT. A supercapacitor is prepared by putting two sheets of nanocomposite paper together at the cellulose exposed side and using the MWNTs on the external surfaces as electrodes. (c) Photographs of the nanocomposite units demonstrating mechanical flexibility. Flat sheet (top), partially rolled (middle), and completely rolled up inside a capillary (bottom) are shown (See Color Plates)

devices including supercapacitors, Li-batteries, and supercapacitor–battery hybrids. This robust integrated thin film structure allows not only good electrochemical performance, but also the ability to function over a large range of mechanical deformation and temperatures, and can utilize a wide variety of electrolytes. Furthermore, because the CNTs are parts of a cellulose nanocomposite, there are stable, integrated, macroscopic devices and the CNTs are immobilized.

12.2 Bioapplications of Carbon Nanotubes

In recent years, we have witnessed the development of nanotechnology and the wide array of resulting products utilizing nanotechnology. An important development of nanotechnology, the CNT, can serve as a model nanomaterial for developing biological diagnostics and therapeutics. Currently, many problems exist with larger biomaterial drug delivery systems such as low efficacy and a lack of specificity (Labhasetwar, 2005; Lacerda et al., 2006). CNTs have unique properties and may offer solutions to a wide array of the existing problems in the field of biomaterials.

One main focus of the bioapplications of CNTs is in the area of drug delivery systems. Currently, many modern protein drugs need to be administered intravenously because of the harsh digestive conditions of the stomach and the sensitivity of these drugs to low pH and proteolytic conditions (Venkatesan et al., 2005). Researchers are currently investigating ways to stabilize protein-based drugs on carbon nanotubes to solve this problem. Similar stability concerns arise in gene delivery to directly encode the proteins within the cells. Many studies have been conducted to understand how CNTs are biodistributed when administered intravenously, orally, and implanted into animals (Lacerda et al., 2006). Both *in vitro* and *in vivo* systems have been used to investigate biodistribution.

Spherical nanoparticles (e.g., gold nanoparticles, quantum dots, silica nanospheres) preceded the introduction of CNTs. These are easier to functionalize and are good visual indicators as well as vehicles for enzyme immobilization, DNA transfection, biosensors, and drug delivery. Drugs can also be integrated into biodegradable polymer nanospheres (Martin and Kohli, 2003). When CNTs looking like hollow cylinders were introduced, they immediately became attractive substitutes to replace spherical nanoparticles. Researchers have used functionalized CNTs for DNA delivery (Pantarotto et al., 2004), SWNTs for RNA delivery (Lu et al., 2004), CNTs for protein delivery (Kam and Dai, 2005), and fullerene CNTs (Ajayan, 1999) along with silica CNTs for gene delivery (Chen et al., 2005).

CNTs have become important nanomaterials in the field of pharmaceutical and therapeutic engineering due to several interesting advantages. Their first advantage is that they have a large inner void volume, which can take up and hold drugs for delivery. The release of the drug from this inner compartment can be controlled by the open ends of tube. Second, both the inner and outer surfaces of CNTs can be modified using specific chemical or biochemical functionalization that can afford a

platform for loading drugs. Third, CNTs can facilitate the safe transportation of concealed drug cargo into the cell within its inner core. Holding the drug in the inner core of the tube can protect it from degradation, aggregation, and can also serve to reduce its side effects by keeping it concealed from the body (Son et al., 2007a, b).

12.2.1 Pharmacological Strategy of CNTs in Drug Delivery

12.2.1.1 Uptake, Distribution, Metabolism, and Elimination of CNTs

Pharmacological strategy of CNTs generally relies on four main critical issues: (1) preparation of nanovectors, (2) uptake, (3) function, and (4) elimination (Fig. 12.4). The physicochemical characteristics of CNTs including size, shape, aggregation, chemical composition, surface functionalization, and solubility play an important role in the biodistribution and pharmacokinetics of nanomaterials (Champion et al., 2007; Kostarelos, 2003; Lacerda et al., 2006; Nishiyama, 2007; Oberdörster et al., 2005; Radomski et al., 2005)

12.2.1.2 Transport of CNTs with Functionalization Chemistry

Nanomaterials have three main advantages in drug delivery because of their small size. First, they are highly useful for *intravenous* injection. Second, they can result in less

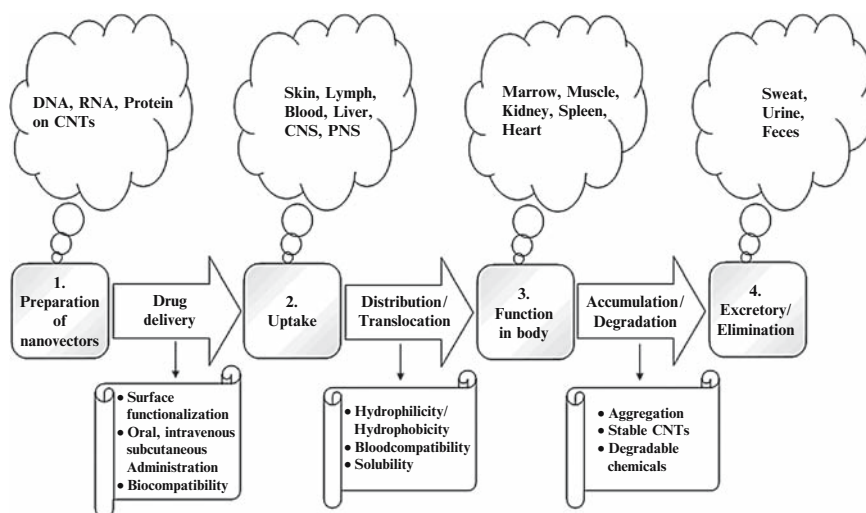


Fig. 12.4 Pharmacological strategy for use of carbon nanotubes (CNTs)

irritation at injection sites. Third, they can penetrate the membranes of the targeted cells (Polizu et al., 2006). Indeed, well-functionalized CNTs and their derivatives are considered one of the most promising nanovectors for biomedical and biotechnological applications. The transport of CNTs combined with proper functionalization chemistry and intrinsic optical properties of CNTs might already lead to their application in drug delivery and cancer therapy (Bianco et al., 2005; Bottini et al., 2007; Kam et al., 2004, 2006; Kam et al., 2005; Kong et al., 2005; Singh et al., 2005; Yinghuai et al., 2005).

Singh et al. (Singh et al., 2005) explored the use of three different types of functionalized CNTs as DNA delivery vehicles. Positively charged, ammonium-functionalized, single-walled and multiwalled CNTs, and lysine-functionalized, single-walled carbon nanotubes were tested for their ability to deliver plasmid DNA. All three types of functionalized CNTs tested demonstrated the ability to attach to DNA, transport it into cells, and upregulate the expression of the marker genes. Singh et al. (2005) also found that while larger CNT surface area allowed the best DNA attachment, DNA attachment was not necessary for gene expression. CNT–DNA delivery systems were successful in both *in vitro* and *in vivo* experiments and these results are promising for future drug delivery applications.

Xiao et al. (2007) has found that short oxidized MWNTs conjugated with fluorescent label were able to cross the cellular membrane of multidrug-resistant cells and these fluorescently labeled MWNTs are not pumped out by P-glycoprotein. Thus, these MWNTs show promise for drug delivery against cells with multidrug resistance, which may be important in treating drug-resistant forms of cancer in the future.

12.2.1.3 Importance of Biocompatibility and Blood Compatibility of CNTs

The use of CNTs as carriers for pharmaceutical applications can be considered only if these carriers are safe for patients. The relevant issues go well beyond the biocompatibility and blood compatibility of CNTs as carriers, and also involve CNT biodistribution and the reliable and reproducible production of CNT carriers (Ferrari, 2005).

Biocompatibility and blood compatibility of CNTs are very important because the lack of those properties has prevented the widespread use of CNTs in biomedical engineering (Dumortier et al., 2006; Kam et al., 2005; Lam et al., 2004; Singh et al., 2006; Sugibayashi et al., 1977, 1979a, b; Worle-Knirsch et al., 2006). Our laboratory recently demonstrated that MWNTs modified with heparin show excellent blood compatibility (Murugesan et al., 2006a, b). These studies suggest the possibility of using CNTs with appropriate surface modifications in various *in vivo* biomedical applications including the treatment of cancer (Bekyarova et al., 2005; Murugesan et al., 2007). Moreover, composites (Fig. 12.3) (Pushparaj et al. 2007) that immobilize CNTs can also serve to enhance biocompatibility and reduce toxicity.

Singh et al. (2006) investigated the tissue biodistribution and blood clearance rates of SWNTs in mice. Three different types of SWNTs were tested: functionalized, water-soluble, and ¹¹¹In-labeled DTPA–SWNT. All types exhibited a blood circulation

life of up to 3.5 h and then were rapidly cleared from the systemic blood circulation through renal excretion. Electron microscopy analysis of urine samples showed that the SWNTs were excreted as intact nanotubes and thus were not broken down in the body. No toxic side effects or mortality was observed in this study. These results suggest that chemical modification of CNTs might increase water solubility and diminish some safety concerns of CNTs.

Guo et al. (2007) have used water-soluble MWNTs labelled with ^{99m}Tc for bio-distribution study in mice. There was no sign of renal or other severe acute toxicity responses consistent with the results of Singh et al. (2006). This work also suggests that functionalization of CNTs might improve their biocompatibility of CNTs.

12.2.1.4 CNTs Behave with Their Needle-Like Shape: Nanoneedles

Geng et al. (2007) compared the transport and trafficking of flexible filaments with spherical micelles in mice. They observed that the flexible filaments remained in the bloodstream for up to 1 week, which is ten times longer than the spherical particles. This is thought to be due to the fact that spheres and short filaments are easier for the cell to take up and thus are removed from the blood stream at a faster rate. This work shows that cellular uptake by nanotubes is probably also length-dependant and that shorter nanotubes are taken up by the cells faster than longer nanotubes. By adjusting the length of the nanotubes, it may be possible to prepare personalized delivery systems having a controlled rate of drug deliverability (Geng et al., 2007).

CNTs are nanoneedles capable of crossing the cell membrane without perturbing or disrupting the membrane and localizing in the cytosol or mitochondria (Dumortier et al., 2006). Cai et al. (2007) looked at the *in vitro* toxicity of nanospearing method using primary B lymphocyte cells. They used functionalized CNTs that were too large for normal uptake into cells and placed a ND-Fe-B permanent magnet underneath the cell culture to pull the functionalized CNTs into the cell. This method was successful and resulted in a ~90% entry rate of the functionalized CNTs into the cells. The group then did a number of tests to check cell signaling and cell cycle processes, and confirmed that they were all normal. Thus, nanospearing did not affect the normal cell function and might be used as an efficient delivery system of plasmid DNA, in cell sensors, or in therapeutic drug delivery (Cai et al., 2005, 2007).

Chen et al. (2007) have developed a nanoinjector that injects compounds immobilized on MWNT-atomic force microscopy (AFM) tips into the cells. First, a MWNT-AFM tip was fabricated from a normal AFM tip with an MWNT on one end. Next, a compound of interest was immobilized on the MWNT-AFM tip through a disulfide bond linkage. After MWNT-AFM tip was tapped on the cell, the cantilever was further lowered and the MWNT nanoneedle then penetrated the membrane. Once inside the cell, the disulfide linkage was broken under the cells reducing environment and the compound of interest was released inside the cell. The MWNT-AFM tip was then removed from the cell. In this study, protein was

injected into cells and the intracellular diffusion was good. This technique caused no observable membrane or cell damage. Unfortunately, this technique requires an AFM and only a single cell is injected, thus, its use as a nanoinjector to administer drugs to patients is probably quite far off. If this method can be scaled up in the future, it might be used to attack skin cancer cells or treat dermatological problems (Chen et al., 2007).

12.2.2 Tumor Targeting and Cancer Therapeutics

Since nanoparticles were first used in drug delivery systems in the 1950s, cancer therapy nanotechnology (i.e., treatment, diagnosis, monitoring, and control of biological systems) has been the major focus of this field (Cuenca et al., 2006; Das et al., 2006; Devalapally et al., 2007; Farokhzad and Langer, 2006; Ferrari, 2005; Kateb et al., 2007; Peng et al., 2007; Shao et al., 2007; Tong and Cheng, 2007; Yu et al., 2007).

Kam et al. (2005) showed that single-walled carbon nanotubes can effectively deliver short DNA oligonucleotides to the nucleus of cancer cells *in vitro*, while leaving the other cells untouched. Moreover, selective cancer cell destruction was demonstrated *in vitro* by heating the SWNTs extensively with infrared radiation once inside cells. During this process, no harm was done to the healthy noncancer cells in the sample (Kam et al., 2005). It is very important to understand how to target SWNTs to cancer cells with specific tumor markers, as this would allow the selective targeting of cancer cells without harming normal cells.

Cui et al. (2007) studied SWNTs with the aim of increasing the efficiency of antisense as therapy. SWNTs were used to transport antisense myc into human HL-60 cancer cells. Results showed that the antisense myc-conjugated SWNTs could enter the cells within 15 min and that the cells continued to take up SWNTs for 48 h. The concentration of SWNTs inside the cells then began to decrease after 48 h. The effects of the SWNT conjugates on the cells included inhibition of the proliferation of the HL-60 cells, induction of cell apoptosis, and downregulation of the c-myc gene and C-MYC protein. The results suggest a promising method for killing cancer cells (Cui et al., 2007).

Hilder and Hill (2007), using computational methods, explored the ability of a CNT to take up the anticancer drug cisplatin. They discovered that the minimum CNT radius required for the uptake of cisplatin is about 4.785 Å, which is a bit smaller than a (9,5) nanotube. They also found that in their simulation, the maximum suction energy occurs with a (11,4) nanotube having a radius of 5.3 Å. These computational methods suggest the feasibility of "loading" CNTs with specific drugs and transporting them to a specific target (Hilder and Hill, 2007).

Liu et al. (2007) discovered that polyethylene glycol (PEG)ylated SWNTs are stable *in vivo* and demonstrate long blood circulation times and low uptake by the reticuloendothelial system. This group linked PEGylated SWNTs to an arginine-glycine-aspartic acid peptide, which was able to effectively target tumors in mice.

Once the SWNTs were delivered to the tumor, they could be heated by laser irradiation to destroy the tumor. This group also noted that they did not observe any obvious toxicity in the mice when injected with SWNTs up to dosages of 2 mg/kg. However, they found that the rate of excretion of SWNTs was very low. Thus, long-term studies are needed to investigate toxicity issues (Liu et al., 2007).

Yu et al. (2007) observed oxidized MWNTs and gonadotropin-releasing hormone (GnRH) by themselves to be nontoxic to prostate cancer cells even in large doses. However, when the GnRHs were immobilized onto the surface of MWNTs, they showed the ability to enter prostate cancer cells and exhibit toxicity. In contrast, while MWNTs and GnRHs also entered cells, they showed no toxicity. Characterization of the MWNT–GnRH by elemental analysis revealed that only 0.7% of the MWNT surface area was modified with GnRH. These results show that a small modification of relatively nontoxic MWNTs can yield an anticancer nanomaterial (Yu et al., 2007).

Kateb et al. (2007) investigated the differences in internalization of MWNTs into microglia, phagocytic brain cells, and glioma, brain cancer cells. The group also investigated the ability of siRNA and DNA to be wrapped onto the MWNTs and transported into the cells for gene therapy. The results showed that the MWNTs were capable of delivering DNA and siRNA into both cell types, but deliver more material to the phagocytic cells than to the tumor cells. The MWNTs were also found to be relatively nontoxic. These MWNTs have potential to be used for either brain cancer therapy or they could be used for gene therapy of specific brain cell types to solve other brain-related diseases (Kateb et al., 2007).

Shao et al. (2007) made use of the IGF1R and HER2 surface receptors on breast cancer cells to develop a novel antibody–antigen method for selective destruction of breast cancer cells. Antibodies against IGF1R and HER2 cancer receptors were first immobilized onto SWNTs that selectively killed all the cancer cells. This technology demonstrates a beneficial new technology that could help many breast cancer patients (Shao et al., 2007).

Feazell et al. (2007) successfully produced an SWNT-based drug delivery system for delivering platinum(IV) anticancer drug to the interior of the cells. Substrate was first attached to SWNTs through disulfide linkages. Once these SWNTs are taken up by the cell through clathrin-dependent endocytosis, they enter the reducing environment of the endosomes causing the disulfide linkages to break by allowing them to selectively release their cargo inside the cell. This group monitored the intracellular location of the SWNTs by attaching a fluorescein-based fluorophore to them. Unfortunately, this approach does not discriminate which cells the drugs are delivered too. Thus, the toxic anticancer drugs are delivered to all cells, just like in standard chemotherapy and such results would certainly be very unpleasant for a patient (Feazell et al., 2007).

McDevitt et al. (2007) reported that multiple copies of tumor-specific monoclonal antibodies were covalently attached to the carbon nanotubes. These tumor-specific antibodies should allow the carbon nanotubes to specifically target tumor cells. This will undoubtedly be beneficial to a patient and will most likely cause reduced side effects. These specific tumor-targeting CNTs may also have reduced

toxicity because they are only going to their targeted cell locations and not distributed throughout the body (McDevitt et al., 2007).

12.3 Toxicity Studies of CNTs and *In Vivo* Challenges

Although CNTs have been widely investigated as drug delivery carriers over the past few years, the toxicology and potential environmental hazards of pristine (unmodified) CNTs or ones modified with organic, biological, or inorganic reagents have been less studied. CNT exposure can be deliberate, as in the case of a nanodiagnostic or nanotherapeutic, or accidental, as in the case of environmental pollution from the manufacture or disposal of CNTs. The issue of CNTs toxicity was first raised in 1998 (Service, 1998). Huczko and Lange (2001) used patches in human volunteers and tested rabbit eyes to assess dermal toxicity on CNTs. They also investigated intratracheal instillation in male guinea pigs in 2001 (Huczko et al., 2001). Pulmonary toxicity assessment of SWNTs in mice was done by Warheit et al. (2004) and Lam et al. (2004) in 2004 and more extensive toxicological and pharmacological studies were reported by Kostarelos group since 2005 (Bianco et al., 2005; Kostarelos et al., 2007; Lacerda et al., 2006; Singh et al., 2005, 2006).

The main risks for human health are believed to be associated with the inhalation of nanoparticles (Hoet et al., 2004; Nohynek et al., 2007). Nanoparticles, less than 100 nm, can be easily suspended in the air and behave just like gas molecules and can be accumulated wherever an airstream takes them. It can be initially deposited by inhalation in the nose and throat and might potentially cause cancers such as nasal cancers. After inhalation, it can also penetrate beyond the bronchus deep into the alveolar region of the lung. From the lung CNTs can enter the blood stream reaching various cells including bone marrow, liver, kidneys, spleen, and heart (Bell; Lam 2006; Maynard, 2006; Tsuji et al., 2006). CNTs within the lung can also be phagocytized by macrophages that can carry them up the muco-ciliary carpet to be coughed out or swallowed, thus, entering the gastrointestinal tract.

The contact of nanoparticles with human skin is another concern when considering the potential human health risks of CNTs (Nohynek et al., 2007). It can penetrate the skin, reach to bloodstream, and be taken by cells, tissues, and organs. For example, if gloves are not worn when handling CNTs, dermal toxicity can take place and very fine nanoparticles might also penetrate the skin through resulting in transdermal delivery.

While nanomaterials as nanomedicines and nanodiagnostics and other applications of nanotechnology to healthcare are promising, the toxicology of nanomaterials is not yet clearly understood (Farokhzad and Langer, 2006; Moghimi et al., 2005). The toxicity of any nanoparticles is related to particle size, surface area, surface reactivity, surface treatment or coatings, aggregation stage, and the method of manufacture. The toxicity of CNTs can be modified by CNT functionalization, coating, length, or aspect ratio, SWNTs versus MWNTs and agglomeration during CNT formulation, use, and disposal (Helland et al., 2007).

CNTs have been studied for cancer therapies despite the fact that these have been shown to accumulate to toxic levels within the organs of diverse animal models and different cell lines (Fiorito et al., 2006; Tong and Cheng, 2007). The molecular and cellular mechanisms for toxicity of carbon nanotubes have not been fully clarified. Furthermore, toxicity must be examined on the basis of multiple routes of administration (i.e., pulmonary, transdermal, ocular, oral, and intravenous) and on multiple species mammals, lower terrestrial animals, aquatic animals (both vertebrates and invertebrates), and plants (both terrestrial and aquatic). A basic set of tests for risk assessment of nanomaterials has been put forward (Nano risk framework).

Toxicology of CNTs can generally be defined as unexpected harmful effects of CNTs, which arise from four main factors: (1) impurities in pristine CNTs such as amorphous carbon and Co, Fe, Ni, Mo (metallic compounds), (2) the intrinsic toxicity of the surface, sometimes toxicity itself can be useful for cancer therapies, (3) the concentration of CNTs, and (4) the high surface area. One advantage of nanometer scale of CNTs is that many individual cylindrical CNTs can be prepared from a few milligrams of material. Furthermore, surface area issues depend on degree of bundling and aggregation of CNTs (Donaldson et al., 2004; Lacerda et al., 2006).

Overall, the safety of CNTs need to be clearly understood because there are three main concerns related to their pathogenicity: (1) these may have more toxicity than larger biomaterials, (2) these might behave like asbestos and other pathogenic fibers that have toxicity associated with their needle-like shape, and (3) these are basically graphitic and are generally believed to be biopersistent (Donaldson et al., 2006; Li et al., 2007a, b; Maynard et al., 2004).

Newly developed injectable CNTs will require both *in vitro* and *in vivo* testing to determine biocompatibility, blood compatibility, mechanical stability, and safety (Pearce et al., 2007). Here, we review the current articles on toxicity of CNTs and *in vivo* barriers.

12.3.1 Inhalation Exposure and Dermal Toxicity to Human Health

CNTs exist as airborne particulate aggregates in size small enough to be respirable. We are all exposed to CNTs due to their natural occurrences in significant levels in our environment (Lam et al., 2006; Murr et al., 2004). Because commercial interest in CNTs has led to the development of mass production and handling facilities, the risks of inhalation exposure need to be better clarified. CNTs can additionally penetrate the body through the skin and through oral intake (Donaldson et al., 2006). Moreover, occupational exposure may occur during the handling or manufacturing processes of incorporating CNTs into fabrics, plastic, rubbers, reinforced structures, composite materials, and household commodities (Lam et al., 2006; Maynard et al., 2004).

Maynard et al. (2004) have discussed concerns about inhalation exposure by SWNTs becoming airborne during the handling. With sufficient agitation unrefined SWNTs can result in the entry of fine particles into the air at concentrations of up to $53 \mu\text{g}/\text{m}^3$ (Maynard et al., 2004).

Li et al. (2007) studied pathological lesions induced by MWNTs in bronchi and alveoli of mice. His group tested toxicity of MWNTs by intratracheal instillation and inhalation. After inhalation of aerosolized MWNTs, they observed that (1) aggregates of MWNTs in the bronchi were adhered to the lining wall of bronchi, (2) larger-size aggregates of MWNTs were distributed in bronchi and smaller-size ones distributed in alveoli, and (3) no inflammatory cells were covered or accumulated around them. In addition, this group noticed that the pathological lesions in inhalation groups were very different with that in intratracheal instillation groups because of three main reasons: (1) aerosolized MWNTs delivered by inhalation were physiologic and active, (2) nonrespirable MWNTs particles could not bypass muco-ciliary system, and (3) aerosolized MWNTs were slowly and regularly inhaled into the airways and alveoli over a relatively long period (Li et al., 2007).

The inhalation exposure CNT toxicology study by Li et al. (2007a, b) was significant because dispersion of CNTs in air for inhalation studies is troublesome and CNTs have a tendency to aggregate together. Thus, before this work it was difficult to perform definitive inhalation studies.

Commercial interest in CNTs has led to the development of mass production and handling facilities. Risks of exposure by various routes need to be clarified because CNTs may penetrate the body through the skin as well as the lung and gut (Donaldson et al., 2006). Even if our understanding of local, chronic, and metabolic toxicity through the skin penetration is not clear, there is a broad consensus that CNTs can enter through the skin and distribute throughout the body (Nohynek et al., 2007; Tsuji et al., 2006).

12.3.2 Studies on Angiogenesis and Toxicity in Chick Eggs

The first report of the anti-angiogenesis activity associated with carbon materials such as MWNTs, fullerenes, and graphite was investigated by our laboratory (Murugesan et al., 2007). We studied the anti-angiogenic effects of a variety of carbon-based materials including graphite, MWNTs, and fullerenes in a model where vascular endothelial growth factor (VEGF) and basic fibroblast growth factor (FGF2) were used to induce angiogenesis in a chick chorioallantoic membrane (CAM) model (Fig. 12.5) (Murugesan et al., 2007). No toxicity of any of the carbon-based materials was observed in the fertilized chick eggs and on this basis we conclude that carbon materials inhibited FGF2- and VEGF-induced angiogenesis, and they had little effect on basal angiogenesis in the absence of these growth factors. This assay is very interesting because MWNTs can also be loaded with anticancer agents through either by chemical or by physical attachment methods. Therefore, the intrinsic anti-angiogenic activity of MWNTs through the interference with growth

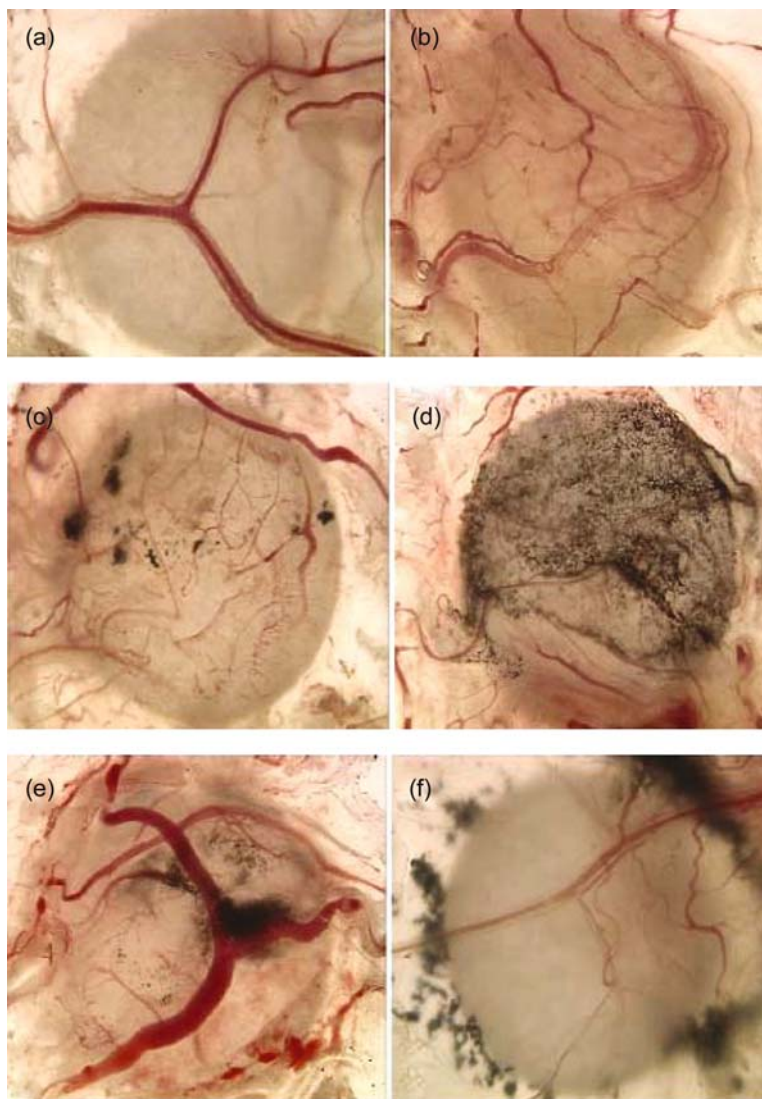


Fig. 12.5 Representative microscopic images of (a) PBS control, (b) FGF2, (c) FGF2 – multi-walled carbon nanotubes (MWNTs) (100 μ g), (d) FGF2 – graphite (100 μ g), (e) FGF2 – fullerene (100 μ g), and (f) FGF2 – MWNTs (1 mg) treated CAM models (*See Color Plates*)

factors might afford a synergistic cancer-treating strategy. Most interesting is also the possibility of using chick eggs for the *in vivo* evaluation of nanoparticle toxicity. This unique system offers an *in vivo* evaluation without the complicating effects of excretion. Moreover, since this is a developmental model, it offers insight in the impact of nanomaterials on development and teratogenicity.

12.3.3 *Translocation – Biodistribution in Mice*

There are a number of articles on the distribution of water-soluble functionalized and radiolabeled CNTs in mice, but these studies have provided conflicting results (Helland et al., 2007). Wang et al. (2004) showed that hydroxylated SWNTs with radioactive iodine-125 atoms passed easily through many compartments were accumulated in liver, kidney, spleen, and except the brain throughout the whole mouse body following the accumulation particularly in bone. Singh et al. (2006) investigated the tissue biodistribution and blood clearance rates of SWNTs and have showed that chelated diethylenetriaminepentaacetic and indium-111-labeled, water-soluble SWNTs or MWNTs, were excreted mainly *via* a renal route with no uptake in the liver and spleen in mice after 24h. The results of Deng et al. (2007) differ from those of Wang et al. (2004) and Singh et al. (2006). Deng and coworkers used taurine-functionalized MWNTs as a carrier and showed high accumulation of MWNTs in the liver with low uptake. Guo et al. (2007) labeled water-soluble MWNTs with ^{99m}Tc and reported that these MWNTs were excreted predominantly in the urine and feces, which is similar to the results of Wang et al. (2004). In this study, however, there was no sign of renal or other severe acute toxicity responses.

These four studies on functionalized CNTs may differ from each other because their functionalized groups may have a strong influence on the behavior of CNTs in mice. Despite these differences, the pharmacokinetic profiles provided are valuable in the development of diagnostic and therapeutic applications for CNTs (Deng et al., 2007; Helland et al., 2007).

12.3.4 *The Effect of Aggregation, Functionalization, and Purity of CNTs*

The effect of CNT aggregation has been shown to play an important role in *in vitro* studies. Unfortunately, it is difficult to define the proportion of large CNT aggregates, finely dispersed CNTs, and impurities (amorphous, graphitic carbon particles, etc.) in a solution of CNTs (Raja et al., 2007). The concentration of CNTs in solution needs to be carefully considered and varied to obtain reliable information on cell viability, cell growth, and cellular uptake. The effect of CNT aggregates and associated non-aggregated CNTs have been related to parameters such as aggregate/particle dimensions, dosage, and duration of exposure (Raja et al., 2007). Cell growth was enhanced when the aggregates were removed from CNT solutions having concentrations below 0.1 mg/ml. In contrast, at concentrations above 0.1 mg/ml removing the aggregates by filtration had no beneficial effect on cell growth.

Many challenging problems remain for the biological application of CNTs. These include addressing solubility issues, difficulties in separating and testing individual CNTs, and the organic functionalization of CNTs, through strong acid oxidation to introduce hydroxyl and carboxyl groups required for covalent attachment of organic

compounds (Bianco and Prato, 2003; Bottini et al., 2006; Liu et al., 1998). The toxicity comparison between pristine CNTs and oxidized CNTs has been studied by Bottini et al., who reported that oxidized MWNTs were more toxic than pristine CNTs. The effect on the degree of functionalization of SWNTs has been investigated as well (Sayes et al., 2006). The result of this study demonstrates that the degree of sidewall functionalization is inversely related to the SWNT cytotoxicity. SWNTs in aqueous suspension were also shown by optical and atomic force microscopy to precipitate onto cellular membranes possibly increasing cytotoxicity.

The toxicity of carbon nanomaterials is complicated by many factors that can alter the behavior of nanoparticles. These include, but are not limited to the surface coating, exposure to UV radiation, aggregation, and proper dispersion. Studies conducted on the toxicity of nanomaterials also need to report the purity of these materials, as it seems to play a key role in toxicity. Fiorito et al. (2006) examined highly purified SWNTs and carbon-fullerenes (concentration 30 and 60 $\mu\text{g}/\text{ml}$) that contained no catalytic metals. These SWNTs, fullerenes, and graphite particles showed no inflammatory response when contacted with mammalian cells. The low nitric oxide release levels and low amounts of reactive oxygen species (ROS) were comparable to those observed for control graphite. Pure SWNTs and pure carbon-fullerenes result in less phagocytic activity by human and murine macrophages than pure graphite. Cell toxicity was also much lower with SWNTs and carbon-fullerenes than with graphite (4% for SWNTs, 2% for fullerenes, and 25% for graphite after 48 h, respectively). Previous findings suggesting SWNTs cause toxicity and increased ROS may be attributable to contaminants such as graphite particles and/or catalytic metals present in impure SWNTs (Fiorito et al., 2006).

12.3.5 In Vitro Studies

Unnecessary animal testing can be avoided by relying on *in vitro* studies as the first stage acute toxicity and cytocompatibility test for injectable materials (Pearce et al., 2007). Many researchers have utilized *in vitro* studies to screen the cellular response to CNTs (Raja et al., 2007) and to investigate the various CNT–mammalian cell interactions such as oxidative stress (Manna et al., 2005; Shvedova et al., 2003, 2007), antiproliferative effects (Cui et al., 2005; Garibaldi et al., 2006), decreased cell adhesion (Cui et al., 2005), apoptosis (Bottini et al., 2006; Cui et al., 2005; Jia et al., 2005), and necrosis (Jia et al., 2005). A summary of these *in vitro* studies are presented in Table 12.1.

12.3.6 In Vivo Studies and Their Challenging Issues

CNTs as therapeutic or diagnostic agents need to penetrate *in vivo* barriers including the tissue endothelium, cell membranes, perinuclear membranes, and nuclear

Table 12.1 *In vitro* toxicity studies (2005–present)

Type of CNTs (suspended amount)	Cell line	Exposure duration	Toxicity	Reference
SWNTs, MWNTs, acid-treated SWNTs with reduced metal catalyst content (5–100µg/ml)	NR 8383, and human A549 lung cells	24h	Metal impurities associated with commercial nanotubes are responsible for the toxic biological effects of CNTs CNTs possess no acute toxicity in pulmonary epithelial and macrophage cells	Pulskamp et al. (2007)
SWNTs (7.5, 15, 30µg/ml)	Human MSTO-211H cells	3 days	Micron-size SWNT-agglomerates were more cytotoxic than well-dispersed SWNT-bundles	Wick et al. (2007)
SWNTs (1.56–800µg/ml)	Human A 549 cells	1 day	SWNTs have low acute toxicity against A549 cells	Davoren et al. (2007)
Pristine MWNTs, oxidized MWNTs (40 and 400µg/ml)	Human T lymphocyte cells	5 days	The oxidized MWNTs were found to be more toxic At high concentrations of 400µg/ml, both pristine and oxidized CNTs were shown to induce apoptosis in human T-cells	Bottini et al. (2006)
Iron-rich (non-purified) SWNTs and (2) iron-stripped (purified) SWNTs (0.12–0.5 mg/ml)	RAW 264.7 macrophages	2h	The presence of iron in SWNT might play an important role in determining redox-dependent responses of macrophages.	Kagan et al. (2006)
SWNT-phenyl-SO ₃ H, SWNT-phenyl-(COOH) ₂ , SWNT-phenyl-SO ₃ Na, underivatized SWNT stabilized in 1% Pluronic F108 (3µg/ml–30mg/ml)	Human dermal fibroblasts (HDF)	48h	The SWNT samples become less cytotoxic as the degree of sidewall functionalization increases The sidewall functionalized SWNT samples are substantially less cytotoxic than surfactant stabilized SWNTs	Sayes et al. (2006)

(continued)

Table 12.1 (continued)

Type of CNTs (suspended amount)	Cell line	Exposure duration	Toxicity	Reference
SWNTs (1.5625–200 µg/ml)	Human embryo kidney (HEK) 293 cells	5 days	The SWNTs showed significant toxicity against the HEK293 cells by inhibiting their proliferation (antiproliferative effects), inducing apoptosis, and decreasing their adhesion abilities	Cui et al. (2005)
MWNTs (0.1, 0.2, and 0.4 mg/ml)	Human epidermal keratinocytes (HEK) cells	1, 2, 4, 8, 12, 24 and 48 h.	MWNTs can induce an irritation response and can enter cells by localizing themselves within cytoplasmic vacuoles	Monteiro-Riviere et al. (2005)
SWNTs (0–100 µg/ml)	HeLa, H1299, and A 549 cells	3.5 days	SWNTs inhibit cell proliferation and show an adverse effect on keratinocytes	Manna et al. (2005)
SWNTs (1.41–226.00 µg/cm ²)	Adult guinea pig alveolar macrophages	6h	The relative cytotoxicity as follows: SWNTs > MWNTs > C ₆₀ , which implies that the size of the materials is related to their cytotoxicity	Jia et al. (2005)
MWNTs (1.41–22.60 µg/cm ²)				

membranes to reach their target and to be eliminated after administration (Lacerda et al., 2006). Various drug delivery systems have been designed to efficiently deliver drugs, antigens, and genes through *in vivo* barriers. Desired pharmacological activity of nanomaterials is often accompanied by deleterious side effects, which results in limiting the pharmaceutical applications of CNTs. Thus, toxicological issues of CNTs must be carefully assessed and addressed.

Although CNTs can be excreted and could be cleared from the body, the bioapplications of CNTs is somewhat limited because they are not biodegradable (Harrison and Atala, 2007). The wide size distribution of CNTs as well as the difficulty in controlling distribution between bundled CNT aggregates and individual tubes can significantly affect biodistribution, targetability, and drug release from

CNTs (Badaire et al., 2005; Bandyopadhyaya et al., 2002; Fan et al., 2007; Lacerda et al., 2006; Maeda et al., 2006; O'Connell et al., 2001, 2002; Regev et al., 2004; Richard et al., 2003; Wu et al., 2006; Yurekli et al., 2004; Zheng et al., 2003a, b). Structurally and chemically identical CNTs are difficult to produce in large amounts and impurities are often present, which can cause problems for their pharmaceutical and clinical applications.

Pristine CNTs are hydrophobic and cause a lack of solubility in biological aqueous fluids such as blood. The poor solubility of CNTs in blood stream poses a major challenge to *in vivo* studies making behavior of CNTs difficult to predict and control (Kam et al., 2005; Zheng et al., 2003a, b). Therefore, modification of CNT surface to introduce hydrophilic, functional groups has been utilized in pharmaceutical applications (Lacerda et al., 2006). However, insufficient *in vivo* evaluation of both pristine and surface-modified CNTs has been performed to answer essential questions on CNT toxicology. Additional *in vivo* studies also required to devise the best method of administration, means of uptake, metabolism, and elimination of CNTs. The *in vivo* studies on CNTs performed to date are presented in Table 12.2.

12.4 Discussion and Conclusion

CNTs are of importance as useful bio-nanomaterials for pharmaceutical applications and biomedical engineering. However, despite the contribution of CNTs to bio-nanomaterials for pharmaceutical applications, the potential risks of CNTs about the exposure to human health have not been adequately assessed. Toxicology issues associated with CNT inhalation, dermal toxicity, pulmonary, biodistribution, biocompatibility, blood compatibility, and elimination need to be addressed prior to their pharmacological application in humans.

The effects of size surface area, shape, purity method of synthesis, charge, surface coating, functionalized groups, and aggregation need to be carefully considered when assessing potential risks of CNT toxicity. Toxicology studies on CNTs should be accompanied by improved control in manufacturing and improved analysis before CNTs can be successfully used for pharmaceutical applications.

For decades, researchers have anticipated how individual nano-sized molecules could be manipulated to achieve diagnostic and therapeutic aims. Nanotechnology to assemble nanodevices, and nanobots from CNT building blocks may be possible one day. Tumor-targeting system using CNTs in cancer therapies faces formidable challenges including the delivery efficacy, enhanced targeting selectivity, and the avoidance of biophysical barriers. Those advances in bio-nanotechnology will require enormous efforts in the field of pharmaceutical engineering, but one day may allow us to successfully target cancer.

For CNTs to fulfill their promise as drug carriers in therapeutic applications, and in nanomedicine, a number of questions need to be successfully addressed: (1) How stable and persistent will CNTs be after administration? (2) Can CNTs be made sufficiently soluble in water? (3) Are CNTs sufficiently biocompatible or blood

Table 12.2 *In vivo* studies (2004–present)

Type of CNTs (injected amount)	Animal species	Method of administration	Exposure duration	Toxicity	Year/Reference
MWNTs (0.05 mg/mouse)	Female Kunming mice	Intratracheal instillation	8 days, 16 days, and 24 days	The aggregates led to inflammation in the lining walls of the bronchi and severe destruction to the alveoli	Li et al. (2007)
Aerosolized MWNTs (32.61 mg/m ³)	Female Kunming mice	Inhalation	8 days, 16 days, and 24 days	Most of the aggregations of MWNTs in the alveoli were smaller than those in the bronchi. The aggregations induced proliferation and thickening of alveolar walls	Li et al. (2007)
SWNTs (10 or 40 µg/mouse)	Male C57BL/6 mice	Single intratracheal instillation	7 days, 28 days, and 60 days	mtDNA damage was accompanied by changes in aortic mitochondrial glutathione and protein carbonyl levels	Li et al. (2007)
DTPA-SWNTs or DTPA-MWNTs labelled with ¹¹¹ In (0.06 or 0.4 mg/mouse)	Female BALB/c mice	Intravenous administration	30 min, 3 h, and 24 h	No toxic side effects, accumulation, or mortalities were observed. CNTs were removed from systemic blood circulation through the renal excretion route	Singh et al. (2006)
Ground or unground MWNTs (0.2 or 5 mg/rat)	Female Sprague–Dawley rats	Intratracheal instillation	2 months, 3 days, 15 days, 60 days	Both ground MWNTs and unground MWNTs induced inflammation and fibrotic reactions and increased TNF-α production	Muller et al. (2005)
MWNTs (0.1 mg of clusters of CNTs/rat)	Male Wistar strain rats	Administration in the subcutaneous tissue in the thoracic region bilaterally in each rat	1 and 4 weeks	Inflammation around 825-CNTs was stronger than that around 220-CNTs	Sato et al. (2005)
SWNT soot (1 or 5 mg/kg)	Male Crl:CD (SD)IGS BR Rats	Intratracheal instillation	24 h, 1 week, 1 month, and 3 months	No severe inflammatory responses such as necrosis, degeneration, or neutrophil infiltration were observed	Warheit et al. (2004)
Raw SWNTs or purified HiPco SWNTs or Arc-SWNTs (0.1 or 0.5 mg/mouse)	Male mice B6C3F ₁	Intratracheal instillation	7 and 90 days	A non-dose-dependent series of multifocal granulomas Induced dose-dependent epithelioid granulomas	Lam et al. (2004)

compatible? (4) How can CNTs be made to penetrate through cells to reach tumor targets? (5) How will CNTs be eliminated after they perform their function even though they are not biodegradable? So far the answers to these questions coming from many different laboratories are not clear. Additional research is required to develop the best methods for CNT administration, promoted uptake, enhanced metabolism, and controlled clearance.

The pharmacological applications of CNTs are highly challenging because of the toxicology issues discussed in this chapter. We conclude that the pharmacological application of CNTs appropriately modified to display improved biocompatibility should provide extraordinary opportunities to accelerate and assist the development of modern drug delivery systems particularly for tumor targeting and cancer therapy only if toxicological issues are adequately addressed.

References

- Ajayan PM (1999) Nanotubes from carbon. *Chem Rev* 99:1787–1799.
- Alyautdin R, Gothier D, Petrov V, Kharkevich D, Kreuter J (1995) Analgesic activity of the hexapeptide dalargin adsorbed on the surface of polysorbate 80-coated poly(butyl cyanoacrylate) nanoparticles. *Eur J. Pharm Biopharm* 41:44–48.
- Alyautdin RN, Petrov VE, Langer K, Berthold A, Kharkevich DA, Kreuter J (1997) Delivery of loperamide across the blood-brain barrier with polysorbate 80-coated polybutylcyanoacrylate nanoparticles. *Pharm Res* 14:325–328.
- Alyautdin RN, Tezikov EB, Ramge P, Kharkevich DA, Begley DJ, Kreuter J (1998) Significant entry of tubocurarine into the brain of rats by adsorption to polysorbate 80-coated polybutylcyanoacrylate nanoparticles: an in situ brain perfusion study. *J Microencapsul* 15:67–74.
- Arthursson P, Edman P, Laakso T, Sjöholm I (1984) Characterization of polyacryl starch microparticles suitable as carrier for proteins and drugs. *J Pharm Sci* 73:1507–1513.
- Arthursson P, Edman P, Sjöholm I (1985) Biodegradable microspheres II: immune response to a heterologous and an autologous protein entrapped in polyacryl starch microparticles. *J Pharmacol Exp Ther* 255–260.
- Atala A, Bauer SB, Soker S, Yoo JJ, Retik AB (2006) Tissue-engineered autologous bladders for patients needing cystoplasty. *LANCET* 367:1241–1246.
- Badaire S, Zakri C, Maugey M, Derre A, Barisci JN, Wallace G, Poulin P (2005) Liquid crystals of DNA-stabilized carbon nanotubes. *Adv Mater* 17:1673–1676.
- Bandaru PR (2007) Electrical properties and applications of carbon nanotube structures. *J Nanosci Nanotechnol* 7:1239–1267.
- Bandyopadhyaya R, Nativ-Roth E, Regev O, Yerushalmi-Rozen R (2002) Stabilization of individual carbon nanotubes in aqueous solutions. *Nano Lett* 2:25–28.
- Bazile D, Prud'homme C, Bassoulet MT, Marlard M, Spenlehauer G, Veillard M (1995) Stealth Me.PEG-PLA nanoparticles avoid uptake by the mononuclear phagocytes system. *J Pharm Sci* 84:493–498.
- Becker C, Jakse G (2007) Stem cells for regeneration of urological structures. *Eur Urol* 51:1217–1228.
- Bekyarova E, Ni Y, Malarkey EB, Montana V, McWilliams JL, Haddon RC, Parpura V (2005) Applications of carbon nanotubes in biotechnology and biomedicine. *J Biomed Nanotechnol* 1:3–17.
- Bell TE (2006) Understanding Risk Assessment of Nanotechnology. Available at http://nano.gov/Understanding_Risk_Assessment.pdf

- Bertling WM, Gareis M, Paspaleeva V, Zimmer A, Kreuter J, Nürnberg E, Harrer P (1991) Use of liposomes, viral capsids, and nanoparticles as DNA carriers. *Biotechnol Appl Biochem* 13:390–405.
- Bianco A, Prato M (2003) Can carbon nanotubes be considered useful tools for biological applications? *Adv Mater* 15:1765–1768.
- Bianco A, Kostarelos K, Partidos CD, Prato M (2005) Biomedical applications of functionalised carbon nanotubes. *Chem Commun* 2005:571–577.
- Birrenbach G, Speiser PP (1976) Polymerized micelles and their use as adjuvants in immunology. *J Pharm Sci* 65:1763–1766.
- Bottini M, Bruckner S, Nika K, Bottini N, Bellucci S, Magrini A, Bergamaschi A, Mustelin T (2006) Multi-walled carbon nanotubes induce T lymphocyte apoptosis. *Toxicol Lett* 160:121–126.
- Bottini M, Magrini A, Dawson MI, Rosato N, Bergamaschi A, Mustelin T (2007) Noncovalently silylated carbon nanotubes decorated with quantum dots. *Carbon* 45:673–676.
- Branemark PI, Breine U, Johansson B, Roylance PJ, Röckert H, Yoffey JM (1964) Regeneration of bone marrow. *Acta Anat* 59:1–46.
- Brigger I, Morizet J, Aubert G, Chacun H, Terrier-Lacombe MJ, Couvreur P, Vassal G (2002) Poly(ethylene glycol)-coated hexadecylcyanoacrylate nanospheres display a combined effect for brain tumor targeting. *J Pharmacol Exp Ther* 303:928–936.
- Cai D, Mataraza JM, Qin ZH, Huang ZP, Huang JY, Chiles TC, Carnahan D, Kempa K, Ren ZF (2005) Highly efficient molecular delivery into mammalian cells using carbon nanotube spearing. *Nat Methods* 2:449–454.
- Cai D, Doughty CA, Potocky TB, Dufort FJ, Huang Z, Blair D, Kempa K, Ren ZF, Chiles TC (2007) Carbon nanotube-mediated delivery of nucleic acids does not result in non-specific activation of B lymphocytes. *Nanotechnology* 18: Art. No. 365101.
- Capila I, Linhardt RJ (2002) Heparin – Protein interactions. *Angew Chem Int Ed* 41:391–412.
- Chai C, Leong KW (2007) Biomaterials approach to expand and direct differentiation of stem cells. *Mol Ther* 15:467–480.
- Champion JA, Katare YK, Mitragotri S (2007) Making polymeric micro- and nanoparticles of complex shapes. *Proc Natl Acad Sci USA* 104:11901–11904.
- Che GL, Lakshmi BB, Fisher ER, Martin CR (1998) Carbon nanotubule membranes for electrochemical energy storage and production. *Nature* 393:346–349.
- Chen CC, Liu YC, Wu CH, Yeh CC, Su MT, Wu YC (2005) Preparation of fluorescent silica nanotubes and their application in gene delivery. *Adv Mater* 17:404–407.
- Chen X, Kis A, Zettl A, Bertozzi CR (2007) A cell nanoinjector based on carbon nanotubes. *Proc Natl Acad Sci USA* 104:8218–8222.
- Couvreur P, Kante B, Roland M, Guiot P, Bauduin P, Speiser P (1979) Polycyanoacrylate nanocapsules as potential lysosomotropic carriers: preparation, morphological and sorptive properties. *J Pharm Pharmacol* 31:331–332.
- Cuenca AG, Jiang HB, Hochwald SN, Delano M, Cance WG, Grobmyer SR (2006) Emerging implications of nanotechnology on cancer diagnostics and therapeutics. *Cancer* 107:459–466.
- Cui DX, Tian FR, Ozkan CS, Wang M, Gao HJ (2005) Effect of single wall carbon nanotubes on human HEK293 cells. *Toxicol Lett* 155:73–85.
- Cui DX, Tian FR, Coyer SR, Wang JC, Pan BF, Gao F, He R, Zhang YF (2007) Effects of anti-sense-myc-conjugated single-walled carbon nanotubes on HL-60 cells. *J Nanosci Nanotechnol* 7:1639–1646.
- Das M, Mardiyani S, Chan WCW, Kumacheva E (2006) Biofunctionalized pH-responsive microgels for cancer cell targeting: rational design. *Adv Mater* 18:80–83.
- Davoren M, Herzog E, Casey A, Cottineau B, Chambers G, Byrne HJ, Lyng FM (2007) In vitro toxicity evaluation of single walled carbon nanotubes on human A549 lung cells. *Toxicol In Vitro* 21:438–448.
- Deng X, Jia G, Wang H, Sun H, Wang X, Yang S, Wang T, Liu Y (2007) Translocation and fate of multi-walled carbon nanotubes in vivo. *Carbon* 45:1419–1424.
- Devalapally H, Shenoy D, Little S, Langer R, Amiji M (2007) Poly(ethylene oxide)-modified poly(beta-amino ester) nanoparticles as a pH-sensitive system for tumor-targeted delivery of

- hydrophobic drugs: part 3. Therapeutic efficacy and safety studies in ovarian cancer xenograft model. *Cancer Chemother Pharmacol* 59:477–484.
- Donaldson K, Stone V, Tran CL, Kreyling W, Borm PJA (2004) Nanotoxicology. *Occup Environ Med* 61:727–728.
- Donaldson K, Aitken R, Tran L, Stone V, Duffin R, Forrest G, Alexander A (2006) Carbon nanotubes: a review of their properties in relation to pulmonary toxicology and workplace safety. *Toxicol Sci* 92:5–22.
- Dumortier H, Lacotte S, Pastorin G, Marega R, Wu W, Bonifazi D, Briand JP, Prato M, Muller S, Bianco A (2006) Functionalized carbon nanotubes are non-cytotoxic and preserve the functionality of primary immune cells. *Nano Lett* 6:1522–1528.
- Eberli D, Atala A (2006) Tissue engineering using adult stem cells. *Method Enzymol* 420:287–302.
- Edman P, Ekman B, Sjöholm I (1980) Immobilization of proteins in microspheres of biodegradable polyacryldextran. *J Pharm Sci* 69:838–842.
- Endo M, Kim YA, Hayashi T, Nishimura K, Matusita T, Miyashita K, Dresselhaus MS (2001) Vapor-grown carbon fibers (VGCFs) – Basic properties and their battery applications. *Carbon* 39:1287–1297.
- Eriksson E and Branemark PI (1996) Osseointegrated from the Perspective of the Plastic Surgeon. *Plast Reconstr Surg* 93:626–637.
- Fan XB, Tan J, Zhang GL, Zhang FB (2007) Isolation of carbon nanohorn assemblies and their potential for intracellular delivery. *Nanotechnology* 18: Art. No. 195103.
- Farokhzad OC, Langer R (2006) Nanomedicine: developing smarter therapeutic and diagnostic modalities. *Adv Drug Deliver Rev* 58:1456–1459.
- Feazell RP, Nakayama-Ratchford N, Dai H, Lippard SJ (2007) Soluble single-walled carbon nanotubes as longboat delivery systems for Platinum(IV) anticancer drug design. *J Am Chem Soc* 129:8438–8439.
- Ferrari M (2005) Cancer nanotechnology: opportunities and challenges. *Nat Rev Cancer* 5:161–171.
- Fiorito S, Serafino A, Andreola F, Bernier P (2006) Effects of fullerenes and single-wall carbon nanotubes on murine and human macrophages. *Carbon* 44:1100–1105.
- Folkman J, Langer R, Linhardt RJ, Haudenschild C, Taylor S (1983) Angiogenesis inhibition and tumor regression caused by heparin or a heparin fragment in the presence of cortisone. *Science* 221:719–725.
- Frackowiak E (2007) Carbon materials for supercapacitor application. *Phys Chem Chem Phys* 9:1774–1785.
- Frackowiak E, Gautier S, Gaucher H, Bonnamy S, Beguin F (1999) Electrochemical storage of lithium multiwalled carbon nanotubes. *Carbon* 37:61–69.
- Frackowiak E, Metenier K, Bertagna V, Beguin F (2000) Supercapacitor electrodes from multiwalled carbon nanotubes. *Appl Phys Lett* 77:2421–2423.
- Frimberger D, Lin HK, Kropp BP (2006) The use of tissue engineering and stem cells in bladder regeneration. *Regen Med* 1:425–435.
- Gardner RL (2007) Stem cells and regenerative medicine: principles, prospects and problems. *C R Biol* 330:465–473.
- Garibaldi S, Brunelli C, Bavastrello V, Ghigliotti G, Nicolini C (2006) Carbon nanotube biocompatibility with cardiac muscle cells. *Nanotechnology* 17:391–397.
- Geng Y, Dalhaimer P, Cai SS, Tsai R, Tewari M, Minko T, Discher DE (2007) Shape effects of filaments versus spherical particles in flow and drug delivery. *Nat Nanotechnol* 2:249–255.
- Gerecht S, Burdick JA, Ferreira LS, Townsend SA, Langer R, Vunjak-Novakovic G (2007) Hyaluronic acid hydrogen for controlled self-renewal and differentiation of human embryonic stem cells. *Proc Natl Acad Sci USA* 104:11298–11303.
- Glück T (1890) Die Invaginationsmethode der Osteo- und Arthroplastik. *Berl Klin Wochenschr Circulation* 33:752–757.
- Glück T (1891) Referat über die Durch das Moderne Chirurgische Experiment Gewonnenen Positiven Resultaten, Betreffende die Naht und den Ersatz von Defekten Höherer Gewebe, Sowie über

- die Verwerthung Resorbirbarer und Lebendiger Tampons in der Chirurgie. *Arch Klin Chir* 41:186.
- Goldberg M, Langer R, Jia XQ (2007) Nanostructured materials for applications in drug delivery and tissue engineering. *J Biomat Sci-Polym E* 18:241–268.
- Goldman L, Coussens C (2005) Implications of Nanotechnology for Environmental Health Research, Roundtable on Environmental Health Sciences, Research and Medicine, The National Academies Press.
- Gref R, Minamitake Y, Peracchia MT, Trubetskoy V, Torchilin V, Langer R (1994) Biodegradable long-circulating polymeric nanospheres. *Science* 263:1600–1603.
- Gulyaev AE, Gelperina SE, Skidan IN, Antropov AS, Kivman GY, Kreuter J (1999) Significant transport of doxorubicin into the brain with polysorbate 80-coated nanoparticles. *Pharm Res* 16:1564–1569.
- Guo J, Zhang X, Li Q, Li W (2007) Biodistribution of functionalized multiwall carbon nanotubes in mice. *Nucl Med Biol* 34:579–583.
- Gurny R (1981) Preliminary study of prolonged acting drug delivery system for the treatment of glaucoma. *Pharm Acta Helv* 56:130–132.
- Gurny R, Peppas NA, Harrington DD, Banker GS (1981) Development of biodegradable and injectable lattices for controlled release of potent drugs. *Drug Devind Pharm* 7:1–25.
- Harrison BS, Atala A (2007) Carbon nanotube applications for tissue engineering. *Biomaterials* 28:344–353.
- Helland A, Wick P, Koehler A, Schmid K, Som C (2007) Reviewing the environmental and human health knowledge base of carbon nanotubes. *Environ Health Perspect* 115:1125–1131.
- Henrymichelland S, Alonso MJ, Andremont A, Maincen P, Sauzieres J, Couvreur P (1987) Attachment of antibiotics to nanoparticles-preparation, drug-release and antimicrobial activity in vitro. *Int J Pharm* 35:121–127.
- Hilder TA, Hill JM (2007) Modelling the encapsulation of the anticancer drug cisplatin into carbon nanotubes. *Nanotechnology* 18: Art. No. 275704.
- Hillmyer MA (2007) Materials science – Micelles made to order. *Science* 317:604–605.
- Hoet PH, Brüske-Hohlfeld I, Salata OV (2004) Nanoparticles – known and unknown health risks. *J Nanobiotechnol* 2:1–15.
- Huczko A, Lange H (2001) Carbon nanotubes: experimental evidence for a null risk of skin irritation and allergy. *Fullerene Sci Technol* 9:247–250.
- Huczko A, Lange H, Calko E, Grubek-Jaworska H, Droszcz P (2001) Physiological testing of carbon nanotubes: are they asbestos-like? *Fullerene Sci Technol* 9:251–254.
- Iijima S (1991) Helical microtubules of graphitic carbon. *Nature* 354:56–58.
- Jan E, Kotov NA (2007) Successful differentiation of mouse neural stem cells on layer-by-layer assembled single-walled carbon nanotube composite. *Nano Lett* 7:1123–1128.
- Jia G, Wang HF, Yan L, Wang X, Pei RJ, Yan T, Zhao YL, Guo XB (2005) Cytotoxicity of carbon nanomaterials: single-wall nanotube, multi-wall nanotube, and fullerene. *Environ Sci Technol* 39:1378–1383.
- Kagan VE, Tyurina YY, Tyurin VA, Konduru NV, Potapovich AI, Osipov AN, Kisin ER, Schwegler-Berry D, Mercer R, Castranova V, Shvedova AA (2006) Direct and indirect effects of single walled carbon nanotubes on RAW 264.7 macrophages: role of iron. *Toxicol Lett* 165:88–100.
- Kam NWS, Dai HJ (2005) Carbon nanotubes as intracellular protein transporters: generality and biological functionality. *J Am Chem Soc* 127:6021–6026.
- Kam NWS, Jessop TC, Wender PA, Dai HJ (2004) Nanotube molecular transporters: internalization of carbon nanotube-protein conjugates into mammalian cells. *J Am Chem Soc* 126:6850–6851.
- Kam NWS, O'Connell M, Wisdom JA, Dai HJ (2005) Carbon nanotubes as multifunctional biological transporters and near-infrared agents for selective cancer cell destruction. *Proc Natl Acad Sci USA* 102:11600–11605.
- Kam NWS, Liu ZA, Dai HJ (2006) Carbon nanotubes as intracellular transporters for proteins and DNA: an investigation of the uptake mechanism and pathway. *Angew Chem Int Ed* 45:577–581.

- Karp JM, Yeh J, Eng G, Fukuda J, Blumling J, Suh KY, Cheng J, Mahdavi A, Borenstein J, Langer R, Khademhosseini A (2007) Controlling size, shape and homogeneity of embryoid bodies using poly(ethylene glycol) microwells. *Lab Chip* 7:786–794.
- Kateb B, Van Handel M, Zhang L, Bronikowski MJ, Manohara H, Badie B (2007) Internalization of MWCNTs by microglia: possible application in immunotherapy of brain tumors. *Neuroimage* 37:S9–S17.
- Ke PC, Qiao R (2007) Carbon nanomaterials in biological systems. *J Phys-Condens Mat* 19: Art. No. 373101 SEP 19 2007.
- Kong H, Luo P, Gao C, Yan D (2005) Polyelectrolyte-functionalized multiwalled carbon nanotubes: preparation, characterization and layer-by-layer self-assembly. *Polymer* 46:2472–2485.
- Kopf H, Joshi, RK, Soliva, M, Speiser, P (1976) Studium der Mizellpolymerisation in Gegenwart niedermolekularer Arzneistoffe. 1. Herstellung und Isolierung der Nanpartikel, Restmonomerenbestimmung, physikalisch-chemische. *Daten Pharm Ind* 38:281–284.
- Kopf H, Joshi, RK, Soliva, M, Speiser, P (1977) Studium der Mizellpolymerisation in Gegenwart niedermolekularer Arzneistoffe. 2. Bindungsart von inkorporierten niedermolekularen Modellarzneistoffen an Nanopartikel auf Polyacrylamid-Basis. Restmonomerenbestimmung, physikalisch-chemische. *Daten Pharm Ind* 39:993–997.
- Kostarelos K (2003) Rational design and engineering of delivery systems for therapeutics: biomedical exercises in colloid and surface science. *Adv Colloid Interface* 106:147–168.
- Kostarelos K, Lacerda L, Pastorin G, Wu W, Wieckowski S, Luangsivilay J, Godefroy S, Pantarotto D, Briand JP, Muller S, Prato M, Bianco A (2007) Cellular uptake of functionalized carbon nanotubes is independent of functional group and cell type. *Nat Nanotechnol* 2:108–113.
- Kramer PA (1974) Albumin microspheres as vehicles for achieving specificity in drug delivery. *J Pharm Sci* 63:1646–1647.
- Kreuter J (2007) Nanoparticles – a historical perspective. *Int J Pharm* 331:1–10.
- Kumar A, Murugesan S, Pushparaj V, Xie J, Soldano C, John G, Nalamasu O, Ajayan PM, Linhardt RJ (2007) Conducting organic-metallic composite submicrometer rods based on ionic liquids. *Small* 3:429–433.
- Labhasetwar V (2005) Nanotechnology for drug and gene therapy: the importance of understanding molecular mechanisms of delivery. *Curr Opin Biotechnol* 16:674–680.
- Lacerda L, Bianco A, Prato M, Kostarelos K (2006) Carbon nanotubes as nanomedicines: from toxicology to pharmacology. *Adv Drug Deliver Rev* 58:1460–1470.
- Lam CW, James JT, McCluskey R, Hunter RL (2004) Pulmonary toxicity of single-wall carbon nanotubes in mice 7 and 90 days after intratracheal instillation. *Toxicol Sci* 77:126–134.
- Lam CW, James JT, McCluskey R, Arepalli S, Hunter RL (2006) A review of carbon nanotube toxicity and assessment of potential occupational and environmental health risks. *Crit Rev Toxicol* 36:189–217.
- Langer R (1998) Drug delivery and targeting. *Nature* 392:5–10.
- Langer R (2001) Perspectives: drug delivery – drugs on target. *Science* 293:58–59.
- Langer R (2007) Editorial: Tissue engineering – perspectives, challenges, and future directions. *Tissue Eng* 13:1–2.
- Langer R, Vacanti JP (1993) Tissue engineering. *Science* 260:920–926.
- Langer R, Linhardt RJ, Hoffberg S, Larsen AK, Cooney CL, Tapper D, Klein M (1982) An enzymatic system for removing heparin in extracorporeal therapy. *Science* 217:261–263.
- Levenberg S, Huang NF, Lavik E, Rogers AB, Itskovitz-Eldor J, Langer R (2003) Differentiation of human embryonic stem cells on three-dimensional polymer scaffolds. *Proc Natl Acad Sci USA* 100:12741–12746.
- Li JG, Li WX, Xu JY, Cai XQ, Liu RL, Li YJ, Zhao QF, Li QN (2007a) Comparative study of pathological lesions induced by multiwalled carbon nanotubes in lungs of mice by intratracheal instillation and inhalation. *Environ Toxicol* 22:415–421.
- Li Z, Hulderman T, Salmen R, Chapman R, Leonard SS, Young SH, Shvedova A, Luster MI, Simeonova PP (2007b) Cardiovascular effects of pulmonary exposure to single-wall carbon nanotubes. *Environ Health Perspect* 115:377–382.

- Linhardt RJ, Ampofo SA, Fareed J, Hoppensteadt D, Mulliken JB, Folkman J (1992) Isolation and characterization of human heparin. *Biochemistry* 31:12441–12445.
- Liu J, Rinzler AG, Dai HJ, Hafner JH, Bradley RK, Boul PJ, Lu A, Iverson T, Shelimov K, Huffman CB, Rodriguez-Macias F, Shon YS, Lee TR, Colbert DT, Smalley RE (1998) Fullerene pipes. *Science* 280:1253–1256.
- Liu YF, Wang HF (2007) Nanomedicine – Nanotechnology tackles tumours. *Nat Nanotechnol* 2:20–21.
- Liu Z, Cai WB, He LN, Nakayama N, Chen K, Sun XM, Chen XY, Dai HJ (2007) In vivo biodistribution and highly efficient tumour targeting of carbon nanotubes in mice. *Nat Nanotechnol* 2:47–52.
- Lohse DL, Linhardt RJ (1992) Purification and characterization of heparin lyases from *Flavobacterium heparinum*. *J Biol Chem* 267:24347–55.
- Lu Q, Moore JM, Huang G, Mount AS, Rao AM, Larcom LL and Ke PC (2004) RNA Polymer Translocation with Single-Walled Carbon Nanotubes. *Nano Lett* 4:2473–2477.
- Maincent P, Le Verge R, Sado P, Couvreur P, Devissaguet JP (1986) Disposition kinetics and oral bioavailability of vincamine-loaded polyalkyl cyanoacrylate nanoparticles. *J Pharm Sci* 75:955–958.
- Maeda Y, Kanda M, Hashimoto M, Hasegawa T, Kimura S, Lian YF, Wakahara T, Akasaka T, Kazaoui S, Minami N, Okazaki T, Hayamizu Y, Hata K, Lu J, Nagase S (2006) Dispersion and separation of small-diameter single-walled carbon nanotubes. *J Am Chem Soc* 128:12239–12242.
- Manna SK, Sarkar S, Barr J, Wise K, Barrera EV, Jejelowo O, Rice-Ficht AC, Ramesh GT (2005) Single-walled carbon nanotube induces oxidative stress and activates nuclear transcription factor-kappa B in human keratinocytes. *Nano Lett* 5:1676–1684.
- Martin CR, Kohli P (2003) The emerging field of nanotube biotechnology. *Nat Rev Drug Discov* 2:29–37.
- Maynard AD (2006) Nanotechnology: assessing the risks. *Nano Today* 1:22–33.
- Maynard AD, Baron PA, Foley M, Shvedova AA, Kisin ER, Castranova V (2004) Exposure to carbon nanotube material: aerosol release during the handling of unrefined single-walled carbon nanotube material. *J Toxicol Environ Health A* 67:87–107.
- McDevitt MR, Chattopadhyay D, Kappel BJ, Jaggi JS, Schiffman SR, Antczak C, Njardarson JT, Brentjens R, Scheinberg DA (2007) Tumor targeting with antibody-functionalized, radiolabeled carbon nanotubes. *J Nucl Med* 48:1180–1189.
- Michael RN (2006) The History of Dental Implants. *US Dentistry* 24–26.
- Michaelis K, Hoffmann MM, Dreis S, Herbert E, Alyautdin RN, Michaelis M, Kreuter J, Langer K J (2006) Covalent linkage of apolipoprotein E to albumin nanoparticles strongly enhances drug transport into the brain. *Pharmacol Exp Ther* 317:1246–1253.
- Moghimi SM, Hunter AC, Murray JC (2005) Nanomedicine: current status and future prospects. *Faseb J* 19:311–330.
- Monteiro-Riviere NA, Nemanich RJ, Inman AO, Wang YYY, Riviere JE (2005) Multi-walled carbon nanotube interactions with human epidermal keratinocytes. *Toxicol Lett* 155:377–384.
- Muller J, Huaux F, Moreau N, Misson P, Heilier JF, Delos M, Arras M, Fonseca A, Nagy JB, Lison D (2005) Respiratory toxicity of multi-wall carbon nanotubes. *Toxicol Appl Pharmacol* 207:221–231.
- Murr LE, Bang JJ, Esquivel EV, Guerrero PA, Lopez A (2004) Carbon nanotubes, nanocrystal forms, and complex nanoparticle aggregates in common fuel-gas combustion sources and the ambient air. *J Nanopart Res* 6:241–251.
- Murugesan S, Mousa S, Vijayaraghavan A, Ajayan PM, Linhardt RJ (2006a) Ionic liquid-derived blood-compatible composite membranes for kidney dialysis. *J Biomed Mater Res B Appl Biomater* 79:298–304.
- Murugesan S, Park TJ, Yang HC, Mousa S, Linhardt RJ (2006b) Blood compatible carbon nanotubes – Nano-based neoproteoglycans. *Langmuir* 22:3461–3463.
- Murugesan S, Mousa S, O'Connor LJ, Lincoln DW, Linhardt RJ (2007) Carbon inhibits vascular endothelial growth factor- and fibroblast growth factor-promoted angiogenesis. *Febs Letters* 581:1157–1160.

- Na K, Kim S, Park K, Kim K, Woo DG, Kwon IC, Chung HM, Park KH (2007) Heparin/poly(L-lysine) nanoparticle-coated polymeric microspheres for stem-cell therapy. *J Am Chem Soc* 129:5788–5789.
- Nepal D, Geckeler KE (2007) Proteins and carbon nanotubes: close encounter in water. *Small* 3:1259–1265.
- Nie SM, Xing Y, Kim GJ, Simons JW (2007) Nanotechnology applications in cancer. *Annu Rev Biomed Eng* 9:257–288.
- Nishiyama N (2007) Nanomedicine – Nanocarriers shape up for long life. *Nat Nanotechnol* 2:203–204.
- Niu CM, Sichel EK, Hoch R, Moy D, Tennent H (1997) High power electrochemical capacitors based on carbon nanotube electrodes. *Appl Phys Lett* 70:1480–1482.
- Nohynek GJ, Lademann J, Ribaud C, Roberts MS (2007) Grey goo on the skin? Nanotechnology, cosmetic and sunscreen safety. *Crit Rev Toxicol* 37:251–277.
- Oberdörster G, Oberdörster E, Oberdörster J (2005) Nanotoxicology: an emerging discipline evolving from studies of ultrafine particles. *Environ Health Perspect* 113:823–839.
- O’Connell MJ, Boul P, Ericson LM, Huffman C, Wang YH, Haroz E, Kuper C, Tour J, Ausman KD, Smalley RE (2001) Reversible water-solubilization of single-walled carbon nanotubes by polymer wrapping. *Chem. Phys. Lett.* 342:265–271.
- O’Connell MJ, Bachilo SM, Huffman CB, Moore VC, Strano MS, Haroz EH, Rialon KL, Boul PJ, Noon WH, Kittrell C, Ma JP, Hauge RH, Weisman RB (2002) Smalley RE Band gap fluorescence from individual single-walled carbon nanotubes. *Science* 297:593–596.
- Ostomel TA, Shi QH, Tsung CK, Liang HJ, Stucky GD (2006) Spherical bioactive glass with enhanced rates of hydroxyapatite deposition and hemostatic activity. *Small* 2:1261–1265.
- Pantarotto D, Singh R, McCarthy D, Erhardt M, Braind J-P, Prato M, Kostarelos K Bianco A (2004) Functionalized Carbon Nanotubes for Plasmid DNA Gene Delivery. *Angew Chem Int Ed* 43:5242–5246.
- Patel HRH (2007) The stem cell revolution: a biologic nanotechnology. *Eur Urol* 51:1173–1174.
- Pearce AI, Richards RG, Milz S, Schneider E, Pearce SG (2007) Animal models for implant biomaterial research in bone: a review. *Eur Cells Mater* 13:1–10.
- Peng WD, Anderson DG, Bao YH, Padera RF, Langer R, Sawicki JA (2007) Nanoparticulate delivery of suicide DNA to murine prostate and prostate tumors. *Prostate* 67:855–862.
- Peracchia MT, Vauthier C, Puisieux F, Couvreur P (1997) Development of sterically stabilized poly(isobutyl 2-cyanoacrylate) nanoparticles by chemical coupling of poly(ethylene glycol). *J Biomed Mater Res* 34:317–326.
- Peracchia MT, Fattal E, Desmaele D, Besnard M, Noel JP, Gomis JM, Appel M, d’Angelo J, Couvreur P (1999) Stealth PEGylated polycyanoacrylate nanoparticles for intravenous administration and splenic targeting. *J Control Release* 60:121–128.
- Polizu S, Savadogo O, Poulin P, Yahia L (2006) Applications of carbon nanotubes-based biomaterials in biomedical nanotechnology. *J Nanosci Nanotechnol* 6:1883–1904.
- Pulskamp K, Diabate S, Krug HF (2007) Carbon nanotubes show no sign of acute toxicity but induce intracellular reactive oxygen species in dependence on contaminants. *Toxicol Lett* 168:58–74.
- Pushparaj VL, Manikoth SM, Kumar A, Murugesan S, Ci L, Vajtai R, Linhardt RJ, Nalamasu O, Ajayan PM (2007) Flexible nanocomposite thin film energy storage devices. *Proc Natl Acad Sci USA* 104: 13574–13577.
- Radomski A, Jurasz P, Alonso-Escolano D, Drews M, Morandi M, Malinski T, Radomski MW (2005) Nanoparticle-induced platelet aggregation and vascular thrombosis. *Brit J Pharmacol* 146:882–893.
- Raja PMV, Connolly J, Ganesan GP, Ci LJ, Ajayan PM, Nalamasu O, Thompson DM (2007) Impact of carbon nanotube exposure, dosage and aggregation on smooth muscle cells. *Toxicol Lett* 169:51–63.
- Rao CNR, Satishkumar BC, Govindaraj A, Nath M (2001) Nanotubes. *Chemphyschem* 2:78–105.

- Ratner BD, Schoen FJ, Hoffman AS, Lemons JE, Hoffman A (2004) *Biomaterials Science: An Introduction to Materials in Medicine*, 2nd ed. Elsevier, New York.
- Regev O, ElKati PNB, Loos J, Koning CE (2004) Preparation of conductive nanotube-polymer composites using latex technology. *Adv Mater* 16:248–251.
- Reilly RM (2007) Carbon nanotubes: potential benefits and risks of nanotechnology in nuclear medicine. *J Nucl Med* 48:1039–1042.
- Richard C, Balavoine F, Schultz P, Ebbesen TW, Mioskowski C (2003) Supramolecular self-assembly of lipid derivatives on carbon nanotubes. *Science* 300:775–778.
- Sato Y, Yokoyama A, Shibata K, Akimoto Y, Ogino S, Nodasaka Y, Kohgo T, Tamura K, Akasaka T, Uo M, Motomiya K, Jeyadevan B, Ishiguro M, Hatakeyama R, Watari F, Tohji K (2005) Influence of length on cytotoxicity of multi-walled carbon nanotubes against human acute monocytic leukemia cell line THP-I in vitro and subcutaneous tissue of rats in vivo. *Mol Biosyst* 1:176–182.
- Sayes CM, Liang F, Hudson JL, Mendez J, Guo WH, Beach JM, Moore VC, Doyle CD, West JL, Billups WE, Ausman KD, Colvin VL (2006) Functionalization density dependence of single-walled carbon nanotubes cytotoxicity in vitro. *Toxicol Lett* 161:135–142.
- Scheffel U, Rhodes BA, Natarajan TK, Wagner HN Jr (1972) Albumin microspheres for study of the reticuloendothelial system. *J Nucl Med* 13:498–503.
- Service RF (1998) Nanotubes: The Next Asbestos? *Science* 281:941.
- Shao N, Lu S, Wickstrom E, Panchapakesan B (2007) Integrated molecular targeting of IGF1R and HER2 surface receptors and destruction of breast cancer cells using single wall carbon nanotubes. *Nanotechnology* 18: Art. No. 315101.
- Shvedova AA, Castranova V, Kisin ER, Schwegler-Berry D, Murray AR, Gandelsman VZ, Maynard A, Baron P (2003) Exposure to carbon nanotube material: assessment of nanotube cytotoxicity using human keratinocyte cells. *J Toxicol Environ Health A* 66:1909–1926.
- Shvedova AA, Kisin ER, Murray AR, Gorelik O, Arepalli S, Castranova V, Young SH, Gao F, Tyurina YY, Oury TD, Kagan VE (2007) Vitamin E deficiency enhances pulmonary inflammatory response and oxidative stress induced by single-walled carbon nanotubes in C57BL/6 mice. *Toxicol Appl Pharm* 221:339–348.
- Singh R, Pantarotto D, McCarthy D, Chaloin O, Hoebeke J, Partidos CD, Briand JP, Prato M, Bianco A, Kostarelos K (2005) Binding and condensation of plasmid DNA onto functionalized carbon nanotubes: toward the construction of nanotube-based gene delivery vectors. *J Am Chem Soc* 127:4388–4396.
- Singh R, Pantarotto D, Lacerda L, Pastorin G, Klumpp C, Prato M, Bianco A, Kostarelos K (2006) Tissue biodistribution and blood clearance rates of intravenously administered carbon nanotube radiotracers. *Proc Natl Acad Sci USA* 103:3357–3362.
- Son SJ, Bai X, Lee SB (2007a) Inorganic hollow nanoparticles and nanotubes in nanomedicine. Part 1. Drug/gene delivery applications. *Drug Discov Today* 12:650–656.
- Son SJ, Bai X, Lee SB (2007b) Inorganic hollow nanoparticles and nanotubes in nanomedicine. Part 2: imaging, diagnostic, and therapeutic applications. *Drug Discov Today* 12:657–663.
- Speiser P, Khanna SC (1970) Perlpolymerisate, eine neue perorale Darreichungsform und ihre Beeinflussung durch Arzneistoffe. *Präpar Pharm* 6:1–4.
- Sugibayashi K, Morimoto Y, Nadai T, Kato Y (1977) Drug-carrier property of albumin microspheres in chemotherapy. I. Tissue distribution of microsphere-entrapped 5-fluorouracil in mice. *Chem Pharm Bull* 25:3433–3434.
- Sugibayashi K, Akimoto M, Morimoto Y (1979a) Drug-carrier property of albumin microspheres in chemotherapy III. Effect of microsphere-entrapped 5-fluorouracil on ehrlich ascites-carcinoma in mice. *J Pharmacobio-Dynam* 2:350–355.
- Sugibayashi K, Morimoto Y, Nadai T, Kato Y, Hasegawa A, Arita T (1979b) Drug-carrier property of albumin microspheres in chemotherapy. II. Preparation and tissue distribution in mice of microsphere-entrapped 5-fluorouracil. *Chem Pharm Bull* 27:204–209.

- Tasis D, Tagmatarchis N, Bianco A, Prato M (2006) Chemistry of carbon nanotubes. *Chem Rev* 106:1105–1136.
- Thompson KP (2007) Near vision accommodating intraocular lens with adjustable power. U.S. patent No. 5,607,472. Retrieved on 2007-02-04.
- Tong R, Cheng JJ (2007) Anticancer polymeric nanomedicines. *Polym Rev* 47:345–381.
- Tsuji JS, Maynard AD, Howard PC, James JT, Lam CW, Warheit DB, Santamaria AB (2006) Research strategies for safety evaluation of nanomaterials, part IV: risk assessment of nanoparticles. *Toxicol Sci* 89:42–50.
- Venkatesan N, Yoshimitsu J, Ito Y, Shibata N, Takada K (2005) Liquid filled nanoparticles as a drug delivery tool for protein therapeutics. *Biomaterials* 26:7154–7163.
- Viswanathan G, Murugesan S, Pushparaj V, Nalamasu O, Ajayan PM, Linhardt RJ (2006) Preparation of biopolymer fibers by electrospinning from room temperature ionic liquids. *Biomacromolecules* 7:415–418.
- Wang HF, Wang J, Deng XY, Sun HF, Shi ZJ, Gu ZN, Liu YF, Zhao YL (2004) Biodistribution of carbon single-wall carbon nanotubes in mice. *J Nanosci Nanotechnol* 4:1019–1024.
- Warheit DB, Laurence BR, Reed KL, Roach DH, Reynolds GAM, Webb TR (2004) Comparative pulmonary toxicity assessment of single-wall carbon nanotubes in rats. *Toxicol Sci* 77:117–125.
- Wei W, Sethuraman A, Jin C, Monteiro-Riviere NA, Narayan RJ (2007) Biological properties of carbon nanotubes. *J Nanosci Nanotechnol* 7:1284–1297.
- Wick P, Manser P, Limbach LK, Dettlaff-Weglikowska U, Krumeich F, Roth S, Stark WJ, Bruinink A (2007) The degree and kind of agglomeration affect carbon nanotube cytotoxicity. *Toxicol Lett* 168:121–131.
- Widder K, Flouret G, Senyei A (1979) Magnetic microspheres: synthesis of a novel parenteral drug carrier. *J Pharm Sci* 68:79–82.
- Widder KJ, Marino PA, Morris RM, Howard DP, Poore GA, Senyei AE (1983a) Selective targeting of magnetic albumin microspheres to the Yoshida sarcoma: ultrastructural evaluation of microsphere disposition. *Eur J Cancer Clin Oncol* 19:141–147.
- Widder KJ, Morris RM, Poore GA, Howard DP, Senyei AE (1983b) Selective targeting of magnetic albumin microspheres containing low-dose doxorubicin: total remission in Yoshida sarcoma-bearing rats. *Eur J Cancer Clin Oncol* 19:135–139.
- Worle-Knirsch JM, Pulskamp K, Krug HF (2006) Oops they did it again! Carbon nanotubes hoax scientists in viability assays. *Nano Lett* 6:1261–1268.
- Wu GT, Wang CS, Zhang XB, Yang HS, Qi ZF, He PM, Li WZ (1999) Structure and lithium insertion properties of carbon nanotubes. *J Electrochem Soc* 146:1696–1701.
- Wu Y, Hudson JS, Lu Q, Moore JM, Mount AS, Rao AM, Alexov E, Ke PC (2006) Coating single-walled carbon nanotubes with phospholipids. *J Phys Chem B* 110:2475–2478.
- Xiao H, Yang LS, Zou HF, Yang L, Le XC (2007) Analysis of oxidized multi-walled carbon nanotubes in single K562 cells by capillary electrophoresis with laser-induced fluorescence. *Anal Bioanal Chem* 387:119–126.
- Yang J, Yamato M, Nishida K, Ohki T, Kanzaki M, Sekine H, Shimizu T, Okano T (2006) Cell delivery in regenerative medicine: the cell sheet engineering approach. *J Control Release* 116:193–203.
- Yinghuai Z, Peng AT, Carpenter K, Maguire JA, Hosmane NS, Takagaki M (2005) Substituted carborane-appended water-soluble single-wall carbon nanotubes: new approach to boron neutron capture therapy drug delivery. *J Am Chem Soc* 127:9875–9880.
- Yu BZ, Yang JS, Li WX (2007) In vitro capability of multi-walled carbon nanotubes modified with gonadotrophin releasing hormone on killing cancer cells. *Carbon* 45:1921–1927.
- Yu X, Munge B, Patel V, Jensen G, Bhirde A, Gong JD, Kim SN, Gillespie J, Gutkind JS, Papadimitrakopoulos F, Rusling JF (2006) Carbon nanotube amplification strategies for highly sensitive immunodetection of cancer biomarkers. *J Am Chem Soc* 128:11199–11205.
- Yurekli K, Mitchell CA, Krishnamoorti R (2004) Small-angle neutron scattering from surfactant-assisted aqueous dispersions of carbon nanotubes. *J Am Chem Soc* 126:9902–9903.
- Zheng M, Jagota A, Semke ED, Diner BA, Mclean RS, Lustig SR, Richardson RE, Tassi NG (2003a) DNA-assisted dispersion and separation of carbon nanotubes. *Nat Mater* 2:338–342.

- Zheng M, Jagota A, Strano MS, Santos AP, Barone P, Chou SG, Diner BA, Dresselhaus MS, McLean RS, Onoa GB, Samsonidze GG, Semke ED, Usrey M, Walls DJ (2003b) Structure-based carbon nanotube sorting by sequence-dependent DNA assembly. *Science* 302:1545–1548.
- Zolle I, Hosein F, Rhodes BATK, Wagner HN Jr (1970) Human serum albumin microspheres for studies of the reticuloendothelial system. *J Nucl Med* 11:379.
- Nano risk framework. Available at www.nanoriskframework.com

Chapter 13

Solubility of Fullerenes in Fatty Acids Esters: A New Way to Deliver *In Vivo* Fullerenes. Theoretical Calculations and Experimental Results

Franco Cataldo^{1,2}

Abstract The biological effects of fullerenes and, in particular, of C_{60} have been recognized since long time. One of the problems which hindered the application of fullerenes in medicinal chemistry regards their insolubility in water and water-based fluids. In the present chapter it is reported that C_{60} and C_{70} fullerenes are soluble in vegetable oils, in general, in esters of fatty acids and in free fatty acids. These results pave the way in the utilization of vegetable oils as vehicles in the delivery of fullerenes for both topical applications and internal use (e.g., intramuscular injection).

It is shown that the solubility of fullerenes in vegetable oils can be predicted and justified on the basis of the solubility parameters of C_{60} and C_{70} and of the glycerol esters of fatty acids. A detailed procedure for the calculation of the solubility parameters of fullerenes and vegetable oils by group increment is reported.

The solubility of C_{60} and C_{70} in a series of vegetable oils, namely: olive, sunflower, peanut, soybean, linseed and castor oil, has been determined quantitatively spectrophotometrically. Additionally, the solubility of C_{60} and C_{70} has been determined quantitatively in the methyl esters of brassica oilseed and only qualitatively in molten cow butter, molten stearic acid and molten behenamide. The experimental results show that the solubility of fullerenes appears to be dependent on the unsaturation level of the fatty acids composing the vegetable oils being lower in oils with higher unsaturation level. The solubility has been found dependent also on the polarizability parameter of the vegetable oils.

The stability of C_{60} and C_{70} solutions in vegetable oils has been studied in air and under inert atmosphere, after thermal processing and under the action of UV radiation. In all cases it has been found that C_{60} and C_{70} are prone to form adducts with the fatty acid chains of the vegetable oils. The adducts are formed both by radical and Diels-Alder mechanisms. The pharmaceutical valency and potential of such adducts has also been discussed.

¹Tor Vergata University, Rome, Italy

²Actinium Chemical Research, Via Casilina 1626/A, 00133 Rome, Italy
Email: cdcata@flashnet.it

Keywords Adducts, C₆₀, C₇₀, esters of fatty acid, excipients, fatty acids, fullerenes, glycerol esters of fatty acids, grafting, group increment method, solubility, solubility parameter, vehicles for drug delivery, vegetable oils, triglycerides

13.1 Introduction

One of the most promising applications of fullerenes is in biochemistry and medicinal chemistry (Wilson, 2000; Tabata et al., 1997; Dugan et al., 2000; see also other chapters of the present book). For such application the biocompatible solubility of C₆₀ is mandatory. Therefore, a lot of efforts have been made in preparing fullerene derivatives with functional groups able to permit the C₆₀ dissolution in water and similarly, also the encapsulation of C₆₀ into host–guest complexes, for instance, with cyclodextrin (Braun et al., 1994; Cataldo, 2002). In this specific context it came quite unexpected the discovery of C₆₀ solubility in various vegetable oils (Braun et al., 2007; Cataldo and Braun, 2007). This implies the possible utilization of fatty acids esters of glycerol for the delivery of fullerene or its derivatives into living organisms or its topical use on skin. Furthermore, it has been observed (Sayes et al., 2005) that C₆₀ fullerene exerts a cytotoxic activity just on the cell membranes through a lipid peroxidation mechanism. This fact offers a possibility for the realization of the idea of the “magic bullet”, i.e., a chemical, which selectively can destroy only the undesired cells leaving untouched the “normal cells” (Guanti et al., 2005).

The solubility of C₆₀ fullerene in numerous solvents was studied since when these molecules become available in bulk quantities (Ruoff et al., 1993; Beck and Mandi, 1997). Similarly, attention was paid to the solubility of C₇₀ (Sivaraman et al., 1994). Numerous papers appeared in the literature on this specific subject and among the most recent and complete surveys it should be mentioned the works of Korobov and Smith (2000), Marcus et al. (2001) and Makitra et al. (2003). In general, it was reported that fullerenes are soluble in solvents with low dielectric constant, large refractive indices and large molecular volume (Ruoff et al., 1993). A correlation with solvent polarizability and fullerene solubility has also been proposed (Sivaraman et al., 1994). Murthy and Geckeler (2001) have correlated the fullerene solubility with the solvent to fullerene molar volume ratio. Particularly surprising are the works of Heymann (1996a, b), where it was shown an increasing solubility of fullerenes in a series of straight chain alcohols: the solubility of both C₆₀ and C₇₀ grows dramatically from methanol to 1-octanol, hence by increasing the size of the solvent molecules and by reducing their hydrophilic character. Liu et al. (2005) have reported that C₆₀ dissolves in ionic liquids.

Despite the numerous modelling works on the subject (e.g. Sivaraman et al., 2001; Huang, 2005) and the great interest on the solubility of fullerenes in hydrophilic solvents, in water and in biologically active solvents for the potential application of fullerenes as drugs, none was able to predict that C₆₀ and C₇₀ fullerenes

are soluble in fatty acid esters and primarily in fatty acids triglycerides such as olive oil (Braun et al., 2007) and in a series of other vegetable oils such as linseed, sunflower and soybean oil (Cataldo and Braun, 2007). The solubility of C_{60} was discovered not only in methyl esters of fatty acids such as the methyl ester of brassica oilseed (Cataldo and Braun, 2007), but also in other long-chain molecules such as fatty amides as we will show in this chapter.

This chapter shows that the solubility of C_{60} and C_{70} fullerenes can be predicted from the solubility parameter of these two molecules and the calculated solubility parameters of fatty acids and their esters. Furthermore, the solubility of C_{60} and C_{70} fullerenes in a series of vegetable oils and fatty acid esters will be presented and discussed.

13.2 Experimental

13.2.1 *Materials and Equipment*

Fullerenes were high purity grades (99 + %) from Southern Chemicals LLC. Vegetable oils were commercially available oils from olive, linseed, soybean, sunflower, peanut and castor. A methyl ester of brassica oilseed also was employed.

The solubility was determined spectrophotometrically on a Shimadzu UV160A using the reference quartz cuvette filled with pure vegetable oil under testing and the sample cuvette filled with the solution of C_{60} or C_{70} in a given vegetable oil.

13.2.2 *Solubility Determination*

In a typical procedure, about 40 mg of fullerene (C_{60} or C_{70}) was stirred with 15–17 g of oil at room temperature. After 3 days of stirring at room temperature the solution was left overnight before filtering it through a paper filter “Rapida A”. The filtered solution was then employed for the spectrophotometric determination of solubility. In the case of C_{60} -saturated solutions, there was no necessity to dilute the solution before the spectrophotometric measurement. Thus, the measurement was made by reading the absorbance at 530 nm using an averaged molar extinction coefficient of $724 M^{-1} cm^{-1}$ (Catalan et al., 1995). Instead, the spectrophotometric determination of C_{70} solubility always required a dilution with fresh oil before measurement. In general, 5 ml of filtered saturated solution was diluted to 50 ml prior to measurement. A molar extinction coefficient of $\epsilon = 28,444 M^{-1} cm^{-1}$ was used at 379 nm or $\epsilon = 15,166 M^{-1} cm^{-1}$ at 469 nm (Sivaraman et al., 1994).

13.3 Results and Discussion

13.3.1 The Solubility Parameter

The solubility parameter has been defined by Hildebrand and Scott (1950) as:

$$\delta = [(\Delta H_{\text{vap}} - RT) / V_m]^{0.5} \quad (13.1)$$

The evaporation enthalpy ΔH_{vap} was taken as the parameter of the cohesion energy between molecules minus the thermal energy needed to separate them (RT) divided by the molar volume V_m . So, equation (13.1) can be re-written as:

$$\delta = [(E_{\text{coh}}) / V_m]^{0.5} \quad (13.2)$$

The cohesive energy E_{coh} of a substance in a condensed state is defined as the increase in internal energy ΔU per mole of substance if all the intermolecular forces are eliminated.

Hansen (2007) has shown that the solubility parameter proposed by Hildebrand and Scott does not take into account the contribution of polar forces and hydrogen bonding, therefore, a more complex solubility parameter has been proposed:

$$\delta^2 = \delta_d^2 + \delta_p^2 + \delta_h^2 \quad (13.3)$$

derived from the contribution of three components of the cohesive energy:

$$E_{\text{coh}} = E_d + E_p + E_h \quad (13.4)$$

respectively due to the contribution of dispersion and polar forces plus an hydrogen bonding contribution.

It is possible to calculate the solubility parameter and the solubility parameter components of almost all molecules and polymers by a group contribution method (Van Krevelen, 1990; Bicerano, 1996). For this purpose, as explained by Van Krevelen (1990) it is useful to introduce the molar attraction constant simply defined as:

$$\varphi = (E_{\text{coh}} V_m)^{0.5} \quad (13.5)$$

A set of equations has been proposed by Van Krevelen (1990) for the calculation of the solubility parameter components using the molar attraction by a group contribution methodology:

$$\delta_d = (\sum \varphi_d) / V_m \quad (13.6)$$

$$\delta_p = (\sum \varphi_p^2)^{0.5} / V_m \quad (13.7)$$

$$\delta_h = \left[\left(\sum E_h \right) / V_m \right]^{0.5} \quad (13.8)$$

The total solubility parameter can be calculated as follows:

$$\delta_t = \left[\delta_d^2 + \delta_p^2 + \delta_h^2 \right]^{0.5} \quad (13.9)$$

It can be observed from equation (13.8) that the hydrogen bond parameter δ_h cannot be calculated from the molar attraction, but directly from the hydrogen bonding energy E_h (Van Krevelen, 1990).

13.3.2 The Solubility Parameter of C_{60} and C_{70} Fullerenes

Fullerenes are highly symmetrical molecules free from any polar groups. For such types of molecules equations (13.7) and (13.8) give $\delta_p = \delta_h = 0$. Therefore, the solubility parameter of fullerenes calculated according to Van Krevelen (1990) can be calculated from equation (13.6).

The density of C_{60} and C_{70} fullerenes is known from literature (Beckhaus et al., 1994) being 1.76 and 1.69 g/ml, respectively. Thus, the molar volume of C_{60} and C_{70} is as follows:

$$V_{C_{60}} = 409.5 \text{ ml/mol}$$

$$V_{C_{70}} = 497.5 \text{ ml/mol}$$

It is interesting to note that such molar volumes can be calculated also by group increments using the van der Waals molar volume for a carbon atom, which is 6.95 ml/mol (Van Krevelen, 1990).

Thus, the calculated molar volumes are:

$$V_{C_{60}} = 417.0 \text{ ml/mol}$$

$$V_{C_{70}} = 486.5 \text{ ml/mol}$$

Both calculated values are in fair agreement with the experimental value. Therefore, with this approach it is possible to calculate also the molar volumes of higher fullerenes, whose density is not known. Table 13.1 reports the calculated molar volumes for a series of fullerenes.

Knowing the fullerene molar volume, either the experimental or the calculated value, it is quite straightforward the calculation of the solubility parameter by substituting the tabulated φ_d values for group increments in equation (13.6).

The calculation should consider the number of hexagonal rings present in the fullerene molecule. It is known that each stable fullerene cage is characterized for having 12 pentagons and a number of hexagons, which depends on the total number of carbon atoms present in the cage according to the Euler's relation:

$$N^* + 2(10 + \xi) \quad (13.10)$$

Table 13.1 Solubility parameters of fullerenes

Fullerene	Molar volume (ml/mol)	Calc. molar volume (ml/mol)	Hexagons (number of)	Solub. param (MPa) ^{1/2}
C ₆₀	409.5	417.0	20	19.5
C ₇₀	497.5	486.5	25	19.4
C ₇₆		528.2	28	20.1
C ₇₈		542.1	29	20.2
C ₈₂		569.9	31	20.4
C ₈₄		583.8	32	20.5
C ₉₀		625.5	35	20.7

where N^* is the number of carbon atoms in the fullerene cage and ξ is the number of hexagons in the fullerene structure.

Thus, for example, for C₆₀ fullerene that has 20 hexagons, the calculation of the solubility parameter is:

$$\delta_d(C_{60}) = (\Sigma\varphi_d)/V_m = [(70 \times 60) + (190 \times 20)]/409.5 = 19.5 \text{ MPa}^{1/2} \text{ (or } J^{1/2} \text{ cm}^{-3/2}) \quad (13.11)$$

In fact, the tabulated φ_d value for each sp² hybridized carbon atom is 70 J^{1/2} cm^{3/2} mol⁻¹, while the φ_d value for each hexagonal ring is 190 J^{1/2} cm^{3/2} mol⁻¹. Thus, for C₇₀, which has 25 hexagonal rings the calculation is:

$$\delta_d(C_{70}) = (\Sigma\varphi_d)/V_m = [(70 \times 70) + (190 \times 25)]/497.5 = 19.4 \text{ MPa}^{1/2} \text{ (or } J^{1/2} \text{ cm}^{-3/2}) \quad (13.12)$$

In the fullerene case, $\delta_d = \delta_t$.

The calculated values found are in fair agreement with the solubility parameter found experimentally by Sivaraman et al. (1994) who reported $\delta_t(C_{60}) \approx \delta_t(C_{70}) \approx 18 \text{ MPa}^{1/2}$. Furthermore, Hansen and Smith (2004) have reported an experimental solubility parameter $\delta_d(C_{60}) = 19.7 \text{ MPa}^{1/2}$ in excellent agreement with the calculated value reported in equation (13.11). Strangely enough, Hansen and Smith (2004) have reported also the $\delta_p(C_{60}) = 2.9 \text{ MPa}^{1/2}$ and a $\delta_h(C_{60}) = 2.7 \text{ MPa}^{1/2}$ so that the total solubility parameter $\delta_t(C_{60}) = 20.1 \text{ MPa}^{1/2}$ calculated according to equation (13.9). However, both for structural and for symmetry considerations Van Krevelen (1990) has suggested that $\delta_p = \delta_h = 0$ in the case of high symmetry molecules like C₆₀, which are free from polar substituents.

Table 13.1 reports the solubility parameters of a series of fullerenes. Higher fullerene homologues up to C₉₀ are predicted to have a solubility parameter $\delta_t \approx \delta_d \approx 20 \text{ MPa}^{1/2}$, thus, not far from the value calculated for the most common fullerenes C₆₀ and C₇₀.

13.3.3 *The Solubility Parameter of Fatty Acids and Fatty Acids Esters of Glycerol*

Being a mixture of different fatty acids esters of glycerol, the calculation with group increment of the solubility parameter of vegetable oils presents some

difficulties. Furthermore, no data are available on the solubility parameters of such oils even in a comprehensive book on solubility parameter such that of Hansen (2007).

The approach employed for the calculation of the solubility parameters of fatty acids and fatty acid esters with the group increment technique according to the Van Krevelen (1990) method has involved the following steps. First of all the density ρ of fatty acids or of a given vegetable oil such as olive oil was taken from literature (Martinenghi, 1963). In the case of vegetable oils, the average molecular weight ω of their fatty acids mixture was considered in the calculation of the molar volume. The value of ω was taken from literature (Martinenghi, 1963).

The general equation for the calculation of the three components of the vegetable oils are:

$$\delta_d = (\sum_i x_i \varphi_{di}) / (\omega \rho^{-1}) \quad (13.13)$$

$$\delta_p = (\sum_i x_i \varphi_{pi}^2)^{0.5} / (\omega \rho^{-1}) \quad (13.14)$$

$$\delta_h = [(\sum_i x_i E_{hi}) / (\omega \rho^{-1})]^{0.5} \quad (13.15)$$

where x_i is the weight fraction of a given component of a vegetable oil (considered always as triglyceride).

Let us consider, for example, the approximate composition of olive oil: we have considered 0.2% of glyceryl trimyristate, 13% of glyceryl tripalmitate, 0.8% of glyceryl tripalmitoleate, 2.5% of glyceryl tristearate, 73.3% of glyceryl trioleate, 9% of glyceryl trilinoleate, 0.3% of glyceryl triarachidate, 0.7% of glyceryl trilinolenate and 0.2% of glyceryl eicosenoic acid. For each triglyceride the relative values $\sum \varphi_d$, $(\sum \varphi_p^2)^{0.5}$ and $\sum E_h$ have been calculated. Then, these values were multiplied by the weight fraction of each triglyceride present in the oil as shown in equations 13–15 and divided by the molar volume of the oil. The results of such calculation are shown in Table 13.2. Table 13.3 reports the average composition of the vegetable oils studied in the present work. From the data in Table 13.3 the solubility parameters of the vegetable oils reported in Table 13.2 have been calculated.

The data in Table 13.2 show that, as expected the polar and hydrogen-bonding component is more pronounced in the case of free fatty acids rather than in vegetable oils, where the fatty acids are all locked as glyceryl esters. An exception is offered by castor oil, which is characterized by a high content of ricinoleic acid, a fatty acid with one hydroxyl group attached to the chain. Thus, its hydrogen-bonding component is rather high than any other vegetable oil considered.

Table 13.2 Solubility parameters of fatty acid and vegetable oils

	δ_d (MPa) ^{1/2}	δ_p (MPa) ^{1/2}	δ_h (MPa) ^{1/2}	δ_t (MPa) ^{1/2}	$\Delta\delta_d$ (°) using calc. δ_d (C ₆₀)	$\Delta\delta_t$ (°) using calc. δ_t (C ₆₀)	$\Delta\delta t$ (°) using Hansen δ data
Myristic acid	16.1	5.6	9.0	19.2	11.1	0.3	7.7
Palmitic acid	15.5	4.8	8.3	18.3	10.4	1.2	7.3
Stearic acid	15.6	4.3	7.9	18.0	9.8	1.5	6.8
Oleic acid	16.3	4.7	8.2	18.8	10.0	0.7	6.7
Linoleic acid	16.1	4.8	8.2	18.7	10.1	0.8	6.8
Linolenic acid	16.0	4.8	8.3	18.7	10.2	0.8	7.0
Olive oil	16.2	1.5	4.7	16.9	5.9	2.6	4.3
Soybean oil	15.4	1.5	4.6	16.2	6.3	3.3	4.9
Sunflower oil	16.0	1.5	4.7	16.7	6.0	2.8	4.4
Peanut oil	15.3	1.5	4.6	16.1	6.4	3.4	5.0
Linseed oil	15.7	1.5	4.7	16.4	6.2	3.1	4.7
Castor oil	15.8	1.2	9.1	18.3	9.9	1.2	7.7
Brassica oil	16.2	1.5	4.4	16.9	5.7	2.6	4.1
Glyceryl trioleate	16.1	1.5	4.7	16.9	6.0	2.6	4.3
Glyceryl tristearate	17.0	1.6	4.7	17.7	5.6	1.8	3.6

^aCalculated according to equation (13.17).

^bCalculated according to equation (13.18).

^cCalculated according to equation (13.16).

13.3.4 Solubility Criteria from Solubility Parameter Comparison of Fullerenes in Fatty Acids and Fatty Acid Esters of Glycerol

There are many different solubility criteria available in order to establish the solubility of a certain molecule in a given solvent. Hansen (2007) and Hansen and Smith (2004) have made extensive review of such criteria. For simplicity of the mathematical treatment we prefer to follow the criteria proposed by Van Krevelen (1990) for the solubility of a polymer in a solvent. The first point is that we assume that C₆₀ and C₇₀ are polymeric forms of elemental carbon and treat them on these terms. To predict the solubility according to Van Krevelen (1990), the difference in the solubility parameters between solute and solvent should conform to the following equation:

$$\Delta\delta = [(\delta_{d, \text{fullerene}} - \delta_{d, \text{solvent}})^2 + (\delta_{p, \text{fullerene}} - \delta_{p, \text{solvent}})^2 + (\delta_{h, \text{fullerene}} - \delta_{h, \text{solvent}})^2]^{1/2} < 5\text{MPa}^{1/2} \quad (13.16)$$

Since according to our calculations $\delta_{p, \text{fullerene}} = \delta_{h, \text{fullerene}} = 0$, the above equation simplifies as follows:

$$\Delta\delta = [(\delta_{d, \text{fullerene}} - \delta_{d, \text{solvent}})^2 + (\delta_{p, \text{solvent}})^2 + (\delta_{h, \text{solvent}})^2]^{1/2} \quad (13.17)$$

The results of such calculations are reported in Table 13.2 (third column from right) and suggest that C₆₀ (and C₇₀) are not soluble or only slightly soluble in molten free

Table 13.3 Composition of vegetable oils studied in the present work^a

Fatty acid	Chain length	Unsaturation	Brassica oilseed (%)	Sunflower (%)	Soybean (%)	Linseed (%)	Olive (%)	Peanut (%)	Castor (%)
Myristic	C ₁₄	NONE	0.5		0.3	0.9	0.2		
Palmitic	C ₁₆	NONE	2.8	3.6	9.8	4.5	13.3	8.3	
Palmitoleic	C ₁₆	1 at C ₉					0.8		0.5
Stearic	C ₁₈	NONE	1.2	2.9	2.4	6.3	2.5	3.1	1.4
Arachidic	C ₂₀	NONE	0.9	1.6	0.9	0.3	0.3	2.4	
Behenic	C ₂₂	NONE	0.6	0.4				3.1	
Lignoceric	C ₂₄	NONE	0.7						
Hexadecenoic	C ₁₆	1 at C ₈	2.5						
Oleic	C ₁₈	1 at C ₉	15.5	34.0	28.9	26.2	73.0	56.0	7.4
		1 at C ₉							
Ricinoleic	C ₁₈	1 OH at C ₁₂							87.0
Linoleic	C ₁₈	1 at C ₉ ; C ₁₂	11.0	57.5	50.7	14.7	9.0	26.0	3.1
Linolenic		1 at C ₉							
		C ₁₂ ; C ₁₅	7.6		6.9	47.0	0.7		
Eicosenoic	C ₂₀	1 at C ₁₁	3.5						
Erucic	C ₂₂	1 at C ₁₃	52.2						
Others			1.0		0.1	0.1	0.2	1.1	0.6

^aFrom Martinenghi (1963).

fatty acids, but are expected to be soluble in glyceryl esters of fatty acids and their mixtures since the $\Delta\delta$ value is close to $5\text{MPa}^{1/2}$ with the exception of the case of castor oil, where the fullerenes are not expected to be soluble.

In Table 13.2 also another calculation has been considered comparing the total solubility parameters of the solvents and the fullerenes. In the case of fullerenes $\delta_{d, \text{ fullerene}} = \delta_{t, \text{ fullerene}}$ and

$$\Delta\delta_t = [(\delta_{t, \text{ fullerene}} - \delta_{t, \text{ solv}})^2]^{1/2} \quad (13.18)$$

with equation (13.18) it is expected that C_{60} and C_{70} fullerenes are easily soluble both in a series of fatty acids and in a series of glyceryl esters of fatty acids. The prediction made in such a way is confirmed by the experimental evidence, which is shown in Table 13.4. In fact both C_{60} and C_{70} are soluble in a series of different glyceryl esters of fatty acids, but also in molten stearic acid, a free fatty acid (in the latter case it was not possible to determine the solubility).

The last column in the right of Table 13.2 shows $\Delta\delta$ values obtained using equation (13.16) and the published solubility parameters of C_{60} proposed by Hansen and Smith (2004), i.e. $\delta_d(C_{60}) = 19.7\text{MPa}^{1/2}$, $\delta_p(C_{60}) = 2.9\text{MPa}^{1/2}$ and a $\delta_h(C_{60}) = 2.7\text{MPa}^{1/2}$. By substituting these values in equation (13.16) together with the calculated δ_d , δ_p and δ_h values for the glyceryl esters of fatty acids as well as the values for the free fatty acids one obtains $\Delta\delta$ values, which suggest solubility of fullerenes in glyceryl esters of fatty acids since $\Delta\delta < 5$ with the exclusion of castor oil. Additionally, last column in the right of Table 13.2 suggests that fullerenes are not soluble or slightly soluble in free fatty acids. Instead, it has been found experimentally that fullerenes are soluble also in free fatty acids and even in fatty acids amides like behenamide as reported in Table 13.4.

Based on these considerations, it appears that the best calculation approach for the prediction of the solubility of fullerenes in free fatty acids and in fatty acids derivatives is granted by equation (13.18), but simply because we are reasoning a posteriori. It is evident from our calculations that the surprising solubility of fullerenes in free fatty acids and glyceryl esters of fatty acids, or which is the same in vegetable oils, was not easily predictable and expected on the basis of theoretical considerations. Only the intuition of Braun et al. (2007) (see also Cataldo and Braun, 2007) has led to this important discovery, which may have implications and applications in medicine, cosmetics and possibly also in other fields.

13.3.5 Experimental Solubility of C_{60} and C_{70} Fullerenes

The solubility of C_{60} in vegetable oils was initially found very low. For instance, in olive oil a value of 6 mg/l has been reported (Braun et al., 2007). Further work has reported that the solubility of C_{60} in a series of vegetable oils is instead at the level of 100–200 mg/l (Cataldo and Braun, 2007). The differences may be, at least in part, ascribed to the different analytical procedures employed, but certainly they

Table 13.4 Solubility of C₆₀ and C₇₀ in natural glyceryl esters of fatty acids and derivatives

Oil or solvent	C ₆₀ solubility (mg/l)	C ₇₀ solubility (mg/l)	C ₆₀ solubility (mol fract. × 10 ⁴)	C ₇₀ solubility (mol fract. × 10 ⁴)	C ₆₀ solubility (molarity × 10 ³)	C ₇₀ solubility (molarity × 10 ³)	δ (MPa) ^{1/2}
Olive	909	1035	12.00	11.71	1.261	1.231	16.9
Castor	392	636	5.36	7.45	0.544	0.756	18.3
Peanut	751	852	10.25	9.97	1.042	1.013	16.1
Brassica ^a	859	1034	12.65	13.05	1.192	1.230	16.9
Sunseed	522	867	6.95	9.89	0.724	1.031	16.7
Soybean	495	<u>753</u>	6.77	8.82	0.687	0.896	16.2
Linseed	365	727	4.87	8.31	0.506	0.865	16.4
Molten cow butter	Soluble	Soluble					
Molten stearic acid	Soluble	Soluble					
Molten behenamide	Soluble	Soluble					
Toluene ^b			4.71	1.8	4.44	1.70	18.2
1,3,5-trimethylbenzene ^b			3.28	2.43	2.36	1.75	18.0
1,2-dichlorobenzene ^b			38.0	40.2	34.2	35.7	20.5
1,3-dichlorobenzene ^b			23.1	25.4	19.2	22.3	20.5
Tetralin ^b			30.1	20.1	22.2	14.6	19.9
N-hexane ^b			0.084	0.02	0.064	0.015	14.9
Dodecane ^b			0.325	0.27	0.143	0.12	16.1
Carbon tetrachloride ^b			0.43	0.14	0.44	0.14	17.8

^aMethyl ester.^bFrom Korobov and Smith (2000).

are due to the different conditions employed in the preparation of the solutions. For instance, Braun et al. (2007) stirred the fullerene/oil mixture (about 15 mg in 5 ml of oil) for 72 hours at room temperature and then determined the solubility by liquid chromatography. On the other hand, Cataldo and Braun (2007) stirred the fullerene/oil mixture (30 mg in 50 ml of oil) for a shorter time (2 hours) but at a much higher temperature (75°C). The solubility determination was made at room temperature on the cooled solution and found two orders of magnitude higher than that originally reported by Braun (2007). It turned out, however, that heating a vegetable oil with C₆₀ fullerene causes a reaction between the solute and the solvent. Spectrophotometric evidences have already been published about the reactivity of fatty acid esters with C₆₀ (Cataldo and Braun, 2007). Therefore, in the present work, the C₆₀ fullerene solubility has been redetermined in a more rigorous procedure and also the C₇₀ solubility has been determined for the first time: the data are reported in Table 13.4. In each determination about 40 mg of C₆₀ or C₇₀ fullerenes was mechanically stirred for 3 days at room temperature with about 15 g of oil. After settling and filtration, the solubility was determined spectrophotometrically and found to be about 4.5 times the values reported previously for C₆₀ (Cataldo and Braun, 2007). As shown in Table 13.4, if the solubility of C₆₀ and C₇₀ is expressed in terms of mol fraction ($\times 10^4$) or in terms of molarity ($\times 10^3$), then one discovers that the solubility level of these molecules in the triglycerides of fatty acids is comparable or even better to the solubility in some good solvents like toluene and trimethylbenzene, but still considerably lower than the fullerenes solubility in certain chlorobenzene derivatives. In any case such result comes as a complete surprise. One thing is to predict the solubility level with the solubility parameter; another matter is to have found unexpectedly high solubility levels for fullerenes in fatty acids esters.

Previously (Cataldo and Braun, 2007), it has been noted the interesting correlation between C₆₀ fullerene solubility and the unsaturation level of the fatty acids present in the vegetable oils and measured by the “iodine number”, an analytical test, which determines the number of double bonds present in the oil by the addition of iodine (Martinenghi, 1963). This correlation is confirmed for C₆₀ also with the new measurements and is extendable also to C₇₀. The correlation is shown in Fig. 13.1 and suggests that the solubility S expressed in milligrams per litre (mg/l) is linked to the iodine number of the oil (NI) according to the following equations:

$$S_{C_{60}} = -5.46(\text{NI}) + 1307 \quad (13.19)$$

and

$$S_{C_{70}} = -2.85(\text{NI}) + 1221 \quad (13.20)$$

These equations suggest that C₆₀ is more sensitive to the degree of unsaturation of the oil employed as solvent than C₇₀. Additionally, a limiting solubility value for the fully saturated triglycerides (those with NI = 0) can be predicted from equations

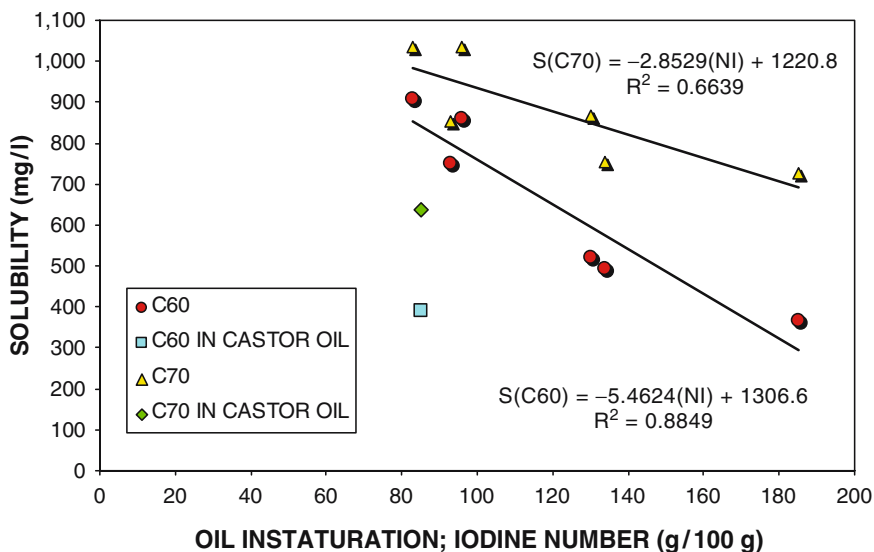


Fig. 13.1 The solubility of C_{60} and C_{70} fullerene is maximum in vegetable oils with lower level of unsaturation (i.e. number of double bonds) and decreases as the insaturation level grows. Having a peculiar chemical structure, castor oil cannot be included in the correlation rule (*See Color Plates*)

(3.19) and (13.20) to be $\approx 1,300$ mg/l for both fullerenes. In fact, as shown in Table 13.4, both C_{60} and C_{70} fullerenes have been found to be easily soluble also in molten cow butter, a largely saturated mixtures of triglycerides with iodine number between 25 and 35 g/100g. Furthermore, C_{60} and C_{70} are easily soluble also in molten stearic acid, a C_{16} free fatty acid (not a triglyceride) having NI = 0. Similarly, an easy solubility of C_{60} and C_{70} was observed in molten behenamide, a fully saturated fatty acid with 22 carbon atoms in the chain whose terminal carboxyl group has been converted into an amide group.

At first glance the relationship between fullerene solubility and fatty acids unsaturation may appear as a surprise. However, it should be noticed that the unsaturation level of vegetable oils correlates also with their refractive index (Martinenghi, 1963). Thus, following the approach of Sivaraman et al. (1994), it is possible to show the change in solubility as function of the polarizability parameter of the solvent defined as:

$$P_p = [(n^2 - 1)/(n^2 + 2)] \quad (13.21)$$

Thus, by plotting the log of the fullerene molar fraction $\times 10^7$ ($\text{Log } \chi$) against the polarizability parameter of the various oils one obtains a reasonable linear correlation, which shows the same trend of the unsaturation level. Such a graph is shown in Fig. 13.2 and suggests that the fullerene molar fraction decreases by increasing the polarizability parameter.

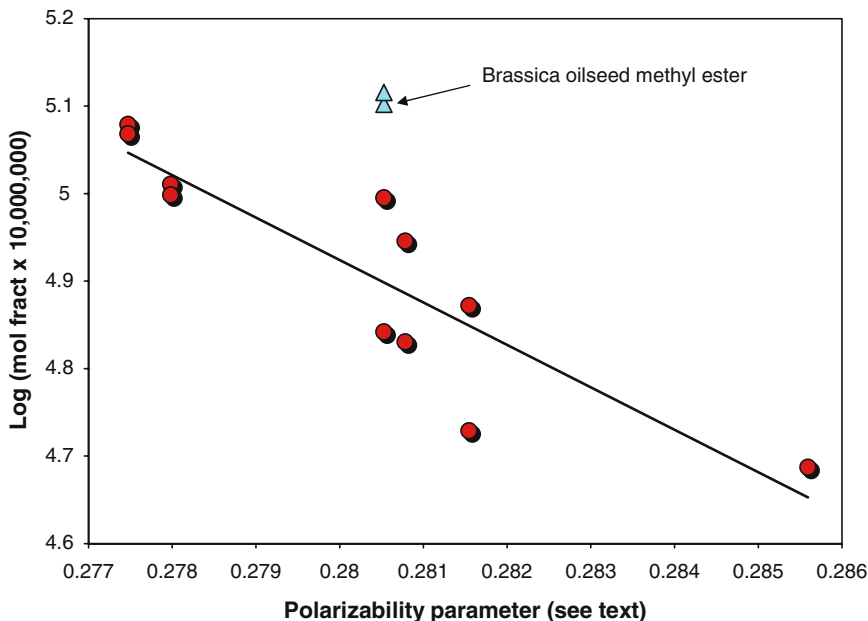


Fig. 13.2 Variation of Log (Mole Fraction $\times 10^7$) with the polarizability parameter $P_p = [(n^2 - 1)/(n^2 + 2)]$ for both C_{60} and C_{70} in various triglycerides of fatty acids. The triangles refer to C_{60} and C_{70} dissolved in methyl ester of brassica oilseed (See Color Plates)

13.3.6 Stability of the C_{60} and C_{70} Fullerenes Solutions in Vegetable Oils

When C_{60} fullerene is dissolved in vegetable oils, its electronic absorption spectra show a new absorption band, which is not present in the spectrum of pristine fullerene in other solvents (see Fig. 13.3). The new band appears at 435 nm almost in all fatty acid esters tested as solvents (Cataldo and Braun, 2007). Curiously, the intensity of this band at 435 nm depends just on the unsaturation level of the fatty acids present in the ester, being more intense in oils with higher unsaturation and hence higher iodine number (in decreasing order: linseed > sunflower ~ soybean) and is much less intense with oils having lower iodine number such as olive oil and biodiesel. The explanation of such behaviour is based on the fact that the addition is favoured by fatty acids with at least two double bonds or more in their chains. In other words, olive oil and brassica oilseed have only 10% content of linoleic acid (see Table 13.3) while the other oils, which instead display a stronger band at 435 nm have all a high levels of linoleic acid and linseed oil has also a high level of linolenic acid with three double bonds. The addition may require the presence of at least two double bonds since it is assumed to be a Diels-Alder type addition reaction. Although the double bonds of linoleic and linolenic acids are not conjugated, moderate thermal processing in the presence of catalysts or the action of light can

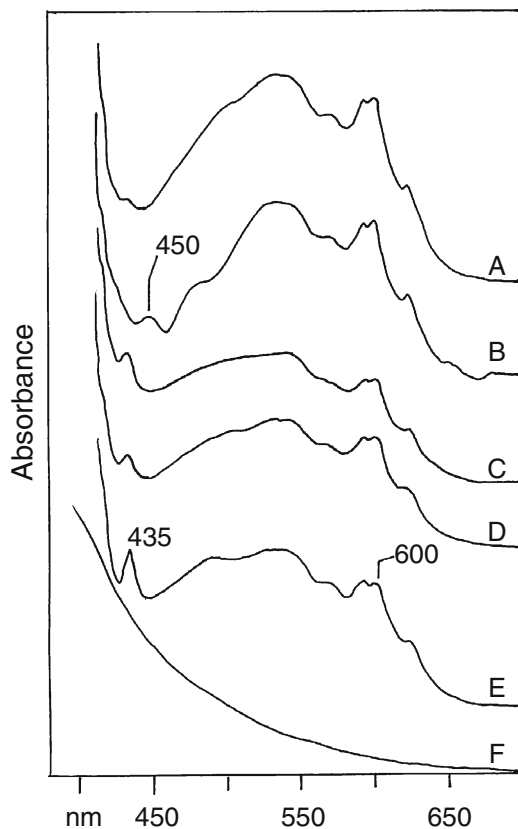
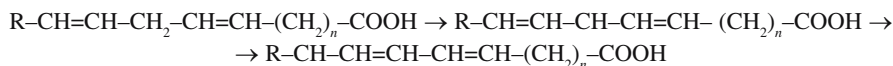


Fig. 13.3 Electronic absorption spectra of C_{60} fullerene dissolved in: (A) brassica oilseeds methyl ester (biodiesel); (B) olive oil; (C) sunflower oil; (D) soybean oil; (E) linseed oil; (F) linseed oil and C_{60} fullerene after heating at 150°C for 15 minutes

cause the slippage of the double bonds to a conjugated position. Fullerenes are highly prone to undergo the Diels-Alder addition reactions where they act essentially as dienophile rather than as dienes (Taylor, 1999).

Additionally, it should be observed that the thermal oxidability and oxidative polymerization of the unsaturated fatty acids follows the trend linolenic > linoleic > oleic >> palmitoleic (Martinenghi, 1963). The oxidation involves, as first step, the abstraction of a hydrogen atom in allylic position to the double bonds. Certainly, this process is favoured in the case of fatty acids with two or more unconjugated double bonds where the formation of a free radical by allylic hydrogen abstraction leads quite necessarily to double bonds slippage with formation of conjugated double bonds:



Thus, the addition of fullerenes to the fatty chains cannot be exclusively through a Diels-Alder mechanism, but involves also a radical mechanism.

The new absorption band at 435 nm in the C_{60} spectrum has been attributed to the 1,2 addition to the fullerene cage to the fatty acid chains either across to the double bonds by a Diels-Alder addition or, more simply, by radical addition (Cataldo and Braun, 2007). Thus, fatty acid esters are able to not only dissolve C_{60} , but also react with this molecule causing the addition of the fatty chain to the fullerene cage. In fact, the bands at 435 nm shown in Fig. 13.3 appear only when C_{60} is stirred at 75°C for a couple of hours in the esters of fatty acids. Only for olive oil the new band appears much weaker than in the other cases and displaced at 450 nm (Fig. 13.3B). Since this oil contains chlorophyll, the displacement may be probably due also to a charge-transfer interaction between C_{60} and chlorophyll or with other impurities.

On standing in air, at room temperature the C_{60} fullerene solutions in vegetable oils are not stable, but change their colour from violet to reddish. The electronic absorption spectra show a gradual increase in the absorption band in the visible initially in the range between 450 and 550 nm. Similar results are obtained both by heating the solutions in air or under nitrogen. In the latter case prolonged heating is needed to achieve the same results. Heating C_{60} solutions in linseed or other oils for 15 minutes at 150°C (in air) causes the entire spectrum of C_{60} in the visible to disappear completely as shown in Fig. 13.3F.

Contrary to C_{60} , C_{70} solutions in vegetable oils prepared at room temperature do not display any new absorption band in their visible spectra and show also a better stability than C_{60} solutions. In fact, after 1 week in air a diluted solution of C_{70} in methyl ester of brassica oilseed shows only slight spectral changes: essentially a reduction in the intensity of the band originally located at 469 nm, which after “ageing” appears at about 467 nm and a less-pronounced reduction in the intensity of the band at 379 nm. In any case, these changes should be interpreted in terms of slower reaction of C_{70} with the solvent oil. Heating C_{70} solutions in sunseed or linseed oil at 160°C for 1–2 hours under argon flow causes profound changes in the visible part of the electronic absorption spectra: the band originally located at 469 nm disappears completely in linseed oil solution or is reduced dramatically in intensity and shifted to shorter wavelengths in the case of sunseed oil solution. A brown colour develops in both cases from the original reddish colour. It is evident that also C_{70} reacts with the fatty acid chains of the solvent as in the case of C_{60} , although the reaction appears slower and seems to require longer times or slightly more drastic conditions.

The stability of C_{60} and C_{70} solutions in vegetable oils has been examined also towards the action of UV light. A C_{60} solution in linseed oil has been irradiated in a quartz reactor with UV light from a 12 W low-pressure Hg lamp having its main emission at 254 nm under N_2 . In less than 1 hour irradiation, all the visible part of the electronic spectrum of C_{60} with bands at about 530 and 600 nm have been bleached. Simultaneously, a growth in absorption intensity as function of the irradiation time has been observed at about 410 nm.

Irradiation of C_{70} solution in peanut oil under the same conditions just described for C_{60} fullerene in linseed oil after 70 minutes of irradiation causes the partial reduction of the intensity of the band at 464 nm and of a shoulder at 398 nm.

The spectral changes undergone by C_{60} and C_{70} solutions in vegetable oils appear very similar to those observed by thermal processing. Therefore, the interpretation is the same: grafting of fullerene molecule onto fatty acid chains.

13.3.7 Potential Application of Vegetable Oils as Vehicle for Drug Delivery of Fullerenes and Fullerene Derivatives

The solubility of C_{60} and C_{70} fullerenes in vegetable oils will permit to employ these molecules for topical use in creams, lotions and ointments, which are adsorbed by skin. Vegetable oils, especially olive oil, are considered excellent excipients for injectable preparation where the active principle is soluble in fats. Their absorption in the subcutaneous tissues is slow and limited and ensures a gradual release of the active principle (Adami, 1960).

The C_{60} and C_{70} reactivity with the vegetable oils at first glance could appear as an obstacle in the use of fullerene solutions in vegetable oils. Apart from the fact that one could use fully saturated fatty acids derivatives as vehicle for fullerenes delivery, which are not reactive with them, the formation of adducts between the unsaturated fatty acids and fullerenes could be exploited not only in the stabilization of the systems fullerenes–vegetable oils, but also in the alteration and, may be in the attenuation of the fullerene reactivity in *in vivo* and in a very gradual release of the fullerenes–fatty acids derivatives in living systems.

13.4 Conclusions

We have confirmed from the earlier observations (Braun et al., 2007; Cataldo and Braun, 2007) that C_{60} fullerene is soluble in vegetable oils, which are glycerol esters of fatty acids. The solubility levels in a series of vegetable oils have been determined and revised in comparison with earlier determinations. For the first time the solubility of C_{70} fullerene have been determined in vegetable oils and found comparable to those found for C_{60} . According to the most recent determinations the solubility of C_{60} and C_{70} in fatty acid esters expressed in molarity or in mole fractions are even higher than the fullerene solubility in common solvent like toluene (Table 13.4). It has been confirmed that the solubility of both C_{60} and C_{70} fullerene is affected by the unsaturation level of the fatty acids composing the vegetable oils. Higher solubility being observed in most saturated oils (Fig. 13.1). The fullerenes solubility appears also related to the polarizability parameters of the vegetable oils: lower values of the polarizability parameters imply higher solubility values (Fig. 13.2).

A theoretical justification of the surprising solubility of C_{60} and C_{70} fullerenes in vegetable oils has been proposed in terms of solubility parameter of fullerenes and vegetable oils. It has been shown that the solubility parameter of C_{60} and C_{70} fullerenes can be calculated by a group increment approach following Van Krevelen

(1990). The calculated solubility parameter derived from the Van Krevelen approach has been compared with the experimental solubility parameters of C_{60} and C_{70} reported in the literature and derived experimentally. An excellent agreement has been found between the calculated and the experimental δ_d values. A comparison with the calculated solubility parameter of the vegetable oils, under certain conditions, permits to show that a good solubility of fullerenes in glycerol esters of fatty acids can be expected. Fullerene solubility in molten free fatty acids can be predicted on the basis of solubility parameters comparison and it has been verified by dissolving C_{60} and C_{70} in molten fatty acids.

It has also been found a certain level of reactivity between C_{60} and C_{70} with the unsaturated fatty acids. The electronic absorption spectra show evidences that C_{60} or C_{70} are grafted onto the fatty chains when the fullerene solutions in vegetable oils are left for days in air, by heating the solutions under N_2 , Ar and air, or by UV irradiation of the solutions in inert atmosphere.

In any case the discovery of the solubility of C_{60} and C_{70} in vegetable oils paves the way in the utilization of these molecules in biology, biochemistry and medicinal chemistry, since the vegetable oils can be used as vehicles of excipients of fullerenes. The formation of adducts between fullerenes and vegetable oils appears as a further opportunity to be exploited in the application of such derivatives in medicinal chemistry.

References

- Adami E (1960) *Pharmacology and Pharmacotherapy*. Istituto Editoriale Cisalpino, Milan, p. 1124.
- Beck MT, Mandi G (1997) Solubility of C_{60} . *Fullerene Sci. Technol.* 4:509–515.
- Beckhaus HD, Verevkin S, Ruchardt C, Diederich F, Thilgen C, ter Meer HU, Mohn H, Muller W (1994) C_{70} is more stable than C_{60} : experimental determination of the heat of formation of C_{70} . *Angew. Chem. Int. Ed. Engl.* 33:996–998.
- Bicerano J (1996) *Prediction of Polymer Properties*, 2nd ed. Marcel Dekker, New York.
- Braun T, Mark L, Ohmacht R, Sharma U (2007) Olive oil as biocompatible solvent for pristine C_{60} . *Fullerenes Nanotechnol. Carbon Nanostruct.* 15:311–314.
- Braun T, Buvári-Barcza A, Barcza L, Konkoly-Thege I, Fodor M, Migali B (1994) Mechanochemistry: a novel approach to the synthesis of fullerene compounds. Water soluble Buckminster fullerene - gamma- cyclodextrin inclusion complexes via solid-solid reaction. *Solid State Chem.* 74:47–51.
- Catalan JS, Laynez JL, Jagerovic N, Elguero J (1995) The colors of C_{60} solutions. *Angew. Chem. Int. Ed. Engl.* 34:105–107.
- Cataldo F, Braun T (2007) Solubility of C_{60} fullerene in long chain fatty acid esters. *Fullerenes Nanot. Carbon Nanostruct.* 15:331–339.
- Cataldo F (2002) Encapsulation of C_{60} fullerene in γ -cyclodextrine. *Polym. Degrad. Stabil.* 77:111–120.
- Dugan LL, Lovett E, Cuddihy S, Ma BW, Lin TS, Choi DW (2000) Carboxyfullerenes as neuro-protective antioxidants. Chapter 11 in *Fullerenes: Chemistry, Physics and Technology*, edited by Kadish K.M. and Ruoff, R.S. Wiley-Interscience, New York.
- Guanti G, Banfi L, Basso A, Riva R (2005) From natural to rationally designed artificial enediynes: towards new anticancer antibiotics activable at will. Chapter 19 in *Polyynes: Synthesis,*

- Properties and Applications, edited by Cataldo, F. Taylor & Francis/CRC Press, Boca Raton, FL.
- Hansen CM, Smith AL (2004) Using Hansen solubility parameters to correlate solubility of C_{60} fullerene in organic solvents and in polymers. *Carbon* 42:1591–1597.
- Hansen CM (2007) *Hansen Solubility Parameters: A User's Handbook*. CRC press/Taylor & Francis, Boca Raton, FL.
- Heymann D (1996a) Solubility of fullerenes C_{60} and C_{70} in seven n-alcohols and their deduced solubility in water. *Fullerene Sci. Technol.* 5:291–310.
- Heymann D (1996b) Solubility of C_{60} in alcohols and alkanes. *Carbon* 34:627–631.
- Hildebrand JH, Scott RL (1950) *The Solubility of Non-Electrolytes*. Reinhold, New York.
- Huang JC (2005) Multiparameter solubility model of fullerene C_{60} . *Fluid Phase Equil.* 237:186–192.
- Korobov MV, Smith AL (2000) Solubility of the fullerenes. In: Kadish KM, Ruoff RS (eds.) *Fullerenes: Chemistry, Physics and Technology*. Wiley-Interscience, New York.
- Liu H, Tao G, Evans DG, Kou Y (2005) Solubility of C_{60} in ionic liquids. *Carbon* 43:1782–1785.
- Makitra RG, Pristanskii RE, Flyunt RI (2003) Solvent effects on the solubility of C_{60} fullerene. *Russ. J. General Chem.* 73:1227–1232.
- Marcus Y, Smith AL, Korobov MV, Mirakyan AL, Avramenko NV, Stukalin EB (2001) Solubility of C_{60} fullerene. *J. Phys. Chem. B* 105:2499–2506.
- Martinenghi GB (1963) *Tecnologia Chimica Industriale degli Oli Grassi e Derivati*, 3rd ed. Ulrico Hoepli, Milan (in italian).
- Murthy CN, Geckeler KE (2001) Solubility correlation of C_{60} fullerene in different solvents. *Fullerenes Nanotechnol. Carbon Nanostruct.* 9:477–486.
- Ruoff RS, Tse DS, Malhotra R, Lorents DC (1993) Solubility of C_{60} in a variety of solvents. *J. Phys. Chem.* 97:3379–3383.
- Sayes CM, Gobin AM, Ausman KD, Mendez J, West JL, Colvin VL (2005) Nano- C_{60} cytotoxicity is due to lipid peroxidation. *Biomaterials* 26:7587–7595.
- Sivaraman N, Dhamodaran R, Kaliappan I, Srinivasan TG, Vasudeva Rao PR, Mathews CK (1994) Solubility of C_{70} in organic solvents. *Fullerene Sci. Technol.* 2:233–246.
- Sivaraman N, Srinivasan TG, Vasudeva Rao PR, Natarajan R (2001) QSPR modelling for solubility of fullerene (C_{60}) in organic solvents. *J. Chem. Inf. Comput. Sci.* 41:1067–1074.
- Tabata Y, Murakami Y, Ikada Y (1997) Antitumor effect of poly(ethylene glycol)-modified fullerene. *Fullerene Sci. Technol.* 5:989–1007.
- Taylor R (1999) *Lecture Notes on Fullerene Chemistry. A Handbook for Chemists*. Imperial College Press, London.
- Van Krevelen DW (1990) *Properties of Polymers. Their correlation with chemical structure, their numerical estimation and prediction from additive group contributions*, 3rd ed. Elsevier, Amsterdam.
- Wilson SR (2000) Biological aspects of fullerenes. Chapter 10 in *Fullerenes: Chemistry, Physics and Technology*, edited by Kadish K.M. and Ruoff, R.S. Wiley-Interscience, New York.

Chapter 14

New Approach to QSPR Modeling of Fullerene C₆₀ Solubility in Organic Solvents: An Application of SMILES-Based Optimal Descriptors

A.A. Toropov^{1*}, B.F. Rasulev¹, D. Leszczynska², and J. Leszczynski¹

Abstract Optimal descriptors, calculated with simplified molecular input line entry system (SMILES), have been used for modeling solubility of fullerene C₆₀ in organic solvents. Local and global attributes of the SMILES have been involved in the modeling algorithm. Local attributes represent symbols, which are images of chemical elements (“O”, “N”, “Cl”, “Br”, etc) or chemical environment (double bonds, i.e., the “=”; triple bonds, i.e., “#”, etc.) Global SMILES attributes are expressed as number of a given chemical element in given SMILES as well as superposition of chemical elements (for instance, SMILES contains both “Cl” and “Br”). Statistical characteristics of the derived model are given by $n = 92$, $r^2 = 0.8865$, $q^2 = 0.8807$, $s = 0.363$, $F = 703$ (training set); and $n = 30$, $r^2 = 0.9069$, $q^2 = 0.8932$, $s = 0.399$, $F = 273$ (test set).

Keywords Optimal descriptor, QSPR, SMILES, Solubility fullerene C₆₀

14.1 Introduction

Many areas of computational chemistry are gaining permanent place as dependable research techniques by providing reliable descriptions of structures and properties of chemical compounds. Due to improvements of hardware and accessibility of many commercial programs a theoretical study supplements experimental investigations and provides new accurate data when experiments are not available. Such

¹Computational Center for Molecular Structure and Interactions, Department of Chemistry

²Department of Civil and Environmental Engineering, Jackson State University, 1400 J. R. Lynch Street, P.O. Box 17910, Jackson, MS 39217, USA

*Correspondence to: Email: aatoropov@yahoo.com

progress is especially important for new areas (nanotechnology), where commercial applications in many cases precede basic research on structures and properties of new species.

Among many theoretical approaches, the quantitative structure–property/activity relationships (QSPR/QSAR) methods in conjunction with experimental data pave the way to characterization of properties of new compounds. Properly calibrated such methods provide tools for the prediction of physicochemical parameters (QSPR) and/or biological activity (QSAR) for substances, which have not been yet examined in experiments (Wiener, 1947a, b, 1948a, b; Randic and Basak, 1999, 2001; Randic and Pompe, 2001a, b; Basak et al., 2001).

Taking into account wide utilization of fullerenes in many aspects of nanotechnology (Prylutsky et al., 2003; Colbert and Smalley, 1999; Wood, 2004; Sivaraman et al., 2001; Faulon and Carla, 2003; Faulon et al., 2004; Danauskas and Jurs, 2001; Kiss et al., 2000; Franco et al., 2007) one can see the necessity of development of predictive models for their physicochemical properties. Among such properties is their solubility. Solubility of fullerene is not only an important technological characteristic, but also an ecological characteristic (Franco et al., 2007).

Recently, the QSPR modeling has been examined as an efficient tool for predicting solubility of fullerene C_{60} in organic solvents (Toropov et al., 2007a, b). The simplified molecular input line entry system (SMILES) (Weininger et al., 1988, 1990; Weininger et al., 1989) has been used as elucidation of solvent molecular structure. The above models have been based on optimization of correlation weights of local SMILES attributes. Perspectives of the optimization of correlation weights of global SMILES attributes for predictive QSPR/QSAR modeling have also been studied by Toropov et al., 2005a, b; Toropov and Benfenati, 2007a, b. Applications of the SMILES for QSPR/QSAR analysis have been recently described in Bologna et al. (2005), Olah et al. (2004), Kurup (2003), and Vidal et al. (2005).

It is to be noted that the QSPR/QSAR analysis of nanosubstances based on elucidation of molecular structure by the molecular graph is ambiguous due to a large number of atoms involved in these molecular systems. Under such circumstances the chiral vector can be used as elucidation of structure of the carbon nanotubes (Toropov et al., 2007c). The SMILES-like representation information for nanomaterials is also able to provide reasonable good predictive models (Toropov and Leszczynski, 2006a).

In this chapter, the genesis of SMILES-based descriptors (as well as perspectives of utilization of these characteristics for QSPR/QSAR analyses) is discussed. We concluded that in fact the SMILES-based optimal descriptors are derivatives of the graph-based optimal descriptors. In fact the SMILES-based descriptors are calculated with scheme that is similar to the well-known additive scheme (Zinkevich et al., 2004), but instead of contributions for the molecular fragments (chemical elements, different kinds of cycles, covalent bonds, etc.) contributions for the SMILES fragments (c, C, n, N, Cl, Br, =, #, etc.) are using.

14.2 Flexible Descriptors

Flexible optimal descriptors have been defined as specific modifications of adjacency matrix, by means of utilization of nonzero diagonal elements (Randic and Basak, 1999, 2001; Randic and Pompe, 2001a, b). These nonzero values of matrix elements change vertex degrees and consequently the values of molecular descriptors. As a rule, these modifications are aimed to change topological indices. The values of these diagonal elements must provide minimum standard error of estimation for predictive model (that is based on the flexible descriptor) of property/activity of interest.

14.3 Optimization of Correlation Weights of Local Graph Invariants

In the case of above-mentioned flexible descriptors a variation of contributions for each atom (vertex in molecular graph) takes place. In the case of optimization of correlation weights of local graph invariants (OCWLI), the variations of contributions for each atom together with contributions for each value of vertex degree or extended connectivity (Toropov and Schultz, 2003; Toropov and Roy, 2004; Toropov et al., 2004a) as well as the nearest neighboring codes (Toropov and Toropova, 2004; Toropova and Benfenati, 2004) in the hydrogen-filled molecular graph are examined. The OCWLI based on so-called graph of atomic orbitals has been studied (Toropov et al., 2001, 2005b, 2006b). The graph of atomic orbitals represents an attempt to take into account the structure of chemical elements for QSPR/QSAR analyses. A comparison of the hydrogen-filled molecular graph and the graph of atomic orbitals has shown that the graph of atomic orbitals can improve predictive QSPR/QSAR models (Toropov and Toropov, 2001, 2002; Castro et al., 2004). Optimal descriptor represents a mathematical function of the correlation weights of graph invariants. Numerical values of the correlation weights, which produce as large as possible correlation coefficient values between property/activity of interest and the descriptor can be calculated by Monte Carlo method optimization procedure (Toropov et al., 2004b, c; Toropov and Benfenati, 2006a–c).

14.4 Optimization of Correlation Weights of Local and Global Graph Invariants

Examples of the global graph invariants are represented by the number and size of cycles, and the total number of chemical elements in a molecule. The number of oxygen and/or nitrogen atoms can be (in the first approximation) a measure of

probability of hydrogen bond interactions. By taking into account these global invariants, QSPR/QSAR, one can improve models based on the correlation weights of local and global graph invariant for calculation of the optimal descriptors (Toropov et al., 2004b, c; Toropov and Benfenati 2006a–c).

14.5 Optimization of Local SMILES Attributes

In fact, both molecular graph and SMILES notation have the same aim. The goal of these two approaches is to provide transparent and suitable information for analysis of molecular structures. Thus, optimization of correlation weights of symbols from the SMILES lines can be utilized for QSPR/QSAR modeling similar to optimal descriptors calculated with the molecular graph. This possibility has been examined in a series of studies (Toropov et al., 2005a, b; Toropov and Benfenati 2007a, b). The results of this work have shown that optimization of SMILES attributes can be utilized for predicting property/activity of interest. It is to be noted that for this purpose the SMILES-based modeling should be using not isolated symbols but an attribute of SMILES (in other words, attribute of molecular system that is represented by SMILES). For instance, it is not proper to separate the “Cl” into “C” and “l”.

14.6 Optimization of Local and Global SMILES Attributes

In the discussed methodology a superposition of chemical elements in molecule can modify property/activity of a given substance. Physicochemical and topological aspects of molecular structure can be reflected by special (0,1)-code (Toropov and Benfenati, 2007a). An essence of the code is as follows: first, this code is a sequence of symbols of fixed length; second, each position (number in the sequence) is an indicator of presence (“1”) or absence (“0”) of a given chemical element or a molecular feature, such as the “=”, “#”, etc. By the Monte Carlo method the correlation weights of these codes (global SMILES attributes) can be calculated. An improvement of such a model (based on optimal descriptors) for a training set is assured. However, improvement of such a model for an external test needs verification for each considered case.

14.7 QSPR Modeling of the Fullerene C₆₀ Solubility in Organic Solvents

Recently, we performed theoretical study of solubility of C₆₀ in various solvents (Toropov et al., 2007a). In this study, the extended experimental data on fullerene C₆₀ solubility in organic solvents was taken from Huanxiang et al. (2005).

The solubility is expressed as logarithm of molar fractions $\log(S)$. A recommended partition of the data into training and test sets is also taken from the mentioned paper. Six outliers described in Huanxiang et al. (2005) were removed from the considerations. SMILES notations of organic solvents for this study have been obtained with ACD/ChemSketch software (<http://www.acdlabs.com/>) according to CAS numbers from US National Library of Medicine (<http://toxnet.nlm.nih.gov/>).

Optimal descriptor used for the QSPR modeling of the C₆₀ solubility is expressed as:

$$DCW = \sum CW(A_k) \quad (14.1)$$

where A_k is the local or global SMILES attribute; $CW(A_k)$ is the correlation weight of the SMILES attribute A_k .

Local SMILES attributes were defined according to hierarchy: first, system is attempting to detect attributes of four symbols, i.e., “[N+]” or “[O-]”; second, system is attempting to detect attributes of two symbols, i.e., “Cl” or “Br”; third, all others are attributes of one symbol.

Global SMILES attributes were defined as (% ,0,1,2,3)-code of six symbols: s1, s2, s3, s4, s5, and s6. The first symbol (s1) is “%”. This symbol indicates: this SMILES attribute is global. The s2 is descriptor of a presence of fluorine: “0” means “F” symbol is absent in the SMILES; “1” means there is one “F” symbol; “2” means there are two “F” symbols; finally “3” means that there are three or more “F” symbols in the SMILES; the s3, s4, s5 are the same descriptors for “Cl”, “Br”, and “O”, respectively; the s6 is the descriptor for the “(” symbol in the SMILES. The brackets are tools to reflect the branching of molecular skeleton (Weininger, 1988, 1990; Weininger et al., 1989). Thus, “(” and “)” are indicators of the same phenomenon. These SMILES attributes (i.e., brackets) have common correlation weight.

Having numerical data on the optimal correlation weights, one can calculate DCW for the training and the test sets. Using data on the training set one can derive model for the fullerene C₆₀ solubility:

$$\text{Log}(S) = C0 + C1.DCW \quad (14.2)$$

A verification of predictive ability of the model that is performed with equation (14.2) can be carried out with the external test set.

Statistical characteristics of QSPRs obtained by the SMILES-based descriptors in three runs of the Monte Carlo optimization are presented in Table 14.1. One can see from Table 14.1 that statistical quality of these models is reproduced in all the three runs of optimization.

Numerical data on the correlation weights and numbers of SMILES attributes in the training and test sets are presented in Table 14.2. One can see from Table 14.2 that two SMILES attributes are absent in the training set. Their correlation weights are defined as being equal to zero. In other words, these attributes are removed from the modeling process.

Table 14.1 Statistical characteristics of the models for fullerene C₆₀ solubility for three runs of the Monte Carlo optimization of the correlation weights of SMILES attributes

Probe	Training set ($n = 92$)				Test set ($n = 30$)			
	R^2	Q^2	s	F	R^2	R^2_{pred}	S	F
1	0.8865	0.8807	0.363	703	0.9069	0.8932	0.399	273
2	0.8837	0.8777	0.367	684	0.9025	0.8879	0.406	259
3	0.8858	0.8801	0.364	698	0.8930	0.8765	0.423	234

Table 14.2 Numerical data on correlation weights of local and global SMILES attributes; numbers of the A_k in training (N_{TRN}) and test (N_{TST}) sets

Attributes (A_k)	CW(A_k) in probe 1	CW(A_k) in probe 2	CW(A_k) in probe 3	k	N_{TRN}	N_{TST}
#	-2.6016461	-2.5986056	-3.4862621	1	1	1
(0.2093995	0.1659505	0.0824541	2	94	26
/	-0.0156713	0.0894500	-0.1154285	3	11	1
1	1.0651715	1.0932344	1.4752185	4	106	32
2	0.5263217	0.5945445	0.6906432	5	14	4
3	-1.8784870	-1.7947064	-2.5743374	6	2	0
=	0.3934758	0.2663370	0.6124806	7	18	5
C	0.5148396	0.4520616	0.8413836	8	283	108
Br	2.5620012	2.5158141	3.4159916	9	26	9
Cl	1.7749851	1.5231909	2.2821480	10	43	11
F	0.3656031	1.1929635	0.9542705	11	1	0
I	4.0462834	3.8553666	5.9503702	12	8	2
N	1.1456203	1.0305655	1.7647230	13	7	1
O	0.5493972	0.3248952	-0.3621346	14	11	7
S	0.5408299	0.3253056	1.1709910	15	2	0
\	0.5211589	0.5815902	0.5637991	16	9	1
c	0.8532568	0.7987998	1.2393025	17	250	80
n	-0.1733716	-0.3880977	0.2269415	18	2	0
s	1.8984978	1.6407885	3.2297841	19	2	0
[N+]	-0.1390942	0.5800894	1.0874254	20	2	1
[O-]	1.3032660	0.3409595	-0.4187749	21	2	1
%00000	2.4042403	2.0797108	1.5954503	22	33	9
%00001	1.7803458	1.5333361	1.1540129	23	8	2
%00002	1.6688723	1.4901379	1.4655293	24	3	2
%00003	3.2981562	3.2516798	4.0867204	25	1	0
%00010	1.3236084	1.2053285	1.4736846	26	7	3
%00011	-0.3750841	-0.3428479	-0.5216306	27	2	0
%00021	-0.2289067	-0.0464214	0.8252090	28	1	1
%00022	0.2722272	0.5818007	1.8594682	29	1	0
%00030*	0.0	0.0	0.0	30	0	1
%00100	1.9710013	1.5270429	1.4667766	31	5	2
%00101	0.6897823	0.3601910	0.2221391	32	1	1
%00102	0.9277824	0.7214552	0.8331393	33	1	0
%00200	2.5816923	2.0488264	2.6446995	34	3	3
%00201	0.9004507	0.5330969	0.6883955	35	2	0
%00301	2.8261014	2.4023359	3.6643559	36	2	0
%01000	2.1427273	1.9170425	1.7340723	37	3	2
%01001	1.2756027	1.1035174	0.9448016	38	3	0

(continued)

Table 14.2 (continued)

Attributes (A _k)	CW(A _k) in probe 1	CW(A _k) in probe 2	CW(A _k) in probe 3	<i>k</i>	N _{TRN}	N _{TST}
%01002*	0.0	0.0	0.0	39	0	1
%01100	3.0662712	2.7154404	3.4031325	40	2	0
%01101	0.0948678	-0.0325986	-0.2831004	41	1	0
%02000	2.5561431	2.4553739	2.7232887	42	4	0
%02001	1.1844248	1.2290197	1.0468828	43	1	1
%03001	2.0000821	2.2683842	2.4175066	44	1	2
%03002	0.1732203	0.5569948	0.5184356	45	6	0
%10000	1.3312122	0.0645285	0.1598626	46	1	0

*Attributes which are absent in the training set. Their correlation weights are zero.

Table 14.3 An example of the DCW calculation with equation (14.1). SMILES = 'CC = 1CCCCC = 1'; CAS = 591-49-1 DCW = 8.9254121

A _k	CW(A _k) in run 1	<i>k</i>
C	0.5148396	8
C	0.5148396	8
=	0.3934758	7
1	1.0651715	4
C	0.5148396	8
=	0.3934758	7
1	1.0651715	4
%00000	2.4042403	22

An example of calculation of the DCW with correlation weights obtained in the first run of the Monte Carlo optimization is shown in Table 14.3.

Experimental values of the fullerene C₆₀ solubility, values of the DCW for organic solvents under consideration, and the details of partition of the data into the training and test sets are shown in Table 14.4. The considered model is displayed in Figs.14.1 and 14.2, for training and test sets, respectively. The model of the fullerene C₆₀ solubility obtained in the first run of the Monte Carlo method optimization is as follows:

$$\text{Log}(S) = -7.2375(-0.0166) + 0.3492(-0.0016) \text{ DCW} \quad (14.3)$$

$$n = 92, r^2 = 0.8865, q^2 = 0.8807, s = 0.363, F = 703(\text{training set})$$

$$n = 30, r^2 = 0.9069, q^2 = 0.8932, s = 0.399, F = 273(\text{test set})$$

Statistical characteristics of six-parameter model from Ref. 37 are described by the following parameters: $n = 122, r^2 = 0.892, s = 0.366, F = 159$.

Table 14.4 Experimental and calculated values of the fullerene C₆₀ solubility (run 1 of the Monte Carlo optimization)

CAS No	Structure	DCW	Expr	Calc	Expr-Calc
Training set (<i>n</i> = 92)					
109-66-0	CCCCC	4.9784383	-6.1	-5.499	-0.601
110-54-3	CCCCCCC	5.4932779	-5.1	-5.319	0.219
111-65-9	CCCCCCCC	6.5229571	-5.2	-4.960	-0.240
26635-64-3	CC(C)CCCCC	6.3178616	-5.2	-5.031	-0.169
124-18-5	CCCCCCCCCCC	7.5526363	-4.7	-4.600	-0.100
112-40-3	CCCCCCCCCCCC	8.5823155	-3.5	-4.241	0.741
493-01-6	C1CCC2CCCCC2C1	10.7356227	-3.3	-3.489	0.189
493-02-7	C1CCC2CCCCC2C1	10.7356227	-3.5	-3.489	-0.011
137-43-9	BrC1CCCC1	9.2375435	-4.2	-4.012	-0.188
542-18-7	ClC1CCCC1	9.1370930	-4.1	-4.047	-0.053
108-85-0	BrC1CCCC1	9.7523831	-3.4	-3.832	0.432
626-62-0	IC1CCCC1	11.6699043	-2.8	-3.162	0.362
5401-62-7	BrC1CCCC1Br	12.9250753	-2.6	-2.724	0.124
110-83-8	C1\C = C/CCC1	8.5225843	-3.8	-4.261	0.461
108-87-2	CC1CCCC1	8.1384605	-4.5	-4.396	-0.104
6876-23-9	CC1CCCC1C	8.6533001	-4.6	-4.216	-0.384
75-09-2	ClCCl	6.6209529	-4.6	-4.925	0.325
56-23-5	ClC(Cl)(Cl)Cl	8.6255983	-4.4	-4.225	-0.175
74-95-3	BrCBr	8.2205343	-4.5	-4.367	-0.133
75-25-2	BrC(Br)Br	11.4457436	-3.2	-3.241	0.041
74-88-4	Cl	6.9653633	-4.2	-4.805	0.605
74-97-5	BrCCl	7.9180971	-4.2	-4.473	0.273
74-96-4	BrCC	5.5626817	-5.2	-5.295	0.095
75-03-6	CCl	7.4802029	-4.5	-4.625	0.125
79-34-5	ClC(Cl)C(Cl)Cl	9.1404379	-3.1	-4.046	0.946
107-06-2	ClCCCl	7.1357925	-5.0	-4.746	-0.254
71-55-6	CC(Cl)(Cl)Cl	7.3654528	-4.7	-4.665	-0.035
540-54-5	CCCCl	5.4622312	-5.6	-5.330	-0.270
107-08-4	CCCl	7.9950425	-4.6	-4.446	-0.154
75-29-6	CC(C)Cl	5.0139056	-5.9	-5.487	-0.413
75-26-3	BrC(C)C	5.2151013	-5.4	-5.416	0.016
75-30-9	CC(C)I	7.7899470	-4.8	-4.517	-0.283
78-87-5	CC(Cl)CCl	6.6977128	-4.9	-4.899	-0.001
142-28-9	ClCCCCl	7.6506321	-4.8	-4.566	-0.234
78-75-1	BrC(C)CBr	7.9877709	-4.3	-4.448	0.148
627-31-6	ICCCl	12.0413259	-3.4	-3.033	-0.367
96-11-7	BrC(CBr)CBr	12.4754228	-2.9	-2.881	-0.019
96-18-4	ClCC(Cl)CCl	9.2883552	-4.0	-3.994	-0.006
513-36-0	CC(C)CCl	5.5287452	-5.4	-5.307	-0.093
513-38-2	CC(C)Cl	8.3047866	-4.3	-4.337	0.037
507-19-7	BrC(C)(C)C	6.3867400	-5.0	-5.007	0.007
540-49-8	Br\C = CBr	10.1711675	-3.7	-3.686	-0.014
127-18-4	Cl/C(Cl) = C/(Cl)Cl	9.5025711	-3.8	-3.919	0.119
513-37-1	C/C(C) = CCl	6.4277086	-4.5	-4.993	0.493
71-43-2	c1ccccc1	9.6541241	-4.0	-3.866	-0.134
95-47-6	Cc1ccccc1C	10.6838033	-2.9	-3.507	0.607
108-38-3	Cc1cccc(C)c1	10.4787078	-3.3	-3.578	0.278
526-73-8	Cc1cccc(C)c1C	10.9935474	-3.1	-3.399	0.299
95-63-6	Cc1cc(C)c(C)cc1	11.3008729	-2.5	-3.291	0.791

(continued)

Table 14.4 (continued)

CAS No	Structure	DCW	Expr	Calc	Expr-Calc
Training set (<i>n</i> = 92)					
108-67-8	Cc1cc(C)cc(C)c1	11.3008729	-3.5	-3.291	-0.209
527-53-7	Cc1cc(C)c(C)c(C)c1	13.8637954	-2.4	-2.396	-0.004
119-64-2	c1ccc2CCCCc2c1	12.7661259	-2.5	-2.780	0.280
103-65-1	CCCc1ccccc1	11.1986429	-3.5	-3.327	-0.173
98-82-8	CC(C)c1ccccc1	10.9935474	-3.6	-3.399	-0.201
104-51-8	CCCCc1ccccc1	11.7134825	-3.4	-3.147	-0.253
98-06-6	CC(C)(C)c1ccccc1	11.8157125	-3.7	-3.111	-0.589
462-06-6	Fe1ccccc1	8.9466991	-4.1	-4.113	0.013
108-90-7	Clc1ccccc1	11.1675962	-3.0	-3.338	0.338
108-86-1	Brc1ccccc1	11.7828863	-3.3	-3.123	-0.177
95-50-1	Clc1ccccc1Cl	13.3559971	-2.4	-2.574	0.174
108-36-1	Brc1cccc(Br)c1	13.6931359	-2.6	-2.456	-0.144
694-80-4	Clc1ccccc1Br	14.6531413	-2.4	-2.121	-0.279
108-37-2	Clc1cc(Br)ccc1	12.1005369	-3.0	-3.012	0.012
120-82-1	Cl/C1 = C/C(Cl)C(Cl)C = C1	13.3374097	-2.8	-2.580	-0.220
100-42-5	C = Cc1ccccc1	11.0772791	-3.2	-3.369	0.169
98-95-3	[O-][N+](=O)c1ccccc1	9.5468209	-3.9	-3.904	0.004
100-47-0	N#Cc1ccccc1	8.7129379	-4.2	-4.195	-0.005
100-66-3	COc1ccccc1	9.6377290	-3.1	-3.872	0.772
100-52-7	O = Cc1ccccc1	10.0312048	-4.2	-3.735	-0.465
103-71-9	O = C = N/c1ccccc1	11.5546296	-3.4	-3.203	-0.197
99-08-1	O = [N+](O-) c1cccc(C)c1	10.9815934	-3.4	-3.403	0.003
108-98-5	Sc1ccccc1	10.1949540	-3.0	-3.677	0.677
100-39-0	BrC1c1ccccc1	12.2977259	-3.1	-2.943	-0.157
30583-33-6	ClC(Cl)(Cl)c1ccccc1	14.1004970	-3.0	-2.314	-0.686
90-12-0	Cc2ccc1c1ccccc12	14.6346343	-2.2	-2.127	-0.073
28804-88-8	Cc1c2ccccc2ccc1C	15.1494739	-2.1	-1.947	-0.153
605-02-7	c1cc(c2ccccc2c1)c3ccccc3	15.2772660	-1.9	-1.903	0.003
64-17-5	CCO	2.9026848	-7.1	-6.224	-0.876
71-36-3	CCCCO	3.9323640	-5.9	-5.864	-0.036
71-41-0	CCCCCO	4.4472036	-5.3	-5.685	0.385
67-64-1	CC(C) = O	2.5311067	-7.0	-6.354	-0.646
68-12-2	CN(C)C = O	3.6767270	-5.3	-5.954	0.654
110-01-0	C1CCCS1	7.1347716	-5.4	-4.746	-0.654
110-02-1	c1cccs1	9.8461083	-4.4	-3.799	-0.601
554-14-3	Cc1cccs1	10.3609479	-3.0	-3.619	0.619
872-50-4	O = C1CCCN1C	8.1166427	-3.9	-4.403	0.503
110-86-1	c1cccn1	8.6274957	-4.0	-4.225	0.225
91-22-5	c1cccc2cccn12	13.0931663	-2.9	-2.665	-0.235
62-53-3	Nc1ccccc1	10.7997444	-3.9	-3.466	-0.434
100-61-8	CNc1ccccc1	11.3145840	-3.8	-3.286	-0.514
121-69-7	CN(C)c1ccccc1	11.6243281	-3.2	-3.178	-0.022
4904-61-4	C1C = C/CCC = C/CC/C = CC1	13.4095487	-2.7	-2.555	-0.145
Test set, <i>n</i> = 30					
629-59-4	CCCCCCCCCCCCC	9.6119947	-4.3	-3.881	-0.419
110-82-7	C1CCCCC1	7.6236209	-5.3	-4.575	-0.725

(continued)

Table 14.4 (continued)

CAS No	Structure	DCW	Expr	Calc	Expr-Calc
Training set ($n = 92$)					
591-49-1	CC = 1CCCCC = 1	8.9254121	-3.8	-4.121	0.321
2207-01-4	CC1CCCCC1C	8.6533001	-4.6	-4.216	-0.384
1678-91-7	CCC1CCCCC1	8.6533001	-4.3	-4.216	-0.084
67-66-3	ClC(Cl)Cl	8.2586760	-4.8	-4.354	-0.446
106-93-4	BrCCBr	8.7353739	-4.2	-4.187	-0.013
106-94-5	BrCCC	6.0775213	-5.2	-5.115	-0.085
109-64-8	BrCCCB	9.2502135	-4.2	-4.007	-0.193
78-77-3	CC(C)CB	5.7299409	-4.9	-5.237	0.337
507-20-0	CC(C)(C)Cl*	4.6719415	-5.7	-5.606	-0.094
558-17-8	CC(C)Cl	8.6121121	-4.4	-4.230	-0.170
79-01-6	Cl/C = C(/Cl)Cl	9.6724790	-3.8	-3.860	0.060
108-88-3	Cc1cccc1	10.1689637	-3.4	-3.686	0.286
106-42-3	Cc1ccc(C)cc1	10.4787078	-3.3	-3.578	0.278
488-23-3	Cc1ccc(C)c(C)c1C	11.8157125	-2.9	-3.111	0.211
100-41-4	CCc1cccc1	10.6838033	-3.4	-3.507	0.107
135-98-8	CCC(C)c1cccc1	11.5083870	-3.6	-3.219	-0.381
591-50-4	Ic1cccc1	13.7004075	-3.5	-2.453	-1.047
541-73-1	Clc1ccc(Cl)c1	12.4030778	-3.4	-2.906	-0.494
583-53-9	Br1cccc1Br	14.9555785	-2.6	-2.015	-0.585
88-72-2	O = [N+](=[O-])c1cccc1C	10.0616605	-3.4	-3.724	0.324
100-44-7	ClCc1cccc1	11.6824358	-3.4	-3.158	-0.242
90-13-1	Clc2ccc1cccc12	15.6332668	-2.0	-1.778	-0.222
2586-62-1	Cc2ccc1cccc1c2Br	16.7633965	-2.1	-1.384	-0.716
71-23-8	CCCO	3.4175244	-6.4	-6.044	-0.356
111-27-3	CCCCCO	4.9620432	-5.1	-5.505	0.405
111-87-5	CCCCCCCCO	5.9917224	-5.0	-5.145	0.145
107-13-1	C = CC#N	2.8862091	-6.4	-6.230	-0.170
111-96-6	COCCOCCO*	4.7372292	-5.2	-5.583	0.383

*SMILES with attributes absent in the training set, these attributes have CW = 0.0.

Different statistical characteristics of the model for the fullerene C_{60} solubility are obtained without of the global SMILES attributes. Their values are as follows: $n = 92$, $R^2 = 0.8613$, $Q^2 = 0.8538$, $s = 0.401$, $F = 559$ (training set); $n = 30$, $R^2 = 0.8900$, $R^2_{\text{pred}} = 0.8742$, $s = 0.436$, $F = 227$ (test set).

It is to be noted that in fact the optimal descriptors examined in the present study are topological characteristics. In other words, no information, except the topology of solvent molecules and experimental values of the fullerene C_{60} solubility, has been used.

In order to gain an understanding of which fragments of the studied solvents contributed significantly to solubility of C_{60} we reviewed the details of all the SMILES attributes. For example, triple bond (symbol - #) is very rare in occurrence in training set (only one time). Thus, this attribute is uninformative, although has large negative contribution to solubility (promoter of solubility lowering). Branching - “(”, is a stable promoter of solubility improvement. A cycle (“1” - one cycle and “2” - two

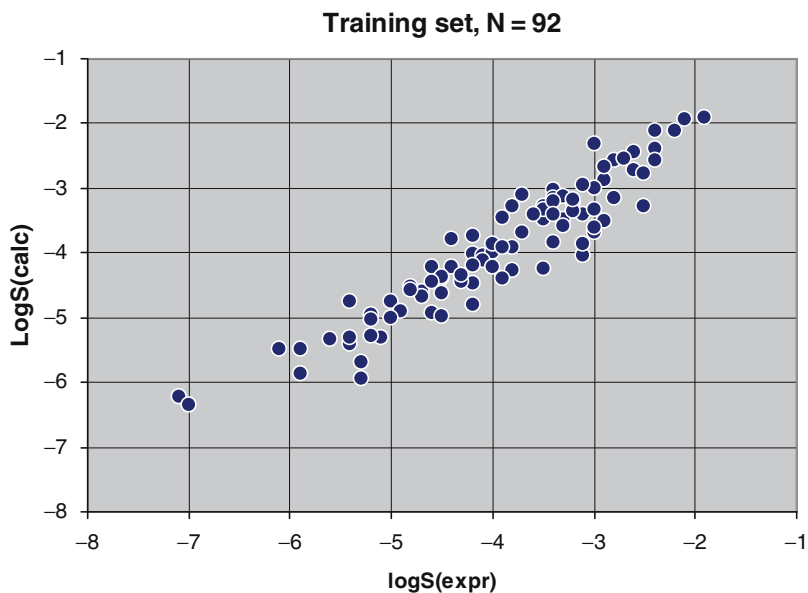


Fig. 14.1 A plot of experimental versus calculated (with equation (14.3)) values of fullerene solubility for the training set

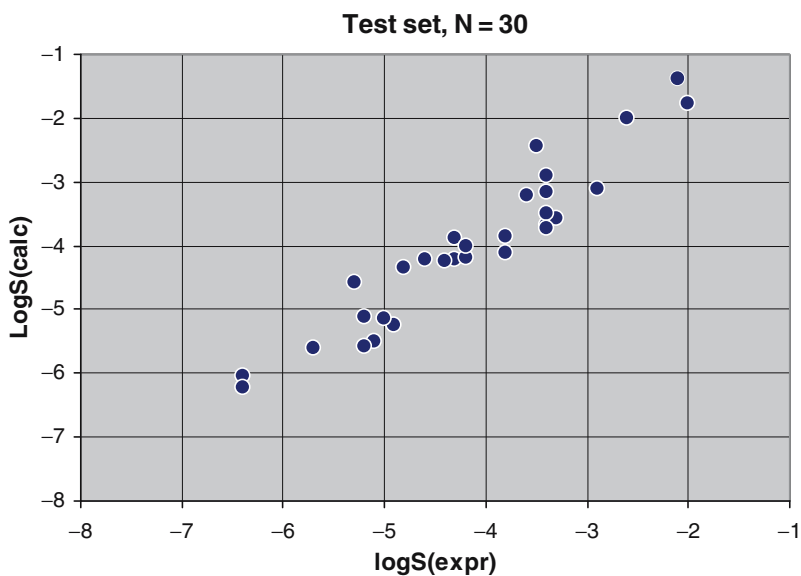


Fig. 14.2 A plot of experimental versus calculated (with equation (14.3)) values of fullerene solubility for the test set

cycles), promotes the solubility improvement, whereas “3” cycles – has negative effect on solubility, but appears only two times in the training set. Double bond – “=”, is a promoter of solubility improvement and its occurrence in the training set is very frequent. Attributes “Br”, “Cl”, “F”, “I”, “O”, “N”, and “S” have the positive contribution to the solubility, i.e., improve solubility, but “N” in sp² hybridization has not clear effect. It has both contributions – positive and negative. In the case of global attributes, global attribute where there are no “F”, “Cl”, “Br”, “O”, and “(” groups – it increases solubility. The presence of only “(” group, branching, also increases solubility. In addition, the presence of “Br” in global attributes promotes solubility. It should be noticed that the value of global attributes needs to be estimated from two points of view. First, a stability of effect (+ or –) and second – number of occurrences in the training set should be considered. From this point of view, the global attribute %03002 (3 and more “Cl” groups and “2” – two branches in skeleton) – has no obvious contribution to solubility. The obtained contributions provide an “unstable” solution that in the some cases increases solubility, but in other cases decreases it.

The above analysis provides better understanding of a complex phenomenon related to solubility of C₆₀ in various organic solvents. We believe that similar dependences are also valid for different types of fullerenes.

14.8 Conclusions

This comprehensive study establishes basis for further modeling of nanomaterials using SMILES-based approach. In particular, we conclude that:

1. SMILES-based optimal descriptors can be utilized as a tool for prediction of the fullerene C₆₀ solubility.
2. Correlation weights of the global SMILES invariants improve statistical quality of the fullerene C₆₀ solubility model for both the training and the test set.

Acknowledgments The authors would like to thanks for support the High Performance Computational Design of Novel Materials (HPCDNM) – Contract #W912HZ-06-C-0057 and the Development of Predictive Techniques for Modeling Properties of NanoMaterials Using New OSPR/ASAR Approach Based on Optimal NanoDescriptors – Contract #W912HZ-06-C-0061 Projects funded by the Department of Defense through the U.S. Army Engineer Research and Development Center, Vicksburg, MS.

References

- Basak SC, Mills DR, Balaban AT, Gute BD (2001) Prediction of mutagenicity of aromatic and heteroaromatic amines from structure: A hierarchical QSAR approach. *J. Chem. Inf. Comput. Sci.* 41: 671–678.
- Bologa C, Allu TK, Olah M, Kappler MA, Opre TI (2005) Descriptor collision and confusion: Toward the design of descriptors to mask chemical structures. *J. Comp-Aid. Mol. Des.* 19: 625–635.

- Castro EA, Toropov AA, Nesterova AI, Nabiev OM (2004) QSPR modeling aqueous solubility of polychlorinated biphenyls by optimization of correlation weights of local and global graph invariants. *CEJC* 2: 500–523.
- Colbert DT, Smalley RE (1999) Fullerene nanotubes for molecular electronics. *Trend. Biotechnol.* 17: 46–50.
- Danauskas SM, Jurs PC (2001) Prediction of C₆₀ solubilities from solvent molecular structures. *J. Chem. Inf. Comput. Sci.* 41: 419–424.
- Faulon J-L, Carla J (2003) Churchwell the signature molecular descriptor. 2. Enumerating molecules from their extended valence sequences. *J. Chem. Inf. Comput. Sci.* 43: 721–734.
- Faulon J-L, Collins MJ, Carr JR (2004) The Signature molecular descriptor. 4. canonizing molecules using extended valence sequences. *J. Chem. Inf. Comput. Sci.* 44: 427–436.
- Franco A, Hansen SF, Olsen SI, Butti L (2007) Limits and prospects of the incremental approach and the European legislation on the management of risks related to nanomaterials. *Regul. Toxicol. Pharm.* 48: 171–183.
- Huanxiang L, Xiaojun Y, Ruisheng Zh, Mancang L, Zhide H, Botao F (2005) Accurate quantitative structure-property relationship model to predict the solubility of C₆₀ in various solvents based on a novel approach using a least-squares support vector machine. *J. Phys. Chem. Sect B.* 109: 20565–20571.
- Kiss IZ, Mandi G, Beck MT (2000) Artificial neural network approach to predict the solubility of C₆₀ in various solvents. *J. Phys. Chem. Sect A* 104: 8081–8088.
- Kurup A (2003) C-QSAR: A database of 18,000 QSARs and associated biological and physical data. *J. Comp-Aid. Mol. Des.* 17: 187–196.
- Olah M, Bologa C, Opre TI (2004) An automated PLS search for biologically relevant QSAR descriptors. *J. Comp-Aid. Mol. Des.* 18: 437–449.
- Prylutsky Yu. I, Yashchuk VM, Kushnir KM, Golub AA, Kudrenko VA, Prylutska SV, Grynyuk II, Buzaneva EV, Scharff P, Braun T, Matyshevska OP (2003) Biophysical studies of fullerene-based composite for bio-nanotechnology. *Mater. Sci. Eng. Sect C* 23: 109–111.
- Randic M, Basak SC (1999) Optimal molecular descriptors based on weighted path numbers. *J. Chem. Inf. Comput. Sci.* 39: 261–266.
- Randic M, Basak, SC (2001) New descriptor for structure-property and structure-activity correlations. *J. Chem. Inf. Comput. Sci.* 41: 650–656.
- Randic M, Pompe M (2001a) The variable connectivity index ${}^1\chi^f$ versus the traditional molecular descriptors: A comparative study of ${}^1\chi^f$ against descriptors of CODESSA. *J. Chem. Inf. Comput. Sci.* 41: 631–638.
- Randic M, Pompe M (2001b) The variable molecular descriptors based on distance related matrices. *J. Chem. Inf. Comput. Sci.* 41: 575–581.
- Sivaraman N, Srinivasan TG, Vasudeva PR (2001) QSPR modeling for solubility of fullerene (C₆₀) in organic solvents. *J. Chem. Inf. Comput. Sci.* 41: 1067–1074.
- Toropov AA, Benfenati E (2004) QSAR modelling of aldehyde toxicity against a protozoan, *Tetrahymena pyriformis* by optimization of correlation weights of nearest neighboring codes. *J. Mol. Struct. (Theochem)* 679: 225–228.
- Toropov AA, Benfenati E (2006a) QSAR models of quail dietary toxicity based on the graph of atomic orbitals. *Bioorg. Med. Chem. Lett.* 16: 1941–1943.
- Toropov AA, Benfenati E (2006b) QSAR models for *Daphnia* toxicity of pesticides based on combinations of topological parameters of molecular structures *Bioorg. Med. Chem.* 14: 2779–2788.
- Toropov AA, Benfenati E (2006c) Correlation weighting of valence shells in QSAR analysis of toxicity. *Bioorg. Med. Chem.* 14: 3923–3928.
- Toropov AA, Benfenati E (2007a) Optimisation of correlation weights of SMILES invariants for modelling oral quail toxicity *Eur. J. Med. Chem.* 42: 606–613.
- Toropov AA, Benfenati E (2007b) SMILES as an alternative to the graph in QSAR modelling of bee toxicity. *Comput. Biol. Chem.* 31: 57–60.
- Toropov AA, Leszczynski J (2006) A new approach to the characterization of nanomaterials: Predicting young's modulus by correlation weighting of nanomaterials codes. *Chem. Phys. Lett.* 433, 29: 125–129.

- Toropov AA, Roy K (2004) QSPR modeling of lipid-water partition coefficient by optimization of correlation weights of local graph invariants. *J. Chem. Inf. Comput. Sci.* 44: 179–186.
- Toropov AA, Schultz TW (2003) Prediction of aquatic toxicity: Use of optimization of correlation weights of local graph invariants. *J. Chem. Inf. Comput. Sci.* 43: 560–567.
- Toropov AA, Toropova AP (2001) Prediction of heteroaromatic amine mutagenicity by means of correlation weighting of atomic orbital graphs of local invariants. *J. Mol. Struct. (Theochem)* 538: 287–293.
- Toropov AA, Toropova AP (2002) QSPR modeling of complex stability by optimization of correlation weights of the hydrogen bond index and the local graph invariants. *Russ. J. Coord. Chem.* 28: 877–880.
- Toropov A, Toropova A (2004) Nearest neighboring code and hydrogen bond index in labeled hydrogen-filled graph and graph of atomic orbitals: Application to model of normal boiling points of haloalkanes. *J. Mol. Struct. (Theochem)* 711: 173–183.
- Toropov AA, Toropova AP, Nesterova AI, Nabiev OM (2004a) Prediction of alkane enthalpies by means of correlation weighting of Morgan extended connectivity in molecular graphs. *Chem. Phys. Lett.* 384: 357–363.
- Toropov AA, Toropova AP, Nesterova AI, Nabiev OM (2004b) QSPR modeling of complex stability by correlation weighing of the topological and chemical invariants of molecular graphs. *Russ. J. Coord. Chem.* 30: 611–617.
- Toropov AA, Kudyshekin VO, Voropaeva NL, Ruban IN, Rashidova S.Sh. (2004c) QSPR modeling of the reactivity parameters of monomers in radical copolymerizations. *J. Struct. Chem.* 45: 945–950.
- Toropov AA, Toropova AP, Mukhamedzhanova D, Gutman I (2005a) Simplified molecular input line entry system (SMILES) as an alternative for constructing quantitative structure-property relationships (QSPR). *Indian J. Chem. Sect. A.* 44: 1545–1552.
- Toropov AA, Toropova AP, Gutman I (2005b) Comparison of QSPR models based on hydrogen-filled graphs and on graphs of atomic orbitals. *Croat. Chem. Acta* 78: 503–509.
- Toropov AA, Leszczynska D, Leszczynski J (2007a) QSPR study on solubility of fullerene C₆₀ in organic solvents using optimal descriptors calculated with SMILES. *Chem. Phys. Lett.* 441: 119–122.
- Toropov AA, Leszczynska D, Leszczynski J (2007b) Predicting water solubility and octanol water partition coefficient for carbon nanotubes based on the chiral vector. *Comp. Biol. Chem.* 31: 127–128.
- Vidal D, Thormann M, Pons M (2005) LINGO, an efficient holographic text based method to calculate biophysical properties and intermolecular similarities. *J. Chem. Inf. Model.* 45: 386–393.
- Weininger D (1988) SMILES, a chemical language and information system. 1. Introduction to methodology and encoding rules. *J. Chem. Inf. Comput. Sci.* 28: 31–36.
- Weininger D (1990) SMILES. 3. DEPICT. Graphical depiction of chemical structures. *J. Chem. Inf. Comput. Sci.* 30: 237–243.
- Weininger D, Weininger A, Weininger L (1989) SMILES. 2. Algorithm for generation of unique SMILES notation. *J. Chem. Inf. Comput. Sci.* 29: 97–101.
- Wood J (2004) C₆₀ boosts performance: *Nanotech. Mat. Today* 7: 12–13.
- Wiener H (1947a) Structural determination of paraffin boiling points. *J. Am. Chem. Soc.* 69: 17–20.
- Wiener H (1947b) Correlation of heats of isomerization, and differences in heats of vaporization of isomers, among the paraffin hydrocarbons. *J. Am. Chem. Soc.* 69: 2636–2638.
- Wiener H (1948a) Relation of the physical properties of the isomeric alkanes to molecular structure. Surface tension, specific dispersion, and critical solution temperature in aniline. *J. Phys. Chem.* 52: 1082–1089.
- Wiener H (1948b) Vapor pressure-temperature relationships among the branched paraffin hydrocarbons. *J. Phys. Chem.* 52: 425–430.
- Zenkevich I, Moeder M, Koeller G, Schrader S (2004) Using new structurally related additive schemes in the precalculation of gas chromatographic retention indices of polychlorinated hydroxybiphenyls on HP-5 stationary phase. *J. Chromatogr. A* 1025: 227–236.

Chapter 15

Functionalized Nanomaterials to Sense Toxins/Pollutant Gases Using Perturbed Microwave Resonant Cavities

Aman Anand^{1*}, J.A. Roberts¹, and J.N. Dahiya²

Abstract This chapter provides an overview of the techniques and methods involving electromagnetic resonators to study the interactions of gas molecules with nanomaterials substrates. A resonant cavity operating in TE_{011} mode was employed by the author(s) to characterize the nature of interactions of a range of weakly polar to nonpolar gas molecules with carbon nanotubes loaded in the cavity. Microwave resonant cavities are special electromagnetic resonators that can have a very high quality factor, which enhances the sensitivity of the apparatus as compared to standard electrical tank circuits. By measuring shifts in the resonant frequency of these circuits and by calculating the pressure broadening of the resonant peaks, the technique developed offers a highly effective means to quantify the amount of foreign agents perturbing these resonant cylinders. By functionalizing the nanomaterials with specific antibodies and loading them as wicks in these cylinders, the technique can be engineered into a very sensitive and unique chemical and biological sensor prototype.

Keywords Carbon nanotubes, chemical and biological sensors, microwave resonance, resonant cavities

15.1 Introduction

Resonant cavities are well-known, highly sensitive devices that have been used to make measurements of fundamental properties of matter in all its phases (Hong, 1974). A resonant cavity can be considered to be multiple inductor capacitor resistance

¹Department of Physics, University of North Texas, Denton, TX 76203, USA

²College of Science and Mathematics, Southeast Missouri State University, Cape Girardeau, MO 63701, USA

*Correspondence to: Email: aman@unt.edu

(LCR) circuits connected in parallel. In this chapter, we present an overview of the study done to quantify the nature of interactions of the gas molecules with the nano-materials that act as loads in these resonant cavities. The microwave spectral response of these cavities containing different gases possessing different indices of refraction provide encyclopedic signatures of interactions of these gases in a complex dielectric medium. The cavities were loaded with different types of materials (carbon-based, silica gel, and cotton fibers). Upon energizing the cavities in their fundamental modes, a non-destructive study was performed to investigate the perturbation response of the load with several different gases. The frequency range of 9.1–9.8 GHz was used in the experiment to study the changes in the dielectric properties of the load due to the gases as well as to quantify the nature of absorption/adsorption of these gases by the nanomaterials loaded in the resonant cavities. The fact that different substrate materials interact differently with select gases enabled the study to provide information on the effect of various forces such as van der Waals (VdW) and other exchange forces that have significant contributions in the interaction behavior of gaseous molecules with the substrates.

15.2 Brief Electromagnetic Theory of Microwave Resonant Cavities

Waveguides and cavities offer an efficient method of transferring electrical energy into special media by varying electromagnetic fields, either in free space or in a contained environment. Extensive experimental, as well as theoretical, studies have been done in the past using various geometries and materials loading electromagnetic devices. Transmission lines, waveguides, and cylindrical and spherical resonators have found many applications in industries today (Harvey, 1963). These devices are highly efficient in storing energies with minimal losses, depending upon the materials used to construct them. Skin depth and Ohmic losses are two major factors in considering the leakage of the fields (Air Force manual Radar Circuit Analysis, 1950). In order to properly design electromagnetic devices solutions of Maxwell's electromagnetic wave equations with appropriate boundary conditions within these devices must be used.

The experiment in this discussion employed a cylindrical resonant cavity, which is formed by closing the ends of a cylindrical waveguide with conducting plates on its ends as shown in Fig. 15.1 (Montgomery, 1947).

A cylindrical microwave resonant cavity can be considered to be N LCR circuits arranged in parallel, where N tends to infinity. The cavity is constructed by $\lambda/4$ sections of such circuits as described in the Air Force manual Radar Circuit Analysis (1950).

In cylindrical resonant cavities there exist Electric (E) and Magnetic (B) fields orthogonal to each other. Eigenvalue solutions of the wave equation subjected to proper boundary conditions are called the modes of resonance and are labeled as either transverse electric (TE_{lmn}) or transverse magnetic (TM_{lmn}). The subscripts l, m, n define the patterns of the fields along the circumference and the axis of the cylinder. Formally, these l, m, n values are the number of full-period variations of E_r

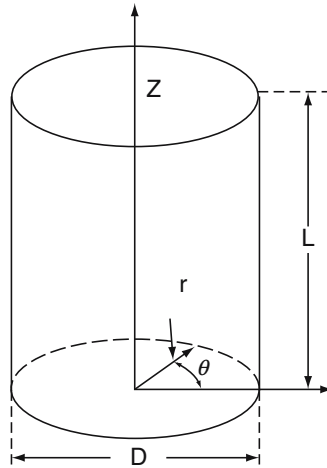


Fig. 15.1 A sketch of a cylindrical geometry coordinate system for a cylindrical resonant cavity. The dimensions are determined by the range of frequencies to be used in the studies

with respect to θ , number of half-period variations of E_θ with respect to r , and number of half-period variations of E_r with respect to the z -axis, respectively (Montgomery, 1947). In this investigation, the cylinder was tuned to oscillate in its fundamental TE_{011} mode. This convention will be used for future references in this work for the purpose of discussions.

The resonant cavities are tuned with a shorting plunger in order to obtain a selective mode frequency. The cylinders were coated with silver in order to minimize losses due to stray fields and other ohmic losses. Very high quality factor of around 20,000 can be obtained. Due to such high quality factors, the resonant devices are very sensitive to perturbation response when loaded with any external medium. Depending upon the permittivity, as well as permeability of the sample, the response of these resonant cavities will have a shift in their resonant frequencies as well as changes in their quality factors. Whenever the samples are loaded in the intense electric field of the cavity, Slater’s perturbation theory (Slater, 1941) states that the shift in the resonant frequencies and change in the Q values of the resonator can then be expressed by Equations (15.1) and (15.2), respectively, as given below

$$\frac{\delta f}{f_r} \approx -\frac{(\epsilon' - 1)}{2} \frac{\int_{\Delta v} \bar{E}^* E^* dV}{\int_V \bar{E}^* E^* dV} \tag{15.1}$$

where δf is the shift from the resonant frequency, ϵ' is the real part of the dielectric constant, Δv is the volume of the sample perturbing the cavity, and dV is the cavity volume, and

$$\Delta\left(\frac{1}{Q}\right) = \varepsilon'' \frac{\int_V \overline{E}^* \overline{E}^* dv}{\int_V \overline{E}^* \overline{E}^* dV} \quad (15.2)$$

where ε'' is the imaginary part of the dielectric constant and Q is the quality factor of the resonator.

The above two equations then tells us that by measuring the amount of shift in the resonant frequency and by quantifying the amount of change in the quality factor of these resonators, it is possible to determine the nature and amount of material loading the cavities. Under no load conditions the resonant frequency is scaled by the dielectric constant of free space/air or vacuum depending upon the pressure conditions of these resonators. It is only when a medium with a dielectric constant (ε') different from free space is introduced within the cavity that the natural resonant frequency gets scaled as defined by equation (15.1). Also, the quality factor, which is a measurable quantity of the imaginary part of the dielectric behavior of the material, is a measure of loss. Hence, the entire concept of measuring any deviation from the unperturbed state of the medium is thus obtained from these two measurable quantities.

15.3 Can We Use This Information to Make Sensor to Detect Toxins?

In order to show how the properties of the cavity can be used to develop a chemical/biological sensor, the nature of sensor needs to be outlined. What is a sensor? In simplistic terms, it is a device that is equipped with proper electronics to quantify changes in a given state of a system. It may be an accelerometer of an automobile, emission gas temperature of a jetliner, environment, bio-metabolism of living bodies, space storms, etc. What is required is a way to detect subtle “**changes**.”

The sensors must determine and quantify these changes and specify the nature of change and transmit or store information in a logical manner for proper counter-measures. An efficient and a reliable detector of a person wearing cologne or perfume is the nose. Can an electronic device be designed to mimic this property?

The natural diffusion of those aromatic compounds and essential oils quickly is detected. What is not observed is the diffusion phenomenon of Brownian motion. The ability to be able to determine which brand of cologne or perfume fragrance is in the immediate environment and how widely it is spread is not easy to be achieved. When a device is able to respond to these fundamental events of change, and is able to signaturize them, the information retrieved is what basically constitutes a sensor response.

Similarly, when the electromagnetic signals that constitute a set of orthogonally coupled Electric (**E**) and Magnetic field (**B**) vectors are introduced inside a geometrical boundary, which in the case in a cylindrical resonant cavity, electro-dynamics comes into the play. Solutions to the Maxwell's equations according to the

appropriate boundary conditions then define the nature of oscillations, resonance, and any impedance losses within these cylinders. By being able to tune these resonant cavities to operate in a specific mode, we are then able to define the natural state of resonance in a particular dominant mode, which can be either electric or magnetic. The experiment described below demonstrates some unique and selective results with the resonant cavities.

15.4 The Experiment

15.4.1 *Experimental Setup and Sensitivity of the Apparatus*

Figure 15.2a shows two tunable cylindrical resonant cavities that were phase-locked to each other for this investigation. These two cavities were maintained under high vacuum conditions in order to avoid any contamination from the environment. In this experimental setup an empirical study was made to observe and characterize the nature of interactions of various gases, both weakly polar as well as nonpolar gases, with the various substrates (S1–S5) as listed in Table 15.1. The two resonant cavities shown in Fig. 15.2a served the purpose of making comparative studies. A cavity containing no load was used as the reference cavity to characterize the nature of perturbation response of only the gas molecules, whereas, on the other hand, the second cavity was loaded with different substrates (S1–S5) progressively and the same gases were cycled through them. Six different experiments were made to characterize the responses of the cavities when gases were cycled through them.

The microwave source used in this study was a microwave network analyzer model IFR 6845 shown in Fig. 15.2b (Microwave network analyzer). Integrated into this single instrument is a synthesized source, a three-input scalar analyzer, and a synthesized spectrum analyzer. Complete engineering details of this equipment is beyond the scope of this document, but the basic function of this instrument is to generate a constant

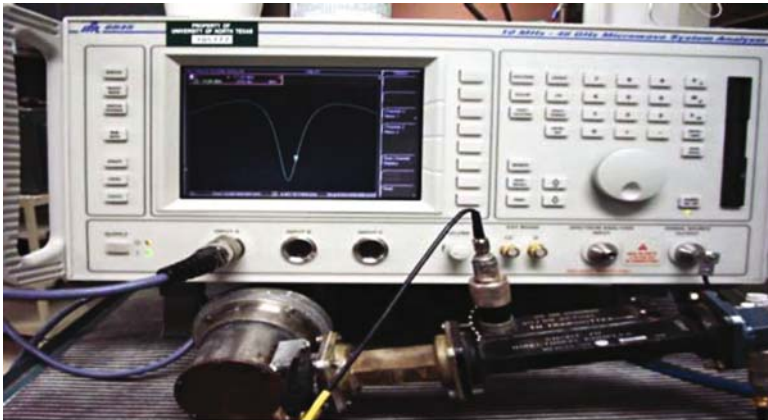
Table 15.1 Various substrates that served as gas absorbers that were loaded in the test cavity shown in Fig. 15.2a

Labeled	Various substrates in amorphous as well as fibrous forms loaded for each experiment	Form/shape/properties
S1	Untreated single-walled carbon nanotubes (SWCNT)	Amorphous powder, chirality (7.5 and 6.5) semiconducting mixed with conducting
S2	Thermally treated nanotubes	Just as S1
S3	Activated charcoal	Granular crystals
S4	Silica gel	Amorphous granules
S5	Cotton fibers	Cotton medical grade



a

Fig. 15.2a Two tunable vacuum tight cylindrical resonant cavities that were phase-locked and their impedance were matched using the impedance tuning coil. The plungers seen on the top were to aid us in tuning these cylinders to resonate in TE_{011} mode (See Color Plates)



b

Fig. 15.2b IFR6845 series microwave network analyzer used as the synthesized source to generate and feed the microwaves into the resonant cavities (See Color Plates)

(CW) output of microwaves capable of sweeping 10 MHz to 47 GHz. Depending upon the physical dimensions of the resonator and their coupling with the source, this spectrum analyzer can operate to detect the microwave absorption profile of the resonator either in the reflection or in the transmission mode. In this work the frequency range

used to sweep the resonator was between 9.1 and 9.8 GHz. The synthesized source has low phase noise and 1 Hz frequency resolution. The crystal detector used to detect the absorption profile usually produces an output current such that the current–voltage characteristic is represented by $I \propto V^2$. The output power can be approximately related to the square of the input power; hence, a small power that is input into the cavity containing some load will produce a relatively large change in the output signal. This engineering principle made it relatively simple to study the effects of both low and high concentrations of gases absorbed onto the substrate.

The test cavity loaded with substrates as labeled below and the reference cavity that was void of any substrate were then completely degassed and a vacuum was maintained around the order of 10^{-5} Torr. During individual experimental runs, fixed pressures of gases (carbon monoxide, carbon dioxide, oxygen, hydrogen, freon-13, fluorine, chlorine, and ammonia) were progressively cycled through the two resonators, and their dielectric response in both test and reference cavities was collected for spectroscopic investigation.

From the response of each substrate it is thus possible to calculate the electric displacement density (\mathbf{D}) due to the polarization of the material when subjected to \mathbf{E} vector.

Even though the presence of a dielectric material in an Electric (\mathbf{E}) field involves phenomenon at the atomic scale, it is possible to represent the overall macroscopic effect from equations (15.1) and (15.3).

$$\begin{aligned} D &= \epsilon_o \left(1 + \frac{P}{\epsilon_o E} \right) E \\ &= \epsilon_o \epsilon_r E \end{aligned} \tag{15.3}$$

where D is the electric displacement and P is the polarization of the material, ϵ_r is the relative dielectric constant of the material whose real and imaginary parts can be found by simply measuring the shift in the frequency and changes in the full width of the profile at half power maximum (full width half maximum [FWHM]) by using equations (15.1) and (15.2), respectively.

Thus, it is shown how experimentally these signature changes in the spectroscopic profile of the medium tell us about the scalability of the resonance with the amount of dielectric material introduced into it.

Hence, by using the above design it is possible to sensitively (parts per million – few parts per billion) detect any changes in the resonators unperturbed response (Fig. 15.3). The remaining task is to find specificity in these changes. These changes can be due to any foreign material; until we are able to specify what material, the sole purpose of the sensor remains half complete. The next phase of the experiment is to find out how to eliminate the role of the vacuum only and to introduce chemical selectivity of the resonator for a specific toxin.

It was found that for different pressures of different gases and different types of nanomaterials, there were different responses in the shifts of the probe signal for each cycle of gassing and degassing of the cavity. This preliminary work suggests

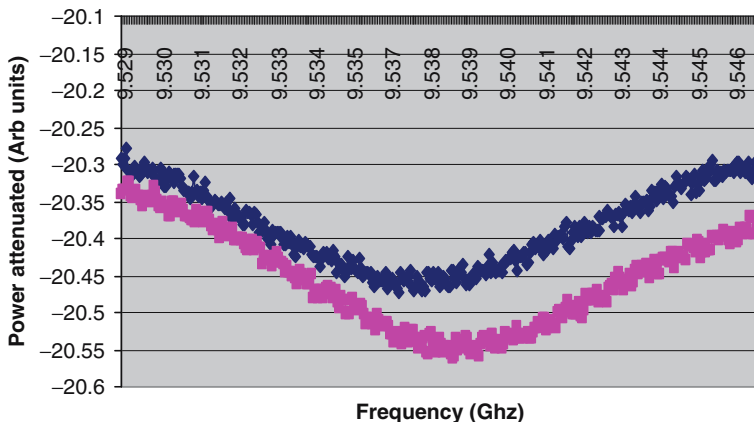


Fig. 15.3 A typical frequency response curve obtained due to the introduction of air into the resonant cavities. Shown above in pink is a typical absorption profile of the resonator under vacuum, and in blue is the shift of the resonant frequency to a lower value upon introducing air into the system (See Color Plates)

that microwave spectroscopy of the complex medium of gases and carbon nanotubes can be used as a highly sensitive technique in studying the complex dielectric response of different polar as well as nonpolar gases when subjected to intense electromagnetic fields within the cavity. In order to introduce the specificity of this prototype, defining the role of carbon nanotubes is imperative. Through experimental runs performed, it was determined that of all the substrates (S1–S5), carbon nanotubes show selective molecular sieving for specific gases. The results of these investigations recorded elsewhere (Anand et al., 2005; Anand, 2007) indicate that due to huge surface area to mass ratio of these novel materials, nanotubes have demonstrated excellent adsorption properties. It was interesting to note that the resonant cavities without any substrates loaded, showed no or very little response of adsorption due to surface adhesion of molecules on their walls, whereas, the cavities with very little amounts of substrates, showed significant adsorption of gas upon cycling. Out of all the substrates, single-walled carbon nanotubes showed maximum adsorption for all the gases and the amount of adsorption of these nanotubes were different for different gases.

15.4.2 Specificity That Completes the Functionality of Sensing

The resonant cavities discussed in section 15.4.1 demonstrated their sensitivity for any foreign agents introduced into them. The cavity that holds no substrates acts as a reference device which is subjected to the same conditions as the test cavity containing chemically functionalized nanotubes in it. When subjected to a certain toxin, which has a high degree of reactivity towards the functionalized nanomaterial the result will be a specific by-product with a certain degree of polarizability

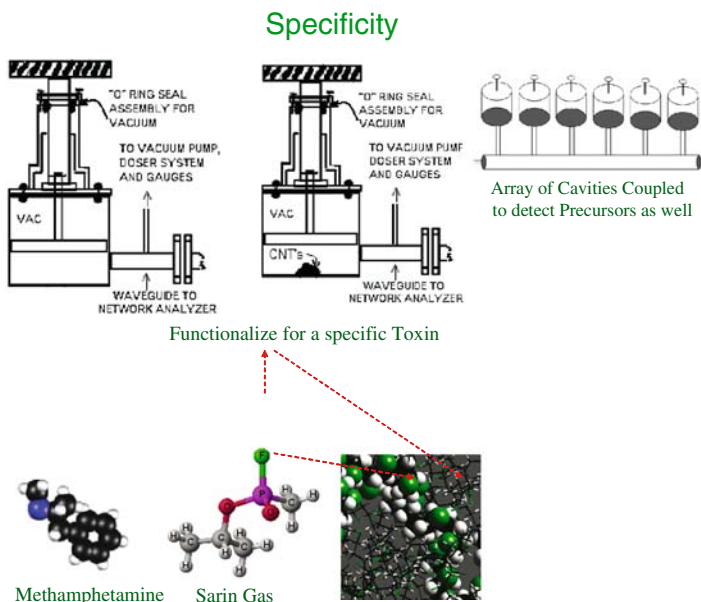


Fig. 15.4 Functionality of the prototype for specific detection (*See Color Plates*)

and dielectric response. This by-product response will be absent in the reference cavity. Thus, by measuring the resolution of shift in the frequencies of both (test and reference) cavities, it is possible to determine the specific toxin that invaded the boundaries of the prototype. The algorithmic procedure of detection capabilities of this prototype is shown in the schematic form in Fig. 15.4.

Figure 15.4 shows the loading and cycling of the samples when the resonant cavities with and without chemically functionalized sniffing wick get perturbed with the foreign agent. Both cavities show different responses to the dielectric medium. Designate the reference cavity (CR) and test cavity with functionalized nanotubes (CTFN) in their natural resonance having frequency F_{ocr} and F_{octfn} subjected to Toxin X.

In the procedure F_{ocr} is scaled due to the new dielectric material of X and this frequency is F_{1cr} . From this ΔF_{cr} is given by:

$$\Delta F_{cr} = F_{ocr} - F_{1cr} \quad (15.4)$$

Similarly, when CTFN is perturbed with the same Toxin X, simultaneously, there is a chemical change in the environment of the CTFN, but not in CR.

Where $X +$ functionalized bonds on nanotubes produces a by-product Y inside CTFN. The new Y will scale the frequency of CTFN due to its own dielectric properties resulting in a new frequency designated as F_{yctfn} . The resultant ΔF_{ctfn} is then given by:

$$\Delta F_{ctfn} = F_{octfn} - F_{yctfn} \quad (15.5)$$

The ratio of equations 15.4 and 15.5 is basically the resultant response, which is specific to the nature of the perturber, implying:

$$\frac{\Delta f_{cr}}{\Delta f_{ctfn}} \rightarrow X \quad (15.6)$$

Similarly, when arrays of these test resonant cavities loaded with functionalized wicks for various toxins are phase-locked to the reference cavity as shown in Fig. 15.5 they can act as detectors for targeting various toxins as well as their precursors through an array of suitably tuned cavities with specifically functionalized nanotubes. By using the approach as demonstrated in this document, it has been shown that the apparatus can be used to successfully detect low levels of toxin vapors associated with the drug “Methamphetamine,” in a laboratory-controlled environment. Some of the results of this study are highly sensitive in nature and are not reported in this document. These results can be obtained by other avenues.

Besides the two main characteristics of sensitivity as well as specificity of a sensor, the industrial, military, and other standards demand the device to be portable, economical, autonomous, and power efficient. In order to address some of these characteristics, the authors in their respective laboratories have been working on improving the design of the prototype, as shown in Figs. 15.6 and 15.7, respectively. The necessary electronics consisting of local oscillators, beat oscillators, smaller cavities, mixers, and phase-locking loops have been assembled in prototypes. As of this date the device needs further evaluation in an operational environment to establish a set of encyclopedic data and for comparison with unknown toxins.

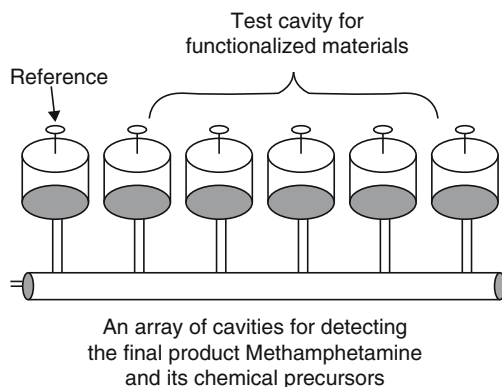


Fig. 15.5 Arrays of cavities phase-locked to the reference cavity and loaded with functionalized wicks to specifically determine the toxin and its precursors

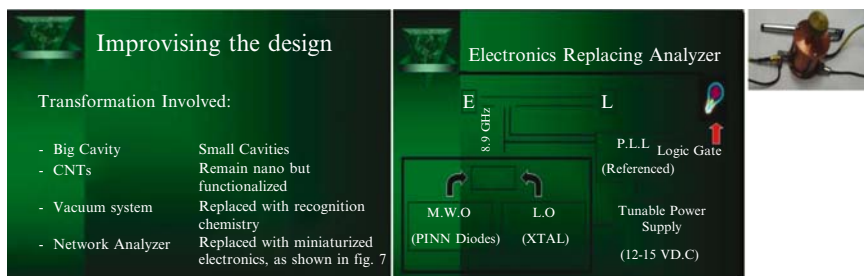


Fig. 15.6 (left) and 15.7 (right) The figures shown above describe the necessary steps taken to introduce portability into the sensor prototype. Shown on the right is the schematic involved in phase-locking the empty (E) and the loaded (L) cavity energized with a 12 V DC current-driven microwave diode. A typical electromagnetic mixer circuit has also been developed. The cavity shown at the far right is a significantly smaller than the test cavity and is comparable to today's cellular phones (*See Color Plates*)

15.5 Conclusion

The results described in this chapter provide an overview of the experimental investigation of gas interactions with carbon nanotubes inside a resonant cavity. An innovative concept of a chemical and biological sensor prototype has also been described. Using the principle of selective functionalization of carbon nanotubes, the scalability of this prototype can be extended to demonstrate sensing in military and chemical and biological industries to detect lethal, less lethal, and other industrial gases. The sensor industry is a multi-billion dollar industry world-wide and sensors have been researched for over a century. Investigators in many nations are working on sensor concepts to develop a “fool-proof” design of sensors/actuators to reduce false-positives in its operations. It is beyond the scope of this document to list all the types of sensor researches that have been done, but with the advancement in nanotechnology and development of novel nanomaterials, there exist several references in the literature (Anand, 2007; Rosa et al., 2004; Poncharal et al., 1999; Babic et al., 2003; Reulet et al., 2000; Zhao, 2001; Ye et al., 1999; Weber et al., 2000; Torrens, 2004; Insepov et al., 2006) that involve the application of nanomaterials to develop various kinds of sensors to detect toxins. It is proposed that with the further development of nanotechnology, and advancement in antibody research, there will be advancement in functionalization chemistry, which can be incorporated in sensor design to develop products with wide applications.

References

Anand A (2007) studying interactions of gas molecules with nanomaterials loaded in a microwave resonant cavity, Ph.D. dissertation, University of North Texas, Texas, USA.

- Anand A et al. (2005) Select gas absorption in carbon nanotubes, loading a resonant cavity to sense airborne toxin gases. *Nucl. Instrum. Meth. Phys. Res. B* 241: 511–516.
- Babic B, Furer J, Sahoo S, Farhangfar Sh, and Schonberger C (2003) Intrinsic thermal vibrations of suspended doubly clamped single-wall carbon nanotubes. *Nano Lett.* 3:1577.
- Harvey AF (1963) *Microwave engineering*. Academic Press, London, Ch. 5, p. 196.
- Hong KH (1974) *Microwave Properties of Liquids and Solids Using a Resonant Microwave Cavity as a Probe*, Ph.D. dissertation, University of North Texas, Texas, USA.
- Microwave network analyzer purchased through Naval Grant number – ONR-N00013-03-0880
- Montgomery CG (1947) *Technique of microwave measurement*. McGraw-Hill, Cleveland, p. 294.
- Poncharal P, Wang ZL., Ugarte D., et al. (1999) *Science* 283: 1513.
- Radar Circuit Analysis, U.S. Air Force radar manual. Washington, 1950, Ch. 10.
- Reulet B, Kasumov AYu, Kociak M, Deblock R, Khodos II, Gorbatov YuB, Volkov VT, Journet C, and Bouchiat HL (2000) Acoustoelectric effects in carbon nanotubes. *Phys. Rev. Lett.* 85: 2829–2832.
- Rosa HMC, Carmen KMF, and Wen JL (2004) *Nanotechnology* 15: S672–S677.
- Slater JC (1941) *Microwave electronics*. *Rev. Mod. Phys.* 441.
- Torrens F (2004) Effect of type, size, and deformation on the polarizability of carbon nanotubes from atomic increments. *Nanotechnology* 15: S259–264.
- Weber SE, Talapatra S, Journet C, Zambano A, and Migone AD (2000) Determination of the binding energy of methane on single-walled carbon nanotube bundles. *Phys. Rev. B.* 61: 19.
- Ye Y et al. (1999) Hydrogen adsorption and cohesive energy of single walled carbon nanotubes. *Appl. Phys. Lett.* 74: 16.
- Zeke Insepov, Dieter Wolf, and Ahmed Hassanein (2006) Nanopumping using carbon nanotubes. *Nanoletters* 6 (9): 1893.
- Zhao, J. (2001) Gas molecules adsorption on carbon nanotubes. *Mat. Res. Soc. Symp. Proc.* 633: A13.48.1.

Chapter 16

Cellular Nanotubes: Membrane Channels for Intercellular Communication

Raquel Negrão Carvalho and Hans-Hermann Gerdes*

Abstract Cells of living organism communicate in many different ways with their neighbor cells. This is accomplished by, for example, the secretion of signaling molecules or the formation of proteinaceous pores, referred to as gap junctions, between physically attached cells. In addition to these long-known communication routes, a novel mechanism was discovered recently based on de novo formation of membrane nanotubes, which facilitate the delivery of biological molecules and organelles between cells. Interestingly, chemists have been developing artificial carbon-based nanostructures with a similar architecture for communication with cells and delivery of clinically interesting drugs. Along with every new developed technology involving the use of foreign compounds in biomedical applications, concerns emerge on the biocompatibility and toxicity at the cellular level. This is particularly true for nano-sized materials, whose effects are yet to be thoroughly determined *in vivo*. Biocompatibilization of synthetic compounds may be done more efficiently if naturally occurring structures are taken as models.

Keywords Tunneling nanotube, TNT, cellular communication, intercellular transport

Abbreviations CNT, Carbon nanotube; F-actin, Filamentous actin; TNT, Tunneling nanotube

16.1 Structure and Formation of Tunneling Nanotubes

Tunneling nanotubes (TNTs) were first described in cultured rat pheochromocytoma PC12 cells as thin continuous membranous channels that span the shortest distance between connected cells (Fig. 16.1) (Rustom et al., 2004). They have a diameter between 25 and 200nm, a length up to several tens of micrometers, and they are extended above the substratum and not in contact with it (reviewed in Gerdes et al.

Department of Biomedicine, University of Bergen, Jonas Lies vei 91, Bergen 5009, Norway

*Correspondence to: Email: hans-hermanngerdes@biomed.uib.no

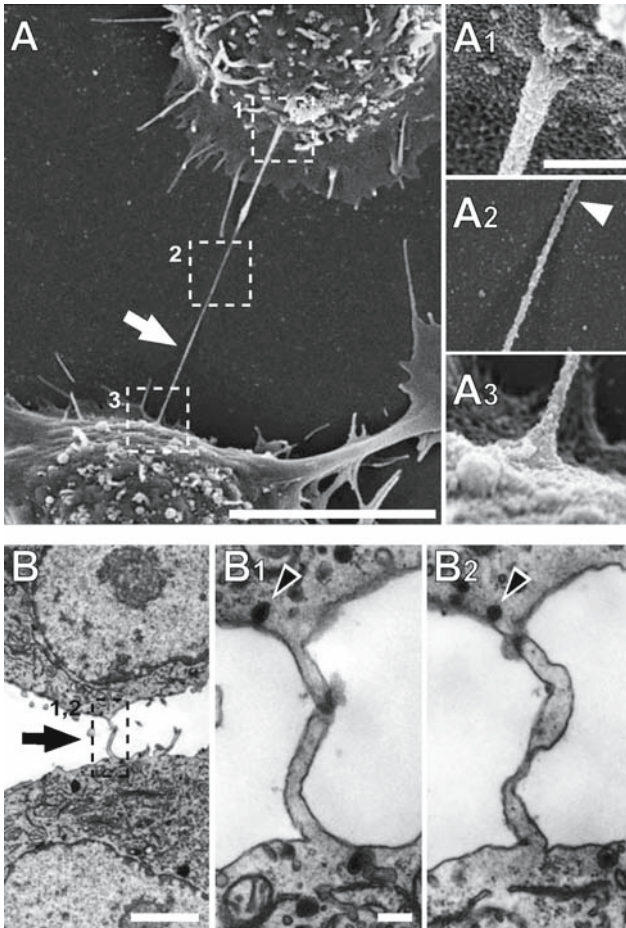


Fig. 16.1 Ultrastructure of tunneling nanotubes (TNTs). (A) Scanning electron microscopic (SEM) or (B) transmission electron microscopic (TEM) image of a tunneling nanotube connecting two cultured PC12 cells. The boxed areas in (A) and (B) are shown as higher magnification images (insets A1–A3, B1, B2). (B1) and (B2) represent consecutive 80nm sections, which demonstrate membrane continuity between the connected cells. Bars: 10 μ m (A); 2 μ m (B); 200nm (insets A1–A3, B1, B2) (Modified from Rustom et al., 2004)

(2007)). Branched TNTs occur occasionally between cultured cells with a typical angle of 120° between the different tubular junctions (Önfelt et al., 2004; Rustom et al., 2004). The interior of TNTs is filled with a bundle of filamentous actin (F-actin) over the entire length of the nanotube (Rustom et al., 2004), while for some cells an additional type of thicker nanotube connectors (with a diameter up to 1 μ m), containing both F-actin and microtubules, was found (Önfelt et al., 2006). Live-cell imaging has provided the basis for the current proposed mechanisms for de novo formation of TNTs. Frequently, a filopodia-like protrusion from one cell may come into contact with the plasma membrane or a filopodium from another cell, and a

straight membrane tube is formed at the shortest distance between the connected cells. Alternatively, TNTs can emerge when two cells in close contact diverge (Önfelt et al., 2004; Rustom et al., 2004; Gerdes et al., 2007). Since their discovery, diverse intercellular membrane nanotubes have been described for different cell types, and the idea of broad structural and functional heterogeneity for this type of nanotube-mediated cell-to-cell communication is emerging (Gerdes and Carvalho, 2008; Gurke et al., 2008; Davis and Sowinski, 2008).

The discovery of TNTs may end up challenging the established cell theory concept of a cell as the primary unit of life in animals, if future studies can reveal a role of TNT-mediated communication in fundamental cellular processes. In the plant kingdom the multicellular organism is already considered the primary unit of life, driven by the role of plasmodesmata, cytoplasmic channels interconnecting plant cells, in processes such as cellular differentiation and development (reviewed in Baluška et al. (2004)).

16.2 Artificial Membrane Nanotubes

TNTs are fragile structures, prone to disruption by mechanical stress, chemical fixation, and prolonged light exposure during widefield microscopy (Rustom et al., 2004; Koyanagi et al., 2005; Watkins and Salter, 2005). These characteristics have made it difficult to analyze the molecular composition as well as the physical properties of such singular naturally occurring tubules. Despite these constraints, important information can be obtained from studies on model artificial membrane tubes such as those created by pulling tethers from synthetic lipid vesicles or cellular plasma membrane (Fig. 16.2). The morphology of such tubes resembles that of

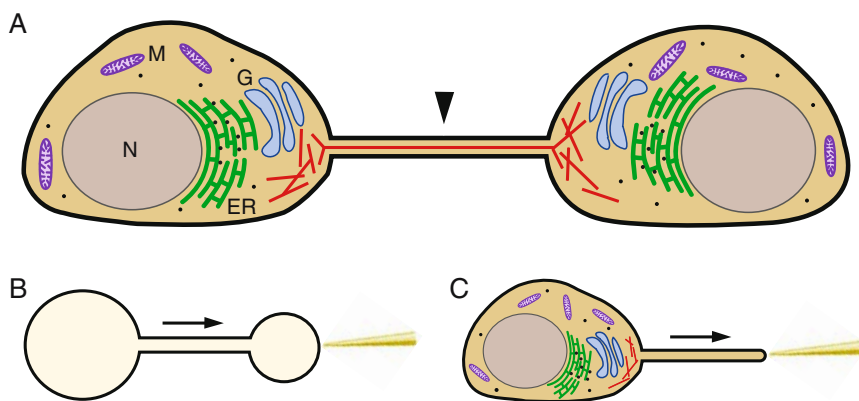


Fig. 16.2 Schematic representation of cellular and artificial membrane nanotubes. (A) Two cells are connected by a tunneling nanotube (arrowhead) containing a bundle of filamentous actin (red line). N (grey), nucleus; M (purple), mitochondrion; ER (green), endoplasmic reticulum; G (blue), Golgi apparatus. (B) Lipid nanotube connecting two lipid vesicles formed by pulling a membrane tether. (C) Membrane tether pulled from the plasma membrane of a cell (*see Color Plates*)

TNTs and it seems reasonable that the same physical laws govern the common shape in both structures. Both TNTs and artificial lipid tethers are straight tubes spanning the shortest distance between two connected points, which hints that this invariable geometry may be energetically favorable. The diameter of a nanotube extracted from membranes is determined by the balance between the bending rigidity and the tension of the membrane, and is typically in the range of 40–400 nm (Karlsson et al., 2001), comparable to TNTs. Similar Y-shaped junctions naturally found in TNTs can be produced artificially by pulling of tethers from lipid vesicles (Karlsson et al., 2002; Lobovkina et al., 2006) and even from straight TNTs (Pontes et al., 2007). Geometrical calculations estimate that this symmetric three-way nanotube junction has the lowest energy (Yin and Yin, 2006).

Formation of membrane tubes by directly pulling tethers from cell membranes requires an initial rise in the force elongation profile, to overcome the increased bending energy of the plasma membrane and the strength of the membrane–cytoskeleton links that need to be disrupted (Li et al., 2002). Alternatively, it was also shown that tubular budding in lipid vesicles can be induced by adding strong anisotropic amphiphilic molecules, which accumulate at the buds and cause a spontaneous curvature and tubular initiation. Under these conditions a direct pulling mechanical force was no longer required (Yamashita et al., 2002). Acquisition of specific proteins that drive membrane curvature has also been associated with tubule formation *in vitro* (Farsad et al., 2001) and *in vivo* (Razzaq et al., 2001). In contrast to artificial membrane tethers, TNTs are not hollow cylindrical membrane tubes, but contain bundles of F-actin attached to the cortical actin cytoskeleton. Thus, it is likely that actin polymerization plays a role in the outward pushing of the plasma membrane and nanotube formation *in vivo* as it is known for the extension of filopodia (Faix and Rottner, 2006). This is also consistent with the observation that the action of molecular motors bound to the bilayer of lipid giant unilamellar vesicles is sufficient to generate membrane tubes (Roux et al., 2002; Koster et al., 2003). In addition, elongation of plasma membrane nanotubes requires a membrane flow from the cell plasma membrane into the growing tube and it is suggested that cells maintain a membrane reservoir (e.g., ruffles, invaginations), controlled by the cytoskeleton, to provide a buffer against membrane tension over several micrometers of tube elongation (Raucher and Sheetz, 1999; Sun et al., 2005). This is also true when nanotubes are formed from lipid bilayer vesicles, where a slight rehydration of the vesicles by increasing the osmotic strength of the aqueous suspension is necessary to provide the bilayer reservoir (Evans et al., 1996).

16.3 Tunneling Nanotubes Are Conduits for the Delivery of Molecules

The current knowledge of TNTs points to their main function being in facilitating the unidirectional intercellular transport of biological molecules either by providing a channel for diffusion of small cytoplasmic molecules or by containing the neces-

sary motors for an active transport of membrane containers. Passive diffusion is likely to be the mechanism for the transfer of calcium fluxes observed between dendritic cells and THP-1 monocytes (Watkins and Salter, 2005), but on the other hand, the small molecule calcein with only 400Da could not be seen passing through TNTs between PC12 cells (Rustom et al., 2004). This suggests that the structural heterogeneity of TNTs in different cells may determine the size exclusion limit of the channel or reflect the existence of a gating mechanism for the transfer of specific molecules. Different membrane containers can travel along TNTs and into the connected cell. TNTs were observed to traffic small organelles belonging to the endosomal/lysosomal system between PC12 cells (Rustom et al., 2004), NRK cells (Rustom et al., 2004), immune cells (Önfelt and Davis, 2004) and human prostate cancer cells (Vidulescu et al., 2004), and mitochondria between neonatal rat cardiac myocytes and human endothelial progenitor cells (Koyanagi et al., 2005). The mechanism by which such organelles are shipped along the interior of TNTs, tightly filled with bundles of F-actin, is still unknown, but is likely to be an active process. The presence of the actin-associated motor protein myosin Va inside TNTs (Rustom et al., 2004; Zhu et al., 2005), partially co-localizing with organelles (Rustom et al., 2004), further supports the involvement of an actin-/myosin-driven transport associated with the movement of organelles inside the TNTs. In addition, a slow transfer of several plasma membrane components including membrane proteins and lipid molecules has been described (Rustom et al., 2004; Watkins and Salter, 2005). Diffusion rates of membrane components in TNTs are likely to be lowered by the tight interactions between the membrane and the F-actin. Conversely, pulling tethers from cell membranes uncouples the lipid bilayer from the membrane-associated cytoskeleton and results in higher diffusion rates for integral membrane proteins in the tether than those observed in the plasma membrane (Berk et al., 1992).

Finally, it has been speculated that TNTs could represent a general mechanism for the intercellular spread of pathogens. In this respect, bacteria and retroviruses were seen to attach to the outer membrane and surf along the nanotubes towards connected cells, where they could be internalized (Önfelt et al., 2006; Sherer et al., 2007). Furthermore, the human immunodeficiency virus type 1 (HIV-1) was shown to move within nanotubes to infect connected cells (Sowinski et al., 2008).

16.4 Bio-Inspired Tuning of Carbon Nanotubes

It is interesting to know how the morphology of man-made carbon nanotubes (CNTs) resembles that of the nature-made TNTs with similar high length to diameter ratios. At the same time, it is evident that the material composite of both structures, lipid membranes in the case of TNTs versus graphitic backbone in the CNTs, is completely different and this determines their properties (Table 16.1) and applications. TNTs have a support of actin filaments enveloped within a tube of lipidic membrane that can easily be disrupted by mechanical and other stress conditions. TNTs are also very flexible and dynamic structures and their lifetime can range

Table 16.1 Comparison of major properties of tunneling nanotubes and carbon nanotubes

	TNT	CNT
Lifetime	Temporary	Stable
Elasticity	Flexible	Rigid
Strength	Fragile	High mechanical strength
Diameter	25–200 nm	0.4–2 nm (SWCNT) 1.4–100 nm (MWCNT)
Length	5–100 μ m	20–1,000 nm (SWCNT) 1–several μ m (MWCNT)
Conductivity	Ionic	Electrical, thermal
Transport mechanism	Diffusion or active transport through tunneling nanotubes	Diffusion or endocytotic uptake of carbon nanotubes

SWCNT, single-walled carbon nanotube; MWCNT, multiwalled carbon nanotube.

from minutes to hours. During the time of interconnecting a cell pair, TNTs can serve as a pathway for diffusion of ions and small molecules, while bigger molecules or organelles are likely to be transported by an active mechanism. By contrast, CNTs have rigid backbones made of graphite that accounts for their stability and high mechanical strength. In addition, CNTs have singularly high electrical and thermal conductivity properties that can be exploited in therapeutic applications. They are also easily internalized into cells, which is suggested to occur either by diffusion across the lipid bilayer of the cell membrane (Pantarotto et al., 2004) or by endocytosis (Kam et al., 2006). By attachment of interesting molecules to the surface of CNTs, these devices can be efficient transporters *in vivo*. Thus, CNTs are able to translocate nucleic acids and proteins (Kam and Dai, 2005; Kam et al., 2006) as well as drug molecules (Wu et al., 2005) into living cells.

Due to their unique nano-based properties, CNTs are considered as one of the most promising nanomaterials with applications in biomedicine and pharmacology. This includes their exploitation in diagnostics, tissue engineering, and drug delivery. With respect to the latter, the same idea of straight tubular structures interacting with living cells and delivering molecules of interest are behind both CNTs and TNTs. However, the central issue in applying CNTs to living organisms is their biocompatibility. Naked CNTs are hydrophobic and prone to nonspecific adhesion, properties that increase the chance of toxic effects. To overcome these obstacles, researchers have modified the surface of CNTs by introducing non-covalent modifications (Klumpp et al., 2006), to improve the solubility and reduce the associated toxicological responses. Furthermore, concerns on CNT uptake and toxicity have driven studies where biological molecules like proteins (Dutta et al., 2007; Zhang et al., 2007) were used to functionalize the nanomaterial surfaces. Despite the fact that these coatings certainly improved the trafficking and tolerance of CNTs in biological systems, it becomes evident that such modifications have their limits in real biological environments.

In light of these constraints, perhaps the best strategy to further improve the properties of CNTs for medical applications could be to exploit the cellular principles as blueprints. Natural systems use lipid membranes as a universal host matrix, which

possess a large number of membrane proteins, receptors, and channels to fulfill the manifold host functions ranging from signal transduction to transport of molecules across the membranes. In this respect, the recently discovered TNTs with their striking similarity to the nano-sized morphology of CNTs could be most instructive in understanding the basic principles of delivery of substances into cells.

Given the fact that the very first encounter of a CNT with a cell is through the cellular plasma membrane and because membrane translocation is such an important step in any drug delivery strategy, one has to consider how and why nature has designed membranes. Cellular membranes are natural barriers that allow the coexistence of several compartments with specific molecules and specific functions inside. They also provide the matrices for a wide number of integral or attached proteins to associate with their substrates or binding partners. In addition, nature has developed versatile environments at the cellular surface that allow molecular recognition events to guide selective internalization of molecules. Most of these membrane features are expected to be present in cellular TNTs. De novo formation of TNTs is accomplished by an outgrowing of cellular extensions in the direction of neighboring cells presumably following a chemo-tactical guidance. Direct contact of the protrusion with the plasma membrane of the neighboring cell is likely to involve recognition of special plasma membrane molecules that precede the final fusion event. Molecular sensing and recognition events by the CNTs are often required if these nanomachines are to be used in biomedical applications. This can be achieved by attachment of molecules that modify and functionalize the CNT surface.

Thus, from a cell biological point of view, it would be most promising to use molecules present in the natural membrane environments of, for example, TNTs for the biocompatibilization of CNTs and their selective recognition at the cellular level. A major breakthrough in this direction has been the demonstration that coating of CNTs with lipid bilayers results in an efficient and biocompatible barrier between the nanotube surface and the surrounding solution (Artyukhin et al., 2005). In addition, lipid molecules in such a structure were able to diffuse along the bilayer plane much like in a normal cell membrane (Artyukhin et al., 2005). As a second major step, it would be interesting to extend this bio-inspired approach by including selected membrane protein receptors on such an artificial system. These should include membrane proteins, which recognize specific cell surface receptors and thus enable CNTs to selectively interact with certain cell types. This could be of great importance for cancer treatment where a selective targeting mechanism for tumor cells is essential to avoid harmful side effects of the therapy on healthy tissue. In this respect, receptor ligand molecules attached to CNTs have already been proven to recognize selectively the respective binding partners of viruses (Zhang et al., 2007) or tumor cells (Kam et al., 2005; McDevitt et al., 2007).

In addition to molecules providing a cell type-specific targeting, extra signaling molecules could be included to direct the CNTs to cellular compartments such as the nucleus or the mitochondrion. The way nature accomplishes the selective intracellular distribution of molecules is by using targeting signals that are recognized at the surface of specific cellular organelles. The use of signal sequences could be extended to intentionally determine the fate of molecules delivered by CNTs.

We envision that researchers developing strategies for carbon nanotube-based *in vivo* delivery of nanomedicines can benefit from taking into consideration the physiology and function of existing cellular mechanisms for the selective delivery of molecules. It can be expected that further characterization of the molecular composition and transport machinery inside TNTs will help to elucidate the structure and function of these curious ways of intercellular transport up to the tissue level. Understanding how nature functions will provide the ideas and tools to design smart nanoscaled devices for medical and pharmacological applications.

Acknowledgments We would like to thank Steffen Gurke and João Barroso for critical comments on the text and the Norwegian Research Council for financial support (project number 164959/V40).

References

- Artyukhin AB, Shestakov A, Harper J, Bakajin O, Stroeve P, Noy A (2005) Functional one-dimensional lipid bilayers on carbon nanotube templates. *J. Am. Chem. Soc.* 127: 7538–7542.
- Baluška F, Volkmann D, Barlow PW (2004) Eukaryotic cells and their cell bodies: Cell theory revised. *Ann. Bot. (Lond)* 94: 9–32.
- Berk DA, Clark A, Jr., Hochmuth RM (1992) Analysis of lateral diffusion from a spherical cell surface to a tubular projection. *Biophys. J.* 61: 1–8.
- Davis DM, Sowinski S (2008) Membrane nanotubes: dynamic long-distance connections between animal cells. *Nat. Rev. Mol. Cell Biol.* 9: 431–436.
- Dutta D, Sundaram SK, Teegarden JG, Riley BJ, Fifield LS, Jacobs JM, Addleman SR, Kaysen GA, Moudgil BM, Weber TJ (2007) Adsorbed proteins influence the biological activity and molecular targeting of nanomaterials. *Toxicol. Sci.* 100: 303–315.
- Evans E, Bowman H, Leung A, Needham D, Tirrell D (1996) Biomembrane templates for nanoscale conduits and networks. *Science* 273: 933–935.
- Farsad K, Ringstad N, Takei K, Floyd SR, Rose K, De Camilli P (2001) Generation of high curvature membranes mediated by direct endophilin bilayer interactions. *J. Cell Biol.* 155: 193–200.
- Faix J, Rottner K (2006) The making of filopodia. *Curr. Opin. Cell Biol.* 18: 18–25.
- Gerdes H-H, Bukoreshtliev NV, Barroso JF (2007) Tunneling nanotubes: A new route for the exchange of components between animal cells. *FEBS Lett.* 581: 2194–2201.
- Gerdes H-H, Carvalho RN (2008) Intercellular transfer mediated by tunneling nanotubes. *Curr. Opin. Cell Biol.* doi: 10.1016/j.ceb.2008.03.005.
- Gurke S, Barroso JF, Gerdes H-H (2008) The art of cellular communication: tunneling nanotubes bridge the divide. *Histochem. Cell Biol.* 129: 539–550.
- Kam NW, Dai H (2005) Carbon nanotubes as intracellular protein transporters: Generality and biological functionality. *J. Am. Chem. Soc.* 127: 6021–6026.
- Kam NW, Liu Z, Dai H (2006) Carbon nanotubes as intracellular transporters for proteins and DNA: An investigation of the uptake mechanism and pathway. *Angew Chem. Int. Ed. Engl.* 45: 577–581.
- Kam NW, O’Connell M, Wisdom JA, Dai H (2005) Carbon nanotubes as multifunctional biological transporters and near-infrared agents for selective cancer cell destruction. *Proc. Natl. Acad. Sci. USA* 102: 11600–11605.
- Karlsson A, Karlsson R, Karlsson M, Cans AS, Strömberg A, Ryttsén F, Orwar O (2001) Networks of nanotubes and containers. *Nature* 409: 150–152.
- Karlsson M, Sott K, Davidson M, Cans AS, Linderholm P, Chiu D, Orwar O (2002) Formation of geometrically complex lipid nanotube-vesicle networks of higher-order topologies. *Proc. Natl. Acad. Sci. USA* 99: 11573–11578.

- Klumpp C, Kostarelos K, Prato M, Bianco A (2006) Functionalized carbon nanotubes as emerging nanovectors for the delivery of therapeutics. *Biochim. Biophys. Acta* 1758: 404–412.
- Koster G, VanDuijn M, Hofs B, Dogterom M (2003) Membrane tube formation from giant vesicles by dynamic association of motor proteins. *Proc. Natl. Acad. Sci. USA* 100: 15583–15588.
- Koyanagi M, Brandes RP, Haendeler J, Zeiher AM, Dimmeler S (2005) Cell-to-cell connection of endothelial progenitor cells with cardiac myocytes by nanotubes: A novel mechanism for cell fate changes? *Circ. Res.* 96: 1039–1041.
- Li Z, Anvari B, Takashima M, Brecht P, Torres JH, Brownell WE (2002) Membrane tether formation from outer hair cells with optical tweezers. *Biophys. J.* 82: 1386–1395.
- Lobovkina T, Dommersnes P, Joanny JF, Hurtig J, Orwar O (2006) Zipper dynamics of surfactant nanotube Y junctions. *Phys. Rev. Lett.* 97: 188105.
- McDevitt MR, Chattopadhyay D, Kappel BJ, Jaggi JS, Schiffman SR, Antczak C, Njardarson JT, Brentjens R, Scheinberg DA (2007) Tumor targeting with antibody-functionalized, radiolabeled carbon nanotubes. *J. Nucl. Med.* 48: 1180–1189.
- Önfelt B, Davis DM (2004) Can membrane nanotubes facilitate communication between immune cells? *Biochem. Soc. Trans.* 32: 676–678.
- Önfelt B, Nedvetzki S, Yanagi K, Davis DM (2004) Cutting edge: Membrane nanotubes connect immune cells. *J. Immunol.* 173: 1511–1513.
- Önfelt B, Nedvetzki S, Benninger RK, Purbhoo MA, Sowinski S, Hume AN, Seabra MC, Neil MA, French PM, Davis DM (2006) Structurally distinct membrane nanotubes between human macrophages support long-distance vesicular traffic or surfing of bacteria. *J. Immunol.* 177: 8476–8483.
- Pantarotto D, Briand JP, Prato M, Bianco A (2004) Translocation of bioactive peptides across cell membranes by carbon nanotubes. *Chem. Commun. (Camb)*: 16–17.
- Pontes B, Viana NB, Campanati L, Farina M, Neto VM, Nussenzveig HM (2007) Structure and elastic properties of tunneling nanotubes. *Eur. Biophys. J.* [Epub ahead of print]
- Raucher D, Sheetz MP (1999) Characteristics of a membrane reservoir buffering membrane tension. *Biophys. J.* 77: 1992–2002.
- Razzaq A, Robinson IM, McMahon HT, Skepper JN, Su Y, Zehhof AC, Jackson AP, Gay NJ, O’Kane CJ (2001) Amphiphysin is necessary for organization of the excitation-contraction coupling machinery of muscles, but not for synaptic vesicle endocytosis in *Drosophila*. *Genes Dev.* 15: 2967–2979.
- Roux A, Cappello G, Cartaud J, Prost J, Goud B, Bassereau P (2002) A minimal system allowing tubulation with molecular motors pulling on giant liposomes. *Proc. Natl. Acad. Sci. USA* 99: 5394–5399.
- Rustom A, Saffrich R, Markovic I, Walther P, Gerdes H-H (2004) Nanotubular highways for intercellular organelle transport. *Science* 303: 1007–1010.
- Sherer NM, Lehmann MJ, Jimenez-Soto LF, Horensavitz C, Pypaert M, Mothes W (2007) Retroviruses can establish filopodial bridges for efficient cell-to-cell transmission. *Nat. Cell Biol.* 9: 310–315.
- Sun M, Graham JS, Hegedüs B, Marga F, Zhang Y, Forgacs G, Grandbois M (2005) Multiple membrane tethers probed by atomic force microscopy. *Biophys. J.* 89: 4320–4329.
- Sowinski S, Jolly C, Berninghausen O, Purbhoo MA, Chauveau A, Köhler K, Oddos S, Eissmann P, Brodsky FM, Hopkins C, Önfelt B, Sattentau Q, Davis DM (2008) Membrane nanotubes physically connect T cells over long distances presenting a novel route for HIV-1 transmission. *Nat. Cell Biol.* 10: 211–219.
- Vidulescu C, Clejan S, O’Connor KC (2004) Vesicle traffic through intercellular bridges in DU 145 human prostate cancer cells. *J. Cell. Mol. Med.* 8: 388–396.
- Watkins SC, Salter RD (2005) Functional connectivity between immune cells mediated by tunneling nanotubes. *Immunity* 23: 309–318.

- Wu W, Wieckowski S, Pastorin G, Benincasa M, Klumpp C, Briand JP, Gennaro R, Prato M, Bianco A (2005) Targeted delivery of amphotericin B to cells by using functionalized carbon nanotubes. *Angew Chem. Int. Ed. Engl.* 44: 6358–6362.
- Yamashita Y, Masum SM, Tanaka T, Tamba Y, Yamazaki M (2002) Shape changes of giant unilamellar vesicles of phosphatidylcholine induced by a de novo designed peptide interacting with their membrane interface. *Langmuir* 18: 9638–9641.
- Yin Y, Yin J (2006) Geometric conservation laws for cells or vesicles with membrane nanotubes or singular points. *J. Nanobiotechnol.* 4: 6.
- Zhang YB, Kanungo M, Ho AJ, Freimuth P, van der Lelie D, Chen M, Khamis SM, Datta SS, Johnson AT, Misewich JA, Wong SS (2007) Functionalized carbon nanotubes for detecting viral proteins. *Nano Lett.* 7: 3086–3091.
- Zhu D, Tan KS, Zhang X, Sun AY, Sun GY, Lee JC (2005) Hydrogen peroxide alters membrane and cytoskeleton properties and increases intercellular connections in astrocytes. *J. Cell Sci.* 118: 3695–3703.

Index

A

Acetylcholine esterase (AChE)
inhibition of, 9
Aggregation, 139, 164, 168, 251, 301
Allantoic fluid, 109
Alzheimer disease, 52, 268
Anaphylaxis inhibition, 5
Antibody, 30, 186, 296
Antisense therapy, 295
Apoptosis, 3, 15, 69, 70, 97, 188
hydrogen peroxide-induced, 4
inhibition of, 70
Artificial hip, 284
Artificial membrane, 365
Asbestos 298
Atomic force microscopy (AFM), 165, 294

B

Ballistic conduction, 226
Biomaterial, 283
Biomimetic polymer, 185
Biopolymer, 255
Blood preparation, 108
Boundary element method, 205

C

Calixarene, 124
Cancer
intraoperative hyperthermic
chemoperfusion, 238
nano-therapeutics, 224
radiotherapeutic treatment, 175
solid tumor, 234
therapy, 36, 89, 95, 295
brain cancer therapy, 296
chemotherapy, 235
hyperthermic therapy, 223, 234

Carbon nanohorn, 232, 249
Carbon nanomaterial toxicity, 251,
268, 300
Carbon Nanotube (CNT), 2, 23, 181, 224,
232, 289
adsorption properties, 28, 187, 358
adverse effect, 41
aggregation, 253, 301
alignment, 196, 204
anti-angiogenesis activity, 299
antifouling action, 209
application, paper battery, 287
bioapplication
diagnostics and therapeutics, 291
biocompatibility, 182, 188, 293
biocompatible electrode array, 211
biomolecule-CNT nanocomposite, 28,
182, 206, 290
boron doping, 36, 233
capillary filling, 247
cell penetration endocytosis, 31, 192, 281
cellular imaging, 207, 270
cellular uptake, 31, 190, 268, 292
chemical functionalization, 182, 203, 206,
289, 290, 293, 301
clustering, 175
covalent functionalisation, 25, 186, 289
defect functionalisation, 28
encapsulation, 26, 174, 186
sidewall functionalisation, 28, 29, 302
crack toughness resistance enhancer, 194
cytotoxicity, 188, 268, 302
dendrimer modified single walled CNT, 207
dispersion, 37, 42, 183, 202
DNA encapsulation, 26, 183
double walled, 232, 242
drug delivery system, 36, 182, 206, 256,
291, 296, 304
drug encapsulation, 249

- Carbon Nanotube (CNT) (*cont.*)
- electrical conductivity, 210, 233
 - increase, 196
 - as electrochemical biosensor, 210
 - electromagnetic radiation absorption, 242
 - energy-storage device, 290
 - fluorescent labeled, 36, 246, 293
 - functionalization
 - in situ* polymerization, 202
 - plasma polymerization, 203
 - gene therapy, 206, 296
 - heat capacity, 233
 - heparin derivative, 293
 - heparin-coated, 286
 - hopping transport, 198
 - hydrogen storage, 210
 - in photovoltaic device, 200
 - indium-labelled, 42, 301
 - inhalation, 42, 298
 - lipid bilayers coating, 369
 - lysine-functionalized, 293
 - magnetic field alignment, 201, 247
 - mechanical strength, 233, 368
 - metallic, 25, 234, 289
 - multi-walled CNT, 24, 193, 232, 242, 289
 - nanobomb, 244
 - nitrogen doping, 233
 - non covalent functionalization, 183, 186, 193, 244, 368
 - amylose, 26
 - cyclodextrin, 26
 - double-stranded DNA, 26, 37, 183
 - PEG, 27, 37, 40, 186, 190, 194, 209, 295
 - single-strand DNA, 26, 183
 - supramolecular, 25, 138
 - optical properties, 199
 - polymer-CNT composite
 - electrical conductivity, 196, 210
 - positively charged CNT, 37, 293
 - peptide, 27, 293
 - as potential diagnostic tool, 24
 - as potential drug carrier, 24, 37, 286, 305
 - as potential therapeutic agent, 24, 247, 254, 286
 - production by
 - arc chamber method, 233
 - arc-discharge, 25
 - chemical vapor deposition, 25, 204, 233
 - laser ablation, 25, 233
 - pulmonary toxicity, 42, 297
 - purification by
 - agarose electrophoresis, 183
 - centrifuge method, 183
 - chromatography, 25
 - microfiltration, 25
 - microwave irradiation, 25
 - oxidation, 25, 203
 - radiolabeled derivative, 42, 294, 301
 - renal excretion, 42, 207, 213, 294
 - resiliency and resistivity, 233
 - semi-conducting, 234
 - single-walled toxicity, 269
 - single-walled CNT, 24
 - solubility, 25, 194
 - ^{99m}Tc labelled, 294
 - tensile strength enhancer, 193
 - thermal ablation, 242, 247
 - thermal conductivity, 200, 233, 289
 - thermal stability enhancer, 212
 - tissue engineering, 211, 368
 - toxicity, 41, 188, 207, 213, 252, 269, 297, 368
 - dyspnea, 189
 - fibrosis, 47, 227, 251, 253
 - toxicology, 188, 283, 297
 - transport, 292
 - ultrashort single walled, 174
 - gadolinium filling, 175
 - water contract angle, 195
- Cell, 363
- communication, 365
 - artificial lipid tether, 366
 - cycle, 96, 188
 - membrane disruption, 9
 - viability, 6, 41, 270, 281, 296
 - MTT assay, 96, 125, 127, 133, 269
 - resazurin reduction test, 147
 - WST assay, 269
- Cellular distribution, 14, 135, 140, 270, 369
- Cellular internalisation (see also cellular uptake), 39
- caveolae-mediated endocytosis, 31
 - clathrin-mediated endocytosis, 31
 - nanoneedle, 33
 - passive diffusion, 31
 - phagocytosis, 31
- Central nervous system (CNS), 64, 288
- Cohesion energy, 320
- Computed tomography, 164, 270, 279
- Conductivity, 196, 200, 210, 289
- Correlation weight
 - global graph invariant, 339
 - local graph invariant, 339
- Cycloaddition, 29, 36, 59, 90
- Cyclodextrine, 124, 318
- Cytochrome *c*, 3, 26, 66
 - fullerene binding to, 8

D

- Delivery, 10, 33, 36, 206, 234, 240, 247, 286, 292, 333, 366
 - actin-/myosin-driven transport, 367
- Dendrofullerene, 2, 9, 55, 58, 65
- Descriptor, 338
 - flexible, 339
- Dielectric constant, 353
- Diels-Alder addition, 330
- Diethylenetriaminepentaacetic acid, 7, 99, 164, 293, 301
- Diffusive conduction, 226
- Dimensionality
 - one-dimensional object, 225
 - two-dimensional object, 225
 - three-dimensional object, 225
- DNAzyme
 - covalent functionalization, 27
 - non covalent functionalization, 244
 - oxidative treatment, 244
- Drug delivery
 - amphotericin B, 36
 - carborane, 36
 - doxorubicin, 37, 227, 238, 240
 - erythropoietin, 11, 37
 - methotrexate, 36
- Drug delivery system, 24
 - poly (lactic acid) nanoparticle, 288
 - poly(acryl-starch) microparticle, 288
 - polyacrylic bead, 288
- Dye, 36, 80, 108, 119, 186

E

- Electric displacement density, 357
- Electron energy loss spectroscopy, 273, 275, 276
- Electron microscopy, 14, 26, 95, 107, 110, 166
- Electron paramagnetic resonance, 5, 64, 88, 96, 126
- Electron tomography, 14, 95, 273, 279
- Electron transfer, 4, 52, 81, 86, 88, 124, 135, 164
- Electrophilic addition, 29
- Electrophoresis, 8, 110, 114, 183
- Endonuclease inhibition, 10
- Energy transfer, 83, 88, 124, 235
- Energy-filtered transmission electron microscopy, 14, 95, 279
- Enhanced permeability and retention (EPR), 226
- Enzyme-linked immunosorbent assay (ELISA), 35
- Erythrocyte, 7, 92, 127
- Evaporation enthalpy, 320
- Excretion, 42, 171, 207, 296

F

- Fatty acid, 13, 87, 227, 317, 322, 324
- Filamentous actin, 364
- Fluorescence resonance energy transfer
 - in biocatalyst system, 207
 - luminescence, 207
- Fluorination, 29, 174
- Folic acid, 244
- Fullerene
 - accumulation, 7, 13, 99, 124
 - administration by inhalation, 14
 - agglomerate formation, 111
 - aggregate, 12, 58, 62, 66, 82, 95, 124, 140, 143, 164, 171, 230, 252
 - batochromic shift, 172
- Bingel reaction, 54
- biological application, 4, 5, 8, 9, 11, 14, 139
 - antioxidant properties, 2, 14, 52, 62, 144, 149, 152
 - cell protection, 2, 21
 - antibacterial activity, 9, 13
 - antiinflammatory activity, 5
 - antimicrobial inactivation, 82, 93
 - DNA cleavage, 6, 90, 133, 145
 - drug delivery, 10, 240, 333
 - enzymatic inhibition, 9
 - neuroprotection, 52, 73
 - photodynamic therapy, 6, 54, 67, 73, 80, 88, 90, 98, 108, 112, 124, 235
 - photosensitizer, 79, 82, 88, 108, 118, 124, 241, 254
 - radical scavenger, 4, 6, 65, 139, 229
 - viral inactivation, 9, 92, 108, 111
- bisaddition, 59
- bis-methanophosphonate, 7, 92
- C₆₀/PVP complex, 6, 88, 139, 142, 144
- cluster, 14, 58, 63, 66, 95, 141, 164, 169, 228
- complex with cyclodextrin, 6, 53, 88, 92, 124, 131, 141, 241, 318
- complex with calixarene, 6, 53, 124
- cyclopropanation, see also Bingel reaction, 54
- cytotoxicity, 7, 15, 100, 160, 268
- di-malonic acid (DMA-C₆₀), 7, 92
- 1, 3-dipolar cycloaddition, 59, 94
- e, e, e*-tris-malonic acid (C₃), 3, 54, 65
 - as anticancer agent, 8
- encapsulation, 53, 171, 318
- endohedral, 11, 157
- excited triplet state, 80, 87
- fullerol/fullerenol, 12, 14, 53, 64, 67, 92
- fulleropyrrolidine, 5, 54, 59, 66, 95
- functionalization, 14, 53, 228, 241

- Fullerene (*cont.*)
- gadofullerene, 157
 - hexa-adduct FHP1, 96
 - hypochromic shift, 142
 - immobilization
 - aminopropylaerosyl, 125
 - antracenaliminopropylaerosyl, 125
 - insolubility, 52, 119, 140, 167
 - intrinsic toxicity, 3
 - irradiation, 14, 88, 91, 111, 124, 131, 332
 - lipid peroxidation, 13, 91, 126, 252, 269
 - lipid-membrane-incorporate fullerene, 141
 - membrane penetration, 135, 151
 - membranotropic activity, 142, 151
 - metallofullerene
 - biodistribution, 166, 171
 - cell viability, 166
 - Gd@C₆₀, 167
 - Gd@C₈₂, 162
 - intermolecular aggregation, 168
 - lanthanide, 172
 - separation, 161
 - sublimation, 161
 - mutagenicity, 90
 - nanoC₆₀, 141
 - nanoclustering, 165, 170, 176
 - nanoparticle, 12, 225
 - preparation, 14
 - nitroxide malonate methanofullerene, 5
 - oligodeoxynucleotide conjugate, 91
 - oxidative stress, 6, 268, 281
 - paclitaxel derivative
 - anticancer activity, 11
 - PEG conjugate, 7, 12, 92, 98, 99, 124, 133, 173
 - pentaaryl derivative, 62
 - photocytotoxic effect, 96
 - photophysics, 84
 - as photosensibilizer, 142
 - phototoxicity, 95, 148
 - pollution due to, 12
 - pulmonary toxicity, 14
 - quantum yield, 84, 88, 93, 241
 - radical sponge, 6
 - radiolabeled derivative, 95
 - solubility modeling, 337
 - sugar ball derivative, 62
 - sulfobutyl derivative, 9, 53, 64, 67, 88
 - suspension, 7, 13, 53, 68, 108, 111, 141
 - toxicity, 3, 14, 68, 91, 100, 141, 152, 160, 171, 229, 252, 268
 - teratogenic activity, 69
 - trans3, trans3, trans3*-C₆₅(COOH)₆ (D₃), 3, 54
 - water-soluble derivative, 2, 51, 140
 - C₇₀, 14, 59, 66, 83, 91, 145, 161, 228, 317, 321
- G**
- Gadodiamide, 173
 - Gadolinium, 7, 11, 99, 157
 - chelate complex, 157
 - high paramagnetic moment, 158
 - toxicity, 158
 - Gene delivery, 11, 37, 291
 - transfection, 11, 28, 39
 - Gene silencing, 40
- H**
- Heart valve, 285
 - Hemagglutinating activity, 109
 - Hemolysis, 91, 127
 - HIV reverse transcriptase
 - inhibition of, 9
 - HIV-Protease
 - fullerene binding to, 8
 - inhibition of, 9
 - Hydrodynamic diameter (D_H), 168
 - pH dependency, 168
 - Hydrodynamic radius, 164
 - Hydrogel, 210, 255, 286
 - Hyperthermia, 234, 236
 - Hypoxene, 149
- I**
- Imaging study, 270
 - cell contrast, 271
 - confocal microscopy, 270, 278
 - electron tomography, 95, 279
 - heavy metal stain, 272
 - sample preparation, 271
 - Immune system, 226
 - Immunological response, 33, 187
 - immunopotential, 35
 - vaccine
 - foot-and-mouth disease virus (FMDV), 35
 - Indium 42, 301
 - Influenza virus
 - inactivation of, 10, 108, 144
 - Infrared radiation, 245, 295
 - Internal energy, 320
 - Intraocular lens, 285
 - Intraperitoneal hyperthermic chemoperfusion, 254

Iodine, 125, 174, 301
Irradiation, 14, 88, 108, 111, 124, 131, 332
 laser irradiation, 296

J

Jablonsky diagram, 83, 232

L

Lanthanide, 160
Laser light scattering
 dynamic and static, 12, 164, 168
Lipid hydroperoxide, 87, 92
Liposome, 7, 91, 97, 135, 141

M

Magnetic particle, 288
Magnetic resonance imaging (MRI), 7, 12,
 100, 157
 diamagnetic relaxation rate, 159
 long-circulating agent, 160
 paramagnetic contrast agent
 spin relaxation time decreasing, 158
 relaxivity, 12, 159, 169
Membrane structure damage, 94
Microwave, 351
 resonance cavity, 352
 spectral response, 352
Mitochondrial succinate dehydrogenase, 133
Molar volume, 320
Molecular dynamics, 26, 37, 183, 205, 269
Molecular rotational motion, 164

N

N,N-dimethyl-fulleropyrrolidinium salt,
 9, 88, 93
NADH, 85, 88, 124, 135
Nanoinjector
 AFM tip, 294
Nanomedicine, 24, 305
Nanotechnology, 23, 80, 182, 224, 287
Necrosis, 15, 99, 124
Nephrogenic systemic fibrosis, 159
Nuclear magnetic resonance, 157, 228
 spin-lattice relaxation time (T₁), 158
 spin-spin relaxation times (T₂), 158
Nucleic acid, 37
 DNA therapeutics, 39
 RNA therapeutics, 40
 small-interference RNA, 40, 206, 296
Nucleophilic addition, 29

O

Oil, 317
 castor, 323
 iodine number, 328
 olive, 319
 soybean, 319
Optically driven actuator, 212

P

Parkinson's disease, 52, 69, 268
Peptide delivery, 11, 33
Perturbation theory, 353
Photodynamic therapy, 6, 79, 123, 235
 drawback
 light inaccessibility, 236
 sunlight hypersensitivity, 236
 photofrin, 81, 88, 98, 235, 256
 photosensitizer, 79, 81, 108, 124, 235
 phthalocyanine, 82
 porphyrin, 81
 tumor, 98
Photoinactivation, 92, 93, 109
Photoirradiation
 DNA degradation, 131
Photoluminescence, 230
Plasma polymerization, 203
Plasmid DNA, 27, 293
Polarization, 357
Polymerase, 10, 183
Polyvinylpyrrolidone, 6, 88, 142
Pyrene, 28, 135, 186

Q

Quantitative structure-property/activity
 relationship (QSPR/QSAR), 338
Quantum dot, 203, 207, 211, 249, 287
Quencher, 67, 92

R

Radical addition, 29, 332
Radioisotope delivery, 160, 172, 175
Reactive oxygen species, 2, 6, 14, 52, 67, 80,
 92, 119, 144, 235, 286, 302
 quenching mechanism, 51, 72
Refractive index, 329
Relaxivity, 159
 concentration dependency, 173
 metal-centered dependence, 164
 rotational correlation, 170
 solution pH dependence, 163
 unpaired spin dependence, 164

Relaxivity (*cont.*)

- water interstitial confinement correlation, 170
- water proton (r_1), 157

Resonant cavity, 351

- electromagnetic theory, 352

S

Scanning electron microscopy, 165, 201

Sensor, 183, 200, 210, 230, 354

Simplified molecular input line entry system (SMILES), 337

Solubility parameter, 320, 324

Solvent polarizability, 318

Structure-impact relationship, 65

Super-capacitor, 199

Superoxide dismutase, 15, 64, 68, 86, 149

Surface plasmon resonance (SPR), 11, 35, 242

T

Taq enzyme, 184

 ^{99m}Tc , 294, 301

Thermogravimetric analysis, 174

Toxin, detection, 354

Transfection, 11, 28, 39, 166

Transmission electron microscopy (TEM), 33, 95, 168, 270, 272, 275, 279

- cryo-TEM, 168

- elastic scattering, 273

- energy-filtered, 275

- high-angle annular dark-field scanning, 272

- high resolution TEM, 26, 29, 189, 201

- inelastic scattering, 273

- low-loss energy-filtered, 267

Triglyceride, 323

Tunneling nanotube (TNT), 363, 366

V

Virus, 35, 107, 369

- enveloped virus, 108

- photodynamic inactivation, 10, 92, 108, 111

- surface membrane fragmentation, 112

- viral contamination, 108

- viral titer, 109

Color Plates

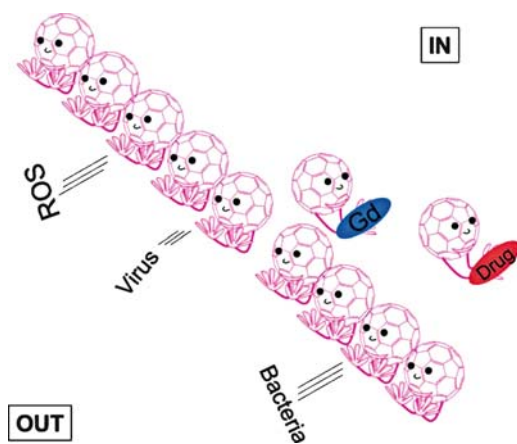
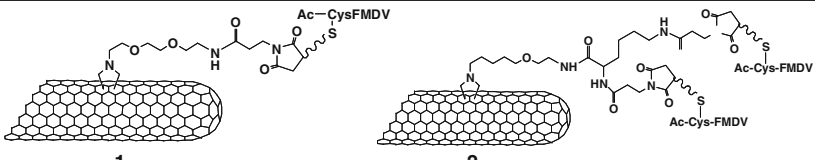
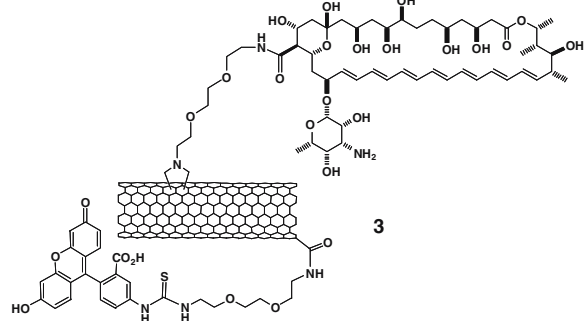
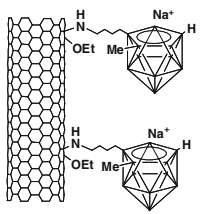
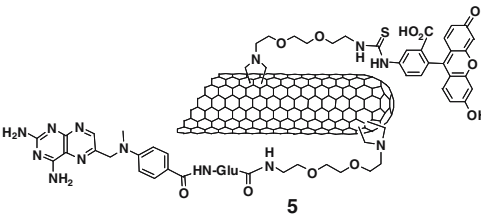
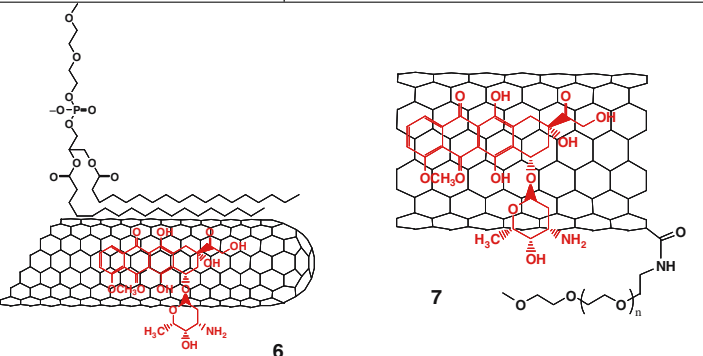


Fig. 1.5 Fullerene's activity

Table 2.1 Structures of carbon nanotubes (CNTs) conjugated to several therapeutic agents

 <p style="text-align: center;">1 2</p> <p style="text-align: center;">Peptide-vaccine delivery (Pantarotto et al. 2003a and 2003b) (FMDV peptide corresponds to the 141-159 region of the viral envelope protein VP1 from foot-and-mouth disease virus)</p>	
 <p style="text-align: center;">3</p> <p style="text-align: center;">Antibiotic delivery (Wu et al. 2005)</p>	
 <p style="text-align: center;">4</p> <p style="text-align: center;">Cancer therapy (Yinghui et al. 2005)</p>	 <p style="text-align: center;">5</p> <p style="text-align: center;">Cancer therapy (Pastorin et al. 2006)</p>
 <p style="text-align: center;">6 7</p> <p style="text-align: center;">Cancer therapy (Liu et al. 2007a, Ali-Boucetta et al. 2008)</p>	

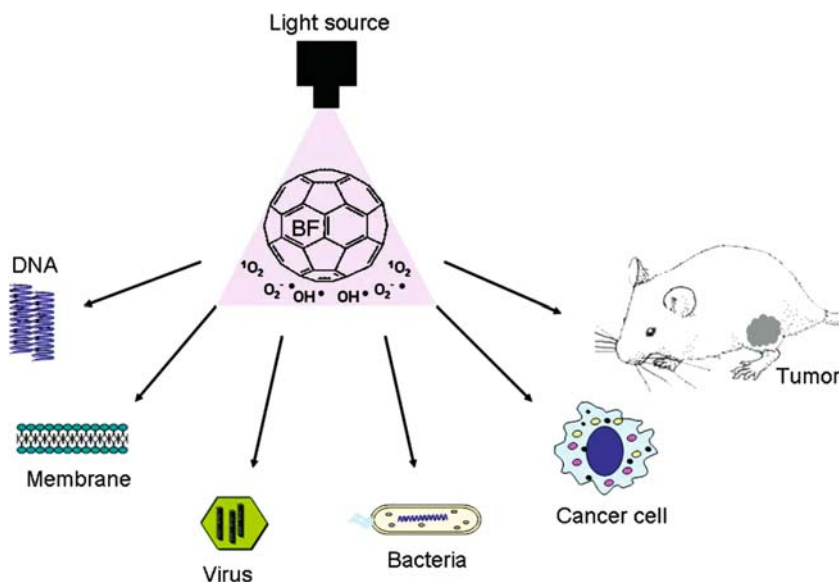


Fig. 4.1 Schematic outline of the possible applications of fullerenes as PDT sensitizers covered in this review

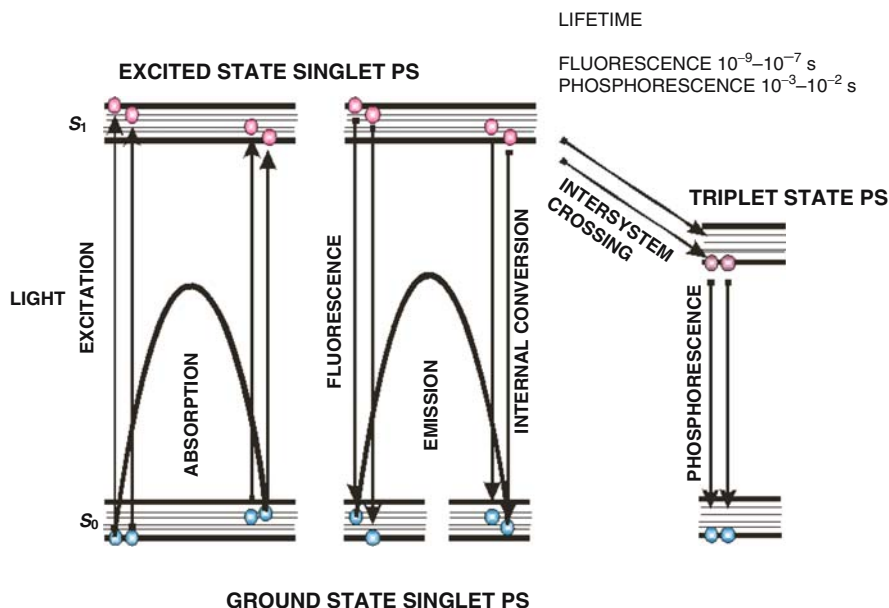


Fig. 4.3 Jablonsky diagram illustrating absorption of a photon by the ground-state singlet photosensitizer that gives rise to the short-lived excited singlet state. This can lose energy by fluorescence (negligible in case of fullerenes), internal conversion to heat, or by intersystem crossing the long-lived triplet state. The triplet state can undergo photochemistry as shown in Fig. 4.4

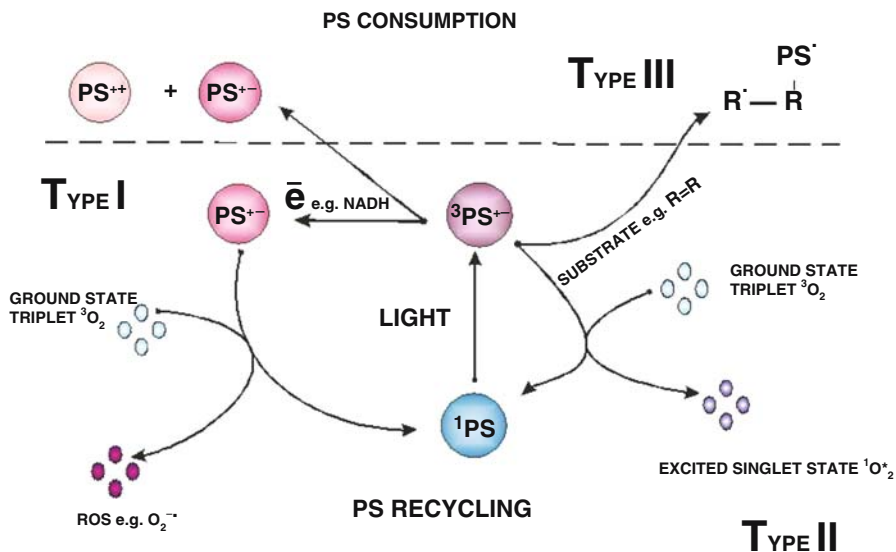


Fig. 4.4 Schematic representation of Type I, Type II, and Type III photochemical mechanisms thought to operate in PDT

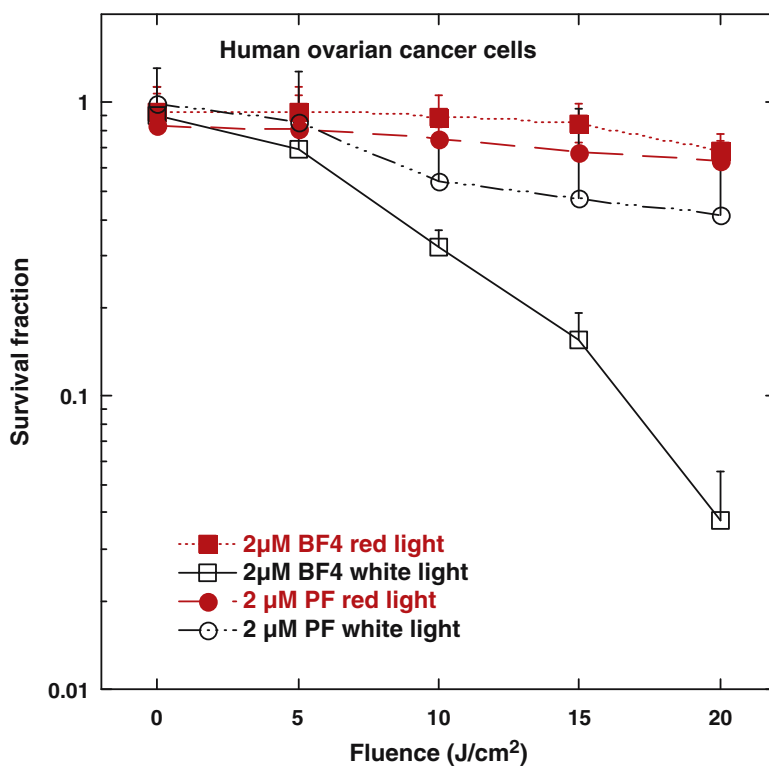


Fig. 4.9 Comparison of PDT-induced killing in human ovarian cancer cells by **BF4** or Photofrin both incubated for 24h at 2 μ M concentration and illuminated with red (630nm) or white light (400–700nm)

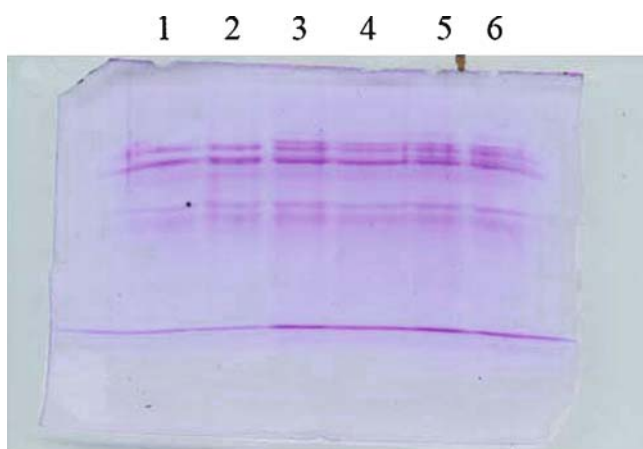


Fig. 5.6 Electrophoresis pattern of proteins of blood serum. Lanes 1–3: intact serum, lanes 4–6 serum after 6 h of irradiation

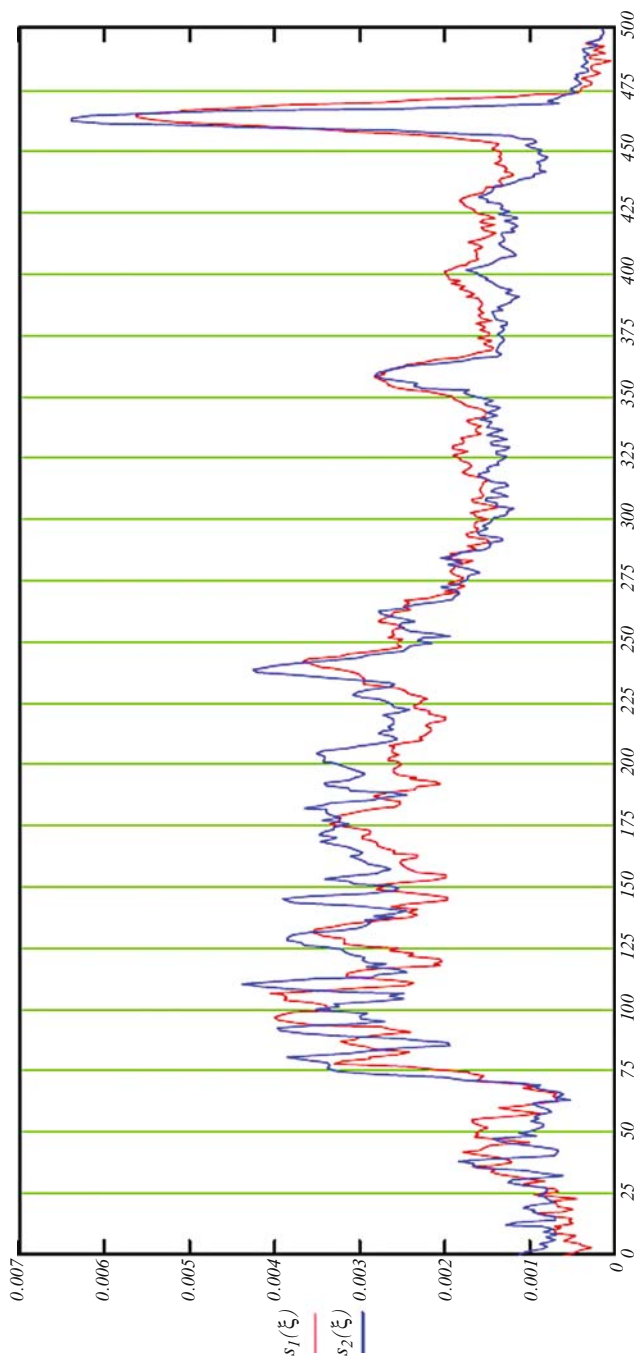


Fig. 5.7 Photometric representation of electrophoresis results. Allantoinic fluid before (red) and after (blue) 6 h of irradiation

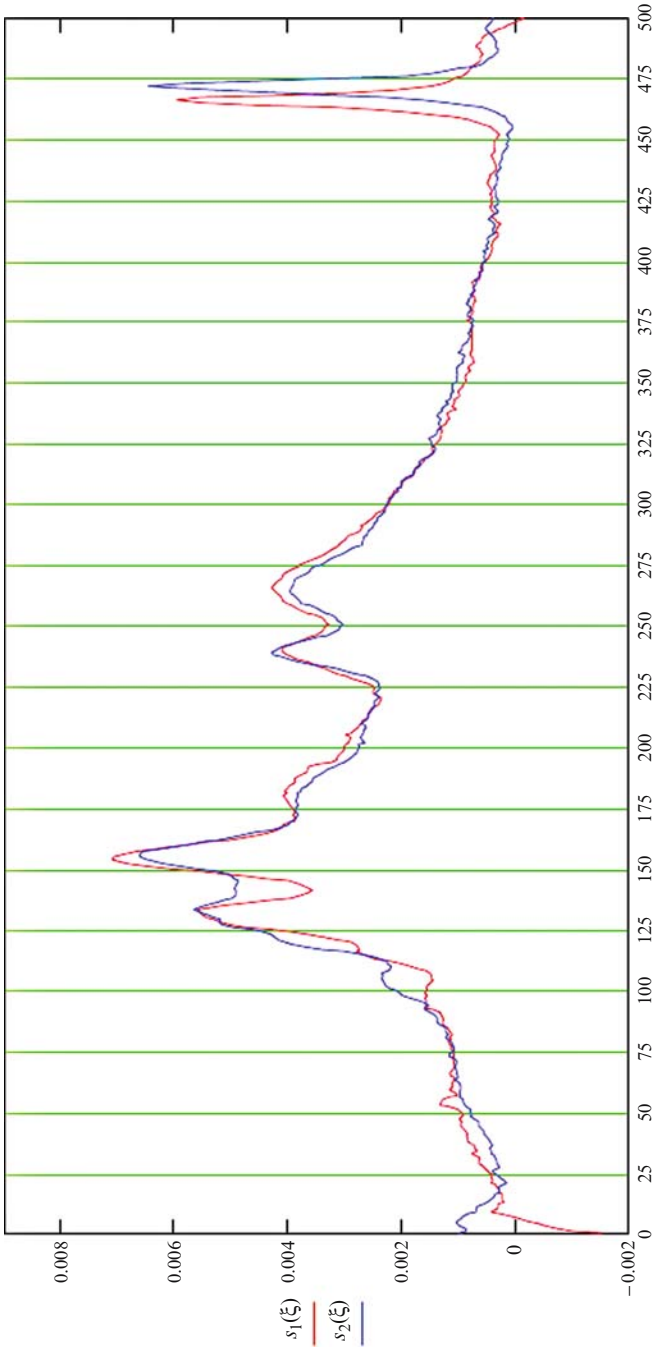


Fig. 5.8 Photometric representation of electrophoresis results. Blood serum before (red) and after (blue) 6 h of irradiation

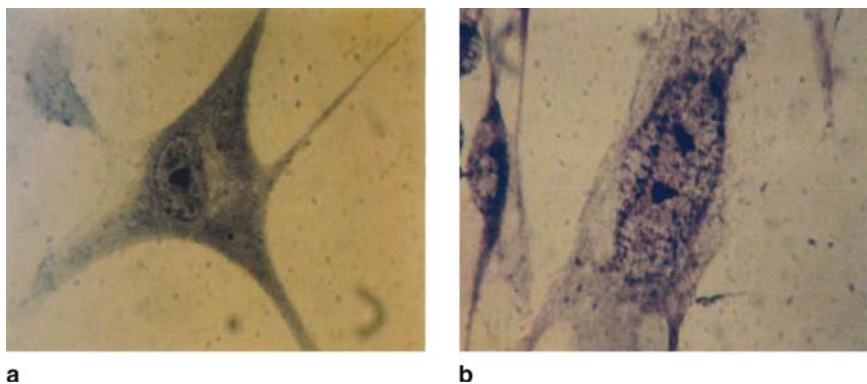


Fig. 7.4 Normal human embryonic fibroblasts grown on fullerene on the surfaces (FoS) before (A) and after 30 min illumination with halogen lamp 45 mW/cm^2 (B). Magnification $1,200\times$

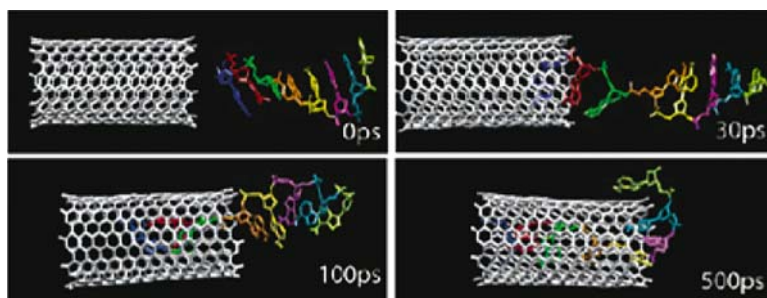


Fig. 9.1 Simulation snapshots of a DNA oligonucleotide (8 adenine bases) interacting with a (10,10) carbon nanotube at 0, 30, 100, and 500 ps. Water molecules are not displayed for clarity (Chaudhary et al., 2006. With permission from American Chemical Society)

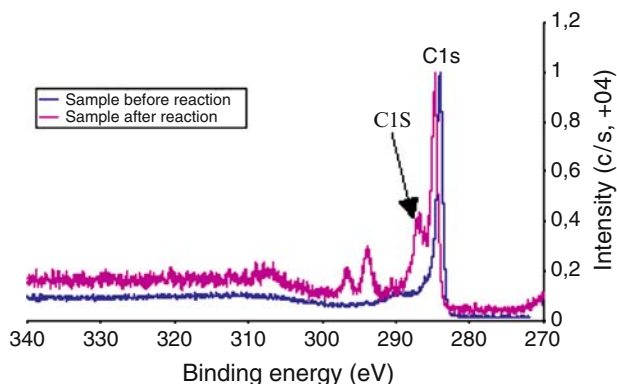


Fig. 9.3 The result of C1s binding energy intensity of samples before (lower curve) and after (upper curve) PCR reaction. The left peaks represent the binding energy intensity of C 1s of SWCNTs after PCR reaction; the right-most peak represents the binding energy intensity of C 1s of SWCNTs before reaction. The graph shows that the C 1s peak of SWCNTs moves towards the left with the emergence of two C 1s peaks, indicating enhanced binding energy after PCR reaction (Chen et al., 2001. With permission from IOP Publishing)

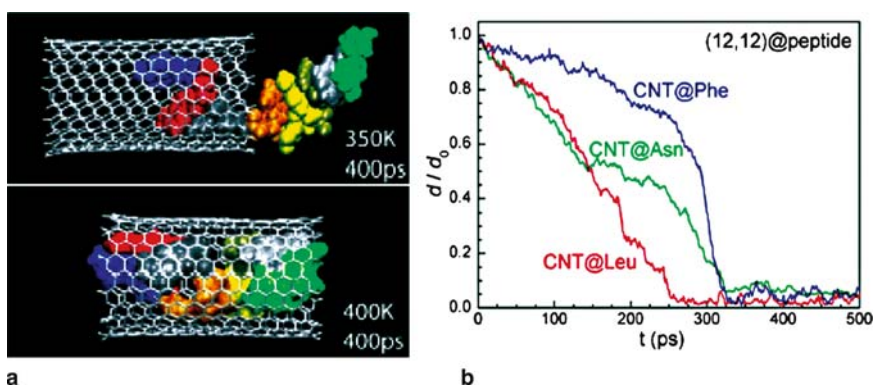


Fig. 9.4 (a) Snapshot of peptide being filled into CNT; (b) normalized COM distances between polypeptide and CNT as function of simulation time (d_0 is the initial COM distance) (Dillon et al., 1997. With permission from American Materials Research Society)

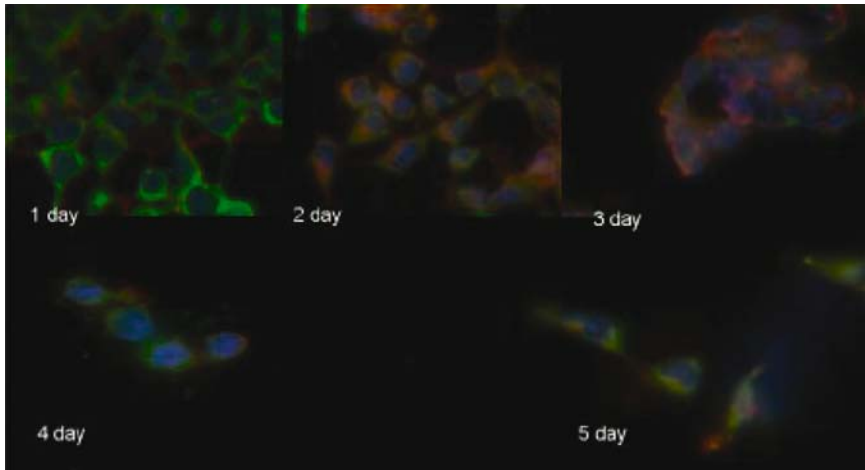


Fig. 9.7 Indirect immunofluorescent staining of SWCNTs-treated HEK293 cells for day 1–5 by fluorescent microscopy ($\times 630$). Green: cadherin; red: collagen; blue: cellular nucleus staining with DAPI. The expression levels of cadherin and collagen IV in cells decreased gradually as the culture days increased; HEK293 cells gradually detached from the cell populations as the culture days increased (Grunlan et al., 2004. With permission from Elsevier)

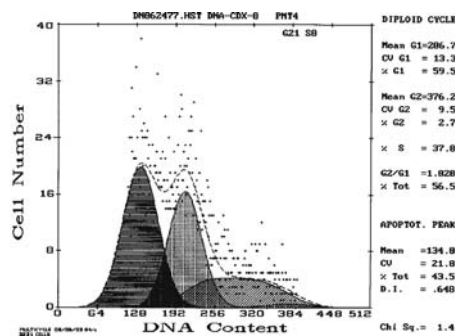


Fig. 9.8 Apoptosis of HEK293 cells induced by SWCNTs. B1: DNA electrophoresis of cells cultured with 25 $\mu\text{g/ml}$ SWCNTs for 1–5 days, *M* molecular marker, no. 1–5 denote the results of cells cultured for day 1–5, respectively; B2: DNA electrophoresis results of control cells cultured for day 1–5; C: the cell cycle distribution of HEK293 cells cultured with 25 $\mu\text{g/ml}$ SWCNTs for 4 days, the percentage of sub-G1 cells (apoptosis cells) was 43.5%. (Grunlan et al., 2000. With permission from Elsevier)

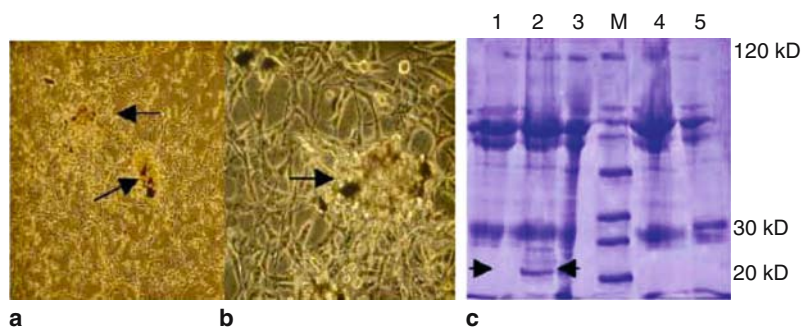


Fig. 9.9 Responses of HEK293 to single-walled carbon nanotubes. (A) SWCNTs were aggregated together and surrounded by HEK293 cells ($\times 200$). (B) The aggregated SWCNTs were surrounded by secretion from HEK293 cells ($\times 400$). (C) SDS-PAGE result showed that some 20–30 kD proteins existed in the supernatants of HEK293 cells with 25 g/ml SWCNTs. *M* is protein marker; the no. 1–5 denote the results for HEK293 cells cultured with SWCNTs for 1–5 days, respectively, showing some small secreted proteins were only detected on the day 2 and day 3 after SWCNTs were added inside the cell culture (Grunlan et al., 2000. With permission from Elsevier)

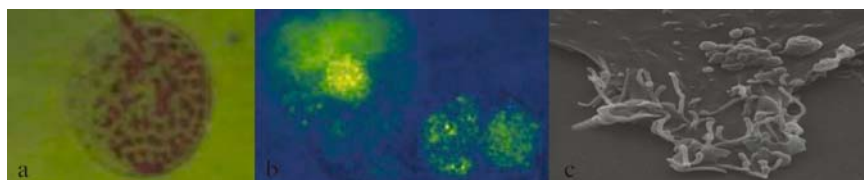


Fig. 9.10 SWCNTs attached to the surface of cells and located within cells **a**. SWCNTs attached to the surface of cells; **b**. SWCNTs labeled with Cy3 located within cells; **c**. Some protuberances appeared on the cell surface after cells are stimulated by SWCNTs. Right picture is control. Bar is 10 μm (With permission from American Scientific publisher)

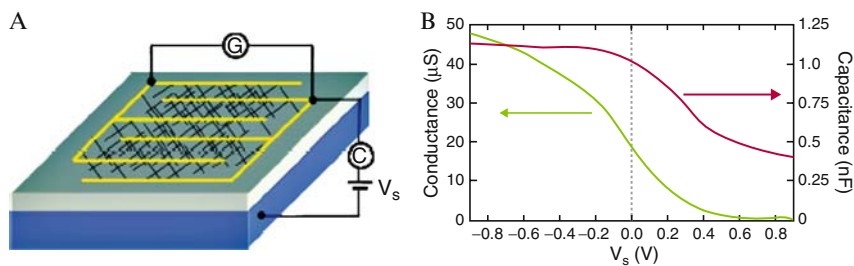


Fig. 9.18 (a) Schematic of the device, which was designed for simultaneous measurement of the SWNT network capacitance and conductance. (b) Dependence of the network capacitance (red) and conductance (green) on the substrate voltage, V_s . The network capacitance is approximately 1/4 the value of the capacitance for a parallel-plate capacitor with an equivalent area and oxide thickness (Kong et al., 2003. With the permission from American Chemical Society)

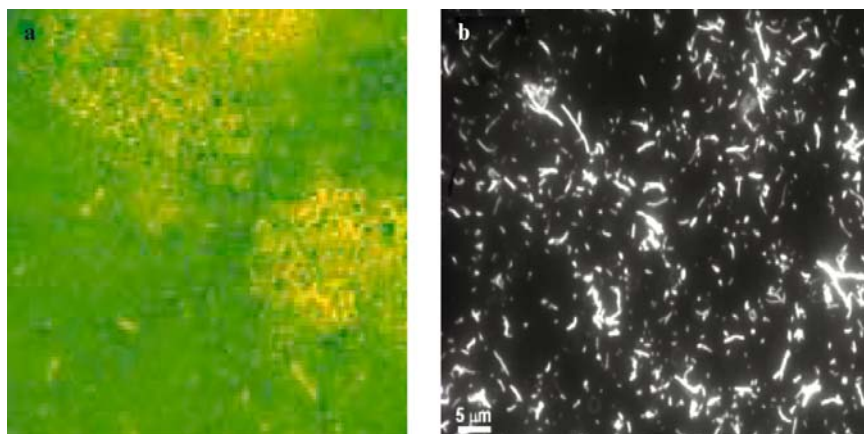


Fig. 9.20 Luminescent carbon nanotubes (a) Cy3 labeled antisense myc-modified SWCNTs; (b) quantum dots-modified MWCNTs (With permission from American Scientific publisher and Wiley-VCH)

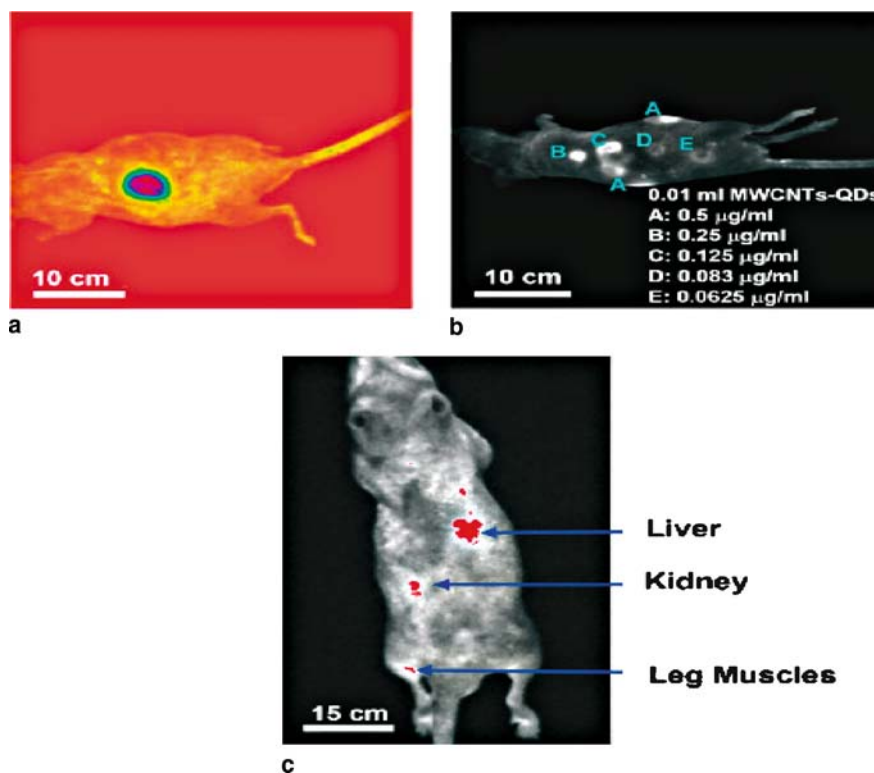


Fig. 9.21 In vivo images of MWCNTs-QDs ($0.5 \mu\text{g ml}^{-1}$ in PBS) in mice injected at different body regions: a) MWCNTs attached with CdSe/ZnS quantum dots (emission of 600 nm) at middorsal location; b) MWCNTs attached with CdSe/ZnS quantum dots at ventrolateral locations, the suspensions were diluted by PBS at various concentrations as indicated (A through E); c) MWCNTs attached with InGaP/ZnS quantum dots (emission of 680 nm, $0.25 \mu\text{g ml}^{-1}$ in PBS) in liver, kidney, and leg muscles. All images were taken successfully in 2 min under epi-UV illuminator with excitation of 435nm. (Shi et al. 2007). Published with permission from Wiley-VCH

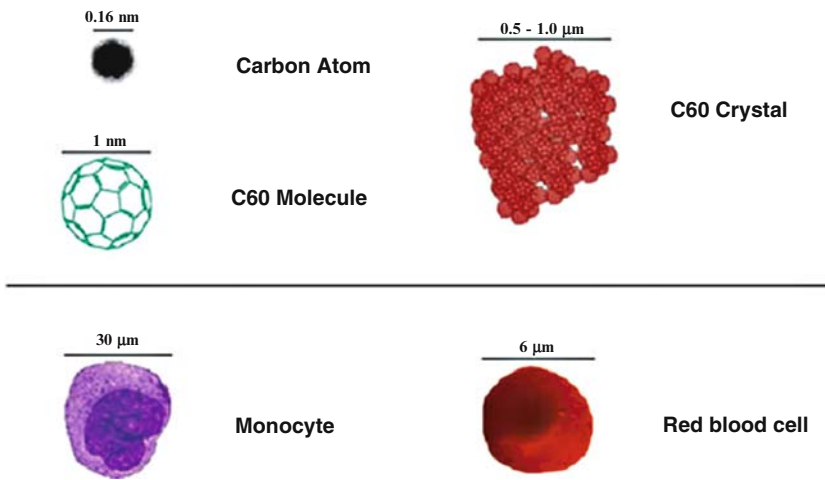


Fig. 10.1 Comparative sizes of one carbon atom, one molecule of C_{60} fullerene, a typically sized aggregate of C_{60} fullerene, a red blood cell, and a large immune system cell, a monocyte

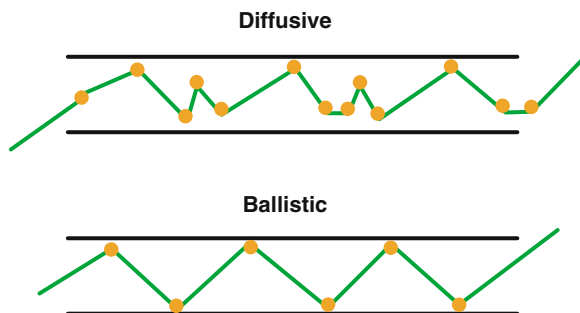


Fig. 10.2 Diffusive versus ballistic transport of electrons

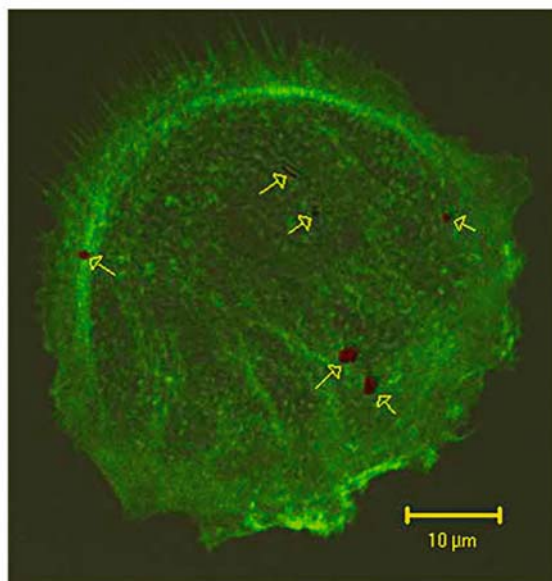
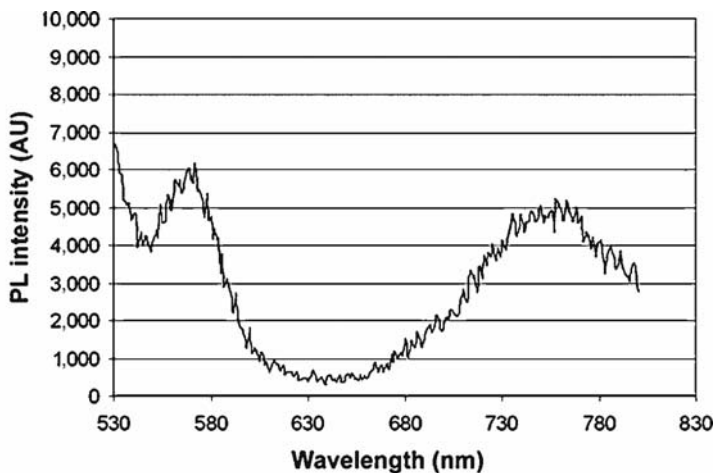


Fig. 10.5 Photoluminescence spectra of dissolved C_{60} . The peak at 750 nm is the photoluminescence signature of the material. Photoluminescent C_{60} aggregates can be visualized within cells and exhibit a vivid red signature which is easily detectable (Levi et al., 2006)

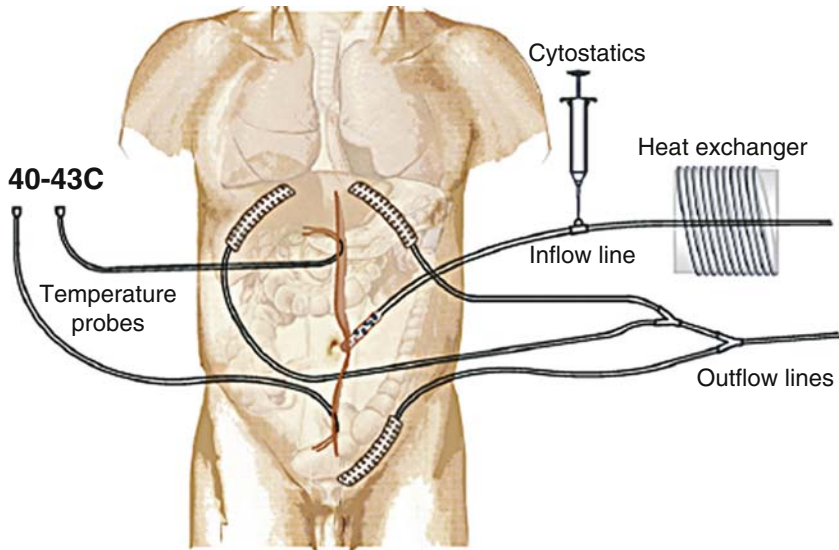


Fig. 10.9 Circuit diagram for intraperitoneal hyperthermic chemoperfusion. Warmed chemotherapeutic agents are circulated through the abdomen and temperature at the inflow and outflow ports are continuously monitored (Reprinted from Reingruber et al., 2007. With permission from Elsevier)

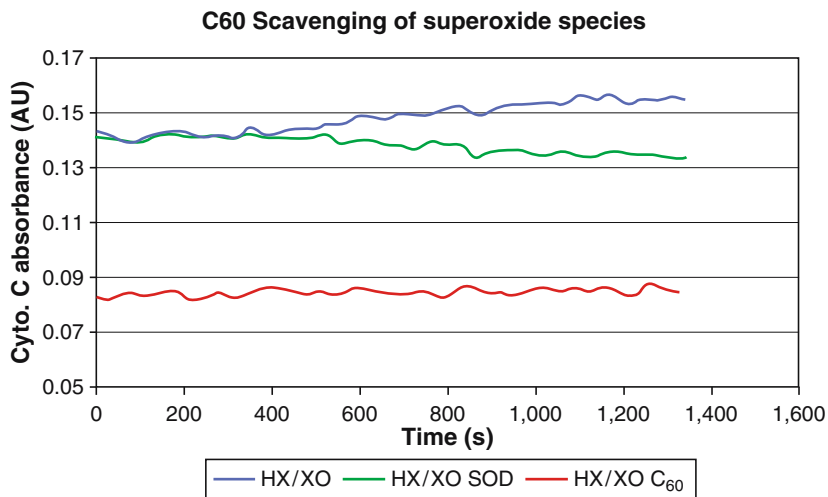


Fig. 10.10 C₆₀ is a very effective scavenger of superoxide species. The standard superoxide scavenger, superoxide dismutase, is not nearly as effective

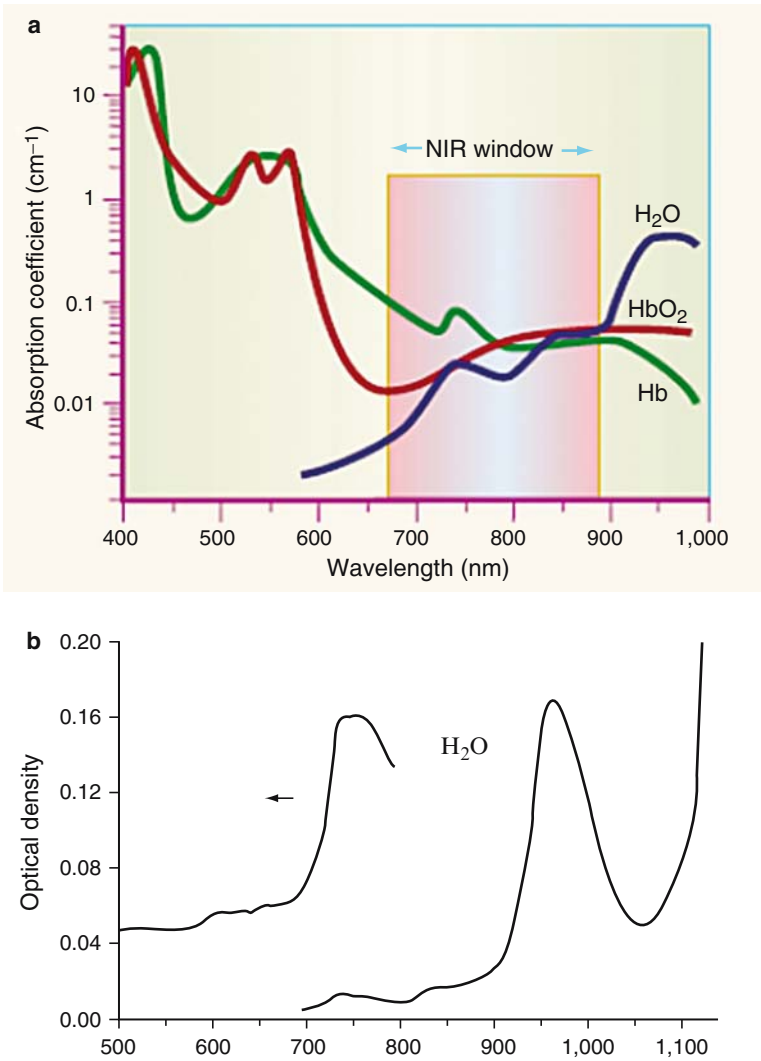


Fig. 10.12 The most efficient regions for nanotube absorption lie where water and hemoglobin have absorption minima: between 700 and 900 nm and around 1,100 nm (Braun and Smirnov 1993; Reprinted from Weissleder, 2001. With permission from Elsevier)

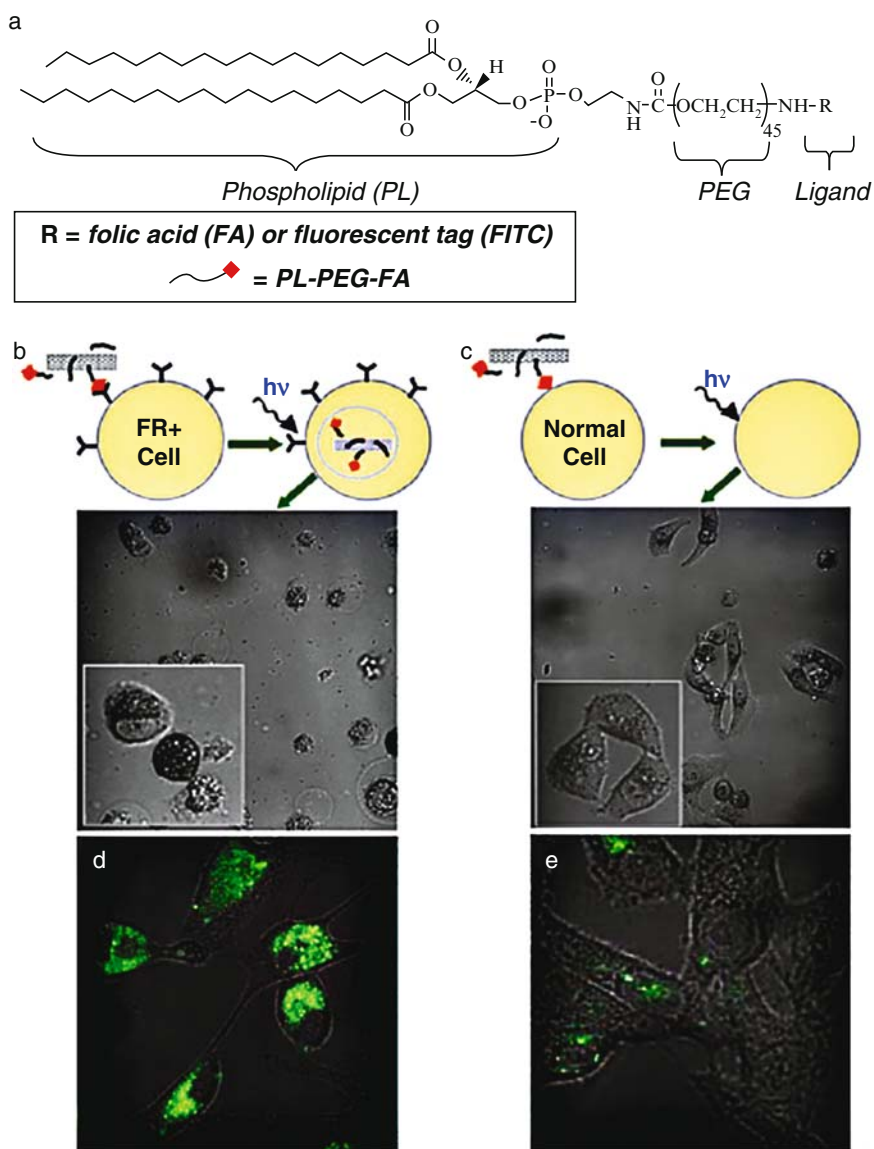


Fig. 10.14 Folic acid can be conjugated onto nanotubes fluorescently labeled nanotubes to target cells expressing folic acid receptors (a,b,c). Nanotubes conjugated with folic acid display a fluorescent signature indicating that nanotubes are internalized by cells expressing folic acid receptors (d). Without the folic acid conjugate, there is very little distribution of nanotubes within the cells as attributed by the lack of fluorescent signature in (e) (Reprinted from Kam et al., 2005. With permission from the National Academy of Sciences, USA)

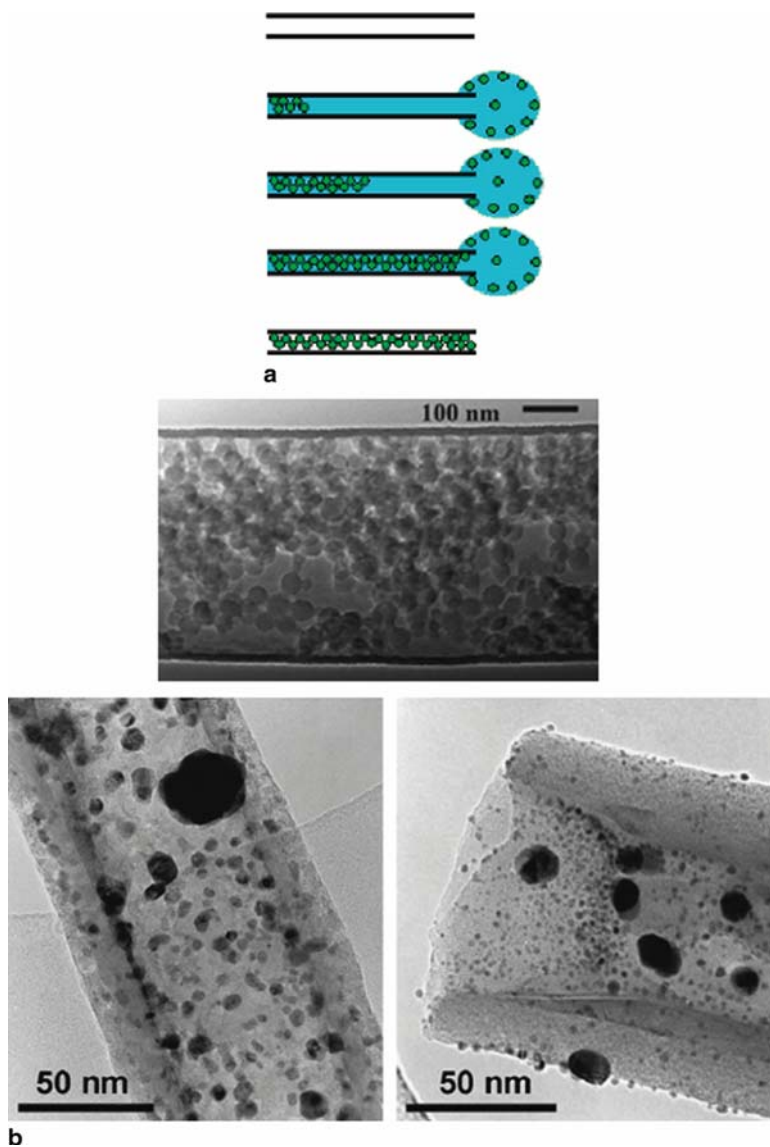


Fig. 10.15 The methods for capillary filling of nanotubes involves dispersal of the agent in a liquid capable of flowing into the nanotube followed by subsequent evaporation of the solvent to leave particles inside the tube. Nanotubes have been filled with polystyrene spheres and palladium nanocrystals using this method (Reprinted from Kim et al., 2005. With permission from American Chemical Society; Reprinted from Tessonnier et al., 2005. With permission from Elsevier)

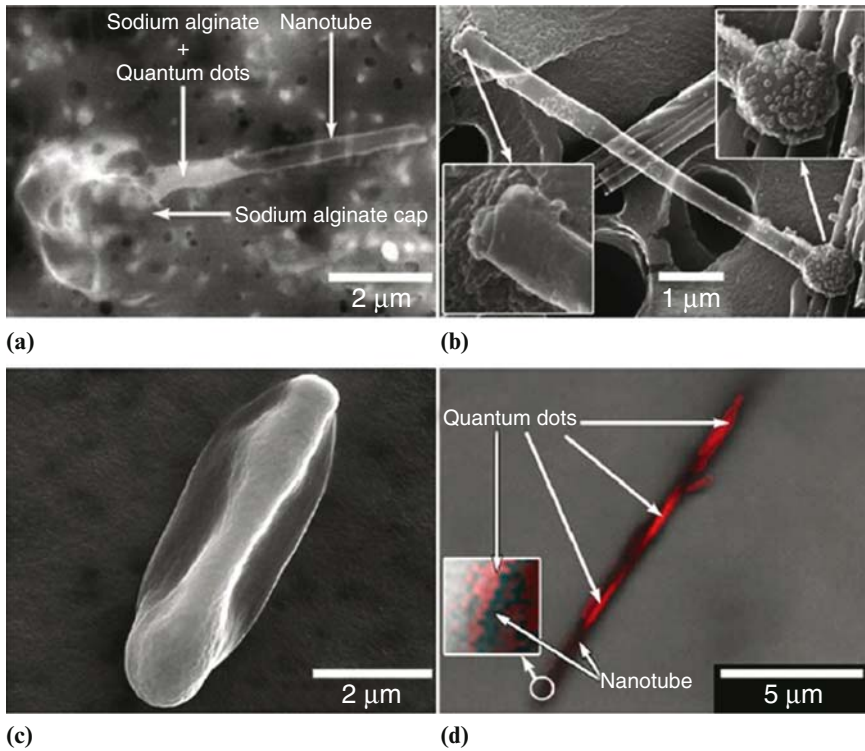


Fig. 10.16 Carbon nanotubes filled with quantum dots in a sodium alginate carrier solvent. The alginate encloses the dots into the tubes by sealing the tube ends. A large majority of excess alginate around the tubes was removed by repeated washing (Reprinted from Nadarajan et al., 2007. With permission from Elsevier)

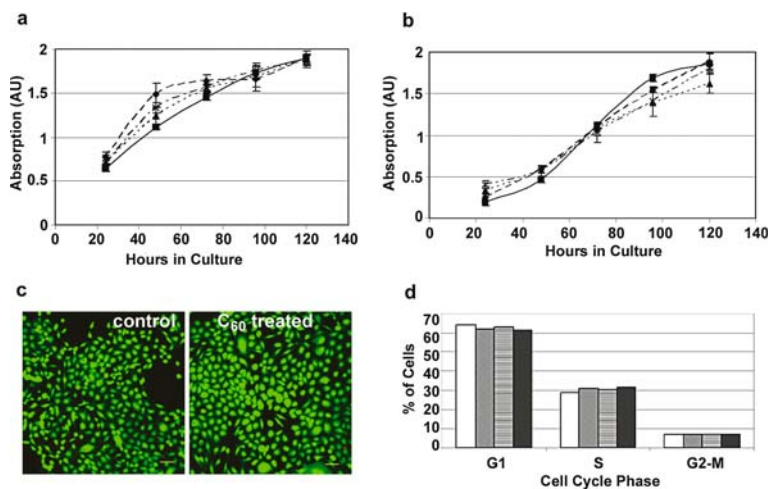


Fig. 10.19 Lack of toxic effects of C₆₀ fullerene on breast epithelial cells. C₆₀ does not inhibit cell proliferation. MCF 10A and (A) MDA MB 231 (B) breast cancer cell lines were cultured either in the absence or presence of methanol C₆₀ and cell proliferation was assayed by crystal violet staining. ♦ Control, no C₆₀, ■ 10 μg C₆₀, ▲ 50 μg C₆₀, X 250 μg C₆₀. (C). MDA MB 231 cells were simultaneously stained with calcein and ethidium using a live-dead assay kit. Lack of red-colored cells and the presence of cells stained in green indicate the lack of toxicity (D). MDA MB 231 cells were either untreated (open box) cultured with varying amounts 10 (gray ■), 50 (patterned ■) and 100 μg (filled ■) of C₆₀ for 48 h and analyzed for cell cycle progression by flow cytometry (Levi et al., 2006)

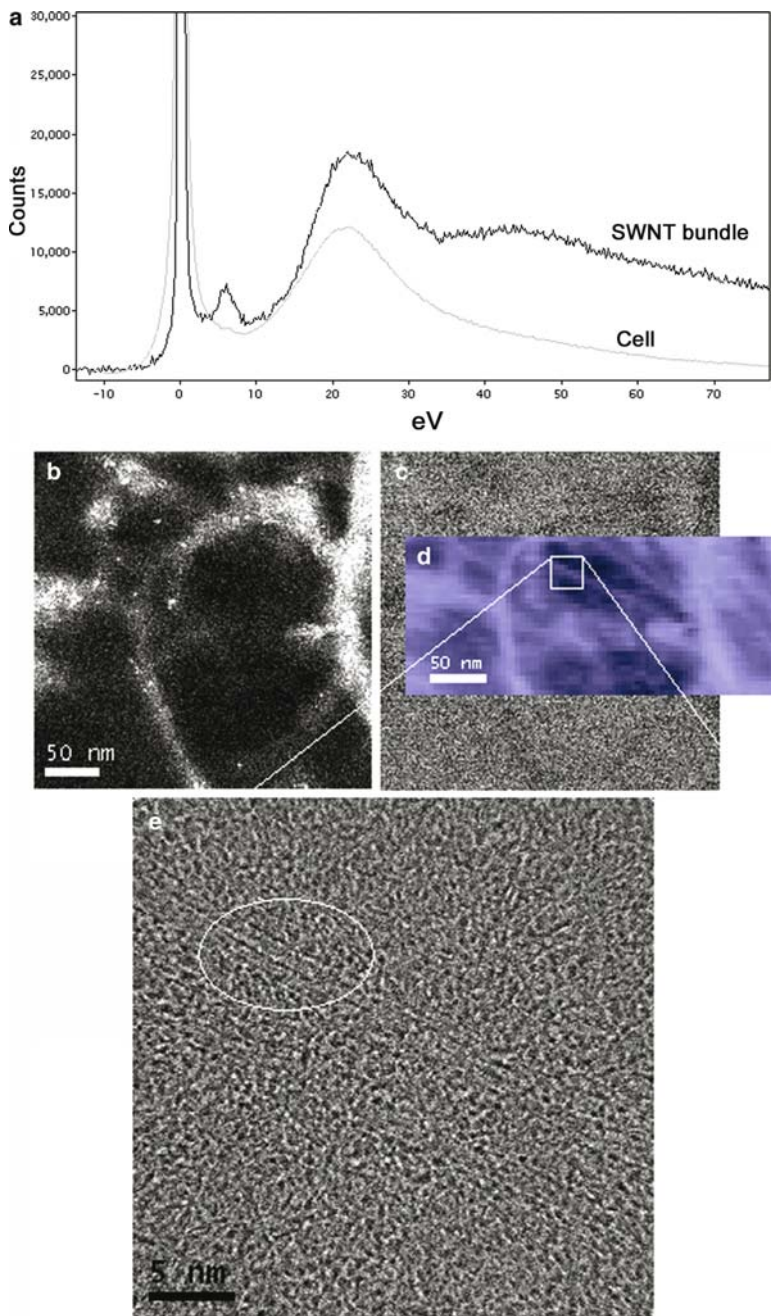


Fig. 11.4 (a) (c) Low-loss EELS spectra of SWNT bundles and the cell alone. The π - π^* transition at ~ 6 eV can be seen clearly only from the bulk of the SWNT bundle, it also exhibits a slightly higher bulk plasmon energy which is clearly visible when mapped as in (d). (b) HAADF image of SWNT bundles with Fe catalyst particles. Fe particles give bright contrast in HAADF image so allow SWNT bundles to be identified. (c) The corresponding bright field image showing no visible features in the same area. (d) Area of interest picked out with plasmon peak map from Fig. 11.1b). (e) High-resolution bright field imaging of the boxed area shows several SWNTs across the image (c). Diameter of SWNT indicated by arrows is 1.2 nm

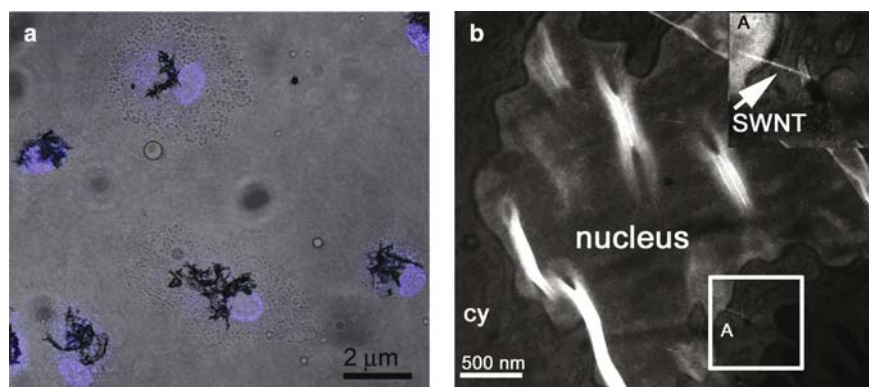


Fig. 11.5 (a) Confocal microscope image of HMMs exposed to AgI@SWNT at 3 days confirming inclusion of SWNT bundles inside the nucleus (blue). (b) HAADF-STEM image of PbO@SWNTs crossing the nuclear membrane into the nucleus (inset from boxed region A) (40 nm thick section, unstained)

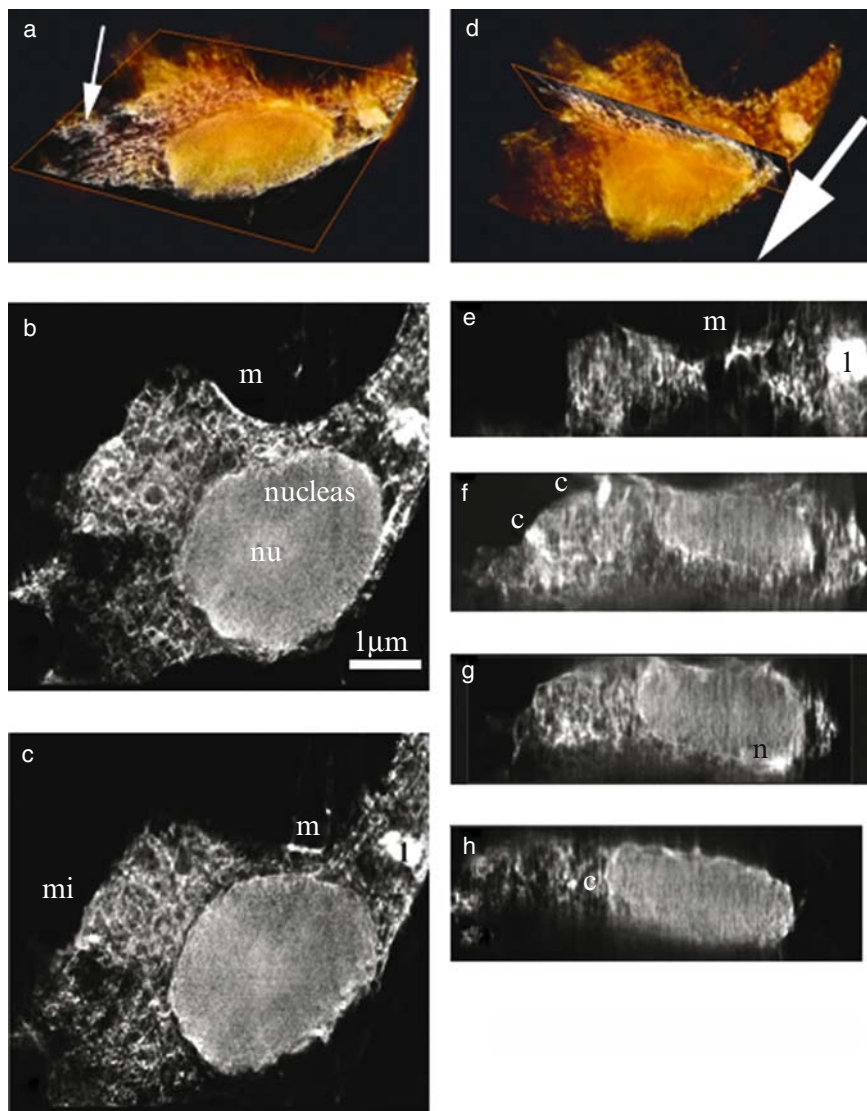


Fig. 11.6 A series of horizontal (b–c) slices and vertical slices (e–h) through a HAADF-STEM reconstruction of a freeze-dried whole cell exposed to C_{60} for 24 h. Slices are $\sim 0.15 \mu\text{m}$ apart. (a) Voltex reconstruction of the same cell showing a horizontal orthoslice through the 3-D reconstruction. (d) Vertical orthoslice through the Voltex reconstruction. Slices through the reconstruction illustrate membranes (m), the nucleus (n), the cytoplasm (c), and secondary lysosomes (l). Several distributions of particles with the cell are revealed at each height through the reconstructed cell

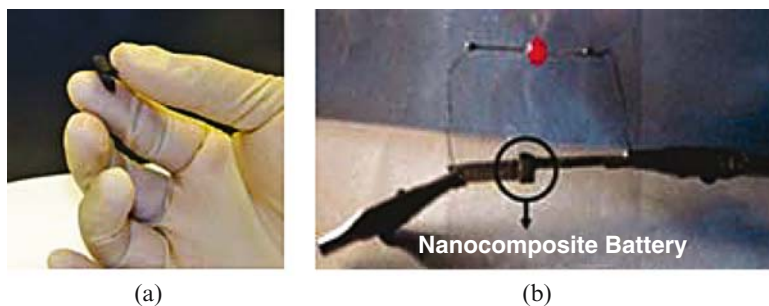


Fig. 12.2 A foldable, bendable battery; paper invention which can be inserted under the skin as a pacemaker and powered in part by bodily fluids. (a) A postage-stamp-sized battery as thin as paper, (b) the flexible nanocomposite film battery used to glow a red light-emitting diode (LED)

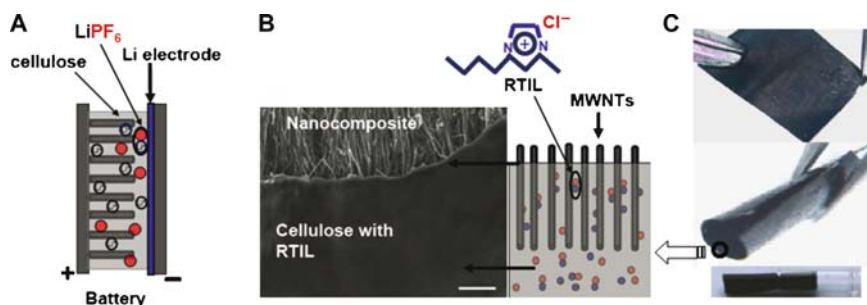


Fig. 12.3 Fabrication of the nanocomposite paper units for battery. (a) Schematic of the battery assembled by using nanocomposite film units. The nanocomposite unit comprises LiPF_6 electrolyte and multiwalled carbon nanotube (MWNT) embedded inside cellulose paper. A thin extra layer of cellulose covers the top of the MWNT array. Ti/Au thin film deposited on the exposed MWNT acts as a current collector. In the battery, a thin Li electrode film is added onto the nanocomposite. (b) Cross-sectional SEM image of the nanocomposite paper showing MWNT protruding from the cellulose-RTIL ([bmIm] [Cl]) thin films (scale bar, $2\mu\text{m}$). The schematic displays the partial exposure of MWNT. A supercapacitor is prepared by putting two sheets of nanocomposite paper together at the cellulose exposed side and using the MWNTs on the external surfaces as electrodes. (c) Photographs of the nanocomposite units demonstrating mechanical flexibility. Flat sheet (*top*), partially rolled (*middle*), and completely rolled up inside a capillary (*bottom*) are shown

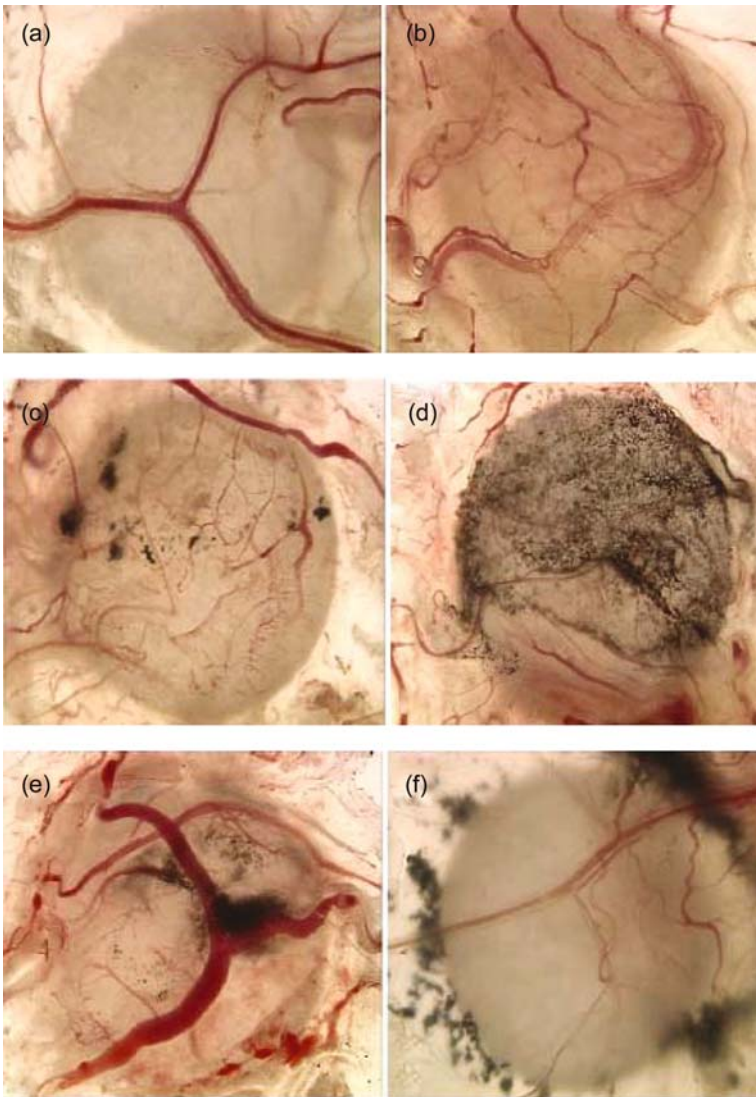


Fig. 12.5 Representative microscopic images of (a) PBS control, (b) FGF2, (c) FGF2 – multi-walled carbon nanotubes (MWNTs) (100 μg), (d) FGF2 – graphite (100 μg), (e) FGF2 – fullerene (100 μg), and (f) FGF2 – MWNTs (1 mg) treated CAM models

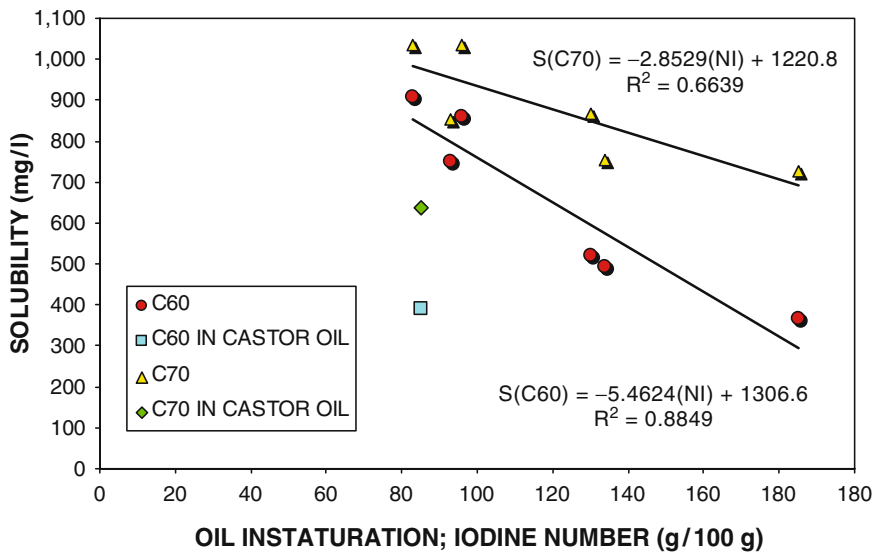


Fig. 13.1 The solubility of C_{60} and C_{70} fullerene is maximum in vegetable oils with lower level of unsaturation (i.e. number of double bonds) and decreases as the insaturation level grows. Having a peculiar chemical structure, castor oil cannot be included in the correlation rule

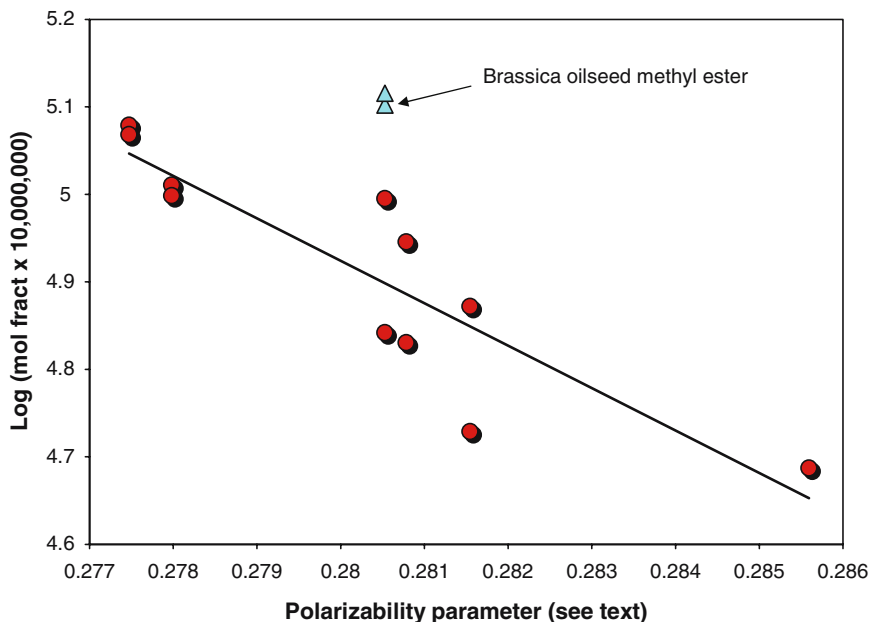
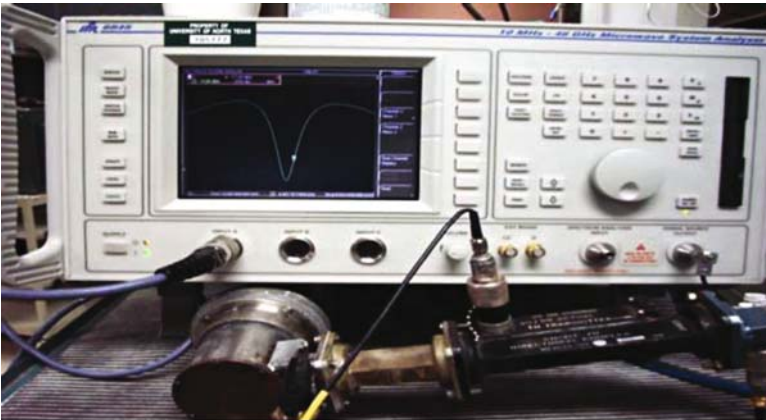


Fig. 13.2 Variation of Log (Mole Fraction $\times 10^7$) with the polarizability parameter $P_p = [(n^2 - 1) / (n^2 + 2)]$ for both C_{60} and C_{70} in various triglycerides of fatty acids. The triangles refer to C_{60} and C_{70} dissolved in methyl ester of brassica oilseed



a

Fig. 15.2a Two tunable vacuum tight cylindrical resonant cavities that were phase-locked and their impedance were matched using the impedance tuning coil. The plungers seen on the top were to aid us in tuning these cylinders to resonate in TE_{011} mode



b

Fig. 15.2b IFR6845 series microwave network analyzer used as the synthesized source to generate and feed the microwaves into the resonant cavities

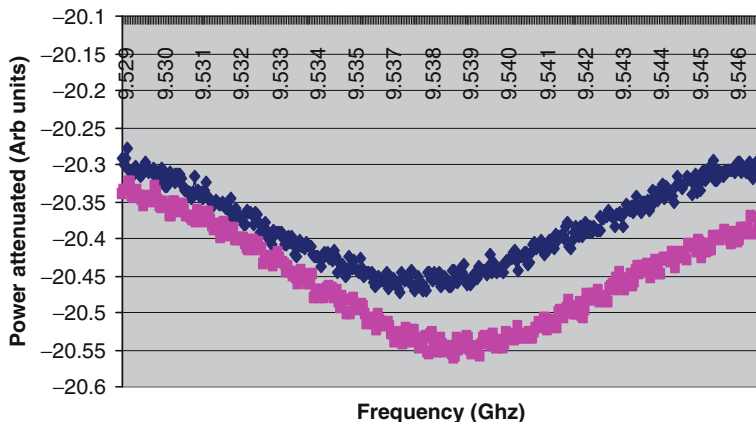


Fig. 15.3 A typical frequency response curve obtained due to the introduction of air into the resonant cavities. Shown above in pink is a typical absorption profile of the resonator under vacuum, and in blue is the shift of the resonant frequency to a lower value upon introducing air into the system

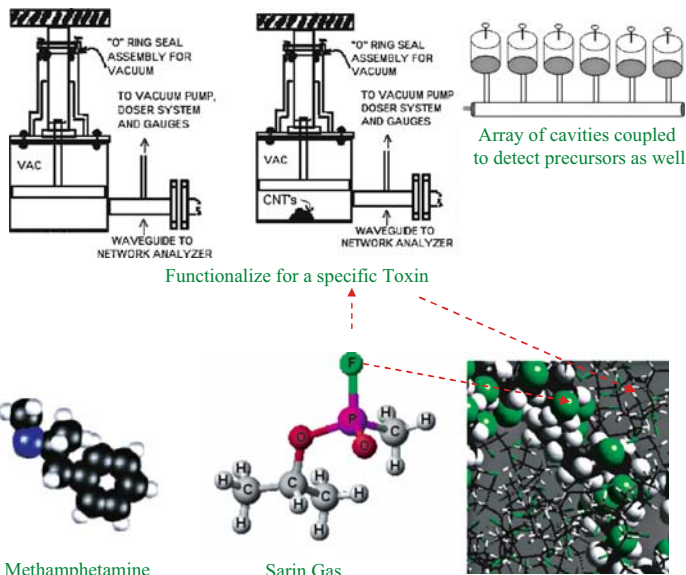


Fig. 15.4 Functionality of the prototype for specific detection

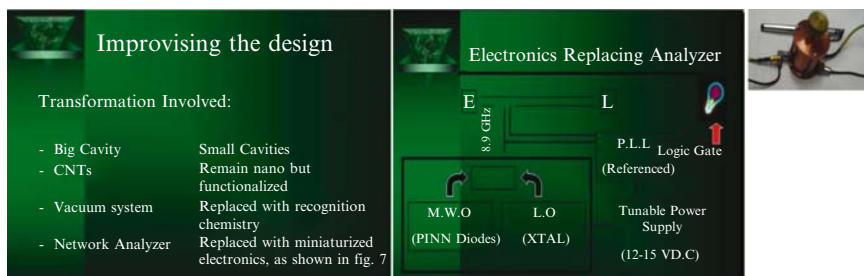


Fig. 15.6 (left) and 15.7 (right) The figures shown above describe the necessary steps taken to introduce portability into the sensor prototype. Shown on the right is the schematic involved in phase-locking the empty (E) and the loaded (L) cavity energized with a 12 V DC current-driven microwave diode. A typical electromagnetic mixer circuit has also been developed. The cavity shown at the far right is a significantly smaller than the test cavity and is comparable to today's cellular phones

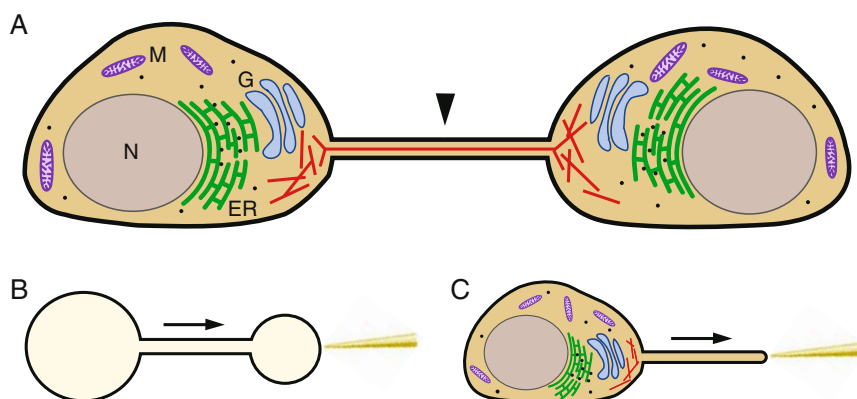


Fig. 16.2 Schematic representation of cellular and artificial membrane nanotubes. (A) Two cells are connected by a tunneling nanotube (arrowhead) containing a bundle of filamentous actin (red line). N (grey), nucleus; M (purple), mitochondrion; ER (green), endoplasmic reticulum; G (blue), Golgi apparatus. (B) Lipid nanotube connecting two lipid vesicles formed by pulling a membrane tether. (C) Membrane tether pulled from the plasma membrane of a cell